John Villadsen
Jens Nielsen
Gunnar Lidén

Bioreaction Engineering Principles

Third Edition

Springer

Bioreaction Engineering Principles

John Villadsen • Jens Nielsen • Gunnar Lidén

Bioreaction Engineering Principles

Third Edition

Springer

John Villadsen
Department of Chemical
and Biochemical Engineering
Technical University of Denmark (DTU)
Lyngby, Denmark
jv@kt.dtu.dk

Gunnar Lidén
Department of Chemical Engineering
Lund University
Lund, Sweden

Jens Nielsen
Systems Biology
Chalmers University of Technology
Gothenburg, Sweden
nielsenj@chalmers.se

ISBN 978-1-4419-9687-9 e-ISBN 978-1-4419-9688-6
DOI 10.1007/978-1-4419-9688-6
Springer New York Dordrecht Heidelberg London

Library of Congress Control Number: 2011931856

Preface

In early 2009, we were approached by Springer Verlag, the company that had absorbed Kluwer Academic/Plenum Publishers. The second edition of our textbook "*Bioreaction Engineering Principles*" was now sold out, and we were asked to prepare a third edition.

With very little hesitation we accepted the offer.

Since 2003 the book has been used as course-book, in European universities and also in North and South America, in the Far East, and in Australia. We wished not only to revise the text, but also to write a book that would appeal to students at the best universities, at least until 2020. In short courses given at major Biotech companies we have also found that some of the material in the previous editions could be used right away to give the companies a better understanding of their processes and to propose better design of their reactors. This acceptance of the book by the industrial community prompted us to include even more examples relevant for design of processes and equipment in the industry. The changes that have been made since the second edition are outlined in the first, introductory chapter of the present edition.

Our initial enthusiasm to embark on a complete revision of the text was mollified by the duties imposed on two of us (J.N. and G.L.) in handling large research groups and with the concomitant administration. One of us (J.V.) had much more time available in his function as senior professor, and he became the main responsible person for the work during the almost 2 years since the start of the project. But we are all happy with the result of our common efforts – "*Tous pour un, un pour tous*."

Some chapters have been read and commented by our colleagues. Special thanks are owed to Prof. John Woodley for commenting on Chaps. 2 and 3, and to Prof. Alvin Nienow for long discussions concerning the right way to present Chap. 11. The former Ph.D. students, Drs. Mikkel Nordkvist and Thomas Grotkjær have kindly given comments to many of the chapters.

We also thank Ph.D. student Saeed Sheykshoaie at Chalmers University who redrew many of the figures in the last rush before finishing the manuscript. Ph.D. student Jacob Brix at DTU has often assisted J.V. with his extensive knowledge of "how to handle the many tricks of Word."

Lyngby, Denmark — John Villadsen
Gothenburg, Sweden — Jens Nielsen
Lund, Sweden — Gunnar Lidén

Contents

List of Symbols

Symbols that are defined and used only within a particular Example, Note, or Problem are not listed. It should be noted that a few symbols are used for different purposes in different chapters. For this reason, more than one definition may apply for a given symbol.

a	Cell age (h)
a	Specific interfacial area (m^2 per m^3 of medium)
a_d	Specific interfacial area (m^2 per m^3 of gas–liquid dispersion)
a_{cell}	Specific cell surface area (m^2 per gram dry weight)
$\mathbf{A}$	Matrix of stoichiometric coefficients for substrates, introduced in (7.2)
$b(y)$	Breakage frequency (h^{-1})
$\mathbf{B}$	Matrix of stoichiometric coefficients for metabolic products, introduced in (7.2)
c_i	Concentration of the ith chemical compound (kg m^{-3})
c_i^*	Saturation concentration of the ith chemical compound (kg m^{-3})
$\boldsymbol{c}$	Vector of concentrations (kg m^{-3})
C_{ij}	Concentration control coefficient of the jth intermediate with respect to the activity of the ith enzyme
C_i^J	Flux control coefficient with respect to the activity of the ith enzyme
$\mathbf{C}^*$	Matrix containing the control coefficients defined in (6.34)
d_b	Bubble diameter (m)
δ_f	Thickness of liquid film (m)
d_{mean}	Mean bubble diameter (m)
d_{mem}	Lipid membrane thickness (m)
d_s	Stirrer diameter (m)
d_{Sauter}	Mean Sauter bubble diameter (m), given by (10.18)
D	Dilution rate (h^{-1}), given by (3.1)
D_{max}	Maximum dilution rate (h^{-1})
D_{mem}	Diffusion coefficient in a lipid membrane (m^2 s^{-1})
D_{eff}	Effective diffusion coefficient (m^2 s^{-1})

D_i	Diffusion coefficient of the ith chemical compound ($m^2\ s^{-1}$)
e_0	Enzyme concentration (g enzyme L^{-1})
E_g	Activation energy of the growth process in (7.28)
E	Mixing efficiency, defined in (11.1)
$\mathbf{E}$	Elemental matrix for all compounds
$\mathbf{E}_c$	Elemental matrix for calculated compounds
$\mathbf{E}_m$	Elemental matrix for measured compounds
$f(\mathbf{y},t)$	Distribution function for cells with property $\mathbf{y}$ in the population (8.1)
$\mathbf{F}$	Variance–covariance matrix
g	Gravity ($m\ s^{-2}$)
G	Gibbs free energy (kJ mol^{-1})
G^0	Gibbs free energy at standard conditions (kJ mol^{-1})
ΔG_{ci}	Gibbs free energy of combustion of the ith reaction component (kJ mol^{-1})
ΔG_d	Gibbs free energy of denaturation (kJ mol^{-1}) (7.29)
ΔG^0_{ci}	Gibbs free energy of combustion of the ith reaction component at standard conditions (kJ mol^{-1})
ΔG^0_f	Gibbs free energy of formation at standard conditions (kJ mol^{-1})
Gr	Grashof number, defined in Table 10.6
h	Test function, given by (3.54)
$h(y)$	Net rate of formation of cells with property y upon cell division (cells h^{-1})
$h^+(y)$	Rate of formation of cells with property y upon cell division (cells h^{-1})
$h^-(y)$	Rate of disappearance of cells with property y upon cell division (cells h^{-1})
H_A	Henry's constant for compound A (atm L mol^{-1})
ΔH_{ci}	Enthalpy of combustion of the ith reaction component (kJ mol^{-1})
ΔH^0_f	Enthalpy of formation (kJ mol^{-1})
$\mathbf{I}$	Identity matrix (diagonal matrix with 1 in the diagonal)
$\mathbf{J}$	Jacobian matrix (9.102)
k_0	Enzyme activity (g substrate [g enzyme]$^{-1}$ h^{-1})
k_i	Rate constant (e.g., kg kg^{-1} h^{-1})
k_g	Mass transfer coefficient for gas film (e.g., mol atm^{-1} s^{-1} m^{-2})
k_l	Mass transfer coefficient for a liquid film surrounding a gas bubble ($m\ s^{-1}$)
k_la	Volumetric mass transfer coefficient (s^{-1})
k_s	Mass transfer coefficient for a liquid film surrounding a solid particle ($m\ s^{-1}$)
K_a	Acid dissociation constant (mol L^{-1})
K_l	Overall mass transfer coefficient for gas–liquid mass transfer ($m\ s^{-1}$)
K	Partition coefficient
K_{eq}	Equilibrium constant
K_m	Michaelis constant (g L^{-1}) (6.1)
m	Amount of biomass (kg)

m_{ATP} Maintenance-associated ATP consumption (moles ATP [kg DW]$^{-1}$ h^{-1})
m_s Maintenance-associated specific substrate consumption (kg [kg DW]$^{-1}$ h^{-1})
$M_n(t)$ The nth moment of a one-dimensional distribution function, given by (8.9)
n Number of cells per unit volume (cells m^{-3}) (8.1)
N Stirring speed (s^{-1})
N_A Aeration number, defined in (11.14)
N_f Flow number, defined in (11.6)
N_p Power number, defined in (11.10)
p Extracellular metabolic product concentration (kg m^{-3})
p_A Partial pressure of compound A (e.g., atm.)
$p(\boldsymbol{y},\boldsymbol{y}^*,t)$ Partitioning function (8.5)
P Dimensionless metabolic product concentration
P Permeability coefficient (m s^{-1})
P Power input to a bioreactor (W)
P_g Power input to a bioreactor at gassed conditions (W)
$\mathbf{P}$ Variance–covariance matrix for the residuals, given by (3.48)
Pe Peclet number, defined in Table 10.6
q_A^t Volumetric rate of transfer of A from gas to liquid (mol L^{-1} h^{-1})
q_x Volumetric rate of formation of biomass (kg DW m^{-3} h^{-1})
$\mathbf{q}$ Volumetric rate vector (kg m^{-3} h^{-1})
$\mathbf{q^t}$ Vector of volumetric mass transfer rates (kg m^{-3} h^{-1})
Q Number of morphological forms
Q Heat of reaction (kJ mol^{-1})
Q_t Fraction of repressor-free operators, given by (7.47)
Q_2 Fraction of promotors being activated, given by (7.53)
Q_3 Fraction of promoters, which form complexes with RNA polymerase, in (7.55)
r_i Specific reaction rate for species i (kg [kg DW]$^{-1}$ h^{-1})
r Enzymatic reaction rate (Chap. 6) (g substrate L^{-1} h^{-1})
r_{ATP} Specific ATP synthesis rate (moles of ATP [kg DW]$^{-1}$ h^{-1})
$\mathbf{r}$ Specific reaction rate vector (kg [kg DW]$^{-1}$ h^{-1})
$\mathbf{r}_s$ Specific substrate formation rate vector (kg [kg DW]$^{-1}$ h^{-1})
$\mathbf{r}_p$ Specific product formation rate vector (kg [kg DW]$^{-1}$ h^{-1})
$\mathbf{r}_x$ Specific formation rate vector of biomass constituents (kg [kg DW]$^{-1}$ h^{-1})
$\mathbf{r(y,t)}$ Vector containing the rates of change of properties, in (8.2)
R Gas constant (=8.314 J K^{-1} mol^{-1})
R Recirculation factor (Sect. 9.1.4)
$\mathbf{R}$ Redundancy matrix, given by (3.41)
$\mathbf{R_r}$ Reduced redundancy matrix

Re	Reynolds number, defined in Table 10.6
s	Extracellular substrate concentration (kg m^{-3})
$\mathbf{s}$	Extracellular substrate concentration vector (kg m^{-3})
s_f	Substrate concentration in the feed to the bioreactor (kg m^{-3})
S	Dimensionless substrate concentration
ΔS	Entropy change (kJ mol^{-1} K^{-1})
Sc	Schmidt number, defined in Table 10.6
Sh	Sherwood number, defined in Table 10.6
t	Time (h)
t_c	Circulation time (s) (11.7)
t_m	Mixing time (s) (11.3)
T	Temperature (K)
$\mathbf{T}$	Matrix in (5.11). $\mathbf{T}^T$, the transform of $\mathbf{T}$, is the stoichiometric matrix
$\mathbf{T}_1$	Matrix corresponding to calculated fluxes (5.12)
$\mathbf{T}_2$	Matrix corresponding to measured rates (5.12)
u_b	Bubble rise velocity (m s^{-1})
u_i	Cybernetic variable, given by (7.36)
u_s	Superficial gas velocity (m s^{-1})
$\mathbf{u}$	Vector containing the specific rates of the metamorphosis reaction (kg kg^{-1} h^{-1})
v	Liquid flow (m^3 h^{-1})
v_e	Liquid effluent flow from the reactor (m^3 h^{-1})
v_f	Liquid feed to the reactor (m^3 h^{-1})
v_g	Gas flow (m^3 h^{-1})
v_i	Flux of internal reaction i in metabolic network (kg [kg DW]$^{-1}$ h^{-1})
v_{pump}	Impeller induced flow (m^3 s^{-1}) (11.6)
$\mathbf{v}$	Flux vector, i.e., vector of specific intracellular reaction rates (kg [kg DW]$^{-1}$ h^{-1})
V	Volume (m^3)
V_d	Total volume of gas–liquid dispersion (m^3) (10.16)
V_g	Dispersed gas volume (m^3) (10.16)
V_l	Liquid volume (m^3)
V_y	Total property space (8.2)
w_i	Cybernetic variable, given by (7.47)
x	Biomass concentration (kg m^{-3})
X	Dimensionless biomass concentration
X_i	Concentration of the ith intracellular component (kg [kg DW]$^{-1}$)
$\mathbf{X}$	Vector of concentrations of intracellular biomass components (kg [kg DW]$^{-1}$)
$\mathbf{y}$	Property state vector
Y_{ij}	Yield coefficient of j from i (kg j per kg of i or C-mol of j per kg of i)
$Y_{x\mathrm{ATP}}$	ATP consumption for biomass formation (moles of ATP [kg DW]$^{-1}$)
Z_i	Concentration of the ith morphological form (kg [kg DW]$^{-1}$)

Greek Letters

α_{ji} Stoichiometric coefficients for substrate i in intracellular reaction j
β_{ji} Stoichiometric coefficient for metabolic product i in intracellular reaction j
$\dot{\gamma}$ Shear rate (s^{-1})
γ_{ji} Stoichiometric coefficient for intracellular component i in intracellular reaction j
$\dot{\gamma}$ Shear rate (s^{-1}), defined in (11.24)
Γ Matrices containing the stoichiometric coefficients for intracellular biomass components
$\boldsymbol{\delta}$ Vector of measurement errors in (3.43)
Δ Matrix for stoichiometric coefficients for morphological forms
ε Gas holdup (m^3 of gas per m^3 of gas–liquid dispersion)
ε Porosity of a pellet
ε_{ji} Elasticity coefficients, defined in (6.27)
$\boldsymbol{\varepsilon}$ Vector of residuals in (3.46)
$\mathbf{E}$ Matrix containing the elasticity coefficients
η Dynamic viscosity (kg m^{-1} s^{-1})
η Internal effectiveness factor, defined in (9) of Note 6.2
π_i Partial pressure of compound i (atm)
θ Dimensionless time
κ_i Degree of reduction of the ith compound
μ Specific growth rate of biomass (h^{-1})
μ_{max} Maximum specific growth rate (h^{-1})
μ_q Specific growth rate for the qth morphological form (kg DW [kg DW]$^{-1}$ h^{-1})
ρ_{cell} Cell density (kg wet biomass [m^{-3} cell])
ρ_l Liquid density (kg m^{-3})
σ Surface tension (N m^{-1})
σ^2 Variance
τ Space time in reactor (h)
τ Shear stress (N m^{-2}), defined in (11.25)
τ_p Tortousity factor, used in (6.23)
Φ_n Thiele modulus for reaction of order n (2) and (5) in Note 6.2
Φ_{gen} Generalized Thiele modulus, Note 6.2
$\psi(X)$ Distribution function of cells (8.8)

Abbreviations

AcCoA	Acetyl co-enzyme A
ADP	Adenosine diphosphate
AMP	Adenosine monophosphate
ATP	Adenosine triphosphate
CoA	Coenzyme A
DHAP	Dihydroxy acetone phosphate
DNA	Deoxyribonucleic acid
E_c	Energy charge
EMP	Embden–Meyerhof–Parnas
FAD	Flavin adenine dinucleotide (oxidized form)
FADH	Flavin adenine dinucleotide (reduced form)
FDA	Food and Drug Administration
F6P	Fructose-6-phosphate
F1,6P	Fructose 1,6 diphosphate
GAP	Glyceraldehyde triphosphate
2 PG	2-phosphoglycerate
3 PG	3-phosphoglycerate
1,3 DPG	1,3 diphosphoglycerate
GTP	Guanosine triphosphate
G6P	Glucose-6-phosphate
HAc	Acetic acid
HLac	Lactic acid
LAB	Lactic acid bacteria
MCA	Metabolic control analysis
MFA	Metabolic Flux Analysis
NAD+	Nicotinamide adenine dinucleotide (oxidized form)
NADH	Nicotinamide adenine dinucleotide (reduced form)
NADP+	Nicotinamide adenine dinucleotide phosphate (oxidized form)
NADPH	Nicotinamide adenine dinucleotide phosphate (reduced form)
PEP	Phosphoenol pyruvate
PP	Pentose phosphate
PSS	Protein synthesizing system
PTS	Phosphotransferase system
PYR	Pyruvate
P/O ratio	Number of molecules of ATP formed per atom of oxygen used in the oxidative phosphorylation
RNA	Ribonucleic acid
mRNA	Messenger RNA

rRNA	Ribosomal RNA
tRNA	Transfer RNA
RQ	Respiratory quotient
R5P	Ribose-5-phosphate
TCA	Tricarboxylic acid
UQ	Ubiquinone

List of Examples

Chapter 6

Chapter 7

Chapter 8

Chapter 9

Chapter 10

Chapter 11

List of Tables

Chapter 11

List of Notes

Chapter 7

Chapter 8

Chapter 9

Chapter 10

Chapter 11

Chapter 1
What Is This Book About?

Looking back to the introductory Chap. 1 of the first and second editions of *Bioreaction Engineering Principles*, we still find that the schematic representation of topics in Fig. 1.1 adequately describes what we believe should be the focus of the third edition.

Throughout the text we emphasize that the design of bioprocesses should be based on modeling of the system. A quantitative approach in which fundamental results from the biosciences is combined with core disciplines from the engineering sciences will lead to the best design of the bioprocess.

It is our sincere hope that the book will find readers from the combined community of microbiologists, biochemists, and chemical engineers. The combined expertise of these scientists constitutes what could be called the *biochemical engineer*. In many universities, Departments of Chemical Engineering have been renamed as Departments of Chemical and Biochemical Engineering in realization of the need for engineers and scientists who are able to tackle the challenge of transforming the astounding discoveries of the biosciences into new industrial processes which will make an impact on all levels of our daily lives. The formation of biochemical engineers is by no means an easy task, since the qualities of two very different academic cultures, Bioscience and Chemical Engineering Science, must be combined without losing the essential qualities of either of the two.

Both the student of Chemical Engineering and the student of one of the Biosciences will be trained to recognize new possibilities within their field of study and to exploit their inventiveness. This results in academic papers that give new fundamental insights and in patents for new procedures or processes. But the approach of the chemical engineer is – generally speaking – that of modeling the process, and thereafter set into motion a recursive process of experimental studies and further modeling analysis. The bioscientist with a much broader basis in factual knowledge and laboratory techniques is – again generally speaking – more likely to pursue deep studies of a particular system, uncovering layer after layer of the Truth about this specimen of Life.

J. Villadsen et al., *Bioreaction Engineering Principles*,
DOI 10.1007/978-1-4419-9688-6_1,

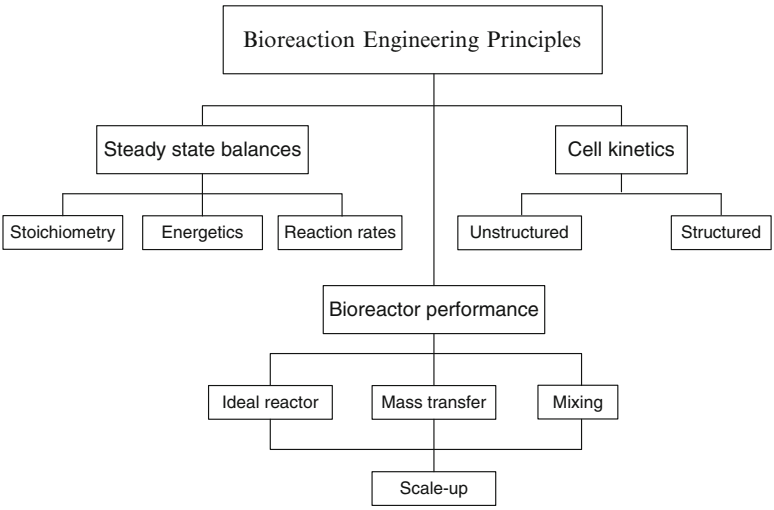

Fig. 1.1 Topics of bioreaction engineering (adapted from first edition (1993) of the book)

The authors of the present textbook have taught the subject of bioreaction engineering to many generations of students, both in their home universities and in courses at foreign universities. The classes have invariably been composed of students with either a strong background in Chemical Engineering – Transport phenomena, Unit operations, and Reaction Engineering – or with an extensive training in experimental techniques in the Biochemistry laboratory, underpinned by studies of heavy tomes on Biochemistry and Biology. Through comments to the first and second edition of our textbook we have learnt to appreciate the difficulties of many biostudents in tackling model building and even rather simple mathematical topics. We have also learnt that "true" chemical engineering students have little or no appreciation of the hard work it takes to learn even the fundamentals of metabolism and molecular biology.

The biostudents *must* learn to apply mathematics and numerical simulation, at least up to a certain level. Otherwise the methodologies used in Metabolic Flux Analysis, Metabolic Control Analysis, and Data Analysis will remain the prerogative of physicists and engineers. Similarly, the engineering students *must* spend time to become familiar with the core disciplines of the biosciences. Otherwise, their modeling studies will be faulted by the Bioscience community, and their biorelated papers, published in secondary journals, will have little or no real value for society.

In this third edition of *Bioreaction Engineering Principles*, we have tried to build bridges between the two communities. Chapter 2 gives a short, but in our opinion sufficient introduction to metabolism in microorganisms, and through the following chapters we build further on this basis. Our short primer in cell physiology can in no sense replace the detailed picture of physiology and biology offered by full size textbooks on these topics, but the student will be encouraged to improve his status by consulting these texts.

Matrix algebra is necessary to understand, even on a superficial level, the concepts discussed in papers on Systems Biology, and we introduce matrix-based Metabolic Flux Analysis in Chap. 5. But the subject is introduced slowly after simple networks have been studied by methods that require very little beyond basic algebra. Similarly, at the end of Chap. 3, methods that are necessary to evaluate the quality of experimental data are discussed, but only after many examples where elemental and redox balances are used to analyze steady-state rate data and to derive the stoichiometry of bioreactions. When in Chap. 6 reactions catalyzed by immobilized enzymes are treated, one must apply some basic concepts from transport phenomena. Diffusion into the pellets is treated with the help of detailed examples. The objective is to give the reader an understanding of the topic which is on the par with that given in standard texts on Chemical Reaction Engineering.

The book has more than 100 examples and notes. The Examples will help the reader to better understand the text while topics which extend the text, sometimes by pointing to applications in different areas, are treated in Notes. The teaching of the examples is further extended into the Problem sections of each chapter. Some of the examples and problems are simple illustrations of the text, while others are detailed quantitative studies relevant for building up a further understanding of bioreactions, both for use in scientific studies and for design of equipment. The design examples often refer to the collaboration of the authors with major bio-tech companies – suitably reformulated if necessary. Hopefully these design examples demonstrate that Bio-reaction Engineering, by combining core subjects from Chemical Engineering and the Bio-Sciences, contributes to secure bioprocesses a prominent place in the process industry.

For the casual reader of the text the Examples and Notes may give quick introduction to the philosophy of the textbook. Therefore lists of examples and notes are given right after the list of Contents. Also included is a list of the Tables. In the tables the student may find many valuable and often used data, just as the examples will be useful for a reader who wishes to obtain information concerning a particular research topic.

The third edition is in fact more like a complete rewriting of the second edition than a revision of the edition from 2003. In Chap. 2, we have decided to give a broad introduction to all the final products that can be derived from sugar and indirectly also from lignocellulosic biomass. The intention is to make the student enthusiastic about the whole area of bioreactions while at the same time introducing the primary metabolism of microorganisms bit by bit. We hope that the review of the potential of industrial production based on renewable materials is an unbiased and fair account of this fascinating area.

In the new edition, Chaps. 3 and 4 introduce concepts of value for bioremediation studies. There is no reason why the environmental engineer should not see his problems in the light of a more general discussion of mass balances treated with the aid of elemental and redox balances, and with suitable reference to the thermodynamics of the ecosystems.

Chapter 6 has now developed into a general overview of enzyme-catalyzed systems. Both the fundamental aspects of enzyme kinetics and the application of

free or immobilized enzymes in scientific studies and in industrial practice are covered. The last Sect. 6.4 of the chapter deals with Metabolic Control Analysis, a concept used in strain improvement by targeted changes in the metabolic pathways. The results of this section can be used equally well to optimize ordinary enzyme processes with several enzymatic reactions.

In Chap. 7, a central chapter of the book, the reader is guided from the simplest unstructured models for cell kinetics through to the fascinating molecular level kinetics that is involved in catabolite repression and in transport through the cell membrane.

Chaps. 9–11 deal with the design of bioreactions. The ideal (i.e., well mixed) reactor is the subject of Chap. 9, and while some material from the second edition has been left out the chapter now deals also with new reactor types, and the important fed-batch mode of operation is treated in more detail with respect to both chemical and mass-transfer limited reactions. Chapter 11 now offers a hands-on introduction to the problems of scale-up which in general are caused by inadequate mixing of the medium. The purpose is not to give a manual on mixing equipment and the empirical foundation for design of such equipment. Rather some general concepts of mixing are highlighted, for example, that the quality of mixing may be improved by clever design, but the power input to any mixing system basically determines the mixing time through application of the same relations derived from fluid dynamics.

A one-semester course based on our text should include Chap. 2, Sect. 3.1–3.5 and Sect. 5.1–5.3.2. This will give the students enough competence to derive stoichiometries from carefully examined experimental data and from simple network models. Many design problems – especially those in which the economic feasibility of a proposed process is to be determined – can be treated with this background in biochemistry and bioenergetics.

The design of steady-state stirred tank reactors and fed-batch reactors in Chap. 9 is, of course essential, and Chaps. 10 and 11 give an input from textbooks in chemical and mechanical engineering that will make the design of real bioreactors trustworthy.

Chaps. 6 and 8 might be included in a two-semester course, or they could be used as basis for short courses on enzyme reactions and on population-based models for bioreactions (essentially the basis is the same as that used for a course in reactive dissolution or precipitation of solids).

Finally Chap. 4 is a short introduction to Chemical Thermodynamics. Very simple calculations useful for, e.g., heat-exchanger design are treated, but the insight that thermodynamics will give in the feasibility of pathway reactions and in the functioning of essential life processes is, indeed valuable in its own right.

In conclusion, it is seen that the contents of the book follow the main route in analysis of bioreactions that was indicated in Fig. 1.1.

The authors wish for all those who spend time with our text that some useful experience is the reward for their efforts, be they students or industrial employees.

1.1 Note on Nomenclature

The nomenclature used in this edition is the same as that used in previous editions and shown in the "List of Symbols." Deviations from the listed symbols may appear, but only if the meaning of a shorter nomenclature is quite clear.

As in previous editions, we insist on using the symbol r for the specific rate of bioreactions (e.g., in units of kg converted (kg biomass h)$^{-1}$) since the cell is the reactor, and IUPAC defines the rate per kg (or m^3) reactor by the letter r. In mass balances for bioreactors the volume V of the reactor vessel is introduced. We use the letter q to designate the rate of the reaction per unit of V. The nomenclature is introduced in Sect. 3.1.1 together with the basic mass balances for the reactor.

To designate the specific growth rate of biomass we shall use both the standard symbol μ (in units of, e.g., kg biomass produced (kg biomass h)$^{-1}$) or r_x, a useful nomenclature when several specific rates are discussed together.

Yield coefficients (in units of, e.g. (kg/kg)) are designated by Y_{ij} where index j is the compound in the numerator and i is the compound in the denominator. This definition is explained in Sect. 3.2.

Chapter 2
Chemicals from Metabolic Pathways

For the past 80–90 years petroleum and natural gas have served as raw materials for the majority of the finished products of our daily lives. After World War II these raw materials decisively substituted coal, and they have been the foundation of an enormous increase in material wealth and welfare throughout the World.

A few basic raw materials, petroleum, natural gas, +S from oil or natural gas, and $O_2 + N_2$ from air, generate first primary (or platform) chemicals, next secondary (commodity) chemicals, then intermediates, and finally the finished products of virtually all industries that provide consumer goods.

The aromatic fraction of petroleum delivers *platform chemicals*, such as propylene, ethyl benzene, cyclohexane, and cumene. These are used to synthesize *secondary chemicals* such as styrene, adipic acid, caprolactam, acetone, and terephthalic acid; and these in turn are raw materials for the *polymer industry* that produces textiles, packaging for food products, appliances, and communication equipment (pencils, inks, computer casings, optical fiber). The aliphatic fraction of petroleum contains other platform chemicals (iso-butylene, butadiene, etc.) that supplement the aromatic fraction to produce intermediates for the abovementioned industries. The *transportation sector* directly receives consumer goods from C_5 to C_{14} aliphatic compounds, while products such as antifreeze and gasoline additives are derived by chemical processing of petroleum platform chemicals.

Natural gas and cracked naphtha deliver other platform chemicals (ethylene, propylene, CO/H_2, NH_3) for the *solvent industry* (methanol, ethanol, ethylene glycol, etc.), for the polymer industry (formaldehyde, polyethylene, polypropylene, PVC), and for *fertilizers*.

Together the platform chemicals from petroleum and natural gas are combined to give most of the products of the *health and hygiene industry*, the *housing industry*, and the exploding *recreation industry*. Except for the input from the mining and the forest industry, and the inorganic platform chemicals (such as cement and phosphates) it is, indeed, hard to imagine the modern world without the crucial input from oil and gas.

J. Villadsen et al., *Bioreaction Engineering Principles*,
DOI 10.1007/978-1-4419-9688-6_2,

It is, however, known to every observant citizen that we have to prepare for a different world, a future in which petroleum can only be used as a raw material for a few platform chemicals (mostly aromatics), and where even natural gas will run scarce. The use of the calorific value of oil and gas for heating and cooling, or for producing electricity will need to be sharply reduced, if not banned. The transportation sector will have to find solutions where gasoline is substituted by other means of vehicle propulsion.

This is the challenge for all modern societies, and at the same time it is likely to be the most brilliant opportunity for science in the 21st century.

In the following, the special role of the **biorefinery** in this quest for new solutions to the raw material challenge will be outlined.

2.1 The Biorefinery

By analogy with the role of the oil refinery, where the raw materials, such as petroleum, natural gas, S, O_2 and N_2, are converted in a series of chemical steps to consumer goods, the role of the biorefinery is to convert raw materials originating in the agricultural sector into *the same* final consumer goods.

Food and feed products are, and will remain the primary products of agriculture. Nevertheless, for many years to come a certain fraction of the primary products from agriculture, such as sugar from beets or cane and starch from grain, potatoes and other storage compounds of plants will be processed into chemicals and transportation fuels – a striking example is the conversion of almost 40% of the enormous cane sugar production of Brazil into bioethanol. The main driver for this development has previously been surplus production of primary agricultural products in the Americas and in Europe. This has resulted in very costly programs where farmers were sometimes subsidized to reduce production. As long as in some parts of the world the production capacity for primary agricultural products remains much higher than the market can absorb, nonfood utilization, also for biofuels, will have a considerable and positive socioeconomic benefit.

The future lies in additional utilization of the huge quantities of waste products from agriculture and forestry – straw, corn cobs, sugarcane bagasse, and forest industry residues – supplemented by household and other waste products of modern society. Typically, one ton of straw is produced per ton of grain.

Hence, *cellulose*, *hemicelluloses, and lignin*, collectively known as *lignocellulosic biomass*, will become an important raw material for the biorefinery.

Cellulose is an unbranched, crystalline microfibril constructed from 7,000 to 15,000 α-D glucose molecules. Embedded in hemicelluloses it acts as reinforcement like iron rods in concrete to give strength to cell walls. Hemicelluloses are composite, branched polysaccharides, polymerized from 500 to 3,000 D-C_5 sugar units to an amorphous structure of xylan, arabinoxylan, glucomannan, and others. In contrast to cellulose, hemicelluloses are relatively easily hydrolyzed by acid treatment or by enzymes to form C_5 monomers, with the C_5 sugar D-xylose being the most abundant pentose derived from many materials.

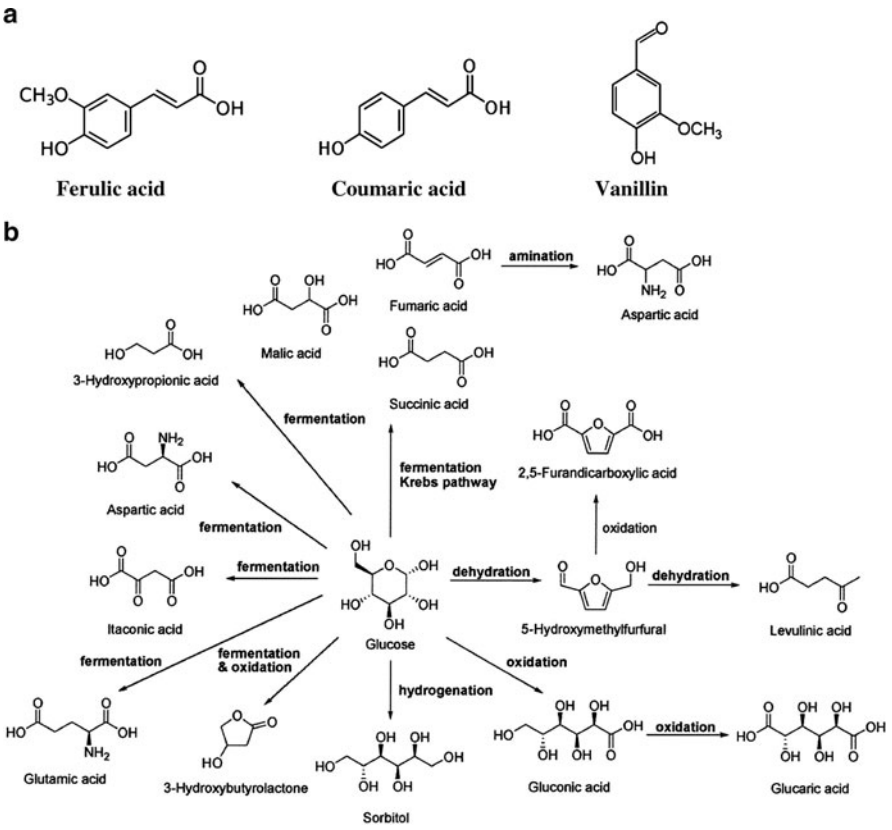

Fig. 2.1 (**a**) Chemicals from lignin. The three compounds all have antioxidant properties that may have possible health effects. They can be used to synthesize other flavor compounds and pharmaceuticals. (**b**) The 12 building blocks derived from the sugars that result by hydrolysis and saccharification of lignocellulusic biomass, exemplified by glucose (Murzin and Leino (2008))

Lignin is an amorphous hydrophobic polymer into which the cellulose microfibrils are embedded. It adds chemical resistance to the network of hemicelluloses and cellulose, but has a number of other functions such as regulating the flow of liquid in the living plant. The building blocks of the very complex lignin polymer change from one lignocellulosic biomass to another, but generally they are of aromatic character, dominated by derivatives of phenyl propane. Figure 2.1a shows three commercially valuable products that can be obtained by hydrolysis of lignin.

2.1.1 Ethanol Production

Given the massive political interest in substituting part of the petroleum-based transportation fuels with fuels derived from cheap and plentiful renewable

resources – about 10^{10} tons/year of lignocellulosic biomass appears to be relatively readily available worldwide – the subject of ethanol production from biomass has been treated in numerous journal papers, books, and pamphlets published by national and international organizations. The three recent reviews (Lin and Tanaka 2006; Hahn-Hägerdahl et al. 2006; Lynd et al. 2008) give short, but well-balanced accounts of the prospects of ethanol production, technological as well as economic, from Japan, Sweden, and the USA.

In March 2009, the price of natural gas was 4.0 US \$/10^6 BTU (=3.7 US \$/10^9 J, or 0.19 US \$/kg based on a heating value of 22200 BTU/lb (ethane)), but the prices fluctuate wildly – the average for 2008 was 0.40 US \$/kg – while the price of cellulosic crops ("energy crops") was about 0.050 US \$ kg or about 2.3 US \$ 10^9 J based on a heat of combustion of 0.023×10^9 J kg^{-1}.

Thus, from the point of view of calorific value, energy crops, even at a much lower cost per J, might seem to have little to offer compared with the user friendly natural gas. Neither is an ethanol price (March 2009) of 1.72 US \$/gallon (0.63 US \$/kg or 21 US \$/10^9 J) very encouraging compared with the relative heating value of either natural gas or energy crops, especially since a yield of ethanol by total conversion of the sugars in lignocellulosic biomass is at most 0.5 kg ethanol/kg biomass. Therefore, when considering ethanol production from biomass one must definitely put a value on the residue in order to get a reasonable economy in the overall process. As will be discussed shortly this is done for all the integrated biomass-to-ethanol processes that are currently examined.

As could be expected, in the heated debate on the socioeconomic benefits of converting biomass to ethanol, the fiscal incentives that subsidize bioethanol are said to be a major incentive for the industry. The raw material is usually considered as waste with no value – or a negative value when considering the environmental costs of burning it on site. Still, the net cost of collecting agricultural waste and transporting it to a central processing facility, added to the capital and running costs of the industrial installation must, at the present, seem discouraging, unless some incentive is given to the entrepreneurs.

For example, using agricultural waste to produce a *liquid fuel* by pyrolysis in an oven directly attached to the equipment that harvests the crop is an appealing, low cost alternative. When the pyrolysis is controlled at about 500°C, and the vapors from the pyrolysis oven are rapidly quenched, 70–80% of the heating value of straw or bagasse can be retrieved. The raw *bio-oil* has a low sulfur content, but it contains about 30% water, is highly oxygenated (10–40% O), and is much too acidic. New research (Bridgewater and Peacocke 2000; Holmgren et al. 2008; Bech 2008) is building up a technology for refining the raw pyrolysis oil, and in numerous patents (e.g., Bech and Dam-Johansen 2006) mobile units for collecting and pyrolysing the biomass are described. According to Holmgren et al. (2008) the raw pyrolysis oil can be refined in a one- or two-step hydrogenation process into a perfectly suitable naphtha or diesel range fuel. The carbon recovery in the liquid fuel is about 45% compared to 25–30% by conversion of wood or corn stover to ethanol with the hemicelluloses as a byproduct. The production cost of refined pyrolysis oil is in the range of 1.7–2.1 US \$/gallon fuel. This is still much too high compared to the

price of raw pyrolysis oil (≈0.35 $/gallon), but the technology is in its infancy, and no large-scale production of pyrolysis oil has as yet been realistically evaluated.

Production of ethanol from lignocellulosic biomass involves a number of steps. Pretreatment of milled or finely cut biomass to open up the structure for further hydrolysis, saccharification of the biomass, and separation of C6/C5 sugars from lignin (Hahn-Hägerdahl et al. 2006). Finally, part or all of the sugars is converted into ethanol. Estimates of the ethanol production cost depend on the nature of the biomass feed (softwood, perennial grass crops, straw, bagasse, etc.), on the process, and on the final product distribution. In some processes, the goal is to ferment all the sugars, either in one or in several steps, and the wastewater is treated in an anaerobic bacterial fermentation to yield biogas. Lignin may be used in further processes in the biorefinery, or it may be burnt to provide heat for the heavy evaporation duties involved in producing almost water-free ethanol based on the 4–8 wt% effluent from the fermentation, and perhaps to turn all the residual in the wastewater into a combustible fuel. The cost of fermenting the C5 sugars is higher than for the C6 sugars, and a good alternative to total conversion of the sugars is to use the C5 and mineral-rich residue from a C6 fermentation with yeast as an excellent cattle feed.

The IOGEN demonstration unit in Ottawa converts 1.5 tons of wheat straw per hour and utilizes both the C5 and the C6 sugars to make a rather weak (4–5 wt%) ethanol solution while the Danish IBUS concept, DONG-Inbicon, produces an 8 wt % ethanol solution from the C6 sugars of steam-treated wheat straw, and with a co-production of a mineral-rich C5 molasses for cattle feed. After pilot scale experiments from 2004, DONG-Inbicon inaugurated in 2009 a demonstration plant for conversion of 4 ton h^{-1} wheat straw to ethanol and C5 molasses. Similar demonstration units have sprung up in many countries. Of particular interest is the large number of straw-based Indian units, inspired and promoted since the 1980s by the "father" of Indian biotechnology, T.K. Ghose. Common to all these envisaged designs for full scale plants is that they incorporate projected advances in both biological and physical process steps. The interest is centered on the hydrolysis step which is at present dreadfully slow compared with the fermentation step (5–7 days in the IOGEN process + 3 days in a separate fermentation step). Hydrolysis of the polymers to C6/C5 sugars is done with cocktails of enzymes with at least three kinds of cellulase activities (endogluconase, exogluconase, and cellobiose), but unless the biomass is properly pretreated large quantities of enzymes must be added. In the Inbicon process (in which only the C6 sugars are converted to ethanol), the enzymatic prehydrolysis liquefaction takes only 5–7 h, and is followed by a *simultaneous saccharification* and *fermentation* (SSF) process to give a *total* hydrolysis + fermentation time of 6 days.

Pretreatment of the raw biomass by hot water, perhaps with the addition of O_2 in "Wet Oxidation" which removes most of the lignin, by steam, by dilute acid, or with a concentrated NH_3 solution has been used to open up the polymer matrix, and to make it more accessible to cellulases. Especially the Ammonium Fiber Expansion (AFEX) method, originally developed in the 1980s with liquid NH_3 soaking the dry biomass, followed by a sudden pressure release, appears to have a high

potential for significantly reducing the hydrolysis time for straw materials. Sendich et al. (2008) summarizes recent progress in the AFEX method. A strong NH_3–H_2O solution is used, and effective recovery of the NH_3 is described. The water/dry biomass ratio is as low as 0.4 with significant implications for the downstream processes.

SSF of pretreated biomass appears to be the correct procedure, despite the difference between optimal hydrolysis temperature (≈50°C) and fermentation temperature (≈33°C) in current processes. The inhibition of the enzymes by the products of the depolymerization process, e.g., glucose and cellobiose (two glucose molecules linked by a $\beta(1 \rightarrow 4)$ bond), is avoided when the sugar is immediately converted to ethanol (Gauss et al. 1976; Olofsson et al. 2008). The ethanol can probably be removed continuously by a moderate stripping of the medium with CO_2, especially at hypobaric fermentor pressure, say 0.5 bar. These low temperature ethanol separation methods could possibly open up for recovery of intact enzymes from the stillage.

The progress of large biotech companies such as Novozymes and Genencor in the construction of new and more potent enzyme cocktails for saccharification, and the selection of robust, ethanol tolerant strains of the yeast *Saccharomyces cerevisiae* will undoubtedly lead to a several fold reduction of the dosage of hydrolytic enzymes. Together with a strong R&D investment to optimize the process design one may hope that the hydrolysis time will be significantly reduced, and finally be able to match the fermentation time of the C6 sugars.

Fermentation of the C5 sugars with yeast presents a problem, and consortia of different bacteria have been used to convert the C5 sugars to ethanol in a second fermentation step. Many bacteria are able to ferment all lignocellulose-derived sugars to ethanol. In Problem 2.3, and in Chap. 5, butanol and acetone are seen to be lucrative products of another bacterial fermentation where the production organism is *Clostridium acetobutylicum*. But bacteria tend to produce mixed acids rather than ethanol (see Fig. 2.5), and they work best at neutral pH (6–7), where they are more susceptible to infection than yeast which works at mildly acidic pH (4.8–6). Their major disadvantage is that they are not nearly as tolerant to ethanol as *S. cerevisiae*. Thus, even the excellent bacterium *Zymomonas mobilis* which is able to produce ethanol in nearly stoichiometric amounts from glucose tends to be severely inhibited by ethanol concentrations above 3 wt%, while new industrial strains of *S. cerevisiae* tolerate more than 15 wt% ethanol.

If one decides to sell the residue from the C6 fermentation as animal feed, the currently slow and incomplete fermentation of C5 sugars in conventional yeasts is not a problem. The value of the cattle feed can be greatly improved if the C5 sugars are converted to biomass with about 70% protein. The company Microbiogen (http://www.microbiogen.com) in Sydney, Australia, has in a long screening program developed an industrial yeast, that by aerobic cultivation quantitatively converts the C5 sugars to yeast biomass, also in the harsh environment of hydrolyzed lignocellulose.

If the goal is to utilize all the sugars for ethanol production then new yeast strains must be engineered. Strong and persistent research efforts toward this goal have

been made by many research groups, see e.g., Hahn-Hägerdahl et al. (2007) and Wisselink et al. (2009). One important breakthrough has been the expression of a fungal xylose isomerase into yeast. This enzyme permits direct isomerization of xylose into xylulose, and an almost simultaneous fermentation of xylose and glucose is obtained (van Maris et al. 2006). In the 2009 paper by Wisselink et al., it is shown that long-term stable co-fermentation of several C5 sugars and glucose can be ensured by *evolutionary engineering*. This is the same strategy used by, e.g., Microbiogen to convert C5 sugars to high value animal feed: A sustained evolutionary pressure is applied to the culture to change the phenotype of the original strain in the desired direction. Problem 2.2 discusses how C5 and C6 sugars are directed to the main metabolic pathways of *S. cerevisiae* through the same feed-line.

When all the evidence from scientific journals[1] is considered together with news releases from reputable biotech companies, it does seem that the goal of producing ethanol from lignocellulosic biomass at a price comparable with gasoline from oil is within reach.

It will be prudent to complement the massive bioscience research effort toward an optimal conversion of lignocellulosic biomass into ethanol with an effort to optimize the engineering design of units that produce ethanol from sugar and starch, the "first generation ethanol processes." Neither the fermentors nor the downstream processes are yet fully optimized, and process intensification as well as energy savings in the up-concentration of dilute ethanol solutions (e.g., using heat pumps) could well lead to a substantial reduction of the production price of ethanol from starch.

With proper foresight these technical improvements will be ready to implement when corn stover, straw, wood chips, or bagasse are included as raw materials for ethanol production.

First generation ethanol processes are typical *mature* processes, just as most processes in the petroleum/gas-based refinery, and a 5% reduction of production costs would be significant. Conversion of biomass to ethanol or to pyrolysis oils must at present (2010) be regarded as *immature* technical processes, defined as processes where the processing costs to final consumer goods are at least equal to the raw material costs. In the oil refinery, the processing cost is only on the order of 20–30% of the raw material cost. The challenges of the production process is the reason why the final price of ethanol from biomass is at present higher than the price of starch-based ethanol, despite the very low price of raw material delivered at the processing site.

The obvious immaturity of the biomass-based processes is, of course the incentive for the massive research commitment by industry and by governments. Without indulging in wishful thinking it is predictable that the cost of enzymes for hydrolysis of biomass will be much reduced if microorganisms such as the fungus *Trichoderma reesei* can be seeded on an optimally pretreated biomass to produce the cellulases for saccharification. The simultaneous fermentation of C5 and C6 sugars at a large scale will eventually also become economically feasible, also in fermentation media that

[1]Older references such as Maiorella et al. (1984) should, however, not be neglected. This seminal paper has recently been honored by being reprinted in *Biotechnol Bioeng* (2009).

contain inhibitors released from the pretreatment of the raw material. Finally, the whole engineering of the production system will be subjected to intensive studies by industry to achieve lower capital costs, smaller energy expenditure, and cheap recycling of the process water.

These improvements of Second Generation ethanol processes will be necessary if the political will to support bio-fuels is to be sustained.

The commitment of land to cultivation of energy crops will be decided on the "land use yield." At present, this parameter is stated to be 135 GJ ha^{-1} for lignocellulosic biomass, 85 GJ ha^{-1} for corn kernels, and only 18 GJ ha^{-1} for soy beans. Considerable efforts are, however, made to improve the utilization of the *whole* biomass from energy crops. Also the introduction of new crops for biodiesel production, and the – rather speculative – development of processes where microorganisms with high lipoid content are cultured in large scale, may make also biodiesel production feasible from a socioeconomic perspective. In the mean time, the use of waste materials such as yellow grease, lard, and tallow may quite soon develop into a cheap, large-scale source of biodiesel.

The predictions are, that by a skillful combination of first and second generation bioethanol processes, the production cost of ethanol will decrease to 1.4–0.8 US $/gallon (Sendich et al. 2008).

In the long run, the burgeoning Brazilian production of ethanol from cane sugar will increase dramatically when the 80% of the plant that is not sugar is utilized for ethanol production. Then, undoubtedly, Brazil will develop a large chemical industry where most of the sugar is used to produce chemicals, while maintaining a large export of ethanol. Very recently (October 2010), a large, well-funded project has been initiated with this end goal in mind. Characteristically, the project partners are Petrobras, the national Brazilian oil company, and Novozymes, a major producer of industrial enzymes.

In fact, as discussed in the next section, pure sugar is much more valuable as a raw material for chemical production rather than when converted to a biofuel. Exactly the same arguments are used to motivate a substantial change in the final use of the oil and gas raw materials, from transportation fuels and for heating purposes to an almost exclusive use in the chemical industry.

2.1.2 Production of Platform Chemicals in the Biorefinery

By analogy with the raw materials such as petroleum and natural gas in the oil refinery, the biorefinery operates with cellulose, hemicellulose, lignin, starch, sucrose, vegetable oils, and fats as raw materials. The sugar polymers are converted to mono- or dimeric sugars: glucose, fructose, sucrose, lactose, galactose, xylose, and arabinose, which serve as platform chemicals together with starch.

The triglycerides from oils and fats deliver other platform chemicals, glycerol and fatty acids. After esterification with aliphatic alcohols the fatty acids are used as biodiesel while the byproduct, glycerol has a great potential as a building block.

Glycerol will become an attractive byproduct from biodiesel production. Among the many promising processes in which glycerol is the raw material one can mention a process in which two enzymes are used. In a suitable membrane reactor construction which allows the two enzymes to be separated, 2 mol of glycerol can be converted to 1 mol of 1,3-propane diol and 1 mol of dihydroxy acetone ($CH_2OH–CO–CH_2OH$). One glycerol molecule is oxidized, and the other is reduced. The result is two compounds, each of which has a much higher value than glycerol.

When the considerable difficulties associated with downstream processing of the monomers derived from lignin have been solved this raw material can be used to synthesize a number of aromatic compounds as exemplified by Fig. 1.1a. In the near future, lignin is likely to be combusted to provide process heat. All the biopolymers can also be pyrolyzed to SynGas ($H_2 + CO$) or to pyrolysis oil as discussed in Sect. 2.1.1. In the following only glycerol and the sugars derived from biopolymers will be considered as building blocks.

In 2004, a group of researchers at Pacific Northwest National Laboratory (PNNL) and National Renewable Energy Laboratory (NREL) in the USA made a detailed screening of sugars as potential candidates for building blocks, secondary chemicals, and intermediates to produce final consumer goods in the industry sectors which have traditionally been served by the petroleum industry.[2] Starting with more than 300 candidates the group arrived at a final set of 12 building blocks, Table 2.1. As argued by Werpy and Petersen (2004), all 12 building blocks have a high potential for substituting building blocks derived from oil and gas.

The first three building blocks are made from sugars by simple chemical processes. *Glucaric acid* is a representative of the many, so-called aldaric acids $COOH–(CHOH)_n–COOH$ which are produced from sugar by mild oxidation. Thus, glucaric acid is obtained from D-glucose or D-gulose by oxidation with dilute

Table 2.1 Twelve sugar-based building blocks suggested by Werpy and Petersen (2004)

Glucaric acid
2,5 Furan dicarboxylic acid
Levulinic acid
Itaconic acid
1,4 Diacids (succinic, fumaric and malic)
3 Hydroxy propionic acid
Glycerol
3-Hydroxybutyrolactone
Xylitol and arabinitol
Sorbitol
Aspartic acid
Glutamic acid

[2]Another (comprehensive) report is from OECD ("The application of Biotechnology to Industrial sustainability – a Primer") (1998:ISBN 92-64-16102-3) and 2001. Newer reviews are Haveren et al. (2008), Clark (2007), and Kamm and Kamm (2007).

nitric acid. *Levulinic acid* (CH_3–CO–$(CH_2)_2$–COOH) results when starch is boiled in dilute sulfuric acid. *2,5 Furan dicarboxylic acid* is obtained by oxidative dehydration of C6 sugars, e.g., glucose and *3-hydroxybutyrolactone* by oxidative degradation of starch.

Sugar alcohols, *sorbitol* (CH_2OH–$(CHOH)_4$–CH_2OH) and the corresponding C5 alcohols *xylitol* and *arabinitol* can be produced by chemical hydrogenation of, respectively, glucose, xylose, and arabinose.

1,4 Di-carboxylic acids (succinic acid, fumaric acid and malic acid), *3 hydroxy propionic acid*, and the two amino acids *aspartic acid* and *glutamic acid* are all metabolites from metabolic pathways, and they are more easily produced from sugars by fermentation than by chemical routes.

Finally, *itaconic acid* (methylene succinic acid, COOH–CH_2–C (=CH_2)–COOH) is produced either by distillation of citric acid (COOH–CH_2–C(COOH) OH–CH_2–COOH), a fermentation product with a yearly production volume of about one million tons, or it can result directly from certain fungal fermentations.

The list of 12 building blocks in Table 2.1 can, if desired, be reduced further since several of the compounds can be synthesized from other compounds on the list. Thus, glutamic acid is the starting point of the biosynthesis of a family of amino acids, including aspartic acid, and the fermentation can be conducted such that aspartic acid or lysine is the final amino acid product. In Sect. 2.5, it will be shown that the amino acids can also be used as intermediates in the production of polymers.

Figure 2.1b summarizes the description of the synthesis pathways from lignocellulosic biomass to the 12 building blocks. Glucose is shown as the starting point for the synthesis, but other sugars resulting from enzymatic hydrolysis and saccharification of biomass could also have been used.

Directly aimed toward *polymers* is the Cargill-Dow lactic acid to polylactide facility (180,000 annual ton production) inaugurated in 2002 in Blair (Nebraska).

Since 2006 (at Loudon, TN) DuPont and Tate & Lyle produce annually 45,000 ton 1,3-propane diol by fermentation of hydrolyzed corn starch. In 2008 Novozymes and Cargill initiated a cooperation to produce 3-hydroxy propionic acid (CH_2OH–CH_2–COOH) directly by fermentation from glucose. The goal is to produce acrylic acid (propenoic acid, CH_2=CHCOOH) by fermentation, rather than chemically from propylene – see Problem 2.7.

The production of polymers from biobased raw materials will be further discussed, in this chapter, and in Chaps. 5, 6, and 9.

It is interesting that together the building blocks in Table 2.1 offer a collection of reactive functional groups, –OH, –CHO, –CO, –COOH, and –NH_2. With at least two of these present in a particular building block this is an attractive platform for building other compounds with a C3, C4, C5, or C6 carbon backbone. This property is of course also found in the raw materials, the sugars, whereas ethanol with only one reactive group has much less value as a platform chemical.

The reactivity of the building blocks makes it possible, mostly by chemical routes, to synthesize, e.g., a whole array of secondary chemicals which in their turn can also substitute oil-based building blocks for almost all conventional, and many new, biodegradable polymers, such as polylactides. Environmentally friendly

solvents such as esters of lactic acid (COOH–CHOH–CH_3) and aliphatic alcohols, as well as conventional solvents (butanol, acetone, etc.) are readily available as end products of central metabolic pathways. Whole families of pharmaceuticals, exemplified by penicillins and cephalosporins, are produced by fermentation. No chemical route is competitive for these bulk chemicals. Finally, specialty drugs, produced in small quantities but at high unit price, are synthesized by microorganisms. Therapeutic proteins and polyketides are examples of products that can only be produced by bioroutes.

In the following, we shall examine the metabolic pathways that lead from the raw material, sugar, to the desired end products, and a few examples of complete synthesis paths will be discussed. The goal is to understand the general rules of carbon flow in the main arteries of the immensely complicated metabolic network of any living organism. Nothing in the network structure was developed by nature without serving a purpose. Biochemistry and biology has given us an understanding of the purpose of the major pathways, but we are still a long way from understanding the whole, tightly regulated network. Learning from the pathways and guessing their interconnections are the way forward to design new organisms that serve our needs better. It is through systematic research where new sets of experiments are devised to obtain a better understanding of the rationale for the observed phenomena that we shall eventually reap the full benefit of what living cells offer to us. *Physiological Engineering, Metabolic Engineering, Systems Biology* – new names are constantly coined for this scientific endeavor – is a happy marriage between the biosciences and the engineering sciences.

In the perspective of this textbook all the tools discussed in the following chapters serve the purpose of understanding how to exploit as fully as possible the flux of carbon through the pathways and to engineer the fluxes by quantitative means. Ultimately, we shall have the perfect organism, optimized with respect to its performance in the reactor as well as in the subsequent down-stream processes toward the final product.

2.2 The Chemistry of Metabolic Pathways

In a metabolic pathway a substrate (input reactant) is converted by a series of enzymatic reactions to a final product. All the carbon in the substrate can end up in the final product or it may partly be lost through a number of *diverging* pathways which branch off from the main pathway.

Carbon can also be fed into the pathway by *converging* pathways.

Any of the intermediates of the pathway may be *excreted* from the cell and can be recovered from the *medium* (sometimes called the *fermentation broth*) from which the cell receives its substrates. Both processes occur by *transport* through the cell membrane.

The final product of the pathway can serve as a substrate for one or more pathways, and the notion of a separate pathway is more or less fictitious in the overall picture of a highly connected *metabolic network*. Several pathways have been named after

the persons who discovered and studied the set of reactions leading from the substrate to the "final" product of the pathway: EMP pathway (Embden, Meyerhof, Parnas + several other contributors), Krebs cycle, Entner–Duodoroff pathway, but other names are also used such as *Glycolysis* (*lysis* = degradation (of glucose)) for the EMP pathway and *TCA cycle* (Tri Carboxylic Acid) for the Krebs cycle. We shall largely use the latter names.

In the first pathway to be discussed (Sect. 2.2.2), the glycolysis pathway, the substrate is *glucose*, but through pathways which converge into glycolysis other sugars, galactose, lactose, mannose, and C5 sugars such as xylose can also serve as a carbon source.

The product is the keto acid, *pyruvic acid* (CH_3–CO–COOH). No carbon is lost in the form of CO_2[3] When furthermore no metabolic intermediates are drained away from the pathway as substrates in other reactions, one obtains two molecules of pyruvic acid[4] from one glucose molecule. Since the net formula for glucose is $C_6H_{12}O_6$ the overall stoichiometry – with respect to carbon – is:

$$C_6H_{12}O_6 \rightarrow 2C_3H_4O_3 \tag{2.1}$$

It is obvious that two H_2 have been lost in the conversion from glucose to pyruvic acid, i.e., the net result of the pathway is an oxidation of the glucose, the first step toward the ultimate combustion of glucose to six molecules of CO_2 in the *catabolic metabolism*.

In the following Sect. 2.2.1, the *purpose* of glycolysis as seen from the point of view of the microorganism will be discussed, and in Sect. 2.2.3 it will be shown how the organism compensates for the loss of *reducing power* associated with the oxidation of glucose to pyruvic acid in glycolysis.

2.2.1 The Currencies of Gibbs Free Energy and of Reducing Power

The conversion of a substrate to a final product through a sequence of chemical reactions will only take place if all the reactions in the sequence are thermodynamically favored in the desired direction. The change in free energy ΔG_R for each reaction must be *negative*. As will be discussed in Chap. 4, a reaction A → B which is thermodynamically unfavorable may still proceed in the indicated direction if it runs

[3]Although CO_2 is obviously a metabolic product we shall use "lost carbon" ("lost" for further metabolism) for this compound.

[4]In figures we usually show the non-dissociated metabolites. At the pH at which most fermentations take place we have the anions: pyruvate, acetate, glutamate, CH_3COCOO^-, CH_3COO^-, etc. rather than the free acids. NH_3 occurs as NH_4^+. When we write stoichiometries (e.g., (2.1)) it is simpler to use the non-dissociated molecules. The need to add acid or base to keep the desired pH is implicitly assumed. In Chap. 4 the ionic forms will have to be used.

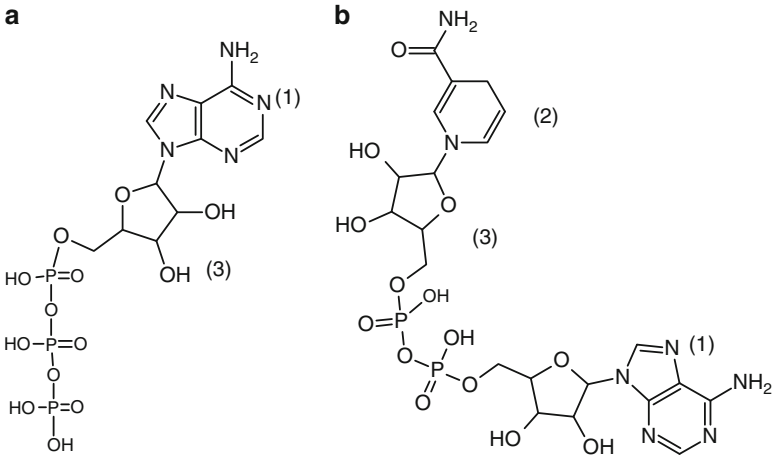

Fig. 2.2 (**a**) The "currency" of free energy, ATP. (**b**) The currency of catabolic reductive power, NADH. In ATP a purine derivative (six amino purine = adenine) (*1*) is attached to the 1′ carbon of the C5 sugar, ribose (*3*). The tri-ester with H_3PO_4 is formed at the 5′ carbon of the sugar. The ribophosphate structure of ATP is also found in NADH, but one of the phosphate groups is substituted with another nucleotide where nicotine amide (*2*) is attached to the 1′ carbon of the C5 sugar. In NAD^+ the 1′ nitrogen in the pyridine ring is positively charged while at the 4′ carbon one H is removed (i.e., the net effect is the removal of "H_2")

in parallel with another reaction C → D that is accompanied by a sufficient loss of free energy to make the sum of the two reactions occur with a negative ΔG_R.

In cell reactions, the reaction C → D is in most cases the hydrolysis of an energy-rich compound adenosine triphosphate (ATP), Fig. 2.2a.

Hydrolysis of ATP removes one molecule of phosphoric acid (or rather one HPO_4^{2-}), and the diphosphate ADP is formed. At the same time, a free energy "package" worth about 30.5 kJ mol^{-1} (at "standard conditions" which will be discussed in Chap. 4) is made available for A → B to proceed against its thermodynamically preferred direction as long as $\Delta G_{A\rightarrow B} < 30.5$ kJ mol^{-1}.

Within the cell, the ratio ATP/ADP is tightly regulated as long as the environment is kept stable, i.e., when the culture grows at *steady state*, the so-called *balanced growth*. Any use of ATP to "help" an energetically unfavorable reaction A → B must be balanced by other reactions $A_i \rightarrow B_i$ which have as sufficiently large, negative ΔG_R ($<<-30.5$ kJ mol^{-1}), and which will still proceed even when ATP is formed besides the main product B_i. The picture of ATP as an energy "currency," continuously exchanged between the thousands of metabolic reactions, is quite suggestive.

Nicotinamide adenine (NADH) dinucleotide, Fig. 2.2b, is the corresponding reductive power currency in the many reactions of the network of (mostly) *catabolic* reactions. The loss of reductive power from a metabolite is counteracted by an increase in NADH:

$$RH_2 + NAD^+ \rightarrow R + NADH + H^+ \qquad (2.2)$$

Generally speaking, the redox carrier serves as a *cofactor* for the enzyme that converts RH_2 to R.

As an example the *redox balanced* overall pathway reaction (2.1) from glucose to pyruvic acid should read

$$C_6H_{12}O_6 + 2NAD^+ \rightarrow 2C_3H_4O_3 + 2NADH + H^+ \tag{2.3}$$

In one of the reactions in glycolysis (reaction (6) in Fig. 2.4: glyceraldehyde-3 phosphate → 1,3 diphosphoglycerate), NAD serves as a cofactor, picking up the H_2 when the triose is oxidized.

On the level of the cell, the ratio NADH/NAD is tightly regulated for a cell culture in balanced growth. Consequently, the sum of all the rates of network reactions that produce NADH is matched with the sum of rates of reactions which consume NADH, just as the sum of rates of ATP producing reactions is matched with the sum of rates of ATP consuming reactions. These two constraints on the rates of pathway reactions in the (necessarily limited) network, with which we decide to represent the totality of the metabolic network of a cell, will be used in Chap. 5 in *Metabolic Flux Analysis* to obtain relationships between the rates of cellular reactions.

As one may guess, the picture of energy transfer and of redox transfer in metabolic networks is not as simple as described here. There are other "currencies" of energy transfer, such as guanosine triphosphate (GTP) which structurally resembles ATP, except that the purine derivative guanosine is used instead of adenine. In certain catabolic reactions, GTP is produced rather than ATP (e.g., in one of the TCA reactions, Fig. 2.7), and GTP is primarily used in protein synthesis. The energy content of the two molecules is the same, and they are easily converted to each other.

Also there are several currencies of redox power besides NADH. Of particular interest is NADPH. The structure of NADPH is the same as that of NADH in Fig. 2.2b, except that a third phosphate ester is attached to the 2′ carbon of the ribose next to the adenine.

Whereas NADH is produced and consumed in cell reactions connected with energy (ATP) production, *the catabolic reactions*, NADPH is (mainly) produced in reactions which lead to synthesis of building blocks for production of more cell mass, and consumed in the reactions which eventually lead to production of proteins and genetic material, RNA and DNA, the *anabolic reactions*.

Many organisms (e.g., *Escherichia coli*, the preferred workhorse of many industrial companies) are able to convert NADH to NADPH and vice versa

$$NADH + NADP^+ \rightarrow NADPH + NAD^+ \tag{2.4}$$

The reaction is catalyzed by an oxido-reductase, *NADPH: NAD transhydrogenase*.

Occasionally, it may be desirable to convert NADH to NADPH, especially in anaerobic fermentations, and reaction (2.4) may become useful. A typical case is the production of fuel-ethanol, where glycerol is an undesired byproduct that must

be produced by the yeast cell in order to satisfy the NADH balance (see Sect. 3.3). In a study by Nissen et al. (2001), the *E. coli* gene for transhydrogenase was inserted in *S. cerevisiae* in order to introduce an alternative NADH sink, and hereby eliminate glycerol production. A potential 5% increase of ethanol yield was expected. However, the strategy did not work, since the NADPH/NADP ratio is higher than the ratio of NADH/NAD, and consequently the reaction runs in the opposite direction, and this resulted in an increased NADH production in the cell, leading to a larger glycerol production.

Another important redox carrying dinucleotide is $FADH_2$, flavin adenine dinucleotide, which plays a role as a cofactor for the enzyme *ATP synthase* in *oxidative phosphorylation*. $FADH_2$ is mainly produced in the TCA cycle, Fig. 2.7, reaction (7).

Other redox carriers such as PQQ, pyrroloquinoline quinine, are used as cofactors in specific reactions, e.g., in the oxidation of methanol to formaldehyde by the enzyme methanol dehydrogenase. It is a key player in the production of single cell protein (SCP) from natural gas or methanol (Matsushita et al. 2002).

Besides their role as redox carriers in metabolic networks the redox cofactors play a part as anti-oxidant vitamins, e.g., in the human body.

All these complex organic molecules function either as donors of H_2 or acceptors of H_2, and one molecule of the cofactor can be interpreted as "H_2." Only in a few cases the H_2 will actually be liberated as molecular hydrogen.

Some reactions use one cofactor while others use a different cofactor. Structurally related cofactors can be converted between each other, e.g., NADH to NADPH (2.4). Although the cofactors are different and have different properties it is often possible in simple calculations to operate with only one common representative for all of them. Thus, if in *Metabolic Flux Analysis* all the anabolic reactions are lumped into one reaction there is, as will be discussed in Chap. 5, a small net-production of redox power. This is written as "NADH" in the stoichiometry for biomass formation, but the small positive production of redox is the result of a large consumption of NADPH and an approximately equal production of NADH. Since both NADH and NADPH are produced from their oxidized counterpart by the same consumption of substrate (sugar), the overall rate of substrate consumption is the same. In more sophisticated analyses, e.g., in the quantitative study of amino acid production by fermentation, the distinction between different cofactors needs to be maintained.

Whereas the net consumption, or production, of redox cofactors in a pathway can always be deduced from the level of reduction of the substrate and the product from the pathway, this is not so for the energy production.

Thus, the net reaction (2.1) does not reveal how much free energy in the form of ATP has been produced, although as will be seen in Chap. 5 oxidative pathways will generally produce free energy. Whether a pathway reaction will produce ATP by hydrolysis of high energy phosphate bonds depends on the enzyme used in the reaction.

Thus *kinases* will produce free energy, ATP, while *hydrolases* will produce enthalpy, which is transferred to the medium as heat.

The only way to find out whether a particular reaction produces ATP (or any other product) is to consult one of the metabolic network encyclopedias which are

now available on the Internet, e.g., EXPASY-Molecular Biology Server, subsection Biological Pathways, see http://www.expasy.ch., KEGG (Kyoto Encyclopedia of Genes and Genome, http://www.genome.jp/kegg/), and http://www.brenda-enzymes.org/, an excellent database for enzyme properties.

2.2.2 *Glycolysis*

In order to produce more biomass the necessary nutrients (or substrates) must be available. Nutrients can roughly be divided into (1) carbon source, (2) energy source, (3) nitrogen source, (4) minerals, and (5) vitamins. The energy source ensures supply of the necessary Gibbs free energy for cell growth, and often the carbon and energy sources are identical. The most common carbon and energy source is glucose, but carbohydrates such as maltose, sucrose, dextrins, or starch are frequently used. Many cells can also use organic acids, e.g., acetic acid or lactic acid, alcohols or polyols, such as glycerol, as carbon and energy source. A few microorganisms grow on hydrocarbons and on CO_2 (as do plant cells), but using H_2 as an energy source.

In Sect. 2.2.7, we shall return to the subject of cellular requirements for nutrients, and in Table 2.5 typical media used in industrial fermentation are listed (Fig. 2.3).

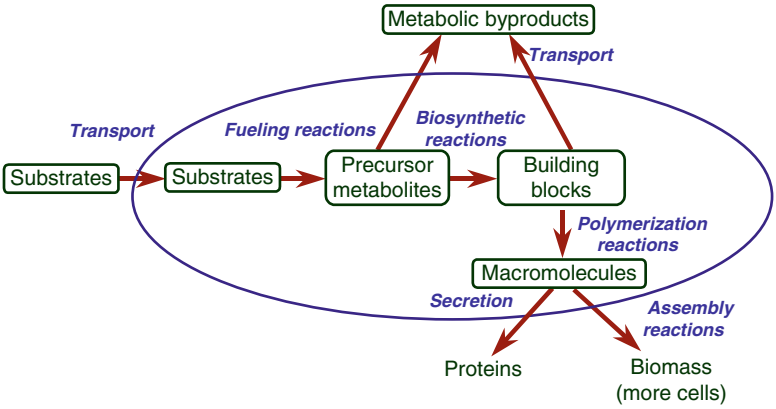

Fig. 2.3 Overview of reactions and processes involved in cellular growth and product formation. Substrates are taken up by the cells by transport processes and converted into precursor metabolites via fueling reactions. The precursor metabolites are converted to building blocks, and these are polymerized to macromolecules. Finally, macromolecules are assembled into cellular structures such as membranes, organelles, etc. that make up the functioning cell. Precursor metabolites and building blocks may be secreted to the extracellular medium as metabolites, or they may serve as precursors for synthesis of metabolic end products. The cell may also secrete certain macromolecules – primarily proteins that can act as hydrolytic enzymes, and some cells may also secrete polysaccharides

We shall first study the generation of energy from sugars, the most common carbon and energy source for microorganisms. The "standard" sugar substrate is *glucose*. This is taken up by the cell either by *passive diffusion* or by various forms of *active transport*, using free energy in the form of ATP to mediate the transport process. In *group translocation*, the glucose molecule is phosphorylated to an activated glucose, *glucose-6 phosphate*, at its passage from the medium through the cell membrane to the *cytosol*, the fluid inside the cell. The activation of the glucose molecule occurs by transfer of phosphate from an activated molecule further down in the path of glucose metabolism. The donor is *phosphoenolpyruvate* (PEP), see Fig. 2.4b, and the process is used for fast glucose transfer by many bacteria such as *lactic acid bacteria* and *E. coli*.

The metabolic pathway by which most living cells create energy from growth on sugars is the EMP-pathway, Figure 2.4a, b, and the end product of the pathway is pyruvate (2.1).

Using yeast as an example, the first reaction of the pathway (1) is the phosphorylation of intracellular glucose to glucose-6 phosphate (G6P) using one ATP (i.e., an energy package of 30.5 kJ) per mole of glucose. Next follows a reversible conversion (2) of G6P to fructose-6 phosphate (F6P), and a further activation of the sugar (3) is achieved by donation of one ATP to F6P to form fructose-1,6 diphosphate (F1,6P).

F1,6P is highly energized and splits by reaction (4) into two *trioses*, dihydroxyacetone phosphate (DHAP) and glyceraldehyde-3 phosphate (GAP). Since DHAP is a symmetrical molecule the position of the phosphate molecule is not specifically indicated, whereas the GAP that results from G6P is phosphorylated in the 3-position, i.e., furthest away from the aldehyde group, see Fig. 2.4a(f).

The entry point to the pentose phosphate pathway (PP), Fig. 2.8, is from G6P (b). F6P and GAP formed in the PP pathway join the two pools (d) and (f) in Fig. 2.4a and are metabolized further in the EMP pathway.

G6P and F6P are used for the production of storage carbohydrates (glycogen and trehalose), and of cell wall components (chitin and glucans). GAP is used for the production of lipids.

The two trioses are connected by a fast reversible reaction (5). When we are looking at the energy production by the EMP pathway we assume that consumption of sugar in the pathway that leads from the DHAP is blocked. Hence all the carbon ends up in GAP and is further metabolized from this intermediate. In a real fermentation the ratio between the pools of GAP and the DHAP is, of course, controlled by the relative rates of consumption of the two compounds.

An interesting observation, of relevance to the discussion of labeled carbon atoms in Chap. 5, is that a glucose molecule labeled in position 1 (i.e., $^{13}C_1$-glucose) will lose 50% of its labeling after the split at F1,6P. GAP is obtained from carbon atoms 1–3, while DHAP stems from carbons 4–6. The GAP obtained from DHAP by the fast reaction (5) is unlabeled, and the resulting concentration of labeled molecules (in the C_3-position of GAP) is only half of what it was in the glucose. This topic is discussed further in Sect. 5.3.3.

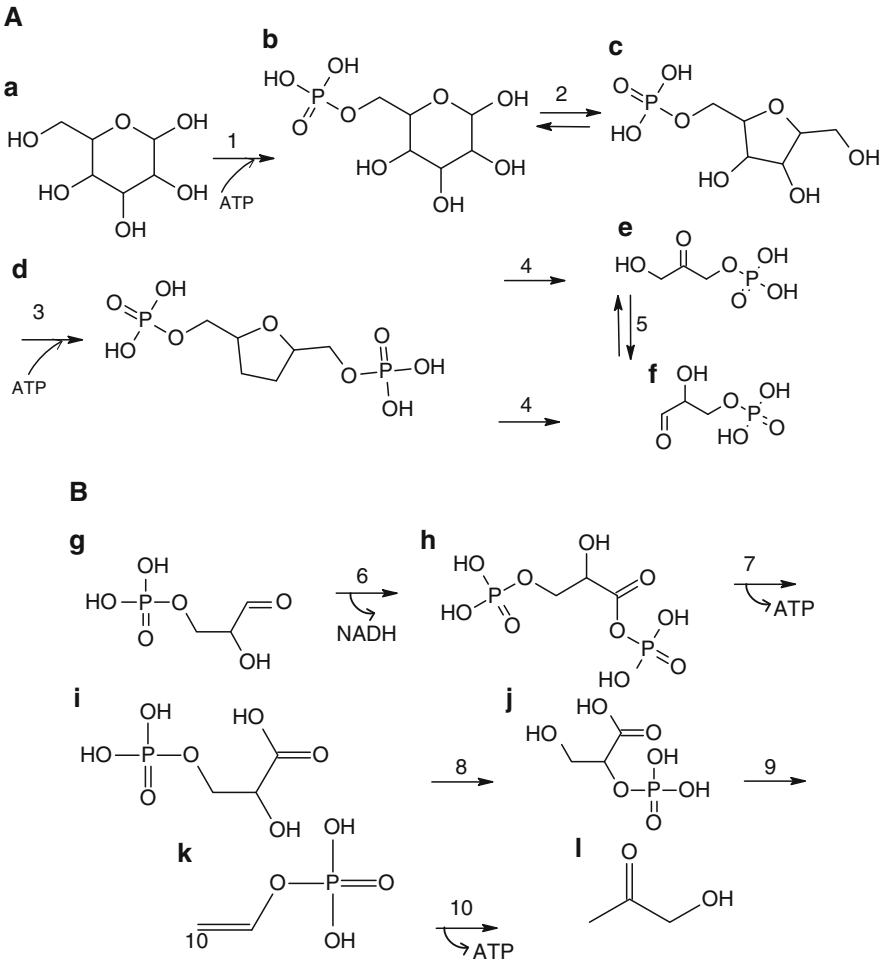

Fig. 2.4 (**A**) The first part of the EMP pathway, until the hexose is split into two trioses. (a) Glucose, (b) glucose 6 phosphate (G6P), (c) fructose 6 phosphate (F6P), (d) fructose 1,6 diphosphate (F1,6P), (e) dihydroxyacetone phosphate (DHAP), and (f) glyceraldehyde 3-phosphate (GAP). The reactions are catalyzed by (*1*) hexokinase, (*2*) phosphohexose isomerase, (*3*) phosphofructokinase, (*4*) aldolase, (*5*) triosephosphate isomerase. (**B**) Reactions of the EMP pathway from GAP (g). (h) 1,3 Diphosphoglycerate (1,3 DPG), (i) 3-phosphoglycerate (3 PG), (j) 2-phosphoglycerate (2 PG), (k) phosphoenolpyruvate (PEP), and (l) pyruvate (PYR). The respective enzymes are (*6*) 3-phosphoglyceralde-hydehydrogenase, (*7*) 3-phosphoglycerate kinase, (*8*) phosphoglycerate mutase, (*9*) enolase, and (*10*) pyruvate kinase. Carbon is drained off from the 3PG and PEP pools (in both cases for amino acids)

The pathway from G6P to pyruvate can also work in the opposite direction. This is called *gluconeogenesis* ("new glucose synthesis"). When small molecules such as a primary alcohol (ethanol) or a carboxylic acid (lactic acid (HLac), formic acid or acetic acid), all products from glycolysis, are used as carbon source, the reactions of Fig. 2.4a, b from G6P to pyruvate must be traced in the opposite direction in order to

synthesize the precursor metabolites that are drained away from the EMP pathway when it operates in its normal direction from glucose to pyruvate. These branch points away from the EMP pathway are indicated in the caption to Fig. 2.4a, b.

The *purpose* of the EMP pathway is, as mentioned previously, to create energy for biosynthesis reactions. When Fig. 2.4a, b is studied from this perspective the result is *that 2 mol ATP is produced for each mole glucose that is converted to 2 mol pyruvate*. In reactions 1–3 the glucose molecule is energized to provide free energy for the split of F1,6P in reaction (4). When calculating the maximum ATP yield in the pathway all DHAP is funneled back into the glycolysis pathway, and each GAP produces two ATP when metabolized to pyruvate. The net result is consequently two ATP, when no carbon is lost to produce metabolites other than pyruvate.

As discussed in Sect. 2.2.1, an overall redox balance on the pathway from glucose to pyruvate reveals that two redox packages (NADH) are synthesized by reduction of the oxidized form of the cofactor when glucose is metabolized to pyruvate (2.3). In Fig. 2.4b, we identify reaction (6) where each of the two aldehydes, GAP, is oxidized to diphosphoglycerate (1,3 DPG), a carboxylic acid, as the reaction in which NADH is synthesized.

Whereas the redox production in the pathway can be deduced by considering the substrate and the final product of the pathway, there is no easy way to find the amount of ATP produced or consumed in the pathway. As indicated at the end of Sect. 2.2.1, one must consult the pathway diagrams, either in textbooks or on the net. For the EMP pathway ATP is produced in reactions (7) and (10) which are both catalyzed by *kinases*. When sufficient energy is stored in an activated metabolic intermediate, kinases release an energy package, generally as ATP. Other hydrolyzing enzymes, *hydrolases*, release energy as *heat*, and this happens when the free energy change of the reaction is insufficient to allow an ATP to be synthesized – see Fig. 5.1 and also the discussion in Chap. 4, where glycerol 3-phosphate hydrolase is used as an example. Generation of heat instead of ATP is certainly practical in many circumstances (in humans to maintain the body temperature), but it is of little use when the organism needs free energy for growth.

The gluconeogenetic path from pyruvate to G6P requires ATP. If a waste product from glycolysis, e.g., ethanol, is used as a substrate rather than glucose, then the precursors from the EMP pathway can only be synthesized if the substrate is also consumed in ATP generating reactions. This is where *respiration* (Sect. 2.2.5) plays a crucial role.

Only reactions (1), (3), and (10) in glycolysis are, as will be seen in Table 4.2, accompanied by large losses of free energy. At physiologically relevant conditions, reactions (6)–(9) have a ΔG that varies between -2.7 and $+2.7$ kJ mol^{-1}. Hence they can easily be reversed, when NADH is provided for reaction (6).

Many of the glycolytic reactions are reversible, and they are thermodynamically favored when the energy status (ATP and NADH) of the cell is high. Reactions (1), (3), and (10) are, however, not reversible. Other enzymes can carry out reactions similar to reactions (1) and (3), but without production of ATP. Reversal of the almost irreversible reaction (10) follows a circuitous route that involves metabolites from the TCA cycle.

In a similar fashion, the reactions from DHAP to glycerol can be reversed at high ATP and NAD level. It is noteworthy that the conversion of glycerol to glycerol 3-phosphate (G3P) is catalyzed by a kinase that requires ATP while as indicated above the hydrolysis of glycerol phosphate by a hydrolase liberates no ATP.

G6P, the final product of gluconeogenesis is used either as a substrate for the PP pathway or it is stored as poly-carbohydrates, e.g., *glycogen* $(\alpha\text{-D glucose})_n$, in yeast. This serves as a final energy source if glucose or degraded macromolecules are unavailable.

The reversal of the metabolic pathways when carbon compounds of the right structure, e.g., proteins and lipids are degraded and serve as alternate sources of building blocks and energy is, of course of preeminent importance in nutrition. But in the context of the present text, where the objective is to present ways of producing chemicals from renewable resources, the pathways that depend on sugars as substrate are in focus. Hence gluconeogenesis will not be given much attention in the following.

As a final note on glycolysis it is worth noting that the two ATP gained by *substrate level phosphorylation*, the reactions that convert glucose to pyruvate, *is generally the only source of free energy obtained in anaerobic fermentations*. Apart from certain anaerobic reactions, such as the conversion of acetyl-phosphate (Acetyl-P) (see Fig. 2.5a, b) to acetic acid, HAc, all further free energy generation must come from respiration, and respiration requires molecular oxygen, i.e., an *aerobic* fermentation process.

2.2.3 *Fermentative Metabolism: Oxidation of NADH in Anaerobic Processes*

At the exit from the EMP pathway 2 mol of ATP and 2 mol of NADH have been produced for each mole of glucose converted to 2 mol of pyruvate.

The ATP is used to drive other, energetically unfavorable processes, but the NAD consumed must be regenerated.

In *anaerobic* fermentation this occurs by reduction of the catabolic product, pyruvate. Figure 2.5a, b shows how *E. coli* and *lactic bacteria* sp. manage this task.

Apart from minor differences (the enzymes of the two bacteria can be slightly different, but they have the same function) the pathways from pyruvate to the final products, lactate, formate (or CO_2), acetate, and ethanol, are identical for most Gram-negative (e.g., *E. coli*) and Gram-positive bacteria (e.g., lactic acid bacteria).

At the first branch point, pyruvate is *either* reduced to lactic acid

$$CH_3COCOOH + NADH(= ''H_2'') \rightarrow CH_3CHOHCOOH(\text{lactic acid, HLac}), \tag{2.5}$$

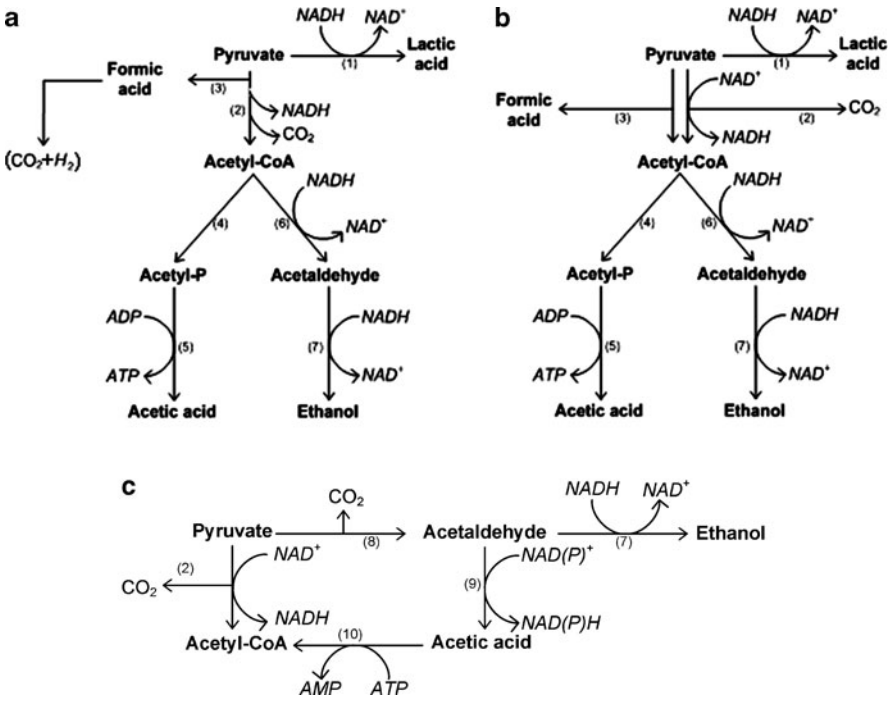

Fig. 2.5 Fermentative pathways for oxidation of NADH in bacteria. Only the main fermentative products are shown. The enzymes are (*1*) lactic acid dehydrogenase; (*2*) pyruvate dehydrogenase; (*3*) pyruvate-formate lyase; (*4*) phosphate acetyltransferase; (*5*) acetate kinase; (*6*) acetaldehyde dehydrogenase, (*7*) alcohol dehydrogenase. (**a**) The fermentative (or mixed acid) metabolism of *Escherichia coli*. (**b**) The fermentative metabolism of lactic acid bacteria. (**c**) Fermentative metabolism in the yeast *Saccharomyces cerevisiae*. (*2*) Pyruvate dehydrogenase, (*7*) alcohol dehydrogease (ADH), (*8*) pyruvate decarboxylase, (*9*) acetaldehyde dehydrogenase, (*10*) acetyl-CoA synthase. The notation NAD(P)H means that acetaldehyde dehydrogenase can use either NAD^+ or $NADP^+$ as cofactor. Note that yeast does not contain lactate dehydrogenase and therefore does not produce lactic acid

or pyruvate splits into two molecules, acetyl-coenzyme-A, AcCoA, and either formic acid (HCOOH) or CO_2. The cofactor, coenzyme-A, CoA (Fig. 2.6), is used in the synthesis of AcCoA.

$$CH_3COCOOH + CoA \rightarrow HCOOH + AcCoA \tag{2.6}$$

$$CH_3COCOOH + CoA \rightarrow CO_2 + AcCoA + NADH \tag{2.7}$$

When the lower part of the metabolic network is inactive, i.e., lactic acid is the only fermentation product, we have *homo-lactic fermentation*. The overall anaerobic

Fig. 2.6 Coenzyme-A (CoA)

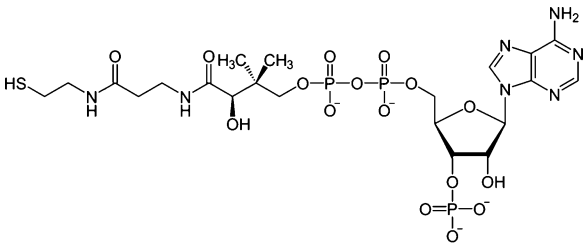

metabolism of glucose to the final product, lactic acid, which is excreted from the cells to the medium is

$$C_6H_{12}O_6 \rightarrow 2C_3H_6O_3(2\,\text{mol of lactic acid}) + 2\text{ATP} \tag{2.8}$$

When both the upper and the lower part of the network are active we have *mixed-acid fermentation*. Lactic acid, together with formic acid or CO_2, acetic acid (HAc) and ethanol, are the normal metabolic products, but under certain conditions both pyruvate and acetaldehyde can be excreted from the cell. CO_2 is produced in lactic acid bacteria by (2.7), and in *E coli* possibly also (together with H_2) by decarboxylation of formic acid.

In mixed acid metabolism of glucose the overall reaction is more complicated than (2.8):

$$C_6H_{12}O_6 \rightarrow \alpha\text{HLac} + \beta\text{HCOOH} + \gamma CO_2 + \delta\text{HAc} + \varepsilon C_2H_5OH + (2+\delta)\text{ATP} \tag{2.9}$$

The stoichiometric coefficients in (2.9) are not fixed quantities as in (2.8), but they change with the environment, i.e., the conditions under which the fermentation is carried out. If the substrate, glucose, is available at high concentration in the medium, then all the coefficients β to ε are practically zero (homo-lactic fermentation), but for very low glucose concentrations in the medium, a large part of the carbon flux from pyruvate is diverted toward the products in the lower part of the network. The term "very low glucose concentration" is quantified in Chap. 7 to be in the mg L^{-1} (ppm) range. In Chaps. 3 and 5, the ratios between the coefficients in (2.9) will be determined by carbon and redox balances.

Coenzyme A, CoA, is a large organic molecule with a structure similar to ATP (Fig. 2.2a). At the end of the long chain on the left is a thiol group that can form thioesters with carboxylic acids. It plays a crucial role, both in catabolic reactions and in anabolic reactions, e.g., in the synthesis of long-chain fatty acids.

Acetyl-CoA, abbreviated to AcCoA, is the ester with acetic acid, HAc.

$$CH_3COOH + \text{CoA} \rightarrow CH_3CO - S - \text{CoA}(\text{Acetyl CoA}) + H_2O \tag{2.10}$$

Acetyl-CoA is converted to Acetyl-P and CoA by reaction with phosphate (P):

$$\text{Acetyl CoA} + P \rightarrow CH_3CO\,O\,PO_3(\text{Acetyl} - P) + \text{CoA} \tag{2.11}$$

Finally, Acetyl-P is hydrolyzed by acetate kinase, to give acetic acid (HAc) + ATP. Thus, if the only metabolic product from anaerobic degradation of glucose could be HAc, the ATP yield per molecule of glucose would double, from two to four ATP per glucose. It is, however, impossible[5] in anaerobic fermentation to have "homo-acetic" metabolism of glucose ($\delta = 2$ in (2.9)) since the other product, HCOOH or CO_2, from the breakdown of pyruvate is less reduced than HAc, and ethanol which is more reduced than HAc must necessarily accompany the formation of HAc. The detailed discussion of this topic is deferred to Chap. 5.

Figure 2.5c shows the, apparently, much simpler looking reduction of pyruvate to final products in the anaerobic fermentation of glucose by the *eukaryote, S. cerevisiae*.

All EMP pathway reactions take place in the cytosol. The decarboxylation (8) of pyruvate to acetaldehyde is followed by reduction (7) to ethanol also takes place in the cytosol. As a side reaction the acetaldehyde can be oxidized to HAc (9), and the final metabolic products, ethanol and HAc are excreted to the medium from the cytosol.

Yeast is a so-called "higher" organism than the bacteria (*prokaryotes)*. The metabolism takes place in different compartments of the cell. One such compartment, separate from the cytosol, is the *mitochondrion* where the TCA cycle reactions (Sect. 2.2.4) occur. In Fig. 2.5c reaction (2) transfers part of the pyruvate to the mitochondria where it is converted to AcCoA with the stoichiometry (2.7).

In reaction (10), HAc is activated to cytosolic AcCoA which may either be used for lipid production in the cytosol, or it may be transferred to mitochondrial AcCoA for further use in mitochondrial processes.

To sum up: *In yeast the anaerobic fermentation of glucose has ethanol as its main product*:

$$C_6H_{12}O_6 \rightarrow 2C_2H_5OH + 2CO_2 + 2ATP \tag{2.12}$$

Other metabolic products of anaerobic yeast fermentation are HAc, acetaldehyde, and TCA cycle metabolites. All these compounds are more oxidized than ethanol. Some NADH must be consumed in a side reaction in order to balance the total NADH production since only the NADH from the EMP pathway is taken care of by reaction (7) in Fig. 2.5c. The pathway in which the extra NADH is consumed is that leading from dihydroxyacetone phosphate, DHAP, to glycerol[6]:

$$(CH_2OP)COCH_2OH + NADH \xrightarrow{(1)} CH_2OP\,CHOH\,CH_2OH \xrightarrow{(2)} (CH_2OH)_2CHOH \tag{2.13}$$

[5]Metabolism is full of surprises: Lengeler et al. (1999, p. 285) describes the anaerobic metabolism of glucose by to three HAc + four ATP. What happens is that CO_2 from decarboxylation of pyruvate is reduced to Acetyl-P using the two NADH created in the EMP pathway.

[6]To save space in writing the stoichiometries only the reduced form of the redox carrier and the activated form (ATP) of the energy carrier are shown in this chapter. H_2O is generally left out. The stoichiometric coefficient for H_2O can be found from an O and an H balance (see Chap. 3).

Reaction (1) is catalyzed by glycerol 3-phosphate dehydrogenase.[7] The hydrolysis reaction (2) is catalyzed by the non-ATP-generating glycerol 3-phosphatase (also called glycerol 1-phosphatase).

The metabolism of glucose to glycerol via the DHAP pathway is summarized as:

$$C_6H_{12}O_6 + 2ATP + 2NADH \rightarrow 2CH_2OH\,CHOH\,CH_2OH \qquad (2.14)$$

As a result of the discussion in Sects. 2.2.2 and 2.2.3, we have learnt how glucose, the preferred substrate of most microorganisms is converted by *anaerobic* fermentation to final metabolic products, some of which are of considerable economic value. Equations (2.8), (2.9), and (2.12) are examples of redox balanced overall pathways, while (2.14) requires balancing by other metabolic pathways. Production of ATP is of course the purpose of the processes when seen from the perspective of the organism.

Other sugars such as fructose, mannose, sucrose, lactose, and xylose can also be used as substrates. The transport processes whereby sugars are taken up to the cell by "facilitated" or by "active" transport will be discussed in Sect. 7.7. Inside the cell disaccharides hydrolyze to monosaccharides (sucrose to glucose and fructose, lactose to glucose and galactose), and phosporylation of one of the hexoses takes place while the other may be excreted. Certain C5 sugars, such as xylose are easily utilized by bacteria while their utilization by yeast is difficult, leading to a very slow fermentation.

The important question of general carbon and energy source utilization is generally outside the scope of this text and it will only be addressed in problems.

2.2.4 *The TCA Cycle: Provider of Building Blocks and NADH/FADH$_2$*

The main entry point to the tri-carboxylic acid cycle (TCA cycle) is via AcCoA which is synthesized by reaction (2.7) from pyruvate, the product of the EMP pathway. To understand the working of the TCA cycle one can imagine that one pyruvate enters through reaction (1) in Fig. 2.7, while another pyruvate enters via

[7]There are actually two cytosolic enzymes coded by different genes, GDPH1 and GDPH2. One enzyme is concerned with redox regulation in the cell whereas the other gives osmotolerance to the yeast when it grows in high salt concentrations (or at very high glucose concentration, e.g., in wine making). The glycerol production at the expense of some ethanol and biomass increases the quality of many wines, and yeast with overexpression of the gene is used by some winemakers (Remize et al. 1999). In the present text we are only concerned with the redox regulation role of GDPH to counteract the production of less reduced metabolic products, especially succinic acid, and the production of NADH when glucose is converted to biomass.

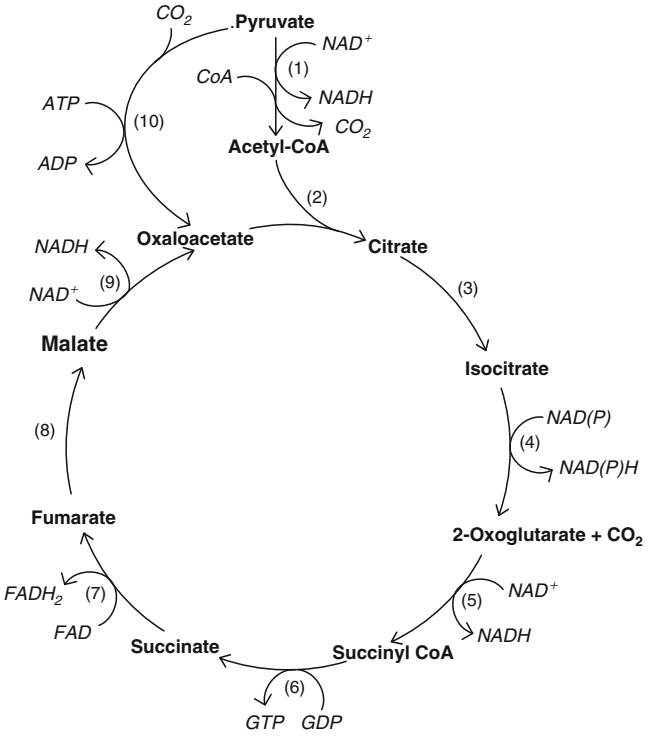

Fig. 2.7 The TCA cycle and the pyruvate carboxylation shunt. To simplify the diagram CoA is not shown. The enzymes are (*1*) pyruvate dehydrogenase; (*2*) citrate synthase; (*3*) aconitase; (*4*) isocitrate dehydrogenase; (*5*) 2-oxoglutarate dehydrogenase; (*6*) succinate thiokinase; (*7*) succinate dehydrogenase; (*8*) fumarase; (*9*) malate dehydrogenase; (*10*) pyruvate carboxylase. In Chap. 5 (Fig. 5.9) the "glyoxylate shunt" will be discussed. The shunt connects isocitrate and malate by the reactions: isocitrate → succinate + glyoxylate, and glyoxylate + AcCoA → malate, using the enzymes (11) isocitrate lyase and (12) malate synthase. Glyoxylic acid is CHO–COOH

the "side door," reaction (10), where it is carboxylated to oxaloacetate. By reaction (2) in Fig. 2.6 citric acid is synthesized, (2.15):

$$\text{Pyruvic acid} + CO_2 \xrightarrow{(10)} \text{Oxaloacetic acid} \xrightarrow{(2)} \text{Citric acid} + \text{pyruvic acid} \qquad (2.15)$$

Following the TCA reactions clockwise from citric acid, the six-carbon tricarboxylic acid is converted by a series of oxidation reactions[8] to the four-carbon

[8]Note in Fig. 2.7 that there are two forms of isocitrate dehydrogenase. One form which is located only in the mitochondria uses NAD^+ as cofactor, the other is located both in the cytosol and in the mitochondria, and it uses $NADP^+$ as cofactor. Equation (2.16) is written for the first form and holds for yeast, while bacteria must operate with the $NADP^+$ requiring cytosolic enzyme. In fact this becomes an advantage when we produce, e.g., amino acids in bacteria, since the NADPH obtained in reaction (4) in Fig. 2.7 is needed in the biosynthesis of the amino acid (see Sect. 2.4).

dicarboxylic acid, oxaloacetic acid. Two carbons are lost to CO_2 if none of the intermediates is drained off the cycle to enter into other pathways, e.g., synthesis of amino acids. The net result is that *one pyruvate is completely ground up to form 3 CO_2*. The oxaloacetate is ready to accept a new pyruvate for the next round of the cycle.

Thus, if no intermediates from the TCA cycle are used for other purposes the net result of one turn of the TCA cycle is:

$$CH_3CO\,COOH \xrightarrow{(+3H_2O)} 3CO_2 + 4NADH + FADH_2 + GTP \tag{2.16}$$

Five redox packages (=5"H_2") and one energy package (GTP, see Sect. 2.2.1) are produced in addition to the "waste product" CO_2.

In *aerobic* processes, and if the microorganism has a functioning *respiration system*, the redox carriers are oxidized by the use of molecular O_2, and large amounts of ATP are produced.

In *anaerobic* processes, the TCA cycle functions exclusively to produce building blocks for cell synthesis. The activity of the TCA cycle will be very low, and the cycle is likely to operate both clockwise and counter-clockwise in order to balance the redox equivalents produced on the right hand side of the cycle with those consumed counter-clockwise on the left hand side.

In the TCA cycle, one finds several of the sugar-based building blocks for the bio-based production of bulk chemicals in Table 2.1 and Fig. 2.1b. Succinic acid is a raw material for the polymer industry, 2-oxoglutarate and oxaloacetic acid are starting points for production of amino acids, and citric acid is one of the most important products of the food industry with an annual production of more than 1 M ton.

When one of the TCA cycle intermediates is desired to be the main product of the fermentation the microorganism is selected or engineered to give a high flux away from the TCA cycle at the right point. Thus, *Asperillus niger*, a filamentous fungus which is the main work-horse for production of citric acid, is operated such that very little carbon is allowed to pass further than to citrate. This means that building blocks for cell synthesis such as 2-oxoglutarate, succinic acid, and oxaloacetate are formed at a minimum rate, just enough to keep the culture alive. The cell functions more or less as a complex catalyst that converts glucose to citric acid.

In Chaps. 3 and 4, it will be shown that the ratios between the production rates of different end products are quantified by *yield coefficients*. Hence, in citric acid production the yield of citric acid on glucose is desired to be as high as possible, at the expense of the yield of biomass on glucose. Some carbon must, as mentioned above be used to maintain vitality of the cell culture, and in *Aspergillus* which produces the main part of its ATP by respiration, even the most efficient citric acid process must allow a certain production of NADH/$FADH_2$ in the TCA cycle.

By the same arguments it is not optimal in an amino acid production process to allow the TCA cycle to use almost all the glucose fed to the organism. In lysine production, it is desirable to have a high flux to 2-oxaloglutarate from where

the carbon is drained off to form glutamate, the primary amino donor for the biosynthesis of most amino acids (see (2.22) and (2.23)).

Some glucose has to be diverted to form the redox carrier NADPH which is used in the amino acid synthesis pathways. The primary source of NADPH is the pentose phosphate (PP) pathway, Sect. 2.2.6, and the ratio between the carbon flow to the PP pathway and to the TCA cycle via pyruvate must be fine-tuned to get the best yield of lysine on glucose.

The main entry to the TCA cycle is, as mentioned earlier, by reaction (2) in Fig. 2.7. Another entry point is by reaction (10), carboxylation of pyruvate, which was used to illustrate how the cycle regenerates oxaloacetate after consumption of one pyruvate molecule. The entry to the reductive part of the TCA cycle via pyruvate (PYR) to oxaloacetate (OOA) is useful when only the metabolites in this branch are needed, e.g., in anaerobic processes.

A similar shunt from OOA to PEP plays a part in gluconeogenesis where the high energy barrier from PYR to PEP must be overcome. OOA, a degradation product from amino acids, is decarboxylated to PEP using one GTP. The reverse reaction PEP to OOA proceeds without the use of ATP.

Besides the cyclic path between oxaloacetate and the last two metabolites of the EMP pathway there are other cycles and shunts in the TCA cycle. The tasks of the TCA cycle are many, and it has to operate properly both for prokaryotes where all TCA cycle reactions occur in the cytosol and for eukaryotes where the TCA cycle reactions occur in the mitochondria, and substrates and products have to be transferred between the cytosol and the mitochondria. Furthermore, the TCA cycle must operate both for conversion of glucose to products, and for synthesis of glucose from the products, i.e., for supplying essential nutrients to fasting animals.

To appreciate the full significance of the many variations in TCA cycle metabolism the reader must consult standard texts in biochemistry. In the present context where synthesis of products from sugars is the main theme, the important duties of the TCA cycle are summarized as follows:

1. Deliver NADH and $FADH_2$ as substrates for respiration.
2. Deliver metabolites that will be used as building blocks for cell synthesis.

2.2.5 *Production of ATP by Oxidative Phosphorylation*

The bacteria and the yeast *Saccharomyces cerevisiae* discussed in Fig. 2.5a–c are all *facultative anaerobes*. This means that *E. coli, lactic acid bacteria* (there are many families), and *S. cerevisiae*, are able to grow both in the presence of molecular O_2 (*oxic growth*) and without O_2 (*anoxic growth*). This is a great advantage in industrial fermentation, since both the aerobic and the anaerobic fermentation paths can be used in the screening for the best production organism.

Other microorganisms (all of them prokaryotes) will die in the presence of O_2. These are called *obligate anaerobes*, and examples are *Clostridium* sp., the soil bacteria *Actinomyces*, and methanogenic bacteria.

The facultative anaerobes can generate free energy (ATP) by the use of O_2 as an electron acceptor. The obligate anaerobes can use other electron acceptors such as SO_4^{2-}, NO_3^-, and metal ions (e.g., Fe^{3+}), or in the case of methanogens, fatty acids, which are reduced to CH_4.

The evolutionary advantage of facultative anaerobes is that (besides the other electron acceptors) they can also use O_2, an abundantly available compound in the atmosphere and in the marine environment. Evolution has provided these organisms with protection agents against the lethal byproducts of oxic growth, e.g., the enzymes *catalase* and *manganese-superoxide dismutase* which are able to scavenge the toxic oxygen radicals that are formed in small quantities in aerobic metabolism.

Once O_2 is available, the facultative anaerobes are able to switch very rapidly from anaerobic to aerobic growth. The changes in metabolism, which are tightly regulated to avoid a dramatic and unhealthy utilization of building blocks from cell synthesis to an "energy feast," are found in many places in the metabolic network. Thus the operation of the TCA cycle will be almost exclusively in the clockwise direction in Fig. 2.7. The fermentative pathways, Fig. 2.5a–c, are down-regulated, and the activity of some enzymes, e.g., pyruvate formate lyase, (3) in Fig. 2.5 a, b, is immediately quenched. In *E. coli*, this has the effect that the pyruvate is degraded, not in the fermentative pathways to give formic acid, ethanol, and acetic acid, but in respiration via the TCA cycle. Lactic acid bacteria which lack an essential part of the electron transfer chain, *cytochrome-c*, produce AcCoA via reaction (2). The total two NADH per glucose which is thus generated can be oxidized in the presence of molecular O_2 using the enzyme *NADH-oxidase*, and as described in Sect. 2.2.3, the lactic acid bacteria can now gain four ATP per mole of glucose and secrete HAc as the only fermentation product. In contrast to *S. cerevisiae* almost all other yeasts are *obligate aerobes*, i.e., they *only* grow in the presence of O_2.

With this introduction to oxic growth we shall now turn to *oxidative phosphorylation* (or *respiration*), the mechanism by which evolutionarily privileged organisms (including humans) are able to reap much more energy from consumption of glucose.

A glucose molecule that has been completely metabolized to CO_2 in glycolysis and through the TCA cycle has obtained a total of 12 reduced redox cofactors:

$$C_6H_{12}O_6 \rightarrow 6CO_2 + 2NADH + (8NADH + 2FADH_2) + 2ATP + GTP \quad (2.17)$$

The oxidized forms of the cofactors are regenerated through a series of steps in the respiratory chain, the so-called *oxidative phosphorylation* process:

$$NADH + 1/2\,O_2 \rightarrow NAD^+ + (P/O)_{NADH}ATP \quad (2.18)$$

$$FADH_2 + 1/2\,O_2 \rightarrow FAD + (P/O)_{FADH_2}ATP \quad (2.19)$$

In Chap. 4, it will be shown that the oxidation of NADH to NAD and H_2O at physiological conditions is accompanied by a change in free energy of about 220 kJ. The activation of 1 mol of ADP to ATP requires 30.5 kJ free energy at "standard conditions," and in Chap. 4 the free energy needed to produce 1 mol of ATP

at physiological conditions will be discussed. At standard conditions and at a thermodynamic efficiency of 100%, about 7 mol of ATP should be synthesized per mole of NADH oxidized. Studies of the electron transfer chain in the respiratory system conducted over the last 70 years have shown that *theoretically* three ATP should be synthesized by reaction (2.18) if all (three) steps in the electron transfer chain are used, while $FADH_2$ which passes through only the last two steps of the chain has a *theoretical* yield of two ATP.

Since the stoichiometric coefficient P/O for ATP (called "the P/O number") is at most 3 the conversion of H_2 to H_2O has a theoretical thermodynamic efficiency of $91.5/220 = 0.42$.

Still, 42% is a remarkable efficiency compared to the efficiency of free energy ("electricity") generation in even the most elaborate modern H_2-based fuel cells. The efficiency is even more remarkable when considering that the $NADH/FADH_2$ originates from "combustion" of glucose to CO_2, a process which human ingenuity cannot hope to replicate with a thermodynamic efficiency that even approaches that of the microbial metabolism.

In actual fermentation practice, the theoretical P/O ratio of (2.18) and (2.19) is not obtained. Experimental studies of aerobic yeast fermentation (to be discussed in Chap. 5) have shown that an overall P/O number of 1.2–1.3 is obtained.

Also with the lower values for P/O, an ATP generation of about $1.25 \times 10 = 12.5$ mol ATP/mol glucose in the respiration of yeast cells is a remarkable improvement on the two ATP gained by glycolysis of glucose to pyruvate and further to ethanol.

In fact, oxidative phosphorylation, whether it is carried out in the space between the cell membranes in *E. coli* or in the mitochondria of eukaryotes, is a remarkable "invention" of nature that permits living organisms with a functioning respiratory chain to consume much less sugar than those organisms which must create all their growth energy by substrate level phosphorylation.

The regulation of the carbon utilization in the cell that was mentioned in the introduction to Sect. 2.2 prevents all the carbon being diverted to an unnecessary and potentially dangerous overproduction of ATP by respiration. Both *E. coli* and yeast have an *overflow metabolism*. At high glucose flux down the EMP pathway (i.e., a high glucose concentration in the medium) some of the pyruvate is directed toward the fermentative pathways. *E. coli* will produce acetate, formate, and ethanol when the glucose concentration in the medium exceeds a certain low level, and at the same time the oxygen consumption reaches an upper, constant level (see Example 7.3).

In yeast fermentation it has been shown that even at low glucose concentration there is a substantial flow of pyruvate into the fermentative pathway in Fig. 2.5c, but up to a critical (also quite low) level of glucose the carbon is shunted back into the mitochondria by reaction (10) in Fig. 2.5c and degraded in the TCA pathway. When the critical glucose level is reached the oxygen uptake rate becomes constant, and an increasing portion of the carbon ends up as ethanol. This is called the *Crabtree effect*, and it sets in also when there is plenty of oxygen available. A corresponding phenomenon, the *Pasteur effect*, is seen when oxygen is scarce, and some of the

carbon *must* be sent toward ethanol. The Pasteur effect is consequently not a metabolic overflow mechanism, but results from an inadequate O_2 supply.

The Crabtree effect will be discussed several times in this text, first in Example 3.5.

The biology and the complicated biochemistry that ensures a highly efficient free energy production in the respiratory system has been the subject of a vast number of theoretical and experimental studies during the last 60 years. In the context of this textbook it is probably enough to be familiar with the few major results outlined above. In Chap. 4, the thermodynamics of the electron transport chain and the reactions by which ATP is generated will be briefly touched upon to give some understanding of the fascinating work of the brilliant scientists who contributed to our present knowledge of the system. There are still some ambiguities in the more or less accepted explanations, and further study of respiration is surely going to reveal new layers of fundamental research problems.

2.2.6 *The Pentose Phosphate Pathway: A Multipurpose Metabolic Network*

The pentose phosphate (PP) pathway shown in Fig. 2.8 is in reality a network of tightly regulated reactions. There is one entry point, G6P, from the EMP pathway and at several points metabolites from the pathway, identical to those formed in the EMP pathway (F6P and three GAP), are sent back to the energy creating EMP pathway. Metabolites are drained off the PP pathway to be used as substrates for production of key products in cellular metabolism. NADPH, a product from the first two reactions of the PP pathway is used to provide reducing power in a number of anabolic reactions. Two ribulose-5 phosphate (Ru5P) molecules react to form ribose-5 phosphate (R5P) and xylulose-5 phosphate (Xu5P). The ten carbons in R5P and Xu5P are "reshuffled" to one 7-carbon sugar, sedoheptulose phosphate (S7P), and the 3-carbon GAP, which may, again through a reshuffling process, produce F6P and a 4-carbon sugar, erythose-4 phosphate (E4P).

In long pathways, and interacting with different amino acids, R5P is converted to adenine and guanine ribonucleotides which we recognize in the structures of the energy and redox carriers of Fig. 2.2. Genetic material (RNA and DNA) are products of polymerization reactions of these compounds. E4P is one of the substrates for synthesis of the aromatic amino acids, phenylalanine, tyrosine, and tryptophan. Hence, in the industrial production of pharmaceuticals (L-DOPA and related products from tyrosine, and artificial sweeteners from phenylalanine) the PP pathway is engineered to give a high yield of E4P compared to the other products of the pathway.

The many different purposes of the PP pathway explain the complexity of the constituent reaction network. In a situation where cellular growth is at a minimum the carbon flux into the PP pathway at G6P is very low, and the full potential for production of energy and of primary metabolites such as lactic acid and ethanol from glucose is realized. When production of amino acids is desired, NADPH is the

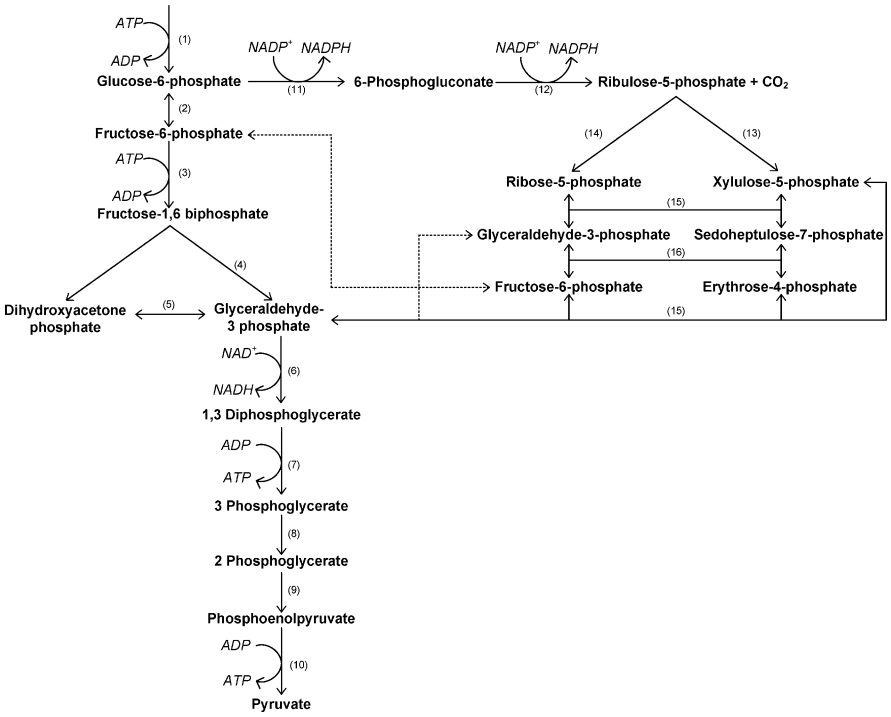

Fig. 2.8 The Pentose Phosphate pathway (PP) seen as an appendix to the EMP pathway (Fig. 2.4a, b, reactions (*1*)–(*10*)). The enzymes in the PP pathway are (*11*) G6P dehydrogenase, (*12*) 6-phosphogluconate dehydrogenase, (*13*) ribulosephosphate 3-empimerase, (*14*) ribosephosphate isomerase, (*15*) transketolase, and (*16*) transaldolase. Transaldolase can catalyze two reactions (**1**) interconversion of xylulose 5-phosphate and ribose 5-phosphate to GAP and sedoheptulose 7-phosphate and (**2**) interconversion of xylulose 5-phosphate and erythrose 4-phosphate to GAP and F6P. Carbon that is not used in the PP pathway reenters the EMP pathway as GAP and F6P

main product of the PP pathway, and the remainder of the carbon is sent back to the EMP pathway as GAP and F6P:

$$3\text{G6P} \rightarrow 6\text{NADPH} + 3\text{CO}_2 + 2\text{F6P} + \text{GAP} \tag{2.20}$$

The F6P can return to G6P via the reversible reaction between F6P and G6P, and more CO_2, GAP, and NADPH are produced in a new round of the *oxidative* part of the PP pathway.

The net result of recycling F6P produced by (2.20) until all F6P is used up is that 3/2 G6P is metabolized to 9 CO_2 and 18 NADPH while 3/2 G6P is metabolized to 3 GAP, i.e., that

$$\text{C}_6\text{H}_{12}\text{O}_6 \xrightarrow{\text{ATP}} 6\text{CO}_2 + 12\text{NADPH}, \text{ and } 2\text{C}_6\text{H}_{12}\text{O}_6 \xrightarrow{\text{ATP}} 4\text{GAP} \tag{2.21}$$

Thus, in circumstances where much NADPH is needed, the PP pathway serves the same purpose as the combined EMP and TCA cycle pathways: One carbon atom

of glucose is combusted to give one CO_2. The free energy in the glucose carbon is preserved in either two NADPH or two NADH.

The application of the two products in cell metabolism is very different. NADPH is used in synthesis reactions, but cannot provide growth energy for the cell by respiration. Only NADH can serve this purpose.

2.2.7 *Summary of the Primary Metabolism of Glucose*

In Sects. 2.2.2–2.2.6, the degradation of glucose through a number of pathways has been followed. All the pathways, except perhaps the PP pathway, serve the purpose of releasing energy for growth of the microorganism, while building blocks for synthesis of cell mass components are drained off the catabolic pathways at rates that depend on the conditions of the fermentation.

In the EMP pathway several intermediate metabolites are diverted to form building blocks, e.g., 3-PG in Fig. 2.4b to form the amino acid *serine*, and serine is used to synthesize other amino acids. Likewise, in anaerobic yeast fermentation it is difficult to avoid a flux via DHAP to glycerol in order to remove NADH. The carbon that leaves the EMP pathway and the TCA cycle is lost for energy production.

The fermentative pathways, Sect. 2.2.3, are necessary in anaerobic fermentations to remove NADH produced in the EMP pathway. Their final products, HLac, ethanol, formic acid, and HAc are not used as building blocks for cell synthesis, and from the perspective of the organism these *primary metabolites* must be considered as waste products.

In many industrial processes, the objective is to maximize the production of primary metabolites and other compounds that are not needed in anabolic catabolism.

Catabolism can be almost decoupled from anabolism, and then the primary metabolic metabolites are the sole sinks for the sugar substrate. For many hours after the biomass concentration has grown to a suitable level and feed of an essential nonsugar substrate has been stopped, the biomass continues to produce the desired product using the ATP that is always obtained as part of the sugar metabolism to "maintain" the organism (see Sect. 5.2) and possibly also to supply ATP for continued production of the metabolite.

Feed of the nitrogen source is typically stopped, and synthesis of new functional biomass becomes impossible. For many hours thereafter, a lactic acid bacterium continues to produce HLac from the sugar source, *Xanthomonas campestris* continues to produce xanthan gum, and an engineered strain of *Bacillus subtilis* synthesizes hyaluronic acid, another moderate molecular weight polysaccharide used in the surgery and in the cosmetics industry.

The processes involved in the "natural life" of an organism, i.e., the anabolic metabolism to produce and maintain a viable cell, and the catabolic metabolism needed to produce energy to sustain the anabolic processes, are together named the *primary metabolism* of the organism. A few of the pathways of primary metabolism have been introduced in the previous sections. Obviously, a standard text in Biochemistry (e.g., Voet and Voet 1995) must be studied to get even a superficial

picture of the whole genome scale primary metabolism. The pathways introduced in this chapter are, however, sufficient to give at least some biochemical background for the quantitative treatment of carbon flux distribution in microorganisms (Chaps. 3–5) and the kinetics of bioreactions (Chaps. 7 and 9).

The literature refers to *secondary metabolism* (or *special metabolism*) along with the primary (or *basic*) metabolism. In secondary metabolism, metabolic products are synthesized in (often very long) pathways which are not absolutely necessary to maintain vitality of a culture *in normal circumstances*. β-Lactam antibiotics (penicillins), pigments, flavors, and the large group of polyketides (including many antibiotics) are filed under the common heading of secondary metabolites. It is difficult to make a clear distinction between metabolites of the primary and secondary metabolism, since some of the "secondary" metabolites and their pathways may play as a yet undiscovered role for the "normal" life of the organism. But definitely, when one of the secondary metabolites is the desired product, the pathways to its formation have to be carefully explored, and key enzymes must be identified and over-expressed in order to get an acceptable yield of the product. This is a major task for Systems Biology, and it requires much experimental and theoretical work.

In Sect. 2.3, a number of primary and secondary pathways are described in somewhat more detail. The goal is not to obtain a hands-on knowledge of how the pathways operate and how they can be optimized, but rather to give a glimpse of the complexity of microbial metabolism.

The discussion of the primary metabolism is supplemented by Tables 2.2–2.4 in which typical building blocks and the requirement for redox and energy carriers are listed.

Table 2.2 Precursor metabolites and some of the building blocks synthesized from the precursors

Precursor metabolite	Building blocks	Amount required (μmol (g DW)$^{-1}$)
Glucose-6-phosphate (G6P)	UDP-glucose, UDP-galactose	205
Fructose-6-phosphate (F6P)	UDP-*N*-acetylglucosamine	71
Ribose-5-phosphate (R5P)	Histidine, tryptophane, nucleotides	898
Erythrose-4-phosphate (E4P)	Phenylalanine, tryptophane, tyrosine	361
Glyceraldehyde-3-phosphate (GAP)	Backbone of phospholipids	129
3-Phosphoglycerate (3GP)	Serine, Cysteine, Glycine, Nucleotides, Choline,	1,496
Phosphoenolpyruvate (PEP)	Phenylalanine, tryptophane, tyrosine	519
Pyruvate (PYR)	Alanine, isoleucine, valine	2,833
Acetyl-CoA (AcCoA)	Lipids	3,747
2-Oxoglutarate (2OG)	Arginine, glutamate, glutamine, proline	1,079
Succinyl-CoA (SuCoA)	Hemes	–
Oxaloacetate (OOA)	Aspartate, asparagine, isoleucine, methionine, threonine, lysine, nucleotides	1,787

A number of important industrial products are found in the list of building blocks. The last column shows the amount of precursor metabolites needed to synthesize 1 g (dry weight = DW) of *Escherichia coli* (Lengeler et al. 1999, p. 115)

Table 2.3 Composition of *E. coli* cells grown at 37 °C on a glucose minimal medium at a specific growth rate $r_x = \mu = 1.04$ g cell formed per gram cell per hour (Ingraham et al. 1983), and the corresponding requirements for ATP and NADPH

Species	Content (g (g DW)$^{-1}$)	ATP (μmol (g DW)$^{-1}$)		NADPH (μmol (g DW)$^{-1}$)	
Protein	0.55	29,257	(21,970)	11,523	(0)
RNA	0.20	6,796	(2,146)	427	(0)
rRNA	0.16				
tRNA	0.03				
mRNA	0.01				
DNA	0.03	1,240	(450)	200	(0)
Lipid	0.09	2,836	(387)	5,270	(0)
Lipopolysaccharide	0.03	470	(125)	564	(0)
Peptidoglycan	0.03	386	(193)	193	(0)
Glycogen	0.03	154	(154)	0	(0)
Building blocks	0.04				
Total	1.00	41,139	(25,425)	18,177	(0)

Numbers in parenthesis for ATP and NADPH are for growth at the same conditions, but on a rich medium that contains all the necessary building blocks (amino acid, nucleotides, fatty acids, etc.). The ratio between NADPH and (NADP + NADPH), the anabolic reduction charge, is usually around 0.5, indicating a need for "preparedness" for the reductive macromolecular synthesis. The corresponding ratio for catabolic reduction charge NADH/(NADH + NAD^+) is small (<0.1) since the oxidized form of the redox carrier must be in ample supply. Data from Ingraham et al. (1983)

Table 2.4 Measured concentrations of AMP, ADP, and ATP in a continuous culture of *Lactococcus lactis*, a common lactic acid bacterium

Specific growth rate (h^{-1})	Substrate	[AMP]	[ADP]	[ATP]	Total adenylate pool	Energy charge
0.03	Glucose	12	17	25	54	0.62
0.48	Glucose	17	23	52	92	0.69
0.69	Glucose	15	27	50	92	0.69
0.15	Maltose	5	8	20	33	0.73
0.32	Maltose	12	23	41	76	0.69
0.58	Maltose	17	26	44	87	0.66

The data are given for different specific growth rates μ (Sjöberg and Hahn-Hägerdahl, 1989). Concentrations are in μmol (g DW)$^{-1}$. The energy charge is defined as $E_c = ([ATP] + (1/2)[ADP])/$total adelynate pool. The value of E_c is about 0.9 in healthy *E. coli* cells (Lengeler et al. 1999, p. 124), which makes the numbers in the table seem rather small, especially at high μ

Table 2.2 shows that the drain of carbon to form building blocks is relatively modest from EMP pathway intermediates, except perhaps from 3GP. Most building blocks are synthesized with pyruvate, AcCoA, and TCA cycle intermediates as precursors. Especially, AcCoA is seen to be an important precursor for the formation of fatty acids and acetyl groups. Pyruvate and the TCA cycle precursors are almost exclusively used to form amino acids as building blocks for protein synthesis.

Table 2.3 shows that protein synthesis requires much ATP, and the difference in ATP consumption between a so-called "minimum medium" and a "complex

medium" is surprisingly small. The reason is that polymerization of amino acids to form protein is very costly in ATP while the production of amino acids from precursor metabolites is relatively cheap.

2.3 Examples of Industrial Production of Chemicals by Bioprocesses

Any medium used as a feed for a fermentation process should satisfy the following requirements:

It should contain a carbon, nitrogen, and energy source.
It should contain all essential minerals and growth factors to ensure rapid growth and a high yield of the desired product.
It should be of a consistent quality and be readily available throughout the year.
It should as far as possible not cause operational problems, neither in the fermentation process (foaming, reduction of mass transfer from a gas phase), nor in the downstream processing.

In the industrial production of biochemicals, cheap media obtained as byproducts from the agricultural sector are used. Sometimes the complex media contain growth factors that promote growth or give the right flavor to the product (such as molasses for bakers' yeast production and for production of rum).

Table 2.5 lists some typical complex media components used in the fermentation industry together with some typical fermentation products. Sugar cane juice is a natural "full" substrate used in fermentations, especially in Brazil.

A defined medium contains all the substances needed for growth and in standardized concentrations following a recipe that may change from organism to organism and depends on whether the fermentation process is aerobic or anaerobic. Lactic acid bacteria which are unable to synthesize certain amino acids are supplied with these in the medium (in Nature the bacteria import the amino acids from degraded proteins in the surroundings). Anaerobically growing yeast needs a supplement of ergosterol (an essential component of cell membranes) and unsaturated fatty acids which can be synthesized by the yeast only at aerobic conditions. A defined medium may also contain defined concentrations of, e.g., an antibiotic for which the producing strain has been made resistant. This serves to ensure that the "wild-type" strain of the organism is kept at bay. The wild-type strain usually grows faster than the "production strain" with its heavy burden of overproducing a desired metabolite or a foreign protein, and it would otherwise out-compete the producing strain in the "fight" for the (limiting) substrate.

The defined media are much more costly than most complex media, but the seasonal variation of the composition of complex media can give quality variations in the product. The purification of the product may become a problem for complex media, and the risk of contamination (e.g., with toxins) is always present.

Table 2.5 Typical complex media used in the fermentation industry

Medium	Contents	Origin	Typical application
Corn steep liquor	Lactate, amino acids, minerals, vitamins	Starch processing from corn	Antibiotics
Corn starch	Starch, glucose	Corn	Ethanol, industrial enzymes
Barley malt	Starch, sucrose	Barley	Beer, whiskey
Molasses	Sucrose, raffinose, glucose, fructose, betain	Sugar cane or sugar beet	Bakers' yeast, ethanol
Pharma media	Carbohydrates, minerals, amino acids, vitamins, fats	Cotton seed	Antibiotics
Serum	Amino acids, growth factors	Serum	Recombinant proteins
Whey	Lactose, proteins	Milk	Lactic acid
Yeast extract	Peptides, amino acids, vitamins	Yeast	Enzymes

Corn steep liquor is a byproduct of the corn wet-milling industry. The shelled and air-cleaned corn is soaked ("steeped") counter-currently in water for about 45 h, whereby the structure is softened and partly broken down. The water leaving the process at the point of entry of the corn contains up to 50 wt% solids. It is combined with gluten and fibers and sold as fermentation medium (Ligget and Koffler, 1948)

In scientific studies, defined media (and often defined *minimal* media) are generally preferred since the quantity of specific components in the medium is known, and this makes it easier to apply mass balances for individual atoms (C or N) and to interpret the results.

2.3.1 Amino Acids

The production of amino acids is one of the oldest industrial bioprocesses. The production scale of these low value added products is huge, and the processes have been optimized both from an engineering standpoint (low energy input, efficient downstream recovery, and purification processes), and from a biological standpoint (detailed analysis of the metabolic pathways, followed by strain modifications, whereby the carbon flux has been directed toward the desired product).

The amino acids of Table 2.6 are traditionally classified into two groups, *essential* and *nonessential*. Mammals, including humans, are unable to synthesize certain amino acids which must therefore be supplied in the diet. These are the *essential* amino acids. In contrast, *nonessential* amino acids are synthesized, also in mammals, either directly from one of the common precursor metabolites of Table 2.2, 3-phosphoglycerate, pyruvate, 2-oxoglutarate and oxaloacetate, or indirectly, e.g., tyrosine can also be synthesized by hydroxylation of phenylalanine.

One may argue that arginine is a nonessential amino acid since it is actually synthesized in human cells, but in too small quantity to satisfy the needs of growing children. Similarly, histidine must be supplemented in diets for children, but is not

Table 2.6 The 20 physiologically important (L-) amino acids and their net-chemical formula (based on the undissociated acids)

Essential	Nonessential
Arginine ($C_6H_{14}N_4O_2$)	Alanine ($C_3H_7NO_2$)
Histidine ($C_6H_9N_3O_2$)	Aspargine ($C_4H_8N_2O_3$)
Isoleucine ($C_6H_{13}NO_2$)	Aspartate ($C_4H_7NO_4$)
Leucine ($C_6H_{13}NO_2$)	Cysteine ($C_3H_7NO_2S$)
Lysine ($C_6H_{14}N_2O_2$)	Glutamate ($C_5H_9NO_4$)
Methionine ($C_5H_{11}NO_2S$)	Glutamine ($C_5H_{10}N_2O_3$)
Phenylalanine ($C_9H_{11}NO_2$)	Glycine ($C_2H_5NO_2$)
Threonine ($C_4H_9NO_3$)	Proline ($C_5H_9NO_2$)
Tryptophan ($C_{11}H_{12}N_2O_2$)	Serine ($C_3H_7NO_3$)
Valine ($C_5H_{11}NO_2$)	Tyrosine ($C_9H_{11}NO_3$)

They all contain the elements C, H, N, and O. Cysteine and methionine also contain S. Phenylalanine and tyrosine contain a benzene ring, tryptophan an indol ring, and histidine an imidazol ring. All four aromatic amino acids have the amino acid, serine (2-amino-3-hydroxy propionic acid), in the 1′ position on the ring. The other 16 amino acids are derived from aliphatic carboxylic acids. In the text the name of the amino acid is given without the (L-)

needed for adults. Milk proteins contain all the essential amino acids in an ideal mixture for human diets.

Bacteria have an amino acid profile almost identical to that of salmon, chicken, pigs, and cattle. This is the reason why SCP, actually dried and heat-treated bacterial cells, is able to supply all the essential amino acids to the feed of these animals when the main protein source of the feed is suboptimal in its amino acid profile. SCP is a fine substitute for fish meal, a product that becomes difficult to obtain due to overfishing of the seas. It is also almost free of phosphorous (less environmental burden in aquacultures). Due to its industrial production from simple substrates its availability does not depend on the seasons, and it never contains toxins. SCP production is treated in Chap. 3, Chap. 5, and in problems to Chap. 9.

Glutamic acid and monosodium glutamate (MSG), $COOH–(CH_2)_2–HC(NH_2)–COONa$, is one of the largest volume chemicals produced by fermentation, with an annual production of 1.5 M ton. Glutamic acid is used in many sauces and in cheese, while MSG is used as a general flavor enhancer in the food industry. Glutamic acid is at a main junction in the cell synthesis of amino acids and in the degradation of proteins. The direct, and usually dominant path to glutamate is by reductive amination of 2-oxoglutarate, a TCA cycle metabolite produced from the precursor pyruvate. $NADP^+$ is generally used as the cofactor of reaction (4) in Fig. 2.7, but a variant of the enzyme, isocitrate dehydrogenase, accepts NAD^+ as cofactor (see footnote to Fig. 2.7). This direct path from 2-oxoglutarate to glutamate is called the *GDH-path* after the name of the enzyme, glutamate dehydrogenase (GDH).

The nitrogen required is often present in the medium as NH_4^+, and is taken up by the cell as NH_3. One ATP is used to transport the proton back to the medium. *GDH* has a low affinity for NH_3. This means that the saturation constant K_m for uptake of NH_3 by the enzyme is high (see Chap. 6), and the enzyme is therefore only effective at high intercellular concentration of NH_3.

A second synthesis route to glutamate is via glutamine, (NH_2)–CO–$(CH_2)_2$–HC (NH_2)–COOH, an amide of glutamic acid. Glutamine is formed from glutamate and NH_3 using the enzyme *glutamine synthetase* (GS), which has a much lower K_m for NH_3 uptake than GDH and therefore works also at low $[NH_3]$ in the cell, i.e., at nitrogen limitation in the medium. It does, however, require an extra ATP, and consequently the energy source, glucose, must be available in sufficient amounts.

The second step is the reaction between glutamine and 2-oxoglutarate using the enzyme *glutamine oxoglutarate aminotransferase* (GOGAT) to give two molecules of glutamate. The net effect of the *GS–GOGAT* pathway (2.22), (2.23) is that one glutamate has been synthesized from 2-oxoglutarate at low concentration of NH_4^+ in the medium, but at the expense of an ATP besides that needed to transport NH_4^+ over the cell membrane to form NH_3 inside the cell and transport H^+ back.

$$2-\text{oxoglutarate} + NH_3 + \text{NAD(P)H} \rightarrow (\text{glutamate}),\ \textit{GDH path} \tag{2.22}$$

$$\text{glutamate} + NH_3 + \text{ATP} \rightarrow \text{glutamine}, \textit{GS path} \tag{2.23}$$

$$\text{glutamine} + 2-\text{oxoglutarate} + \text{NADPH} \rightarrow 2\ \text{glutamate}, \textit{GOGAT path}.$$

Other amino acids can be synthesized from the corresponding oxo-acids (e.g., alanine, CH_3–$HC(NH_2)$–COOH) by amination of pyruvate), but only at high-medium concentrations of NH_4^+ due to high values of the dissociation constant K_m.[9]

A much better method is to use *transamination* of the oxo-acid with glutamate or glutamine as the NH_3 donor since the K_m value for the transamination reaction is much smaller than that for the direct amination. In this way, a large pool of glutamate or glutamine in the cell is used to feed the synthesis of other amino acids.

One example from the many amino acid synthesis paths where transamination via glutamate or glutamine is a key step is that of *Aspartate* from glutamate and the precursor molecule oxaloacetic acid. The enzyme is *aspartate(amino)transferase*:

$$\text{Oxaloacetate(OOA)} + \text{Glutamate} \rightarrow \text{Asparate}(\text{COOH} - \text{CH}_2 - \text{HC}(\text{NH}_2) - \text{COOH}) + 2-\text{oxoglutarate} \tag{2.24}$$

From aspartate and following a long path in which one pyruvate is incorporated, one finally arrives at *Lysine*:

$$\text{Aspartate} + \text{pyruvate} + 3\text{NADPH} + NH_3 \rightarrow \text{Lysine}(\text{COOH} - \text{HC}(\text{NH}_2) - (\text{CH}_2)_3 - \text{CH}_2 - \text{NH}_2) + CO_2 \tag{2.25}$$

[9] In a very interesting process Hols et al. (1999) have used genetic engineering to convert a homo (lactic)fermenting *Lactococcus lactis* to become a homo(alanine) fermenting organism. Since alanine has a much higher sales price than lactic acid this is a splendid idea. The paper does, however, show that very high NH_3 concentrations are needed.

Actually, along the path from aspartate to lysine one encounters a branch point at the metabolite piperidine-2,6 dicarboxylate. From this branch point there are two branches that meet again at the final intermediate, meso-2,6 diaminopimelate, before lysine. One branch, the one summarized in (2.25), is a direct shunt from one branch point to the other. The second branch (the Succinyl CoA branch) has many steps, involves transamination by means of a second glutamate molecule, and interacts with the TCA cycle reaction between succinyl CoA and succinic acid. The direct path gives the highest yield of lysine on glucose, but it works best at high NH_3 level, where the facilitation of uptake of the second NH_3 by means of the glutamate/2-oxoglutarate cycle is not needed.

The synthesis of the enormously important amino acid lysine with an annual production of 1.1 M ton has of course given rise to an equally impressive scientific literature. A comprehensive reference is Wittmann and Becker (2007). Recently, Kjeldsen and Nielsen (2009) published a *genome scale* reconstruction of the *Corynebacterium glutamicum* metabolic network. In the increasing body of genome scale pathway reconstructions all supposedly relevant pathway reactions are included, but without specifying the finer (and usually unknown) details.

2.3.2 Antibiotics

The biosynthesis of amino acids is used as an example of the numerous chemicals that can be produced from the primary metabolism of microorganisms, either directly or after chemical transformation outside the cell. Many more examples will be discussed in the text or in problems.

Antibiotics are examples of *secondary metabolites*. As was mentioned in the introduction to Sect. 2.3, secondary metabolites do not have a direct function in the normal growth of the cell culture, but the production of any of the antibiotic chemicals is the cellular response to *stress signals*. Organisms competing with, e.g., a penicillin producing microorganism for a limited resource will have their capability to proliferate disrupted by penicillin secreted from the cell of the penicillin producer. Penicillin acts as an inhibitor of formation of peptidoglycan cross links in the cell walls of the competing organism.

Obviously penicillin and other antibiotics with this defense mechanism cannot have any effect on viral infections, since viruses have no cell wall. Likewise they are of little use in combating most fungal infections – e.g., penicillin cannot be used to treat either influenza or ring worm. Its predominant role in human and veterinary medicine is for treatment of bacterial infections.

Although penicillin and other antibiotics have no direct effect on the cells of animals, including humans, all antibiotics can provoke sometimes violent allergic reactions.

Continued use of the first antibiotics on the market has also spawned defensive mechanisms in many bacteria. Penicillin resistance was observed already in the 1950s and has led to the development of a continuous stream of new antibiotics.

Table 2.7 Four classes of antibiotics

Category	Examples	Application	Producer
β-Lactams	Penicillins, cephalosporins	Bacterial infections	Filamentous fungi
Polyketides	Erythromycin, tetracyclines	β-Lactam resistant infections	Actinomycetes (soil bacteria)
Glycopeptides	Teicoplanin	Last resort treatment bacterial infection	Actinomycetes
Antracyclines	Daunorubicin	Chemotherapy	Actinomycetes

The classification of natural products into categories and with respect to applications is difficult, but the listing in the table is at least indicative

Table 2.7 gives a rough classification of antibiotics currently on the market, and Fig. 2.9 shows how two of the early penicillin products, penicillin G and V, are synthesized.

The first step in the biosynthesis of β-lactams is the condensation of L-α amino adipic acid, L-cysteine, and L-valine to form the tripeptide α-aminoadipyl-cysteinyl-valenine, ACV. It is interesting that valine is incorporated as D-valine. The enzyme *ACV Synthase* (ACVS) has several functions: It forms the two peptide bonds and it epimirizes L-valine to the D-valine bound in ACV.

The next step is an oxidative ring closure of LLD-ACV to form isopenicillin N (IPN) which has the characteristic structure of β-lactams. The β-lactam ring is the square with three carbons and one nitrogen in the center of the molecule.

The enzyme *isopenicillin N synthetase* (IPNS) uses free oxygen as electron acceptor. IPN is not in itself a potent antibiotic compound, but based on IPN all the commercial penicillins and cephalosporins can be produced. The side chain (aminoadipic acid) can be cleaved off by the enzymatic action of an *acetylase* to form the "nucleus," 6-APA, which in itself has no antibacterial effect, but is an important commercial product used for the synthesis of other, more active β-lactams than (LLD)-IPN. In the presence of an *acyltransferase* (AT), the commercial products penicillin G and V are formed when benzyl-CoA or phenoxybenzyl-CoA (i.e., the organic acids activated by coupling to CoA) is added. Methicillin and oxacillin are examples of penicillins with other side chain organic acids.

All penicillins are susceptible to the action of β-lactamases secreted by bacteria as a defense mechanism, and over the last 60 years the pharmaceutical industry has struggled to invent new antibiotics that can effectively combat penicillin resistant bacteria. The defense mechanisms of the bacteria have become ever more ingenious as a result of the wholesale application of β-lactams in human and veterinary medicine. The deactivation of penicillin by cleaving off the side chain is supplemented by the gradual appearance of bacterial enzymes that disrupt the β-lactam ring, and the battle to stay ahead of the bacterial defense mechanisms has led to new lines of antibiotics.

The *cephalosporins* are synthesized by filamentous fungi related to *Penicillium crysogenum*, but also in different bacteria. In the last step of the biosynthesis the five member thiazolidine ring next to the β-lactam ring is expanded (using an *expandase* enzyme) to a six member dihydrothiazine ring (Fig. 2.10).

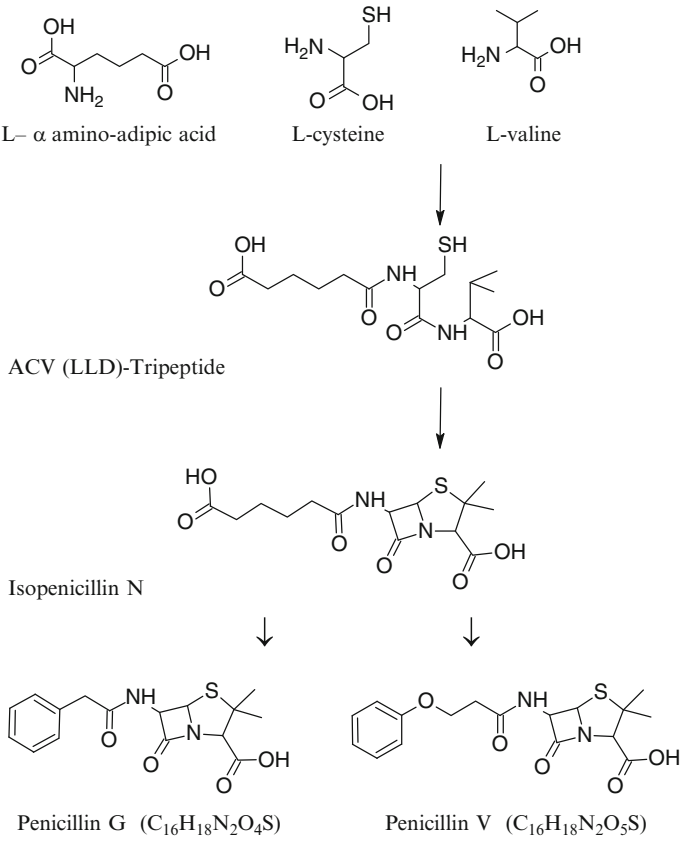

Fig. 2.9 The biosynthetic pathway in *Penicillium crysogenum* from the three amino acid precursors to penicillin. The enzymes involved are ACV synthase, isopenicillin N synthase, and isopenicillin *N* acyltransferase. In the last step adipic acid is exchanged with phenylacetic acid or phenoxy acetic acid to produce, respectively, penicillin G and V

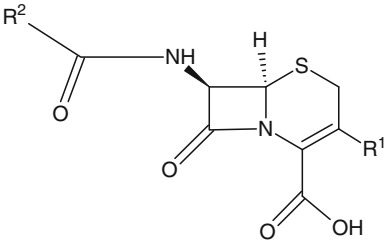

Fig. 2.10 The structure of cephalosporins. In new generations of cephalosporins R^1 and R^2 are very complicated side groups

The cephalosporins are also not immune to the action of β-lactamases, but their broad applicability to fight both Gram-positive and Gram-negative bacteria has won them a strong position in the antibiotics market through the development of several new "generations" of antibiotics with the general structure shown in Fig. 2.10.

The urge to develop new antibiotics that are immune to the very effective defense systems of many microorganisms (e.g., *Staphylococcus aureus*, the infamous organism that causes sometimes life-threatening infections in hospitals – about 500,000 cases each year in US hospitals) has spawned new categories of antibiotics which have a completely different structure from that of β-lactams.

A particularly numerous and varied category is the *microlides* and the *tetracyclines* which belong to the huge group of natural products called *polyketides*. All polyketides are synthesized by very complex *polyketide synthase* enzymes. In a series of chain elongation steps from CoA, activated carboxylic acids are formed, and then condensed to extremely complicated organic compounds. The synthesis mechanism has only been discovered during the last 20 years (Gokhale et al. 1999; Arora et al. 2005), and new polyketides, some with no known origin in nature, are now being synthesized by highly automated biosynthetic processes.

The polyketides have a very broad spectrum of activities: antimicrobial, antifungal, antiparasitic, and antitumor. Still, ever more complex drugs must be invented to combat the inevitable emergence of resistance. Combination of several antibiotics, e.g., glycopeptides in combination with β-lactams, is one way to fight multiresistant organisms (e.g., the use of clavulanic acid, a β-lactamase *inhibitor*, to support the action of β-lactams).

One unfortunate complication is that the new and very effective antibiotics become increasingly toxic to the patients, and they must be administered with great caution. The antracyclines are typical last-resort drugs used to combat life-threatening illnesses such as breast cancer.

The story of antibiotics, from the first observation by Alexander Fleming in 1928 of the antibacterial effect of a *Penicillium* fungus to the multibillion dollar antibiotics industry 80 years later is, indeed, fascinating. Historical accounts of the victory of antibiotics over illnesses and infections that were previously life threatening, followed by the sad aftermath of misuse of antibiotics, must be among the most educating in the whole history of science.

There is no doubt that antibiotics production is synonymous with the story of the development of modern Biochemical Engineering. Fermentation equipment has grown to huge tanks of sizes up to several hundred cubic meters, and many standard down-stream operation processes were developed to capture antibiotics from very dilute solutions and to purify the products to satisfy stringent regulatory requirements.

Antibiotics production has also been a huge money maker for the pharmaceutical industry during the last 60 years. Cephalosporins have gradually replaced penicillins, but as the production of both standard drugs has moved to China and India, prices have declined, and nonbrand antibiotics have put considerable pressure on the original producers. Furthermore, the use of antibiotics in veterinary medicine has been restricted, and the prophylactic use of antibiotics for humans is sternly discouraged.

Still, the value of antibiotics production in 2008 was in the range of 25,000 M US $, just about the level in 1995 (Nielsen 1997). The price of standard penicillins is now as low as 5–8 US $/kg which classifies these pharmaceuticals as commodity chemicals.

2.3.3 Secreted Proteins

Although the production of pharmaceutical proteins by mammalian cells is considered to be outside of what we have defined to be the scope of the present text, many industrial enzymes and some pharmaceutical proteins are produced by standard fermentation technology, using a small selection of microorganisms as producers. These large-scale industrial processes are studied and designed, using the same set of quantitative tools as are applied in the production of simple metabolites with *Lactococcus lactis, E. coli, B. subtilis, S. cerevisiae*, and *A. niger* or *oryzae* as production organisms. Also, it is relevant to introduce the foremost business area of some of the most important biotech companies, Novozymes, Genencor, Genentec, Amgen, Novo Nordisk, Sanofi-Aventis, Merck, Roche, and Eli Lilly.

The most common industrial enzymes are hydrolytic enzymes that degrade macromolecules to monomers that may serve as carbon, energy, and nitrogen sources. They are secreted by a wide variety of microorganisms. Among the most frequently secreted enzymes are *proteases* (for degradation of proteins) and *peptidases* (for degradation of peptides). The biggest production volume is obtained in *amylases* (degradation of starch), *xylanases* (degradation of xylans), and *cellulases* (degradation of cellulose), the three types of enzymes discussed in Sect. 2.1 for the production of ethanol from biomass.

Through the secretion of enzymes some microorganisms are able to grow on very complex nutrients, and the ability of microorganisms to decompose leaves and other plant materials plays an important role in the overall carbon cycle. The ability of microorganisms to secrete enzymes has been exploited for many centuries, particularly in the food and feed industry. Thus, *Aspergillus oryzae*, an efficient producer of the starch degrading enzymes α-*amylase* and *glucoamylase*, has been used for more than thousand years in the Far East for koji-sauce production. Furthermore, the secretion of proteases and peptidases by lactic acid bacteria plays an important role in many dairy processes. Primarily, hydrolysis of proteins and peptides ensures a supply of carbon and energy sources as well as amino acids. Secondly, the hydrolysis of many proteins and peptides is important for proper flavor development. Since the 1950s enzymes have also been used in detergents to improve the washing process, and with the help of enzymes many industrial processes, e.g., the treatment of cotton, have become truly "green" processes, with little impact on the environment and large savings in process energy compared to conventional processes. An overview of the application of industrial enzymes is found at http://www.novozymes.com. The majority of the industrial enzymes are produced, using a small selection of well-studied host cells into which foreign genes are encoded.

The possibility to introduce foreign genes into a microbial host by genetic engineering, and hereby to produce a specific protein in high amounts, also paved the way for a completely new route to pharmaceutical proteins. The first biopharmaceutical proteins (human insulin and human growth hormone) were produced in recombinant *E. coli*, but soon followed the exploitation of other expression systems such as *S. cerevisiae* (used by Novo Nordisk for production of about 50% of the global

market for human insulin), insect cells, and mammalian cells (Chinese hamster ovary cells and hybridoma cells). Today approximately 100 protein drugs, largely recombinant proteins and monoclonal antibodies that are often referred to as biotech drugs or biologics, produce revenues of hundreds of million US $. The biochemical processes underlying the synthesis of a successful *heterologous protein* in a given host cell are quite complex. There are many post-translational modifications, and the secretory pathway may involve many individual steps. Production of a given protein drug is specific for the host system and as mentioned at the start of this section even a brief overview of the subject is far beyond the scope of the present text.

2.4 Design of Biotech Processes: Criteria for Commercial Success

When a microorganism or cell type has been identified to produce an interesting compound there are a number of considerations to be made before an economically viable, industrial process can be realized. In companies with a solid experience in the design and scale-up of fermentation processes, new processes are introduced relatively fast, especially if the product is not a pharmaceutical. Thus, in recent years Novozymes has successfully introduced three to four completely new processes each year, starting in the laboratory, and carrying the R&D work all the way through to industrial scale production.

Development of a fermentation process can roughly be divided into four phases. First the product is identified, and its potential sales value over a prescribed lifetime is closely evaluated. In the case of a pharmaceutical, identification of a potential product may be a result of the random screening for different therapeutic effects by microbial metabolites, e.g., by high throughput screening of secondary metabolites from *Actinomycetes*, or it may be the result of a targeted identification of a novel product, e.g., a peptide hormone with known function. Outside the pharmaceutical sector the product may also be chosen after a random screening procedure, e.g., screening for a novel enzyme to be used in detergents, or it may be chosen in a more rational fashion. With the rapid progress in genomic sequencing programs, it is now possible to search for new target proteins directly in the sequenced genomes by skillful use of *bioinformatics*.

When the product has been identified, the next step is to choose or construct the specific strain to be used for production, and thereafter follows design of the process. This involves choosing an appropriate fermentation medium and the optimal process conditions. In parallel with the design of the production process further research, e.g., clinical tests, is done in order to have the product approved. When the strain has been constructed one of the first aims is therefore to produce sufficient cell material for further research, and this is typically done in pilot plant facilities. For a pharmaceutical compound sufficient material must be produced for clinical trials. For other products it may be necessary to carry out tests of the product and examine any possible toxic effects. The final steps are concerned with

product approval by the proper authorities. Then, perhaps 5 years after starting the process, follows construction of the production facility, sometimes by retrofitting of an existing plant to save on capital costs.

In the next sections, we consider some of the different aspects of process development as an introduction to the more detailed quantitative analysis that will be treated in the remainder of the book.

2.4.1 Strain Design and Selection

A key step in the development of a fermentation process is to choose an appropriate strain. In the past, this choice was normally obvious after the product had been identified, e.g., *Penicillin chrysogenum* was chosen for penicillin production since this was the organism that was first identified to produce penicillin. With the introduction of recombinant DNA technology it is, however, now possible to choose almost any host organism for the industrial production. Thus, strains of *E. coli* have been constructed that can produce ethanol at a high yield, and a recombinant strain of *Penicillin chrysogenum* can now be used directly to produce 7-ADCA (a precursor used for synthesis of cephalosporins) by fermentation. The choice of strain depends a lot on tradition within the company (e.g., Novozymes favors *B. subtilis* over *E. coli*), and most companies use a small set of favorite organisms to produce many different products. For production of a heterologous protein by expression of a foreign gene in a given organism, it is also necessary to consider many other aspects, e.g., whether the protein will be correctly folded and glycosylated.

Table 2.8 gives an overview of the advantages/disadvantages of different cellular systems for the production of recombinant proteins. Although optimization of the process continues even after large-scale production has started, it is important to choose a good host system from the beginning, particularly in the production of pharmaceuticals. The introduction of new strains requires a new approval of the process, and the associated costs may prevent the realization of a new process even though engineering wisdom tells that the over all process economy could be much improved.

As indicated in Table 2.8 the choice of expression system depends on many factors, but the main factors are (1) the desirability of post-translational modification and secretion, (2) the stability of the protein in question, and (3) the projected dose of protein per patient (which determines whether the cost of the drug becomes critical). Thus, for proteins used in large doses, such as human insulin, it is important that the production costs are kept low, which requires an expression system with a high productivity, i.e., *E. coli* or *S. cerevisiae*. For very complex molecules such as tissue plasminogen activator (tPA) and erythropoietin (EPO) it is, however, not possible to obtain sufficiently active compounds in microbial systems, and here a higher (mammalian) eukaryotic expression system is required.

Table 2.8 Pros and cons of different production organisms for recombinant proteins

Host	Advantages	Disadvantages
Bacteria (*E. coli*)	Wide choice of cloning vectors Gene expression easy to control Large yields possible Good protein secretion	Post-translational modifications lacking High endotoxin content Protein aggregation (inclusion bodies)
Yeast (*Saccharomyces cerevisiae*)	Generally regarded as safe (GRAS) No pathogens for humans Large scale production established Some post-translational modifications are possible	Less cloning vectors available Glycosylation not identical to mammalian glycosylation Genetic base is still less solid than is the case for *E. coli*
Filamentous fungi	Experience with large scale production Source of many industrial enzymes Excellent protein secretion	High level of heterologous protein expression is as yet not achieved Genetics only recently characterized
Mammalian cells	Same biological activity as natural protein Expression vectors available	Cells difficult to grow in reactors Expensive Slow growth and low productivity
Cultured insect cells	High level of gene expression possible Post-translational modification possible	Not always 100% active proteins Mechanisms largely unknown

2.4.2 *Criteria for Design and Optimization of a Fermentation Process*

The criteria used for design and optimization of a fermentation process vary with the product to be synthesized. Thus, the criteria used for a high volume/low value added product are normally completely different from the criteria used for a low volume/high value added product. For products belonging to the first category (which includes most whole cell products, all primary metabolites, many secondary metabolites, most industrial enzymes, and most polysaccharides) the three most important design parameters are:

- Yield of desired product on substrate (typical unit: g product per g substrate)
- Productivity (typical unit: g product per L reactor volume per hour)
- Final titer (typical unit: g product per L reactor volume)

Yield of product on the substrate is very important for high volume/low cost products since the raw materials often account for a significant part of the total costs. Thus in penicillin production, the costs of glucose alone may account for up to 15% of the total production costs. In Table 2.5 it was argued that the right choice

of fermentation medium could have a large influence not only on product yield and production cost, but also on product quality.

Productivity is important since this ensures an efficient utilization of the production capacity, i.e., the bioreactors. It is of no avail that certain bacteria are able to give a high yield of ethanol on sugar when the production rate of ethanol is very low. Especially in an expanding market, it is important to step up the productivity as has been demonstrated by Novozymes where a huge increase in production has been achieved and many new processes have been developed since 2000 with very little new capital investment.

Final titer is of importance for the further treatment of the fermentation medium, e.g., purification of the product. Thus, if the product is present at a very low concentration at the end of the fermentation it may be very expensive even to extract it from the medium with a satisfactory yield. Again the production of ethanol is a good example. Well designed strains of *S. cerevisiae* are now able to work efficiently at an ethanol concentration that surpasses 10 wt%, a limit that is far from being reached in bacterial fermentations where 4–5 wt% ethanol often stops the fermentation.

Sometimes it is important to consider both an aerobic process and an anaerobic process. The aerobic process may have higher productivity, but it requires more process energy.

In Chap. 3, we shall start the quantitative treatment of reaction rates and yield coefficients, the key design parameters for product yield on substrate and productivity of the process. Qualitatively, these concepts are illustrated in Fig. 2.3 which is a representation of the overall conversion of substrates into metabolic products and biomass components (or total biomass). In Sect. 3.1, the rate of consumption of any substrate is seen to be determined by measurement of the concentration of the substrate in the medium. Similarly, the rates of formation of metabolic products and biomass are determined from measurements of the corresponding concentrations. It is therefore possible to determine the rate of all flows in and out of the total pool of cells. The inflow of a substrate is normally referred to as the substrate uptake rate and the outflow of a metabolic product is normally referred to as the product formation rate. Clearly, the product formation rate is a direct measure of the productivity of the culture. Furthermore, the yield coefficient of any product is defined as the ratio of product formation rate and the substrate uptake rate. The yield coefficient quantifies the efficiency in the overall conversion of the substrate to the product of interest.

In the production of novel pharmaceuticals, which typically belong to the category of low volume/high value added products the abovementioned design parameters are normally not that important. For these processes time-to-market and product quality is generally much more important, and change of the process after implementation is often complicated due to a requirement of FDA approval. In the initial design phase it is, however, still prudent to remember the three design criteria: *Yield, Productivity*, and *Final Titer*. Especially the requirement for high final titer is important since the cost of purification (or "downstream processing") may account for more than 90% of the total production costs.

2.4.3 Strain Improvement

A key issue in process optimization is to improve the properties of the applied strain since the overall conversion of substrates to the product of interest is primarily determined by the properties of the microorganism. The cell may be conceived as a small chemical factory, and through engineering of the pathways it may be possible to redirect the carbon fluxes such that the yield and sometimes also the productivity increases. Engineering of the cellular pathways is done by making changes in the genome of the organism. This may lead to different expressions of the enzymes that catalyze the individual biochemical reactions or processes.

Traditionally, strain improvement through introduction of mutations was done through random mutagenesis and selection of strains with improved properties. This is well illustrated by the industrial penicillin production, where introduction of new strains has resulted in an increase of productivity by a factor of more than 100 between 1962 and 2000. The improvements are the results of large strain development programs, some carried out by the major penicillin producing companies and some by companies dedicated to develop new and better strains for the industry in general. Similar success stories are recorded for improvements in the properties of bakers' yeast, *S. cerevisiae*, and in other microorganisms applied for the production of industrial enzymes or metabolites.

The development of better producing organisms is, unfortunately, accompanied by a decrease in strain stability of the industrial strains. They will all mutate spontaneously to strains with a much reduced productivity, and this, as we shall see in Chap. 9 prevents the use of continuous cultivation in most of the important industrial fermentation processes. A typical example of strain reversion is studied by Christensen et al. (1995). An industrial strain of *P. crysogenum* was subjected to continuous culture for 500 h. For the first 150 h the penicillin V concentration in the exit from the reactor was constant, but over the next 200 h it decreased to a level of only 35% of the initial concentration. Clearly, the high producing strain had reverted to a much poorer strain. The reversion was also visually observed by a gradual change in the color of the spores from green to white. A similar case is studied for the teicoplanin producer *Actinoplanes teichomyceticus* (see Problem 9.7).

Today the genome of many of the favorite industrial "work-horses" has been sequenced, and in combination with the rapid development of recombinant DNA technology it has become possible to apply a rational, directed approach to strain improvement. This is often referred to as *metabolic engineering*, but terms such as molecular breeding or cellular engineering are also used. Several different definitions have been given for metabolic engineering, but they all convey the message that is captured in the definition: *The directed improvement of product formation or cellular properties through modifications of specific biochemical pathways or by introduction of new pathways using recombinant DNA technology*.

Among the applications of metabolic engineering are:

- *Heterologous protein production*. Examples are found in the production of pharmaceutical proteins (hormones, antibodies, vaccines, etc.) and in the

production of novel enzymes. As a first step, the heterologous gene needs to be inserted in the production host. Subsequently, the protein synthesis pathway must often be engineered, e.g., to have an efficient glycosylation or secretion of the protein. In some cases, it may also be necessary to engineer the strain to obtain an improved productivity.

- *Extension of substrate range*. In many industrial processes, it is interesting to extend the substrate range for the applied microorganism in order to use cheaper or more efficient substrates. Initially, the pathway (or enzyme) for uptake and metabolism of the desired substrate is inserted. Subsequently, it is important to ensure that the substrate is metabolized at a reasonable rate, and that the metabolism of the new substrate does not result in the formation of undesirable byproducts. This may in some cases involve extensive pathway engineering.
- *Pathways leading to new products*. It is desirable to use a given, well-studied host for production of many different products. This can be achieved by extending existing pathways from other organisms. An example is the import into *E. coli* of the yeast pathway from DHAP to glycerol, and of the pathway from glycerol to propane 1,3-diol from *Klebsiella pneumonica*. These are key features of the DuPont-Genencor process to produce the diol. Another approach is to generate completely new pathways through gene shuffling or by other methods of directed evolution. In both cases, it is often necessary to further engineer the organism to improve the rate of production and eliminate byproduct formation.
- *Pathways for degradation of xenobiotics*. Many organisms naturally degrade xenobiotics (i.e., compounds that are foreign to the body and to cells), but each organism is usually specific for a given substrate. Thus a consortium of bacteria, collected from an oil field or from a spot where seepage of bitumen from the ground is observed, is likely to be useful for cleaning up oil spills. In bioremediation it is attractive to work with only a few organisms, each of which is able to degrade a wide variety of compounds. This may be achieved either by inserting pathways from other organisms or through engineering of the existing pathways.
- *Engineering of cellular physiology for process improvement*. In the industrial exploitation of microorganisms or higher organisms one may engineer the cellular physiology for process improvement, e.g., make the cells tolerant to low oxygen concentration, less sensitive to high glucose concentrations, improve their morphology, or increase their ability to flocculate. In cases where the underlying mechanisms are known this can be achieved by metabolic engineering. This may involve expression of heterologous genes, disruption of genes, or over-expression of homologous genes.
- *Elimination or reduction of by-product formation*. In many industrial processes byproducts are formed. This constitutes a problem, not only because carbon is lost to formation of the byproducts, but also because the byproducts may be toxic to the organism, or necessitate a major effort to separate the byproduct from the desired product because it is toxic (e.g., oxalic acid from citric acid) or interferes with filtration and other downstream processes. Thus, polysaccharides severely interfere with membrane separation processes. In some cases the byproducts can be eliminated through simple gene disruption, but in other cases the formation of the

byproduct is essential for the overall cellular function, and disruption of the pathway leading to the byproduct may be lethal for the cell, e.g., when the pathway from DHAP to glycerol is knocked out in an attempt to improve the ethanol yield in anaerobic cultivation of yeast. It is often necessary to analyze a large part of the metabolic network in order to devise a safe strategy for reduction of the byproduct formation.

- *Improvement of yield or productivity*. In many industrial processes, especially in the production of low-value added products, it is important to continuously improve the yield and/or productivity. In simple cases this can be achieved by inserting additional gene copies of what is believed to be a key enzyme in the pathway. In other cases the pathways leading to the product of interest have many enzymatic steps which influence each other by feed back and feed forward control mechanisms (see Chap. 6), and a given pathway may even interact with other pathways through the global regulatory system of the organism. Now the single-enzyme manipulation is doomed to failure, and a much more involved analysis of the metabolism is needed to find prospective improvements of the process. Finally, in some cases the limitation is not in the actual pathway, and it may therefore be necessary to engineer the whole central carbon metabolism. This is, however, very difficult to do. For example, it is very difficult to achieve a higher carbon flux through the EMP pathway, due to the tight regulatory structure of the pathway.

Besides application of these tools from the biosciences, the design and proper operation of an industrial plant for low-value added products require a deep technical insight into many of the disciplines that together make up the science of chemical engineering: stoichiometric analysis, modeling of reaction kinetics, transport phenomena, bioreactor design, and unit operations. In this textbook we will, as announced in Chap. 1, highlight the chemical engineering disciplines that are associated with bioreactions and give a quantitative description of a given phenotype of a cell. It will be shown how the organism operates in, and interacts with the technical equipment. A comprehensive treatment of metabolic engineering is given in Stephanopoulos et al. (1998) while the engineering tools of the bioindustry are discussed in quite a few available texts.

2.5 The Prospects of the Biorefinery

In Sect. 2.1.2, the review by Werpy and Petersen (2004) was used to illustrate the enthusiasm that embraces any discussion of the prospects of the biorefinery to substitute chemical routes from oil and gas to commodity chemicals with “green” or “sustainable” routes based on the action of microorganisms or the enzymes produced by these.

Sects. 2.2–2.4 have shown how microorganisms can serve as chemical factories that basically convert solar energy harbored in the raw materials, sugar or starch,

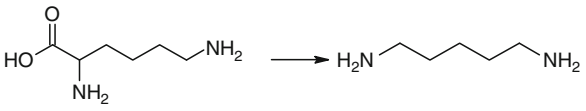

Fig. 2.11 A diamino pentane is the result of lysine production after one gene change

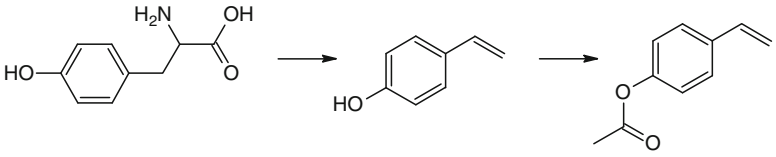

Fig. 2.12 Tyrosine is chemically converted to *p*-hydroxystyrene or *p*-acetoxystyrene

into a multitude of products, both commodity chemicals such as the metabolites of the TCA cycle and amino acids, and the much higher valued pharmaceuticals.

The "natural" products of metabolism are not the only products that can be produced by microorganisms. In Sect. 2.4, it was shown how genetic engineering of "a favorite organism" can make it produce a desired compound, and even synthesize compounds (e.g., certain polyketides) that are not found (or not yet discovered) in nature. These "strange" compounds may have an enormous value in the treatment of human diseases.

Much simpler "tricks" than those used in polyketide chemistry are, however, available and are frequently revealed in the patent literature. Most of these tricks are based on single gene-modifications of standard microorganisms.

Thus, as has been discussed in Sect. 2.3.1 lysine is a huge commodity chemical produced by fermentation. The polymer industry might be more interested in the amines that can be produced by decarboxylation of lysine (Fig. 2.11).

The reason is that the diamine (Cadaverine) can form macromolecules by amide formation with a large number of dicarboxylic acids.

C. glutamicum, the best producer of lysine (partly because it prevents decarboxylation of the product) is modified by inserting the gene for L-lysine decarboxylase from *E. coli*. Now *C. glutamicum* produces L-lysine as before, but as an extra step the acid is decarboxylated and cadaverine is exported to the medium Mimitsouka et al. (2007) and Tateno et al. (2009). Naturally the process is patented (by BASF).

Tyrosine is produced as an intermediate in the neuro-pharma industry. But the biosynthesis toward tyrosine passes through a number of intermediates that could be withdrawn for production of other valuable chemicals.

The DuPont Company has demonstrated that tyrosine can be chemically converted in a two-step process to very valuable monomers for production of adhesives (Fig. 2.12).

The process, described in US patent application 0213569 (2007), comprises the treatment of tyrosine with an aqueous solution of HBr and $NaNO_2$ followed by conversion, using an alkaline catalyst, of the isomeric mixture of brominated tyrosine intermediates to either of the two styrene compounds. The patent is an excellent

illustration of the symbiosis of a fermentation process and organic chemical synthesis which makes a few changes in the metabolite to obtain the desired product. An overview of the possibilities of processes by which fermentation is coupled with classical chemistry is given by Murzin and Leino (2008).

Interestingly, it has recently been shown that *p*-hydroxystyrene can also be produced directly from glucose without ever obtaining the L-tyrosine (Verhoef et al. 2009). A *Pseudomonas putida* strain, originally designed to produce phenol and *p*-coumaric acid from glucose (see Fig. 2.1), was engineered for efficient production of *p*-hydroxystyrene by inserting the genes for the enzymes *L-phenylalanine/L-tyrosine ammonia lyase* and *p-coumaric acid decarboxylase*. Here, we see an example of the combination of metabolic capabilities of two microorganisms to produce a desired product in one synthesis process.

The conclusion from the few examples shown here is that only the imagination of the industrial or academic researcher sets the limit to what can be produced in the biorefinery. Once an interesting organic compound has been identified, the tools of bioinformatics are used to screen for a suitable host organism which from genome-scale models is known to have the capability to produce the compound or can be genetically engineered to do so by gene transfer from other organisms. The steps of Sect. 2.4 are followed to increase the yield and productivity of the selected construct, and suitable cultivation conditions are found through laboratory and pilot plant experiments.

Problems

Problem 2.1. A number of process designs for large-scale production of ethanol are available on the net. IOGEN, DONG-Inbicon, a Danisco-DuPont scheme, supported by U. Tennessee and several others can be found. Make an analysis of the different schemes. What products are made? What is the saccharification process? How well are down-stream processes designed with respect to total energy minimization?

What is the current market price for ethanol in bulk, and how well does it match the production cost of ethanol from lignocellulosic biomass?

References: Lynd et al. (2008), Lin and Tanaka (2006), Sendich et al. (2008), and also material from the biotech companies Novozymes and Genencor.

Problem 2.2. Consult the literature to find profiles for batch cofermentation of glucose and xylose by a "wild-type" yeast strain *S. cerevisiae*, and also by better yeast strains. Observe the *sequential* utilization of the sugars.

1. How has *S. cerevisiae* been engineered in the group of Hahn-Hägerdahl to obtain a more rapid conversion of xylose? Describe the redox reactions used and comment on the difficulties of the process.
2. Compare the process of (1) with that of the Delft group of scientists (Wesselink et al. 2009).

Problem 2.3. Butanol (1-butanol, and perhaps even better iso-butanol) can become an excellent transportation fuel.

On the net you will find many recent proposals for the production of butanol by fermentation (e.g., a huge project by BP and DuPont). Give an account of the advantages of producing butanol rather than ethanol, and also outline some of the disadvantages.

Several papers from 2007/2009 review the biosynthesis of butanol: Lee et al. (2008), Atsumi et al. (2008), Sillers et al. (2008), as well as the history of butanol production by fermentation, Villadsen (2007). Older literature references are given in Chap. 5.

You will notice that the pathway to butanol, acetone, and butyric acid is an extension of the fermentation pathways in Fig. 2.5a, b, starting with dimerization of AcCoA.

1. Write the pathways which lead to the products in the "solvents fermentation process."
2. What are the key issues in the process?
3. How can the formation of butyric acid be (almost) suppressed, and what is the maximum yield of butanol on glucose obtained according to the references?
4. Find the bulk prices of 1-butanol and of technically pure glucose syrup obtained by liquefaction of starch. What is the added value of converting glucose syrup to butanol when the reported yields are used in the calculation?

Problem 2.4. Using the diagrams in a standard text on biochemistry or the much more detailed diagrams on the net you are required to write down the whole pathway from glucose to L-lysine and to L-tyrosine. This will give you an impression of the complexity of the biochemistry, but you will also notice that many parts of the total paths to the two amino acids are similar.

Problem 2.5. In Werpy and Petersen (2004), (Table 2.1), you will find diagrams that show how succinic acid can be used to produce a large number of chemicals.

1. Indicate the chemical processes needed to make these chemicals from succinic acid as a starting material. Could some of the chemicals also have been formed from other building blocks?
2. Look in recent literature for papers from the group of Sang Yup Lee at KAIST for exciting work toward production of succinic acid by fermentation. What are the issues of importance in order to get a high yield on glucose, a high productivity, and a high titer? Is the limited solution of succinic acid in aqueous solutions a problem?

Problem 2.6. In eukaryotes NAD^+ is produced in the mitochondria as a result of respiration. NAD^+ is needed in the cytosol (the EMP pathway). By which process is the NAD^+ transferred from the mitochondria to the cytosol? The answer is found by consultation of standard textbooks on Biochemistry.

Problem 2.7. Since 2008 Cargill and Novozymes have collaborated to develop an entirely bio-based route to acrylic acid (2-propenoic acid), which is the basis for

production of the hugely important acryl-based polymers. Central to their effort is to produce 3-hydroxy propionic acid (see Fig. 2.1b), which by dehydration of the alcohol gives acrylic acid.

Based on two major publications, Straathof et al. (2005) and Henry et al. (2010), you are required to review the research that within less than a decade has led to identification of the best metabolic routes to 3-hydroxy propionic acid, one of the projected platform chemicals in Werpy and Petersen(2004).

A thorough study of this problem will teach you how front-line biotech companies use all the suggestions discussed in Sect. 2.4.3 for strain development, and of pathway engineering in particular.

References

Arora, P., Archana, V., Saxena, P., Mohanty, D., and Golkhale. R.S., (2005). Promiscuous fatty acid CoA ligases produce Acyl-CoA and Acyl-SNAC precursors for polyketide synthesis. *J. Am. Chem. Soc*., **127**, 9388–9389.

Atsumi, S., Cann, A.F., Connor, M.R., Shen, C.R., Smith, K.M., Brynildsen, M.P., Chou, K.J.Y., Hanai, T., and Liao, J.C., (2008). Metabolic engineering of *E. coli* for 1-butanol production. *Metabolic Eng*., **10**, 305–311.

Bech, N. and Dam-Johansen, K., (2006) WO 2006/117005 and 6.

Bech, N., (2008). In situ flash pyrolysis of straw, PhD thesis, Department of Chemical and Biochemical Engineering, DTU.

Bridgewater, A.V. and Peacocke, G.C.V., (2000). Fast pyrolysis processes for biomass, *Renewable, Sustainable Energy Reviews*, **4**, 1–73.

Christensen, L.H., Henriksen, C..M., Nielsen, J,, Villadsen, J., and Egel-Mitani, M., (1995). Continuous cultivation of *Penicillium crysogenum*: Growth on glucose and penicillin production. *J. Biotechnol*., **42**, 95–107.

Clark, J.E., (2007). Green chemistry for the 2nd generation biorefinery-sustainable chemical manufacturing based on biomass. *J.Chem. Technol. Biotechnol.* **82**, 603–609.

Gauss, W.F., Suzuki, S., and Takagi, M., (1976). Manufacture of alcohol from cellulosic materials using plural ferments. US patent 3990944.

Gokhale, R.S., Tsuji, S.Y., Cane, D.E., and Khosla, G., (1999). Dissecting and exploiting intermodular communication in polyketide synthases. *Science*, **284**, 482–485.

Hahn-Hägerdahl, B., Galbe, M., Gorwa-Grauslund, M.F., Lidén, G., Zacchi, G., (2006). Bioethanol – the fuel of tomorrow from the residues of today. *Trends in Biotechnology*, **24**, 549–556.

Hahn-Hägerdahl, B, Karhumaa, K., Fonseca, C., Spencer-Martins, I. and Gorwa-Grauslund, M.F., (2007). Towards industrial pentose fermenting yeasts. *Appl. Microbiol. Biotechnol*., **74**, 937–953.

Haveren, J van, Scott, E.L., and Sanders, (2008). Bulk chemicals from biomass. *Biofuels, Bioprod. Bioref*., **2**, 41–57.

Henry, C.S., Broadbelt, L.J., and Hatzimanikatis, V., (2010). Discovery and analysis of novel metabolic pathways for the biosynthesis of industrial chemicals: 3-hydroxypropanoate, *Biotechnol Bioeng*, **106**, 462–473.

Holmgren, J., Marinangeli, R., Elliott, D. and Bain, R., (2008). Consider upgrading pyrolysis oils into renewable fuels. *Hydrocarbon Processing*, September 2008.

Hols P., Kleerebezem M., Schanck A., Ferain T., Hugenholtz J., Delcour J., and de Vos W., (1999). Conversion of *Lactococcus lactis* from homolactic to homoalanine fermentation through metabolic engineering, *Nature Biotechnology*, **17**, 588–592.

Ingraham, J.L., Maaløe, O., and Neidhardt, F.C., (1983). Growth of the Bacterial Cell. Sinnauer Associates, Sunderland, UK.

Kamm, B., and Kamm, M., (2007). Biorefineries-Multi Product Processes, *Adv. Biochem. Engin./ Biotechnol*., **105,** 175–204.

Kjeldsen, K.R., and Nielsen, J., (2009). In silico genome-scale reconstruction and validation of the *Corynebacterium glutamicum* metabolic network. *Biotechnol. Bioeng*., **102**, 583–597.

Lee, S.Y., Park, J.H, Jang, S.H., Nielsen, L.K., Kim, J., and Jung, K.S., (2008). Fermentative butanol production by *Clostridia*. *Biotechnol. Bioeng*., **101**, 209–228.

Lengeler, J.W., Drews, G., and Schlegel, H.C. (editors), 1999. Biology of Procaryotes. Georg Thieme Verlag, Stuttgart, DE.

Ligget, R.W. and Koffler, H., (1948). Corn Steep Liquor in Microbiology. *Bacteriol. Rev*. **12**, 297–311.

Lin, Y., and Tanaka, S., (2006). Ethanol fermentation from biomass resources: current state and prospects. *Appl Miocrobiol Biotechnol*, **69**, 627–642.

Lynd, Lee R., Laser, M.S., Bransby, D., Dale, B.E., Davison, B., Hamilton, R., Himmel, M., Keller, M., McMillan, J.D., Sheehan, J., and Wyman, C.E., (2008). How biotech can transform biofuels. *Nature Biotechnology*, **26**, 169 – 172.

Maiorella, B.L., Blanch, H.W., and Wilke, C.R., (1984). Economic evaluation of alternative ethanol fermentation processes. Reprinted in *Biotechnol. Bioeng*. (2009), **104**, 421–443.

Matsushita, K., Toyama, H., Yamada, M., and Adachi, O., (2002). Quinoproteins: Structure, function and biotechnological applications. *Appl. Microbiol. Biotechnol*., **58**, 13–22.

Mimitsouka, T., Sawai, H., Hatsu, M., and Yamada, K., (2007). Metabolic engineering of *Corynebacterium glutamicum*for cadaverin fermentation, *Biosci Biotechnol Biochem*, **71**, 2130–2135.

Murzin, D.Y., and Leino, R., (2008). Sustainable chemical technology through catalytic multistep reactions. *Chem Eng Research and Design*, **86**, 1002–1010.

Nielsen, J., (1997). Physiological engineering aspects of *Penicillin chrysogenum*. World Scientific Publishing Company, Singapore.

Nissen, T.L., Anderlund, M., Nielsen, J., Villadsen, J., and Kielland-Brandt, M., (2001). Expression of a cytoplasmic transhydrogenase in *S. cerevisiae* results in formation of 2-oxoglutarate due to depletion of the NADPH pool. *Yeast*, **18**, 19–32.

Olofsson, K., Bertilsson, M., and Lidén, G., (2008). A short review of SSF – An interesting process option for ethanol production from lignocellulosic feedstocks. *Biotechnol for Biofuels*, **1**:7.

Remize, F., Roustan, J.L., Sablayrolles, J.M., Barre, P., and Dequin, S., (1999). Glycerol overproduction by engineered *S. cerevisiae* wine yeast strains leads to substantial changes in by-product formation and to a stimulation of fermentation rate in stationary phase. *Appl. Environ. Microbiology*. **65**, 143–149.

Sendich E., Laser, M., Kim, S., Alizadeh, H., Laureano-Perez, L., Dale, B., and Lynd, L., (2008). Recent process improvements for the AFEX process and resulting reductions in minimum ethanol selling price. *Bioresource Technology*, **98**, 8429–8435.

Sillers, R., Chow, A., Tracy, B., and Papoutsakis, E.T., (2008). Metabolic engineering of the non-sporulating, non-solventogenic *Clostridium acetobutylicum* strain M 5 to produce butanol without acetone demonstrate the robustness of the acid-formation pathways and the importance of the electron balance. *Metabolic Eng*., **10**, 321–332.

Sjöberg, A., and Hahn-Hägerdahl, B., (1989). β-glucose-1-phosphate, a possible mediator for polysaccharide formation in maltose-assimilating *Lactococcus lactis*. *Appl. Environ. Microbiol*. **55**, 1549–1554.

Stephanopoulos, G.N., Aristidou, A.A., and Nielsen, J., (1998). Metabolic Engineering, Principles and Methodologies. Academic Press, London.

Straathof, A.J.J., Sie, S., Franco, T.T., and van der Wielen L.A.M., (2005). Feasibility of acrylic acid production by fermentation, Appl Microbiol Biotechnol, **67**, 727–734.

Tateno, T., Okada, Y., Tscuchidate, T., Tanaka, T., Fukoda, H., and Kondo, A., (2009). Direct production of cadaverine from soluble starch using *Corynebacterium glutamicum* coexpressing α-amylase and lysine decarboxylase, *Appl Microbiol Biotechnol*, **82**, 115–121.

van Maris, A., Abbott, D., Bellissimi, E., van den Brink, J., Kuyper, S.M., Luttik, M., Wesseling, H., Scheffers, W., van Dijken, J., and Pronk, J., (2006). Alcoholic fermentation of carbon sources in biomass hydrolysates by *S. cerevisiae*: current status. *Antonie van Leeuwenhoek*, **90,** 391–418.

Verhoef, S., Wiercks, N., Westerhof, R.G.M., de Winde, J.H., and Ruijssenaars, H.J., (2009). Bio-production of p-hydroxystyrene from glucose by solvent tolerant bacterium *Psudomonas putida* S 12 in a two-phase water-decanol fermentation. *Appl. Environ. Microbiol.*, **75**, 931–936.

Villadsen, J., (2007). Innovative technology to meet the demands of the White Biotechnology revolution of chemical production. *Chem. Eng. Sci.,* **62**, 6957–6968.

Voet, D., and Voet, J.G., (1995). Biochemistry (2nd edition) Wiley, New York.

Werpy, T.A, and Petersen, G, (Editors), (2004). Top value added chemicals from biomass. Volume 1 Results of screening for potential candidates from sugars and synthesis gas. Produced by PNNL and NREL for the US Department of Energy.

Wisselink, H.W., Toirkens, M.J., Wu, Q., Pronk, J.T., and van Maris, A.J.A., (2009). Novel evolutionary approach for accelerated utilization of glucose and arabinose mixtures by engineered *S. cerevisiae* strains. *Appl. Environ. Microbiol*, **75**, 907–914.

Wittmann, C., and Becker, J., (2007), The L-lysine story: From metabolic pathways to industrial production. In "Amino acid Biosynthesis-Pathway, Regulation and Metabolic Engineering", p. 39–70 (Ed. V.F. Windish). Springer Verlag, Berlin.

Chapter 3
Elemental and Redox Balances

In Chap. 2 we painted a picture of the potential of Biotechnology as the provider of a great many of the chemicals used in our daily life. Now, in small steps the quantitative tools for analysis of the cellular reactions will be introduced. First, the *rates* of cellular reactions will be determined by application of *mass balances* to data obtained in *steady-state continuous* bioreactors. The rates to be calculated are not for individual pathway reactions, e.g., the conversion of pyruvate to acetaldehyde and further to ethanol in Fig. 2.5c. Rather, the rates are calculated based on the difference between the inlet to the reactor and the effluent from the reactor in the medium concentration of one of the substrates, e.g., glucose, or one of the products, e.g., ethanol or biomass. Consequently, the rate of ethanol production calculated from the experiment is the net result of all the cell reactions that produce and consume ethanol, the so-called *excretion rate* of ethanol from the cells to the medium. Similarly, the rate of glucose consumption, the *uptake rate* of glucose, is the sum of glucose consumption in all cell reactions that consume glucose.

It goes without saying that the picture of cell metabolism obtained by these simple calculations is very incomplete. One would like to know the rate of glucose consumption or the rate of, e.g., lysine production in individual pathways in order to understand how the cell metabolism functions and to promote, by genetic manipulations, the channeling of substrates into the pathways that give an optimal yield of a desired product.

Biochemical Networks and the subject of *Metabolic Flux Modeling*, in which the distribution of glucose to different pathways or the production (or loss) of a product in different pathways is obtained, will be treated in Chap. 5. Still, the so-called *Black Box* model of cell metabolism that is obtained from measurement of net inflow and outflow concentrations of reactants and products is very valuable. It permits the overall conversion of reactants to products to be described by *one single stoichiometric equation*. The coefficients of this equation, the *Yield coefficients*, determine the economic feasibility of the process. For example, the yield coefficient of lysine on glucose (g lysine per g glucose) combined with the price per unit mass of lysine and glucose immediately determines whether the process stands a chance of being economically viable.

J. Villadsen et al., *Bioreaction Engineering Principles*,
DOI 10.1007/978-1-4419-9688-6_3,

Interestingly, the much more detailed analysis of Chap. 5 eventually leads back to a Black Box model for the conversion of substrates to products. But with the added insight obtained by Metabolic Flux Modeling one is able to predict the means by which cell metabolism has to be changed in order to funnel more of the substrate into pathways that give a higher yield of the desired product, i.e., to change the yield coefficients of the overall Black Box model in a desired direction.

In general, the Black Box approach requires no biochemical information at all. One simply measures the incoming and exit flows of substrates and products to calculate rates of production and consumption. With the added information obtained from the metabolic pathways of Chap. 2 it is only natural that more information can be retrieved based on the same amount of experimental work, and this is why the methodology of Chap. 5 gives much more insight in cell physiology than what is obtained in the present chapter.

It is, however, important to recognize that the rates obtained either in Chap. 3 or 5 are *steady-state* rates which represent the outcome of the process *only* at the steady-state conditions applied in the particular experiment, e.g., at the rate at which medium flows through the given reactor volume. When the experimental conditions are changed a new set of steady-state rates is obtained, and based on the collection of steady-state rates one may start to build *kinetic expressions* by correlating, e.g., the rate of glucose consumption with the concentration of glucose in the effluent from the continuous reactor. This kinetic modeling exercise can be used in bioreactor *design*. A kinetic expression is, however, tied to a particular stoichiometry, and if the stoichiometry changes, then the kinetic expression which is tied to a particular overall Black Box stoichiometry must fail. An example of a steady-state metabolism that changes with increasing flow of medium through the reactor is the overflow metabolism discussed for both bacteria and yeast in Sect. 2.2.5. The collection of steady-state rates obtained at different steady-state flow rates will show that new metabolites appear when the flow rate increases beyond a critical value, and the concept of a single kinetic expression for the steady-state rate data becomes invalid. Here, the more detailed description of Chap. 5 can be used since the individual metabolic paths to, e.g., biomass and ethanol are recognized, and competing reactions to different end products can be distinguished in much the same way as "a main reaction" and different "side reactions" are distinguished in conventional reaction engineering.

In Chap. 7, it will become abundantly clear that kinetic modeling of bioreactions is far more complicated than the modeling of "normal" chemical reactions. One set of kinetic expressions will be obtained based on steady-state experimental data while completely different expressions will result when the reactor is subject to rapidly changing environmental conditions, e.g., if the inlet flow is suddenly changed.

The complexity of bioreactions compared to normal chemical reactions is one of the challenges of Bioreaction Engineering: In contrast to conventional chemical reactions the living cell reacts on many different levels. A sudden upset of the environmental conditions activates hidden regulatory mechanisms in the cell metabolism with time constants that can vary between milliseconds and hours.

New pathways are opened up and others shut down during transient operation of the reactor, and the kinetics obtained on the basis of only steady-state experiments becomes invalid.

3.1 The Continuous, Stirred Tank Reactor

A very efficient bioreactor setup for analysis of overall conversion rates in bioprocesses is the continuous, stirred tank reactor, which is schematically shown in Fig. 3.1. There are two feed ports, one for liquid feed and one for gaseous feed. In the liquid reaction medium the reactants, called *substrates*, are converted to *biomass* and *metabolic products*. Cells and metabolic products dissolved in the aqueous medium leave the reactor through the liquid effluent. Gas-phase substrates such as oxygen are fed to the reactor through a gas distributor and dissolved in the medium from which they are taken up by the cells. Gaseous products such as carbon dioxide leave through the headspace of the reactor (exhaust gas). When the liquid feed rate v (L h^{-1}), the gas feed rate v_g (L h^{-1}), the medium volume V (L) and the concentrations of substrates in the liquid and gas feed streams are independent of time, i.e., when all the input variables to the system have constant values, we will expect all the output variables, i.e., biomass concentration and activity of the cells as well as the concentration of metabolic products in liquid and gas effluents to have constant values. The bioreactor is operating in a *steady-state continuous mode*. In a large majority of cases all the output variables have time independent values when the feed variables are constant, but there are exceptions, and these exceptions can have considerable scientific and practical interest as will be qualitatively discussed in Note 3.1 and considered again in Chaps. 7 and 9.

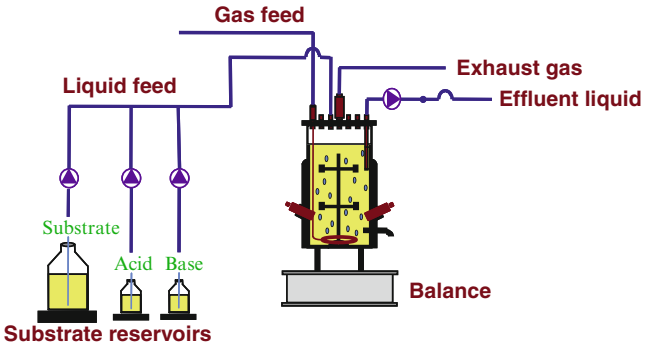

Fig. 3.1 A continuous, stirred tank bioreactor with feed of a liquid medium from a substrate reservoir and a feed of gaseous medium through a sparger. pH is typically kept constant by adding acid or base from separate reservoirs

Note 3.1 *Time-dependent output with constant values of input variables.* Sometimes, a time-independent set of input variables does not lead to time-independent output variables.

- Some microbial cultures seem unable to reach steady state in a certain range of (time independent) operating conditions. All outputs oscillate with an oscillation time that depends on the input variables. This is further discussed in Chaps. 7 and 8.
- The cells may suddenly, and for no apparent reason, change their behavior. A product – it could be penicillin – is suddenly not being produced at the same constant rate, which has been measured for many hours of apparently steady-state operation. After a relatively short period the cells may totally have lost their ability to produce a particular metabolic product. This is typically caused by strain reversion of the highly efficient industrial producer (see Christensen et al. 1995 and Example 9.11). In other cases, the cells may become "sick" and die. A cell count of viable cells will show a gradually diminishing fraction of viable cells, i.e., cells that are able to grow. All these cases are typically a consequence of occurrence of natural mutations, which may be followed by selection of the mutated cells in the bioreactor.

The experimenter is likely to become surprised (and frustrated) by observing an unsteady-state output from what should be a steady-state continuous bioreactor. Still, the unexpected results may offer opportunities for challenging research, and the observation of irregular behavior in well-controlled laboratory reactors can prevent later disasters when the laboratory results are to be used in an industrial scale process. Thus, the observation of oscillating reactions indicates that the kinetics of the overall reaction is of a kind, which does not always admit to a steady-state output, even when the input is constant – a situation also encountered in chemical reaction engineering. The gradual cessation of synthesis of a desired product indicates that the cell environment has changed in a subtle fashion which it will take much experimental effort to explore. A slight difference in medium sterilization or in the protocol for inoculation of the reactor, a change to a different batch of yeast extract used as nitrogen source in the feed medium – and a host of other perturbations could all lead to loss of productivity. Events observed in the steady-state laboratory culture could also have their origin in the genome of the cell – a slight change in the expression of certain genes could lead to a cascade of events observed on the macroscopic level in the reactor.

These observations – which as stated initially are not commonplace – do, however, show that experimental studies of biological reactions try to extract useful information from a system, which in principle is not at all observable. It is vastly more complex than the gas-phase reaction catalyzed by a solid catalyst, a standard topic in textbooks on chemical reaction engineering. An almost infinite possibility of reaction paths with a hierarchal control structure which fine-tunes the active paths in response to a changing environment, to the age of the culture, or to signals that we have not even begun to explore is the standard scenario of cell reaction studies.

Besides setting the substrate concentrations to certain values in the liquid and the gas feed streams, the attainment of a steady-state continuous culture requires that v_g, and especially v, the feed rate of the liquid feed, are set to constant values relative to the medium volume V in the reactor. Using gas flow meters v_g/V is controlled at a given set point to obtain a certain gas flow rate – often specified in terms of v.v.m. – volume gas per volume liquid per minute. The ratio between v

and V is one of the most important input variables in bioreactors. The ratio is called the *dilution rate* and is measured in units of reciprocal time, usually h^{-1}.

$$\text{Dilution rate } = D = \frac{v}{V}, \tag{3.1}$$

where D is the *space velocity* or the reciprocal of the holding time, the terms used in conventional chemical reaction engineering.

To attain a constant D several different control strategies may be used:

- The volume of the reaction medium or the weight of reactor and medium is measured with a frequency of, e.g., 10 min^{-1} and the liquid feed rate v is controlled to give a certain set-point for V. When D is fixed in this way, i.e., by controlling one input variable v by means of the measured value of another input variable V the reactor is said to operate as a *chemostat*. This is how most laboratory continuous, stirred tank reactors are operated.

Control of D can also be achieved by measurement of one of the output variables:

- In the *turbidostat* v is manipulated at a constant V to obtain a constant, measured biomass concentration x (g L^{-1}) in the effluent. In this way, a certain value of D is obtained which corresponds to the set point value of x.
- The feed of a nutrient (e.g., glucose) can be manipulated to obtain a certain pH in the effluent. Many bioreactions produce or consume protons, and by separating the nutrient feed from the alkali/acid feed used to neutralize the proton production the rate of the bioreaction can likewise be controlled. This is the *pH-auxostat*.
- Measurements of the effluent concentration of one of the metabolic products, e.g., ethanol in fermentations with *Saccharomyces cerevisiae*, can also be used to obtain the D value, which corresponds to a given set point for the effluent concentration (or the rate of production) of one of the products. This is called a *productostat* (Andersen et al. 1997).

These three strategies (which are called "closed loop control" strategies by control engineers) are used together with a more or less detailed mathematical model of the process, which occurs in the bioreactor. As in any textbook treatment of stirred tank reactors it is assumed that by efficient stirring of the medium the effluent concentrations of biomass and metabolic products will be identical to those found at any point in the reactor. The reactor is then called an *ideal bioreactor*. Unless the steady state to be explored is unstable, all four strategies can be used to reach a desired steady state. The choice of strategy should ideally depend on the sensitivity of the steady state to changes in the variable used to establish the control policy. The strategy, which gives the highest sensitivity, should be chosen – although chemostat operation is used in the large majority of investigations, probably by force of habit.

As seen in Fig. 3.2 the biomass concentration in the effluent from a steady-state aerobic cultivation of *S. cerevisiae* on glucose is virtually independent of D at small

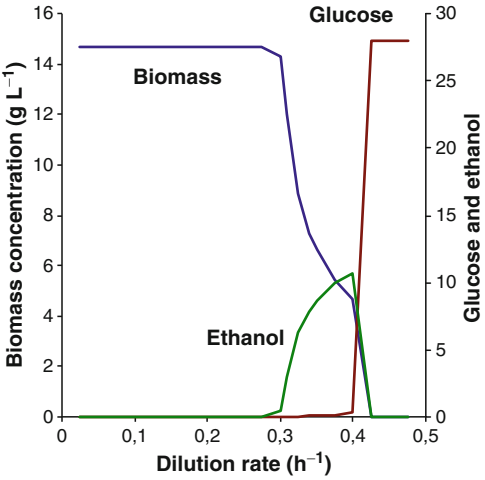

Fig. 3.2 Schematic view of the concentration profiles of biomass, ethanol, and glucose at different dilution rates in a continuous, stirred tank bioreactor containing the yeast *S. cerevisiae*

values of D. Consequently, a steady state at a small D cannot be accurately fixed in a turbidostat. The substrate concentration s in the effluent may well vary significantly on a relative scale (we shall see in Chap. 7 that s is proportional to D at small D) but it is difficult to measure the small substrate concentration accurately enough to fix v or D at the desired value. Operation of the bioreactor as a chemostat should therefore be the preferred strategy. At a steady state with a high D value, close to the so-called wash-out value, the substrate concentration has increased significantly, and the biomass concentration has decreased from its high and almost constant value at small D. Here the turbidostat is working very well since even small variations in D give rise to large changes in x, and the steady state is pinpointed by basing the control on a given set point for x. The chemostat is totally unsuited near wash out, but the pH-auxostat is also very satisfactory (Pham et al. 1999), since the rate of proton production is strongly coupled (sometimes even proportional) to the value of biomass production. Around the so-called critical dilution rate D_{crit} where ethanol production sets in the ethanol concentration p (or the ethanol production rate) depends strongly on D. Here a productostat is the ideal control strategy (Lei et al. 2001). Control of x or of the respiratory quotient, the ratio between oxygen consumption and carbon dioxide production, are less sensitive near D_{crit}, and the chemostat is unsuited since one cannot control v accurately enough to obtain a steady state with a desired p.

It always takes patience to reach a steady state in a continuous, stirred tank reactor, and the time constant for the transient between one steady state and the next varies with the steady state. It takes on the order of five holding times, i.e. $5...D^{-1}$, to attain a new steady state, and the measured rates can be far off their true steady-state values if the approach to the new steady state is not within 95–99%. The time between steady states is not wasted since the transient itself contains much information on the physiology of the organism. For a dilution rate close to the critical dilution rate D_{crit} where ethanol starts to be produced in aerobic yeast fermentation, Lei et al. 2001 obtained a steady state within five holding times using the

productostat control strategy, while Postma et al. (1989) obtained a transient time between steady-state D values of close to $50\,D^{-1}$, probably because of latent instability of the control strategy (chemostat) that was used when D is close to D_{crit}.

The despair of experimenters who have waited many hours to obtain a steady state in continuous, stirred tank reactors, when the pH control for no apparent reason fails or a rubber tube breaks, is all too well known. Likewise, the loss of plasmids, leading to gradual loss of productivity of the culture, is a well-known source of frustration. Still, the steady-state continuous reactor is the ideal equipment for physiological studies – and also to obtain trustworthy data for design of an industrial production. The set of steady-state data is the foundation of a quantitative treatment of bioreactions, and deeper layers of metabolic response are revealed in the transients from one steady state to the next. These transient experiments give the necessary input for the modeling of nonideal reactors in which the effects of spatial in-homogeneities of, e.g., glucose or oxygen on the performance of industrial bioreactors are investigated (see Sect. 11.2). Without at least a semiquantitative knowledge of how rapidly a change in, e.g., a vitamin concentration changes the production rate of a desired metabolite, the detailed calculations of flow patterns in the bioreactor obtained by computational fluid dynamics are of little value.

3.1.1 *Mass Balances for an Ideal, Steady-State Continuous Tank Reactor*

Based on the measured feed and effluent concentrations in the continuous tank bioreactor of Fig. 3.1, the reaction rates are easily calculated from steady-state mass balances for the bioreactor. Thus all three equations (3.2)–(3.4) express that at steady state (no mass accumulation) the mass of the compound produced by the reaction is equal to the difference in mass of the compound between the liquid feed and the outlet from the reactor.

$$q_{s_i} V + v\left(s_{i,\text{f}} - s_i\right) = 0, \tag{3.2}$$

$$q_{p_i} V + v\left(p_{i,\text{f}} - p_i\right) = 0, \tag{3.3}$$

$$q_{\text{x}} V + v(x_{\text{f}} - x) = 0, \tag{3.4}$$

where q_i *is the volumetric production rate*, i.e., the mass of compound i produced per volume reactor and per unit time. s_{i} and p_{i} are the concentrations of substrate i and metabolic product i, respectively. x is the concentration of the biomass. Subscript f indicates the concentration of the variable in the liquid feed to the bioreactor. In (3.2) the difference $(s_{i,f} - s_i)$ is positive, and the production rate q_{s_i} is of course negative. We find it most logical to work only with production rates (positive or negative) rather than introducing a separate term for rates of consumption. Consequently, the definitions in (3.2)–(3.4) are used throughout the text.

With a gaseous substrate or product (3.2) and (3.3) are slightly modified

$$\left(q_{\mathrm{s}_i}^t + q_{\mathrm{s}_i}\right) V + v\left(s_{i,\mathrm{f}} - s_i\right) = 0, \tag{3.5}$$

$$\left(q_{\mathrm{p}_i}^t + q_{\mathrm{p}_i}\right) V + v\left(p_{i,\mathrm{f}} - p_i\right) = 0, \tag{3.6}$$

In (3.5) and (3.6) q_{i} is again the rate of production of the component by the biochemical reaction, whereas q_i^t is the rate at which the component is transferred from the gas phase to the liquid medium, which is given by:

$$q_{\mathrm{s}_i}^t = k_{\mathrm{l}}a\left(s_i^* - s_i\right), \tag{3.7}$$

$$q_{\mathrm{p}_i}^t = k_{\mathrm{l}}a\left(p_i^* - p_i\right), \tag{3.8}$$

where $k_{\mathrm{l}}a$ is a mass transfer coefficient which may depend on the fermentation medium and on the component being transferred, but it always depends on the agitation of the liquid medium or the construction of the sparger used to introduce the gas. s_i^* and p_i^* are the concentrations of components in the liquid which are in equilibrium with the gas phase. Both depend on the partial pressure of the component in the gas phase, on the medium temperature, pH, etc., as will be further discussed in Chap. 10.

$$s_i^* = H_{\mathrm{s}_i}\pi_{\mathrm{s}_i}; \quad p_i^* = H_{\mathrm{p}_i}\pi_{\mathrm{p}_i} \tag{3.9}$$

In (3.9), π_{s_i} and π_{p_i} are the partial pressures in the gas phase ($=y_i P$ where y_i is the molar fraction of the component in the gas phase and P the total pressure), and H_{i} is a so-called Henry's law coefficient, which as described above is dependent on the medium and on the operating conditions. A typical unit for H is mol (L atm)$^{-1}$.

Finally, the gas-phase partial pressures are given from mass balances for the gas phase between the gas inlet and the head space:

$$q_{\mathrm{s}_i}^t = \frac{1}{RT}\left(v_{\mathrm{gf}}\pi_{\mathrm{s}_i,\mathrm{f}} - v_{\mathrm{g}}\pi_{\mathrm{s}_i}\right) = k_{\mathrm{l}}a\left(s_i^* - s_i\right)V, \tag{3.10}$$

In (3.10) $v_{\mathrm{g,f}}$ and v_{g} are the inlet and outlet volumetric gas flow rates, and the left hand expression is therefore the difference in molar flow of the gas phase component between the gas inlet and the head space. $v_{\mathrm{g,f}}$ is different from v_{g} if the volumetric production rate of gaseous products is different from the consumption rate of gaseous substrates, or if liquid phase components, typically water, are stripped off from the medium.

The correct use of the mass balances (3.5)–(3.8) and (3.10) is illustrated in Example 3.4 and in Problem 3.1. There are many pitfalls in the calculation of gas phase transfer rates, and terribly wrong results for, e.g., the oxygen consumption rate will result unless these pitfalls are avoided.

From measurements of the concentrations of the reactants at a fixed value of the input variable D, the reaction rates can always, and quite easily, be determined by correct use of the mass balances. Equations (3.2)–(3.4) are used for liquid phase components, and (3.5)–(3.10) when the component is exchanged with a gas phase.

In an experiment used to determine the reaction rates a number of the variables in the mass balances are usually zero or very close to zero.

- Typically, there is neither biomass nor product in the feed streams:

$$x_{\mathrm{f}} = p_{i,\mathrm{f}} = \pi_{\mathrm{p}_{i,\mathrm{f}}} = 0. \tag{3.11}$$

- Components transferred from the gas phase are typically only sparingly soluble. In particular, this is true for oxygen and also for natural gas, the carbon and energy source used in modern single-cell protein (SCP) production. Typically, at normal pressure $s^*_{\mathrm{O}_2} \cong 1\,\mathrm{mM}$ and $s_{\mathrm{O}_2} = 10 - 20\ \mu\mathrm{M}$ while the corresponding values for s_{CH_4} are a little lower. Thus in (3.7) and (3.10) s_{i} can be set to zero. In other aerobic bioreactions s_{O_2} has to be a sizeable fraction of $s^*_{\mathrm{O}_2}$ – perhaps 10% for penicillin fermentation and even higher for baker's yeast production.

In (3.2)–(3.4) q_{i} is the volumetric production rate, i.e., the mass of compound i produced per volume reactor and per unit time. The rates of the bioreactions, i.e., of the reactions within the cell, conventionally measured as mass of component i produced per unit weight of cell (rather than per unit volume of cell) and per unit time are

$$r_i = \frac{q_i}{x}. \tag{3.12}$$

Specifically for the biomass:

$$\mu = r_{\mathrm{x}} = \frac{q_{\mathrm{x}}}{x} \equiv \text{the specific growth rate}. \tag{3.13}$$

As mentioned in Chap. 1 we shall stick with these definitions throughout the text. r_{i} are the rates associated with the "real" reactions in the "real" reactor – the cell. This is in accordance with the nomenclature of IUPAC. q_i is primarily used in mass balances set up for the reactor vessel.

3.2 Yield Coefficients

When any particular rate, whether q_i or r_i is scaled with another rate q_j *or* r_j one obtains the *yield coefficient* Y_{ji}.

$$Y_{ji} \equiv \left|\frac{r_i}{r_j}\right| = \left|\frac{q_i}{q_j}\right| \quad \text{and} \quad Y_{ij} = Y_{ji}^{-1}. \tag{3.14}$$

Since the rate of production of all substrates is negative a numerical sign is used in (3.14) to obtain yield coefficients, which are all positive. In our definition of the yield coefficient the first index j in Y_{ji} always refers to the reference rate.[1] Yield coefficients are measured in many consistent set of units, g g^{-1} or mol mol^{-1}, or for carbon-containing compounds C-moles $(C\text{-mole})^{-1}$. As discussed in Sect. 2.4.2 yield coefficients are very important parameters for design and optimization of fermentation processes.

With the above definition of the yield coefficients, a stoichiometric equation for growth of biomass X on one carbon mole CH_2O ($=C_6H_{12}O_6/6$) of glucose as the carbon and energy source can now be written as follows:

$$\begin{aligned} &-\mathrm{CH_2O} - Y_{\mathrm{so}}\mathrm{O_2} - Y_{\mathrm{sn}}\mathrm{NH_3} - Y_{\mathrm{ss_1}}\mathrm{S_1} - \ldots + Y_{\mathrm{sx}}\mathrm{X} + Y_{\mathrm{sc}}\mathrm{CO_2} \\ &+ Y_{\mathrm{sp_1}}\mathrm{P_1} + \ldots + Y_{\mathrm{sw}}\mathrm{H_2O} = 0 \end{aligned} \tag{3.15}$$

Capital letters S_i are used to denote substrates other than glucose, O_2 and the nitrogen source, which in (3.15) is taken to be NH_3. Likewise, capital letters P_i are used for metabolic products other than CO_2. In (3.15) the rates are all scaled by the rate of consumption of glucose in units of 1 C-mole = 30 g. Thus, if $Y_{sn} = 0.05$ then 0.05 moles of NH_3 is consumed every time 30 g = 1 C-mole glucose is consumed by the chemical reaction (3.15). From (3.15), other yield coefficients are easily calculated, e.g., the *respiratory quotient* RQ, which is frequently used in control of industrial scale aerobic cultivations:

$$\mathrm{RQ} = \left|\frac{q_c}{q_o}\right| = \frac{Y_{sc}}{Y_{so}} = Y_{oc}. \tag{3.16}$$

In all stoichiometric calculations in this textbook the chemical formula for the biomass X is written on the basis of one C-mole biomass:

$$\mathrm{X} = \mathrm{CH_aO_bN_cS_dP_e} \ldots \tag{3.17}$$

Likewise, all other carbon-containing species S_1, S_2 …, P_1, P_2… are written on the basis of 1 C-mole. With this convention a carbon balance gives

$$1 + Y_{\mathrm{ss_1}} + Y_{\mathrm{ss_2}} + \cdots = Y_{\mathrm{sx}} + Y_{\mathrm{sc}} + Y_{\mathrm{sp_1}} + Y_{\mathrm{sp_2}} + \cdots \tag{3.18}$$

Water has been included in the general stoichiometry (3.15), but since the reaction is carried out in aqueous solution, and since the concentration of substrates and products rarely exceeds 5 wt%, the water produced adds so little to the total medium that it can often be neglected when calculating the effluent concentrations. If substantial amounts of weak alkali or acid (1–2 M concentration) are added to keep pH constant, this extra feed of water may of course have to be considered. The yield of water by the reaction is in itself of no importance, and in the stoichiometric calculations we shall in general not consider the term Y_{sw} H_2O.

[1] In the literature one often finds another notation for the yield coefficient, namely $Y_{i/j}$ for Y_{ji}.

Table 3.1 Average composition of *S. cerevisiae*

Macromolecule	Elemental composition	Percent by weight	g (C-mole)$^{-1}$
Protein	$CH_{1.58}O_{0.31}N_{0.27}S_{0.004}$	57	22.45
RNA	$CH_{1.25}O_{0.75}N_{0.38}P_{0.11}$	16	34.0
DNA	$CH_{1.15}O_{0.62}N_{0.39}P_{0.10}$	3	31.6
Carbohydrates	$CH_{1.67}O_{0.83}$	10	27.0
Phospholipids	$CH_{1.91}O_{0.23}N_{0.02}P_{0.02}$	10.8	18.5
Neutral fat	$CH_{1.84}O_{0.12}$	2.5	15.8
Pool of cellular metabolites	$CH_{1.8}O_{0.8}N_{0.2}S_{0.01}$	0.7	29.7

The biomass formula (3.17) indicates that a long list of elements appear in the biomass. C, H, O, and N are, however, the dominant elements, while the content of S, P, and of all the trace elements such as Ca, Mg, Na, Fe, Co, etc., is small compared to the N-content. These elements must, however, be present in the feed as, e.g., Na_2SO_4 and K_2HPO_4 to synthesize an active biomass. The composition of *X* is determined by elemental analysis: A sample of dried biomass is ignited and the combustion products are analyzed. The residue is termed "ash," and it consists of inorganic compounds, mostly oxides. The ash content of biomass is usually in the range 4–8 wt%. It follows from the analytical procedure that the oxygen content of the sample cannot be measured, but must be calculated. In most examples of this book calculations are made on the basis of ash-free biomass, but in an experimental study the ash content of the biomass must of course be accounted for. Otherwise, a significant error is introduced, and the calculation of rates is quite sensitive to the composition of the biomass. The composition of ash-free biomass varies somewhat between different organisms, but as seen in Table 3.2 the composition of a given organism varies much more with the growth conditions than between different organisms.

The yeast *S. cerevisiae* growing at glucose-limited conditions with an ample supply of nitrogen source has a macromolecular composition shown in Table 3.1. Based on the weight fractions of the seven main groups of biomass components and their respective formula weight the average composition and formula weight of the biomass can be calculated as follows:

$$X = CH_{1.596}O_{0.396}N_{0.216}S_{0.0024}P_{0.017} \tag{3.19}$$

This[2] corresponds to a formula weight of $M_x = 23.58$ g (C-mole biomass)$^{-1}$.

[2]According to Table 3.1, 100 g biomass contains 57 g protein, or 57/22.45 = 2.539 C-mole.

The same calculation is done for the other 6 constituents of the biomass, and one finds that 100 g biomass corresponds to 4.241 C-mole.

4.241 C-mole biomass contains $0.31 \times 2.539 + 0.75 \times 0.471 + \cdots = 1.678$ mol O, or 1.678/4.241 = 0.396 oxygen atom per C-mol biomass.

The same calculation is done for the other elements of X, and the biomass composition (3.19) results.

Table 3.2 Elemental composition of biomass for several microbial species

Microorganism	Elemental composition	Ash content (w/w%)	Condition
Candida utilis	$CH_{1.83}O_{0.46}N_{0.19}$	7.0	Glucose limited, $D = 0.05\ h^{-1}$
	$CH_{1.87}O_{0.56}N_{0.20}$	7.0	Glucose limited, $D = 0.45\ h^{-1}$
	$CH_{1.83}O_{0.54}N_{0.10}$	7.0	Ammonia limited, $D = 0.05\ h^{-1}$
	$CH_{1.87}O_{0.56}N_{0.20}$	7.0	Ammonia limited, $D = 0.45\ h^{-1}$
Klebsiella aerogenes	$CH_{1.75}O_{0.43}N_{0.22}$	3.6	Glycerol limited, $D = 0.10\ h^{-1}$
	$CH_{1.73}O_{0.43}N_{0.24}$	3.6	Glycerol limited, $D = 0.85\ h^{-1}$
	$CH_{1.75}O_{0.47}N_{0.17}$	3.6	Ammonia limited, $D = 0.10\ h^{-1}$
	$CH_{1.73}O_{0.43}N_{0.24}$	3.6	Ammonia limited, $D = 0.85\ h^{-1}$
Saccharomyces cerevisiae	$CH_{1.82}O_{0.58}N_{0.16}$	7.3	Glucose limited, $D = 0.080\ h^{-1}$
	$CH_{1.78}O_{0.60}N_{0.19}$	9.7	Glucose limited, $D = 0.255\ h^{-1}$
Escherichia coli	$CH_{1.94}O_{0.52}N_{0.25}P_{0.025}$	5.5	Unlimited growth
	$CH_{1.77}O_{0.49}N_{0.24}P_{0.017}$	5.5	Unlimited growth
	$CH_{1.83}O_{0.50}N_{0.22}P_{0.021}$	5.5	Unlimited growth
	$CH_{1.96}O_{0.55}N_{0.25}P_{0.022}$	5.5	Unlimited growth
Pseudomonas fluorescens	$CH_{1.93}O_{0.55}N_{0.25}P_{0.021}$	5.5	Unlimited growth
Aerobacter aerogenes	$CH_{1.83}O_{0.55}N_{0.26}P_{0.024}$	5.5	Unlimited growth
Penicillium chrysogenum	$CH_{1.64}O_{0.52}N_{0.16}$	7.9	Unlimited growth
Aspergillus niger	$CH_{1.72}O_{0.55}N_{0.17}$	7.5	Unlimited growth
Average	$CH_{1.81}O_{0.52}N_{0.21}$	6.0	

Table 3.2 shows the elemental composition of many organisms studied at different conditions and by different authors. Note that the biomass formula calculated in (3.19) from the approximate macromolecular composition is somewhat different from the formula calculated by the – presumably more accurate – elemental analysis.

Compared to the formula weight and composition of biomass calculated from the macromolecular composition (3.19) the compositions listed in Table 3.2 seem to contain an added 0.1 H_2O per C-atom. Tentatively, this could be ascribed to a systematic error in the elementary analysis: Many of the macromolecules contain strongly bound water, which is not completely released when the sample is dried before combustion. When the composition (3.19) is rescaled by adding 0.1 H_2O per C atom one obtains the average in Table 3.2 or

$$X = CH_{1.8}O_{0.5}N_{0.2} \tag{3.20}$$

This corresponds to a formula weight of $M_x = 24.6$ g (C-mole biomass)$^{-1}$. Unless otherwise stated we shall throughout the book use (3.20) as the "standard" formula for biomass. Equation (3.20) is, however, only applicable in "normal" fermentations where the carbon source is the limiting growth factor.

The small discrepancy between biomass composition determined either from the constituents of the biomass (Table 3.1) or by elementary analysis (Table 3.2) has

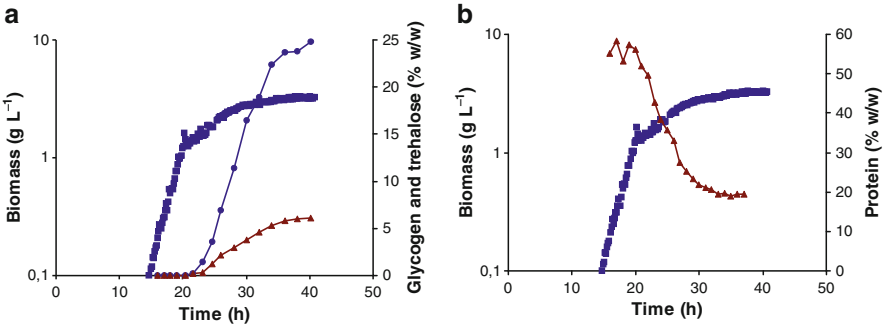

Fig. 3.3 Anaerobic batch cultivation of *S. cerevisiae*. After about 20 h the nitrogen source (NH_3) is exhausted and nitrogen limitation sets in. (**a**) The biomass concentration and the cellular content of the storage carbohydrates trehalose and glycogen. Until about 20 h the biomass grows exponentially. After 20 h the biomass concentration increases further until the glucose is exhausted. The increase is due to formation of glycogen and trehalose which accumulate to, respectively, 25 and 6 wt% of the dry cell mass. (**b**) The cellular content of protein decreases from about 57–20 wt% as the biomass accumulates storage carbohydrates after 20 h fermentation time. The data are from Schulze (1995) and Schulze et al. (1996)

given rise to some discussion in the literature. Lange and Heijnen (2001) gives a detailed, statistical analysis of the experimental results.

As indicated in Table 3.2 the biomass composition depends on the growth conditions. This is further illustrated in Fig. 3.3, which shows results of an anaerobic yeast fermentation carried out in a batch reactor where nitrogen limitation sets in at 20 h after the start of the fermentation. The cells cannot divide when the nitrogen source is used up, but they can still accumulate storage carbohydrates by polymerization of the substrate, glucose. Consequently the biomass concentration keeps increasing until all the glucose is used up. Assuming that no "active", i.e., N-containing biomass is synthesized after depletion of the N-source, the original cells just become bloated with glycogen ($CH_{1.67}O_{0.83}$) and some trehalose ($CH_{1.78}O_{0.89}$). After 40 h, the biomass contains 25 wt% glycogen and 6 wt% trehalose. At the end of the batch fermentation the formula weight of X is 24.57 gL^{-1} and its composition has changed from (3.19) to

$$X = CH_{1.62}O_{0.52}N_{0.155}S_{0.0017}P_{0.012} \tag{3.21}$$

Accumulation of storage carbon compounds in prokaryotes may amount to 70–80% of the total cell weight. A typical example is the accumulation of polyhydroxybutyrate (PHB) in *Ralstonia eutropha* (Lee and Choi 2001) when nitrogen, phosphate, or some other nutrient needed for growth of an active cell is denied to the culture. In these extreme cases the biomass composition approaches that of the storage polymer, e.g., $CH_{1.5}O_{0.5}$ for PHB. On the web page of the company Metabolix, a leader in production of polyhydroxy alkalonates, one obtains information on the current technical and economical status of PHB.

3.3 Black Box Stoichiometries

Equation (3.15) is an attempt to represent all the chemical reactions by which the substrates are converted to biomass and metabolic products by a single chemical equation, a so-called Black Box model. As discussed in the introduction to this chapter, this is an immense simplification since all the biochemical reactions responsible for the overall conversion of substrates to metabolic products and biomass are lumped into a single overall reaction. For certain biological systems the yield coefficients may, however, be constant, even for growth at different growth conditions. Thus, Fig. 3.4 shows the rates of production of ethanol (e), CO_2 (c), biomass (x), and glycerol (g) in a continuous steady- state anaerobic cultivation of *S. cerevisiae* as functions of the rate of consumption of glucose (s), the limiting substrate in all the experiments. A vertical line through any point $(-q_sV)$ on the abscissa will give the amount of products synthesized per hour in the reactor of volume V at the dilution rate which corresponds to $(-q_sV)$. Increasing values of $(-q_sV)$ corresponds to increasing values of the dilution rate $D = v/V$. The four lines very nearly intersect at the origin of the diagram, and by regression the slopes are calculated to have the following values (all in C-mole per C-mole glucose):

$$\frac{q_eV}{-q_sV} = Y_{se} = 0.510; \quad Y_{sc} = 0.275; \quad Y_{sx} = 0.137; \quad Y_{sg} = 0.077. \tag{3.22}$$

Consequently, the stoichiometry is

$$-\mathrm{CH_2O} + 0.510\mathrm{CH_3O_{1/2}} + 0.275\mathrm{CO_2} + 0.137X + 0.077\mathrm{CH_{8/3}O} = 0. \tag{3.23}$$

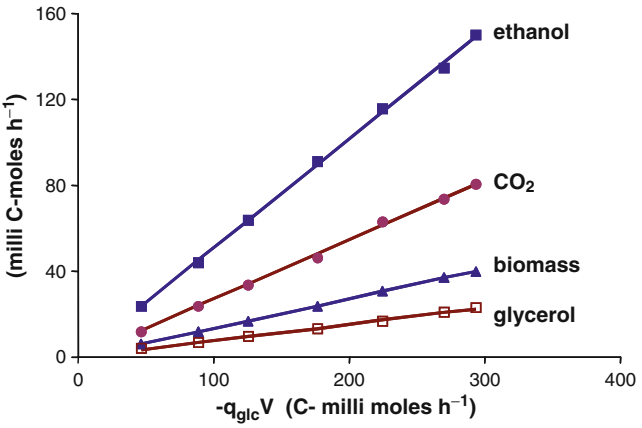

Fig. 3.4 Anaerobic glucose-limited continuous culture of *S. cerevisiae*. Production rate as a function of glucose consumption rate at steady state: total ethanol (liquid and gaseous) (*closed squares*); CO_2 (*closed circles*); biomass (*closed triangles*); glycerol (*open squares*). The lines are calculated by linear regression. The data are adapted from Duboc (1997)

Since $Y_{se} + Y_{sc} + Y_{sg} + Y_{sx} = 0.999$ all significant carbon- containing compounds are accounted for. Except for small amounts of S, P, and minerals Duboc (1997) determined the following biomass formula:

$$X = CH_{1.74}O_{0.60}N_{0.12} \tag{3.24}$$

Only the carbon-containing compounds are included in (3.23). Since no N-containing metabolic products are formed, the nitrogen from the feed appears only in the biomass. Hence the stoichiometric coefficient Y_{sn} is easily found. Thus, in the experiments of Duboc (1997) the nitrogen source was NH_3, and $Y_{sn} = 0.12 \times Y_{sx}$ mol NH_3 (C-mol glucose)$^{-1}$ with the biomass composition of (3.24). The yield coefficient of H_2O, Y_{sw}, is not included either. It can be found from an O or an H balance (in mole H_2O per C-mole glucose):

$$Y_{sw} = 1 - \tfrac{1}{2} \times 0.510 - 2 \times 0.275 - 0.6 \times 0.137 - 0.077 = 0.0358,$$

$$Y_{sw} = 0.5\,(2 + 3 \times 0.0164 - 3 \times 0.510 - 1.8 \times 0.137 - \tfrac{8}{3} \times 0.077) = 0.0377.$$

The two values are identical to within the experimental error. As mentioned earlier, the small amount of water produced by the overall reaction (3.23) has no perceptible influence on the concentration of the reactants. Thus, complete conversion of 1 C-mole glucose = 30 g glucose per liter medium leads to formation of 0.04 mole H_2O, a negligible amount compared to the 55 moles of water initially present per liter medium.

From (3.23), the yield coefficients on biomass produced are easily obtained using (3.14) (on a C-mole per C-mole biomass basis):

$$Y_{xs} = Y_{sx}^{-1} = 7.30; \quad Y_{xe} = Y_{se}Y_{xs} = 3.72. \tag{3.25}$$

Note 3.2 *How to treat ions in the black box model.* Unless otherwise stated the stoichiometries discussed in this book are written with undissociated substrates and reactants, but the stoichiometry could easily be extended to consider charged compounds. Hereby, one would introduce an additional balance, namely the overall charge, but at the same time an additional compound, namely protons, will appear. In reaction (3.15) and in the specific example of reaction (3.23) the nitrogen source (NH_3) is likely to be almost completely protonated at the usual medium pH of 5.5–6 in a yeast cultivation since pK_a is 9.25 for the acid NH_4^+. The ammonium ion is transported across the cell membrane by an active, ATP-consuming mechanism (see Sect. 7.7) and delivered to the cytosol of the cell. The pH of the cytosol is close to neutral and again the dissociation of NH_4^+ is quite small. Nitrogen is, however, incorporated into the cell mass as NH_3, and with this drain of NH_3 away from the equilibrium all the protons of NH_4^+ are liberated and transported back to the medium.

This can be used to determine the specific growth rate $r_x = \mu$, (3.13). In a stoichiometry such as (3.23) with a negligible production of organic acids $q_x = \mu x$ is nearly proportional to the volumetric rate of proton production. Now the volumetric rate of biomass production is calculated by titration of the medium with a concentrated (2–5 M to avoid dilution of

the reactants) KOH or NaOH solution to the fixed pH of the fermentation: $q_x = q_{H^+} \times Y_{nx} (= q_{H^+} \times (0.12)^{-1}$ for the biomass of (3.24)). Finally r_x is determined based on the measured biomass concentration x. Using a separate feed of NH_3 rather than the commonly applied mixed feed containing $(NH_4)_2SO_4$ or some other ammonium salt, one may if desired avoid the high cation concentration of Na^+ or K^+ which is a side effect of titration with the strong bases.

At the end of this section we shall again emphasize that any given stoichiometry such as reaction (3.23) is true only for steady-state operation and usually only for a given set of environmental conditions (pH, T, substrate concentrations). The substrate concentrations s_i in the bioreactor are time independent, and by definition equal to the effluent concentrations in the "ideal" steady state, continuous tank bioreactor – and in no other situation. Since the value of s_i depends on the input variable D, in a fashion to be discussed in Chap. 7, it is very likely that a change in dilution rate leads to a different stoichiometry since the flux of carbon may be distributed differently in the many pathways of the metabolic network. The situation illustrated in Fig. 3.4 is, indeed, very rare. Here, the stoichiometry remains unchanged over the wide range of dilution rates ($0.05 < D < 0.33$ h^{-1}), which corresponds to the substrate utilization rates 0.047 to 0.292 C-moles glucose h^{-1}. The change in stoichiometry around D_{crit} in the aerobic yeast fermentation schematically shown in Fig. 3.2 is a much more typical situation. When D increases above D_{crit} the yield coefficient Y_{se} jumps from virtually zero to a value much closer to the yield coefficient of the anaerobic yeast fermentation given in reaction (3.23) while Y_{sx} decreases rapidly. A complete change in stoichiometry when a "secondary" growth substrate such as NH_3 has been depleted has also been illustrated in Fig. 3.3 in connection with changes in the biomass composition.

3.4 Degree of Reduction Balances

All carbon-containing substrates can be oxidized to CO_2, and relative to this end product of biochemical reactions the substrates and the carbon-containing metabolic products are in a reduced state. A particular route through the metabolic network of a microorganism will convert the substrate, i.e., the input to the pathway, to a product that may be reduced or oxidized relative to the substrate. The pathways diagrams of Chap. 2 provide a great many examples of biochemical reactions that may be part of a pathway or may constitute a whole pathway.

$$-C_6H_{12}O_6 + 2CH_3COCOOH + 2NADH = 0 (\text{glycolysis of glucose to pyruvic acid})$$

$$-C_6H_{12}O_6 + 2CH_3CHOHCOOH = 0((2.8), \text{Lactic acid from glucose})$$

$$-C_6H_{12}O_6 + 2CH_3COOH + 2CO_2 + 4NADH = 0 (\text{Glucose to acetic acid})$$

$$-C_6H_{12}O_6 + CH_3COOH + C_2H_5OH + 2HCOOH = 0(\text{Mixed acid fermentation})$$

$$-C_6H_{12}O_6 - NADH + 2(CH_2OH)_2CHOH = 0((2.14), \text{Glucose to glycerol}) \quad (3.26)$$

$$-C_6H_{12}O_6 + 2C_2H_5OH + 2CO_2 = 0((2.12), \text{Glucose to ethanol})$$

$$-2CH_3COCOOH + 6CO_2 + 8NADH + 2FADH_2 = 0(\text{TCA cycle}, (2.16))$$

$$-C_6H_{12}O_6 + 6CO_2 + 12NADPH = 0((2.21), \text{glucose degradation, PP pathway})$$

$$-2NADH + O_2 = 0(\text{oxidative phosphorylation}, (2.18))$$

The second, fourth, and sixth example in (3.26) shows how redox from the substrate is distributed among the metabolic products. This is called *Metabolite Balancing*.

In the other examples the redox cofactors introduced in Sect. 2.2.1 are involved.

The examples do not include the oxidized form of the redox cofactors, and the production or consumption of energy-carrying compounds (ATP or GTP) has also been omitted in order to focus on the redox balancing of the reactions. Energy balancing is first used in Chap. 5.

All the results in (3.26) were obtained by consultation of the metabolic pathways of Sect. 2.2. Very simple pathways have been chosen as examples, and the reader will have no difficulty in setting up the correct metabolite balances and to add (the correct) redox cofactors where needed.

It is, however, of considerable value to develop a general method by which the redox content of the substrate(s) and the product(s) can be calculated. Hereby the correct number of redox cofactors can be added to the stoichiometric equation in order to satisfy the demand that *in any pathway from a set of substrates to a set of products redox is neither produced nor consumed*.

The methodology described in the following has been applied in different versions by different authors. It was probably first proposed by Erickson et al. (1978), but was very effectively expanded and used in the seminal text by Roels (1983). The following steps are made:

1. Define a redox-neutral compound for each element of interest.
2. We choose H_2O, CO_2, NH_3, H_2SO_4, and H_3PO_4 as the neutral compounds corresponding to the elements O, C, N, S, and P. With this set of neutral compounds, and with a *unit of redox defined as* $H = 1$ one obtains the following redox levels of the five listed elements:

$$O = -2, \quad C = 4, \quad N = -3, \quad S = 6, \quad P = 5 \quad (3.27)$$

3. Now the redox level of any reactant in a biochemical reaction can be calculated.

Examples

(a) Glucose: $6 \times 4 + 12 \times 1 + 6 \times (-2) = 24$
(b) Ethanol: $2 \times 4 + 6 \times 1 + 1 \times (-2) = 12$
(c) Acetic acid (HAc): $2 \times (4 + 2 \times 1 + 1 \times (-2)) = 8$
(d) Lactic acid (HLac): $3 \times (4 + 2 \times 1 + 1 \times (-2) = 12$
(e) Glycerol: $3 \times 4 + 8 \times 1 + 3 \times (-2) = 14$
(f) Lysine (see Table 2.6): $6 \times 4 + 14 \times 1 + 2 \times (-3) + 2 \times (-2) = 28$

4. With this information on the redox level of reactants and products it is easy to redox balance each of the reactions in (3.26):
Examples

(a) Mixed acid fermentation: $(-24) + 8 + 12 + 2 \times 2 = 0$
(b) Glucose to ethanol: $(-24) + 2 \times 12 + 2 \times 0 = 0$
(c) Glucose to HAc: $(-24) + 2 \times 8 + 2 \times 0 + 4 \times 2 = 0$
(d) Glucose to lysine: $(-24) + 28 - 2 \times 2 = 0$

In examples (b) and (c) 1/3 of the carbon in the glucose is lost in the decarboxylation of pyruvate to either acetaldehyde or to AcCoA (see Fig. 2.5). It is important to remember this loss of carbon to CO_2 also when calculating the redox balance. When glucose is converted to lysine all six carbon atoms in glucose are retained in lysine (see the net reaction (2.25)). The four-carbon amino acid aspartate is produced from pyruvate *via* uptake of CO_2 (Fig. 2.7, reaction 10), and CO_2 is liberated in the final step of the lysine synthesis pathway. Hence, in the synthesis of lysine from glucose 4 redox units are gained. As discussed in Sect. 2.2.1 all the redox cofactors correspond to "H_2," and consequently in Example (d) two redox cofactor molecules are used while in (c) four cofactor molecules = 4 NADH are produced. In example (c), we know from Chap. 2 that the cofactor involved in the catabolic reaction of glucose to acetic acid is NADH. *This is not so in general, and to write a proper black-box model for the pathway one must find the correct redox cofactors involved from the net or from biochemistry textbooks.*

The simultaneous appearance of several redox cofactors in a long pathway, e.g., from glucose to lysine, may seem quite confusing to the nonspecialist. Thus, in fact 4 NADPH are used in lysine synthesis from glucose since the aspartate in (2.25) is obtained by transamination of oxalic acid where one NADPH is used. Consequently the two redox cofactors lost in Example (d) result as 2 NADH produced when glucose is converted to two pyruvate molecules in glycolysis – 4 NADPH lost when the two pyruvate are used to synthesize lysine. The two NADH are oxidized to NAD^+ in oxidative phosphorylation (the last of the reactions in (3.26)) while the 4 NADPH must be produced by reaction 8.

In a simplified analysis of pathway networks it does, however, not matter which cofactor is used, since they all stem from the carbon and energy source, usually glucose. One needs one glucose molecule to produce 12 reduced-form redox cofactors. In Chap. 5 where biomass formation is represented by a single reaction we learnt in Chap. 2 that much NADPH is consumed while an even larger amount of NADH is produced. In order to work with the same cofactor in all the pathway

reactions one simply uses "NADH" everywhere in the approximate metabolic models that lead to stoichiometric coefficients in an overall Black Box model. In a more detailed model, for example aiming at finding the smallest possible amount of glucose to make lysine, one must keep track of each of the redox cofactors, unless the organism has a transhydrogenase activity (2.4). If the two NADH cofactors produced in lysine synthesis from glucose could be converted to NADPH an increase in "theoretical yield" of lysine could be obtained (see Problem 5.3).

The different number of carbon atoms in glucose and ethanol makes it a little difficult to appreciate which of the compounds is the most reduced. When each carbon containing compound is written on the basis of one carbon (glucose CH_2O, and ethanol $CH_3O_{0.5}$) it becomes obvious that ethanol (degree of reduction of 6 per carbon) is more reduced than glucose (degree of reduction of 4 per carbon). The reason why the conversion of one C-mole glucose to one C-mole of ethanol is not accompanied by the loss of one NADH is that the carbon yield of ethanol is only 2/3: $CH_2O \rightarrow 2/3\ CH_3O_{0.5} + 1/3\ CO_2$ where CO_2 is redox neutral. When, in Chap. 5 a metabolic model is set up with the constraint that the redox balance and the ATP balance must close for the ensemble of all the pathways that make up the model it is, in fact, much easier to write each individual pathway based on reactants and products scaled to one carbon atom. Now the carbon balance closes for all the pathways as in (3.18), and one avoids the mistakes caused by the splitting up of a molecule into two (glucose to 2 pyruvate in the first equation of (3.26) which can be reformulated to $-CH_2O + CH_{4/3}O + 1/3$ NADH $(+\ 1/3$ ATP$) = 0$). When the compounds are written per C-atom, glucose, HLac and HAc all have the formula CH_2O and a degree of reduction $= 4$. This should not give rise to ambiguities, and if needed one may write the name of the compound after the formula.

Roels (1983) systematically worked with *the degree of reduction per carbon atom in the compound*, and in most of the text we shall use his concept which is also very useful in the calculation of heats of reaction and free energy of reaction (see Chap. 4).

Each of the reactions in (3.26) can easily be rewritten into this form.

We shall use the letter κ for the degree of reduction of a compound per C-mol (or C-atom). Thus κ is, respectively, 4, 14/3, and 6 for glucose, glycerol, and ethanol.

For a "standard" biomass, (3.20), $CH_{1.8}O_{0.5}N_{0.2}$, $\kappa = 4.20$. Normal active biomass always has a somewhat higher degree of reduction than that of the substrate glucose ($\kappa = 4$). Storage carbohydrates such as glycogen ($CH_{1.67}O_{0.83}$) have $\kappa = 4$ while poly-hydroxy butyrate PHB ($CH_{1.5}O_{0.5}$) has $\kappa = 4.5$. Thus, if the organism accumulates glycogen its average degree of reduction is smaller than 4.2, but it is higher than 4.2 if it accumulates the strongly reduced poly-hydoxy alkanoates.

Table 4.3 collects the degree of reduction for a large number of compounds, but it uses a slightly different definition of κ which is based on N_2 as the redox neutral N-compound.

Example 3.1 *Anaerobic yeast fermentation.* We shall examine the stoichiometry of reaction (3.23) a little closer. The pathway leading from glucose to ethanol is redox neutral, (3.26) reaction 6. Production of biomass of composition (3.24) ($\kappa = 4.18$) is, however, not redox neutral since carbon is lost in connection with formation of precursor metabolites (Table 2.2) needed for biomass synthesis, e.g., ribose-5-P, a precursor for synthesis of nucleic acids, and

acetyl-CoA, a precursor for lipid biosynthesis. In both cases reduced cofactors are formed. Conversion of some glucose to the more reduced glycerol counterbalances this biomass-related production of redox equivalents. Using the stoichiometry of reaction (3.23) one obtains the following redox balance:

$$\begin{aligned} &-(4\times 1+0\times 0.0164)+(6\times 0.510+0\times 0.275+4.67\times 0.077+4.18\times 0.137)\\ &=-0.0078\approx 0 \end{aligned} \tag{1}$$

The redox balance (1) is very nearly satisfied. Previously it was shown that the carbon balance is satisfied, and the combined tests confirm to a high degree of certainty that not only have the right compounds of the net reaction been found, but they are also determined in the right ratios.

This result is unusually good, a testimony to the exceptional care with which Duboc conducted his experiments (see, e.g., Problem 3.1). With state-of-the-art laboratory bioreactors and analytical tools (GC, MIMS, HPLC) a carefully designed experiment is expected to account for 98–99% of the carbon, and the degree of reduction balance should close to within 95%, unless the experimental data are highly correlated (see Sect. 3.6 and Chap. 7).

Example 3.2 *Aerobic growth with ammonia as nitrogen source.* Let the stoichiometry of a general, aerobic process with one product P be

$$-S-Y_{\mathrm{sn}}\mathrm{NH_3}-Y_{\mathrm{so}}\mathrm{O_2}+Y_{\mathrm{sx}}X+Y_{\mathrm{sc}}\mathrm{CO_2}+Y_{\mathrm{sp}}P=0 \tag{1}$$

where S is the carbon- and energy substrate $\mathrm{CH}_{s_1}\mathrm{O}_{s_2}$ with degree of reduction κ_s, X is biomass $\mathrm{CH}_{x_1}\mathrm{O}_{x_2}\mathrm{N}_{x_3}$ with degree of reduction κ_x, and P is a product $\mathrm{CH}_{p_1}\mathrm{O}_{p_2}$ with degree of reduction κ_p. With the overall reaction stoichiometry of (1) the carbon, nitrogen, and degree of reduction balances are as follows:

$$Y_{\mathrm{sx}}+Y_{\mathrm{sc}}+Y_{\mathrm{sp}}=1, \tag{2}$$

$$Y_{\mathrm{sn}}=x_3Y_{\mathrm{sx}}, \tag{3}$$

$$\kappa_{\mathrm{x}}Y_{\mathrm{sx}}+\kappa_{\mathrm{p}}Y_{\mathrm{sp}}-\kappa_{\mathrm{s}}-(-4)Y_{\mathrm{so}}=0. \tag{4}$$

Equations (2) and (4) are solved to obtain Y_{sx} and Y_{sp} in terms of Y_{sc} and Y_{so}

$$Y_{\mathrm{sx}}=\frac{(4-\kappa_{\mathrm{p}}\mathrm{RQ})\,Y_{\mathrm{so}}+\kappa_{\mathrm{p}}-\kappa_{\mathrm{s}}}{\kappa_{\mathrm{p}}-\kappa_{\mathrm{x}}}, \tag{5}$$

$$Y_{\mathrm{sp}}=\frac{(\kappa_{\mathrm{x}}\mathrm{RQ}-4)\,Y_{\mathrm{so}}+\kappa_{\mathrm{s}}-\kappa_{\mathrm{x}}}{\kappa_{\mathrm{p}}-\kappa_{\mathrm{x}}}. \tag{6}$$

The respiratory quotient $\mathrm{RQ}=Y_{\mathrm{oc}}$ is given by (3.16)

$$\mathrm{RQ}=\frac{Y_{\mathrm{sc}}}{Y_{\mathrm{so}}} \tag{7}$$

Let the substrate be glucose and the product ethanol. For a standard biomass with $\kappa_x = 4.20$:

$$Y_{sx} = \frac{(4 - 6\text{RQ})Y_{so} + 2}{1.80}; \quad Y_{sp} = \frac{(4.20\text{RQ} - 4)Y_{so} - 0.20}{1.80} \tag{8}$$

In industrial yeast fermentation both Y_{so} and RQ are usually monitored more or less continuously, and (8) can be used to calculate the biomass yield on glucose and the ethanol yield on glucose. Thus for RQ = 3 and $Y_{so} = 0.1$ mole oxygen per C-mole glucose we find

- $Y_{sx} = 0.333$ C-mole biomass per C-mole glucose
- $Y_{sp} = 0.367$ C-mole ethanol per C-mole glucose

For RQ = 1 and $Y_{so} = 1$, one obtains $Y_{sx} = Y_{sp} = 0$, which corresponds to complete combustion of glucose to carbon dioxide according to:

$$-CH_2O - O_2 + CO_2 + H_2O = 0 \tag{9}$$

At these conditions neither biomass nor ethanol is produced.

Example 3.3 *Anaerobic growth of yeast with NH_3 as nitrogen source and ethanol as the product.* The stoichiometry of the overall reaction for anaerobic growth of *S. cerevisiae* with ammonia as the sole nitrogen source was given in (3.23). The degree of reduction balance yields

$$-4 + 4.20\, Y_{sx} + 6\, Y_{sp} = 0 \tag{1}$$

for a standard biomass with $\kappa_x = 4.20$. Typically for yeast fermentation, $Y_{sx} = 0.12$ g (g glucose)$^{-1}$ or 0.15 C mole biomass (C-mole glucose)$^{-1}$. Consequently, the maximum expectable yield of ethanol on glucose is 0.56 C-mole (C-mole glucose)$^{-1}$ even if no glycerol is produced. The bacterium *Zymomonas mobilis* also produces ethanol, and the biomass yield is lower than for yeast fermentation. Typically Y_{sx} is 0.05 g (g glucose)$^{-1}$ or 0.06 C mole (C-mole glucose)$^{-1}$. With the lower biomass yield a higher ethanol yield of $Y_{sp} = 0.624$ C-mole ethanol (C-mole glucose)$^{-1}$ or 94% of the theoretical yield is obtained. The bacterium is consequently a more efficient producer of ethanol than yeast – but yeast (*S. cerevisiae*) has other advantages, e. g., its extreme tolerance for ethanol as discussed in Sect. 2.1.1.

Example 3.4 *Biomass production from natural gas.* The bacterium *Methylococcus capsulatus* grows aerobically with methane or methanol as the sole carbon and energy source. The catabolic pathways are different from those shown in Chap. 2 – in fact few organisms are able to grow on C-1 carbon compounds, see Goldberg and Rokem (1991). The resulting biomass is an excellent protein source, which can be used directly as feed for domestic animals and as feed for fish, e.g., salmon. The protein content of the biomass can amount to 70% of the dry weight (DW). In hydrolyzed form the protein has considerable potential for use in human diets, as a daily supplement in school meals in poor countries or in aid packages sent to catastrophe-stricken countries. The nucleic acids are broken down much faster than the proteins in a short, high temperature treatment of the spray-dried biomass, and consequently long-term negative effects caused by the nucleic acids are avoided when the protein is used for human consumption.

Single-Cell Protein has been produced industrially since the 1950s. The population increase after WW 2 prompted one of the recurrent food crises, and SCP plants were erected in the Soviet Union and in several Western countries, notably the huge Billingham (UK) plant by ICI. Many different substrates were used, oil residues (very dubious!), molasses, ethanol and natural gas, or methanol. The two last substrates are by far the best since infection of the fermentation and contamination of the product is unlikely. The first surge of SCP production was stopped by the oil crisis of the 1970s, except in the Soviet Union where the desire for self sufficiency in animal feed kept several plants alive until the dissolution of the Union. Since the 1990s the rapidly disappearing source of animal protein, fishmeal, has renewed the interest in SCP which (as all microbial protein) has an amino acid-profile that is essentially equal to that of fish (and humans). Norferm, a subsidiary of the Norwegian oil company Statoil, erected an SCP plant of capacity 9,000 ton/year at Tjelbergodden in the vicinity of Trondheim. At the industrial site a methanol plant of capacity about 2,300 ton/day was erected and supplied with CH_4 cleaned to more than 99% from natural gas, a byproduct from the Norwegian oil fields in the North Atlantic. It was chosen to supply the SCP plant with the 99% CH_4 rather than with a small fraction (2.7%) of the methanol produced at the site. The SCP product was used as an excellent feed for salmon in the fish-farms in Western Norway, and the added value of using part of the raw material for this purpose rather than for methanol was substantial. In 2009, high quality fish meal, obligatory for feed of carnivorous fish such as salmon, has become virtually unavailable, and the price has skyrocketed. Consequently, the demand for a clean, industrially produced substitute for fish meal has exploded, and in countries around the world with underused natural gas resources (China, Trinidad & Tobago, Brunei, Libya, and the Emirates) plans for building SCP factories are emerging. Technically speaking, methanol is the simpler substrate for SCP production, and the very large installed capacity for methanol production in a waning market (Trinidad & Tobago produces 20,000 ton methanol/day!) should give methanol an advantage over CH_4 in new plants.

Economic projections show that SCP can substitute a substantial fraction of the demand for high-grade animal protein, which in Europe alone is more than 10^6 tons per year.

With standard biomass ($\kappa_x = 4.20$) and $Y_{CH4x} = 0.8\text{g (g CH}_4)^{-1}$ one obtains:

$$-CH_4 - 1.454O_2 + 0.520X + 0.480CO_2 = 0 \tag{1}$$

If the same C-mole yield of biomass can be obtained from methanol then

$$-CH_3OH - 0.954O_2 + 0.520X + 0.480CO_2 = 0 \tag{2}$$

As expected, half a mole of O_2 is used to oxidize methane to methanol and consequently Y_{so} in (2) is 0.5 smaller than Y_{so} in (1). In reality, the CO_2 production per C-mole X is smaller in (2) than in (1) due to better utilization of the methanol, and this gives a higher biomass yield per C-mole carbon source, but in this example we shall use (2) to illustrate how the steady-state oxygen uptake rate is calculated based on (3.10).

Consider a 10 L continuous bioreactor fed with 600 L dry air h^{-1} at atmospheric pressure and 45°C. The methanol concentration in the reactor is 1 g L^{-1} and the reactor temperature is 45°C.

The volumetric composition of the inlet gas is 79% N_2 (+Ar) and 21% O_2.

The volumetric composition of the O_2 and CO_2 in the dry outlet gas is 18.0% O_2 and 1.70% CO_2.

Based on these data the rates of production of O_2 (negative) and CO_2 can be calculated.

First we find the outlet gas flow v_g relative to the inlet gas flow v_{gf}.

In 100 L of inlet gas 79 L is inert N_2 (+Ar). In 100 L outlet gas the inert content is 100 – 18 – 1.7 = 80.3 L. Hence $v_g < v_{gf}$ (O_2 is consumed and the CO_2 does not add up to the loss of O_2).

$v_g/v_{gf} = 79/80.3 = 0.9838$, and per 10 L reactor volume $600 \times (0.21 - 0.18 \times 0.9838) = 19.75$ L O_2 has been consumed per hour. $600 \times 0.017 \times 0.9838 = 10.03$ L h^{-1} CO_2 has been produced.

At 45°C and atmospheric pressure, 19.75 L $O_2 = 19.75/(318 \times 0.082) = 0.757$ mol O_2.

Consequently $(-q_o) = 0.757/10 = 0.0757$ mol O_2 L^{-1} reactor h^{-1}.

Correspondingly $q_c = 10.03/(318 \times 0.082)/10 = 0.0385$ mol CO_2 L^{-1} h^{-1}.

It is noted that $q_c/(-q_o) = Y_{oc} = RQ = 0.5086$ which is close to the value 0.480/0.954 = 0.503 obtained from the stoichiometry (2). Hence the stoichiometry of (2) is validated and

$\boldsymbol{q_x} = 0.520/0.954 \times 0.0757 = 0.0413$ C-mole biomass L^{-1} h^{-1} = 1.02 g X L^{-1} h^{-1} for standard biomass with $M_x = 24.6$ g C-mole^{-1}.

Here, the oxygen uptake rate has been calculated directly from a mass balance for oxygen between the inlet and the outlet of the reactor. The right hand expression in (3.10), i.e. (3.7) can now be used to find an estimate for the mass transfer coefficient k_la.

Nordkvist et al. (2007) used the following correlation for O_2 saturation concentration in H_2O at 1 bar partial pressure of O_2 (i.e., total pressure $P = 1$ bar + P_{sat} (H_2O at T):

$$s_{O_2}{}^* = 0.0270 \ \exp(1,142/T) \text{ mol } O_2L^{-1} \tag{3}$$

At 45°C, the saturated vapor pressure of H_2O is 71.88 mmHg = 71.88/760 = 0.0946 bar.

From (3) $s_{O_2}{}^* = 0.977$ mmolL^{-1} at 1 bar partial pressure of O_2. Consequently, at atmospheric pressure (1 bar total pressure) $s_{O_2}{}^* = 0.977/(1 + 0.0946) = 0.8925$ mmolL^{-1}.

At the inlet conditions to the reactor the partial pressure of $O_2 = \pi_{O_2} = 0.21$bar.

Thus, if π_{O_2} in all the gas bubbles in the reactor is equal to that in the inlet gas, and the medium concentration of oxygen is $s_{O_2} = 20\mu$M then (3.7) gives

$$\begin{aligned} -q_o &= 75.7 \text{ mmol } O_2L^{-1}h^{-1} \\ &= k_la(0.21 \ \times \ 0.8925 - 0.02) \text{ mmol } O_2L^{-1}h^{-1} \rightarrow k_la = 452\,h^{-1}. \end{aligned} \tag{4}$$

This is a conservative estimate of k_la since the partial pressure of O_2 in the gas bubbles must lie somewhere between 0.18 (based on the outlet conditions) and 0.21. To establish the correct value of k_la one must assume a model for the rate of change of π_{O_2} in the gas bubbles between the inlet and outlet of the reactor. This subject is discussed in Problem 3.1 and in Chap. 10. If an average value of 0.195 is assumed for π_{O_2} (reasonable for relatively small changes in π_{O_2} between inlet and outlet) one would find $k_la = 491$ h^{-1}. A k_la-value of about 500 h^{-1} can easily be obtained in a well-stirred laboratory bioreactor (and also in an industrial bioreactor – see Sect. 11.2). In a final calculation, we shall study what happens if the outlet gas from the bioreactor is not meticulously dried before the composition is measured.

In that case the outlet gas flow from 600 L h^{-1} dry inlet gas flow would be (600 – oxygen consumed + CO_2 produced + the water vapor evaporated into the gas) L h^{-1}.

If one assumes that equilibrium is reached for water between the gas and the liquid phase, the total outlet gas flow would be: $(600 - 19.75 + 10.03 + 0.0946\ v_g)$ L $h^{-1} = (590.28 + 0.0946\ v_g)$ L $h^{-1} \rightarrow v_g = 651.95$ L h^{-1}.

The mole fraction (= volume fraction) of O_2 in v_g would be $(0.21 \times 600 - 19.75)/652 = 0.1630$.

Until now nothing has gone wrong. But *if* one neglects the water evaporated into the gas by its passage of the reactor and still assumes that the outlet gas consists only of inert + O_2 + CO_2, i.e., that $v_g = 590.28$ L h^{-1} ($v_g/v_{gf} = 0.9838$), then one would predict that $600 \times (0.21 - 0.9838 \times 0.1630) = 29.78$ L O_2 h^{-1} had been consumed.

This would lead to an overestimation of $(-q_{O_2})$ by a factor of 29.78/19.75 = 1.50, clearly an unacceptable result.

Since one cannot predict how far toward equilibrium saturation of the gas phase with water one has reached, there is no way to tell the water mole fraction of v_g.

The only sensible conclusion is that *the outlet gas must be thoroughly dried before its composition is measured*. This is easily done by adsorbents or by using the water vapor permeable "Nafion®" tubing between the bioreactor and the measurement point.

The degree of reduction balance can be written as a linear combination of the elemental balances for oxygen and hydrogen. It is therefore clear that the reduction balance does not introduce an additional balance to the system. When all the elemental balances are satisfied then the degree of reduction balance automatically closes. As discussed earlier the use of all the elemental balances is in practice prevented by lack of information on the yield coefficient for water, which cannot be experimentally determined, and it is therefore advantageous to use the degree of reduction balance together with the carbon and nitrogen balances.

3.4.1 Consistency Test of Experimental Data

A major reason for applying both mass and redox balances to experimental data is to check the consistency of the data. While the usefulness of element balances is fairly obvious, the redox balance tells whether the right compounds are included in the Black Box model, and it gives indications of the nature of a missing compound.

Experiments can go wrong for many reasons of which some are listed below.

- Some of the products may go undetected. It was not suspected that they would appear.
- Products thought to remain in the liquid phase are partly stripped to the gas phase.
- The measurement instruments are wrongly calibrated, or they suddenly malfunction.

It may seem strange that a metabolic product is unexpectedly being produced, but the complexity of the metabolic network of microorganisms makes it quite

possible to miss a product unless the biochemical potential of the particular organism has been thoroughly investigated. Thus, the unexpected conversion to gluconic acid of a large fraction of the glucose used as feed in penicillin production was for a long time puzzling (Nielsen et al. 1994). The appearance of oxalic acid at moderately high pH in citric acid fermentation (Example 3.6) can lead to a large economic loss. The example shows how the byproduct formation was discovered and how the *Aspergillus* strain can be improved by genetic engineering to avoid that the problem ever occurs.

Stripping of some ethanol (and of even lower boiling products) from anaerobic fermentations, sparged with N_2 to give a completely O_2 free environment, is a common cause of error in the mass balances. Even at a low liquid phase mole fraction ethanol has a high gas-phase mole fraction. A substantial loss of ethanol may result, especially at low D where the production rate is small while the rate of stripping is more or less independent of D. Refluxing the medium, even with $1 - 2°C$ cooling water is of little help since the heat transfer coefficient is small on the mostly dry gas-phase side of the heat exchanger. Feeding of substrate through the reflux condenser may be a practical way of avoiding this problem, since in that case a wet surface is present on the vapor side of the heat exchanger (Duboc and von Stockar 1998, see Problem 3.1).

Finally instruments, especially flow meters may give rise to systematic errors. When the gas flow to the laboratory bioreactor is low, e.g., 0.1 vvm (volume gas per volume medium per minute), calibration of flow meters can be difficult, and the rate of gas flow v_g is in error. Here a high accuracy of the instrument that determines the concentration of the gas-phase reactant is of course of no help.

Examples 3.5 and 3.6 illustrate how consistency tests may be of great help to check whether the data material is trustworthy.

These tests should clearly be made routinely after each experiment in the experimental program and not retrospectively when all the data have been collected and the experimental equipment is dismantled or is being used for other purposes.

Once the stoichiometric equation (3.15) has been established it will serve as basis for design of the process, and it might have catastrophic effects if the yield coefficients are wrong due to errors in the experimental data that were not discovered by a conscientious analysis of the data.

Example 3.5 *Consistency analysis of yeast fermentation.* One of the first high quality experimental investigations of continuous aerobic yeast cultivation was by von Meyenburg (1969) who worked in professor Fiechters group at ETH, Zürich. Many later papers have used the data, e.g., Bijkerk and Hall (1977), to set up structured kinetic models for aerobic yeast growth.

The data are shown in Fig. 3.5. The stirred tank bioreactor was operated as a chemostat, and the feed was 28 g L^{-1} sterile glucose solution with sufficient NH_3 (NH_4^+) and other substrates to make the culture glucose limited. At low values of D no ethanol is produced, and the biomass concentration is high and approximately constant at 14 g L^{-1}, except perhaps for a slight drop for the lowest D values. At these D values the metabolism is purely respiratory, and the yeast obtains sufficient ATP for growth by complete degradation of glucose to CO_2.

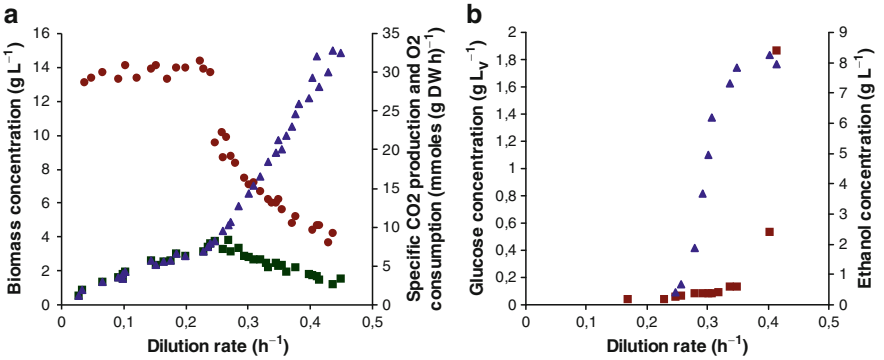

Fig. 3.5 Chemostat cultures of *S. cerevisiae* (von Meyenburg (1969)). (**a**) Data for the biomass concentration (*closed circles*), the specific oxygen uptake rate (*filled squares*), and the specific carbon dioxide formation rate (*filled triangles*). (**b**) Data for the glucose concentration (*filled squares*) and the ethanol concentration (*filled triangles*)

The critical dilution rate D_{crit} is in the vicinity of 0.25 h^{-1}, and above D_{crit} the yeast starts to produce ethanol as shown in Fig. 3.2 and explained in Sect. 2.2.5. Above D_{crit} the mode of fermentation is called respiro-fermentative. RQ increases rapidly, and Y_{sx} decreases.

A semi-quantitative model for the fermentation will be discussed in Example 7.3. Here we will analyze the stoichiometry for different D values, observe the sharp change of stoichiometry around D_{crit} and make a consistency test of the data.

A constant biomass composition $X = CH_{1.83}O_{0.56}N_{0.17}$ ($M_x = 25.17$ g C-mole^{-1}) with 8 wt.% ash is assumed for all D values. In a real situation this assumption must of course be checked.

The Black Box stoichiometry is taken to be:

$$\begin{aligned} &-CH_2O - Y_{sn}NH_3 - Y_{so}O_2 + Y_{sc}CO_2 + Y_{sp}CH_3O_{0.5} \\ &+ Y_{sw}H_2O + Y_{sx}CH_{1.83}O_{0.56}N_{0.17} = 0 \end{aligned} \tag{1}$$

Equation (1) combines one rate, $q_s = q_{glucose}$ and 6 yield coefficients. Glycerol does not appear in aerobic yeast fermentations. The elemental balances for C, H, O and N supply four constraints, and hence three rates must be experimentally determined to identify the system. The data shown in Fig. 3.5 can be used to find the rates of production of glucose, biomass, ethanol, CO_2 and O_2. Hence the system is overdetermined and we can make a consistency test of the data.

Since biomass is the only sink for the nitrogen feed Y_{sn} can be calculated based on Y_{sx}, but unless we measure q_{NH_3} there is no way to prove that $Y_{sn} = 0.17\ Y_{sx}$ or whether an unexpected N-containing compound is produced. It does not help to include q_{NH_3} in the set of measurements together with q_x, since in the Black Box model (1) the two rates are proportional and form a closed set, separate from the other measurements of rates.

Y_{sw} is – as mentioned earlier – uninteresting and probably it cannot be measured accurately enough to be of any value. Water is therefore excluded from the analysis, but at the same time one must drop one of the four elemental balances. However, with a carbon balance, a nitrogen balance and a degree of reduction balance the degrees of freedom is still 3, i.e., three rates must be experimentally determined to identify the system. Thus, when

water is excluded from the stoichiometry one yield coefficient disappears, but also one of the constraints cannot be used.

By excluding water and assuming that Y_{sn} is directly determined from Y_{sx} the remaining variables in the system are [Y_{so}, Y_{sc}, Y_{sp}, Y_{sx}] together with q_s. Two constraints, the carbon and the redox balances can be set up, and three out of the five rates q_o, q_x, q_c, q_p, and q_x must be used to identify the stoichiometry All five rates are available from Fig. 3.5. Three values of D are chosen for further studies, $D = 0.15\ \mathrm{h}^{-1}$ (or any $D < 0.25\ \mathrm{h}^{-1}$, at least within the accuracy of Fig. 3.5), $D = 0.30\ \mathrm{h}^{-1}$ and $D = 0.40\ \mathrm{h}^{-1}$.

$D < 0.25\ \mathrm{h}^{-1}$

At these dilution rates we have: $x = 14\ \mathrm{g\ L}^{-1}$, $s = p \approx 0$, $s_f = 28\ \mathrm{g\ L}^{-1}$, $x_f = 0$.

$$\begin{aligned} Y_{sx} &= \frac{14\ \mathrm{g/L} \times 0.92}{25.17(\mathrm{g/C-mole})} \frac{30(\mathrm{g/C-mole})}{28\ \mathrm{g/L}} \\ &= 0.548\ \mathrm{C-mole\ DW(C-mole\ glucose)}^{-1} \end{aligned} \tag{2}$$

From a carbon balance, we find:

$$Y_{sc} = 1 - Y_{sx} = 0.452\ \mathrm{mol\ CO_2(C-mole\ glucose)}^{-1} \tag{3}$$

and from a generalized degree of reduction balance

$$\begin{aligned} 4 - 4Y_{so} = 4.20Y_{sx} \Rightarrow Y_{so} &= \tfrac{1}{4}(4 - 4.20 \times 0.548) \\ &= 0.425\ \mathrm{mol\ O_2(C-mole\ glucose)}^{-1} \end{aligned} \tag{4}$$

With these values for Y_{sc} and Y_{so}, RQ is calculated to be 1.06, which corresponds well with the measured data for $(-q_0)$ and q_c in Fig. 3.5. For $D < 0.25\ \mathrm{h}^{-1}$ it is observed that r_o and r_c both increase linearly with D and the slope is 30.0 mmol CO_2 per gram DW = 0.03 $\times$ 25.13/0.92 = Y_{xc} = 0.82 mol of CO_2 per C mole of (ash-free) biomass, or

$$Y_{sc} = Y_{sx}Y_{xc} = 0.45\ \mathrm{mol\ CO_2(C-mole\ glucose)}^{-1} \tag{5}$$

This value is nearly the same as that found from the carbon balance in (3), where the calculation is based on measurements of glucose and biomass concentrations. Again it is concluded that there is a consistency in the experimental data. Observe that $(-r_o)$ and r_c are both larger than zero when $D = 0$. This is due to a consumption of glucose for maintenance purposes (see Sect. 5.2.1).

$D > 0.25\ \mathrm{h}^{-1}$

At the two dilution rates $D = 0.3$ and $0.4\ \mathrm{h}^{-1}$ we read the following approximate data on Fig. 3.5:

- $D = 0.3\ \mathrm{h}^{-1} : x = 7.1\ \mathrm{g\ L}^{-1}$ and $p = 4.2\ \mathrm{g\ L}^{-1}$
- $D = 0.4\ \mathrm{h}^{-1} : x = 4.4\ \mathrm{g\ L}^{-1}$ and $p = 8.3\ \mathrm{g\ L}^{-1}$

No attempt is made to smooth the biomass and the ethanol data, and the accuracy is not better than $0.1 - 0.2\ \mathrm{g\ L}^{-1}$.

Both r_c and r_o appear to be well approximated by linear functions in D. By regression the following linear relationships are determined

$$r_c = 116\,D - 20.4 \text{ mmol } CO_2(\text{g DW h})^{-1} \tag{6}$$

$$r_c = -29.1\,D + 15.3 \text{ mmol } O_2(\text{g DW h})^{-1} \tag{7}$$

The decreasing specific rate of oxygen consumption for $D > 0.25\ \text{h}^{-1}$ is not found in other studies where a constant value of $(-r_o)$ for $D > D_{crit}$ appears to fit the data better (see Example 7.3 for further discussion).

For $D = 0.3\ \text{h}^{-1}$ one obtains

$$\begin{aligned} -q_s &= (28 - 0.1) \times 0.3/30 = 0.279 \text{ C} - \text{mole } (\text{L} \times \text{h})^{-1}, \\ q_x &= \frac{7.1 \times 0.92}{25.17} \times 0.3 = 0.07785 \text{ C} - \text{mole } (\text{L} \times \text{h})^{-1}, \\ q_p &= \frac{4.2}{23} \times 0.3 = 0.0548 \text{ C} - \text{mole } (\text{L} \times \text{h})^{-1}, \\ \\ q_c &= 14.40 \times 7.1 \times 10^{-3} = 0.1022 \text{ mol } (\text{L} \times \text{h})^{-1}, \\ -q_o &= 6.57 \times 7.1 \times 10^{-3} = 0.0466 \text{ mol } (\text{L} \times \text{h})^{-1}. \end{aligned}$$

From these data the yield coefficients are calculated. The following table shows results for $D = 0.3\ \text{h}^{-1}$ and also for $D = 0.4\ \text{h}^{-1}$ (all in mole or C-mol per C-mol glucose)

D (h^{-1})	Y_{sx}	Y_{sp}	Y_{sc}	Y_{so}	Y_{sp1}	Y_{se}
0.3	0.279	0.196	0.366	0.167	0.159	0.355
0.4	0.175	0.394	0.312	0.044	0.119	0.513

A carbon balance shows that some carbon is missing in the products for both $D = 0.3$ and $0.4\ \text{h}^{-1}$. The yield coefficient of the missing carbon is shown in the column Y_{sp_1} of the table. A degree of reduction balance yields:

$$\begin{aligned} D = 0.3\,\text{h}^{-1} : &-4 + 4 \times 0.167 + 0.279 \times 4.20 + 0.196 \times 6 + 0.159\kappa_{p_1} = 0 \Rightarrow \kappa_{p_1} \\ &= 6.19 \end{aligned}$$

For $D = 0.4\ \text{h}^{-1}$: $\kappa_{p_1} = 6.09$. Thus, for both cases the degree of reduction for P_1 is close to 6. There is good reason to believe that P_1 is ethanol. The final column of the table shows $Y_{se} = Y_{sp} + Y_{sp_1}$. For the low dilution rate almost half the produced ethanol has been stripped off; for the highest dilution rate only 23%. A loss of carbon of this magnitude is of course unacceptable.

Bijkerk and Hall (1977) mention in their analysis of the von Meyenburg data that "12–13 wt% is missing from the carbon balance." In the analysis given here 16% is missing at $D = 0.3\ \text{h}^{-1}$ and 12% at $0.4\ \text{h}^{-1}$ – both calculated on a C-mole basis. Taking the averages 12.5 wt% and 14% respectively a tentative formula weight of P_1 is calculated by

$$M_{P_1} = \frac{12.5}{14} \times 30 = 26.7\,\text{g}(\text{C} - \text{mole})^{-1}.$$

This does not contradict the strong indication from the redox balance that P_1 is ethanol ($M_p = 23$ g C-mole $^{-1}$), but the loss in wt% ought to decrease with increasing D just as it has been argued that the loss in C-mole% should decrease with increasing D as was also confirmed in our analysis.

Example 3.6 *Citric acid produced by Aspergillus niger*. Citric acid, $C_6H_8O_7$, is an intermediate in the TCA cycle (Fig. 2.7), produced by condensation of AcCoA and oxaloacetate (2.15). It is an enormously important product from the bioindustry (1.7 M tons in 2007), and it is used as an acidulate of soft drinks, as a food preservative, in detergents to soften water by its chelating properties, and in multiple other ways. As carbon source sucrose, cane juice, sugar beet waste, corn steep liquor, and many other (cheap) substrates are used. The most common producing organism is *Aspergillus niger*, but other organisms such as yeast have been applied. Production is usually by fed-batch fermentation (Sect. 9.2.2) in large aerated, stirred tanks, and the filamentous fungus is present as small pellets of entangled mycelium (Sect. 7.6.2). The optimal pH is between 1.8 and 2, and NH_4NO_3 is used as N-source. Production in Europe and in the USA (Tate & Lyle was a major producing company) has almost ceased. Now the cheap bulk chemical is produced in the Far East and in India.

A well-designed citric acid fermentation process can give a carbon yield of 0.6–0.7 on glucose since no other metabolic products such as CO_2 needs to be formed by conversion of the hexose *via* pyruvate (and carboxylation of pyruvate or PEP) to oxaloacetate.

We shall study a typical case with a carbon yield of 68 g citric acid per 100 g glucose at pH = 2.5.

The N-source is NH_4NO_3 and the biomass has the composition $X = CH_{1.8}O_{0.5}N_{0.2}$.

$$-CH_2O - Y_{so}O_2 - Y_{sn}NH_4NO_3 + Y_{sx}X + Y_{sp}CH_{4/3}O_{7/6} = 0 \tag{1}$$

$$Y_{sn} = \tfrac{1}{2}Y_{sx} \times 0.2 \tag{2}$$

The two remaining yield coefficients can be calculated in terms of the known value of Y_{sp}.

$$Y_{sp} = \frac{68/32}{100/30} = 0.6375 \text{ C} - \text{mole citric acid}(\text{C} - \text{mole glucose})^{-1} \tag{3}$$

A carbon balance gives: $-1 + 0.6375 + Y_{sx} = 0$, and consequently $Y_{sx} = 0.3625$. From the nitrogen balance one immediately finds $Y_{sn} = 0.03625$. A degree of reduction balance gives:

$$-4 \times 1 - (-4) \times Y_{so} - 0.03625 \times \kappa_n + 0.3625 \times 4.20 + 0.6375 \times 3 = 0 \tag{4}$$

$\kappa_n = 2 \times (-3) + 4 \times 1 + 3\,(-2) = -8$, and consequently:

$$Y_{so} = \tfrac{1}{4}(4 + Y_{sn}\kappa_n - Y_{sx}\kappa_x - Y_{sp}\kappa_p) = 0.06875 \frac{\text{mol O}_2}{\text{C} - \text{mole glucose}} \tag{5}$$

In an experiment conducted at a higher pH = 5, a lower citric acid yield $Y_{sp} = 0.5375$ C mole (C mole glucose)$^{-1}$ is obtained, but the nitrogen, biomass and oxygen yields are the same ((2), (3), and (5)). Clearly new metabolic product(s) is produced besides citric acid, and from the carbon balance we find:

$$Y_{sp_1} = 1 - 0.3625 - 0.5375 = 0.1. \tag{6}$$

The degree of reduction balance is used in an attempt to identify the compound:

$$\begin{aligned} &-4-(-4)\times 0.06875-(-8)\times 0.03625+0.3625\\ &\times 4.20+0.5375\times 3+0.1\times \kappa_{p1}=0\Rightarrow \kappa_{p1}=3. \end{aligned} \tag{7}$$

The missing metabolic product P_1 does not contain N since Y_{sn} and Y_{sx} are unchanged. A reasonable guess is that P_1 is another TCA cycle metabolite. Both Fumaric acid ($C_4H_4O_4$) and Malic acid ($C_4H_6O_5$) have $\kappa = 3$, but why should these compounds appear? Also 2 CO_2 would have been lost in the process, which would not give a combined degree of reduction of 3 for P_1. An obvious possibility is that some of the precursors to citric acid have been used to make other products in a process that could formally involve decomposition of 0.1 C-mole citric acid to give a total of 0.1 C-mole of these products.

A quick search in the BRENDA enzyme database (http://www.brenda-enzymes.org) shows that *Aspergillus niger* has an oxaloacetate hydrolase (reaction 2 in (8)) with a pH optimum of 7. The database also refers to recent literature in which the enzyme is studied.

It is quite likely that this enzyme which is almost completely inactive at the low pH of 2.5 has been activated at the higher pH of 5, and that P_1 is a mixture of the two byproducts HAc and oxalic acid formed from oxaloacetate which is synthesized by reaction 1 in (8) using the enzyme pyruvate carboxylase.

$$\text{Pyruvate} + CO_2 \xrightarrow{1} \text{oxaloacetate} \xrightarrow{2} \text{acetate} + \text{oxalate} \tag{8}$$

Formally (and omitting the cofactor CoA) the overall process by which some citric acid is lost can be written as

$$\begin{aligned} &-C_6H_8O_7-H_2O+(COOH)_2+2CH_3COOH=0,\quad \text{or per C}-\text{mol citric acid}:\\ &-CH_{4/3}O_{7/6}+1/3CHO_2(\text{oxalic acid})+2/3CH_2O=0(\text{acetic acid}) \end{aligned} \tag{9}$$

Consequently, the mass balance (1) should be modified by including oxalic acid and acetic acid with yield coefficients of 1/30 and 1/15 to explain the results obtained at pH 5.

The presence of even small amounts of the toxic oxalic acid in citric acid used as a food preservative is unacceptable, and industry carefully monitors and controls the pH at 2.5 to 3 to avoid activation of oxaloacetate hydrolase.

An inherently safe method of avoiding oxalic acid contamination is to knock out the (single) gene for oxaloacetate hydrolase in *Aspergillus niger*. A gene deletion in the production organism does not prevent the use of the product citric acid in food. Among several gene modification studies of *A. niger* that have shown how to avoid the danger of oxalic acid formation Pedersen et al. (2000) is a good example. The knock-out strain had the same citric acid yield as the parent strain and the same maximum specific growth rate $\mu_{max} = 0.20\ h^{-1}$.

3.4.2 Redox Balances Used in the Design of Bioremediation Processes

As stated earlier, the main purpose of this text is to supply a quantitative foundation for design of processes in which biomass, sugar, or perhaps natural gas is converted into more valuable end products. Bioremediation has a completely different

purpose, namely the break-down and removal of chemicals from the environment. Although the design of bioreactors for this purpose follows the same principles as those applied in Chaps. 9–11 of the present text, the biochemistry and biology of bioremediation systems constitutes a separate discipline. Hence, subjects relevant to bioremediation will only receive cursory attention, mostly in the form of problems and examples in the different chapters. Still, the application of the basic material of this chapter can be valuable for Environmental Engineers who might recognize that some of their design concepts are based on the general framework of mass and redox balances, although the nomenclature and approach in Environmental Biotechnology often looks different. The removal of cellulosic material from the environment by microbial action is easy to model: Cellulose is degraded to sugars or to fatty acids. In an aerobic waste water plant these compounds are degraded to CO_2. In anaerobic reactors the fatty acids are converted to the final products CH_4 and CO_2 by redox-neutral processes. Thus, by Metabolite Balancing one obtains, e.g.:

$$CH_3COOH \rightarrow CH_4 + CO_2 \quad \text{and} \quad C_3H_7COOH \rightarrow 2.5\ CH_4 + 1.5\ CO_2 \tag{3.28}$$

Metabolite Balancing, the distribution of redox from the substrate into a number of metabolic products, is the result of all biological processes if there are no external sinks of redox. The process is necessarily strictly anaerobic since O_2 would scavenge redox from the system, but the medium must also be free of oxidized ions such as sulfate, nitrate, and Fe^{3+}. Sometimes CO_2 can act as a redox sink, and it is reduced to CH_4, but a potent energy source such as H_2 must be present (the H_2 ends up as H_2O) to overcome the large positive ΔG of the reaction (see Example 4.6). The presence of microorganisms that allow sulfate or nitrate reduction will be treated below. At first the true Metabolite Balancing situation will be discussed. It will be seen that quite complicated calculations on anaerobic bioremediation reactors can be done in analogy to the examples in (3.28).

Note 3.3 *BOD as a unit of redox power*. In anaerobic waste water treatment the redox level of the substrate is defined in terms of BOD (Biological Oxygen Demand), COD (Chemical Oxygen Demand), and TOC (Total Organic Carbon). The major goal of domestic waste treatment is to reduce BOD_n. This is defined as the amount of O_2 required to oxidize all the reduced matter (solids or solutes) in the sample of waste water to redox neutral compounds with the help of a consortium of microorganisms, either naturally present or added as standards. BOD is measured in a sealed reactor at 20°C, and the index n refers to the duration of the experiment. Usually $n = 5$ days, but in Scandinavia $n = 7$ days is used. One might add inhibitors that prevent interference from inorganic N or S (NH_3, S^{2-}, SO_4^{2-}, NO_3^{1-}), and now only the carbonaceous BOD is measured. Afterward, the BOD associated with NH_3 and sulfides can be measured. The dissolved oxygen level in the reactor is measured before and after the experiment to calculate the amount of O_2 used. Typical units for BOD are mg O_2 (L wastewater)$^{-1}$ or kg O_2 ton^{-1}. Typical raw sewage has a BOD of about 300 mg L^{-1} which will be reduced by 95% after 5 days.

A text on waste water treatment or environmental microbiology, e.g., Maier et al. (2000), must be consulted to understand the detailed use of BOD_n. For our purpose, we only need to

consider BOD as the amount of O_2 measured in units of *kg* used by the consortium of microorganisms in the anaerobic waste water plant to convert the organic compounds in the waste water to CO_2, H_2O, Volatile Fatty Acids (usually HAc), and gaseous metabolic products such as CH_4. An example will show how mass balances can be set up and solved for the plant, and BOD is used to express the redox level of the substrate and the products.

Example 3.7 *Design of an anaerobic waste water treatment unit.* The feed to an anaerobic waste water plant operating as a continuous, stirred tank reactor is a mixture of animal fats represented by tri-palmitin, $C_{51}H_{98}O_6$.

The microorganisms (represented as $CH_{1.8}O_{0.5}N_{0.2}$) use the fats as carbon source while the nitrogen source is supplied as NH_3. The output streams from the digester are

1. A gas composed of CH_4 and CO_2.
2. A liquid effluent which contains no residual fats. For simplicity the liquid effluent is assumed to contain only HAc.
3. An effluent stream of solids, assumed to be biomass with 7% ash. The total carbon in the feed stream is 3,180 kg BOD/day.

Effluents 2 and 3 contain, respectively, 330 kg BOD/day and 160 kg biomass (with 7% ash)/day.

Calculate the rates of production of CO_2 and CH_4, and determine the stoichiometry of the total bioreaction.

The degree of reduction of tri-palmitin is $\kappa = 5.686$ per C-atom.

3,180 kg BOD = (3,180/32) kmol O_2 = (3180/32) × (4/5.686) = 69.91 kC-mole tri-palmitin.

Consequently, 69.91 kC-mole tri-palmitin is treated per day in the digester.

Effluent stream 2: 330 kg BOD (as HAc) = 330/32 × (4/4) = 10.31 k C-mole HAc per day.

Effluent stream 3: 160 kg biomass (as $CH_{1,.8}O_{0.5}N_{0.2}$ with 7% ash) = 0.93 × 160/24.6 = 6.05 kC-mole per day. The NH_3 consumed is consequently 0.2 × 6.05 = 1.21 kmol per day.

Total redox balance: $69.91 \times 5.686 = 4 \times 10.31 + 4.20 \times 6.05 + 8 \times R_{CH_4}$

Total C-balance: $69.91 = 10.31 + 6.05 + R_{CH_4} + R_{CO_2}$

R_{CH_4} and R_{CO_2} are the daily production rates of CH_4 and CO_2.

$R_{CH_4} = 41.36\text{kmol} = 41.36$ k mol, and finally: $R_{CO_2} = 12.19\,\text{kC} - \text{mole}$.

The stoichiometry of the Black Box model can be assembled:

(1/51) $C_{51}H_{98}O_6$ + 0.01731 NH_3 → 0.0865 X + 0.1744 CO_2 + 0.1475 HAc + 0.5916 CH_4 (+water)

[The authors acknowledge the assistance of professor Lars K Nielsen, University of Queensland, Australia, for the original formulation of this example which is in his notes for a course in Metabolic Engineering given at UQ].

Under strictly anaerobic conditions certain (obligate anaerobic) bacteria can use inorganic ions as electron acceptors.

One such group of microorganisms is the sulfur-reducing bacteria that are widespread in Nature. They slowly degrade cellulose rich materials while using SO_4^{-2}, SO_3^{-2}, $S_2O_3^{-2}$ or even elemental sulfur as electron acceptor. The sulfur compounds are

reduced to H_2S. Typical sulfur-reducing bacteria such as *Desulphobacter* and *Desulphovibrio* do not incorporate the sulfur (and convert it to sulfur-containing amino acids such as cysteine), but run the sulfur reduction process in parallel with cell growth on a carbon source. The free energy needed to reduce SO_4^{-2} to $H_2S_{(g)}$ ($\Delta G = 775$ kJ/mol at standard conditions – see Sect. 4.1, and also Note 4.1) is obtained by oxidation of a small organic molecule, e.g., lactic acid to acetic acid ($\Delta G = -492$ kJ/mol):

$$2CH_3CHOHCOOH + SO_4^{-2} \rightarrow CH_3COOH + H_2S + 2HCO_3^{-1} \tag{3.29}$$

for which $\Delta G = -209$ kJ (mol $SO_4^{-2})^{-1}$

The same *dissimilatory* reduction mechanism is used when nitrate is the electron acceptor, and the final nitrogen compound is N_2. For a biomass yield of Y_{sx} (C-mol/mol glucose) one obtains the following stoichiometry, where for simplicity the nitrate is written as HNO_3:

$$\begin{aligned} CH_2O + 0.2Y_{sx}NH_3 + 2\alpha HNO_3 \rightarrow\ & Y_{sx}CH_{1.8}O_{0.5}N_{0.2} + \alpha N_2 \\ & + (1 - Y_{sx})CO_2 + Y_{sw}H_2O \end{aligned} \tag{3.30}$$

The efficiency of the denitrification process, calculated as the moles of NO_3^{-1} taken up for each C-mol of glucose can be calculated from a degree of reduction balance:

$$4.20Y_{sx} - 6\alpha = 4 - 2 \times 8\alpha \rightarrow \alpha = (4 - 4.20Y_{sx})/10 \tag{3.31}$$

The process would work up to $Y_{sx} = 0.95$ where all the redox in the glucose is used to make biomass. Much lower biomass yields are of course desired, and 0.8 mol of nitrate can be taken up in the limit of $Y_{sx} = 0$. Here, the waste water treatment unit removes nitrate at the expense of a cheap carbon source, e.g., degraded cellulose which is also present in the waste water. Some denitrifiers (e.g., *Pseudomonas denitrificans*) can reduce nitrate all the way to $NHNH_4^+$, especially at high carbon availability, and the ammonia can be taken up by the organism by *assimilatory* nitrate reduction.

Needless to say, there are also naturally occurring microorganisms that oxidize N and S containing compounds, e.g., NH_3 to nitrate, and sulfides to sulfates. Here oxygen is a substrate, and both biomass formation and oxidation of the inorganic compound are energetically favored. In removal of nitrogen from waste water an aerobic bioreactor is coupled in series with an anaerobic reactor. In the first reactor all NH_4^+ is oxidized to NO_3^{-1}, and in the second the nitrate is reduced to N_2 according to (3.30). Problem 3.7 discusses this dual N-removing process.

Sulfide-oxidizing bacteria are used in the mining industry to access, e.g., CuS in the ore, and $CuSO_4$ is produced without roasting the ore and converting the SO_2 to H_2SO_4.

3.5 Systematic Analysis of Black Box Stoichiometries

In all the examples of Sect. 3.4 there was a single carbon and energy source, a single nitrogen source such as NH_3 (or NH_4NO_3), and usually a single nitrogen free metabolic product apart from CO_2. The yield coefficients could be calculated manually using a carbon – and a degree of reduction balance. In the general case with N substrates and M metabolic products, some of which might contain nitrogen, a more systematic procedure to calculate the stoichiometry is, however, needed.

Let the general stoichiometry be

$$-\mathrm{CH_{a_1}O_{b_1}N_{c_1}} - \sum_{j=2}^{N-1} Y_{\mathrm{s_1 s}_j} S_j - Y_{\mathrm{s_1 o}}\mathrm{O_2} + Y_{\mathrm{s_1 x}} X + \sum_{j=1}^{M-2} Y_{\mathrm{s_1 p}_j} P_j + Y_{\mathrm{s_1 c}}\mathrm{CO_2} + Y_{\mathrm{s_1 w}}\mathrm{H_2O} = 0 \tag{3.32}$$

For each element an equal amount must be present in the substrates and in the products as illustrated by several examples in Sect. 3.4 where the carbon balance was set up using the yield coefficients. The *elemental balances* can, however, also be set up in terms of the volumetric production rates $\mathbf{q}$, and generally this can be specified as:

$$\sum_{j=1}^{N} y_{\mathrm{s}_j} q_{\mathrm{s}_j} + y_x q_x + \sum_{j=1}^{M} y_{\mathrm{p}_j} q_{\mathrm{p}_j} = 0 \tag{3.33}$$

The coefficient y specifies the content of the element in the given compound, e.g., for glucose y is 1 for carbon, 2 for hydrogen and 1 for oxygen. For a standard biomass y is 1 for carbon, 1.8 for hydrogen, 0.5 for oxygen and 0.2 for nitrogen. If an element does not appear in the compound y is zero, e.g., in water y is zero for carbon. Equation (3.33) is one relation between the $M + N + 1$ reaction rates, just as (3.32) is an equation that shows how chemically specified substrates are converted to different specified products. To generalize the four elemental balances we define a matrix $\mathbf{E}$ with 4 rows (representing C, H, O, and N), and N + M + 1 columns. In each column the elemental composition of one of the reaction species is written, i.e., the y for the different reaction species are given. Now (3.33) can be written in compact notation

$$\mathbf{Eq} = \mathbf{0} \tag{3.34}$$

$\mathbf{q}$ is the $N + M + 1$ column vector of volumetric reaction rates. Equation (3.34) provides four constraints between the $N + M + 1$ rates in $\mathbf{q}$, and four of these can consequently be calculated from the remaining $N + M - 3$ rates. If other elements, such as S, appear in some of the reactant compositions (cystein would be a case in point) the extension of (3.32) to contain more rows is obvious, but then at least one additional substrate is included, and the degrees of freedom is not affected.

Let the $N + M - 3$ measured rates be placed in the first $N + M - 3$ positions $\mathbf{q_m}$ of $\mathbf{q}$, and the remaining 4 rates in $\mathbf{q_c}$. Now (3.34) can be rewritten

$$\mathbf{E}_\mathrm{m}\mathbf{q}_\mathrm{m} + \mathbf{E}_\mathrm{c}\mathbf{q}_\mathrm{c} = \mathbf{0}. \tag{3.35}$$

Here $\mathbf{E}_\mathrm{c}$ is a (4×4) matrix whereas $\mathbf{E}_\mathrm{m}$ has 4 rows and $N + M - 3$ columns. Provided that $\det(\mathbf{E}_\mathrm{c}) \neq 0$ the algebraic equation (3.33) is solved to give

$$\mathbf{q}_\mathrm{c} = -(\mathbf{E}_\mathrm{c})^{-1}\mathbf{E}_\mathrm{m}\mathbf{q}_\mathrm{m} \tag{3.36}$$

$(\mathbf{E}_\mathrm{c})^{-1}$ is the inverse of matrix $\mathbf{E}_\mathrm{c}$. Typical cases where the procedure fails due to a singularity in $\mathbf{E}_\mathrm{c}$ is when substrates or products with the same composition per C-mol are included in $\mathbf{E}_\mathrm{c}$, e.g., glucose as a substrate and acetate as a product.

The concept of the systematic procedure is illustrated in Example 3.8.

Example 3.8 *Anaerobic yeast fermentation with CO_2, ethanol, and glycerol as metabolic products.* Consider anaerobic fermentation of *S. cerevisiae* where the metabolic products are [CO_2 (c), ethanol (e), glycerol (g)]. Let the carbon source be glucose and the nitrogen source NH_3. The biomass composition is $CH_{1.61}O_{0.52}N_{0.15}$. There are two substrates, CH_2O and NH_3, four products [$CH_3O_{1/2}$, $CH_{8/3}O$, CO_2, H_2O] in addition to the biomass X. With 7 reacting species and four constraints one needs to measure three rates. The remaining rates can be calculated.

The measured rates are chosen as $\mathbf{q_m} = (q_\mathrm{s}, q_\mathrm{x}, q_\mathrm{g})$ and the calculated rates are then $\mathbf{q_c} = (q_\mathrm{c}, q_\mathrm{n}, q_\mathrm{e}, q_\mathrm{w})$

$$\underbrace{\begin{pmatrix} 1 & 1 & 1 \\ 2 & 1.61 & \frac{8}{3} \\ 1 & 0.52 & 1 \\ 0 & 0.15 & 0 \end{pmatrix}}_{\mathbf{E}_\mathrm{m}} \cdot \underbrace{\begin{pmatrix} q_s \\ q_x \\ q_g \end{pmatrix}}_{\mathbf{q}_\mathrm{m}} + \underbrace{\begin{pmatrix} 1 & 0 & 1 & 0 \\ 0 & 3 & 3 & 2 \\ 2 & 0 & 0.5 & 1 \\ 0 & 1 & 0 & 0 \end{pmatrix}}_{\mathbf{E}_c} \times \underbrace{\begin{pmatrix} q_c \\ q_n \\ q_e \\ q_w \end{pmatrix}}_{\mathbf{q}_\mathrm{c}} = \begin{pmatrix} 0 \\ 0 \\ 0 \\ 0 \end{pmatrix}$$

$$\begin{pmatrix} q_\mathrm{c} \\ q_\mathrm{n} \\ q_\mathrm{e} \\ q_\mathrm{w} \end{pmatrix} = -(\mathbf{E}_\mathrm{c})^{-1}\mathbf{E}_\mathrm{m}\mathbf{q}_\mathrm{m} = \begin{pmatrix} -\frac{1}{3} & -0.3133 & -\frac{2}{9} \\ 0 & -0.15 & 0 \\ -\frac{2}{3} & -0.6867 & -\frac{7}{9} \\ 0 & 0.45 & -\frac{1}{6} \end{pmatrix} \times \begin{pmatrix} q_\mathrm{s} \\ q_\mathrm{x} \\ q_\mathrm{g} \end{pmatrix} \tag{1}$$

$$\begin{aligned} Y_\mathrm{sc} &= \frac{q_\mathrm{c}}{-q_\mathrm{s}} = \frac{-\frac{1}{3}q_\mathrm{s}}{-q_\mathrm{s}} + \frac{-0.3133q_\mathrm{x}}{-q_\mathrm{s}} - \frac{\frac{2}{9}q_\mathrm{g}}{-q_\mathrm{s}} = \tfrac{1}{3} - 0.3133Y_\mathrm{sx} - \tfrac{2}{9}Y_\mathrm{sg}, \\ Y_\mathrm{sn} &= \frac{-0.15q_\mathrm{x}}{-q_\mathrm{s}} = -0.15Y_\mathrm{sx}, \\ Y_\mathrm{se} &= \frac{q_\mathrm{e}}{-q_\mathrm{s}} = \tfrac{2}{3} - 0.6867Y_\mathrm{sx} - \tfrac{7}{9}Y_\mathrm{sg}, \\ Y_\mathrm{sw} &= \frac{q_\mathrm{w}}{-q_\mathrm{s}} = 0.45Y_\mathrm{sx} - \tfrac{1}{6}Y_\mathrm{sg}. \end{aligned} \tag{2}$$

Thus the black box model for this process becomes:

$$\begin{aligned} &-\mathrm{CH_2O} - 0.15Y_{\mathrm{sx}}\mathrm{NH_3} + Y_{\mathrm{sx}}\mathrm{CH_{1.61}O_{0.52}N_{0.15}} + (\tfrac{1}{3} - 0.3133Y_{\mathrm{sx}} - \tfrac{2}{9}Y_{\mathrm{sg}})\mathrm{CO_2} \\ &+ Y_{\mathrm{sg}}\mathrm{CH_{8/3}O} + (\tfrac{2}{3} - 0.6867Y_{\mathrm{sx}} - \tfrac{7}{9}Y_{\mathrm{sg}})\mathrm{CH_3O_{1/2}} + (0.45Y_{\mathrm{sx}} - \tfrac{1}{6}Y_{\mathrm{sg}})\mathrm{H_2O} = 0 \end{aligned} \tag{3}$$

All stoichiometric coefficients are determined from the measured rates q_{s}, q_{x}, and q_{g} – or from q_{s}, Y_{sx}, and Y_{sg}.

It is easily seen that the carbon balance is satisfied:

$$-1 + (\tfrac{1}{3} - 0.3133Y_{\mathrm{sx}} - \tfrac{2}{9}Y_{\mathrm{sg}}) + (\tfrac{2}{3} - 0.6867Y_{\mathrm{sx}} - \tfrac{7}{9}Y_{\mathrm{sg}}) + Y_{\mathrm{sx}} + Y_{\mathrm{sg}} = 0 \tag{4}$$

The degree of reduction balance is automatically satisfied when $\mathrm{H_2O}$ is taken to be one of the reaction species – as is necessary when element balances are used:

$$-4 + 4.12Y_{\mathrm{sx}} + 4\,\tfrac{2}{3}Y_{\mathrm{sg}} + 6 \times (\tfrac{2}{3} - 0.6867Y_{\mathrm{sx}} - \tfrac{7}{9}Y_{\mathrm{sg}}) = 0 \tag{5}$$

In examples as simple as this it is of course not necessary to set the whole mathematical machinery into action. The yield coefficient for $\mathrm{NH_3}$ is immediately given to be 0.15 and if a degree of reduction balance plus a carbon balance is used one obtains

$$\begin{aligned} 1 &= Y_{\mathrm{sx}} + Y_{\mathrm{sg}} + Y_{\mathrm{se}} + Y_{\mathrm{sc}} \\ 4 &= 4.12Y_{\mathrm{sx}} + 4\tfrac{2}{3}Y_{\mathrm{sg}} + 6Y_{\mathrm{se}} \end{aligned} \tag{6}$$

$$\begin{aligned} \begin{pmatrix} Y_{\mathrm{sc}} \\ Y_{\mathrm{se}} \end{pmatrix} &= \begin{pmatrix} 1 & 1 \\ 0 & 6 \end{pmatrix}^{-1} \begin{pmatrix} 1 - Y_{\mathrm{sx}} - Y_{\mathrm{sg}} \\ 4 - 4.12Y_{\mathrm{sx}} - 4\tfrac{2}{3}Y_{\mathrm{sg}} \end{pmatrix} \\ &= \tfrac{1}{6}\begin{pmatrix} 6 & -1 \\ 0 & 1 \end{pmatrix} \begin{pmatrix} 1 - Y_{\mathrm{sx}} - Y_{\mathrm{sg}} \\ 4 - 4.12Y_{\mathrm{sx}} - 4\tfrac{2}{3}Y_{\mathrm{sg}} \end{pmatrix} = \begin{pmatrix} \tfrac{1}{3} - 0.3133Y_{\mathrm{sx}} - \tfrac{2}{9}Y_{\mathrm{sg}} \\ \tfrac{2}{3} - 0.6867Y_{\mathrm{sx}} - \tfrac{7}{9}Y_{\mathrm{sg}} \end{pmatrix} \end{aligned}$$

Basically this is the result obtained in (2). If desired Y_{sw} can be found from an H or an O balance.

Example 3.9 *Production of lysine from glucose with acetic acid as byproduct.* The production of L-lysine ($\mathrm{CH_{7/3}O_{1/3}N_{1/3}}$) using the bacterium *Corynebacterium glutamicum* was discussed in Sect. 2.3.1. With $\mathrm{NH_3}$ as nitrogen source and a standard biomass composition the stoichiometry of the total reaction is given in (1). Some carbon is lost to the undesired byproduct acetic acid.

$$\begin{aligned} &-\mathrm{CH_2O} - Y_{\mathrm{sn}}\mathrm{NH_3} - Y_{\mathrm{so}}\mathrm{O_2} + Y_{\mathrm{sx}}\mathrm{CH_{1.8}O_{0.5}N_{0.2}} \\ &+ Y_{\mathrm{sp_1}}\mathrm{CH_{7/3}O_{1/3}N_{1/3}} + Y_{\mathrm{sp_2}}\mathrm{CH_2O} + Y_{\mathrm{sc}}\mathrm{CO_2} + Y_{\mathrm{sw}}\mathrm{H_2O} = 0 \end{aligned} \tag{1}$$

There are eight rates and four constraints. Four rates can be calculated, and the systematic method (3.36) is perhaps safer to use than the manual calculations based on C and N balances + a redox balance.

Choose q_s, q_{p_1}, q_{p_2} and q_{O_2} as the four measured rates

$$\begin{pmatrix} q_n \\ q_x \\ q_c \\ q_w \end{pmatrix} = -\begin{pmatrix} 0 & 1 & 1 & 0 \\ 3 & 1.8 & 0 & 2 \\ 0 & 0.5 & 2 & 1 \\ 1 & 0.2 & 0 & 0 \end{pmatrix}^{-1} \begin{pmatrix} 1 & 1 & 1 & 0 \\ 2 & \frac{7}{3} & 2 & 0 \\ 1 & \frac{1}{3} & 1 & 2 \\ 0 & \frac{1}{3} & 0 & 0 \end{pmatrix} \begin{pmatrix} q_s \\ q_{p_1} \\ q_{p_2} \\ q_{o_2} \end{pmatrix}$$
$$= \begin{pmatrix} 0.1905 & -\frac{1}{9} & 0.1905 & -0.1905 \\ -0.9524 & -\frac{10}{9} & -0.9524 & 0.9524 \\ -0.0476 & \frac{1}{9} & -0.0476 & -0.9524 \\ -0.4286 & 0 & -0.4286 & -0.5714 \end{pmatrix} \begin{pmatrix} q_s \\ q_{p_1} \\ q_{p_2} \\ q_{o_2} \end{pmatrix} \tag{2}$$

From (2) the yield coefficients in reaction (1) are obtained:

$$\begin{aligned} Y_{sn} &= 0.1905 + \tfrac{1}{9}Y_{sp_1} - 0.1905Y_{sp_2} - 0.1905Y_{so} \\ Y_{sx} &= 0.9524 - \tfrac{10}{9}Y_{sp_1} - 0.9524Y_{sp_2} - 0.9524Y_{so} \\ Y_{sc} &= 0.0476 + \tfrac{1}{9}Y_{sp_1} - 0.0476Y_{sp_2} + 0.9524Y_{so} \\ Y_{sw} &= 0.4286 - 0.4286Y_{sp_2} + 0.5714Y_{so} \end{aligned} \tag{3}$$

It is easily shown that the carbon, nitrogen, and redox balances close:

$$\begin{aligned} 1 &= Y_{sx} + Y_{sp_1} + Y_{sp_2} + Y_{sc} \\ Y_{sn} &= 0.2Y_{sx} + \tfrac{1}{3}Y_{sp_1} \\ -4Y_{so} + 4 &= 4.20Y_{sx} + 4\tfrac{2}{3}Y_{sp_1} + 4Y_{sp_2} \end{aligned} \tag{4}$$

Note that the occurrence of a product (acetate) with the same formula per C-atom as a substrate (glucose) does not disturb the calculations when they appear together in $\mathbf{E}_m$.

Calculations such as these are made as a preliminary to a process design. It is of first importance to see whether a sufficiently high yield of the desired product can be obtained to make the process economically viable.

Based on our simple stoichiometric model, and assuming that Y_{so} must be nonnegative the maximum lysine yield is obtained by setting $Y_{sx} = Y_{sp_2} = 0$ in the redox balance.

$$Y_{so} = \frac{4 - 4\frac{2}{3}Y_{sp_1}}{4} = 1 - \tfrac{7}{6}Y_{sp_1} \tag{5}$$

$(Y_{sp_1})_{max} = (6/7)$ C-mole lysine (C-mole glucose)$^{-1}$ when $Y_{so} = 0$. This result is higher than the true theoretical maximum yield 3/4 which as shown in Sect. 3.4 can only be found by analysis of individual pathways. In this respect, the Black Box model is too crude.

In actual lysine production the biomass yield is far from zero – it is in fact higher than for most aerobic processes. Consequently, the theoretical limit for Y_{sp_1} is not at all approached in practice – but carbon yields of 0.30–0.35 are also economically acceptable. Furthermore, several essential amino acids must be supplied, but the metabolic product lysine obtains its nitrogen directly by uptake of the nitrogen source NH_3 as discussed in Sect. 2.3.1.

3.6 Identification of Gross Measurement Errors

In Sect. 3.5 it was shown that four out of the $N + M + 1$ rates can be calculated based on C, H, O, and N balances – or for simple systems from a carbon and redox balance. It would, however, be a very poor policy to use only the minimum number of rates when fermentation results (at a given set of environmental conditions) are to be interpreted in terms of a stoichiometric equation. First of all compounds may be missing from the stoichiometric equation as was the case in Example 3.6 or their rates of production or consumption may be misjudged due to gross experimental errors as was the case for ethanol which was stripped away in Example 3.5.

But even small – and quite unavoidable – experimental inaccuracies will lead to substantial errors in the calculated rates. The data of Duboc (1997), which were analyzed in Example 3.1, are very accurate. The sum of yield coefficients of products is 0.999 (.23) while the redox balance, (1) in Example 3.1, closes to within 0.008. Still, a calculation of two yield coefficients Y_{sx} and Y_{sg} based on Y_{sc}, Y_{se}, and using the carbon – and the redox balances leads to significant errors due to the ill-conditioned nature of the linear algebraic problem. Inserting the round-off values for Y_{sc} and Y_{se} in (3.22) gives

$$\begin{aligned} &\text{Carbon balance}: \; 1 = 0.275 + 0.510 + Y_{sx} + Y_{sg} \\ &\text{Redox balance}: \; 4 = 0.510 \times 6 + 4.18 Y_{sx} + 4.667 Y_{sg} \\ &\begin{pmatrix} Y_{sx} \\ Y_{sg} \end{pmatrix} = \frac{1}{0.487} \begin{pmatrix} 4.667 & -1 \\ -4.18 & 1 \end{pmatrix} \begin{pmatrix} 0.215 \\ 0.940 \end{pmatrix} = \begin{pmatrix} 0.130 \\ 0.0848 \end{pmatrix} \end{aligned} \tag{3.37}$$

The calculated value of Y_{sx} is close to the measured value of 0.137 while the calculated value of Y_{sg} is woefully different from the experimental value of 0.077. One can certainly determine the rate of glycerol formation with an experimental error, which is smaller than 10% relative.

Experimentally measured rates beyond the minimum $N + M - 3$ rates can be used either to validate the stoichiometry by a qualitative assessment of the difference between measured and calculated values of the four remaining stoichiometric coefficients – as was done in Examples 3.5 and 3.6 – or they may be used, partly or as a whole to obtain better values for all the stoichiometric coefficients in a so-called reconciliation procedure. This is done by least-squares fitting of the coefficients, see also Section 5.3.2. Thus, if L measurements where $N + M - 3 < L \leq N + M + 1$ are used the remaining rates can be calculated as follows:

$$\mathbf{E}_c^T(\mathbf{E}_m \mathbf{q}_m + \mathbf{E}_c \mathbf{q}_c) = \mathbf{E}_c^T \mathbf{E}_c \mathbf{q}_c + \mathbf{E}_c^T \mathbf{E}_m \mathbf{q}_m = \mathbf{0} \tag{3.38}$$

Here (3.35) is multiplied from the left by $\mathbf{E}_c^T$, i.e. by the matrix $\mathbf{E}_c$ where rows and columns are transposed. When $L > N + M - 3$ the matrix $\mathbf{E}_c$ is not quadratic but contains four rows and less than four columns. But the product of $\mathbf{E}_c^T$ and $\mathbf{E}_c$ is a quadratic matrix of order less than four but larger than or equal to zero:

$$[(N+M+1-L)\times 4]\times[4\times(N+M-1-L)]$$
$$=[N+M+1-L]\times[N+M+1-L]$$

Consequently,

$$\mathbf{q}_c=-\left[\mathbf{E}_c^T\mathbf{E}_c\right]^{-1}\left[\mathbf{E}_c^T\mathbf{E}_m\right]\mathbf{q}_m \tag{3.39}$$

The requirement for application of (3.39) is that $\mathbf{E}_c^T\mathbf{E}_c$ has full rank, i.e. rank $(\mathbf{E}_c^T\mathbf{E}_c) = N + M + 1 - L$, or det $(\mathbf{E}_c^T\mathbf{E}_c) \neq 0$.

Inserting (3.39) in (3.35), we get

$$\mathbf{R}\mathbf{q}_m=\mathbf{0} \tag{3.40}$$

In (3.40):

$$\mathbf{R}=\mathbf{E}_m-\mathbf{E}_c\left(\mathbf{E}_c^T\mathbf{E}_c\right)^{-1}\mathbf{E}_c^T\mathbf{E}_m \tag{3.41}$$

The matrix **R** is called the *redundancy matrix* (Heijden et al., 1994a, b), and its rank specifies the number of independent equations in (3.40). Thus, if there are I elemental balances the redundancy matrix contains I – rank (**R**) dependent rows, and if these rows are deleted we obtain rank® independent equations relating the L measured rates:

$$\mathbf{R}_r\mathbf{q}_m=\mathbf{0} \tag{3.42}$$

Here $\mathbf{R}_r$ is the reduced redundancy matrix containing only the independent rows of **R**. If rank (**R**) = 0, the system is not over-determined.

The case $L = N + M + 1$ is obviously not of interest, unless there are experimental errors ("inaccuracies") in the measured data. This case will be treated shortly for the general case of L measurements with L bounded as shown above. Usually some of the rates can, however, not be found with satisfactory precision. q_w is certainly one example, but q_x can be difficult to measure if the medium is strongly colored or contains solid particles as is often the case in industrial fermentations. Consequently, (3.39) can be used to calculate a set of rates $\mathbf{q}_c$ where $\mathbf{q}_c$ contains less than four components when only C, H, O, and N are considered.

We now assume that all the measured rates contain random errors. With $\mathbf{q}_m$ and $\overline{\mathbf{q}}_m$ being the vectors of, respectively, the true and the measured values, we have

$$\overline{\mathbf{q}}_m=\mathbf{q}_m+\boldsymbol{\delta} \tag{3.43}$$

$\boldsymbol{\delta}$ is the vector of measurement errors. It is now assumed that the error vector is normally distributed, with a mean value of zero and with a variance–covariance matrix **F**:

$$\mathbf{E}(\boldsymbol{\delta}) = \mathbf{0} \tag{3.44}$$

$$\mathbf{F} = \mathbf{E}\left[(\overline{\mathbf{q}}_m - \mathbf{q}_m)(\overline{\mathbf{q}}_m - \mathbf{q}_m)^T\right] = \mathbf{E}\left(\boldsymbol{\delta}\boldsymbol{\delta}^T\right) \tag{3.45}$$

E is a matrix with each element being represented by the expected value operator. If the model is correct and there are no measurement errors ($\boldsymbol{\delta} = \mathbf{0}$), all I – rank (**R**) equations in (3.44) will be satisfied, i.e., the elemental balances close exactly. In any real experimental investigation ($\boldsymbol{\delta} \neq \mathbf{0}$) there is a residual in each part of (3.43).

The vector of residuals $\boldsymbol{\varepsilon}$ is given by

$$\boldsymbol{\varepsilon} = \mathbf{R}_r\boldsymbol{\delta} = \mathbf{R}_r(\overline{\mathbf{q}}_m - \mathbf{q}_m) = \mathbf{R}_r\overline{\mathbf{q}}_m \tag{3.46}$$

since from (3.42) $\mathbf{R}_r\mathbf{q}_m = \mathbf{0}$. Since also $\mathbf{E}(\boldsymbol{\delta}) = \mathbf{0}$, the residuals $\boldsymbol{\varepsilon}$ defined in (3.46) have a mean of zero and the variance–covariance matrix for $\boldsymbol{\varepsilon}$ is given by (3.47):

$$\mathbf{E}(\boldsymbol{\varepsilon}) = \mathbf{R}_r\mathbf{E}(\boldsymbol{\delta}) = \mathbf{0} \tag{3.47}$$

$$\mathbf{P} = \mathbf{E}(\boldsymbol{\varepsilon}\boldsymbol{\varepsilon}^T) = \mathbf{R}_r\mathbf{E}(\boldsymbol{\delta}\boldsymbol{\delta}^T)\mathbf{R}_r^T = \mathbf{R}_r\mathbf{F}\mathbf{R}_r^T \tag{3.48}$$

The minimum variance estimate of the error vector $\boldsymbol{\delta}$ is obtained by minimizing the sum of squared errors scaled according to the level of confidence placed on the individual measurements, i.e., to compute,

$$\underset{\delta}{\text{Min}}\,(\boldsymbol{\delta}^T\mathbf{F}^{-1}\boldsymbol{\delta}) \tag{3.49}$$

The solution to the minimization problem in (3.49) is given by

$$\hat{\boldsymbol{\delta}} = \mathbf{F}\mathbf{R}_r^T\mathbf{P}^{-1}\boldsymbol{\varepsilon} = \mathbf{F}\mathbf{R}_r^T\mathbf{P}^{-1}\mathbf{R}_r\overline{\mathbf{q}}_m \tag{3.50}$$

The "hat" specifies that it is an estimate. The estimate in (3.50) coincides with the maximum likelihood estimate, since $\boldsymbol{\delta}$ is normally distributed.[3] Using (3.50) we find an estimate of the measured rates to be given by

$$\hat{\mathbf{q}}_m = \overline{\mathbf{q}}_m - \hat{\boldsymbol{\delta}} = (\mathbf{I} - \mathbf{F}\mathbf{R}_r^T\mathbf{P}^{-1}\mathbf{R}_r)\overline{\mathbf{q}}_m \tag{3.51}$$

I is a unity matrix. In Note 3.4 it is shown that the estimate $\hat{\mathbf{q}}_m$ given by (3.51) has a smaller standard deviation than the raw measurement data $\overline{\mathbf{q}}_m$, and the estimate is therefore likely to be more reliable than the measured data. Application of (3.51) to a set of experimental data is illustrated in Example 3.10.

[3] When δ is normally distributed, the function to be minimized is the same for the least-square minimization problem and for the maximum-likelihood minimization problem. If the error vector is not normally distributed the estimate in (3.50) remains valid for the least-squares minimization problem, whereas it will no longer be the maximum-likelihood estimate (Wang and Stephanopoulos 1983).

Note 3.4 *Variance–covariance matrix of the rate estimates.* The variance–covariance matrix for the rate estimates is given by

$$\hat{\mathbf{F}} = \mathbf{E}\left[(\hat{\mathbf{q}}_\mathrm{m} - \mathbf{q}_\mathrm{m})(\hat{\mathbf{q}}_\mathrm{m} - \mathbf{q}_\mathrm{m})^\mathrm{T}\right] = \mathbf{E}\left[(\hat{\boldsymbol{\delta}} - \boldsymbol{\delta})(\hat{\boldsymbol{\delta}} - \boldsymbol{\delta}^\mathrm{T})\right] \tag{1}$$

$$\mathbf{E}\left[(\hat{\boldsymbol{\delta}} - \boldsymbol{\delta})(\hat{\boldsymbol{\delta}} - \boldsymbol{\delta}^\mathrm{T})\right] = \mathbf{E}(\hat{\boldsymbol{\delta}}\hat{\boldsymbol{\delta}}^\mathrm{T}) - \mathbf{E}(\boldsymbol{\delta}\hat{\boldsymbol{\delta}}^\mathrm{T}) - \mathbf{E}(\hat{\boldsymbol{\delta}}\boldsymbol{\delta}^\mathrm{T}) + \mathbf{E}(\boldsymbol{\delta}\boldsymbol{\delta}^\mathrm{T}) \tag{2}$$

The first term in (2) represents the variance–covariance matrix for $\hat{\boldsymbol{\delta}}$, which by using (3.50) and (3.48) we find to be given by

$$\mathbf{E}(\hat{\boldsymbol{\delta}}\hat{\boldsymbol{\delta}}^\mathrm{T}) = \mathbf{F}\mathbf{R}_\mathrm{r}^\mathrm{T}\mathbf{P}^{-1}\mathbf{E}(\boldsymbol{\varepsilon}\boldsymbol{\varepsilon}^\mathrm{T})(\mathbf{F}\mathbf{R}_\mathrm{r}^\mathrm{T}\mathbf{P}^{-1})^\mathrm{T} = \mathbf{F}\mathbf{R}_\mathrm{r}^\mathrm{T}(\mathbf{P}^{-1})^\mathrm{T}\mathbf{R}_\mathrm{r}\mathbf{F}^\mathrm{T}. \tag{3}$$

For the second term in (2), we find

$$\begin{aligned}\mathbf{E}(\boldsymbol{\delta}\hat{\boldsymbol{\delta}}^\mathrm{T}) &= \mathbf{E}[\boldsymbol{\delta}(\mathbf{F}\mathbf{R}_\mathrm{r}^\mathrm{T}\mathbf{P}^{-1}\boldsymbol{\varepsilon})^\mathrm{T}] = \mathbf{E}[\boldsymbol{\delta}(\mathbf{F}\mathbf{R}_\mathrm{r}^\mathrm{T}\mathbf{P}^{-1}\mathbf{R}_r\boldsymbol{\delta})^\mathrm{T}] \\ &= \mathbf{E}(\boldsymbol{\delta}\boldsymbol{\delta}^\mathrm{T})\mathbf{R}_\mathrm{r}^\mathrm{T}(\mathbf{P}^{-1})^\mathrm{T}\mathbf{R}_\mathrm{r}\mathbf{F}^\mathrm{T} = \mathbf{F}\mathbf{R}_\mathrm{r}^\mathrm{T}(\mathbf{P}^{-1})^\mathrm{T}\mathbf{R}_\mathrm{r}\mathbf{F}^\mathrm{T}\end{aligned} \tag{4}$$

For the third term:

$$\mathbf{E}(\hat{\boldsymbol{\delta}}\boldsymbol{\delta}^\mathrm{T}) = \mathbf{E}[(\mathbf{F}\mathbf{R}_\mathrm{r}^\mathrm{T}\mathbf{P}^{-1}\boldsymbol{\varepsilon})\boldsymbol{\delta}^\mathrm{T}] = \mathbf{E}[(\mathbf{F}\mathbf{R}_\mathrm{r}^\mathrm{T}\mathbf{P}^{-1}\mathbf{R}_\mathrm{r}\boldsymbol{\delta})\boldsymbol{\delta}^\mathrm{T}] = \mathbf{F}\mathbf{R}_\mathrm{r}^\mathrm{T}\mathbf{P}^{-1}\mathbf{R}_\mathrm{r}\mathbf{E}(\boldsymbol{\delta}\boldsymbol{\delta}^\mathrm{T}) = \mathbf{F}\mathbf{R}_\mathrm{r}^\mathrm{T}\mathbf{P}^{-1}\mathbf{R}_\mathrm{r}\mathbf{F}. \tag{5}$$

The fourth term is given by (3.45). By combination of these results we find that the contributions from the first and second term cancel and

$$\hat{\mathbf{F}} = \mathbf{F} - \mathbf{F}\mathbf{R}_\mathrm{r}^\mathrm{T}\mathbf{P}^{-1}\mathbf{R}_\mathrm{r}\mathbf{F}. \tag{6}$$

Since the last term is positive, the variance-covariance matrix for the estimated rates is always smaller than that for the measured rates.

Example 3.10 *Calculation of best estimates for measured rates.* We return to the experimental data of von Meyenburg (1969), which were presented in Example 3.5 (see Fig. 3.5). We want to find better estimates for the measured variables. First consider the data for low dilution rates where no ethanol is formed. In Example 3.13 we will consider the data for higher dilution rates.

At low dilution rates the measured rates are $q_\mathrm{s}, q_\mathrm{o}, q_\mathrm{c}$ and q_x. There are two nonmeasured rates – ammonia utilization q_n and formation of water q_w. Thus, with the biomass composition specified in (1) of Example 3.5 we have

$$\mathbf{E}_\mathrm{m} = \begin{pmatrix} 1 & 0 & 1 & 1 \\ 2 & 0 & 0 & 1.83 \\ 1 & 2 & 2 & 0.56 \\ 0 & 0 & 0 & 0.17 \end{pmatrix}; \qquad \mathbf{E}_\mathrm{c} = \begin{pmatrix} 0 & 0 \\ 3 & 2 \\ 0 & 1 \\ 1 & 0 \end{pmatrix} \tag{1}$$

With a total of six components and four elemental balances, the number of degrees of freedom $\mathbf{F} = 2$, and since four volumetric rates are measured ($K = 4$), the system is over-determined. From (3.41) the redundancy matrix is found to be

$$\mathbf{R} = \begin{pmatrix} 1 & 0 & 1 & 1 \\ 0 & -0.286 & -0.286 & 0.014 \\ 0 & 0.572 & 0.572 & -0.028 \\ 0 & 0.858 & 0.858 & -0.042 \end{pmatrix} \tag{2}$$

with $\text{rank}(\mathbf{R}) = 2$. It is easily seen that the last two rows are proportional to the second row, and we therefore delete these two rows and find the reduced redundancy matrix

$$\mathbf{R}_\text{r} = \begin{pmatrix} 1 & 0 & 1 & 1 \\ 0 & -0.286 & -0.286 & 0.014 \end{pmatrix} \tag{3}$$

At $D = 0.15\,\text{h}^{-1}$ we find the measured volumetric rates to be (all in C-moles or moles; see Example 3.5).

$$\overline{\mathbf{q}}_\text{m} = \begin{pmatrix} -0.140 \\ -0.063 \\ 0.063 \\ 0.079 \end{pmatrix} \tag{4}$$

The vector of residuals is then

$$\boldsymbol{\varepsilon} = \mathbf{R}_\text{r}\overline{\mathbf{q}}_\text{m} = \begin{pmatrix} 1 & 0 & 1 & 1 \\ 0 & -0.286 & -0.286 & 0.014 \end{pmatrix} \begin{pmatrix} -0.140 \\ -0.063 \\ 0.063 \\ 0.079 \end{pmatrix} = 10^{-3} \begin{pmatrix} 2.0 \\ 1.1 \end{pmatrix} \tag{5}$$

There is a fairly good consistency in the data, since the residuals are very small. We will, however, try to obtain even better estimates for the measured rates.

In order to find the variance–covariance matrix, we need to know something about the size of the measurement errors. We will here assume that these errors are uncorrelated and that the relative error in the gas measurements is 10%, whereas it is 5% for the glucose and the biomass measurements. The variance–covariance matrix is therefore:

$$\mathbf{F} = \begin{pmatrix} (0.05 \times 0.140)^2 & 0 & 0 & 0 \\ 0 & (0.10 \times 0.063)^2 & 0 & 0 \\ 0 & 0 & (0.10 \times 0.063)^2 & 0 \\ 0 & 0 & 0 & (0.05 \times 0.079)^2 \end{pmatrix}$$

$$\Downarrow \tag{6}$$

$$\mathbf{F} = 10^{-4} \begin{pmatrix} 0.490 & 0 & 0 & 0 \\ 0 & 0.397 & 0 & 0 \\ 0 & 0 & 0.397 & 0 \\ 0 & 0 & 0 & 0.157 \end{pmatrix}$$

Thus the $\mathbf{P}$ matrix is found from (3.48):

$$\mathbf{P} = \mathbf{R}_r \mathbf{F} \mathbf{R}_r^T = 10^{-4} \begin{pmatrix} 1.044 & -0.111 \\ -0.111 & 0.065 \end{pmatrix}; \quad \mathbf{P}^{-1} = 10^5 \begin{pmatrix} 0.117 & 0.201 \\ 0.201 & 1.887 \end{pmatrix} \tag{7}$$

The estimate for the vector of measurement errors can now be calculated by using (3.50):

$$\hat{\boldsymbol{\delta}} = \mathbf{F} \mathbf{R}_r^T \mathbf{P}^{-1} \mathbf{R}_r \overline{\mathbf{q}}_m = 10^{-3} \begin{pmatrix} 2.2 \\ -2.8 \\ -1.0 \\ 0.8 \end{pmatrix} \tag{8}$$

Consequently, the estimate for the measured rates is:

$$\hat{\mathbf{q}}_m = \overline{\mathbf{q}}_m - \hat{\boldsymbol{\delta}} = \begin{pmatrix} -0.142 \\ -0.060 \\ 0.064 \\ 0.078 \end{pmatrix} \tag{9}$$

It is concluded that the measurements are very good, since the estimated rates differ only slightly from the raw data. It is, however, justified to make the small corrections, and we can next calculate the variance covariance matrix for the estimated rates by using (6) of Note 3.4.

$$\hat{\mathbf{F}} = 10^{-4} \begin{pmatrix} 0.209 & 0.112 & 0.116 & -0.092 \\ 0.112 & 0.154 & -0.152 & -0.041 \\ -0.116 & -0.152 & 0.151 & -0.034 \\ -0.092 & 0.041 & -0.034 & 0.127 \end{pmatrix} \tag{10}$$

It is observed that the diagonal elements in $\hat{\mathbf{F}}$ are smaller than the diagonal elements in $\mathbf{F}$, and the variance of the estimates is therefore smaller than for the raw measurements. The estimates $\hat{\mathbf{q}}_m$ are therefore likely to be more accurate and reliable. Whereas the errors of the raw measurements are uncorrelated, it is observed from (10) that the errors of the estimated rates are correlated through the constraints in (3.40).

In the analysis we have used the volumetric rates, whereas yield coefficients were used in Example 3.5. The present error analysis could, however, just as well be carried out using the yield coefficients (simply replace the volumetric rate vector with a vector containing the yields).

Normally the variance–covariance matrix is assumed to be diagonal, i.e., the measurements are uncorrelated. However, the volumetric rates are seldom measured directly, but they are based on measurements of so-called primary variables, which may influence more than one of the measured volumetric rates. An example is measurement of the oxygen uptake rate and the carbon dioxide production rate, which are based on measurement of the gas flow rate through the bioreactor together with measurement of the partial pressure of the two gases in the exhaust. If there is an error in the measured gas flow rate, this will influence both of the above-mentioned rates, and errors in the measured rates are therefore indirectly correlated. The same objection holds for measurements of many other

volumetric rates, which are in reality obtained by combination of a concentration and a flow-rate measurement. In all these cases of indirect error correction it is difficult to specify the true variance–covariance matrix **F**. Madron et al. (1977) describe a method by which the variance–covariance matrix can be found from knowledge of the errors in the primary variables (see Note 3.5), but even if we know that there is often a certain coupling between measurement errors we will use a diagonal **F** matrix since we can rarely do anything better. The diagonal **F** matrix is preferable, partly because the calculations are simplified but also because we usually know little beyond the order of magnitude of the measurement errors. Thus in some cases **F** is expressed as

$$\mathbf{F} = c\mathbf{I} \tag{3.52}$$

Again **I** is the unity matrix. Inserting (3.52) in (3.51), we obtain

$$\hat{\mathbf{q}}_{\mathrm{m}} = (\mathbf{I} - \mathbf{R}_{\mathrm{r}}^{\mathrm{T}}(\mathbf{R}_{\mathrm{r}}\mathbf{R}_{\mathrm{r}}^{\mathrm{T}})^{-1}\mathbf{R}_{\mathrm{r}})\overline{\mathbf{q}}_{\mathrm{m}} \tag{3.53}$$

This is the classical least-squares estimate. Equation (3.53) is useful in many situations, and its application to the data analyzed in Example 3.10 is illustrated in Example 3.11.

Note 3.5 *Calculation of the variance–covariance matrix from the errors in the primary variables.* Normally the measured rates are determined from several measurements of so-called primary variables, e.g., the volumetric glucose utilization rate in a chemostat is measured from the glucose concentration in the exit stream and the feed flow rate. Specification of the variance-covariance matrix is therefore not straightforward, but Madron et al. (1977) describes a simple approach to find **F**. The measured rates are specified as functions of the primary variables, which are collected in the vector **v** (dimension L^*):

$$q_{\mathrm{m},i} = f_i(\mathbf{v}) \; ; \qquad i = 1, ..., L \tag{1}$$

Generally the functions f_i are nonlinear, but in order to obtain an approximate estimate of the variance and the covariances the functions are linearized. Thus the errors δ_i in the L measured rates are expressed as linear combinations of the errors δ_j^* of the L^* primary variables:

$$\delta_i = \sum_{j=1}^{L^*} \left(\frac{\partial f_i}{\partial v_j}\right)\delta_j^* = \sum_{j=1}^{L^*} g_{ij}\delta_j^*; \quad i = 1, ..., L \tag{2}$$

The sensitivities g_{ji} are collected in the matrix **G** (dimension $L \times L^*$), and the variance–covariance matrix **F** is calculated from

$$\mathbf{F} = \mathbf{G}\mathbf{F}^*\mathbf{G}^{\mathrm{T}} \tag{3}$$

F* is the diagonal matrix containing the L^* variances of the primary variables. The accuracy of the computed variances is limited by the accuracy of the linear approximation in (2) involved in the computation of the sensitivities.

Table 3.3 Values of the χ^2 distribution

	Confidence level $(1 - \theta)$					
Degrees of freedom	0.500	0.750	0.900	0.950	0.975	0.990
1	0.46	1.32	2.71	3.84	5.02	6.63
2	1.39	2.77	4.61	5.99	7.38	9.21
3	2.37	4.11	6.25	7.81	9.35	11.30
4	3.36	5.39	7.78	9.49	11.10	13.30
5	4.35	6.63	9.24	11.10	12.80	15.10

Example 3.11 *Application of the least-squares estimate.* Using (3.53) on the data analyzed in Example 3.10, i.e., $\mathbf{R}_r$ and $\mathbf{q}_m$ are given respectively by (3) and (4) of Example 3.10, we find

$$\hat{\mathbf{q}}_m = \begin{pmatrix} -0.142 \\ -0.060 \\ 0.064 \\ 0.077 \end{pmatrix} \tag{1}$$

This is almost identical with the estimates for the rates found in Example 3.10, where information concerning the measurement errors of the rates was included.

If any components in the residual vector are significantly different from zero, either there must be a significant error in at least one of the measurements or the applied model is not correct. To quantify what is meant by residuals significantly different from zero, we introduce the test function h given by the sum of weighted squares of the residuals, i.e., the residuals are weighted according to their accuracy:

$$h = \varepsilon^T \mathbf{P}^{-1} \varepsilon \tag{3.54}$$

With uncorrelated raw measurements, the test function h is chi-square distributed (see, e.g., Wang and Stephanopoulos 1983). Heijden et al. (1994b) proved that this is also the case for correlated raw data. The degrees of freedom of the distribution is equal to rank($\mathbf{P}$) = rank ($\mathbf{R}$)

The calculated value of h is compared with values of the χ^2 distribution at the given value of rank ($\mathbf{R}$). If at a high enough confidence level $1 - \theta$ one obtains that h is larger than χ^2, then there is something wrong with the data or the model. Table 3.3 is an extract from a table of χ^2 values. Normally a confidence level of at least 95% should be used.

Example 3.12 *Calculation of the test function h.* With the data in Example 3.10, the vector of residuals is given by (5) of Example 3.10 and the test function is found to be

$$h = \varepsilon^T \mathbf{P}^{-1} \varepsilon = 10^{-1} \begin{pmatrix} 2.0 & 1.1 \end{pmatrix} \begin{pmatrix} 0.117 & 0.201 \\ 0.201 & 1.887 \end{pmatrix} \begin{pmatrix} 2.0 \\ 1.1 \end{pmatrix} = 0.364 \tag{1}$$

Since rank (**R**) = 2, the number of degrees of freedom for the χ^2 distribution is 2, and from Table 3.3 it is seen that h is far too small to raise any suspicion about the quality of the measurements.

The test of the data quality is easily carried out, but one cannot conclude from the result that $h > \chi^2$ at, say, the 97.5% level, whether the unsatisfactorily large errors are due to a systematic defect of the data or to large random errors. However, in many cases one may suspect that one of the measurements has a systematic error, and if by leaving this measurement out of the analysis the errors become nonsignificant it is reasonable to assume that this particular measurement contains a systematic error. Thus the approach illustrated above can be used for error diagnosis, but only when the system is over-determined by at least two measurements, i.e., rank (**R**) $\geq$2. Otherwise, when one measurement is left out the system is no longer over-determined, and the analysis cannot be carried out. The concept of eliminating one measurement at a time is very simple, as illustrated in Example 3.13, but it may be time-consuming if no information about the possible source of error is available; i.e., one has to repeat the calculations with each of the measured rates left out of the analysis. A more systematic approach for error diagnosis is found in Heijden et al. (1994a, b).

Example 3.13 *Error diagnosis of yeast fermentation.* We now consider the data of von Meyenburg (1969) for high dilution rates. In Example 3.5 it was concluded that some ethanol was probably missing. As in Example 3.10 we have two nonmeasured rates, ammonia utilization and formation of water, whereas there are five measured rates: consumption of glucose and oxygen and production of carbon dioxide, ethanol, and biomass. Thus

$$\mathbf{E}_m = \begin{pmatrix} 1 & 0 & 1 & 1 & 1 \\ 2 & 0 & 0 & 3 & 1.83 \\ 1 & 2 & 2 & 0.5 & 0.56 \\ 0 & 0 & 0 & 0 & 0.17 \end{pmatrix}; \qquad \mathbf{E}_c = \begin{pmatrix} 0 & 0 \\ 3 & 2 \\ 0 & 1 \\ 1 & 0 \end{pmatrix} \tag{1}$$

The redundancy matrix is found to be

$$\mathbf{R} = \begin{pmatrix} 1 & 0 & 1 & 1 & 1 \\ 0 & -0.286 & -0.286 & 0.143 & 0.014 \\ 0 & 0.571 & 0.571 & -0.286 & -0.029 \\ 0 & 0.857 & 0.857 & -0.429 & -0.043 \end{pmatrix} \tag{2}$$

R has the rank 2; the last two rows are multiples of the second row. The reduced redundancy matrix is thus found to be

$$\mathbf{R}_r = \begin{pmatrix} 1 & 0 & 1 & 1 & 1 \\ 0 & -0.286 & -0.286 & 0.143 & 0.014 \end{pmatrix} \tag{3}$$

At $D = 0.3\ \mathrm{h}^{-1}$ we have the following measured rates from Example 3.5

$$\overline{\mathbf{q}}_m = \begin{pmatrix} -0.279 \\ -0.047 \\ 0.102 \\ 0.055 \\ 0.078 \end{pmatrix} \tag{4}$$

The vector of residuals is:

$$\boldsymbol{\varepsilon} = \mathbf{R}_r \overline{\mathbf{q}}_m = \begin{pmatrix} -0.0440 \\ -0.0067 \end{pmatrix} \tag{5}$$

For the variance–covariance matrix we use the same measurement errors as in Example 3.10, i.e., 10% in the gas measurements and 5% in the medium-based measurements. Consequently

$$\mathbf{F} = \begin{pmatrix} (0.05 \times 0.279)^2 & 0 & 0 & 0 & 0 \\ 0 & (0.1 \times 0.047)^2 & 0 & 0 & 0 \\ 0 & 0 & (0.1 \times 0.102)^2 & 0 & 0 \\ 0 & 0 & 0 & (0.05 \times 0.055)^2 & 0 \\ 0 & 0 & 0 & 0 & (0.05 \times 0.078)^2 \end{pmatrix} \tag{6}$$

$$\mathbf{P} = \mathbf{R}_r \mathbf{F} \mathbf{R}_t^T = 10^{-3} \begin{pmatrix} 0.321 & -0.028 \\ -0.028 & 0.010 \end{pmatrix}; \quad \mathbf{P}^{-1} = 10^5 \begin{pmatrix} 0.041 & 0.111 \\ 0.111 & 1.260 \end{pmatrix} \tag{7}$$

Now we calculate the test function

$$h = \varepsilon^T \mathbf{P}^{-1} \varepsilon = 20.27 \tag{8}$$

Comparison of the calculated h with the values of the χ^2 distribution for rank $(\mathbf{R}) = 2$ shows that there is an overwhelming probability that the data set contains significant deficiencies.

Since rank$(\mathbf{R}) = 2$, it is possible to drop one of the measurements and still have an overdetermined system. We can therefore carry out the error diagnosis described above, i.e., delete one of the measured rates at a time and calculate the test function. The results of this analysis give the test function for each case, i.e., with each of the measured rates deleted from the analysis:

Ethanol	$h = 1.87 \times 10^{-6}$
Carbon dioxide	$h = 19.89$
Oxygen	$h = 9.26$
Biomass	$h = 3.36$
Glucose	$h = 4.41$

When one of the measurements is left out of the analysis, rank$(\mathbf{R}) = 1$, and the test function should therefore be compared with the χ^2 distribution with one degree of freedom. It is evident that when the ethanol measurement is left out, all signs of trouble disappear from the data set. It seems beyond doubt that there is a systematic error in the ethanol measurement, and we can obtain a nice statistical confirmation of the somewhat more qualitative argument of Example 3.5, which strongly indicated that some ethanol was missing from the mass balance. Using (3.50) we find good estimates for the measurement errors

$$\hat{\delta} = 10^{-3} \begin{pmatrix} 0.506 \\ 0.115 \\ 0.811 \\ 0.035 \end{pmatrix} \tag{9}$$

These are small, and correction of the measured rates (not including that of ethanol) is therefore not necessary. Using (3.39), we calculate the three nonmeasured rates (including that of ethanol)

$$\mathbf{q}_c = \begin{pmatrix} q_n \\ q_p \\ q_w \end{pmatrix} = \begin{pmatrix} -0.012 \\ 0.100 \\ 0.076 \end{pmatrix} \tag{10}$$

The calculated volumetric rate of ethanol production is thus 0.100 C-moles of ethanol per liter per hour, which corresponds to 0.357 C-moles of ethanol per C-mole of glucose. This is identical to the sum of Y_{sp} and the calculated Y_{sp1} found in Example 3.5. The method for error diagnosis illustrated here is very simple and quite powerful. It is, however, advisable not to embark on a mechanical error analysis without first using the intuitively simple engineering approach of Example 3.5.

Problems

Problem 3.1 *Rate of oxygen consumption and stripping of ethanol.* Consider a well-stirred laboratory reactor of volume 2 L used for aerobic continuous cultivation of *S. cerevisiae*. The reactor is sparged with $v_{gf} = 1.3$ L air min^{-1}, and the liquid flow rate through the reactor is $v = 0.6$ L h^{-1}. The oxygen volume fraction in v_{gf} is 20.96%, $T = 30°$C, and the total pressure $P = 1$ atm. In questions (a) to (e) it is assumed that $v_g = v_{gf} = 1.3$ L air min^{-1}.

(a) What are the conditions for which the assumption $v_g = v_{gf}$ is satisfied? Determine the rate of oxygen transfer q_o^t when the volume fraction of oxygen in the exhaust gas is 0.1663.

(b) The oxygen tension in the reactor is measured to 25 μM. s_0^* is 1.16 mM when $\pi_o = 1$ atm. Determine the mass transfer coefficient $k_l a$. Different models for the degree of mixing of the gas between bubbles should be considered: No mixing (completely segregated flow of the gas bubbles), partly mixed, and fully mixed (gas phase completely mixed as we would assume is the case for the liquid phase).

(c) Determine for a liquid flow rate $v = 0.6$ L h^{-1} through the reactor the difference between q_o^t and $(-q_o)$ when s_{of} is $\cong 0$. Is it permissible to equate $(-q_o)$ and q_o^t?

(d) The ethanol concentration in the liquid effluent from the reactor is measured to 4.2 g L^{-1}. The inlet concentration is zero. Find the rate of ethanol production (C-moles L^{-1} h^{-1}). Also determine the mole fraction of ethanol in the liquid.

(e) From physical chemistry the following relation is obtained between the liquid mole fraction x and the gas-phase mole fraction y.

$$y_i = \gamma_i x_i \frac{\pi_i^{\text{sat}}}{p} = \frac{\pi_i}{p} \tag{1}$$

where γ_i is the activity coefficient, p is the total pressure, and π_i is the partial pressure of component i in the gas phase. π_i^{sat} is the saturated vapor pressure 78.4 mmHg of ethanol at the system temperature 30°C. The activity coefficient for ethanol in water is quite high. Rarey and Gmehling (1993) give the value 6.61 for γ_i for $x_\text{i} < 0.01$ mol mol^{-1}. Assume that thermodynamic equilibrium is established between ethanol in the liquid phase and ethanol in the gas phase. Determine how much ethanol is being stripped to the gas phase (C-moles L^{-1}h^{-1}) when $v_\text{g} = v_\text{gf} = 1.3$ L min^{-1}. Compare with the ethanol produced by the bioreaction (question "d"). Will the evaporated ethanol have a significant effect on v_g – i.e., will it seriously invalidate the assumption that $v_\text{g} = v_\text{gf}$?

(f) According to the assumption $v_\text{g} = v_\text{gf,}$ the rate of CO_2 production q_c must be equal to $(-q_\text{o})$.

Consequently the rate of biomass production q_x can be calculated for a given glucose consumption rate. Let $(-q_\text{s}) = 0.297$ C-mole L^{-1} h^{-1}.

Calculate q_x and insert in the redox balance. The lack of closure of the redox balance should prompt you to reconsider the assumption $v_\text{g} = v_\text{gf}$.

The redox balance will give you a linear relation between q_c and $(-q_\text{o})$ when you assume that q_p calculated in (e) is correct and that also $(-q_\text{s})$ is correctly measured.

With this relation you can calculate the correct value of $v_\text{gf}/v_\text{c.}$

Now the measured value for the O_2 mol fraction in v_g can be used to calculate a correct value for $(-q_\text{o})$. Determine the correct values of $(-q_\text{o})$, q_x, and q_c, and check that the redox balance now closes.

It would have been somewhat easier if the volume fraction of CO_2 in v_g had been measured! But as seen here, there is enough information in $(-q_\text{s})$, q_p and the measured volume fraction of O_2 in v_g to find the stoichiometric equation.

(g) $\pi_{H_2O}^{\text{sat}}$ is 31.7 mmHg at 30°C. Assume that dry air, 20.96% oxygen is used as feed to the reactor, but one does not bother to dry the exit gas. Assume that thermodynamic equilibrium is reached between the medium (taken to be pure H_2O) and the gas phase, and that $\gamma_{H_2O} = 1$. What is the difference between v_gf and v_g due to water evaporation? Using the correct values for $(-q_\text{o})$ and q_c calculated in (f) you are requested to calculate the measured volume fraction of O_2 in the exit gas which has not been properly dried.

(h) Finally, consider the situation in (g) for a gas flow of 6.5 L min^{-1}, i.e., five times higher than in the previous questions. The exit gas is still assumed to be saturated with H_2O and not being dried before measuring the O_2 mole fraction. Calculate the error in $(-q_\text{o})$ when the exit gas is (wrongly) taken to be only N_2, O_2, and CO_2.

Different messages have hopefully been delivered in this problem:

The difference in oxygen pressure between inlet and outlet must not be too small (i.e., do not use too high v_{gf}).

The off-gas should be dried before π_{O_2} is measured (Christensen et al. 1995).

If a reaction component (here CO_2) can be easily measured, then measure it.

[The present problem is inspired by the experimental investigation of errors in measurement of oxygen uptake rates and ethanol production rates in bioreactors performed by Duboc and von Stockar (1998)].

Problem 3.2 *Single-cell protein from ethane.* The microorganism *Mycobacterium vaccae* is able to grow with ethane as the sole source of carbon and energy and with NH_3 as the nitrogen source. The limiting substrate is ethane, and the yield $Y_{sx} = 23.7$ g dry weight per mole ethane.

Except for small amounts of S and P an elemental analysis of dry cell mass is C, 47.4 wt%; N, 8.30 wt%; H, 7.43 wt%. The ash content is 4.00 wt%, while the oxygen content (which cannot be obtained by the analysis) must be found from a total mass balance. Determine the elemental composition of the ash-free biomass and its formula weight per C-atom.

(a) Calculate Y_{sx} in C-moles (C-mole)$^{-1}$.
(b) Calculate the oxygen consumption Y_{so} mol O_2 (C-mole ethane)$^{-1}$ when it is assumed that CO_2 is the only metabolic product (apart from H_2O). Write the stoichiometry for conversion of ethane to SCP.
(c) Measurements show that 10.44 g DW is formed per mole O_2 consumed. The yield Y_{sx} is that calculated above, but the value of RQ is 0.3805. Show that an extra metabolic product must be formed besides CO_2 (and H_2O). Determine the degree of reduction of this extra metabolic product. Using your general chemical knowledge you should be able to identify the extra metabolic product.

Problem 3.3 *Production of Penicillin V.* Figure 2.9 recaptures the biosynthesis of P = Penicillin V. In the last step of the pathway phenoxyacetic acid forms an amide with the amino group of 6-APA. There are two carbon substrates, glucose (S_1) and phenoxyacetic acid (S_2)

(a) On a C-mole basis what is the yield coefficient Y_{ps2}? Also determine Y_{ps2} in g g^{-1}.
(b) The composition of *Penicillium chrysogenum* is $X = CH_{1.64}O_{0.52}N_{0.16}S_{0.0046}P_{0.0054}$. Determine the oxygen requirement Y_{po} if $Y_{sx} = 0.127$ and $Y_{sp} = 0.194$. Also find RQ.
(c) Make the assumption that during a fed-batch cultivation of penicillin r_p will always be proportional to $r_x = \mu$. Discuss whether this assumption appears to be reasonable. If the assumption holds, then what would be the effect on the specific penicillin production rate if during the cultivation Y_{so} starts to increase.
(d) On line RQ measurement show that during the first 120 h of the production phase (after biomass has been formed during an initial batch phase) RQ = 0.95 to 1.15 with considerable scatter of the data. After 150 h when growth of the

fungus has virtually ceased RQ increases rapidly above 1.20. Discuss probable reasons for this observation. Is it due to break-down of the assumption in question "c"? Are other products formed? Could there be some straightforward experimental error?

Problem 3.4 *Checking an anaerobic mass balance for cultivation of S. cervisiae.* In a steady state, strictly anaerobic chemostat with $V = 1$ L the yeast *S. cerevisiae* grows on a sterile medium with 23 g L^{-1} glucose and 1 g L^{-1} NH_3. The feed rate is $v = 0.1$ L h^{-1}. The biomass composition is $X = CH_{1.76}O_{0.56}N_{0.17}$.

The effluent from the bioreactor has the following composition in g L^{-1}: Glucose (s), 0.048; ammonia (s_n), 0.728; biomass (x), 2.36; ethanol (p_e), 8.85; glycerol (p_g), 2.39. The CO_2 production is measured by a photoacoustic method. The CO_2 concentration in the effluent gas (in the head space) is found to be 2.88 vol.%. On a flow-meter the total gas flow (30°C, 1 atm) is determined to 0.25 L min^{-1}. v_{gf} is assumed to be equal to v_g.

(a) Use the data to set up a carbon balance. Show that the data are not consistent, and calculate the yield coefficient of a missing metabolite.
(b) Calculate the degree of reduction of the missing metabolite. In your opinion what is the source of the error?

Problem 3.5 *Production of poly β-hydroxy butyrate (PHB).* van Aalst et al. (1997) studied the formation of PHB by the bacterium *Paracoccus pantotrophus* in a continuous, stirred tank reactor operated at steady state. When growing under N-limitation but with an excess of the carbon source the organism can build up a large carbon storage that can be used to support active growth when, or if the N-limitation is lifted. This is part of the clean-up cycle in waste water treatment plants, but PHB has an independent and increasing interest as a biodegradeable polymer – in competition with particularly polylactides. Although PHB is a part of the biomass it can just as well be regarded as a metabolic product. Its formula is $P = CH_{1.5}O_{0.5}$ per carbon atom. The remainder of the biomass (the "active" biomass) has the formula $X = CH_{1.73}O_{0.44}N_{0.24}$ per carbon atom. The organism uses acetic acid, CH_3COOH as carbon and energy source. It grows aerobically, and some CO_2 is produced together with X and P.

(a) The result of two experiments, one with N-limitation and one with C-limitation are given below

Dilution rate and effluent concentration of substrates	Production rates in mg L^{-1} h^{-1}		
(D h^{-1}, s_i mg L^{-1})	$-q_s$	q_x	q_p
$D = 0.5$ $s_{HAc} = 70$ $s_{NH_3} = 95$	3,065	1,050	75
$D = 0.1$ $s_{HAc} = 750$ $s_{NH_3} = 10.5$	1,625	260	420

For each of the two experiments determine the yield coefficients in the black box model CH_2O (HAc) $- Y_{sn}$ $NH_3 - Y_{so}$ $O_2 + Y_{sx}$ X + Y_{sp} P + Y_{sc} CO_2 + Y_{sw} $H_2O = 0$.

(b) For each of the two experiments calculate the exit concentrations of X and P when there is no X or P in the feed. Also calculate the inlet concentrations of acetic acid and ammonia.

(c) Could any single kinetic expression describe the results of both experiments?

Problem 3.6 *Comparison between two strains of S. cerevisiae.* Nissen et al. (2001) studied anaerobic cultivation of three different strains of *S. cerevisiae,* TN1, TN26, and TN21 on a defined medium with glucose as carbon and energy source. TN1 is the "standard" haploid strain used in a number of studies by the authors. TN21 is a transformant of TN1 which expresses the transhydrogenase gene *tdh* from *Azotobacter vinlandii* to a high level, 4.53 units mg^{-1}. TN26 is also a transformant of TN1 with the same multicopy expression vector as in TN1, but without ligation of the *tdh* gene. TN26 is consequently genetically identical to TN21, except that it cannot express transhydrogenase. It is therefore unable to equilibrate the reversible reaction between $NADPH/NAD^+$ and $NADH/NADP^+$.

The table below shows product yields from steady state, glucose limited continuous cultivations of the three strains. Note the high accuracy of the data, and also that TN26 behaves exactly as TN1. There are, however, small but significant differences between TN21 and TN26. All data are given as C-mole $(\text{C-mole glucose})^{-1}$.

Product	TN1	TN26	TN21
Ethanol	0.494 ± 0.012	0.493 ± 0.011	0.451 ± 0.011
Glycerol	0.091 ± 0.001	0.093 ± 0.001	0.118 ± 0.001
CO_2	0.275 ± 0.007	0.271 ± 0.007	0.262 ± 0.007
Biomass	0.111 ± 0.002	0.112 ± 0.002	0.102 ± 0.002
Succinate	0.005 ± 0.0003	0.005 ± 0.0003	0.006 ± 0.0003
Pyruvate	0.005 ± 0.0003	0.005 ± 0.0003	0.001 ± 0.0003
Acetate	0.005 ± 0.0003	0.005 ± 0.0003	0.007 ± 0.0003
2-Oxaloacetate	0.002 ± 0.0003	0.007 ± 0.0003	0.045 ± 0.0003
Total	0.988 ± 0.022	0.991 ± 0.021	0.992 ± 0.021

(a) Check the redox balance for TN26 and TN21.

(b) Assume that the missing carbon is ethanol. Repeat the calculation of (a) with this assumption.

(c) Discuss qualitatively the difference between the product profiles for TN26 and TN21. What could be the reason for the higher yield of 2-oxaloacetate? The dominant cofactor for conversion of 2-oxoglutarate to glutamic acid is NAPDH in all three strains.

[The experimental investigation of this problem was mentioned in Sect. 2.2.1]

Problem 3.7 *Simultaneous removal of* NH_4^+ *and* NO_3^{1-} *from waste water.* Biological removal of nutrients from industrial waste water streams can be achieved in so-called integrated waste water treatment systems where variations

in the local environment allow consortia of anaerobic and aerobic microorganisms to live side by side. With a less than perfect aeration there will be anoxic regions within the otherwise aerated reactor, and nitrification (aerobic) of NH_3 to nitrate occurs simultaneously with (anaerobic) denitrification of nitrate to N_2.

Three types of organisms live together:

1. Aerobic organisms that respire the carbon source (e.g., HAc) to CO_2.
2. Aerobic organisms that convert NH_3 to nitrate using CO_2 as carbon source and the oxidation of inorganic N (NH_3) to nitrate as the energy source. These nitrifying organisms belong to the so-called chemolithotrophs (i.e., they fix CO_2 into biomass).
3. Denitrifying organisms that use, e.g., acetate as carbon source and nitrate as electron acceptor (see Example 3.7) producing N_2, biomass, and CO_2.

   (a) Calculate the minimum amount of CO_2 that has to be produced in order for the denitrifiers to produce N_2 by the stoichiometry

$$CH_2O(\text{as acetate}) + Y_{s,HNO_3}HNO_3 \rightarrow Y_{sx}CH_{1.8}O_{0.5}N_{0.2} + Y_{sN_2}N_2 + Y_{sc}CO_2(+\text{water}) \quad (1)$$

   (b) A liquid feed of 500 m^3/day to a continuous, stirred tank reactor contains 5 g L^{-1} COD (presumably as HAc) and 0.3 g L^{-1} N (as NH_3). The O_2 consumption is 2,000 kg/day. The liquid effluent contains 0.2 g COD L^{-1} (as acetate), 1 g biomass L^{-1} ($CH_{1.8}O_{0.5}N_{0.2}$ with 7% ash), no ammonia, but some nitrate (write this as HNO_3, although the pH is much too high for free HNO_3 to be present). The exhaust gas from the plant contains N_2 and CO_2 (if air was used instead of O_2 it would be N_2 in excess of that in the incoming air).

   Calculate the rates of production of N_2 and "HNO_3" in kmol/day.

   Write the complete stoichiometry for the process.

   How would the stoichiometry change if the liquid effluent contained no HNO_3 while the values of Y_{sx} and Y_{so} remained the same as in the previous case?

   Carbon is frequently added to the feed (as HAc) to give enough "power" in the feed. Consequently, it is interesting to see if Y_{s,NH_3} is higher in the variation of the problem.

   COD is measured in the same way as BOD (see Sect. 3.4.2).

[The authors acknowledge the assistance of professor Lars K Nielsen, University of Queensland, Australia, for the original formulation of this problem which is in his notes for a course Metabolic Engineering given at UQ].

Problem 3.8 *Correctly and incorrectly calculated rates of O_2 consumption.* A 1 L working volume fermentor is sparged with air (composition 20.96% O_2, 79.04% N_2 (+Ar)). The gas is dry, and the feed rate is v_{gf} L h^{-1} ($T = 30°C$, $P = 1$ atm).

The exit gas flow is v_g L h^{-1}. It is carefully dried before its composition is measured at 30°C and $P = 1$ atm.

(a) For $v_{gf} = 60$ L h^{-1} the oxygen and carbon dioxide concentrations in v_g are measured to $O_2 = 17.10$ (volume)% and $CO_2 = 6.10\%$.
Calculate $(-q_{O_2})$ (mol h^{-1} (L bioreactor)$^{-1}$) and q_{CO_2}.
Determine the respiratory quotient RQ.
What would be the error in RQ if it was incorrectly assumed that the exit gas flow v_g was equal to the inlet gas flow $v_{gf} = 60$ L h^{-1}?

(b) The feed rate of air is increased to $v_{gf} = 120$ L h^{-1} (same composition, T and P as before). Assume that the mass transfer coefficient $k_l a$ is sufficiently high at $v_{gf} = 60$ L h^{-1} to make the bioreaction entirely controlled by the chemical reaction rate. Then the two gas production rates q_{O_2} and q_{CO_2} are the same as at $v_{gf} = 60$ L h^{-1}.
Calculate the composition of CO_2 and O_2 in the exit gas.

(c) Let the O_2 concentration in the exit gas be measured to 19.00 (volume)% when $v_{gf} = 120$ L h^{-1}. What would be the calculated rate of oxygen consumption $(-q_{O_2})$ if it was incorrectly assumed that $v_g = v_{gf}$?

(d) In the two experiments (a and b) an oxygen probe measures the oxygen tension s_O in the medium to be 25 and 11% of the saturation value s_O* (30°C, medium in equilibrium with air) when v_{gf} is respectively 120 and 60 L h^{-1}. Determine the value of $k_l a$ in the two experiments. Why do you think $k_l a$ is somewhat lower in the 60 L h^{-1} experiment than in the 120 L h^{-1} experiment ?
If v_{gf} is further reduced to 30 L h^{-1} s_O is close to zero. Is it now correct to assume that the true rate of the bioreaction can be calculated based on the composition of O_2 in the exit gas ? What happens when v_{gf} is reduced too much?

(e) The above results were obtained in an aerobic cultivation of *Saccharomyces cerevisiae* in a stirred tank continuous bioreactor with glucose as carbon source and NH_3 as N-source. The gas production rates were measured to: $q_{O_2} = -0.0811 \text{mol } h^{-1}(\text{Lreactor})^{-1}$, and $q_{CO_2} = 0.1515 \text{mol } h^{-1}L^{-1}$.
The glucose feed is 1/3 L h^{-1}(L reactor)$^{-1}$ with $s_f = 36$ g L^{-1}. In the effluent the glucose concentration is $s = 0.15$ g L^{-1}.
The only products are biomass ($X = C\ H_{1.74}\ O_{0.6}\ N_{0.12}$), CO_2 and ethanol.
Determine the stoichiometry for the bioreaction.

Problem 3.9 *The redox content of complex molecules of cyclic and aromatic nature.*

(a) Start with *n*-hexane. How many redox equivalents are contained in this molecule?

(b) Convert *n*-hexane first to cyclohexane and then to benzene. What is the redox content of the two molecules? What is the redox level per carbon atom in benzene?

(c) Convert benzene to *p*-hydroxy benzene. What is the redox content in this molecule?

(d) Now construct 4-hydroxy phenyl pyruvic acid (by addition of pyruvic acid to *p*-hydroxy benzene. Again find the redox content of the molecule.
(e) Finally, convert 4-hydroxy pyruvic acid to tyrosine (Fig. 2.12) by a transamination reaction (Sect. 2.3.1) where one molecule glutamic acid is simultaneously converted to 2-oxoglutaric acid. Confirm the value 4 2/9 for the redox level of tyrosine (per C-atom).

References

Aalst van, M.A., Leeuwen van, M.A., Pot, M.C, Loosdrecht van, M., and Heijnen, J.J, (1997). Kinetic modelling of PHB production and consumption by *Paracoccus pantotrophus* under dynamic substrate supply. *Biotechnol. Bioeng*., **55,** 773–782.

Andersen, M.Y., Pedersen, N., Brabrand, H., Hallager, L., and Jørgensen, S.B. (1997). Regulation of a continuous yeast bioreactor near the critical dilution rate using a productostat. *J. Biotechnol*., **54**, 1–14.

Bijkerk, A.H.E. and Hall, R.J. (1977). A mechanistic model of the aerobic growth of *Saccharomyces cerevisiae*. *Biotechnol. Bioeng*., **19**, 267–296.

Christensen, L.H., Schulze, U., Nielsen, J., and Villadsen, J. (1995). Acoustic gas analysis for fast and precise monitoring of bioreactors. *Chem. Eng. Sci*., **50**, 2601–2610.

Duboc, P. (1997). Transient growth of *Saccharomyces cerevisiae,* a quantitative approach, PhD thesis EFPL (Lausanne).

Duboc, P., and von Stockar, U. (1998). Systematic errors in data evaluation due to ethanol stripping and water vaporization. *Biotechnol. Bioeng*., **58**, 428–439.

Erickson, L.E., Minkevich, I.G., and Eroshin, V.K. (1978). Application of mass and energy balance regularities in fermentation. *Biotechnol. Bioeng*., **20**, 1595–1621.

Goldberg, I. and Rokem, J.S. (1991). *Biology of Methylotrophs*, Butterworth-Heinemann, Boston.

Heijden, R.T.J.M. van der, Heijnen, J.J., Hellinga, C., Romein, B., and Luyben, K., Ch. A.M. (1994a). Linear constraint relations in biochemical reaction systems: I, Classification of the calculability and the balanceability of conversion rates. *Biotechnol. Bioeng*., **43**, 3–10.

Heijden, R.T.J.M. van der, Romein, B., Heijnen, J.J., Hellinga, C., and Luyben, K. Ch. A.M. (1994b). Linear constraint relations in biochemical reaction systems: II, Diagnosis and estimation of gross errors, *Biotechnol. Bioeng*., **43**, 11–20.

Lange, H.C., and Heijnen, J.J. (2001). Statistical reconciliation of the elemental and molecular biomass composition of *Saccharomyces cerevisiae*. *Biotechnol. Bioeng.,* **75**, 334–344.

Lee, S.Y., and Choi, J.I. (2001). Production of microbial polyesters by fermentation of recombinant microorganisms. *Advances in Biochem. Eng*., **71**, 183–207.

Lei, F., Rotbøll, M., and Bay-Jørgensen, S. (2001). A biochemically structured model for *Saccharomyces cerevisiae*. *J. Biotechnol*., **88**, 205–221.

Madron, F., Veverka, V., and Vanecek, V. (1977). Statistical analysis of material balance of a chemical reactor. *A.I.Ch.E. Journal*, **23**, 482–486.

Maier, R.M., Pepper, I.L., and Gerba, C.P., (2000). *Environmental Microbiology*, Academic Press (London, UK).

Meyenburg, K. von (1969). Katabolit-Repression und der Sprossungszyklus von *Saccharomyces cerevisiae*, Dissertation, ETH, Zürich.

Nielsen, J., Johansen, C.L., and Villadsen, J. (1994). Culture fluorescense measurements during batch and fed-batch cultivations with *Penicillium crysogenum*. *J. Biotechnol*., **38**, 51–62.

Nissen, T.L., Anderlund, M., Nielsen, J., Villadsen, J., and Kjelland-Brandt, M.C. (2001). Expression of a cytoplasmic transhydrogenase in *Saccharomyces cerevisiae* results in formation of 2-oxoglutarate due to depletion of the NADPD-pool. *Yeast*, **18**, 19–32.

Nordqvist, M., Nielsen, P.M., and Villadsen, J. (2007). Oxidation of lactose to Lactobionic acid by a *Microdochium nivale* carbohydrate oxidase: Kinetics and operational stability. *Biotechnol. Bioeng.*, **97**, 694–707.

Pedersen, H., Christensen, B., Hjort, C., and Nielsen, J. (2000). Construction and characterization of an oxalic acid nonproducing strain of *Aspergillus niger*. *Metabol. Eng.*, **2**, 34–41.

Pham, H., Larsson, G., and Enfors S.-O. (1999). Modeling of aerobic growth of *Saccharomyces cerevisiae* in a pH-auxostat. *Bioproc. Eng.*, **20**, 537–544.

Postma, E., Verduyn, C., Scheffers, A., and van Dijken, J. (1989). Enzymatic analysis of the Crabtree-effect in glucose limited chemostat cultures of *Saccharomyces cerevisiae*. *Appl. Environ. Microbiology*, **55**, 468–477.

Rarey, J.R., and Gmehling, J. (1993). Computer – operated differential static apparatus for the measurement of vapor-liquid equilibrium data. *Fluid Phase Equilib.*, **83**, 279–287.

Roels, J.A. (1983). *Energetics and Kinetics in Biotechnology*. Elsevier Biomedical Press, Amsterdam.

Schulze, U. (1995). Anaerobic physiology of *S. cerevisiae*. Ph.D. thesis, Department of Biotechnology, DTU.

Schulze, U., Lidén, G., Nielsen, J., and Villadsen, J. (1996). Physiological effect of N-starvation in an anaerobic batch culture of *S. cerevisiae*. *Microbiology*, **142**, 2299–2310.

Wang, N.S. and Stephanopoulos, G. (1983). Application of macroscopic balances to the identification of gross measurement errors. *Biotechnol. Bioeng.*, **25**, 2177–2208.

Chapter 4
Thermodynamics of Bioreactions

The Black Box models of Chap. 3, based as they are on mass balances in continuous steady-state reactors, are the pale reflections of the long biochemical pathways of Chap. 2.

The proper synthesis of the Black Box model will follow in Chap. 5. But before considering the analysis of individual pathways and their combination into a metabolic network, it is profitable to consider whether a given pathway is at all feasible from the standpoint of thermodynamics. Based on the genome of the organism and using computer-aided analysis, one can write up the whole ensemble of fluxes through different pathways toward desired products (the *fluxome*). But are all the possible pathways feasible, i.e., will there be a positive flux through the pathway? A preliminary answer is given by consideration of thermodynamic constraints applied to each of the enzymatic reactions in the pathway. If just one of the reactions in the pathway is accompanied by a large and positive change in free energy ($\Delta G >> 0$) the flux of substrate toward product by that particular pathway is blocked. The product can still be synthesized from the substrate, but a different metabolic path is used. This is why in gluconeogenesis reversal of reaction 10 in Fig. 2.4b has to follow a circuitous route *via* malate, and this is in general the reason why in functioning pathways a large negative ΔG between substrate to the pathway and product from the pathway is "squandered" in many steps, each with a small value of $-\Delta G$.

To give some insight into the role of thermodynamics in pathway engineering, and to avoid needless speculation on improvement of the enzymes in a pathway that would never be functional, a few basic concepts from classical thermodynamics will be reviewed, using glycolysis as an example. Furthermore, the functioning of oxidative phosphorylation which can hardly be understood without recourse to thermodynamics will be sketched. This example is also used to introduce the basic concepts of non-equilibrium thermodynamics, a discipline which can be applied to estimate the *rate* of bioreactions. Finally, some simple calculation methods for the heat release by bioreactions will prove to be of considerable practical value for the design of heat exchangers in bioreactors.

J. Villadsen et al., *Bioreaction Engineering Principles*,
DOI 10.1007/978-1-4419-9688-6_4,

Surely, thermodynamics has a much broader application in bioprocesses than suggested by the above examples. Thermodynamics is applied in the design of complex separation processes where macromolecules (proteins, RNA, or DNA) or large metabolic products (e.g., polyketides) are extracted from the fermentation medium using chromatography, crystallization, or aqueous two-phase media. Membrane separation processes and the fouling of membranes by macromolecules are other topics which cannot be discussed quantitatively without recourse to thermodynamics.

In the context of the main theme of the textbook the examples are, however, restricted to what is considered to be essential to help in the analysis and design of bioreactions.

4.1 Chemical Equilibrium and Thermodynamic State Functions

4.1.1 Changes in Free Energy and Enthalpy

In thermodynamics, a *system* is defined as that part of the universe which is being studied, such as a bioreactor or a cell, whereas the rest of the universe is referred to as the *surroundings*. A system is said to be *open* or *closed* according to whether it can exchange matter and energy with its surroundings. Because living cells take up nutrients, release metabolites, and generate work and heat, they are open systems. The state of a system is defined by a set of *state functions* which besides the free energy G include enthalpy H, equal to the heat absorbed at constant pressure when the only type of work is due to volume change, and entropy S, a measure of the degree of order in the system.

Biochemical reactions occurring within a cell must satisfy the laws of thermodynamics, and according to the second law of thermodynamics (4.1), *spontaneous* processes generally occur in a direction that increases the overall disorder (or entropy) of the system. The total entropy contained in the products is greater than the entropy contained in the reactants, or, mathematically, $\Delta S_R > 0$. Thus, one might say that the process is "entropy driven."

The spontaneity of a process is, however, not be decided by the entropy change alone, and some reactions with $\Delta S_R < 0$ proceed very well. These are *exothermic* reactions, reactions accompanied by a large release of heat Q to the surroundings. These reactions have a large, *negative* increase of the *enthalpy* H of the system: $-\Delta H_R = Q > 0$ – one might say that the reaction is "enthalpy driven." In fact, most *endothermic* reactions ($\Delta H_R > 0$) will not proceed spontaneously, even when $\Delta S_R > 0$, since the change in enthalpy has a much greater influence on ΔG_R than has ΔS_R.

These observations are expressed in (4.1):

$$\Delta G_R = \Delta H_R - T\Delta S_R. \tag{4.1}$$

The process has a *positive affinity*, i.e., it proceeds spontaneously, when $\Delta G_R < 0$.

It is noted that the ΔS_R contribution to ΔG_R is proportional to the absolute temperature T.

Since ΔH_R and ΔS_R are weak functions of T, a process with negative ΔS_R can have a positive affinity at low temperature, but a negative affinity at higher T. An example is the folding of proteins to their native, active form. Both ΔH_R and ΔS_R are negative (the process is exothermic, but the folding increases the "order" of the system). At low temperature the folded protein is stable, while the unfolded, denatured protein is stable at higher temperatures.

In the following a procedure is outlined by which the *value* of ΔG_R for a chemical reaction can be *calculated*. The procedure consists of three steps:

1. A set of standard values for G, H, and S is defined: *All elements in their stable form at* 298.16 K, 1 atm *total pressure, are defined to have* $H = G = 0$. According to the *third law of thermodynamics*, the entropy of a perfect crystal of any element is zero at 0 K. At 25°C = 298.16 K all elements have a positive value of S. The entropy of a compound is found by spectrometry.
2. Next, the thermodynamic properties of *compounds* at standard conditions, G_f, H_f, and S_f, *the free energy, the free enthalpy of formation*, and *the entropy of the compound*, respectively, are determined. In classical thermodynamics, the compound is "built" from its constituent elements, using the appropriate stoichiometry (e.g., 2 H and 1 O to form H_2O). The thermodynamic properties of a compound depend on the state of the compound. Thus (water) ice, liquid, and vapor have different values for G_f, H_f, and S_f.

   The enthalpy of formation, H_f, is experimentally determined by calorimetry, while G_f is calculated using (4.1) together with experimentally determined values for H_f and S_f.

   G_f and H_f are *properties* of the compound. Negative values for G_f and H_f signify that an input of free energy and heat is needed to reverse the reaction, i.e., to recreate the building blocks from the compounds.

   Whereas the building blocks are the elements in classical thermodynamics, it may be practical to use other building blocks for certain compounds. Thus, in biochemistry it is convenient to define G_f for energy carrying and for redox carrying cofactors relative to the G_f of the compounds from which they are synthesized. ATP is synthesized from ADP and free phosphate (P_i), and NADH is synthesized by reduction of NAD. Hence G_f (ATP) and G_f (NADH) are defined as the free energy content of these compounds, above that of their counterparts ADP and NAD.

   With this definition and at standard conditions G_f (ATP) = 30.5 kJ (mol ATP)$^{-1}$. This is the"free energy package" that the co-substrate ATP delivers to a reaction which would not proceed voluntarily without an input of free energy.

   Similarly, at standard conditions G_f(NADH) = 153 kJ (mol NADH)$^{-1}$ This is the energy package that NADH as a co-substrate delivers to a reduction process that without the participation of NADH would always have a positive ΔG_R. The "standard" conditions for which the two free energy packages have the above quoted values will be discussed later (Example 4.3).

3. Finally, the change in free energy of the system by converting a set of reactants to a set of products is found by applying (4.2).

The way in which ΔG_R is calculated by means of the procedures 1–3 mimics the procedure which was introduced in Chap. 3 to balance the redox transfer in chemical reactions: The degree of reduction of the elements was found after a set of compounds had been defined to have zero redox content. Next, the redox level of arbitrary compounds was calculated and finally the stoichiometry of a chemical reaction was balanced, sometimes by adding a redox cofactor on either the substrate or the product side of the reaction.

Equation (4.2) is consequently an analogue of the redox balances of Chap. 3:

$$(\Delta G)_R^0 = \left(\sum_i Y_{sp_i} G_{f,i}\right)_{\text{products}} - \left(\sum_j Y_{ss_j} G_{f,j}\right)_{\text{substrates}}, \tag{4.2}$$

where Y_{sp_i} and Y_{ss_i} are the yield coefficients defined in (3.14) for products and substrates. In (4.2), $G_{f,j}$ is the free energy of formation of the reactants (substrates and products) at the state at which they are present in the reaction.

The standard conditions used to define ΔG_R^0 in (4.2) are *usually* $T = 25°C$, 1 M concentration of reacting species, or partial pressure π_i and $\pi_j = 1$ atm (for gas-phase reactions). But, as indicated in procedure 2 above, a different set of standard conditions is used in aqueous phase biochemical reactions. *Most notably* $[H^+]$ *is defined to be* 10^{-7}.

Extensive tables of G_f, H_f, and S_f are available, and using data from these tables (nowadays present in databases) ΔG_R^0 and ΔH_R^0 can be calculated.

For any chemical reaction carried out at non-standard conditions ΔG_R is related to ΔG_R^0, the free energy of reaction at standard conditions, by

$$\Delta G_R = \Delta G_R^0 + RT \ln K. \tag{4.3}$$

In (4.3), *the mass action fraction* K for the reaction is defined by:

$$K = \frac{\Pi\, p_i^{Y_{p_i}}}{\Pi\, s_i^{Y_{s_i}}}, \tag{4.4}$$

where $\Pi\, s_i^{Y_{s_i}}$ is the product of substrate activities where each activity is raised to the power of the corresponding stoichiometric (or yield) coefficient in the reaction. $\Pi\, p_i^{Y_{p_i}}$ is the corresponding quantity for the products. For reactants in dilute aqueous solutions the activities can be set equal to their molar concentrations. For gas-phase reactants at low total pressure, the activities are equal to the partial pressures in atm.

At equilibrium $\Delta G_R = 0$ and therefore

$$\Delta G_R^0 = -RT \ln K_{eq}. \tag{4.5}$$

In (4.5), K_{eq} is the *equilibrium constant* for the reaction.

Examples 4.1 and 4.2 serve to illustrate the application of the basic formulas (4.1)–(4.5).

Spontaneous processes are said to be *exergonic*, and they could be utilized to do work, e.g., by means of a fuel cell. Processes that are not spontaneous, i.e., with positive ΔG_R, are termed *endergonic*, and they must be driven by an input of free energy. Processes at equilibrium, i.e., the forward and backward processes are exactly balanced, are characterized by $\Delta G_R = 0$.

It is important to note that a large negative value of ΔG_R does not necessarily imply that a chemical reaction will proceed at a measurable rate. Thus, the free energy change of the phosphorylation of glucose to glucose-6-phosphate by ATP is large and negative, but this reaction does not occur just by mixing glucose and ATP. Only when the enzyme hexokinase is added does the reaction proceed. Similarly, most biological molecules, including proteins, nucleic acids, carbohydrates, and lipids, are thermodynamically unstable to hydrolysis, but their spontaneous hydrolysis is insignificant. Only when hydrolytic enzymes are added do the hydrolysis reactions proceed at a measurable rate. Despite their importance in accelerating a reaction, enzymes do not change the ΔG_R for the reaction. As catalysts they can only speed up the attainment of thermodynamic equilibrium, but they do not allow a reaction with a positive ΔG to proceed.

Example 4.1 *Thermodynamic data for H_2O.* In Handbook of Chemistry and Physics one obtains the following standard values for O_2, H_2, and H_2O – all in the gas phase

	G_f^o	H_f^o	S^0
O_2	0	0	205
H_2	0	0	130.6
H_2O	−228.72	−241.95	188.8

G_f^o and H_f^o are in kJ mol^{-1}, S^0 is in J(mol K)$^{-1}$. Since (4.1) is a relation between ΔG, ΔH, and ΔS we can use two of these quantities to calculate the third. Thus, for water at 25°C:

$$\begin{aligned} H_f^o(H_2O)_g &= -228.72 + (188.8 - 130.6 - 0.5 \times 205) \times 0.298 \\ &= -241.93 \text{ kJ mol}^{-1}. \end{aligned}$$

Liquid water has much lower entropy (70.0 J (mol K)$^{-1}$) than gaseous H_2O at the same conditions. Consequently, for formation of liquid water from O_2 and H_2 at 25°C:

$$\Delta H_f^o = -241.95 - 2.436 \times 18 = -285.80 \text{ kJ mol}^{-1},$$

$$\Delta G_f^o = -285.80 - 0.298(70.0 - 130.6 - 102.5) = -237.3 \text{ kJ mol}^{-1}.$$

The heat of vaporization of H_2O at 25°C is 2.436 kJ g^{-1}.

Example 4.2 *Equilibrium constant for formation of H_2O.* For the reaction between ½ O_2 and H_2 to form gaseous water at [25°C, 1 atm]:

$$\ln K_{eq} = \frac{-\Delta G^0}{RT} = \frac{228.72}{0.298 \times 8.315} = \ln \left[\frac{p_{H_2O}}{p_{O_2}^{1/2}\, p_{H_2}} \right]_{eq} = 92.28. \quad (1)$$

For the corresponding reaction where the produced water is in equilibrium with liquid water at 25°C

$$\begin{aligned} \tfrac{1}{2}O_2 + H_2 &\rightarrow (H_2O)_{gas}; \quad \Delta G_1 \\ (H_2O)_{gas} &\leftrightarrow (H_2O)_l; \quad \Delta G_2 = 0 \end{aligned} \tag{2}$$

The total reaction to form water in the liquid phase has $\Delta G_R = \Delta G_1 + \Delta G_2 = \Delta G_1$

$$\Delta G_R = \Delta G_R^0 + RT \ln \frac{23.7}{760} = -228.72 - 8.593 = -237.3 \text{ kJ mol}^{-1} \tag{3}$$

since the partial pressure of H_2O in equilibrium with liquid water at 25°C is 23.7 mmHg. Apart from round-off errors this is the same result as was obtained in Example 4.1 where a standard free energy $G_f\,(H_2O)_{liquid}$ was defined in a reference frame of liquid water at 25°C rather than gaseous water. Similarly, if in a reaction with no liquid water present we can remove the produced water vapor to a partial pressure of 23.7 mmHg while the partial pressures of O_2 and H_2 are kept at 1 atm we can shift the free energy of the gas-phase reaction from −228.7 to −237.3 kJ mol^{-1} H_2O formed.

4.1.2 Free Energy Changes in Bioreactions

Example 4.2 shows that the value of ΔG_R can be pushed in a desired direction by fixing the concentrations (or for gas-phase reactions the partial pressures) of reactants at levels different from those at standard conditions. Since the reaction only proceeds spontaneously when ΔG_R is negative, we may force it thermodynamically by decreasing the product concentrations and increasing the substrate concentrations. For reactions to run inside a living organism, it is therefore important that the levels of substrates and products are allowed to vary without affecting the overall thermodynamic feasibility of the reaction. Hence, the first reaction in a pathway is typically designed by nature to have a large and negative ΔG_R as it may hereby be thermodynamically feasible even when the substrate concentration gets very low. Similarly the last reaction in a pathway also typically has a large and negative ΔG_R to make it thermodynamic feasible even when the product concentration gets very high. This is illustrated for the EMP pathway in Example 4.3.

The typical way in which a pathway reaction is made to proceed in a thermodynamically unfavored direction is by coupling it to a thermodynamically favored reaction. This is where ATP plays a crucial role as a cofactor in pathway reactions. Thus, phosphorylation of glucose to glucose-6 phosphate (G6P) is coupled to the hydrolysis of one ATP molecule to ADP. Reaction (4.7), in which glucose is directly phosphorylated to G6P at pH = 7 has a positive ΔG_R of 13.8 kJ (mol glucose)$^{-1}$, but if ATP with a ΔG of 30.5 kJ (mol ATP)$^{-1}$ when formed from

ADP and P_i is added as a co-substrate to give reaction (4.8), we obtain by application of (4.2) that $\Delta G^0_R = 13.8 - 30.5 = -16.7$ kJ (mol glucose)$^{-1}$ at pH = 7.

$$G^o_f(\text{ATP}) = 30.5 \text{ kJ mol}^{-1} \text{ at } [\text{ATP}] = [\text{ADP}] = [P_i] = 1 \text{ mol L}^{-1}, [H^+] = 10^{-7}, \tag{4.6}$$

$$\text{Glucose} + P_i \rightarrow \text{G6P}; \ \Delta G^0_R = 13.8 \text{ kJ (mol glucose)}^{-1}, \tag{4.7}$$

$$\text{Glucose} + \text{ATP} \rightarrow \text{ADP} + \text{G6P} + P_i = 0; \Delta G^0_R = -16.7 \text{ kJ (mol glucose)}^{-1}. \tag{4.8}$$

Further down in the EMP pathway (Fig. 2.4) ATP is regenerated in two reactions. One is the conversion of phosphoenolpyruvate (PEP) to pyruvate (PYR):

$$\text{PEP} + \text{ADP} + P_i \rightarrow \text{PYR} + \text{ATP}; (\Delta G^0_R = -61.9 - (-30.5) = -31.4 \text{ kJ mol}^{-1}. \tag{4.9}$$

The many individual reactions, which together constitute the EMP pathway net-reaction

$$\text{Glucose} + 2 \text{ NAD}^+ + 2 \text{ ADP} + 2P_i \rightarrow 2 \text{ PYR} + 2\text{NADH} + 2 \text{ ATP} \tag{4.10}$$

will, by careful harnessing of the large release of free energy in some of the reactions, proceed voluntarily although some of the reaction steps have a positive ΔG^0_R. This is the first message of Example 4.3.

The ATP that participates in the reactions is not to be construed as a stationary pool. ATP is formed and consumed all the time, and the turnover frequency is high. Left alone, ATP has a half-life time of a few seconds, or at most a few minutes, depending on the cell type and on the environment. It is tacitly assumed that in steady-state fermentations, the ATP generation in catabolic pathways is always balanced by its consumption in anabolic pathways.

It should finally be remarked that the $\Delta G^0_R = -30.5$ kJ mol^{-1} for the hydrolysis of ATP is not an exact, unchangeable value. In living cells concentrations of ions, coenzymes, and metabolites might vary by several orders of magnitude across the membranes that separate organelles, and the actual ΔG_R may therefore be much different from ΔG^0_R. This also holds for most other biochemical reactions, and one must be extremely careful when evaluating thermodynamic feasibility based exclusively on the ΔG^0 for the reaction. This is the second message of Example 4.3.

Example 4.3 *Free energy changes of reactions in the EMP pathway*. To determine the free energy changes of cellular reactions, it is necessary to know the concentrations of all metabolites and cofactors participating in these reactions. Such data are available only for a few pathways, and thermodynamic considerations are therefore often based solely on standard free energy changes. This may lead to erroneous conclusions since the use of standard free energy changes assumes certain fixed concentrations for reactants and products (those of the standard state) that may be very different from the actual intracellular metabolite concentrations. To illustrate this point, we calculate the free energy change for the reactions in the EMP pathway (see Fig. 2.4). Table 4.1 lists the measured intracellular

Table 4.1 Concentrations (at pH = 7) of intermediates and of cofactors of the EMP pathway in the human erythrocyte

Metabolite/cofactor	Concentration (μM)	Metabolite/cofactor	Concentration (μM)
Glucose (GLC)	5000	2-Phosphoglycerate (2PG)	29.5
Glucose-6-P (G6P)	83	Phosphoenolpyruvate (PEP)	23
Fructose-6-P (F6P)	14		51
Fructose-1,6-bisP (FDP)	31	Pyruvate (PYR)	1,850
Dihydroxyacetone P (DHAP)	138	ATP (ATP^{-4})	138
Glyceraldehyde-3-P (GAP)	18.5	ADP (ADP^{-3})	1,000
1,3 Diphosphoglycerate (1,3 DPG)	60–250	P_i (HPO_4^{2-})	50
3-Phosphoglycerate (3PG)	118	NADH NAD (NAD^+)	1,310

The data are from Lehninger (1975), except for the redox cofactors (Pissara and Nielsen 1997) and for 1,3 DPG (Jovanovic et al. 2006). The correct reactant species for the cofactors are shown in parenthesis

concentrations of the intermediates, the cofactors, and orthophosphate in the human erythrocyte (red blood cells), and Table 4.2 lists the calculated free energy changes.

The first column of Table 4.2 lists the standard free energies of reaction (298.16 K, 1 M concentration of all reactants, except $[H^+]$), of all 10 reactions in the EMP pathway (Fig. 2.4). Column three shows ΔG_R for the reactions at the actual metabolite and cofactor concentrations listed in Table 4.1 and using (4.3).

The intermediate concentrations obviously have a great influence on the free energy of reaction. Thus, for reactions 8 and 4 one obtains the following:

$$\begin{aligned}\Delta G_{R8} &= 4.44 + 298.16 \times 0.008314 \times \ln(29.5/118) = 4.44 - 3.44 = 1.0 \text{ kJ mol}^{-1},\\ \Delta G_{R4} &= 23.97 + 2.479 \times \ln(138 \times 18.5 \times 10^{-6}/31) = 23.97 - 23.31 = 0.66 \text{ kJ mol}^{-1}.\end{aligned} \quad (1)$$

Table 4.2 shows that reactions 1, 3, 10, and perhaps 7 are accompanied by a large, negative ΔG_R. Except perhaps for reaction 6, the last reactions are close to equilibrium, and the enzyme concentrations are probably high enough to bring them to equilibrium (i.e., the flux of the forward and the reverse reactions is much higher than the net flow through the reactions). For reactions with large negative ΔG_R, the activities of the respective enzymes are so low that the equilibrium will never be reached. These reactions are *thermodynamically irreversible* while the close-to-equilibrium reactions will rapidly communicate changes in flux generated by one of the (almost) irreversible reactions through the rest of the pathway.

The reason for the low activity of the enzymes hexokinase, phosphofructokinase, and pyruvate kinase could be that their activity is tightly regulated by the regulatory signal network of the cell, but the large negative ΔG_R permits them to operate also at very low concentration of the substrates, e.g., glucose and FDP, and at high pyruvate concentration. Note that thermodynamically phosphofructokinase is negatively influenced by the energy charge [ATP]/[ADP], an influence which is also reflected in the *kinetics* of the reaction. The analysis shows that the EMP pathway is designed to function at most conditions that the cells may experience in practice.

Table 4.2 Approximate ΔG_R values for the EMP pathway reactions in the human erythrocyte

Reaction	ΔG^0 (kJ mol^{-1})	ΔG (expression)	ΔG (kJ mol^{-1})
Hexokinase	−16.74	$\Delta G^0 + RT \ln \frac{[G6P][ADP]}{[GLC][ATP]}$	−33.3
Glucose-6-P isomerase	1.67	$\Delta G^0 + RT \ln \frac{[F6P]}{[G6P]}$	−2.7
Phosphofructokinase	−14.22	$\Delta G^0 + RT \ln \frac{[FDP][ADP]}{[F6P][ATP]}$	−18.7
Aldolase	23.97	$\Delta G^0 + RT \ln \frac{[DHAP][GAP]}{[FDP]}$	0.7
Triose-P-isomerase	7.66	$\Delta G^0 + RT \ln \frac{[GAP]}{[DHAP]}$	2.7
GAP dehydrogenase	6.28	$\Delta G^0 + RT \ln \frac{[NADH][H^+][1,3DPG]}{[NAD^+][10^{-7}][GAP]}$	1.1 (4.6)
3 PG kinase	−18.83	$\Delta G^0 + RT \ln \frac{[ATP][3PG]}{[ADP][1,3DPG]}$	−10.7 (−14.3)
Phosphoglycerate mutase	4.44	$\Delta G^0 + RT \ln \frac{[2PG]}{[3PG]}$	1.0
Enolase	1.84	$\Delta G^0 + RT \ln \frac{[PEP]}{[2PG]}$	1.2
Pyruvate kinase	−31.38	$\Delta G^0 + RT \ln \frac{[PYR][ATP]}{[PEP][ADP]}$	−23.0

At standard conditions for bioreactions in aqueous media pH = 7, while all other reactants are present in 1 M concentrations. In reactions 6 and 7, the results are shown for the two literature values 60 and 250 μM for [1,3 DPG]. Some references use $T_{standard}$ = 310 K, others 298 K. To avoid further confusion we shall stick to $T_{standard}$ = 25°C

The energy carriers ATP and ADP are in reality fully on ionic form at pH = 7. There are four negative charges on ATP and three on ADP. Thus, hydrolysis of ATP is more correctly written as follows:

$$ATP^{-4} \rightarrow H_2O + HPO_4^{-2} + ADP^{-3} + H^+ = 0. \tag{2}$$

In fact, for pH = 7, [ATP]/[ADP] = 13.4, [P] = 1 mM at physiological conditions (Table 4.2), one obtains by (4.3):

$$\begin{aligned} \Delta G_R(2) &= -30.5 + RT\ln(10^{-3}/13.4) = -30.5 + 8.314 \times 0.298 \times (-9.50) \\ &= -54.0\text{kJ(molATP)}^{-1}. \end{aligned} \tag{3}$$

This means that *54.0 kJ of free energy must be spent to synthesize 1 mol ATP at the physiological conditions that prevail in the cell.*

At acid pH less free energy is spent (e.g., $-54.0 + RT \ln 100 = -42.6$ kJ mol^{-1} at pH = 5).

If in reaction 6 of Table 4.2 the intercellular pH is changed from 7 to 5, the NADH-producing dehydrogenation of GAP would really become a bottleneck with $\Delta G_R = 1.1 + 2.479 \ln 100 = 12.5$ kJ mol^{-1} at the low value 60 μM of [1,3 DPG].

In a healthy culture the intracellular pH does, however, not deviate more than perhaps 0.5 from the standard value of 7. A drastic influence of pH is not really relevant, unless the cell is in great stress due to an abrupt change in the medium pH.

The ambiguous result of a thermodynamic analysis of perhaps the best researched metabolic pathway is, indeed, troublesome. Bottlenecks that could impair the functioning of the pathway which is *known* to operate smoothly in so many organisms can easily be conjured up (e.g., by increasing the very poorly determined value of [1,3 DPG] to 500 μM).

Consequently, a number of recent papers, of which Vojinovic and von Stockar (2009) may be the most comprehensive, have introduced a putative influence of many other species, e.g., $[Mg^{+2}]$ which is known to be necessary for the functioning of enzymes in the EMP pathway. The calculation of ΔG_R for the EMP reactions becomes excessively complicated, and the result depends on a number of equilibrium constants K_i of which few are known from experiments or from ab initio calculations.

It is probably fair to conclude that a very accurate calculation of the ΔG_R values for any pathway is impossible, mostly because the concentrations of intracellular metabolites are not known with sufficient accuracy, and also, they may change a lot with the cultivation conditions.

Still, even an approximate calculation will reveal whether a pathway that would be feasible based on the genomic potential of the organism does, in fact, work in practice. Also, the analysis will give a warning concerning the functioning of a pathway from which by genetic engineering we want to extract a larger amount of a metabolic product: The concentration of pathway intermediate may drastically change as a result of the engineering of the strain From a thermodynamic, as well as from a kinetic point of view the expected increased productivity could be jeopardized.

4.1.3 Combustion: A Change in Reference State

When an organic compound is burnt in oxygen the reaction products are always CO_2, H_2O and sometimes N_2 for nitrogen containing compounds. The thermodynamic data for combustion are found in the same way as data for free energy of formation, enthalpy of formation, and entropy of formation, except that CO_2 (gaseous) and H_2O (liquid) are defined to have zero free energy and enthalpy of combustion at standard conditions 25°C (or 20°C in some tables). The physical state of the compound to be combusted is taken as its natural state at the reference temperature, unless otherwise specified.

Thus, for combustion of H_2 with $½O_2$ to liquid water, the heat of combustion $-\Delta H_c$ is 286 kJ mol^{-1}, and $-\Delta G_c = 237$ kJ mol^{-1} (see Example 4.1). $(-\Delta H_c)$ is larger than $(-\Delta G_c)$ due to the decrease in entropy when the "ordered" H_2O molecule is formed from the "less ordered" O_2 and H_2.

In combustion reactions, and generally in aerobic fermentations the relative difference between ΔG_c and ΔH_c is much smaller than the difference between G_f and H_f, for the reactants, see Example 4.4, and also Example 4.5 for $D = 0.15\ h^{-1}$. This is not true for anaerobic fermentations where the heat of reaction is usually small, but $T\,\Delta S_R$ is large and positive (see Example 4.5 for $D = 0.4\ h^{-1}$). Aerobic fermentation processes are *enthalpy driven*, while anaerobic processes are in general *entropy driven*. There are exceptions to this rule. In the strictly anaerobic *methanogenesis* reaction, Example 4.6, the entropy change is large and *negative*, and a negative value for the ΔG_R of the reaction is only obtained due to a large and negative ΔH_R.

Example 4.4 *Calculation of ΔG_c for ethanol combustion at 25°C, 1 atm.* Combustion of liquid ethanol to the final combustion products of liquid H_2O and gaseous CO_2 occurs by the stoichiometry (1)

$$-(C_2H_5OH)_l - 3O_2 + 2(CO_2)_g + 3(H_2O)_l = 0 \tag{1}$$

The following data are given for formation of CO_2 from $C_{graphite}$ and O_2 and formation of ethanol according to

$$-(2C + 3H_2 + \tfrac{1}{2}O_2) + C_2H_5OH = 0 \tag{2}$$

Compound	H_f^0 (kcal mol^{-1})	G_f^0 (kcal mol^{-1})	S^0 (cal mol^{-1} K^{-1})
CO_2	−94.05	−94.26	51.06
C_2H_5OH	−66.36	−41.79	38.4

Using $S^0 = 1.36$ cal (mole K)$^{-1}$ for $C_{graphite}$, G_f^0 can be calculated from H_f^0 and S^o as in Example 4.1.

$$CO_2: \quad G_f^0 = -94.05 - 0.298 \times (51.06 - 1.36 - 49) = -94.26 \text{ kcal mol}^{-1}, \tag{3}$$

$$\begin{aligned} C_2H_5OH: \; G_f^0 &= -66.36 - 0.298 \times (38.4 - 2 \cdot 1.36 - 3 \times 31.21 - 0.5 \times 49) \\ &= -41.79 \text{ kcal mol}^{-1}. \end{aligned} \tag{4}$$

The heat of combustion of ethanol by (1) is now calculated as the sum of the heat of formation of the $(CO_2)_g$ and the $(H_2O)_l$ that make up the ethanol molecule less the heat of formation of ethanol.

$$\begin{aligned} Q_c = -\Delta H_c &= -66.36 + 2 \times 94.05 + 3 \times 68.28 = 326.6 \text{ kcal} \\ &= 1,367 \text{ kJ (mole ethanol)}^{-1}, \end{aligned} \tag{5}$$

$$\begin{aligned} -\Delta G_c &= 327 + 0.298 \times (2 \times 51.06 + 3 \times 16.72 - 38.4 - 3 \times 49.0) \\ &= 317 \text{ kcal mol}^{-1} = 1,326 \text{ kJ (mole ethanol)}^{-1}. \end{aligned} \tag{6}$$

The values of Q_c and ΔG_c are, indeed, almost the same.

4.2 Heat of Reaction

In large-scale processes, the removal of metabolic heat released is an important factor for the overall reactor design. Since the rates of biological reactions are, generally speaking, low in comparison to heterogeneously catalyzed processes in the chemical industry, it may come as a surprise that heat removal is a problem. However, biological processes run at temperatures very close to the cooling medium temperature (most often cooling water, which at best has a temperature of 5–10°C). This gives a poor heat removal capacity.

For design of heat exchangers one needs to calculate the net heat of reaction when substrates are converted to metabolic products and biomass. Table 4.3 collects heat of combustion data for many of the compounds involved in bioprocesses. As indicated in Example 4.3 the reference state for biochemical reactions is different from that used in "ordinary" chemical reactions: CO_2 is not in the gas phase, but dissolved in water at pH = 7, and for CO_2 as well as other compounds which may take part in acid-base reactions the sum of the ions which are formed at pH = 7 is used as the reference concentration unit. The difference between the "biological" thermodynamic data such as $-\Delta H_c$ in Table 4.3 and those used in chemical thermodynamics is small. Since the values of Table 4.3 are going to be used to find heats of reaction when, e.g., glucose is converted to ethanol and CO_2 the difference in reference state means nothing, or hardly anything. The calculations of Examples 4.2 and 4.4 illustrate how the values in the table may be obtained.

Also included in the table is a column showing the degree of reduction κ^* per carbon atom of the compounds. κ, defined in Sect. 3.4 is identical to κ^* for all compounds which do not contain N, but in relation to combustion calculations it seems more natural to use N_2 rather than NH_3 as the "redox neutral" N containing compound. If the elements S and P appear, the degree of reduction of S and P is set to 6 and 5, respectively, just as in κ. Note in particular that κ^* for "standard" biomass $CH_{1.8}O_{0.5}N_{0.2}$ is 4.80, whereas $\kappa = 4.20$.

The average value of $(-\Delta H_c)/\kappa^*$ for the compounds in Table 4.3 is 115 kJ mol^{-1} with a standard deviation of 6–7 kJ mol^{-1}.

From the additive property of ΔH (and ΔG) one obtains (4.11) for the enthalpy change in the system due to the bioreaction

$$\Delta H = \sum_i Y_{p_i}(-\Delta H_{ci}) - \sum_j Y_{s_j}(-\Delta H_{cj}). \tag{4.11}$$

The heat delivered to the surroundings, the heat of reaction Q, is given by:

$$Q = \sum_j Y_{s_j}(-\Delta H_{cj}) - \sum_i Y_{p_i}(-\Delta H_{ci}) = \sum_j Y_{s_j} Q_{cj} - \sum_i Y_{p_i} Q_{ci}. \tag{4.12}$$

The last column of Table 4.3 shows that ΔH_c (in kJ C-mole^{-1}) is approximately proportional with κ^*, $-\Delta H_c \approx 115\ \kappa^*$, with a standard deviation of 6–7 kJ C-mole^{-1}.

This observation can be used to find the heat of combustion of each compound with an accuracy that is certainly satisfactory for heat exchanger calculations. All that is needed is the chemical formula for the compound and the corresponding value for κ^*.

When the approximation $-\Delta H_{ci} = Q_{ci} = 115\kappa_i^*$ is inserted in (4.11) we find:

$$Q = \left[\sum_j Y_{s_j}\kappa_j^* - \sum_i Y_{p_i}\kappa_i^*\right] \times 115 \text{ kJ (C-mole)}^{-1}. \tag{4.13}$$

Table 4.3 Heat of combustion for various compounds at standard conditions (pH 7, liquid water, CO_2 (dissolved and dissociated in H_2O to HCO_3^{1-}), H_2SO_4 (dissociated, infinite dilution), N_2)

Compound	Formula	Degree of reduction (κ^*) per carbon	$-\Delta H_c^0$ (kJ/mole)	$-\Delta H_c^0$ (kJ/C-mole)	$-\Delta H_c^0/\kappa^*$ (kJ/C-mole)
Formic acid	CH_2O_2	2	255	255	127.5
Acetic acid	$C_2H_4O_2$	4	875	437	109.5
Propionic acid	$C_3H_6O_2$	4.67	1,527	509	109.0
Butyric acid	$C_4H_8O_2$	5.00	2,184	546	109.2
Valeric acid	$C_5H_{10}O_2$	5.20	2,841	568	109.2
Palmitic acid	$(C_{16}H_{32}O_2)_s$	5.75	9,978	624	108.5
Lactic acid	$C_3H_6O_3$	4	1,367	456	114.0
Gluconic acid	$C_6H_{12}O_7$	3.67	2,575	429	117.0
Pyruvic acid	$C_3H_4O_3$	3.33	1,082	361	108.3
Oxalic acid	$C_2H_2O_4$	1	246	123	123.0
Succinic acid	$C_4H_6O_4$	3.50	1,491	373	106.6
Fumaric acid	$C_4H_4O_4$	3	1,335	334	111.3
Malic acid	$C_4H_6O_5$	3	1,328	332	110.7
Citric acid	$C_6H_8O_7$	3	1,961	327	109.0
Glucose	$C_6H_{12}O_6$	4	2,803	467	116.8
Fructose	$C_6H_{12}O_6$	4	2,813	469	117.2
Galactose	$C_6H_{12}O_6$	4	2,805	468	117.0
Sucrose	$C_{12}H_{22}O_{11}$	4	5,644	470	117.5
Lactose	$C_{12}H_{22}O_{11}$	4	5,651	471	117.8
Hydrogen	H_2	2	286		(143.0)
Methane	$(CH_4)_g$	8	890	890	121.2
Ethane	$(C_2H_6)_g$	7	1,560	780	113.8
Propane	$(C_3H_8)_g$	6.67	2,220	740	112.2
Methanol	CH_4O	6	727	727	111.5
Ethanol	C_2H_6O	6	1,367	683	118.0
iso-Propanol	C_3H_8O	6	2,020	673	118.6
n-Butanol	$C_4H_{10}O$	6	2,676	669	112.0
Ethylene glycol	$C_2H_6O_2$	5	1,179	590	142.8
Glycerol	$C_3H_8O_3$	4.67	1,661	554	116.6
Acetone	C_3H_6O	5.33	1,790	597	105.3
Formaldehyde	$(CH_2O)_g$	4	571	571	127.7
Acetaldehyde	C_2H_4O	5	1,166	583	113.7
Urea	CH_4ON_2	6	632	632	105.3
Ammonia	$(NH_3)_g$	3	383		(127.7)
Hydrogen sulfide	$(H_2S)_g$	8	909		(113.6)
Biomass	$CH_{1.8}O_{0.5}N_{0.2}$	4.80	560	560	116.7

Concentration is 1 M for each reactant, except 10^{-7} M for $[H^+]$

If the relation between Q_{ci} and κ^* had been exactly true (4.13) would be identical to (4.12). The errors introduced with (4.13) are *usually* of no importance in engineering calculations – and (4.12) is not either exact. Active biomass may have a degree of reduction κ from just over 4 to perhaps 4.40, and yet the heat of combustion of all kinds of biomass is set to 560 kJ (C-mole)$^{-1}$ in Table 4.3.

Since the reference level for Q_c as well as for the degree of reduction of an element is arbitrary one may just as well apply κ_i instead of κ_i^*in (4.13). Thus (4.13) and (4.14) give identical values for Q

$$Q = \left[\sum_j Y_{s_j}\kappa_j - \sum_i Y_{p_i}\kappa_i\right] \times 115 \text{ kJ (C} - \text{mole)}^{-1}. \tag{4.14}$$

It is perhaps convenient to work with only one set of degrees of reduction, and (4.14) may be easier to remember than (4.13).

For an aerobic process Y_{so} is determined by a degree of reduction balance

$$(-4)Y_{so} = \sum_i Y_{p_i}\kappa_i - \sum_j Y_{s_j}\kappa_j. \tag{4.15}$$

Consequently, (4.15) is identical to (4.16), which is very easy to memorize.

$$Q = 4 \times 115 Y_{so} = 460 Y_{so} \text{ kJ (C} - \text{mole)}^{-1} \tag{4.16}$$

According to (4.16) the heat of reaction should be zero for a fully anaerobic process. This is of course not quite true, even for an anaerobic process using a sugar as substrate, and the result is totally wrong in other systems, e.g., when H_2 is used as energy source and CO_2 as carbon source – see Example 4.6.

In microcalorimeters, heat production rates $q_Q = \mathrm{d}Q/\mathrm{d}t$ of less than 1 mW per L medium can be measured quite accurately, and q_Q can be included in the database as an independent rate measurement. q_Q is, however, strongly correlated to q_{O_2}, and the two measurements should not be included together in the set of independent rate measurements. Several research groups have used microcalorimetry to measure the heat production rate of fermentations, see, e.g., von Stockar et al. 1993.

It should finally be remarked that similar to the relation $Q_{ci} \cong 115\kappa_i^*$there exists an approximate relation (4.17) between $-\Delta G_c$ and κ_i^*. The relation (4.17) is used in the same way as (4.13) to calculate ΔG_c, remembering that $G_{ci} = 0$ for CO_2 dissolved as HCO_3^{1-}, liquid H_2O, N_2, O_2, and H_2SO_4 (at infinite dilution)

$$-\Delta G_{ci} = 94.4\ \kappa_i^* + 86.6 \text{ kJ (C} - \text{mole)}^{-1}. \tag{4.17}$$

Equation (4.17) may be used in approximate calculations of the free energy change in a given (bio-) chemical reaction. For the compounds listed in Table 4.3 the standard deviation of the average (4.17) is also about 6 kJ (C-mole)$^{-1}$.

Example 4.5 *Heat of reaction for aerobic growth of yeast.* Consider the stoichiometry for aerobic yeast fermentation at $D = 0.3\ \mathrm{h}^{-1}$ derived in Example 3.5

$$\begin{aligned}&-(CH_2O + 0.279 \times 0.17NH_3 + 0.167O_2)+\\ &(0.279CH_{1.83}O_{0.56}N_{0.17} + 0.366CO_2 + 0.355CH_3O_{1/2} + 0.275H_2O) = 0.\end{aligned} \tag{1}$$

We now calculate the heat of reaction using (4.12)–(4.16), respectively:

$$Q = 467 + 0.0474 \times 383 - 0.279 \times 560 - 0.355 \times 683 = 86.4 \text{ kJ (C - mole glucose)}^{-1}, \tag{4.12}$$

$$Q = (4 + 3 \times 0.0474 - 4.71 \times 0.279 - 6 \times 0.355) \times 115 = 80.3 \text{ kJ (C - mole glucose)}^{-1}, \tag{4.13}$$

$$Q = (4 - 4.20 \times 0.279 - 6 \times 0.355) \times 115 = 80.3 \text{ kJ (C - mole glucose)}^{-1}, \tag{4.14}$$

$$Q = 460 \times 0.167 = 76.8 \text{ kJ (C - mole glucose)}^{-1}. \tag{4.16}$$

The last result is not equal to the two previous results. The reason is that Y_{so} was determined by an independent measurement of the rate of oxygen uptake, and not from a degree of reduction balance. As shown in Example 3.5, the redox balance based on the measured yield coefficients closes only to within 98%. More than this cannot be expected except in very high quality experiments, and the difference between the calculated Q values reflects the uncertainty which must be expected when using κ_i rather than the tabulated values of Q_{ci}.

Using (4.17) the free energy change accompanying reaction (1) can also be calculated, at least approximately:

$$-\Delta G_c = 94.4\,(4 \times 1 + 3 \times 0.0474 - 4.71 \times 0.279 - 6 \times 0.355) + 86.6\,(1 + 0.0474 - 0.279 - 0.355) = 101.5 \text{ kJ(C - mole)}^{-1}.$$

Using thermodynamic tables one obtains the result $-\Delta G = 107.8$ kJ (C-mole)$^{-1}$. The approximate result is certainly good enough for engineering calculations – first of all it shows that the reaction is strongly thermodynamically favored.

When (4.12) and (4.17) are used to calculate Q and ΔG for all three D-values of Example 3.5 the following results are obtained

D (h^{-1})	*0.15*	*0.30*	*0.40*
Q (kJ (C-mole glucose)$^{-1}$)	195.8	86.4	30.0
	357	310	172
$-\Delta G_c$ (kJ (C-mole glucose)$^{-1}$)	208	102	47
$-\Delta G_c$ (kJ (C-mole biomass)$^{-1}$)	380	366	269

Both Q and $-\Delta G_c$ decrease drastically with D when calculated per (C-mole glucose)$^{-1}$, but especially $-\Delta G_c$ is much less dependent on D when calculated on a C-mole biomass basis.

The results of the table can be complemented by the value $-\Delta G_c = 25$ kJ (C-mole glucose) calculated by use of (4.17) applied to the fully anaerobic yeast fermentation, (3.23). It is clear that the free energy contained in the substrate is predominantly conserved in the fermentation products when anaerobic cultivation is approached.

When the biomass yields Y_{sx} at the four cultivation conditions are compared with the respective values for $-\Delta G_c$, it is also seen that although Y_{sx} certainly decreases with decreasing $|-\Delta G_c|$ it appears that the free energy change is used more effectively at anaerobic or

nearly anaerobic conditions than at fully aerobic conditions: At fully respiratory growth ($D = 0.15\ h^{-1}$) the biomass yield is $0.548/208 = 2.63 \times 10^{-3}$ increasing to $0.137/25 = 5.4 \times 10^{-3}$ (C-mole biomass/C-mole biomass) kJ^{-1} for the data of (3.23).

The increasing effectiveness of the biomass formation process at conditions approaching anaerobicity will be further discussed in Example 5.5, but from a completely different perspective.

Example 4.6 *Anaerobic growth on H_2 and CO_2 to produce CH_4.* The bacterium *Methanobacterium thermoautotrophicum* uses methanogenesis as its catabolic pathway, i.e., it converts H_2 and CO_2 to CH_4, releasing energy in the process. It has an extremely low biomass yield coefficient of about 0.02 C-mole $(\text{mol } H_2)^{-1}$, but a large rate of heat production r_Q, up to 13 W $(\text{g biomass})^{-1}$. The biomass composition of the organism has been experimentally determined to $X = CH_{1.68}O_{0.39}N_{0.24}$ ($\kappa = 4.18$).

Using $Y_{H_2X} = 0.02$ C-mole $(\text{mol } H_2)^{-1}$, the stoichiometry for a black box model is determined from a carbon and a redox balance:

$$-H_2 - 0.260\ CO_2 - 0.0048\ NH_3 + 0.02\ X + 0.240\ CH_4 + 0.511\ H_2O = 0. \tag{1}$$

Schill et al. (1999) made an experimental and theoretical study of this rather strange microorganism for which the growth-associated heat production is inordinately high – as implied by the name of the organism. The reaction temperature was 60°C and to calculate the heat of reaction and the free energy change associated with (1) the thermodynamic data of Table 4.3 must be complemented as follows:

The change in heats of combustion with modest changes of temperature is negligible – e.g., for the heat of combustion of H_2 to form liquid water:

$$\begin{aligned}(-\Delta H_c)_{333K} - (-\Delta H_c)_{298K} &= (7 + \tfrac{1}{2} \times 7 - 9)(333 - 298) + 18(563 - 582)\\ &= -289\ \text{cal mol}^{-1}.\end{aligned} \tag{2}$$

The first term in (2) is $\Delta\alpha\ \Delta T$, where $\Delta\alpha$ is the change in molar specific heat by the reaction. The second term derives from the change in heat of condensation of H_2O between 298 and 333 K

Using the result of Example 4.1

$$(-\Delta H_c)_{333K} = (68,280 - 289)\ \text{cal}\ (\text{mol}\ H_2)^{-1} = 285\ \text{kJ}\ (\text{mol}\ H_2)^{-1}.$$

The change in free energy is much larger. Thus for the combustion of H_2 which at the reaction temperature 333 K is present in a measured concentration $c_{H_2} = 8 \times 10^{-6}$ M in the cytosol of the organism

$$(-\Delta G_c)_{333K} - (-\Delta G_c)_{298K} = -\Delta T \Delta S + RT \ln(H \times c_{H_2}), \tag{3}$$

where H is the Henry's law coefficient 1,250 atm L mol^{-1} for solution of H_2 in water at 60°C, $\Delta T = 35$ K, and ΔS is 39 cal $(\text{mol K})^{-1}$ from Example 4.1 (liquid water).

$$\begin{aligned}(-\Delta G_c)_{333} &= 56,661 - 35 \times 39 - 1.987 \times 333\ \ln 100 = 52.2\ \text{kcal mol}^{-1}\\ &= 219\ \text{kJ mol}^{-1}.\end{aligned} \tag{4}$$

The following table summarizes the thermodynamic data (in kJ (C-mole)$^{-1}$) used by Schill et al. (1999) to calculate the heat of reaction and free energy change associated with (1). The measured concentration of the dissolved gases at 333 K is also shown.

Compound	$-\Delta \boldsymbol{H}_{\mathbf{c}}$ kJ C-mole^{-1}	$-\Delta \boldsymbol{G}_{\mathbf{c}}$ kJ C-mole^{-1}
H_2 (8×10^{-6}M)	285	219
CH_4 (5.7×10^{-4}M)	892	808
CO_2 (1.6×10^{-4}M)	0	−12.8
NH_3 (50 mM)	383	401
Biomass	458	541

Except for the rather low value of $(-\Delta H_c)$ for biomass – the value is calculated from a calorimetric experiment by the authors – the heats of combustion are practically the same as those shown in Table 4.3. We can now calculate ΔH_R and ΔG_R for the stoichiometry (1)

$$\begin{aligned} Q = -\Delta H_R &= 285 + 0.0048 \times 383 - 0.02 \times 458 - 0.240 \times 892 \\ &= 63.6 \text{ kJ } (\text{mol}H_2)^{-1}, \\ -\Delta G_R &= 219 - 12.8 \times 0.260 + 0.0048 \times 401 - 0.02 \times 541 - 0.240 \times 808 \\ &= 12.9 \text{ kJ } (\text{mol}H_2)^{-1}. \end{aligned}$$

It is seen that the heat of reaction is five times higher than the free energy change, and this is quite unusual. The reason for the small $-\Delta G_R$ is that much of the free energy contained in the substrate (H_2) is recovered in the product (CH_4). The entropy change by (4.1) is consequently large and negative.

When ΔH_R and ΔG_R are calculated on the basis of biomass formed ($Y_{sx} = 0.02$ C-mole C-mole^{-1})

$$\begin{aligned} -\Delta H_R &= 3,160 \text{ kJ } (\text{C} - \text{mole biomass})^{-1}, \\ (-\Delta G_R) &= 645 \text{ kJ } (\text{C} - \text{mole biomass})^{-1}, \end{aligned} \tag{4}$$

where the heat of reaction is seen to be about nine times higher than for respiratory growth of yeast on glucose when compared on a C-mole biomass basis (see Example 4.5) while $-\Delta G_R$ is only 70% higher than for respiratory growth of yeast on glucose. One must conclude that *Methanobacterium thermoautotrophicum* grows on CO_2 and H_2 with a very poor thermodynamic efficiency – and also that anaerobic processes are certainly not always associated with a small heat of reaction.

4.2.1 Nonequilibrium Thermodynamics

Cellular systems are open systems where some processes operate far from equilibrium, and others close to equilibrium – as illustrated in Example 4.3. No reaction is at equilibrium since this would stop the net flow through the pathway, and the cell would stop functioning. For many cellular processes thermodynamic driving forces are used directly, e.g., in passive diffusion of substrates across the cytoplasmic membrane, and also if the transport is mediated by a carrier as in facilitated

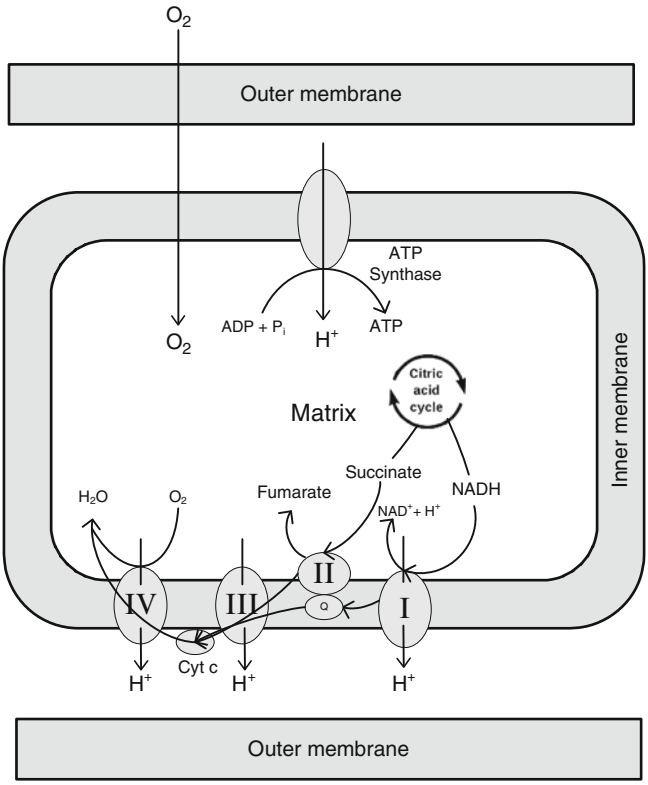

Fig. 4.1 The electron transport chain and oxidative phosphorylation in eukaryotes

diffusion (to be treated in Chap. 7). When the flow is in the direction of the thermodynamic force gradient it is referred to as *conjugate flow*. There are, however, also some important cellular processes where the flow is *non-conjugate*, i.e., the flow is against a thermodynamic driving force. Clearly, non-conjugate flow does not occur voluntarily, but when coupled with a conjugate flow it is possible to drive processes against a thermodynamic driving force.

Non-equilibrium thermodynamics is an extension of classical thermodynamics to non-equilibrium states. It supplies relationships between flows and thermodynamic driving forces, for both conjugate and non-conjugate flows. Additionally, non-equilibrium thermodynamics allows for a quantitative description of processes where conjugate flows are tightly coupled to non-conjugate flows.

An example of a cellular process where conjugate and non-conjugate flows are coupled is the oxidative phosphorylation (see Fig. 4.1), an essential life process for all animals and an option for many microorganisms. In this process protons are transported across the inner mitochondrial membrane (the cytosolic membrane in bacteria) against a proton gradient. The transport of protons is driven by the oxidation of NADH by oxygen, and the coupling of the two processes is tight.

The mitochondria of eukaryotes have an inner membrane that surrounds the mitochondrial matrix and an outer membrane that is in contact with the cytosol. Electrons generated by oxidation of NADH in enzyme complex I are transferred to complex III in the form of a reduced, lipid-soluble carrier that freely diffuses in the membrane. Here they join electrons generated by oxidation of the TCA cycle intermediate succinate. From Complex III electrons are transferred to Complex IV in the form of another, water soluble reduced carrier that moves along the outer, hydrophilic side of the membrane. Finally, in complex IV the electrons are consumed by reduction of molecular O_2 absorbed in the mitochondrial matrix.

Harvesting of the energy generated by oxidation of NADH and succinate occurs by processes which occur across the inner membrane. These processes were named *chemiosmotic coupling* by Mitchell (1966, 1967, 1969) who ascribed pumping of protons *out* of the membrane coupled to an *influx* of protons to the mitochondrial matrix as the source of ATP generation. This theory is contested in a series of papers from 1998 and onwards (Nath, 2002) and an alternative molecular mechanism now known as *Nath's torsional mechanism of energy transduction and ATP synthesis* has been proposed. See Section 4.3.2. An overall view of energy coupling according to the torsional mechanism is illustrated in the papers of Nath cited below.

Furthermore, the process is closely coupled to the phosphorylation of ADP, catalyzed by an ATP synthase that converts ADP and free phosphate into ATP. The process of ATP generation is thermodynamically driven by the oxidation of energy-rich reduced compounds in the *electron transport chain* which is made up of the four enzyme complexes I to IV of Fig. 4.1.

4.2.2 Free Energy Reclaimed by Oxidation in the Electron Transfer Chain

The first of the enzyme complexes on Fig. 4.1 (Complex I = NADH dehydrogenase) oxidizes NADH to NAD^+, and the reductive power harnessed in the two liberated electrons is transferred to Ubiquinol (Q on Fig. 4.1) by the redox process:

$$\left.\begin{aligned} \mathrm{NADH} &\rightarrow \mathrm{NAD^+ + H^+ + 2e^-} \\ \mathrm{Q_{ox} + 2e^-} &\rightarrow \mathrm{Q_{red}} \end{aligned}\right\} \rightarrow \mathrm{NADH + Q_{ox} \rightarrow Q_{red} + NAD^+ + H^+} \quad (4.18)$$

Equation (4.18) is an abbreviated description of the electron transfer to Q. In the equation several intermediate steps are involved.

A second contribution to Q_{red} is received by oxidation of succinate to fumarate (reaction 7 in Fig. 2.7) in Complex II (succinate dehydrogenase + other units that pass the electrons on to Q_{ox}). The reductive power from succinate is transferred to $FADH_2$ and from there to Q_{red}:

$$\left.\begin{aligned} \mathrm{succinate + FAD} &\rightarrow \mathrm{fumarate + FADH_2} \\ \mathrm{FADH_2 + Q_{ox}} &\rightarrow \mathrm{Q_{red} + FAD} \end{aligned}\right\} \rightarrow \mathrm{succinate + Q_{ox} \rightarrow fumarate + Q_{red}} \quad (4.19)$$

A third contribution to Q_{red} is from cytosolic NADH which in the form of $FADH_2$ is transported to the mitochondria via complex II.

In complex III the reductive power is transferred to cytochrome c

$$Q_{red} + (\text{cytochrome c})_{ox} \rightarrow Q_{ox} + (\text{cytochrome c})_{red} \tag{4.20}$$

Finally, in complex IV the electrons from NADH and $FADH_2$, transferred via the reduced compounds Q_{red} and $(\text{cytochrome c})_{red}$, are delivered to O_2:

$$(\text{cytochrome c})_{red} + 1/2O_2 \rightarrow H_2O + (\text{cytochrome c})_{ox} \tag{4.21}$$

The reason for the seemingly complicated transfer of reductive power to Complex IV where it is used to reduce O_2 is that this enzyme complex (cytochrome c oxidase) does not accept NADH or $FADH_2$ as substrates. Likewise, the reductive power from succinate and from cytosolic NADH can only be incorporated via Complex II, while Complex III provides the substrate for Complex IV by transfer of electrons from Q_{red} to $(\text{cytochrome c})_{ox}$. Q as well as cytochrome c serve as virtually loss free and extremely fast conductors of electrons through the electron transfer chain, and between almost stationary, large enzyme complexes.

The standard free energy gains by the reactions (4.18)–(4.20) are, respectively, -69.5, -36.7, and -112 kJ (mol reactant)$^{-1}$ (NADH, Q_{red}, and $(\text{cytochrome c})_{red}$). Each reaction supplies ΔG to support synthesis of ATP (40–55 kJ mol^{-1} at the physiological conditions of the mitochondria, see Example 4.3). Reaction (4.19) supplies only a small complement of free energy (-2.9 kJ mol^{-1}), but the reaction supplies two extra electrons per mol $FADH_2$ that is oxidized, and as will be seen shortly this has a large influence on the ion-transport through the inner membrane of the mitochondria.

The sum of the four contributions to the total free energy gained in the electron transfer chain is around -220 kJ (mol NADH)$^{-1}$ that is oxidized, a value already mentioned in Sect. 2.2.5.

Based on the data in Note 4.1 one can obtain the free energy change that accompanies the reaction

$$NADH + 1/2O_2 + H^+ \rightarrow NAD^+ + H_2O \tag{4.22}$$

by considering the electrochemical cell composed of the following half-reactions:

$$NADH \rightarrow NAD^+ + H^+ + 2e^-, \quad (\text{electron donor with } E_o = -0.315\,\text{V}),$$

$$1/2O_2 + 2H^+ + 2e^- \rightarrow H_2O, \quad (\text{electron acceptor with } E_o = -0.815\,\text{V}),$$

$$\Delta G = -2 \times 96.49 \times (0.815 - (-0.315)) = -218\ \text{kJ}\,(\text{mol NADH})^{-1}.$$

This is the total contribution from NADH in the piecewise calculation given above for the free energy gain from the electron transfer chain. It is clear that the

available free energy is not used with a thermodynamic efficiency of 1, since even at the highest quoted value (55 kJ mol^{-1}) for the required ΔG/mol ATP one would obtain 4 ATP per NADH oxidized, and the literature quotes values between 3 and 2.5 as the maximum possible.

The reason for the incomplete free energy recovery is discussed in Sect. 4.3.2.

Note 4.1 *On the proper use of thermodynamic data from tables*. Free energies for chemical reactions that occur in an aqueous phase are conveniently obtained by measurements of the *Electromotoric Force* (*emf*) of electrochemical cells in which electrons from a donor in one half-cell are transferred to an acceptor in the other half-cell.

There are numerous tables available on half-cell electrode potentials E, and data from these tables can be combined to find the *emf* of the cell defined as

$$\begin{aligned} emf\,(\text{unit : Volt(V)}) = E(\text{electron acceptor couple}) \\ - E(\text{electron donor couple}). \end{aligned} \tag{1}$$

The free energy change ΔG_R associated with the reaction (2) is given by the expression (3):

$$(\text{acceptor})_{ox} + (\text{donor})_{reduced} \rightarrow (\text{acceptor})_{reduced} + (\text{donor})_{ox} \tag{2}$$

$$\Delta G_R = -nF \text{ emf}. \tag{3}$$

In (3) F is Faraday's constant[1] $= 96490$ J V^{-1}, and n is the number of electrons transferred.

One needs to define a standard state for the electrode potentials. In most tables, the standard state is that in which all reactants have activity 1 (temperature = 298.16 K, total pressure = 1 atm). In biological systems it is impractical to work with $a_{H^+} = 1$ ($[H^+] \approx 1$ mol L^{-1}) since most reactions are carried out at pH near 7. In "normal" tables the electrode potential E_o of

$$2H^+ + 2e^- \rightarrow H_2 \quad (pH = 0) \tag{4}$$

is *defined to be 0*. Consequently, the half-electrode potential for reducing H^+ to H_2 at pH = 7 is obtained by applying (4.3) to (3):

$$E^0 = \frac{(\ln 10) \times 14 \times 8.314 \times 298}{2 \times 96,490} = 0.414\text{V}. \tag{5}$$

Similarly, when H_2 *donates* electrons by the reverse of (4) the electrode potential is – 0.414 V.

[1] Each electron transferred from the electron donor to the electron acceptor liberates an energy quantum of 1.602 10^{-19} J per V potential difference. Hence for 1 mol transferred, the liberated energy is $6.023 \times 10^{23} \times 1.602 \times 10^{-19} = 96{,}490$ J/V. This explains (3), as well as the value of Faradays constant.

Table 4.4 Single-electrode potential for electron *acceptors*

Couple	$2H^+/H_2$	$O_2/2\ H_2O$	NAD^+/ NADH	$NADP^+$/ NADPH	CO_2/ CH_4	CO_2/CO	NO_3^-/ NH_4^+
E_o (mV)	414	815	315	319	239	492	−340
Couple	NO_3^-/ NH_2^-	$2NO_3^-$/ N_2	$N_2/2NH_4^+$	SO_4^{2-}/HS^-	SO_4^{2-}/S	S/HS^-	Fe^{+3}/Fe^{+2}
E_o (mV)	−431	824	277	218	200	278	−770

The data are from different references, e.g., Lengeler et al. (1999). Thus, when $2H^+$ accepts two electrons (to form H_2), $E_o = 0.414$ V. When H_2 *donates* two electrons (to form $2H^+$), $E_o = -0.414$ V

Table 4.4 gives some values for single-electrode potentials of *electron acceptor couples*, always at pH = 7. In each case, the number of electrons accepted and donated should be found from the stoichiometry, e.g., 10 electrons accepted in (6)

$$2NO_3^-/N_2: \quad 2NO_3^- + 10e^- + 12H^+ \rightarrow N_2 + 6H_2O \tag{6}$$

Depending on the stoichiometry of the reaction for which we wish to calculate ΔG_R the reactions involved in the above table can act either as electron acceptors or as electron donors.

Hence the cell made up from the two first half-reactions of Table 4.4

$$H_2 \rightarrow 2H^+ + 2e^- \text{ (electron donor, } E_o = -0.414\,\text{V)}$$

$$1/2O_2 + 2e^- + 2H^+ \rightarrow H_2O \text{ (electron acceptor, } E_o = 0.815\,\text{V)}$$

$$\text{determines } \Delta G_R \text{ for the overall reaction } H_2 + 1/2O_2 \rightarrow H_2O \tag{7}$$

When the two stoichiometric equations are added, we obtain the following for ΔG_R using (1)–(3): $\Delta G_R = -2\,F(E_o(\text{acceptor couple}) - E_o(\text{donor couple})) = -2 \times 96.49 \times (0.815 - (-0.414)) = -237.1$ kJ/mol H_2O formed.

When the reverse reaction is considered H^+ is the electron acceptor and H_2O the electron donor.

Now the *emf* of the cell is $[0.414 - (-0.815)]$ V and $\Delta G_R = 237.1$ kJ/mol H_2O consumed.

In Example 4.1 $\Delta G_f^0\ (H_2O)_{liq}$, i.e., ΔG_R for reaction (7) was previously found to be $-4.183 \times 56.666 = -237.1$ kJ/mol $(H_2O)_{liq}$ produced.

The value of the half reaction potential (an intensive property) is independent of the number of electrons transferred, but the number of electrons transferred is, of course, found by balancing the stoichiometries of the half-reactions. Thus, for the half-reactions:

$$\begin{aligned} &SO_4^{-2} + 9H^+ + 8e^- \rightarrow HS^{-1} + 4H_2O \text{ (acceptor, } E_o = 0.218\,\text{V)} \\ &H_2 \rightarrow 2H^+ + 2e^- \text{(donor, } E_o = -0.414\,\text{V)} \end{aligned} \tag{8}$$

The *emf* of the cell is $0.218 - (-0.414) = 0.632$ V.

Consequently, for the reaction

$$4H_2 + SO_4^{-2} + H^+ \rightarrow HS^- + 4H_2O \tag{9}$$

$\Delta G_R = -8 \times 96.49 \times 0.632 = -488$ kJ/SO_4^{-2}, or –122 kJ/H_2 (at pH = 7 and $[SO_4^{-2}] = [HS^{-1}] = [H_2] = 1$ M).

In a natural habitat $[H_2]$ is far smaller than 1 M, say 10^{-5} M, and ΔG_R for (9) is more like – 488 + ln 10 × 298 × 0.008314 × (4 × 5) = −374 kJ. Also, at high $[HS^-]/[SO_4^{2-}]$, pH tends to be much higher than 7 which further reduces $(-\Delta G_R)$.

The example should illustrate, that the correct calculation of the feasibility of a bioreaction (here mediated by the bacterium *Desulfovibrio desulfuricans*) can be quite demanding, since one needs to know the correct concentrations of the reactants, and also whether a product might precipitate.

This is case for $Fe^{+2} \rightarrow Fe^{+3}$ (as $Fe(OH)_3$ at pH = 7), and ΔG_R for the oxidation of Fe^{+2} by O_2 from $\Delta G_R^0 = -1 \times 96.49 \times (0.815 - 0.770) = -4.3$ kJ (mol Fe^{+2}), but at the low $[Fe^{+3}]$ present $\Delta G_R = -97.9$ kJ (mol Fe^{+2})$^{-1}$.

(The solubility product of $Fe(OH)_3$ is SP = $[Fe^{+3}]$ $[OH^-] = 4 \times 10^{-38} \rightarrow [Fe^{+3}] = 4 \times 10^{-17}$ at pH = 7).

A similar reasoning is used to calculate the free energy of ionic species.

$$\text{Consider the reaction } HA \rightarrow H^+ + A^-. \tag{10}$$

If you know G_f^0 for HA (i.e., the value of G_f^0 (HA) in a 1 M aqueous solution of HA) then

$$G_f^0(A^-) = G_f^0(HA) + RT \ \ln 10 \ pK_a. \tag{11}$$

In (11) $pK_a = -\log_{10}(K_a)$, and K_a is the equilibrium constant for the dissociation of HA by (10).

Similarly for the reverse reaction of (10), i.e., the protonation of the base B

$$G_f^0(HB^+) = G_f^0(B) - RT \ \ln 10 \ pK_a. \tag{12}$$

Both formulas are derived from the dissociation constant for H_2O:

$$\begin{aligned} &H_2O \rightarrow H^+ + OH^{-1}, \quad \text{where } K_w = [H^+][OH^-] = 10^{-14} \\ &K_aK_b = 10^{-14} = K_w; \quad pK_a + pK_b = 14. \end{aligned} \tag{13}$$

Thus, for the dissociation of water to H^+ and OH^{1-}, and of H_2S to $HS^- + H^+$ ($pK_a = 6.89$):

$$\begin{aligned} G_f^0(OH^{-1}) &= G_f^0(H_2O)_{aq} + RT \ \ln 10 \times 14 = -237.0 + 79.88 \\ &= -157.1 \text{ kJ mol } OH^{-1}, \\ G_f^0(HS^{-1}) &= G_f^0(H_2S)_{aq} + RT \ \ln 10 \times 6.89 = -27.36 + 39.31 \\ &= 12.0 \text{ kJ mol } HS^{-1}. \end{aligned}$$

4.2.3 Production of ATP Mediated by $F_0 - F_1$ ATP Synthase

In the previous section the source of free energy for production of ATP by

$$ADP^{-3} + HPO_4^{-2} + H^+ \rightarrow ATP^{-4} + H_2O \tag{4.23}$$

has been determined, and the value of the available $-\Delta G^0$ per NADH is calculated.

Figure 4.1 shows that the ATP synthesis occurs in an enzyme complex, the $F_0 - F_1$ ATP synthase that is not in any way in physical contact with the electron transfer chain through which the free energy is produced. This has created a lot of speculation (e.g., that the synthase would be somehow "energized" by the processes occurring in the electron transport chain), but until Peter Mitchell (1961) postulated his *chemiosmotic hypothesis* by which the free energy created by the oxidation of NADH was spent to pump protons across the inner mitochondrial membrane *against* a proton gradient from about a pH of 7 on the inside of the membrane to perhaps pH 6.4 on the outside of the membrane, no really credible explanation for ATP synthesis process was available.

The term "pumping" should not be taken literarily since the inner mitochondrial membrane is impervious to ions. What happens according to Mitchell is that upon attachment of a proton to the surface of one of the enzyme complexes that sticks into the mitochondrial matrix, the enzyme changes conformation, and the proton is detached from the surface of the enzyme that sticks into the intermembrane space.

The free energy spent to pump H^+ across the cell membrane with a positive ΔG:

$$\Delta G = F \times [\Delta\Psi - \ln 10 \times (RT/F)(\mathrm{pH_{outside}} - \mathrm{pH_{inside}})] = F\Delta p, \tag{4.24}$$

where $\Delta\Psi$ is the *membrane potential* [V(mol (H^+ transported)$^{-1}$] which is positive since the potential is more negative on the inside of the membrane. Δp is called the *proton motive force,* composed of an electrical term and a proton diffusion potential. ΔpH is negative since pH is lower (by about 0.6 units) on the outside (positive) side of the membrane than on the (negative) inside of the membrane.

The membrane potential has somewhat different values for different mitochondria, but a value of 0.14 V (mol H^+)$^{-1}$ is not unreasonable.

Hence Δp is approximately $0.14 + 2.303 \times 8.314 \times 298 \times 0.6/96490) = (0.14 + 0.045)$ V mol$^{-1} \approx 0.195$ V mol^{-1}, and the free energy spent to pump protons out of the membrane is $96.49 \times 0.195 = 18.8$ kJ (mol H^+)$^{-1}$. If this free energy is retrieved for ATP synthesis when the protons flow back through the ATP synthase, and if the free energy needed to synthesize ATP at physiological conditions is in the range 40–55 kJ mol^{-1}, then about 3 protons must be pumped out to gain 1 ATP.

Following the chemiosmotic hypothesis, it now remains to find how many protons are pumped out through each of the enzymes of the electron transfer chain. This is an as yet not quite settled question, and a textbook on biochemistry (e.g., Berg et al. 2007) must be consulted to appreciate the conceptual difficulties associated with answering the question. The above reference states that *10 protons*

are pumped out per NADH oxidized (four from Complex I (implying that five protons must be taken from the mitochondrial matrix since one proton is used to form NAD^+), two from Complex III and four from Complex IV), but other texts claim a different number (e.g., a total transfer of 12 H^+, but numbers as low as six protons are also stated in some references). This means that each NADH that is oxidized may contribute with 2.5 to 3 ATP. The contribution from $FADH_2$ that enters the electron transfer chain at Complex III is only six protons, and 1.5 to 2 ATP can be obtained by oxidation of 1 mol of succinate.

We can now conceive the total cyclic process of ATP synthesis, using the large free energy released by oxidation of NADH, as two (scalar) chemical flows, the chemical reactions with, respectively, a positive ΔG (or negative *affinity*) and a negative ΔG (positive affinity), coupled to two vectorially directed flows of protons from the mitochondrial matrix (negative affinity) and of protons to the mitochondrial matrix through the ATP synthetase (positive affinity).

The total rate of free energy dissipation D must be non-negative for the cyclic process to occur, and if we define the rates of the four individual "flow processes" as v_i we obtain

$$D = \sum v_i A_i \geq 0. \tag{4.25}$$

Note 4.2 *50 years of controversy about the chemiosmotic hypothesis may now be resolved.* By the mid twentieth century it was known that ATP was the currency of energy in life processes, but little was known about the processes by which ATP was synthesized in the mitochondria of eukaryotes. The prevalent theory was that ATP was formed by substrate level phosphorylation – the process responsible for energy production at anaerobic conditions.

Peter Mitchell[2] proved that this theory was wrong, and he postulated that an electrochemical potential gradient across biological membranes – here the inner mitochondrial membrane – led to ATP generation. He concluded that the energy gained in transport of *protons* against a concentration gradient would be recovered as ATP when the protons flowed back to the mitochondrial matrix.

His early papers (1961, 1966) were hugely influential, and they spawned many subsequent experimental and theoretical studies, e.g., the derivation in Roels (1983) of the net thermodynamic efficiency of oxidative phosphorylation which was found to be around 70%, a magnificent efficiency for free energy production by "combustion" of H_2.

In almost every current textbook on Biochemistry Mitchell's chemiosmotic hypothesis and its consequences are described in great detail.

[2] Peter D Mitchell (1920–1992) is one of the few "modern" bioscientists who has made his most important discoveries outside of the "teams" that now seem to dominate the field. After an early health-related retirement in 1963 from a readership at Edinburgh he formed a small and more or less privately funded research team with his associate Jennifer Moyle at an old estate in Cornwall that he restored himself. The purpose of the "Glynn foundation" was to promote fundamental biochemical research, and the many important papers from his hand that were rewarded with the Nobel prize in 1978 prove that meaningful research can also be conducted by small teams.

Yet, during the more than 50 years since its conception the chemiosmotic hypothesis, fruitful as it may have been in physiological studies, has repeatedly been subjected to attacks. Experiments that according to the hypothesis should have given a certain answer failed to give the expected answer.[3] The most comprehensive criticism has been put forward by Sunil Nath (at IIT, Delhi).

The main points of Nath's criticism of Mitchell's chemiosmotic hypothesis are summarized below. In the end, this criticism leads Nath (2008, 2010) and Nath and Nath (2009) to formulate a new hypothesis for ATP synthesis based on the torsional mechanism of the $F_0 - F_1$ transmembrane protein (Oster et al. 2000, Jain et al. 2004) in which ATP is synthesized from ADP by reaction (4.23).

1. The transport of a single charged ion (H^+) across the inner mitochondrial membrane should be electro-neutral in the overall sense. Otherwise, huge charges would be created, the electro-neutrality of bulk phases would not hold, and the laws of thermodynamics would be violated (Nath, 2004). The passage of the cation H^+ must be accompanied by the *sequential* translocation of an anion – and Nath postulates succinate as the physiological anion in mitochondria (although other anions/counter-cations could also be translocated).
2. Consequently (4.24) in which H^+ is the sole cause of the electrochemical potential difference between the two delocalized regions- inside and outside the inner mitochondrial membrane- is not true. The *overall* driving force for ATP synthesis is the sum of the electrochemical potentials of the anion and the proton, i.e. $\Delta\mu A + \Delta\mu H$, each of which contributes equally to the energy and driving force to synthesize ATP.
3. According to Nath, translocation of the anion and H^+ does not occur simultaneously, but ordered and sequential (specifically, cation followed by anion on the redox side and anion followed by cation on the ATPase side). There is *no* overall and delocalized electrochemical potential between the two bulk phases on either side of the membrane, but a local and *transient* electrochemical potential in separate access channels for anions and H^+ in the a- and c-subunits of F_0 as the protons pass back to the mitochondrial matrix through the ATP synthase.
4. On the microscopic level, coupling between the anion and the H^+ access channels occurs through energized conformational states of the $F_0 - F_1$ ATP synthtase[4] that are not in equilibrium with the bulk aqueous phases, and non-equilibrium energy storage is mediated within the γ-subunit of the enzyme as torsional energy – from which the name of the new hypothesis is derived. The torsional energy will cause conformational changes

[3] Many of these experiments are commented in Nath (2010) and in the references cited therein.

[4] The enzyme $F_0 - F_1$ ATP synthase consists of two parts, F_o, embedded in the inner mitochondrial membrane, and F_1 that protrudes like a ball on the matrix side of the membrane (as clearly seen on electro micrographs). F_o and the stalk that connects it with F_1 channels the ions back to the mitochondrial matrix while ATP synthesis occurs by the concerted action of the many subunits of F_1. An intuitively appealing description of how ions, in particular protons, from the intermembrane space flow back to the matrix is given by Oster et al. (2000). He finds that protons flow in a helical movement that makes the stem of the F_o rotate. The rotation of the stem "winds up" certain subunits of F_1 as is done by the winch of a crossbow. When sufficient *potential* energy is accumulated the bolt of free energy (=ATP) is released to allow the three part-process of ATP synthesis to proceed: Binding of ADP and free phosphate, ATP synthesis, and finally removal of ATP from F_1 into the mitochondrial matrix.

at the catalytic sites of the protein, and ATP is synthesized through a newly found catalytic cycle in the F_1 portion of the enzyme (Nath, 2002, 2008). The torsional mechanism also includes an in-depth treatment of the elementary events in the F_1 portion of the ATP synthase, and by offering the elusive details of coupling in this fascinating enzyme it takes us beyond the binding change mechanism.

The work of Nath that has led to formulation of a new, unified theory for ATP synthesis and hydrolysis can also be used to formulate new theories for muscle contraction and for other cargo-carrying molecular motors involved in intracellular transport. Eventually the new theory may lead to a fundamental insight into the workings of biological molecular machines, and it may substantially help in the construction of new nanotechnology devices.

Finally, the theory – although already exploited in several experimental studies by Nath and coworkers – opens up a fruitful field of experimental studies of a wide range of problems in biomechanics, perhaps on the impact of malfunction of molecular machines in studies of diseases.

The rather long description of the oxidative phosphorylation process has not been motivated by a desire to give a full account of the process which, important as it is in metabolism, has only a small bearing on the main goal of the text, namely to give an understanding of how biological reactions are used in the production of important chemicals.

It is, however, valuable to introduce some basic tenets of non-equilibrium thermodynamics. Hereby, it is possible to understand how chemical processes combined with transport processes can drive synthesis processes with a large and positive ΔG.

The energy transmission discussed for mitochondria is perhaps the most important example of such processes, and it works in analogy with many key processes in biology: In transport of other ions against concentration gradients, in substrate transport to the cell, and in the essential production of carbohydrates by plants where solar energy is harnessed in ATP, and subsequently utilized in the capture of CO_2 and H_2O.

The subject of energized membrane transport is discussed in Sect. 7.7, especially in Sect. 7.7.2.

Problems

Problem 4.1 *Thermodynamic properties of NH_3 and of NH_4^+.* From a table of thermodynamic data one obtains

$S^0 = 45.77$ cal mol^{-1} K^{-1} for N_2
$S^0 = 46.01$ cal mol^{-1} K^{-1} for $(NH_3)_g$ and 25.1 cal mol^{-1} K^{-1} for $(NH_3)_{liq}$
$H_f^0 = -11.04$ kcal mol^{-1} for $(NH_3)_g$

All values are at standard conditions (298 K). Other data are found in the examples in this chapter.

The heat of condensation of $(NH_3)_g$ is $Q_{cond} = 284.8$ cal g^{-1} at 25°C

For aqueous NH_3 solutions, the equilibrium NH_3 vapor pressure is $8.24x$ where x is the weight % of NH_3 in the solution ($x < 4$ wt%).

(a) Calculate G_f^0 for $(NH_3)_g$ and $(NH_3)_{liq}$ at standard conditions.
(b) Calculate the heat of combustion for $(NH_3)_g$ and for $(NH_3)_{liq}$. Compare with Table 4.3 for $Q_c(NH_3)_g$.
(c) The following relation holds for $x \leq 4$ wt% aqueous solutions of NH_3:

$$\pi_{NH3}(\text{mmHg}) = 8.24x \tag{1}$$

Calculate G_f^0 for a 1 M solution of NH_3 in water.
(d) Calculate G_f^0 for NH_4^+ (kJ mol at $[NH_4^+] = 1$ M).
K_a for $NH_4^+ \rightarrow NH_{3,aq} + H^+$ is $10^{-9.25}$.
(e) Consider the reaction $2NH_4^+ \rightarrow N_2 + 3H_2 + 2H^+$.
Use the table of half-reaction potentials in Note 4.1 to calculate ΔG_R per mol N_2 for the reaction at pH = 7.

Also determine ΔG_R directly from the stoichiometry of the reaction and using the value for G_f^0 (NH_4^+) found in (d). The results should fit to within a few kJ $(\text{mol } N_2)^{-1}$).

Problem 4.2 *Is a lysine yield of 6/7 on glucose possible from a thermodynamic point of view?*. In Example 3.9 a maximum yield of 6/7 C-mole lysine (C-mole glucose)$^{-1}$ was predicted by imposing the constraint that all yield coefficients in (5) of the example should be non-negative. Stephanopolous and Vallino (1991), Vallino and Stephanopolous 1993), and Marx et al. (1996) report that the maximum theoretical yield is only 3/4. The reason could be that ΔG is positive for the reaction:

$$-CH_2O - (2/7)NH_3 + (6/7)CH_{7/3}O_{1/3}N_{1/3} + (1/7)CO_2 + (3/7)H_2O = 0 \tag{1}$$

(a) Use (4.16) to calculate an approximate value for $(-\Delta G_c^0)_{\text{lysine}}$.
(b) Use this value to determine ΔG_R^0 for reaction (1).
(c) Experimental values for ΔG_c and for ΔH_c are difficult to find for lysine, but Morrero and Gani (2001) have calculated ΔG_f^0 and ΔH_f^0 for L-lysine by a group contribution method. Their calculated values are as follows:

$$-G_f^0 = 214 \text{ kJ mole}^{-1} \quad \text{and} \quad -H_f^0 = 450 \text{ kJ mol}^{-1}. \tag{2}$$

Use these data to calculate ΔG_c^0 and ΔH_c^0 for L-lysine. Data for CO_2 and H_2O are taken from the examples of Chap. 4. Note that the difference between ΔG_c calculated in question 1 and question 3 is quite small.
(d) Based on this information: Will reaction (1) have a positive affinity (1)?

Problem 4.3 *The effect of a transhydrogenase reaction in Saccharomyces Cerevisiae*. In Problem 3.6 three different strains of *S. cerevisiae* were compared. The purpose of constructing strain TN21 was to provide the anaerobically growing yeast culture with a sink for NADH. If NADH was converted to NADPH, it was thought that less glycerol would be formed – in TN1 and TN26 glycerol production is the only means of balancing the excess NADH formed in connection with the formation of precursor metabolites like pyruvate and acetyl-CoA. Furthermore, the produced NADPH might substitute NADPH produced in the PP pathway and consequently diminish the glucose loss in this pathway.

(a) Consider the reaction

$$-\text{NADH} - \text{NADP}^+ + \text{NADPH} + \text{NAD}^+ = 0 \qquad (1)$$

which is catalyzed by the transhydrogenase in TN21. Is it reasonable to assume that ΔG^0 is almost zero for reaction (1)? Consult Note 4.1 to calculate ΔG_R.

Based on the data in Tables 2.3 and 4.1, what would be the value of ΔG at the "actual" concentrations of the cofactors?

Would your conclusions be the same when you consider a yeast that vigorously produces ethanol at anaerobic conditions?

(b) Nissen et al. (2001) measured the intracellular concentration of each of the four reactants in (1). Actually only the cytosolic concentrations should have been measured since the inserted transhydrogenase operates only in the cytosol, but the measurements in the table below are thought to give an adequate representation of the relative values of the four nucleotides in the cytosol.

Intracellular concentrations of NAD(H) and NADP(H) in μmol (g DW)$^{-1}$ for the two control strains TN1 and TN26, and for the transhydrogenase-containing strain TN21, sampled during exponential growth in anaerobic batch cultivations. Each measurement was carried out twice.

Strain	NAD^+	$NADP^+$	NADH	NADPH	$NADH/NAD^+$	$NADPH/NADP^+$
TN1	2.87 ± 0.09	0.23 ± 0.01	0.44 ± 0.01	1.21 ± 0.07	0.15 ± 0.01	5.26 ± 0.55
TN26	2.85 ± 0.11	0.24 ± 0.01	0.43 ± 0.01	1.19 ± 0.07	0.15 ± 0.01	4.96 ± 0.52
TN21	2.17 ± 0.07	0.27 ± 0.02	0.54 ± 0.02	0.80 ± 0.10	0.17 ± 0.01	2.96 ± 0.60

Calculate ΔG for reaction (1) using the very consistent data of the table for TN 1 and TN 26 (which should be almost identical).

(c) Based on the results of question 2: what is the expected value of the ratio between the numbers in the last two columns of the table? Does the result for TN 21 correspond to the expected value of the ratio? (A tentative explanation for the answer may be that the ratio $NADH/NAD^+$ is highly controlled by other mechanisms, and that it is not permitted to increase to its equilibrium value) In any event the result of the genetic manipulation of the yeast strain is a total fiasco. The secretion of 2-oxoglutarate observed in problem 3.6 for TN 21 could be a result of the lower NADPH concentration in this strain, since NADPH is the preferred cofactor for conversion of 2-oxaloacetate to glutamic acid.

Problem 4.4 *Nitrification by Nitrosomonas Sp.* Fixation of CO_2 to biomass can be driven by a simultaneous oxidation of NH_3 to nitrite. The overall reaction is

$$\begin{aligned} &-CO_2-(a+0.2)NH_3-(1.5a-1.05)O_2+CH_{1.8}O_{0.5}N_{0.2}\\ &+aHNO_2+(a-0.6)H_2O=0 \end{aligned} \tag{1}$$

Reaction (1) can be divided into two separate chemical reactions which run in parallel:

$$-CO_2-0.2\ NH_3-0.6H_2O+CH_{1.8}O_{0.5}N_{0.2}+1.05\ O_2=0 \tag{2}$$

$$-NH_3-1.5\ O_2+HNO_2+H_2O=0 \tag{3}$$

Determine ΔG for each of the two reactions (1) and (2). Determine the minimum value of parameter a in (1) for the whole process to be thermodynamically feasible. Chemolithotrophic bacteria such as *Nitrosomonas* are thermodynamically quite inefficient. Assume a thermodynamic efficiency of 30% for fixation of CO_2 and calculate the maximum yield of biomass on NH_3.

This problem is inspired by work on Chemolithotrophs by Dr. Lars K. Nielsen at the University of Queensland, Australia.

Problem 4.5 *Heat exchanger calculations.* Consider the aerobic yeast fermentation of Example 3.5 for $D = 0.4\ h^{-1}$.

$$\begin{aligned} &-CH_2O-0.0298NH_3-0.044\ O_2+0.175CH_{1.83}O_{0.56}N_{0.17}+0.312\ CO_2\\ &+0.513CH_3O_{0.5}+Y_{sw}H_2O=0 \end{aligned}$$

(a) The fermentation is carried out in a 100 L stirred tank reactor.
$s_f = 28\ g\ L^{-1}$, $x = 4\ g\ L^{-1}$ (see Fig. 3.5).
The metabolic heat is to be removed via an internal cooling coil with a heat transfer coefficient $U = 500\ W\ m^{-2}\ (°C)^{-1}$.** The inlet cooling water temperature is 10°C, the exit temperature of the cooling water is 20°C, and the fermentation temperature is $T = 30°C$.
Calculate the required heat transfer area A.

(b) Consider $D = 0.25\ h^{-1}$ where growth can be assumed to be fully respiratory. Will heat removal be a problem at this process condition?

(c) Finally, consider a change in the effluent cooling water temperature to 25°C. Calculate the required change in heat transfer area.

Problem 4.6 *Production of lactate from pyruvate.* Pyruvate + $2H^+$ + 2 e^- → lactate; (electron acceptor, $E_o = -0.185$ V)

From Note 4.1, take the oxidation of NADH to NAD^+ as the electron donor reaction.

Calculate ΔG_R^0 for conversion of pyruvate to lactate.

Problem 4.7 *Combined removal of nitrate and ammonia from waste water*. In Sect. 3.4.2, (3.30) the conversion of nitrate and ammonium from waste water by an anaerobic fermentation process was considered.

The reaction between the nitrogen species is given by:

$$3NO_3^- + 5NH_4^- \rightarrow 4N_2 + 2H^+ + 9H_2O \quad (1)$$

(a) Based on the data in Table 4.4 calculate the value of ΔG_R^0 for reaction (1).
(b) The solubility of N_2 in H_2O at 25°C is 0.0170 g L^{-1}. The free energies of ${NO_3}^{1-}$ and ${NH_4}^+$ are, respectively, −108.74 and −79.31 kJ mol^{-1}.

Based on the stoichiometry (1) recalculate ΔG_R^0 at pH = 7, 1 atm total pressure. The two results should differ by no more than a few per cent.

You will find that ΔG_R^0 is negative. Hence, the addition of sugar to the feed is not necessary to provide free energy for the reaction, but it is of course needed to supply a substrate for the (modest) production of biomass.
(c) In a waste water stream at pH = 7 one has measured $[{NO_3}^{1-}] = 10^{-4}$ M and $[{NH_4}^+] = 10^{-4}$ M. Determine the value of ΔG_R for reaction (1) at these conditions.

Problem 4.8 *Can ATP be generated in the conversion of glucose to lactate or from G3P to glycerol?*. The free energy of glucose dissolved in water is $G_f^0 = -908$ kJ mol^{-1}.

Correspondingly, G_f^0 (lactic acid, HLac)) is −523 kJ mol^{-1} and G_f^0 (glycerol) = −665 kJ mol^{-1}.

The value of K_a for HLac → H^+ + Lac^{-1} is $10^{-3.08}$.

(a) Determine ΔG_R for the reaction Glucose → $2Lac^{-1}$ + $2H^+$
Could – ΔG_R be big enough to synthesize 2ATP from ADP?
(b) Determine ΔG_R for the reaction Glucose + 2ATP + 2NADH → 2glycerol + 2ADP + $2NAD^+$ Is there enough free energy to produce one ATP by hydrolysis of glycerol 3-phosphate (G3P) to glycerol?

References

Berg, J. M., Tymocko, J. L., and Stryer, L. (2007). Biochemistry. 6th edition. Freeman and Company, New York.

Channakeshawa, C. (2011). New paradigm for ATP synthesis and consumption. *Journal of Biosciences*, **36**, 3–4 (March 2011).

Jovanovic, S., Jovanovic, N., and Jovanovic, A, (2006). High glucose protects single beating adult cardiomycetes against hypoxia. *Biochem. Biophys. Res. Comm.* **341**, 57–66.

Lengeler, J.W., Drews, G., and Schlegel, H.C. (editors), 1999. Biology of prokaryotes. Georg Thieme Verlag, Stuttgart.

Lehninger, A.E. (1975). Biochemistry, 2nd ed., Worth, New York.

Morrero, J., and Gani, R. (2001). "Group contribution based estimation of pure component properties." *Fluid Phase Equil.* **183/184**, 183–208.

Marx, A., de Graaf, A.A., Wiechert, W., Eggeling, L., and Sahm, H. (1996). "Determination of the fluxes in the central metabolism of *Corynebacterium glutamicum* by NMR combined with metabolite balancing." *Biotechnol. Bioeng.* **49**, 111–129.

Mitchell, P., (1961). Coupling of phosphorylation to electron and hydrogen transfer by a chemiosmotic type of mechanism. *Nature* **191**, 144–148.

Mitchell, P. (1966). Chemiosmotic coupling in oxidative and photosynthetic phosphorylation. *Biol Rev*, **41**, 445–502.

Mitchell, P. and Moyle, J. (1967). Respiration driven protein translocation in rat liver mitochondira. *Biochem. J*, **105**, 1147–1162.

Mitchell, P. and Moyle, J. (1969). Estimation of membrane potential and pH differences across the cristae membrane of rat liver mitochondria. *Eur. J. Biochem.* **7**, 471–484.

Nath, S. (2008). The new unified theory of ATP synthesis/hydrolysis and muscle contraction, its manifold fundamental consequences and mechanistic implications, and its applications in health and disease. *Int. J. Mol. Sci.* **9**, 1784–1840.

Nath, S.S. and Nath, S. (2009). Energy transfer from Adenosine triphosphate. Quantitative analysis and molecular insights. *J. Phys. Chem.* ***B***., **113**, 1533–1537.

Nath, S. (2010). Beyond the chemiosmotic theory: Analysis of key fundamental aspects of energy coupling in oxidative phosphorylation in the light of the torsional mechanism of energy transduction and ATP synthesis. Invited review, parts I and II, *J. Bioenerg. Biomembr.* **42**, 293–300 and 301–309.

Nissen, T.L., Anderlund, M., Nielsen, J., Villadsen, J., and Kjelland-Brandt, M.C. (2001). Expression of a cytoplasmic transhydrogenase in *Saccharomyces cerevisiae* results in formation of 2-oxoglutarate due to depletion of the NADPD-pool. *Yeast*, **18**, 19–32.

Oster, G., Wang, H. and Grabe M. (2000). How F_o-ATPase generates rotary torque. *Phil. Trans. R. Soc. Lond.* **B 355**, 523–529.

Pissara, P.D. and Nielsen, J. (1997). Thermodynamics of metabolic pathways for penicillin production: Analysis of thermodynamic feasibility and free energy changes during fed-batch cultivation. *Biotechnol. Prog.* **13**, 156–165.

Roels, J.A. (1983). Energetics and Kinetics in Biotechnology. Elsevier Biomedical Press, Amsterdam.

Schill, N.A., Liu, J.-S., and von Stockar, U. (1999). "Thermodynamic analysis of growth of *Methanobacterium thermoautotrophicum*". *Biotechnol. Bioeng.* **64**, 74–81.

Stephanopolous, G., and Vallino, J.J. (1991). "Network rigidity and metabolic engineering in metabolic overproduction." *Science*, **252**, 1675–1680.

Vallino, J.J., and Stephanopolous, G. (1993). Metabolic flux distributions in *Corynebacterium glutamicum* during growth and lysine overproduction. *Biotechnol. Bioeng.* **41**, 633–646.

von Stockar, U., Gnaiger, E., Gustafsson, L., Larsson, C., Marison, I., and Tissot, P. (1993). "Thermodynamic considerations in constructing energy balances for cellular growth". *Biochim. Biophys. Acta*, **1833**, 221–240.

Vojinovic, V. and von Stockar U. (2009). Influence of uncertainties in pH, pMg, activity coefficients, metabolic concentrations, and other factors on the analysis of the thermodynamic feasibility of metabolic pathways. *Biotechnol. Bioeng.* **103**, 780–795.

Chapter 5
Biochemical Reaction Networks

Section 2.2 introduced the pathways of cells, and in Chap. 3 the steady-state conversion of substrates to final metabolic products was described using a *single stoichiometric equation*, the black box model. The stoichiometric coefficients, or rather the yield coefficients, because they vary with the cultivation conditions, were determined using mass and redox balances. In Chap. 4, the black box model was examined using the tools of thermodynamics to determine if a given overall reaction was feasible from a thermodynamic perspective. In this chapter, the *network* of pathways through which substrates are converted to products are studied more closely. Specifically, the distribution of carbon from the substrate(s) to the different products is *calculated*.

When the metabolic network is subjected to a quantitative analysis it becomes possible to predict the yield of a specific product Y_{si} on the substrate S, and moreover the analysis will indicate how the metabolism should be changed to *improve* the yield.

The *insight* which is gained through this analysis is of great importance to industrial application of microorganisms as "chemical factories" to produce the final products of the biorefinery. Under different names, physiological engineering, metabolic engineering, and now systems biology, the quantitative treatment of metabolism has revolutionized our approach to the application of microorganisms, and has made it possible to bypass, or at least curtail, the resource-heavy experimental programs that previously determined the time it took from "idea to a marketable new process or product."

Today, a combination of experiments in silico, i.e., model-driven experiments on computers, together with rapid screening of possible future production organisms, conducted on a "laboratory-on-a-chip," have cut down the time it takes to commercially develop a new process from years to a few months.

Figure 5.1 presents a peak at the metabolism from the Biochemical Pathway Map, a comprehensive map of biochemical reactions occurring in all organisms. It shows the reactions at grid-point [D6, E6] of the metabolic map, and the complete map contains thousands of reactions.

In this chapter, we provide the basic concepts used to analyze metabolic networks. The resulting analysis of the metabolism is much more accurate than

J. Villadsen et al., *Bioreaction Engineering Principles*,
DOI 10.1007/978-1-4419-9688-6_5,

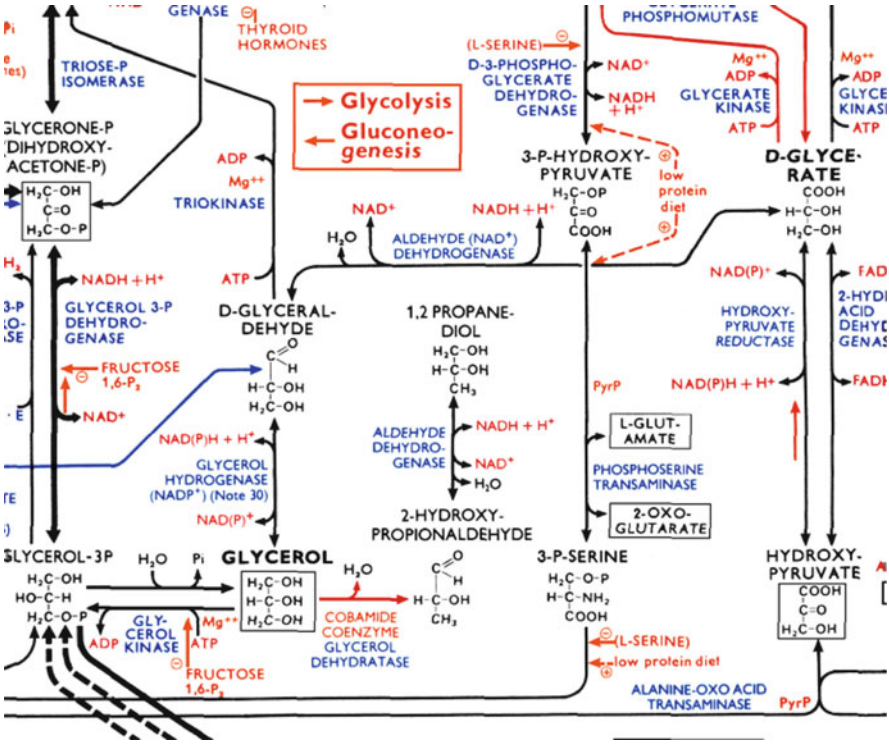

Fig. 5.1 Excerpt from the Biochemical Pathways Map published by the ExPASy Proteomics Server (http://www.expasy.ch). At the bottom of the picture is shown the path from DHAP (dihydroxy acetone phosphate) to glycerol and further to 1,2 propane-diol, an isomer of the 1,3 propane-diol used by DuPont in the Sorona® process (see Sect. 2.1.2 and Problem 5.5). Note the presence of two enzymes in the reaction between glycerol-3P and glycerol, the hydrolase in the direction toward glycerol, and a kinase in the opposite direction

that of the black box model. Still, the black box model applies to the overall yields and rates, and the more detailed analysis should not be seen as a replacement of the black box model, but rather as an extension. Any analysis of experimental data should start with the black box model to check the consistency of the data. If this is not done, a more detailed analysis as presented in this chapter may give a wrong interpretation of how the metabolism of the studied organism is operating.

5.1 Basic Concepts

When calculating the steady-state fluxes through the different branches of a metabolic network we shall use information about the net flows in and out of the cells, i.e., the net rate of production of substrates and metabolic products that can be

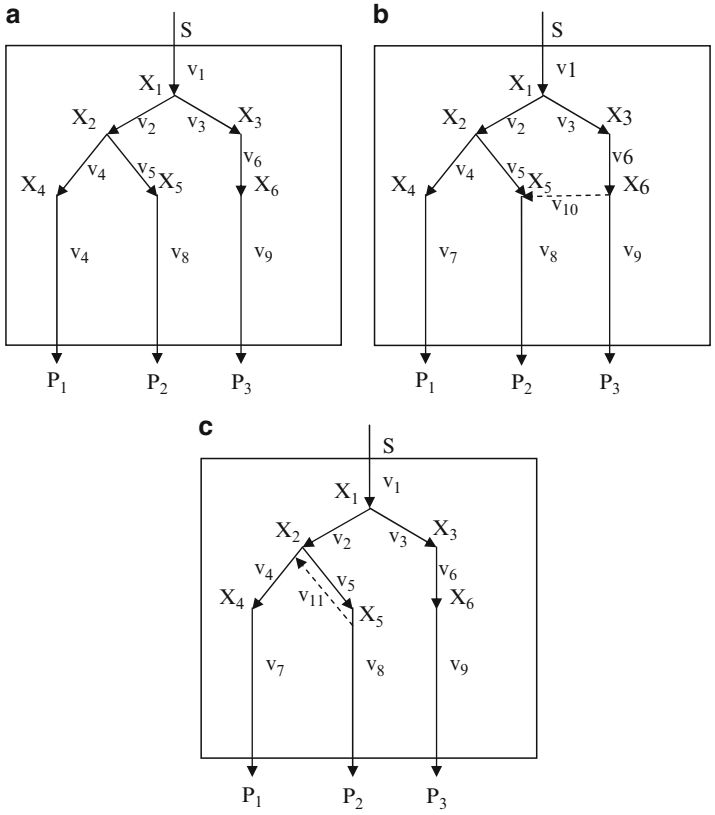

Fig. 5.2 Graph of a metabolic network (**a**) and two variants (**b, c**) of the network

measured as described in Sect. 3.1. These are in reality the only fluxes that can be directly measured, since it is difficult and inaccurate to measure fluxes within the functioning cell. If a cell is pulled apart in order to measure the enzyme activities, the controls imposed on the individual enzymes is lost, and the enzyme activity measured in vitro will therefore not say much about the in vivo flux. Furthermore, in enzyme assays the maximum enzyme activity is typically measured, and in order to identify the actual rate of an enzyme-catalyzed reaction it is necessary to know the substrate concentration, as well as the concentrations of all other metabolites that affect the enzyme reaction rate.

Consider the three variants of a simplified metabolic network shown in Fig. 5.2.

One carbon substrate S is fed to the network at a rate $(-r_s)$, which is equal to the internal rate, or *flux*, v_1, at which carbon is directed toward the first intracellular metabolite pool X_1. The carbon flows from pool X_1 toward the two pools X_2 and X_3. The two fluxes v_2 and v_3 determine the distribution of carbon toward the *metabolic products*, $P_1 + P_2$ and P_3, respectively. At X_2 there is a further distribution of carbon toward P_1 and P_2, respectively.

In Fig. 5.2a, there is no communication between the three branches of the network. In Fig. 5.2c the pools X_2 and X_5 communicate via a reversible reaction for which the rate of $X_2 \rightarrow X_5$ is v_5, while the rate of $X_5 \rightarrow X_2$ is v_{11}.

In Fig. 5.2b, the branches toward P_2 and P_3 communicate through the reaction $X_6 \rightarrow X_5$ with rate v_{10}. If, in Fig. 5.2c, the *net rate* of formation v_5–v_{11} of X_5 from X_2 is considered rather than the individual rates, then Fig. 5.2a, c are identical. The two networks Fig. 5.2b, c still have three products, P_1 to P_3, and one substrate S.

There are six intracellular metabolites, X_1 to X_6, and the network consists of nine intracellular reactions with rates v_1 to v_9 in Fig. 5.2a, with addition of v_{10} and v_{11} in 5.2b, c, respectively. The network (or *graph*) 5.2a has two *diverging* branch points $[X_1, X_2]$. The network 5.2b has three diverging branch points $[X_1, X_2, X_6]$ and one *converging* branch point, X_5. The network 5.2c has one diverging branch point, X_1, and two branch points $[X_2, X_5]$ that are both diverging and converging. A diverging branch point has one input and several outputs, while a converging branch point has several inputs and one output.

The objective of *Metabolic Flux Analysis* is to find the distribution of carbon in the product streams, and next to calculate those production rates P_i that are not given experimentally. If the objective is only to calculate the nonmeasured production rates, the structure of the internal network is not really relevant, besides allowing us to calculate the missing production rates. In this context, the *values* of the individual internal fluxes v_i are as such unimportant. However, the values of v_i are very relevant when the objective is to learn how the cell responds to different perturbations, either genetic or in the environment.

The general assumption that allows us to calculate fluxes in metabolic networks is:

> For all intracellular metabolites the fluxes leading to a given metabolite are balanced with the fluxes leading away from the metabolite. This ensures that in a steady state situation there is no net accumulation of metabolites X_i.

This very general assumption implies that the level of all metabolites stays constant at all times. This is of course not quite the case, but as the turnover of the metabolites is very high, i.e., the fluxes through the metabolite pools are orders of magnitude higher than the metabolite levels, the assumption is valid, except for the first few seconds (or for some metabolites minutes) following environmental perturbations. At the time scale of growth of the cells (typically in the order of hours) the assumption is very reasonable.

When we consider the basic network, Fig. 5.2a with only diverging branches this concept can easily be demonstrated. If the values of $[v_1, v_2, v_4]$ are known then the value of all the other fluxes can be calculated: $v_3 = v_1 - v_2$, $v_5 = v_2 - v_4$, $v_6 = v_9 = v_3$, $v_7 = v_4$, and $v_8 = v_5$. Thus, the vector $\boldsymbol{v} = [v_1, v_2, v_4]$ is a *key* to the solution of the flux distribution problem. Other vectors of *key rates* can be selected, and common to these key vectors is, that all internal rates and the rates of product formation can be determined based on the key rate vectors. The elements of the key rate vector can be internal fluxes v_i, product formation rates r_{pi}, or the substrate consumption rate $-r_s$. Using only r_{pi} and the substrate consumption rate $(-r_s)$ is the most useful choice, since these are easily available experimentally. The network

Fig. 5.2a can in fact be simplified into a network with only three *independent* paths: S to P_1, S to P_2, and S to P_3. The vector $\boldsymbol{V} = [V_1, V_2, V_3]$ symbolizes this reduced network, and product P_i *is only produced in pathway* V_i.

Besides the constraints obtained from the relationships between the internal fluxes v_i, more constraints can be imposed on the network:

1. A total carbon balance shows that the carbon input used to form the key products P_i must equal the carbon fed to the network in S.
2. A redox balance which specifies that the redox generated in one part of the network which is isolated from the rest of the metabolic network, must equal that consumed in the remainder of the network. Thus redox generated in V_1 must be consumed in V_2 and V_3.
3. Similarly an energy balance for an isolated network, Fig. 5.2, must stipulate that ATP generated in one part of the network must be consumed in other parts.

The redox carrier in constraint 2 is usually taken to be NADH, even when the actual pathways use other redox carriers. In a simplified Metabolic Flux Analysis this assumption is permissible since, as considered in Chap. 2, the same amount of carbon source (e.g., glucose) is used to provide reduced cofactors NADH, NADPH, or $FADH_2$, and the yield on the carbon source will be the same. Also in a simplified analysis all energy carriers can be taken to be ATP. These assumptions do not carry over to a more detailed analysis, as shown by the following example.

In (2.25) three NADPH was used to produce lysine from aspartate and pyruvate while two NADH were available after conversion of one molecule of glucose to two molecules of pyruvate. The NADH is converted to NAD^+ in oxidative phosphorylation and serves to generate ATP, but cannot be converted to NADPH. Hence, as discussed in Problem 5.3, the yield of lysine on glucose is smaller than the 6/7 which was calculated in Example 3.9.

We shall now return to the analysis of the network in Fig. 5.2a, where at first it will be assumed that all three rates r_{pi} are measured. For each of the three paths V_i leading from glucose to product P_i a stoichiometric equation, complete with NADH and ATP consumed or produced, is written. In general, we shall write the stoichiometries based on one C-mol P_i. For catabolic reactions the amount of redox and ATP corresponding to the production of one C-mol P_i is taken from the metabolic pathways of Chap. 2 or from the literature. For all these reactions, the stoichiometric coefficients will be exact numbers.

If one of the P_i is biomass with composition $CH_aO_bN_cS_dP_e$ the corresponding stoichiometric equation is of empirical nature. One does not know how much CO_2 that accompanies the formation of one C-mol biomass (mainly from the production of NADPH in the PP-pathway, Sect. 2.2.6), and the amount of ATP used to synthesize biomass from the building blocks is unknown. We shall see in the examples of this chapter that the yield coefficient Y_{xATP} can vary a lot with the cultivation conditions, but the yield coefficient Y_{xc}, the amount of CO_2 produced per C-mol biomass is fairly constant, independent of the organism and the operational conditions. A value Y_{xc} in the range 0.08–0.15 covers most situations, and

furthermore the result of the flux analysis is not sensitive to the value of Y_{sc}, whereas Y_{xATP} has a great influence on the result.

When the steady-state rate of production of the products is measured, one immediately obtains the amount of substrate consumed by adding the three stoichiometric equations. CO_2 and other metabolic products obtained in one or more of the pathways is also found from the stoichiometric equations.

The internal fluxes v_1 to v_9 in Fig. 5.2a can be determined by back-tracking the three net pathways V_i from product to substrate. The relative values of the fluxes will help to predict where metabolic engineering might be used to increase the flux through one net-pathway V_i relative to another.

Although the fluxes v_i are easily obtained from the values of P_i, it is impossible to calculate the size of the metabolite pools X_i. These can, however, be obtained by sophisticated experimental methods discussed in Sect. 9.3.5. The metabolism is instantly quenched by immersion of the culture in liquid N_2, in very cold methanol or in chloroform. Hereafter, the metabolites are extracted from the cells and quantified, e.g., by HPLC.

Finally the analysis, combined with an assumption that in the steady state the net production of ATP in the network must be zero, can be used to determine the ATP consumption in the biomass production pathway. A collection of experiments, conducted at different cultivation conditions (e.g., different dilution rates D), will give an empirical understanding of how Y_{xATP} varies with the cultivation conditions.

In the following, a number of examples will illustrate how the concepts discussed above can be used to analyze networks with only diverging branches.

Before closing the introduction to Metabolic Flux Analysis a few comments will, however, be given to the networks in Fig. 5.2b, c.

If the existence of flux v_{10} is not suspected in the analysis of the network, Fig. 5.2b, some truly strange results may be obtained, e.g., that the ratio between P_2 and P_3 increases dramatically with increasing substrate concentration when the kinetic expression for v_{10} is of higher order than v_9 in the concentration of X_6. The only way in which the existence of v_{10} can be detected and the value of v_{10} measured is if there exist two forms of X_5, one form X_{5a} when the metabolite is synthesized from X_6 and the other form X_{5b} when it is synthesized from X_2. Furthermore, the labeling must be preserved when P_2 is synthesized from either X_{5a} or X_{5b}. Now a measurement of the ratio between P_{2a} and P_{2b} determines the ratio between v_5 and v_{10}, and the new flux v_{10} can be calculated.

If, in Fig. 5.2c only the net flux v_5–v_{11} is used, then the analysis of the network based on measurements of the three P_i is identical to that used for Fig. 5.2a. The existence of the reversible reaction between X_2 and X_5 can only be detected if there exist two distinct forms of X_2, one when X_2 is synthesized from X_1, and the other when X_2 is synthesized from X_5. If the two forms of X_2 can be distinguished in P_1, which is produced from X_2 via X_4, then the ratio between v_5 and v_{11} can be calculated. Possibly P_2 can also be used, but then the reaction $X_2 \rightarrow X_5$ must produce two distinct variants of X_5, depending on whether X_{2a} or X_{2b} is the reactant.

The discovery of a path from X_6 to X_5 can be of great value: Assume in Fig. 5.2b that P_2 is the desired product, and P_1 is undesired – perhaps the presence of P_1 in the

product mixture may even make recovery of P_2 more difficult – then it would be a definite advantage to knock out the path from X_1 to X_2. This would be done by deletion of the gene which codes for the enzyme in the reaction $X_1 \rightarrow X_2$ while over-expressing v_{10}.

Similarly, in Fig. 5.2c one may wish to increase the rate of the reaction $X_2 \rightarrow X_5$ by increasing the level of the enzyme that catalyzes the reaction. If, however, the analysis shows that both v_5 and v_{11} are much larger than the net reaction rate v_5–v_{11} then nothing would be gained, because the reaction $X_2 \rightarrow X_5$ is essentially working in thermodynamic equilibrium.

It is not difficult to imagine more complex networks than those shown in Fig. 5.2. If Fig. 5.2b, c are combined, then all three paths V_1, V_2, and V_3 communicate. The analysis of the network, and the design of suitable experiments to determine the values of all the fluxes, will become quite complicated.

In Sect. 5.1.1, a number of examples will be given to show how networks with diverging branches are analyzed. Since a network consisting of catabolic reactions coupled to a simplified model for biomass formation is well represented by a graph with diverging branches this is an important category. Networks with internal loops and reversible reactions will be treated in Sect. 5.3.

5.1.1 Metabolic Network with Diverging Branches

Consider the following network that represents the catabolic reactions in lactic acid bacteria which were discussed in Fig. 2.4a, b (the EMP pathway) and further in Fig. 2.5b (regeneration of NAD in anaerobic cultivation of lactic acid bacteria).

The network is basically the same as that shown in Fig. 5.2a, but with only six internal fluxes v_i and two internal metabolite pools $X_1 =$ pyruvate and $X_2 =$ AcCoA. There are two diverging branches, and consequently measurement of the three final metabolic products, acetate, ethanol, and lactate defines the network. There are two further metabolic products, CO_2 (from v_3) and formate (from v_4), and the rates of formation of these products are found alongside of the calculation of the fluxes.

The three component net pathway vector $\boldsymbol{V}$ is defined as the pathways $[S \rightarrow P_1, P_2, P_3]$ of the following reactions, when the path v_3 between pyruvate and AcCoA is chosen:

$$\begin{aligned} V_1 &: 3/2\mathrm{CH_2O(glucose)} \rightarrow \mathrm{CH_2O(HAc)} + {}_{1/2}\mathrm{CO_2} + \mathrm{ATP} + \mathrm{NADH} \\ V_2 &: 3/2\mathrm{CH_2O(glucose)} \rightarrow \mathrm{CH_3O_{1/2}(ethanol = e)} + 1/2\mathrm{CO_2} + 1/2\mathrm{ATP} \\ V_3 &: \mathrm{CH_2O(glucose)} \rightarrow \mathrm{CH_2O(HLac)} + 1/3\mathrm{ATP} \end{aligned} \quad (5.1)$$

In all reactions of (5.1) the carbon balance is satisfied. This will also be true for any linear combination of the reactions, and consequently for the network as such, the constraint that we shall always impose on the network is automatically satisfied.

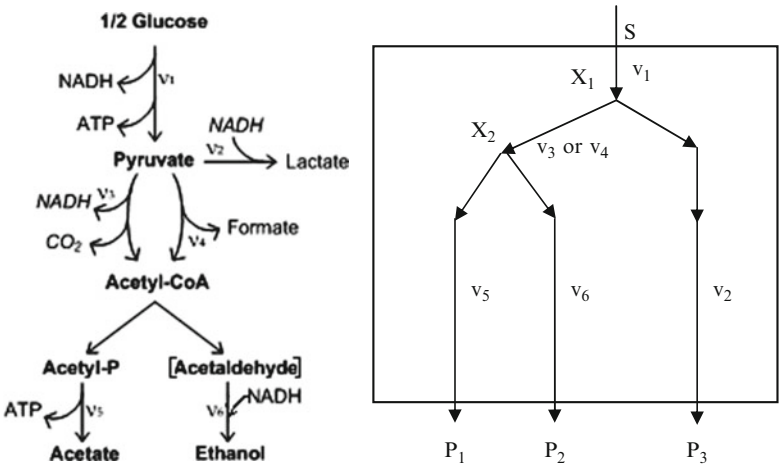

Fig. 5.3 Heterofermentative lactic acid fermentation via pyruvate dehydrogenase (v_3) or pyruvate formate lyase (v_4) to the final products, HAc (P_1), ethanol (P_2), and HLac (P_3). CO_2 is a byproduct of v_3, while formic acid (HCOOH) is a byproduct in v_4. $X_1 =$ pyruvate (PYR) and $X_2 =$ acetyl coenzyme A (AcCoA). $S =$ glucose

The three reaction paths together produce both NADH and ATP. Hence the network of Fig. 5.3 can only be part of a larger metabolic network.

One needs a sink for the ATP produced, and this sink is obviously obtained if a fourth reaction path V_4 with biomass as the final product, P_4, is added to (5.1). Here a large amount of ATP is consumed, but since biomass production is generally accompanied by production of redox (see (5.5) below) this does not help to close the overall NADH balance.

If, however, the path v_4 between pyruvate and AcCoA is chosen one obtains

$$\begin{aligned} V_1 &: 3/2\mathrm{CH_2O(glucose)} \rightarrow \mathrm{CH_2O(HAc)} + 1/2\mathrm{HCOOH} + \mathrm{ATP} + 1/2\mathrm{NADH} \\ V_2 &: 3/2\mathrm{CH_2O(glucose)} \rightarrow \mathrm{CH_3O_{1/2}(e)} + 1/2\mathrm{HCOOH} + 1/2\mathrm{ATP} - 1/2\mathrm{NADH} \\ V_3 &: \mathrm{CH_2O(glucose)} \rightarrow \mathrm{CH_2O(HLac)} + 1/3\mathrm{ATP} \end{aligned} \quad (5.2)$$

Now the overall redox balance closes if $V_1 = V_2$. Since $r_{\mathrm{HCOOH}} = (1/2)\,(V_1 + V_2)$ one obtains that $r_{\mathrm{HAc}} = r_{\mathrm{e}} = r_{\mathrm{HCOOH}}$, all calculated on a C-mol basis.

$(-r_{\mathrm{s}})$ is defined to be 1, and $V_3 = P_3 = \alpha$. The substrate used in V_3 is $(-r_{\mathrm{s}})_3 = \alpha$.

$r_{\mathrm{HAc}} = (1-\alpha)/3 = r_{\mathrm{e}} = r_{\mathrm{HCOOH}}$, and the stoichiometry of the total (black box) model for the catabolism is:

$$\begin{aligned} \mathrm{CH_2O(glucose)} \rightarrow\ & (1-\alpha)[\mathrm{CH_2O(HAc)} + \mathrm{CH_3O_{1/2}(e)} + \mathrm{HCOOH}]/3 \\ & + \alpha\mathrm{CH_2O(HLac)} + (3-\alpha)/6\mathrm{ATP}. \end{aligned} \quad (5.3)$$

One could also specify $r_{\mathrm{HAc}} = P_1 = 1$ and $r_{\mathrm{HLac}} = \beta P_1$. From the NADH balance $P_2 = P_1 = 1$, and $S = 3 + \beta$. Now the stoichiometry of the black box model is given by:

$$\mathrm{C\,H_2O(glucose)} \rightarrow [\mathrm{CH_2O(HAc)} + \mathrm{CH_3O_{1/2}(e)} + \mathrm{HCOOH}]/(3+\beta) + \beta/(3+\beta)\mathrm{CH_2O(HLac)} + (9+2\beta)/(18+6\beta)\mathrm{ATP} \quad (5.4)$$

When α is equated to $\beta/(3+\beta)$ one finds (as expected!) that the two expressions (5.3) and (5.4) are identical. They both express that the network is identified, using two net production rates (S and P_3 in (5.3), and P_1 and P_3 in (5.4)) when one constraint, the NADH balance, is invoked besides the carbon balance, which is automatically satisfied when we write the fluxes V_i as shown in (5.2).

Addition of a fourth path V_4 to the network of Fig. 5.3 is trivial. If this pathway is that by which glucose is converted to biomass X, (5.5), it becomes possible to close the ATP balance, since the three catabolic reactions feed ATP to biomass production. With both the NADH and the ATP balance available as constraints, the addition of the new branch point does not increase the dimension of the network, which is fully identified based on two measured production rates r_i.

$$(\alpha+1)\mathrm{CH_2O(glucose)} \rightarrow \mathrm{X} + \alpha\mathrm{CO_2} + 1/2[4(1+\alpha) - \kappa_x]\mathrm{NADH} - \gamma\mathrm{ATP} \quad (5.5)$$

The coefficient α which represents the loss of carbon as CO_2 in the many reactions that produce building blocks for X is of small importance for the result of the analysis of the metabolic network. A value between 0.08 and 0.14 can be chosen.

The ATP consumption, determined by γ, is much more difficult to specify. We shall see in Example 5.2 that values as low as $\gamma = 1.8$ mol ATP (C-mol X)$^{-1}$ can apply for anaerobic, glucose limited cultures. But when other nutrients, e.g., the N-source, become limiting, γ can be very large. This results in very poor growth of the culture, since the catabolic reactions are not able to supply a sufficient quantity of ATP to support the anabolic reactions. Example 5.5 illustrates this situation. Finally, in fully respiratory growth, a value of γ equal to 0.1 ATP per g biomass produced (i.e., $\gamma \approx 2.5$ mol ATP per C-mol X of formula weight 25 g biomass/C-mol) is used in many references as a "standard." Due to the difficulty of fixing the correct value of γ the energy balance is often rejected as a constraint in network analysis. But if measurements of r_i are available at different cultivation conditions (as in Examples 5.2 and 5.3), the energy balance can be used to estimate γ since other contributions to the balance are usually known from metabolic pathway charts. Eventually, the accumulated knowledge of the variation of γ with the cultivation conditions can be used to select an appropriate value for γ, and this value can be used in situations when less experimental rate data are available.

Example 5.1 *Analysis of the metabolism of lactic acid bacteria.* We shall calculate the fluxes in a network that represents the anaerobic, glucose limited growth of lactic acid bacteria on a defined medium. The catabolism is given by Fig. 5.3, but only the PFL (Pyruvate Formate Lyase) path v_4 between pyruvate and AcCoA is open.

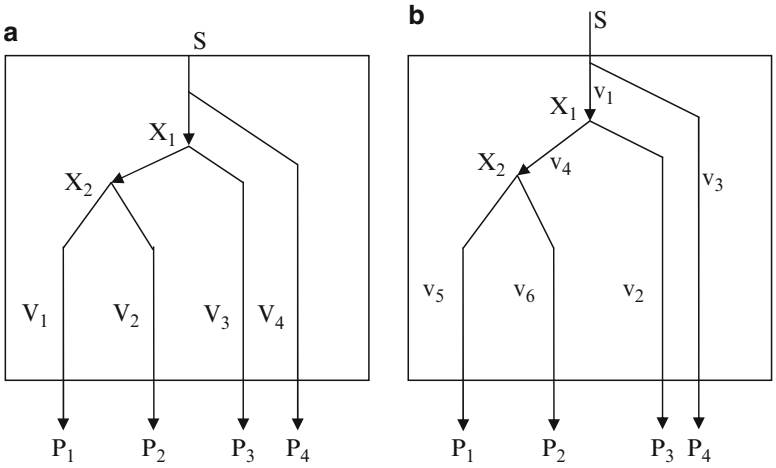

Fig. 5.4 (**a**) The metabolic pathway diagram of Fig. 5.3 (only the path v_4 from X_1 to X_2 is shown) supplemented with a path V_4 from S to biomass ($=P_4$). The internal metabolic pools are $X_2 =$ AcCoA and $X_1 =$ pyruvate. (**b**) The same network as in (**a**), but the paths V_i are shown as made up from the internal paths v_i, e.g., $V_1 = v_1 \rightarrow v_4 \rightarrow v_5$, $V_3 = v_1 \rightarrow v_2$, and $V_4 = v_3$. Biomass is made from many cell reactions, but is symbolized by a split of the flux of S, just inside the cell wall

The coefficients α and γ in (5.5) are chosen as respectively 0.10 mol CO_2 and 2.00 mol ATP per C-mol biomass. The biomass has the composition: $X = CH_{1.8}O_{0.5}N_{0.2}$.

The network has $N = 3$ branch points and $N + 1 = 4$ independent net fluxes V_i, see Fig. 5.4a.

When α and the composition of X are given, a redox balance applied to (5.5) determines β: $\kappa_x = 4.20$ and $1/2(1.1 \times 4 - 4.20) = 0.10$.

We choose r_x and r_{HAc} as the measured production rates, and we apply both the NADH and the ATP balance to determine the two other production rates $r_{EtOH} = r_e$ and r_{HLac}.

$$\begin{aligned} &\text{NADH balance}: 1/2V_1 - 1/2V_2 + 0.1V_4 = 0 \qquad 1/2r_e = 1/2r_{HAc} + 0.1r_x \\ &\qquad\qquad\qquad\qquad \text{or} \qquad\qquad\qquad\qquad (1) \\ &\text{ATP balance}: V_1 + 1/2V_2 + 1/3V_3 - 2V_4 = 0 \quad 1/2r_e + 1/3r_{HLac} = -r_{HAc} + 2r_x \end{aligned}$$

$$\rightarrow r_e = r_{HAc} + 0.2r_x \text{ and } r_{HLac} = -4.5r_{HAc} + 5.7r_x \qquad (2)$$

The missing production rates are

$$\begin{aligned} &r_{HCOOH} = 1/2(r_{HAc} + r_e) = r_{HAc} + 0.1r_x; \\ &r_c = r_{CO_2} = 0.1r_x; \qquad (-r_s) = -1.5r_{HAc} + 7.1r_x \end{aligned} \qquad (3)$$

Closure of the resulting mass balance is easily demonstrated:

$$\begin{aligned} (-1.5r_{HAc} + 7.1r_x) = r_{HAc} + r_x + r_c + (r_{HAc} + 0.2r_x) \\ + (-4.5r_{HAc} + 5.7r_x) + (r_{HAc} + 0.1r_x) \end{aligned} \qquad (4)$$

Similarly for the degree of reduction balance:

$$\begin{aligned} 4(-1.5r_{\mathrm{HAc}} + 7.1r_{\mathrm{x}}) = {} & 4r_{\mathrm{HAc}} + 4.2r_{\mathrm{x}} + 6(r_{\mathrm{HAc}} + 0.2r_{\mathrm{x}}) \\ & + 4(-4.5r_{\mathrm{HAc}} + 5.7r_{\mathrm{x}}) + 2(r_{\mathrm{HAc}} + 0.1r_{\mathrm{x}}) \end{aligned} \tag{5}$$

Both balances are seen to close for any values of $[r_{\mathrm{x}}, r_{\mathrm{HAc}}]$.
If desired the internal fluxes v_i can be calculated based on the production rates r_i.
For example:

$$\begin{aligned} v_4 &= v_5 + v_6 + r_{\mathrm{HCOOH}} = 1.5(r_{\mathrm{HAc}} + r_{\mathrm{e}}) = 3r_{\mathrm{HAc}} + 0.3r_{\mathrm{x}} \\ v_1 &= v_4 + v_2 = -1.5r_{\mathrm{HAc}} + 6r_{\mathrm{x}} = (-r_{\mathrm{s}}) - r_{\mathrm{x}} - r_{\mathrm{c}} = -1.5r_{\mathrm{HAc}} + 6r_{\mathrm{x}} \end{aligned} \tag{6}$$

The black box stoichiometry for conversion of glucose to products is:

$$\mathrm{CH_2O} \rightarrow Y_{\mathrm{sx}}\mathrm{X} + Y_{\mathrm{sc}}\mathrm{CO_2} + Y_{\mathrm{sHAc}} + Y_{\mathrm{se}}\mathrm{EtOH} + Y_{\mathrm{sHLac}}\mathrm{HLac} + Y_{\mathrm{sHCOOH}}\mathrm{HCOOH} \tag{7}$$

In (7) all products are on a C-mol basis. The yield coefficients Y_{si} are found from the rates r_i.

It is remarkable that all six yield coefficients $Y_{ij} = r_j/r_i$ can be found from the rates (2) to (4).

The basis is the two measurements $[r_{\mathrm{x}}, r_{\mathrm{HAc}}]$, while the procedure in Sect. 3.5 must use three measured rates besides the three element balances for C, O, and H. Also the calculations used here are almost trivial while those of Sect. 3.5 are considerably more complicated.

The reason for the significant reduction of both experimental and computational work is, that now *biochemistry* is used to find the right structure of the metabolism (e.g., the stoichiometric coefficient for HCOOH is found automatically from the structure of the pathways), and also we have used the available information on the energy generation and consumption in each pathway.

In (7) neither the stoichiometric coefficient for H_2O, nor that for the N-source is stated. Y_{sn} is of course proportional to Y_{sx}, and if desired $Y_{\mathrm{sH_2O}}$ can be found from an O or an H balance.

One final comment: In the present problem, any two of the seven measurable rates $[r_{\mathrm{x}}, r_{\mathrm{HAc}}, r_{\mathrm{e}}, r_{\mathrm{HLac}}, r_{\mathrm{s}}, r_{\mathrm{HCOOH}}, r_{\mathrm{c}}]$ except the two proportional rates $[r_{\mathrm{x}}, r_{\mathrm{c}}]$ can be chosen as the measured rates $\boldsymbol{r_m}$, and the remaining five rates $\boldsymbol{r_c}$ can be calculated as shown in the example. But the influence of experimental errors on the result $\boldsymbol{r_c}$ is very different for different choices of $\boldsymbol{r_m}$. This is discussed in Note 5.4, and Problem 5.1 exemplifies the importance of using the "right" measurements.

Example 5.2 *Anaerobic growth of Saccharomyces cerevisiae*. Conversion of glucose to biomass and the three metabolic products ethanol (e), acetaldehyde (a), and glycerol (g) is described by the four net fluxes V_i of Fig. 5.5 with stoichiometries stated in (1)

$$\begin{aligned} V_1 = r_{\mathrm{x}}: \ & 1.12\mathrm{CH_2O} \rightarrow \mathrm{X}(\mathrm{CH_{1.74}O_{0.6}N_{0.12}}) + 0.12\mathrm{CO_2} + 0.15\mathrm{NADH} - 2.42\mathrm{ATP} \\ V_2 = r_{\mathrm{a}}: \ & 1.5\mathrm{CH_2O} \rightarrow \mathrm{CH_2O_{1/2}(a)} + 0.5\mathrm{CO_2} + 0.5\mathrm{NADH} + 0.5\mathrm{ATP} \\ V_3 = r_{\mathrm{e}}: \ & 1.5\mathrm{CH_2O} \rightarrow \mathrm{CH_3O_{1/2}(e)} + 0.5\mathrm{CO_2} + 0.5\mathrm{ATP} \\ V_4 = r_{\mathrm{g}}: \ & \mathrm{CH_2O} \rightarrow \mathrm{CH_{8/3}O(g)} - 1/3\mathrm{NADH} - 1/3\mathrm{ATP} \end{aligned} \tag{1}$$

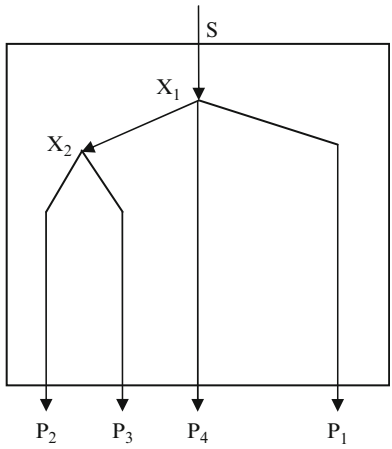

Fig. 5.5 Anaerobic growth of yeast to produce biomass ($X = P_1$) and three metabolic products P_2 = acetaldehyde (a, excreted from the cell), P_3 = ethanol (e) and P_4 = glycerol (g). The metabolite pools are X_1 = 1,6 fructose diphosphate (F1,6P) and X_2 = acetaldehyde (internal). The metabolic pathways V_2 to V_4 are described in Sect. 2.2.3, and graphically in Fig. 2.5c

$$\text{Redox balance} : 0.15V_1 + 0.5V_2 - 1/3V_4 = 0 \tag{2}$$

$$\text{ATP balance} : -2.42V_1 + 0.5V_2 + 0.5V_3 - 1/3V_4 = 0 \tag{3}$$

To determine the four fluxes V_i two measured rates of production P_i must be given.
We choose $V_1(\rightarrow P_1) = r_x$ and $V_2(\rightarrow P_2) = r_a$.
Solution of the two equations (2) and (3) for $V_3 = r_e$ and $V_4 = r_g$ yields:

$$r_g = 0.45r_x + 1.5r_a \quad \text{and} \quad r_e = 5.14r_x \tag{4}$$

Thereafter, the missing production rates r_s and $r_c = r_{CO_2}$ are calculated:

$$-r_s = 1.12r_x + 1.5(r_a + r_e) + r_g = 9.28r_x + 3r_a \tag{5}$$

$$r_c = 0.12r_x + 0.5(r_a + r_e) = 2.69r_x + 0.5r_a \tag{6}$$

The overall carbon and redox balances both close:

$$(-r_s) = 9.28r_x + 3r_a = r_x + r_a + (2.69r_x + 0.5r_a) + (0.45r_x + 1.5r_a) + 5.14r_x$$

$$4(-r_s) = 4.18r_x + 5r_a + 14/3r_g + 6r_e$$

If the (simple) calculations (2)–(6) have been done correctly both balances should, of course, close, but for the beginner it is nice to check the results of the analysis.

It might, in passing, be noted that $V_1(r_x)$ and $V_3(r_e)$ could not have been chosen as basis for analysis of the network. The reason is again that the two rates are proportional ($r_e = 5.14r_x$) and do not constitute a set of two linearly independent rates. The linear dependence between r_x and r_e can be spotted immediately from the structure of the two linear algebraic equations (2) and (3): If the (2×2) coefficient matrix for the two rates to be determined as a linear combination of the remaining rates is singular, then two different rates must be chosen.

It is interesting to compare two special cases:

1. $r_e = 0$.
   In this case r_x is also zero, and the equations boil down to $r_g = 1.5r_a$, $r_c = 1/2r_a$ and $(-r_s) = 1.5r_a$.

   Referring to Figs. 2.4a and 2.5c we find that the glucose flux is divided into two equal fluxes at the branch point of fructose 1,6 diphosphate. The two fluxes continue to glycerol and to the branch point at pyruvate. At pyruvate $0.5CO_2$ is split off, and the remainder ends as acetaldehyde. The overall reaction is

$$CH_2O \rightarrow 0.5CH_{8/3}O + 1/3\ CH_2O_{1/2} + 1/6CO_2 \tag{7}$$

   Hence, the maximum yield of glycerol is 0.5 C-mol per C-mol glucose $= 0.51\ g\ g^{-1}$.

   When, during World War I, Germany had to use as much as possible of its animal and vegetable fat production for food and feed purposes, its ample resources of beet sugar became the source of glycerol for production of explosives. A small flux from acetaldehyde to ethanol was permitted in order to keep the biomass alive, but addition of sulfite to the medium precipitated most of the aldehyde, and glycerol was basically the only metabolic product.

   Today, the process would be run by suppression of alcohol dehydrogenase (ADH), the enzyme that converts acetaldehyde to ethanol.
2. $r_a = 0$.
   Under normal conditions anaerobic yeast fermentation yields very little acetaldehyde, and with the data used above the case $r_a = 0$ will give:

$$9.28CH_2O \rightarrow CH_{1.74}O_{0.6}N_{0.12} + 5.14CH_3O_{1/2} + 0.45CH_{8/3}O + 2.69CO_2 \tag{8}$$

$$Y_{sx} = 0.1077,\ Y_{se} = 0.5539,\ Y_{sc} = 0.2890,\ \text{and}\ Y_{sg} = 0.0485. \tag{9}$$

In Sect. 3.3, a set of very accurate cultivation data was analyzed for a yeast with the biomass composition of the present example. The yield coefficients were determined in (3.23):

$$Y_{sx} = 0.137, \quad Y_{se} = 0.510, \quad Y_{sc} = 0.275, \quad \text{and}\ Y_{sg} = 0.077. \tag{10}$$

The yield coefficients determined from the model are close to those obtained experimentally, but characteristically Y_{sx} is smaller, while Y_{se} and Y_{sg} are larger when determined from the model.

It appears that the model overestimates the rates of the catabolic reactions, relative to the rate of biomass formation.

If $\gamma = Y_{xATP}$ in (5.5) was smaller, then less ATP had to be produced by conversion of glucose to ethanol to support a given rate of biomass synthesis. Since both r_e and r_g are proportional to r_x when $r_a = 0$, then all three yield factors would move toward those obtained experimentally, if a smaller value of γ was used in (5.5).

Repeating the calculations of the example for $\beta = 0.12$, but with γ values smaller than 2.42, reveals that a sharp minimum in the least squares difference between the experimental and the calculated values for the yield coefficients is obtained for $\gamma = 1.8$. This leads to the stoichiometry:

$$CH_2O \rightarrow 0.136X + 0.524\ CH_3O_{1/2} + 0.278\ CO_2 + 0.061\ CH_{8/3}O \tag{11}$$

Changing β to 0.13 and γ to 1.74 gives an even better model prediction:

$$CH_2O \rightarrow 0.138X + 0.516\ CH_3O_{1/2} + 0.276\ CO_2 + 0.070\ CH_{8/3}O \tag{12}$$

The model and the experiments now give almost the same result.

Whether (11), (12) or a model with even better fitted values of β and γ is used, the power of a well-structured metabolic model is obvious. It should be noted that not a single experimental value is necessary to obtain the same result by the model as that obtained in Sect. 3.3.

Example 5.3 *Aerobic growth of Saccharomyces cerevisiae*. In Example 3.5, the data of von Meyenburg were analyzed, and it was found that a substantial part of the ethanol formed when $D > D_{crit}$ had been stripped to the gas phase. When the data at $D = 0.30\ h^{-1}$ and $0.40\ h^{-1}$ is corrected for the missing ethanol one obtains the following table of yield coefficients (all on C-mol basis).

D (h^{-1})	Y_{sx}	Y_{sc}	Y_{so}	Y_{se}
0.15	0.548	0.452	0.425	0
0.30	0.279	0.366	0.167	0.355
0.40	0.175	0.312	0.044	0.513

These data will now be analyzed using a simple model. The model contains two main pathways V_1 and V_2 besides two internal pathways v_3 and v_4, which together lead to CO_2, a metabolic product that is also obtained in the two main pathways. In pathway V_1 biomass X is produced, and in pathway V_2 ethanol.

For $\alpha = 0.10$ in (5.5) one obtains the following stoichiometries for V_1 and V_2:

$$V_1 : 1.10\ CH_2O \rightarrow X(\kappa_x = 4.20) + 0.10\ CO_2 + 0.10\ NADH - \gamma ATP \tag{1}$$

$$V_2 : 1.5\ CH_2O \rightarrow CH_3O_{1/2}(e) + 0.5\ CO_2 + 0.5\ ATP \tag{2}$$

Besides the glucose needed for (1) and (2) some glucose is completely combusted to CO_2 in internal pathway v_3. The NADH produced in this path is combined with the NADH obtained in V_1, and in pathway reaction v_4 all the NADH is oxidized to NAD while producing ATP to support the biomass production in V_1.

First we analyze the main metabolic network – the one that produces biomass and ethanol through pathways V_1 and V_2. With r_x and r_e as the measured rates, the rates of glucose consumption and CO_2 production, $(-r_s)_1$ and $(r_c)_1$, for this part of the metabolism are obtained.

$$\begin{aligned} \text{From pathways } V_1 \text{ and } V_2 \text{ one obtains : } (-r_s)_1 &= 1.1r_x + 1.5r_e \text{ and } (r_c)_1 \\ &= 0.1r_x + 0.5r_e \end{aligned} \tag{3}$$

Next the stoichiometry of the internal pathway reactions is considered:

$$v_3 : CH_2O \rightarrow CO_2 + 2NADH + \varepsilon ATP \text{ with rate} = (-r_s)_2 \tag{4}$$

$$v_4 : O_2 \rightarrow -2\text{NADH} + 2\text{P/O ATP (2.18) with rate}(-r_o) \tag{5}$$

The redox and the energy balances are used to calculate $(-r_s)_2$ and $(-r_o)$ in terms of r_x and r_e:

$$\text{Redox balance} : 0.1r_x + 2(-r_s)_2 - 2(-r_o) = 0 \tag{6}$$

$$\text{ATP balance} : -\gamma r_x + 0.5r_e + \varepsilon(r_s)_2 + 2\text{P/O}(-r_o) = 0 \tag{7}$$

In the energy balance (7) ε is the amount of ATP obtained in the EMP pathway and in the conversion of pyruvate to CO_2 in the TCA cycle. ε is at least 1/3 ATP per C-mol glucose (from the EMP pathway). In the TCA cycle 1 GTP is obtained per pyruvate, or 1/3 ATP per C-mol glucose. GTP is equivalent to ATP as energy currency. When AcCoA is synthesized in the mitochondria from cytosolic HAc (see Fig. 2.5c) the activation of the HAc does, however, require ATP which cancels the "ATP" gained in the TCA cycle. Thus, if a large part of the pyruvate enters the mitochondria via the shunt in Fig. 2.5c, the value of ε is close to 1/3. The largest value of ε is 2/3 per C-atom glucose. The calculations below are, however, almost independent of the value of ε, but they are quite sensitive to the value of γ, the other parameter in (7).

All the redox obtained in the TCA cycle is taken to be NADH. In *S. cerevisiae* NADH does, however, enter the electron transfer chain at the level of Complex II/III in Fig. 4.1, with a theoretical ATP yield of two ATP/($2e^{-1}$). Thus, NADH and $FADH_2$ are equivalent in this organism.

Solving (6) and (7) for $(-r_s)_2$ and $(-r_o)$ yields the following result:

$$(-r_s)_2 = [(\gamma - 0.1\text{P/O})r_x - 0.5r_e]/(\varepsilon + 2\text{P/O}) = (r_c)_2 \tag{8}$$

$$(-r_o) = 0.05r_x + (-r_s)_2 \tag{9}$$

$$\begin{aligned}\text{The total glucose consumption is} : (-r_s) &= (-r_2)_1 + (-r_s)_2 \\ &= 1.1r_x + 1.5r_e + (-r_s)_2\end{aligned} \tag{10}$$

$$\text{The total } CO_2 \text{ produced is} : r_c = 0.1r_x + 0.5r_e + (-r_s)_2 \tag{11}$$

The yield coefficients Y_{sj} of O_2, biomass, ethanol and CO_2 on glucose can be determined as the ratio between $[(-r_o), r_x, r_e, r_c]$, and $(-r_s)$. For given values of $[Y_{sx}, Y_{se}, \text{P/O}, \gamma, \varepsilon]$, one can calculate the yield coefficients $[Y_{so}, Y_{sc}]$ and compare them with the experimental results of the table.

For P/O = 1.25, the value recommended by van Gulik and Heijnen (1995), and $\varepsilon = 0.5$ (halfway between 1/3 and 2/3), one calculates the following values for γ when the three Y_{so} values of the table are compared (by least squares regression) with the calculated values for Y_{so}:

$$D = [0.15(r_e = 0), 0.30, 0.40]\,\text{h}^{-1} \rightarrow \gamma = [2.45, 2.35, 2.17]\ \text{mol ATP(C-mol biomass)}^{-1} \tag{12}$$

From the γ values calculated in (12) it is seen that the ATP consumption associated with the synthesis of one C-mol biomass continuously decreases from the so-called "standard" value of ≈2.5 mol ATP at fully respiratory cultivation toward the much lower value ≈1.8 mol ATP calculated in Example 5.3 for the anaerobic cultivation of *S. cerevisiae*.

The results of (12) were obtained based on a constant value of P/O. The experimental data can, however, also be interpreted in a different way. *If* γ remains at 2.45 mol ATP (C-mol biomass)$^{-1}$ for all three D values, then P/O must increase from 1.25 at $D = 0.15\ h^{-1}$ to about 1.9 at $D = 0.4\ h^{-1}$. This explanation is, however, less convincing, since the lowest γ value = 1.8 is obtained with no oxygen supply at all, and the argument based on an increasing P/O with increasing D is not valid in this case.

We have, however, in Table 3.2 seen that the biomass composition changes with the cultivation conditions. This may affect the ATP cost. Also the maintenance of a constant membrane potential at aerobic growth may require extra ATP in fully aerobic growth.

Speculations concerning the energy costs for different life processes, and the efficiency of the energy producing mechanisms can never lead to any firm conclusions. The energy creating and the energy consuming processes, including *maintenance* of already existing cells, are intimately connected, and their individual contributions cannot be sorted out. In Sect. 5.2 these issues will be discussed.

5.1.2 A Formal, Matrix-Based Description of Metabolic Networks

The analysis of metabolic networks described above works fine as long as the network is small (or it is reduced through lumping of reactions), but as soon as the number of reactions increases it is necessary to have a more stringent formulation of the network model. Such a formalism can be based on the internal fluxes $\boldsymbol{v}$ (e.g., in C-mol per time unit) of Fig. 5.2 rather than on the fluxes $\boldsymbol{V}$ from substrate(s) to metabolic products, which were used in Figs. 5.3–5.6, and mass balances around every internal branch point (i.e., for each internal metabolite) are used as constraints on the fluxes. The rates of production of all metabolic products and substrates are written as linear combinations of the internal fluxes v_i, as exemplified below for the metabolism of glucose by lactic acid bacteria via the pyruvate formate lyase pathway in Fig. 5.4b.

$$\begin{aligned} &(-r_s) = v_1 + 1.1v_3; \quad r_x = v_3; \quad r_{HLac} = v_2; \quad r_{HAc} = v_5; \\ &r_e = v_6; \quad r_{HCOOH} = 1/3v_4; \quad r_c = 0.1v_3 \end{aligned} \tag{5.6}$$

Next four constraints are invoked, which express that there is no accumulation of mass at the two branch points at pyruvate and AcCoA, and that there is no accumulation of NADH and ATP in the network:

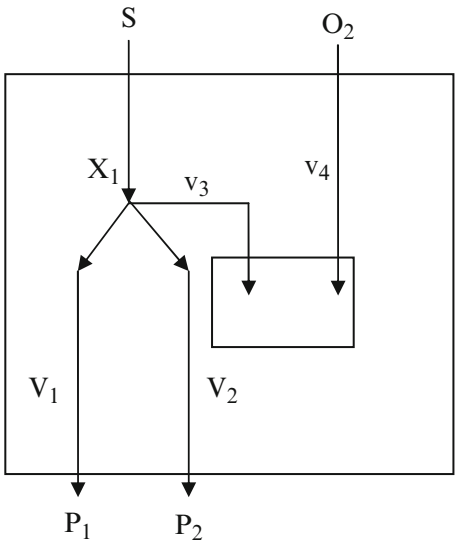

Fig. 5.6 Aerobic growth of yeast to produce biomass $X = P_1$ and ethanol P_2 from glucose S. The metabolite pool X_1 is pyruvate, and part of the glucose is diverted to produce NADH for the oxidative phosphorylation, which takes place in the "inner" box

$$\begin{aligned} r_{\mathrm{PYR}} &= v_1 - v_2 - v_4 = 0; \\ r_{\mathrm{AcCoA}} &= 2/3v_4 - v_5 - v_6 = 0; \\ r_{\mathrm{NADH}} &= 1/3v_1 - 1/3v_2 + 0.1v_3 - v_6 = 0; \\ r_{\mathrm{ATP}} &= 1/3v_1 - 2v_3 + 1/2v_5 = 0 \end{aligned} \tag{5.7}$$

Finally, the production rates $\boldsymbol{r}$ and the internal fluxes $\boldsymbol{v}$ are related by the following equation:

$$\begin{bmatrix} -r_{\mathrm{s}} \\ r_{\mathrm{x}} \\ r_{\mathrm{HLac}} \\ r_{\mathrm{e}} \\ r_{\mathrm{HAc}} \\ r_{\mathrm{HCOOH}} \\ r_{\mathrm{c}} \\ r_{\mathrm{PYR}} \\ r_{\mathrm{AcCoA}} \\ r_{\mathrm{NADH}} \\ r_{\mathrm{ATP}} \end{bmatrix} = \begin{bmatrix} 1 & 0 & 1.1 & 0 & 0 & 0 \\ 0 & 0 & 1 & 0 & 0 & 0 \\ 0 & 1 & 0 & 0 & 0 & 0 \\ 0 & 0 & 0 & 0 & 0 & 1 \\ 0 & 0 & 0 & 0 & 1 & 0 \\ 0 & 0 & 0 & 1/3 & 0 & 0 \\ 0 & 0 & 0.1 & 0 & 0 & 0 \\ 1 & -1 & 0 & -1 & 0 & 0 \\ 0 & 0 & 0 & 2/3 & -1 & -1 \\ 1/3 & -1/3 & 0.1 & 0 & 0 & -1 \\ 1/3 & 0 & -2 & 0 & 1/2 & 0 \end{bmatrix} \cdot \begin{bmatrix} v_1 \\ v_2 \\ v_3 \\ v_4 \\ v_5 \\ v_6 \end{bmatrix} \tag{5.8}$$

The six fluxes v_i are related through the four algebraic equations in (5.7). Hence, if *two* of the six fluxes are selected, the last four can be calculated in terms of the two selected fluxes. The easiest calculation is obtained when two fluxes which are proportional to two different elements of $\boldsymbol{r}$ are selected. In (5.8) there are five such possibilities (but the network is also very simple).

In the following $[v_3, v_5] = [r_x, r_{HAc}]$ are chosen. The four remaining fluxes $[v_1, v_2, v_4, v_6]$ are now calculated as shown in (5.9):

$$\begin{bmatrix} v_1 \\ v_2 \\ v_4 \\ v_6 \end{bmatrix} = \begin{bmatrix} 1 & -1 & -1 & 0 \\ 0 & 0 & 2/3 & -1 \\ 1/3 & -1/3 & 0 & -1 \\ 1/3 & 0 & 0 & 0 \end{bmatrix}^{-1} \times \begin{bmatrix} 0 & 0 \\ 0 & 1 \\ -0.1 & 0 \\ 2 & -1/2 \end{bmatrix} \times \begin{bmatrix} r_x \\ r_{HAc} \end{bmatrix}$$

$$= \begin{bmatrix} 6 & -1.5 \\ 5.7 & -4.5 \\ 0.3 & 3 \\ 0.2 & 1 \end{bmatrix} \times \begin{bmatrix} r_x \\ r_{HAc} \end{bmatrix}. \tag{5.9}$$

Finally, the remaining five nonzero production rates are easily calculated from (5.6):

$$\begin{bmatrix} -r_s \\ r_{HLac} \\ r_e \\ r_{HCOOH} \\ r_c \end{bmatrix} = \begin{bmatrix} 7.1r_x - 1.5r_{HAc} \\ 5.7r_x - 4.5r_{HAc} \\ 0.2r_x + r_{HAc} \\ 0.1r_x + r_{HAc} \\ 0.1r_x \end{bmatrix} \tag{5.10}$$

Equations (5.6)–(5.10) illustrate the application of the method on the network in Example 5.1 (Fig. 5.4b). The results are of course identical to those obtained previously.

The general application of the method is formally given in (5.11)–(5.12).

Here the J columns of matrix $\boldsymbol{T}$ in (5.11) are the stoichiometric coefficients in the J reactions v_i in the metabolic network. The first K rows in $\boldsymbol{T}$ show the distribution of the K substrates in the J internal reactions, while the next M rows show how biomass and metabolic products are formed in the J internal reactions. The last $N+2$ (N being the number of internal nodes – or metabolites) rows of $\boldsymbol{T}$ show how, due to the steady state treatment of the network, internal metabolites are formed in the internal reactions, all with a rate $r_i = 0$. In Example 5.1, $J = 6$, $K = 1$, $M = 6$, and $N = 2$.

$\boldsymbol{T}^T$, the transpose of $\boldsymbol{T}$, is normally called *the stoichiometric matrix*.

$$\boldsymbol{r} = \boldsymbol{T}\boldsymbol{v}, \tag{5.11}$$

In (5.11) $\boldsymbol{r}$ has dimension $(K+M+N+2, 1)$, $\boldsymbol{v}$ $(J, 1)$, and $\boldsymbol{T}(K+M+N+2, J)$.

From the column vector $\boldsymbol{v}$ we pick vector $\boldsymbol{v}_1$ with $J-N-2$ elements. The remainder of $\boldsymbol{v}$ is $\boldsymbol{v}_2$ with $N+2$ elements.

The last $N+2$ rows of matrix $\boldsymbol{T}$, a matrix $\boldsymbol{T}_0$ of dimension $(N+2, J)$, is now divided into two matrices, $\boldsymbol{T}_1$ with dimension $(N+2, N+2)$, and the remainder, $\boldsymbol{T}_2$, of dimension $(N+2, J-N-2)$. $\boldsymbol{T}_1$ is the part of $\boldsymbol{T}_0$ that belongs to $\boldsymbol{v}_2$, while $\boldsymbol{T}_2$ is the part belonging to $\boldsymbol{v}_1$.

$\boldsymbol{v}_2$ can now be found as a function of $\boldsymbol{v}_1$ by the solution of:

$$\boldsymbol{T}_1 \cdot \boldsymbol{v}_2 = -\boldsymbol{T}_2 \cdot \boldsymbol{v}_1 \rightarrow \boldsymbol{v}_2 = -\boldsymbol{T}_1^{-1} \cdot \boldsymbol{T}_2 \cdot \boldsymbol{v}_1 \tag{5.12}$$

Finally, $\boldsymbol{r}$ is found directly from (5.11) as a function of $\boldsymbol{v}_1$, since all elements of $\boldsymbol{v}$ have now been expressed in terms of $\boldsymbol{v}_1$. Some of the elements of $\boldsymbol{r}$ may be equal to

elements in $\boldsymbol{v}_1$, while the others are linear combinations of the elements of $\boldsymbol{v}_1$. A requirement for the use of (5.12) is that $\boldsymbol{T}_1$ is nonsingular, i.e., it has full rank. For simple metabolic networks this is normally the case, but for larger metabolic networks reaction paths with similar overall stoichiometry one may end up with a singular matrix. We shall return to a discussion of this issue.

Note 5.1 *Comparison of the method based on the net fluxes* $\boldsymbol{V}$*, and the method based on the total set of internal fluxes* $\boldsymbol{v}$*.* In Example 5.1 there are $N = 2$ branch points at the specified internal metabolites X_1 and X_2 and one "unspecified" branch point where carbon is drained off to biomass. This establishes $N+2=4$ pathways V_i between the substrate S and $N+2=4$ metabolic products P_i. Each path V_i leads to a product that is *only* formed in that path. The metabolic products P_i are the independent variables of the network which can be fully described using these variables. All other metabolic products are found as linear combinations of the P_i.

Consequently, in Fig. 5.4a there are $N_t = N+1=3$ binary branches and 4 products P_i, where each product is formed in one and only one pathway. There are 2 internal branch points with well defined metabolites (X_1, X_2) while the branch to $P_4 =$ biomass X receives carbon from many donor metabolites along the path from S to X. If the redox and energy balances are used as constraints on the fluxes V_i, the number of independent P_1 needed to define the network is reduced to $N_t-1=2$. The rate of substrate consumption is found from a total carbon balance based on the P_i, and likewise the other metabolic products are found as linear combinations of the P_i. In Figure 5.4b the network is also defined by $N=2$ specified internal branch points, and one unspecified branch point. From each branch point two fluxes emanate. Hence the network is fed by $(-r_s)$ and is made up of $2(N+1) = 6$ internal fluxes v_i. At each of the N *specified internal* branch points (at X_1 and X_2 in Figure 5.4b), a mass balance is set up to express that the internal metabolite concentration stays constant in time. This gives N constraints on the $2(N+1)$ fluxes v_i, and the number of independent fluxes is hereby reduced to $N+2$.

When the redox and energy balances are introduced as extra constraints, the number of independent internal fluxes v_i is further reduced to N. This is the same result as that obtained by analysis of the method based on Figure 5.4a, where $N_t - 1$ net-*production rates* (defined as explained above) were needed to define the network when the two constraints are used.

Although the two methods should give identical results, they are not equally easy to work with. In the "net-flux" method with $N+2$ pathways to $N+2$ products P_i there will always be exactly two extra constraints that can, if desired, be applied to reduce the number of independent rates to N. In the "internal-flux" method one *must* solve a matrix equation of dimension $N+2$ that is set up to express that the net rate of production of the N specified internal metabolites X_i and cofactors ATP and NADH is zero. If one of the cofactor related constraints is not used, then more than N external rates $(-r_s, P_i)$ must be measured to identify the network.

For large N the difference in computational work is considerable. In large networks it also becomes increasingly difficult to see if some of the internal reactions are linearly dependent. If for example both ATP and ADP are included as reaction species with $r_i = 0$ there will be two rows in $\boldsymbol{T}_1$ that are only different in the signs. Hence $\boldsymbol{T}_1$ cannot be inverted. This error is easily avoided by only using one species of a cofactor pair. When some of the reactions in the network are linearly dependent – and this may be difficult to appreciate in large networks as exemplified in Note 5.5 – columns in $\boldsymbol{T}_1$ become linearly dependent, and again $\boldsymbol{T}_1$ cannot be inverted. Here the remedy is to use a different set of fluxes in $\boldsymbol{v}_2$. When computer software is used to solve the flux distribution problem, the software will automatically find a set of

fluxes v_i in $\boldsymbol{v}_2$ for which this problem does not arise, but in manual calculations (*e.g.* in "student exercises") this problem is often frustrating.

The $J-N-2$ independent fluxes v_i are expressed in terms of measured rates r_i (in the example $(v_3, v_5) = (r_x, r_{HAc})$ were used but (r_x, r_c) could not be used). In large networks it is also difficult to see which *rates* are linearly independent, and the basis for calculation of the remaining fluxes fails, since $\boldsymbol{T}_1$ is again singular. The system is said to be *nonobservable* with the chosen set of measured rates.

When the larger computational work and the risk of having to duplicate the computations in the "internal flux" method are considered, this method seems to be much less attractive than the "net-flux" method, at least for manual calculations.

One may claim, that it is easy to set up the stoichiometries of the internal reactions, since the stoichiometric coefficients are immediately known from textbooks or are stored in the computer software (e.g., PYR → 2/3AcCoA + 1/3HCOOH for v_4 in Fig. 5.4b). But the computer is also able to combine the single reactions v_i to one net flow (e.g., V_1 in Fig. 5.4a $= v_1 + v_4 + v_5$ with the combined stoichiometry V_1: $3/2CH_2O \rightarrow HAc + 1/2HCOOH + NADH + ATP$).

From a pedagogical perspective, the "net-flux" method is the easiest to apply and it works well for diverging networks – also when as in Example 5.4 there are many net paths V_i. In large networks with many internal loops it does, however, become increasingly difficult to sort out the valid net paths – see Example 5.7 which is still a very simple example of a metabolic network. Consequently, the general method of Metabolic Flux Analysis based on (5.11) and (5.12) will surely be the right method to use for open-ended network analysis of real biological problems, while the net-flux method serves as a reasonably simple introduction to flux analysis – without much matrix algebra – a subject that is unfortunately shunned by many students.

Example 5.4 *Production of butanol and acetone by fermentation.* In Problem 2.3, the revival of the old (1917) fermentation route to butanol (the main product) and acetone is treated in a literature exercise. In the present example, the metabolic network, a simplification of that proposed by Reardon et al. (1987), is examined by the net flux method.

The left hand side of the figure shows the network based on eight fluxes V_i from S to eight products P_i.

The upper part of the network, until the branch point at AcCoA, is identical to that of Fig. 5.3, except that acetoin (*acn* = 3-hydroxy butanone, CH_3–CO–CHOH–CH_3) is synthesized from pyruvate by decarboxylation of one pyruvate, followed by condensation with another pyruvate to form acetoin and a second CO_2. At the branch point of AcCoA a third reaction takes place, the condensation of two AcCoA to form Aceto-AcCoA = CH_3CO–CH_2CO–S–CoA by pathway reaction v_8. Aceto-AcCoA can either (reaction v_9) decarboxylate to acetone (CH_3COCH_3) + CoA, where the CoA is used to activate butyric acid (HBu) to buturyl-CoA (BuCoA), or it can be reduced (reaction v_{10}) to BuCoA ($CH_3CH_2CH_2CO$–CoA). In reactions v_{11} and v_{12}, BuCoA can be reduced to 1-butanol (BuOH) or hydrolyzed to butyric acid (HBu), by the same reactions shown for AcCoA. One ATP is produced both in reaction v_6 and in v_{12} per molecule of the activated compound.

H_2 is produced by reaction v_{13}. This could result by decarboxylation of HCOOH if pyruvate formate lyase is the active enzyme. If pyruvate dehydrogenase is the active enzyme it could result by dehydrogenation of NADH following NADH → NAD + H_2. The final products are CO_2 and H_2 in the stoichiometric ratio 1:1 if, as is the case for the example, *no* HCOOH is observed in the products. Hence it does not matter by which route pyruvate is converted to AcCoA. In the stoichiometries listed in (1) 1/2HCOOH is assumed to be produced per C-mol carbon in the substrate (glucose) in all the reactions (v_4 to v_{12}) that are being fed via the

decarboxylation of pyruvate to AcCoA. The rate of H_2 production r_{H_2} is equal to the rate of HCOOH production r_{HCOOH} as a byproduct in many of the net-reactions shown in (1) below.

In this example it becomes quite difficult to write the stoichiometries for the internal reactions v_1 to v_{13}. A large number of cofactors are involved, and there are several loops in which AcCoA or BuCoA are recirculated. The result could easily be that incorrect stoichiometric coefficients are used, and that several linearly dependent reactions are included.

The net flux description (right hand diagram of Fig. 5.7) in terms of eight net fluxes V_i to eight products P_i, each of which is only produced by one pathway V_i is, however, quite simple. The redox balance for each pathway is easily checked, and the ATP contribution is found by using the results of previous examples.

$$
\begin{aligned}
&V_1 = r_x : -1.1\,CH_2O + X(CH_2O_{0.5}N_{0.25}) + 0.1CO_2 + 0.075\ NADH - 2.48\ ATP = 0\\
&V_2 = r_{acn} : -1.5\ CH_2O + CH_2O_{1/2} + 1/2\ CO_2 + 1/2\ NADH + 1/2\ ATP = 0\\
&V_3 = r_{HLac} : -CH_2O + CH_2O(HLac) + 1/3ATP = 0\\
&V_4 = r_e : -1.5\ CH_2O + 1/2\ HCOOH + CH_3O_{1/2} - 1/2NADH + 1/2ATP = 0\\
&V_5 = r_{HAc} : -1.5CH_2O + 1/2\ HCOOH + CH_2O(HAc) + 1/2\ NADH + ATP = 0\\
&V_6 = r_{ac} : -2\ CH_2O + CH_2O_{1/3} + 2/3\ HCOOH + 1/3\ CO_2 + 2/3\ NADH + 2/3\ ATP = 0\\
&V_7 = v_{HBu} : -1.5\ CH_2O + CH_2O_{1/2} + 1/2\ HCOOH + 3/4\ ATP = 0\\
&V_8 = r_{BuOH} : -1.5\ CH_2O + CH_{2.5}O_{0.25} + 1/2\ HCOOH - 1/2\ NADH + 1/2\ ATP = 0
\end{aligned}
\tag{1}
$$

The redox and energy balances are

$$
\begin{aligned}
&NADH : 0.075V_1 + 1/2\ V_2 - 1/2\ V_4 + 1/2\ V_5 + 2/3\ V_6 - 1/2\ V_8 = 0\\
&ATP : -2.48\ V_1 + 1/2\ V_2 + 1/3\ V_3 + 1/2\ V_4 + V_5 + 2/3\ V_6 + 3/4\ V_7 + 1/2\ V_8 = 0
\end{aligned}
\tag{2}
$$

Six out of the eight V_i must be measured while the last two can be calculated from (2) as linear combinations of the measured V_i. By inspection it is found that the calculated fluxes cannot be (V_2, V_6) or (V_4, V_8) since matrix $\boldsymbol{T}_1$ of (5.12) will be singular. All other pairs can be used.

We choose (V_3, V_5) as $\boldsymbol{r_c}$, and in (3) these two net flows are found in terms of the remaining six V_i.

$$
\begin{aligned}
V_5 &= r_{HAc} = -0.150V_1 - V_2 + V_4 - 4/3V_6 + V_8\\
V_3 &= r_{HLac} = 7.89V_1 + 3/2V_2 - 9/2V_4 + 2V_6 - 9/4V_7 - 9/2V_8
\end{aligned}
\tag{3}
$$

Now the whole flux distribution problem has been solved by almost trivial manual calculations, and all other metabolic production rates are found as linear combinations of the six independent V_i:

$$
\begin{aligned}
(-r_s) &= 1.1V_1 + 3/2V_2 + v_3 + 3/2V_4 + 3/2V_5 + 2V_6 + 3/2V_7 + 3/2V_8\\
&= 8.765V_1 + 3/2V_2 - 3/2V_4 + 2V_6 - 3/4V_7 - 3/2V_8\\
r_{HCOOH} &= 1/2V_4 + 1/2V_5 + 2/3V_6 + 1/2V_7 + 1/2V_8\\
&= -0.075V_1 - 1/2V_2 + V_4 + 1/2V_7 + V_8 = r_{H_2}\\
r_c &= r_{HCOOH} + 0.1V_1 + 1/2V_2 + 1/3V_6\\
&= 0.025V_1 + V_4 + 1/3V_6 + 1/2V_7 + V_8
\end{aligned}
\tag{4}
$$

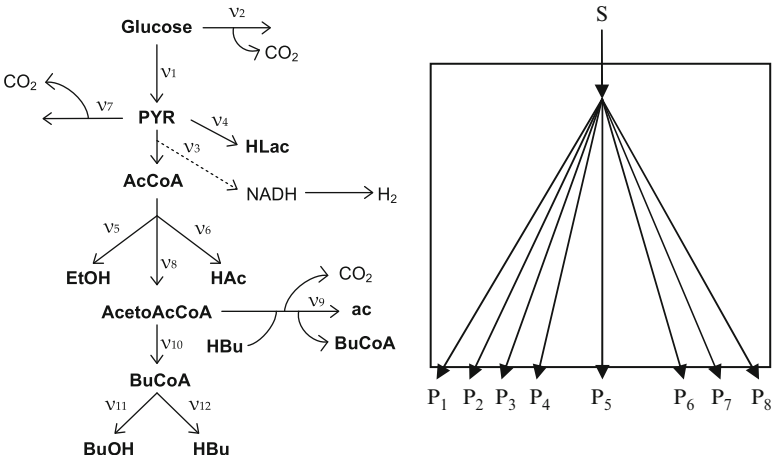

Fig. 5.7 The metabolic network from glucose to solvents in *Clostridium acetobutylicum*

The 13 fluxes v_i are tied together by six relations ($r_{PYR} = r_{AcCoA} = r_{AvcetoAcCoA} = r_{BuCoA} = r_{NADH} = r_{ATP} = 0$) giving a (6×6) matrix $\boldsymbol{T}_1$ in (5.12), and there are quite a few linearly dependent columns in $\boldsymbol{T}$. It can be a frustrating experience for students to pick a valid set of six internal fluxes v_i, especially if they solve the problem using only a pocket calculator. In "professional" metabolic flux analysis this should of course not be an issue.

To illustrate the problems when inexperienced students apply the general method based on (5.12) the following "mistake" is instructive. In Fig. 5.7 there are 13 internal fluxes v_i and there are four internal nodes (PYR, AcCoA, AcetoAcCoA, BuCoA) together with the redox and ATP balances.

Hence one must measure seven production rates to close the problem. [r_s, r_x, r_e, r_{ac}, r_{BuOH}, r_{HBu}, r_{acn}] were chosen by the student group. It was later found that $(-r_s)$ was a linear combination of the other six measured rates. Evidently, one had overlooked a linear dependence between v_{13} and the rates of production of the metabolites below AcCoA, and there were in reality only 12 independent internal fluxes v_i.

5.2 Growth Energetics

5.2.1 Consumption of ATP for Cellular Maintenance

Herbert (1959) showed that what he called "*endogeneous metabolism*" results in a continuous degradation of already formed biomass, and that the total substrate consumption must be calculated as the sum of two terms, one that gives rise to ab initio formation of biomass, while the other is used to regenerate degraded biomass. The rates of the two separate biomass formation reactions are $r_x =$ the observed

specific growth rate μ of the culture, and the rate of formation of biomass from degraded biomass, $r_{xe} = \mu_e$.

$$(-r_s) = Y_{xs}^{true}\mu + Y_{xs}^{true}\mu_e = Y_{xs}^{true}\mu + m_s \tag{5.13}$$

The so-called true yield coefficient, Y_{xs}^{true}, specifies the yield in the conversion of substrate into biomass. Pirt (1965) introduced an empirical correlation identical in form to (5.13), but he collected the product of Y_{xs}^{true} and μ_e in the empirical constant m_s, as shown in the last expression in (5.13). The empirical constant was called the *maintenance coefficient*.

In Sect. 7.3.2 we shall discuss the application of (5.13) for description of cellular processes and show, that despite its empirical nature it gives a good description of the total specific substrate uptake rate. However, the simple linear rate equation does not explain, in a biologically satisfactory way, what the extra substrate consumed for maintenance is in fact used for, i.e., which energy requiring cellular processes do not lead to net formation of biomass. It is not at all clear which cellular processes should be categorized as maintenance processes, but below we list some of the most important processes that are customarily regarded as leading to maintenance substrate consumption:

- *Maintenance of gradients and electrical potential*. In order to ensure proper function of the cell it is necessary to maintain concentration gradients, e.g., a proton gradient across the cellular membrane. Furthermore, it is necessary to maintain an electrical potential across the cellular membrane. These processes require energy (and consequently substrate), but they do not lead to formation of any *new* biomass, and they are therefore typical examples of maintenance processes. We shall see (Note 5.2) that the major part of the maintenance requirement originates in these processes.
- *Futile cycles*. Inside the cells there are pairs of reactions which result in the net hydrolysis of ATP. An example is the conversion of fructose-6-phosphate (F6P) to fructose 1,6-bisphosphate (a reaction that requires ATP) followed by its hydrolysis back to F6P by a phosphatase (a reaction that does not result in ATP formation). This two-step futile cycle represents a very common situation, and in practice the regulatory system of the cell ensures that this futile cycle does not operate, e.g., the phosphatase is repressed in the presence of glucose. However, there are more complex futile cycles that involve a large number of reactions. The result is always a net hydrolysis of ATP. The exact purpose of such futile cycles is not known, but they may serve to generate heat by the hydrolysis of ATP, and hence establish a higher temperature than that of the environment. Since futile cycles result in utilization of energy without net formation of biomass, they may also be considered as maintenance processes.
- *Turnover of macromolecules*. Many macromolecules (e.g., mRNA) are continuously degraded and re-synthesized inside the cell. This does not result in net formation of biomass, but substantial amounts of Gibbs free energy are used, and

turnover of macromolecules is therefore another typical example of a maintenance process.

Utilization of energy, and consequently of substrate, in each of the three processes listed above is likely to be a function of the specific growth rate. When the specific growth rate is high there is a high turnover of macromolecules, and with increasing activity level in the cell it is, e.g., necessary to pump more protons out of the cell. Furthermore, with a higher flux through the cellular pathways there is a larger loss of energy in the futile cycles. This is biologically reasonable, since when the cells grow under limiting conditions, i.e., at low specific growth rate, they will try to use the substrate as efficiently as possible, and the maintenance processes are therefore curtailed. The energy expenditure in maintenance processes is therefore likely to be an increasing function of the specific growth rate. Thus, part of the Gibbs free energy spent in these maintenance processes may be included in the overall yield coefficient Y_{xs}^{true}, and only that part of free energy which is spent at zero-growth rate are included in the maintenance coefficient.

Bauchop and Elsden (1960) introduced the concept of ATP requirements for biomass synthesis via the yield coefficient Y_{xATP} (unit: mmol ATP (g DW)$^{-1}$), and proposed a balance equation (5.14) which is analogous to (5.13):

$$r_{ATP} = Y_{xATP}\mu + m_{ATP} \tag{5.14}$$

r_{ATP} specifies the total formation rate of ATP in catabolic pathways (different from the net formation rate of ATP, which is implicitly assumed to be zero in the equation).

From precise measurements of the metabolic products of the anaerobic metabolism it is possible to calculate the specific formation rate of ATP, i.e., r_{ATP}. This may be used to find experimental values for Y_{xATP} and m_{ATP}, as shown in many studies, e.g., Benthin et al. (1994) for lactic acid bacteria. In aerobic processes a major part of the ATP production originates in the respiration, and the yield of ATP in this process is given by the P/O ratio.

Although the discussion in Sect. 4.3.2 implies that $Y_{NADH,ATP} = P/O$ can be calculated exactly for a given organism, the *operational value* of the P/O is not known since the thermodynamic efficiency of the ATP generation process is never 1 and may vary with the microorganism and perhaps also with the environmental conditions. Detailed empirical studies, e.g., van Gulik and Heijnen (1995), have indicated an operational P/O ratio of 1.2–1.3. The ATP production can therefore not be calculated with the same accuracy in organisms that gain ATP by respiration as is the case for organisms that are only able to produce ATP in fermentative pathways (by substrate level phosphorylation).

In Table 5.1 experimentally determined values for Y_{xATP} and m_{ATP} are collected for a number of microorganisms growing at anaerobic conditions where r_{ATP} could be determined rather precisely. There is a large variation in the experimentally found values. This is explained by the fact that Y_{xATP} depends both on the applied medium and on the macromolecular composition of the biomass, as illustrated by the lower values obtained with growth on a complex medium compared with growth on a minimal medium.

One may also calculate theoretical values for Y_{xATP} from the metabolic network. In Table 2.3, a value of 41 mmol of ATP per gram dry weight was given for *E. coli* synthesis on a minimal medium. If we add 6 mmol of ATP per gram dry weight used in the transport processes (Stouthamer 1979), we obtain a theoretical value for Y_{xATP} of 47 mmol of ATP per gram dry weight for *E. coli*. By comparison it is seen that the experimental value of Y_{xATP} for *E. coli* in Table 5.1 is 2.0–2.5 times larger than the theoretical value. This is a general observation made also for other microorganisms. The reason is that energy used in the maintenance processes is included in Y_{xATP}, as discussed in Note 5.2.

Note 5.2 *Calculation of the total ATP consumption for maintenance.* We want to evaluate the total ATP consumption for maintenance reactions in *E. coli* with growth on a minimal medium. As discussed in the text there is a substantial deviation between the value of Y_{xATP} for *E. coli* in Table 5.1 and the value of 41 mmol (g DW)$^{-1}$ for synthesis of an *E. coli* cell found in Table 2.3. Even if transport of substrates is considered there is, as mentioned above, a large deviation. The difference between the "theoretically" calculated value and the experimentally determined value must be due to the three types of maintenance processes discussed in the text.

Many of the cellular macromolecules are very stable, and it is mainly enzymes and mRNA that are degraded and re-synthesized inside the cell. The half-life of mRNA is of the order of a few minutes, and there are good reasons for this low value. In order to control the synthesis of proteins at the genetic level it is important that mRNA be quite unstable, since otherwise translation of the mRNA would continue even when the enzyme is not needed. Since it is much cheaper from an energetic point of view to synthesize mRNA than protein, it is better for the cell to have a high turnover rate of mRNA rather than synthesize unnecessary protein. The turnover rate of enzymes is not known exactly, and probably it is heavily dependent on the cellular function of the enzyme. If the degradation of mRNA and protein is by first-order processes, the rate of turnover depends on the cellular content of these two components. Since the content of enzymes and mRNA increases with the specific growth rate, the ATP requirement for turnover of macromolecules therefore increases with the specific growth rate. Using a half-life for mRNA of 1 min and a protein half-life of 10 h, the ATP requirement for macromolecular turnover can be calculated to be in the order of 6 mmol ATP (g DW h)$^{-1}$. Consequently, only a minor part of the ATP requirement for maintenance processes can be accounted for by turnover of macromolecules.

Stouthamer (1979) states, that up to 50% of the total energy production during anaerobic growth of *E. coli* is used for maintaining membrane potentials, i.e., maintenance of the thermodynamic and electrochemical gradients across the cytoplasmic membrane. This corresponds to 49–59 mmol of ATP per gram dry weight, and only a minor fraction of the ATP is therefore "lost" in the futile cycles. During aerobic growth, membrane energetization is ensured by the respiration (i.e., the oxidation of NADH), and this at least partly explains why the operational P/O ratio is smaller than the theoretical value.

5.2.2 Energetics of Anaerobic Processes

Anaerobic cultivations are quite simple to analyze from the point of view of energetics. All the free energy that is available for biomass growth is produced in

Table 5.1 Experimentally determined values of Y_{xATP} and m_s for various microorganisms grown under anaerobic conditions with glucose as the energy source

Microorganism	Y_{xATP} (mmol ATP (g DW)$^{-1}$)	m_{ATP} (mmol ATP (g DW h)$^{-1}$)	References
Aerobacter aerogenes	71	6.8	Stouthamer and Bettenhaussen (1973)
Escherichia coli	57	2.3	Stouthamer and Bettenhaussen (1973)
Lactobacillus casei	97	18.9	Hempfling and Mainzer (1975)
Lactobacillus delbruckii	41	1.5	de Vries et al. (1970)
Lactococcus cremoris	72	0	Major and Bull (1985)
(Now called L. lactis)	73	1.4	Otto et al. (1980)
Lactococcus diacetilactis	53	–	Brown and Collins (1977)
Saccharomyces cerevisiae	15–50	18-Jul	Benthin et al. (1994)[a]
	47	–	Brown and Collins (1977)
	71–91	<1	Verduyn et al. (1990)

[a] In their analysis, Benthin et al. (1994) found a large variation in the energetic parameters depending on the (complex) medium composition, see Example 5.5

the EMP pathway (two ATP per glucose molecule), except when fermentation products contain carboxylic acids such as HAc and HBu which give an extra ATP when hydrolyzed from their energized progenitors, Acetyl-P and Buturyl-P.

The obligate anaerobes are, as explained in Sect. 2.2.5 unable to grow in the presence of oxygen, but also facultative anaerobes often lack essential parts of the electron transfer chain and are unable to gain free energy by respiration. Thus, the only advantage that lactic acid bacteria gain by the presence of oxygen is, that this, at least in theory, permits all the carbon from glucose to end up in HAc, and the meager ATP yield of 1/3 ATP/C-mol glucose is doubled to 2/3 ATP/C-mol glucose.

Based on the metabolic models of Sect. 5.1 it is quite easy to estimate how much of the energy gained in the catabolic reactions is captured by the anabolic reactions that lead to a net-production of new biomass, and how much is used for maintenance.

Consider the results of Example 5.1 for a *homofermentative* cultivation of lactic acid bacteria, i.e., when the glucose concentration is high enough to repress the reactions from pyruvate to the mixed acids. Assume the value $\beta = 0.1$ for CO_2 produced per C-mol biomass and the biomass composition $X = CH_{1.8}O_{0.5}N_{0.2}$ used in Example 5.1. Also assume that some O_2 is present to oxidize (by the action of NADH oxidase) the small amount of NADH that accompanies the biomass production.

In this situation, Y_{sx} (C-mol biomass/C-mol glucose) is easily calculated as a function of γ. The flux to HLac must be 3γ higher than the flux to biomass, and $(-r_s) = (1.1 + 3\gamma) r_x$:

$$Y_{sx} = \frac{1}{1.1 + 3\gamma} \tag{5.15}$$

The result obtained in (5.15) is called the *true* biomass yield Y_{xs}^{true}, i.e., it relates the substrate consumption to the formation of *new* biomass. Y_{xs}^{true} is derived using a simple, but still structurally correct model that includes the parameter γ. Our uncertainty concerning the exact energy requirement for synthesis of biomass is expressed through the parameter γ.

The discussion in Examples 5.2 and 5.3 has shown that γ ranges between 2.45 for respiratory growth and 1.8 for growth of yeast on a defined medium (Sect. 2.2.7). There is little reason to believe that very different values for the range of γ would be found for the growth of bacteria. Thus, (5.15) yields [0.120 ($\gamma = 2.45$) $< Y_{sx} <$ 0.154 ($\gamma = 1.8$)], and in analogy with the anaerobic yeast cultivation, Y_{sx} is probably close to the upper end of the range.

For an anaerobic or microaerobic cultivation of *Lactococcus lactis* in a glucose limited, defined medium (the amino acids that the organism cannot synthesize are added in known amounts according to a recipe), the bacteria can grow at a specific growth rate $\mu = r_x = 0.6\ h^{-1}$. Lactic acid is the only metabolic product as long as the glucose concentration in the medium is above about 11 mg L^{-1}. At lower glucose concentrations HCOOH, ethanol, and HAc are produced by the mixed acid metabolism of Fig. 5.3

The yield of biomass is, however, much lower than the value obtained by the metabolic model. Typically, Y_{sx} (experimental) $= Y_{sx}^{obs} = 0.05$–0.03 C-mol/C-mol glucose is found.

From (5.13) one obtains:

$$Y_{sx}^{obs} = \frac{\mu}{(-r_s)} = \frac{\mu}{Y_{xs}^{true}\mu + m_s} \tag{5.16}$$

Inserting $\mu = 0.6\ h^{-1}$, one obtains $m_s = 8.10$ C-mol glucose (C-mol biomass h)$^{-1}$ when [Y_{sx}^{obs}, Y_{xs}^{true}] = [0.05, 0.154] are used as parameters. Since 1 C-mol glucose produces 1/3 mol ATP, the maintenance requirement can also be written as

$$m_s = 1/3 \times 8.10/24.6 = 110\ \text{mmol ATP(g biomass h)}^{-1} \tag{5.17}$$

The number calculated by (5.17) is higher than the numbers (73 or 53) shown in Table 5.1. The derivation of this result is based on (5.15) with a γ value in the same range as found for yeast cultivation. This may well be true when the medium for the lactic acid bacteria cultivation is well supplied with essential amino acids and μ is high. Example 5.5 does, however, show that γ increases dramatically during a batch cultivation of lactic acid bacteria which means that Y_{sx} calculated from (5.16)

also decreases. In any case m_s must be a physiological parameter that is independent of μ as long as the substrate has the same composition. This would not be the case if it is calculated from (5.16) with constant Y_{sx}. In Example 5.5, it is shown that m_s as well as Y_{xATP} may change abruptly when the substrates runs out of an essential component. This situation is discussed below.

When a *complex* nitrogen source (Table 2.5) is used the growth pattern can be much more complicated than observed with a defined medium. The nitrogen source (yeast extract and casein peptone), "a rich N-source," contains all the building blocks and NADPH required for growth, and the experimentally observed Y_{xATP} can be much smaller than the value calculated from a model where a defined medium is assumed. Thus, Benthin (1992) found that $Y_{xATP} = 26$ mmol ATP (g biomass)$^{-1}$ for growth of *Lactococcus lactis* on a complex medium. In the calculation the macromolecular composition of the organism and an analysis of the medium was used. From (5.15):

$$Y_{xATP}^{true} = \frac{1.1 + 3\gamma}{3 \times 24.6} \times 1,000 = 13.55(1.1 + 3\gamma)$$
$$= 26 \text{ mmol ATP(g biomass)}^{-1} \tag{5.18}$$

This corresponds to $\gamma = 0.27$, a value far below the γ values that were used to calculate the ATP requirement for growth on a defined medium.

Growth on complex media is accompanied by phenomena that make the interpretation of experimental results difficult. The medium will contain compounds of very different "value" for growth, and the organism selects the most valuable compounds first. Thus a four-carbon peptide from the yeast extract is imported at the expense of one ATP. After hydrolysis, one limiting amino acid may be incorporated into the biomass. The three other amino acids are re-exported, each with a gain of one ATP. After the most "valuable" components from the medium have been used up growth slows down, and the organism struggles to synthesized essential building blocks from what is left over in the medium (usually the casein peptone), and the value of Y_{xATP} increases drastically.

Example 5.5 *Growth energetics for cultivation of Lactococcus lactis.* *Lactococcus lactis* is used as a starter culture in the dairy industry for the production of butter, yogurt, and cheese. It is also used in some types of fermented sausage and sour bread. *L. lactis* is characterized as a homofermentative Gram-positive bacterium mainly producing lactic acid, but it may produce many other products at conditions of very low sugar concentrations. *L. lactis* is a multiple amino acid auxotroph, i.e., it requires a supply of several amino acids for growth, and it is therefore normally grown on a rich medium. This is a drawback when a detailed analysis of the growth process is to be carried out, since it is difficult to identify the growth-limiting substrate. However, it also means that there is no net production/consumption of NADH and NADPH in connection with biomass synthesis and the overall biomass synthesis reaction can therefore be specified as:

$$a \text{ glucose} + b \text{ nitrogen source} \rightarrow \text{biomass}$$

Here the nitrogen source is a complex mixture of peptides and other nitrogen compounds. a and b are yield coefficients in the overall biomass synthesis process. Since the stoichiometric coefficient for biomass is 1 the forward rate of this reaction is given by the specific growth rate, $r_x = \mu$.

The ATP required to support biomass growth, r_{xATP}, is supplied by the catabolic reactions, which at homofermenative conditions are limited to conversion of glucose to lactic acid. r_{xATP} is given by (5.14). Without maintenance, the glucose requirement would be Y_{xs}^{true}, calculated by (5.18).

To illustrate the validity of the simple model with constant m_s and Y_{xs}^{true} we shall consider experimental data by Benthin et al. (1994), who made a meticulous analysis of the growth and product formation of *L. lactis*. Figure 5.8a shows results from a batch fermentation of this organism. The medium contained 20 g L^{-1} of glucose and 7 g L^{-1} of a complex N source (a mixture of 50% yeast extract and 50% caseine peptone). The biomass concentration was monitored by flow injection analysis (Benthin et al. 1991), and the specific total acid production r_p was measured by monitoring the amount of alkali added to keep the pH constant in the bioreactor. Throughout the batch fermentation the glucose concentration is high, and consequently only lactic acid is produced. It is observed that there are two distinct growth phases. First a phase with rapid growth and specific growth rate μ between 0.3 and 0.7 h^{-1}. This is followed by a phase where the specific growth rate first decreases to about 0.3 h^{-1} and then recovers to about 0.45 h^{-1}. After 12 h the specific growth rate decreases monotonously to a very low value.

By plotting the specific production rate r_p versus the specific growth rate μ (Fig. 5.8b) it is observed that two straight lines appear, one for $\mu > 0.3$ h^{-1}, and one that extends from $\mu = 0.3$ h^{-1} and almost to $\mu = 0$. The lactic acid production is closely correlated to the ATP production (1 mol of ATP per mole of lactic acid produced), and the plot in Fig. 5.8b can therefore be used to estimate Y_{xATP} and m_{ATP} from, respectively, the slope and the intercept.

$$\begin{aligned} \mu > 0.3\,h^{-1} \quad & Y_{xATP} = 15 \text{ mmol ATP}(\text{g DW})^{-1}, \text{ and} \\ & m_{ATP} = 18 \text{ mmol ATP}(\text{g DW h})^{-1} \\ \mu < 0.3\,h^{-1} \quad & Y_{xATP} = 50 \text{ mmol ATP}(\text{g DW})^{-1}, \text{ and} \\ & m_{ATP} = 7 \text{ mmol ATP}(\text{g DW h})^{-1} \end{aligned}$$

In the first growth phase, Y_{xATP} is very low, much below the value of 26 mmol ATP (g biomass)$^{-1}$ calculated by Benthin (1992). In the second growth phase, Y_{xATP} is much higher, but m_{ATP} is lower than in the first growth phase. Here one (or more) compound(s) in the complex nitrogen source has been exhausted, and the cells have to synthesize this (or these) compound(s). The ATP requirement for growth is therefore higher. With the higher ATP requirement for cellular growth, the cell is apparently able to get some savings by reducing the ATP consumption in maintenance processes; i.e., it is able to adjust its behavior to the more hostile environment.

The picture of cell synthesis and maintenance obtained here is definitely more complex than that given by (5.14) with constant values for m_s and Y_{xATP}.

It was not possible to identify the (probably N-containing) compound(s) which caused the change in metabolism at about 7 h, but analysis of the medium throughout the fermentation showed that mainly peptides are metabolized during the first growth phase, whereas both peptides and free amino acids are metabolized in the second growth phase.

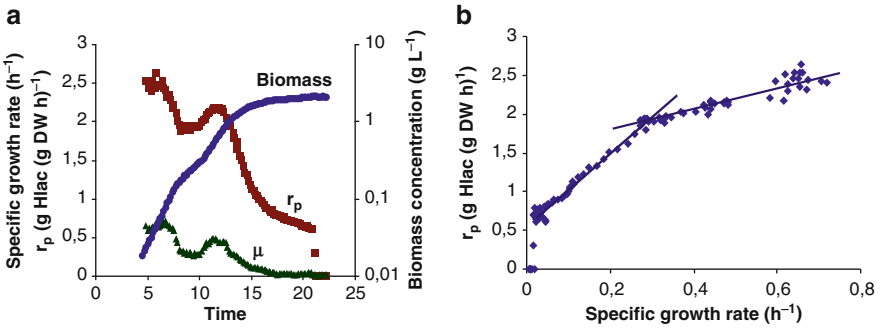

Fig. 5.8 Batch fermentation of *L. lactis* on glucose and a complex nitrogen source. (**a**) Measurements of the biomass concentration (*filled circle*), the specific acid production rate (*filled square*), and the specific growth rate (*filled triangle*). (**b**) Plot of the specific acid production rate versus the specific growth rate

5.2.3 *Energetics of Aerobic Processes*

During aerobic growth it is possible to oxidize part of the energy source completely to carbon dioxide in the TCA cycle. Since much more Gibbs free energy (and consequently ATP) is gained by complete oxidation of the energy source, it is possible to obtain much higher biomass yields from the energy source in an aerobic process than in an anaerobic process. In aerobic processes most of the ATP is formed in the oxidative phosphorylation, and therefore this process has a central position when energetic balances are to be set up.

In aerobic processes the catabolic reactions can be lumped into:

$$CH_2O \rightarrow CO_2 + 2NADH + \varepsilon ATP \tag{5.19}$$

$$2NADH + O_2 \rightarrow 2P/O\ ATP \tag{5.20}$$

$$CH_2O \rightarrow CO_2 + 2NADHP \tag{5.21}$$

In these processes glucose is oxidized to supply free energy and NADPH to the anabolic processes which can be represented by the single reaction (5.22):

$$(1+\alpha)CH_2O \rightarrow X + \alpha CO_2 + 1/2[4(1+\alpha) - \kappa_x]\text{``NADH''} - \gamma ATP \tag{5.22}$$

The reason for including the NADPH required for biomass growth in the simple fashion shown in (5.22) is discussed in previous examples. Table 5.2 shows calculated values of $[Y_{xNADPH}, Y_{xNADH}]$ based on the known composition of several industrially important microorganisms.

Besides the ATP consumption in (5.22) the organism also needs ATP for maintenance, and a fourth catabolic reaction, a combination of (5.19) and (5.20), is needed.

$$CH_2O \rightarrow ATP \rightarrow \text{maintenance} = m_{ATP} \tag{5.23}$$

The analysis of the growth energetics now becomes much more complicated than was the case for anaerobic processes, and in fact the three parameters $\gamma = Y^{\text{true}}_{\text{xATP}}$, P/O, and m_{ATP} cannot all be determined when only one carbon source is used. This is the conclusion of the following analysis.

There are four measurable rates, $\mu = r_{\text{x}}$, r_{c}, $(-r_{\text{s}})$, and $(-r_{\text{o}})$ in the simplest case of no metabolite formation besides CO_2. These are connected by the following three balance equations for ATP, NADH, and NADPH:

$$-r_{\text{s}} = (A + 1 + \alpha + 1/2Y_{\text{xNADPH}})\mu + B = Y^{\text{true}}_{\text{xs}}\mu + m_{\text{s}} \tag{5.24}$$

$$r_{\text{c}} = (A + \alpha + 1/2Y_{\text{xNADPH}})\mu + B = Y^{\text{true}}_{\text{xc}}\mu + m_{\text{c}} \tag{5.25}$$

$$-r_{\text{o}} = (A + 1/2Y_{\text{xNADH}})\mu + B = Y^{\text{true}}_{\text{so}}\mu + m_{\text{o}} \tag{5.26}$$

The parameter α is between 0.08 and 0.14, and ε between 1/3 and 2/3 (see Example 5.3).

The two parameters A and B in (5.24) to (5.26) are given by (5.27) and (5.28).

$$A = \frac{Y_{\text{xATP}} - Y_{\text{xNADH}}\text{P/O}}{\varepsilon + 2\text{P/O}} \tag{5.27}$$

$$B = \frac{m_{\text{ATP}}}{\varepsilon + 2\text{P/O}} \tag{5.28}$$

Equation (5.24) is the same as the linear rate equation (5.13) with the difference that the yields are now obtained in terms of basic cellular energetic parameters. When the units of C-mol (C-mol h)$^{-1}$ are used the values of m_{c} and m_{o} are simply related to m_{s}, i.e., $m_{\text{c}} = 2m_{\text{o}} = m_{\text{s}}$. Values of Y_{xNADH} and Y_{xNADPH} are taken from tables, e.g., Table 5.2.

Inserting the values for *S. cerevisiae* and using a standard biomass with $\kappa_{\text{x}} = 4.20$ yields:

$$\begin{aligned}\alpha &= 4.20 + 2 \times 24.6(15.43 - 8.24) \times 10^{-3} \\ &= 0.138\,\text{mol CO}_2(\text{C - mol biomass})^{-1}\end{aligned} \tag{5.29}$$

This value for the CO_2 production which accompanies biomass production in (5.22) falls nicely in the range (0.08, 0.14) used in previous examples.

With the three parameters α, Y_{xNADH}, and Y_{xNADPH} that belong to the redox balance as known quantities, and $[-r_{\text{s}}, r_{\text{x}}, r_{\text{c}}]$ measured as functions of μ one can determine the parameters A and B from (5.24) to (5.26). The three energetic parameters Y_{xATP}, P/O, and m_{ATP} appear only in A and B, and all three parameters cannot be determined based on measurements with only one substrate.

If, indeed, $[Y_{\text{xATP}}$, P/O, $m_{\text{ATP}}]$ are fundamental parameters for the particular microorganism, new information is obtained when the cultivation is repeated with other substrates, such as acetate, glycerol, ethanol, or citrate. The model

(5.24)–(5.26) will now have yield coefficients that depend in a different way on [Y_{xATP}, P/O, m_{ATP}], and the energetic parameters can all be determined when the yield coefficients are determined experimentally for different substrates.

This is the basis for the studies of growth energetics by van Gulik and Heijnen (1995) and by Vanrolleghem and Heijnen (1998). Their results were used in Example 5.3 in an analysis of aerobic yeast cultivation. Christiansen and Nielsen (2002) did a similar study for *Bacillus clausii*, a well-known host for the production of industrial enzymes. Example 5.6 is a much abbreviated account of their study, which revealed that the organism is severely handicapped due to ineffective oxygen utilization.

Example 5.6 *Energetics of Bacillus clausii*. Due to the ability to secrete large amounts of protein, members of the genus *Bacillus* are widely used as hosts in the fermentation industry for the production of industrial enzymes, fine chemicals, antibiotics, and insecticides. *B. clausii* is a facultative alkalophilic *Bacillus*, which is commercially used in the production of the alkaline serine protease Savinase®, an enzyme used in detergents. In order to design optimal industrial processes a detailed understanding of the bioenergetics, and in particular, the maintenance demands are important. Production of proteases in *Bacilli* is generally a response to poor nutritional conditions, and proteases are therefore typically produced at low specific growth rates. Most industrial fermentations for proteases are therefore operated in the fed-batch mode (see Chap. 9) with very low specific growth rates in the later stages of the process. Here a large part of the carbon source is consumed for maintenance demands, and the growth energetics are of particular importance, since the energy metabolism influences both the yield of biomass and product on substrate. It also determines the oxygen requirement and the removal of the accompanying heat of reaction. The parameters with the most significant influence on growth energetics and oxygen consumption are [Y_{xATP}, P/O, m_{ATP}] as discussed in the text.

Table 5.2 Calculated values of the requirements of NADPH for biomass synthesis and the amount of NADH formed in connection with biomass synthesis[a]

Organism	Y_{xNADPH} (mmol NADPH (g DW)$^{-1}$)	Y_{xNADH} (mmol NADH (g DW)$^{-1}$)	References
E. coli	13.91	16.97	Ingraham et al. (1983)
S. cerevisiae	8.24	15.43	Oura (1983)[b]
P. chrysogenum	8.49	16.00	Nielsen (1997)

[a] Note that the NADPH requirement for growth is considerably higher for the bacterium *E. coli* than for the two fungi. Prokaryotes have a higher lipid and protein content than eukaryotes and a substantial portion of the NADPH is spent in the synthesis of these cell constituents. A more recent textbook, Lengeler et al. (1999), gives a figure of about 19 mmol NADPH per g DW, which is slightly higher than the value specified in this table. The calculations are complicated by the presence of isoenzymes using different cofactors for some of the steps. Therefore, the calculated values should in reality be presented as ranges [see, e.g., Albers et al. (1996)]

[b] See also Albers et al. (1998) for a detailed calculation of the NADH formation in connection with biomass synthesis. The calculations are based on the growth of one specific carbon source (glucose) and one specific nitrogen source (ammonia). Furthermore, a certain composition of the biomass in terms of protein, lipid content, etc. has been used. The original references should be consulted for detailed information

We have seen that all three parameters cannot be determined by using only data from growth on glucose, but by combining data for growth on more than one carbon source with a detailed knowledge on the biomass composition and the central carbon metabolism, all three parameters can be estimated. An important assumption in this approach is that the parameters are conserved properties and do not change with the carbon source used. Christiansen and Nielsen (2002) studied the growth kinetics and energetics in glucose and citrate limited chemostat cultures of *B. clausii* with special focus on the oxygen consumption. The true yield coefficients of glucose, oxygen, and carbon dioxide were obtained from glucose limited chemostats. From experimental results on the amino acid composition of the biomass and the RNA content, supplemented with literature data, a detailed biomass composition was determined, and the building block requirements for biomass formation were calculated. From this analysis, the elemental composition of the biomass was found to be $CH_{1.82}O_{0.55}N_{0.16}$, and the ash content was found to be 6%. Furthermore, the ATP cost for biomass synthesis was calculated to be 16.2 mmol ATP (g DW)$^{-1}$ (or 0.43 mol ATP (C-mole biomass)$^{-1}$) and 19.0 mmol ATP (g DW)$^{-1}$ (or 0.73 mol ATP (C-mole biomass)$^{-1}$) for growth on glucose and citrate, respectively. The cost of biomass synthesis from precursor metabolites is obviously the same for growth on glucose and citrate, but the ATP cost for synthesis of precursor metabolites is different for the two substrates. Thus, it is energetically more expensive to synthesize pyruvate and phosphoenolpyruvate (both precursor metabolites) from citrate than from glucose. In order to account for additional drain of ATP for biomass synthesis a constant value of K_x moles of ATP per C-mole biomass is added to the above-calculated values.

In the following a simplified version of the Christiansen and Nielsen (2002) model is considered. Synthesis of the desired enzyme product was not considered since only a small amount of free energy is used for this purpose. In the model, NADH, NADPH, and $FADH_2$ are lumped into one compound, NADH. In the original model, both NADH and $FADH_2$ were considered, since substantial amounts of $FADH_2$ are formed during growth on citrate, and the P/O ratio (=2) for this compound is smaller than that obtained for NADH. Here, we primarily wish to illustrate the concept of how data from growth on two different substrates can be used to estimate all three energetic parameters, and we therefore apply a less complex model.

In the model, the overall stoichiometry for biomass synthesis for growth on glucose and citrate are:

$$\begin{aligned} 1.148\ CH_2O \rightarrow X(CH_{1.82}O_{0.55}N_{0.16}) + 0.148\ CO_2 \\ +0.176\ NADH - (0.43 + K_x)\ ATP \end{aligned} \tag{1}$$

$$2.025\ CH_{8/6}O_{7/6} \rightarrow X + 1.025\ CO_2 + 0.917\ NADH - (0.73 + K_x)\ ATP \tag{2}$$

The glucose catabolism is ($\varepsilon = 2/3$ in (5.22)):

$$CH_2O \rightarrow 2/3ATP + 2NADH + CO_2 \tag{3}$$

The citrate catabolism is:

$$CH_{8/6}O_{7/6} \rightarrow 4/18ATP + 3/2\ NADH + CO_2 \tag{4}$$

For growth on either one of the substrates, respiration is described by:

$$NADH + 1/2O_2 \rightarrow P/O\ ATP \tag{5}$$

Balances of cofactors and the balances for glucose and citrate in the two models are used to derive the following equations which are analogous to (5.22):

$$-r_{\mathrm{glc}} = \left(1.148 + \frac{(0.43 + K_{\mathrm{x}}) - 0.176\mathrm{P/O}}{2\mathrm{P/O} + 0.667}\right)\mu + \frac{m_{\mathrm{ATP}}}{2\mathrm{P/O} + 0.667} = Y^{\mathrm{true}}_{\mathrm{xglc}}\mu + m_{\mathrm{glc}} \qquad (6)$$

$$-r_{\mathrm{cit}} = \left(2.025 + \frac{(0.73 + K_{\mathrm{x}}) - 0.917\mathrm{P/O}}{1.5\mathrm{P/O} + 4/18}\right)\mu + \frac{m_{\mathrm{ATP}}}{1.5\mathrm{P/O} + 4/18} = Y^{\mathrm{true}}_{\mathrm{xcit}}\mu + m_{\mathrm{cit}} \qquad (7)$$

From chemostat cultures Christiansen and Nielsen (2002) found the following yield coefficients and maintenance coefficient[1]:

- $Y^{\mathrm{true}}_{\mathrm{xglc}} = 1.64$ C - mol glucose (C - mol DW)$^{-1}$
- $m_{\mathrm{glc}} = 0.032$ C - mol glucose (C - mol DW h)$^{-1}$
- $Y^{\mathrm{true}}_{\mathrm{xcit}} = 2.69$ C - mol citrate (C - mol DW)$^{-1}$

Equating the slopes of the straight lines in (6) and (7) with the experimentally determined yield coefficients [$Y^{\mathrm{true}}_{\mathrm{xglc}}$, $Y^{\mathrm{true}}_{\mathrm{xcit}}$] one obtains:

$$1.64 = 1.15 + \frac{(0.43 + K_{\mathrm{x}}) - 0.176\mathrm{P/O}}{2\mathrm{P/O} + 0.667} \qquad (8)$$

$$2.69 = 2.02 + \frac{(0.73 + K_{\mathrm{x}}) - 0.917\mathrm{P/O}}{1.5\mathrm{P/O} + 4/18} \qquad (9)$$

Solving these two equations for K_{x} and P/O, one finds values of 0.708 mol ATP (C-mol biomass)$^{-1}$ corresponding to 26.8 mol ATP (g DW)$^{-1}$ and 0.68, respectively. Furthermore, using the estimated value for the P/O-ratio together with:

$$0.032 = \frac{m_{\mathrm{ATP}}}{2\mathrm{P/O} + 0.667} \qquad (10)$$

the maintenance ATP requirement is obtained as 2.52 mmol ATP (g DW)$^{-1}$. As a consequence of the simpler model applied here, these values deviate slightly from those reported by Christiansen and Nielsen (2002).

The estimated P/O-ratio is quite low and indicates a low thermodynamic efficiency of the oxidative phosphorylation (Sect. 4.3). The consequence is a very high oxygen requirement of *B. clausii*, and this is a serious problem in connection with industrial application.

5.3 Flux Analysis in Large Metabolic Networks

When working toward an overall improvement of the yield of a given product from a certain substrate it is of great help to identify all possible routes (or pathways) between the substrate and the product, and to obtain quantitative information about

[1] The true yield coefficient for citrate is not reported by Christiansen and Nielsen (2002) since they only have data for a single chemostat experiment. Their approach is therefore somewhat more complicated, and to reduce the complexity we have here use a true yield coefficient that has been calculated from their data.

the relative activities of the different pathways involved in the overall conversion. This task is supported by the growing number of organisms for which the genome has been sequenced. In Genome Scale Reconstructions the results from genome sequencing are combined with thermodynamics to see which pathways are feasible, and with literature searches in enzyme data bases to see which enzymes are present and active in thermodynamically feasible pathways of the organism. In *metabolic engineering*, directed genetic changes are introduced in order to reroute the carbon fluxes toward the product of interest. Here, it is essential to know how the different pathways operate at different growth conditions. The in vivo fluxes are the end result of many different types of regulation within the cell, and quantification of the metabolic fluxes therefore represents a detailed phenotypic characterization. Quantification of metabolic fluxes goes hand in hand with identification of the active metabolic network, and methods to quantify fluxes are referred to as *Metabolic Network Analysis* (Christensen and Nielsen 1999).

Metabolic Network Analysis basically consists of two steps:

- Identification of the metabolic network structure (or pathway topology).
- Quantification of the fluxes through the branches of the metabolic network.

The extensive biochemistry literature and biochemical databases available on the web (see, e.g., http://ww.genome.ad.jp) provide much information relevant for identification of the metabolic network structure. Complete metabolic maps with direct links to sequenced genes and other information about the individual enzymes is typically retrieved. Thus, there are many reports on the presence of specific enzyme activities in many different species, and for most industrially important microorganisms the major metabolic routes have been identified. However, in less commonly used organisms the complete metabolic network structure is yet unknown, i.e., some of the pathways carrying significant fluxes have not been identified for the microorganism that is investigated. Here enzyme assays can be used to confirm the presence of specific enzymes and to determine the cofactor requirements, e.g., whether the enzyme uses NADH or NADPH as cofactor. If an analogous enzyme from another organism has a higher activity or a more useful cofactor requirement, it can be imported to the selected production organism, and the engineered organism is subjected to an experimental study to see if it works better than the original strain. The control structure of the organism can well invalidate the result of individual enzyme engineering, and in parallel to the experimental work to find the best operational conditions for the new strain, *sensitivity analysis* of the enzymes in the entire pathway must be conducted. These aspects are treated in Chap. 6, while this chapter deals only with analysis of the steady-state fluxes *in a given network*.

Although enzyme assays are valuable to confirm the presence and activity of a given pathway, they are of limited use for a rapid screen of the totality of pathways in the studied microorganism. For this purpose isotope-labeled substrates are very helpful. Especially, the use of ^{13}C-labeled glucose, followed by an analysis of the labeling pattern of the intracellular metabolites, has proved to be essential for identification of the metabolic network structure. This aspect is discussed further in Sect. 5.3.3.

5.3.1 Expressing the Rate of Biomass Formation

When setting up the metabolic network it is important to specify a reaction (or, as an extension to the treatment in Sect. 5.1 a set of reactions) that with sufficient accuracy describes how biomass is formed. This reaction will specify the drain of precursor metabolites, or of building blocks, if the synthesis of these is included in the model. In some cases the stoichiometry for biomass formation has a significant influence on the analysis, and Note 5.3 shows how the so-called *biomass equation* is set up.

Note 5.3 *Biomass equation in metabolic network models.* Biomass formation is the result of a large number of different biochemical reactions. In Chaps. 2 and 3 we looked at some of the many different reactions that are involved. Biomass synthesis starts with the formation of precursor metabolites (see Table 2.2), which are converted into building blocks (amino acids, nucleotides, lipids, etc.). The building blocks are the monomers in macromolecules, which are the major constituents of biomass (see Table 2.3). The macromolecular composition of a given cell depends on the growth condition, and on the composition of the different macromolecules, e.g., on the amino acids in the proteins. It is therefore not possible to specify a single reaction by which precursor metabolites are converted into biomass. If, for lack of knowledge of the composition of a particular organism, one must use data for a more or less similar organism, one must make the assumption that the macromolecular composition is constant or changes with growth conditions in a similar way as the "standard" organism.

There are three different ways of setting up an equation for formation of biomass with constant macromolecular composition:

1. Direct synthesis from precursor metabolites
2. Direct synthesis from building blocks
3. Synthesis from macromolecules

In some cases a combination of the three approaches is used.

In the first approach, an overall reaction is specified for conversion of precursor metabolites into biomass. Here information compiled in Table 2.2 is used together with information about the costs of ATP, NADPH, and NADH to make biomass from the precursor metabolites. This identifies the stoichiometric coefficients for the different precursor metabolites involved in biomass formation. Reactions leading from the individual precursor metabolites to building blocks are not considered in this model, except perhaps for reactions leading to building blocks that are used for product formation, e.g., the synthesis of valine, cysteine, and α-aminoadipic acid may have to be considered in a model for penicillin production. The synthesis of all other amino acids can be lumped into the overall biomass equation describing formation of biomass directly from precursor metabolites.

In the second approach, the synthesis of most building blocks is considered in the model, and the biomass equation is described as a reaction where building blocks are converted into biomass. The stoichiometric coefficients for the building blocks are calculated based on the amount of different building blocks that is needed for biomass formation. This approach typically results in a substantial increase in the model complexity, since a large number of reactions lead to many different building blocks. Perhaps lumping of reactions that lead to

specific sets of building blocks can be done, but still the number of reactions considered in the model is large. The advantage is, however, that it is relatively easy to identify the different elements of the biomass equation.

In the last approach, reactions for synthesis of the different macromolecules are included in the model, e.g,. reactions for synthesis of proteins, lipids, DNA, RNA, and carbohydrates. The biomass equation is described as a reaction where the macromolecules are converted into biomass, and the stoichiometric coefficients for the macromolecules are given by the macromolecular composition of the biomass. With this approach it is relatively easy to study the influence on the calculated fluxes of the macromolecular composition which directly appears in the biomass equation.

Whichever approach is used one needs substantial information about how biomass is synthesized and on the metabolic costs of the different precursor metabolites, building blocks, and macromolecules. In addition, the costs of ATP, NADPH, and NADH for biomass formation must also be available, and this requires information about the biomass composition. In recent years, this type of information has become available for many microorganisms as part of flux analysis studies. If no information is available for the investigated system one may use data from related organisms. It is always recommendable to calculate the sensitivities of the calculated fluxes to variations in the estimated (or experimentally determined) biomass equation.

5.3.2 *The Network Structure and the Use of Measurable Rates*

When the metabolic network structure has been identified, the next step is to quantify the fluxes through the different branches in the network. In the standard method of quantification of all intracellular rates $\boldsymbol{v}$, balancing the fluxes at all N intracellular branch points is used, and with net fluxes from substrates to products, the $N + 1$ net fluxes $\boldsymbol{V}$ must be balanced, just as was illustrated in Sect. 5.1 for simple networks. The network is identified using measurable nonzero exchange rates between the medium and the cell, i.e., uptake rates for substrates, and production rates for metabolic products and biomass.

As indicated in the discussion of Fig. 5.2 labeled substrates will have to be used to identify converging fluxes in the network as well as reversible intracellular reactions.

1. *Use of directly measurable nonzero rates*. This approach is the same as that discussed for the simple metabolic network models in Sect. 5.1. The minimum number of measured rates necessary to identify the network was discussed there, and the use of more than the minimum number of rates is discussed below.
2. *Use of labeled substrates*. When cells are fed with labeled substrates, e.g., glucose that is enriched for ^{13}C in the first position ($^{13}C_1$), then there will be a specific labeling of the intracellular metabolites. As there are different carbon transitions in the different cellular pathways, the labeling pattern of the intracellular metabolites is a function of the activity of the different pathways. Through measurements of the labeling pattern of the metabolic products, and by application of balances for the individual carbon atoms, additional

constraints are added to the system. As discussed in Sect. 5.3.3 this is used to quantify the fluxes, even when only a few rates are measured.

3. *Use of linear programming*. Unfortunately, in many studies there are not nearly enough measurements to identify the network. Extra constraints can be added, e.g., by assuming that the metabolism strives to optimize growth of the organism. The fluxes $\boldsymbol{v}$ are defined by a set of linear relations between the rates, and optimization of the specific growth rate μ can be accomplished by manipulation of the fluxes $\boldsymbol{v}$, using a standard method from Operational Research, namely linear programming. Comprehensive texts are now available that discuss these methods, and they will not be treated in the present text.

When *more* than the minimum exchange rates are measured, i.e., *the system is over-determined*, all the measured rates can be used to improve the analysis. In the net-flux method measurements of more metabolite production rates than those used in $\boldsymbol{V}$ can be used to validate the model structure or to estimate one or more parameters of the model as illustrated in Example 5.2. In the method based on internal fluxes, extra measurements are used to give improved values for the internal flux vector $\boldsymbol{v}$ as illustrated below.

If, vector $\boldsymbol{v}_1$ in (5.12) contains more than $J-N-2$ elements, say $J-N-2+Q$ elements, in the case where the NADH and the ATP balances are included besides the N mass balances around the specified internal branch points, then matrix $\boldsymbol{T}_1$ has fewer than $N+2$ columns, but still $N+2$ rows. This means that the matrix cannot be inverted.

This problem is easily resolved as already discussed in Sect. 3.6. $\boldsymbol{T}_1$ has dimension $(N+2)\times(N+2-Q)$, and correspondingly $\boldsymbol{T}_2$ has dimension $(N+2)\times(J-N-2+Q)$.

$$\text{Construct matrix } \boldsymbol{T}_1^{\#} = \left(\boldsymbol{T}_1^{\mathrm{T}}\cdot\boldsymbol{T}_1\right)^{-1}\cdot\boldsymbol{T}_1^{\mathrm{T}} \tag{5.30}$$

$(\boldsymbol{T}_1^{\mathrm{T}}\cdot\boldsymbol{T}_1)$ is always a *symmetric* (square) matrix, and $\boldsymbol{T}_1^{\#}$ is defined as the *pseudo inverse* of $\boldsymbol{T}_1$ .This definition of $\boldsymbol{T}_1^{\#}$ derives from the fact that by simple matrix operations:

$$\begin{aligned} T_1^{\#} &= \left(\boldsymbol{T}_1^{\mathrm{T}}\cdot\boldsymbol{T}_1\right)^{-1}\cdot\boldsymbol{T}_1^{\mathrm{T}} = \boldsymbol{T}_1^{-1}\cdot\left(\boldsymbol{T}_1^{\mathrm{T}}\right)^{-1}\cdot\boldsymbol{T}_1^{\mathrm{T}} \\ &= \boldsymbol{T}_1^{-1}, \text{a “pseudo inverse” of } \boldsymbol{T}_1 \end{aligned} \tag{5.31}$$

The symmetric matrix $\left(\boldsymbol{T}_1^{\mathrm{T}}\cdot\boldsymbol{T}_1\right)^{-1}$ has dimension $(N+2-Q)\times(N+2-Q)$.

$$\text{Hence the dimension of } \boldsymbol{T}_1^{\#} \text{ is } (N+2-Q)\times(N+2). \tag{5.32}$$

The product $\boldsymbol{T}_1^{\#}\cdot\boldsymbol{T}_2$ has dimension $(N+2-Q)\times(J-N-2+Q)$, and since $\boldsymbol{v}_1$ has dimension $(J-N-2+Q)\times 1$, then the product

$$\boldsymbol{v}_2 = -\boldsymbol{T}_1^{\#}\cdot\boldsymbol{T}_2\cdot\boldsymbol{v}_1 \text{ has dimension} (N+2-Q)\times 1 \tag{5.33}$$

One correctly obtains a vector $\boldsymbol{v}_2$ with fewer (but better estimated) elements than in the basic procedure of (5.12).

Finally, the $(K+M)\times 1$ vector of nonzero exchange rates $\boldsymbol{r}$ is found as in (5.11), namely as the product of the first $K+M$ rows of $\boldsymbol{T}$ and the intracellular flux vector $\boldsymbol{v}$.

The only condition for success of this procedure is, that $\boldsymbol{T}_1$ has full rank, i.e., that the columns of $\boldsymbol{T}_0$ that belong to $\boldsymbol{v}_2$ are not linearly dependent due to linear dependencies between the intracellular fluxes represented in $\boldsymbol{v}_2$. This requirement is of course also necessary for success of the basic procedure in (5.11) and (5.12).

Note 5.4 *Sensitivity analysis of stoichiometric matrices.* In the solution of the linear algebraic problem $\boldsymbol{A}\cdot\boldsymbol{y}=\boldsymbol{x}$ it is important to pay attention to the system matrix $\boldsymbol{A}$. If $\boldsymbol{A}$ is ill-conditioned, even small errors in $\boldsymbol{x}$ will be magnified in the solution y. One way to check this is through evaluation of the *condition number*, c_p for $\boldsymbol{A}$.

c_p depends on the *norm* that we use to "measure" $\boldsymbol{A}$. Most commonly the "2-norm," $p=2$, is used, and the condition number $c_\mathrm{p}=2$ $(\boldsymbol{A})$ is the Euclidian (or least squares) norm of $\boldsymbol{A}$.

c_2 is calculated (see footnote[2]) as the square root of the ratio between the largest and the smallest eigenvalues σ_i of $\boldsymbol{A}\cdot\boldsymbol{A}^\mathrm{T}$. These eigenvalues are the *singular values* of $\boldsymbol{A}$.

Since $\boldsymbol{A}\cdot\boldsymbol{A}^\mathrm{T}$ is always a symmetric matrix the eigenvalues are real, and

$$c_2\left(|\sigma_{\max}|/|\sigma_{\min}|\right)^{1/2} \tag{1}$$

The error magnification factor given by (1) is an estimate of the true error magnification factor.

In the flux calculation problem the matrix $\boldsymbol{A}$ of interest is $\boldsymbol{T}_1$, the part of $\boldsymbol{T}_0$ in (5.12) that belongs to the calculated part of $\boldsymbol{v}$, namely $\boldsymbol{v}_2$.

The condition number depends significantly on which elements of $\boldsymbol{v}$ are included in the vector $\boldsymbol{v}_1$ of measured elements of the flux vector.

---

[2] Calculation of c_2 as described above follows from the theory of *similarity transformation* of matrices. If, as is the case here $\boldsymbol{T}_1$ has fewer columns than rows, then the product $\boldsymbol{T}_1^\mathrm{T}\boldsymbol{T}_1$ is always a square matrix of dimension equal to the number of columns in $\boldsymbol{T}_1$. The matrix $\boldsymbol{A}$ in (2) therefore contains as eigenvalues the *singular values* σ_i of $\boldsymbol{T}_1$, and c_2 is the square root of the ratio between the largest and smallest of $|\sigma_i|$. $\boldsymbol{T}_1^\mathrm{T}\boldsymbol{T}_1$ is a square matrix of dimension equal to the number of rows in $\boldsymbol{T}_1$. It also has the singular values σ_i of $\boldsymbol{T}_1$ as eigenvalues, but in addition a number of eigenvalues $\sigma_i=0$ that is equal to the difference between the number of rows and columns in $\boldsymbol{T}_1$. These extra eigenvalues are ignored, and therefore it does not matter whether we calculate $\boldsymbol{T}_1^\mathrm{T}\boldsymbol{T}_1$ or $\boldsymbol{T}_1\boldsymbol{T}^\mathrm{T}$ to obtain $\boldsymbol{A}$. But, since the dimension of $\boldsymbol{A}$ is smaller in the first case we shall always as in (2) use $\boldsymbol{T}_1^\mathrm{T}\boldsymbol{T}_1$ when the condition number for a rectangular matrix with fewer columns than rows is calculated by means of the eigenvalues of $\boldsymbol{A}$.

The theory of similarity transformation is used in statistics (Principal Component Analysis, or PCA) to extract "the most important" correlations from large sets of data. In PCA the calculations of the present example are exactly followed, and the "extraction" of results mimics the treatment given to matrix $\boldsymbol{T}_1$.

Thus, if $[v_3, v_5] = [r_x, r_{HAc}] = \boldsymbol{v}_1$ as in the example shown in (5.9):

$$\boldsymbol{A} \cdot \boldsymbol{A}^T = \begin{bmatrix} 1 & -1 & -1 & 0 \\ 0 & 0 & 2/3 & -1 \\ 1/3 & -1/3 & 0 & 0 \\ 1/3 & 0 & 0 & 1/2 \end{bmatrix} \cdot \begin{bmatrix} 1 & 0 & 1/3 & 1/3 \\ -1 & 0 & -1/3 & 0 \\ -1 & 2/3 & 0 & 0 \\ 0 & -1 & 0 & 1/2 \end{bmatrix}$$
$$= \begin{bmatrix} 3 & -2/3 & 2/3 & 1/3 \\ -2/3 & 13/9 & 0 & -1/2 \\ 2/3 & 0 & 2/9 & 1/9 \\ 1/3 & -1/2 & 1/9 & 13/36 \end{bmatrix}$$

The eigenvalues of $\boldsymbol{A} \cdot \boldsymbol{A}^T$ are $\sigma_i = [3.336, 2.3406, 0.08128, 0.01945]$. $c_2 = (333.6/1.945)^{1/2} = 13$.

For other choices of $\boldsymbol{v}_1$, the following results are obtained:

$$\boldsymbol{v}_1 = (v_3, v_6) = (r_x, r_e), (v_3, v_4) = (r_x, r_{HLac}) \text{ and } (v_5, v_6) = (r_{HAc}, r_e) \rightarrow c_2 = 17,\ 9,\ \text{and } 206.$$

For $c = 10^Q$, it is as a rule of thumb required that the experimental data are given with Q accurate digits. Hence two to three digits accuracy is demanded to get meaningful results if $\boldsymbol{v}_1$ is (r_{HAc}, r_e). The two measurements are strongly correlated.

Taking more measurements into $\boldsymbol{v}_1$ will always diminish the influence of experimental errors on the calculated fluxes. Thus if $\boldsymbol{v}_1 = (v_2, v_3, v_5, v_6) = (r_{HLac}, r_x, r_{HAc}, r_e)$ the calculation of $\boldsymbol{v}_2 = (v_1, v_4)$ follows the procedure of (5.30)–(5.33):

$$\boldsymbol{T}_1^T \cdot \boldsymbol{T}_1 = \begin{bmatrix} 1 & 0 & 1/3 & 1/3 \\ -1 & 2/3 & 0 & 0 \end{bmatrix} \cdot \begin{bmatrix} 1 & -1 \\ 0 & 2/3 \\ 1/3 & 0 \\ 1/3 & 0 \end{bmatrix} = \begin{bmatrix} 11/9 & -1 \\ -1 & 13/9 \end{bmatrix} = A \tag{2}$$

$$\boldsymbol{A}^{-1} = (1/62)\begin{bmatrix} 117 & 81 \\ 81 & 99 \end{bmatrix}, \quad \text{and } \boldsymbol{T}_1^{\#} = \boldsymbol{A}^{-1} \cdot \boldsymbol{T}_1^T = (1/62)\begin{bmatrix} 36 & 54 & 39 & 39 \\ -18 & 66 & 27 & 27 \end{bmatrix}$$

$$\boldsymbol{v}_2 = \begin{bmatrix} v_1 \\ v_4 \end{bmatrix} = \begin{bmatrix} 49/62 & 741/620 & 69/124 & 3/2 \\ -9/62 & 513/620 & 105/124 & 3/2 \end{bmatrix} \cdot \begin{bmatrix} r_{HLac} \\ r_x \\ r_{HAc} \\ r_e \end{bmatrix} \tag{3}$$

It is easy to prove that for error-free data one obtains the same results for $[v_1, v_4]$ as in (5.9), e.g.

$$\begin{aligned} \boldsymbol{v}_1 &= 49/62 r_{HLac} + 741/620 r_x + 69/124 r_{HAc} + 3/2 r_e \\ &= 49/62(5.7 r_x - 4.5 r_{HAc}) + 741/620 r_x + 69/124 r_{HAc} \\ &\quad + 3/2(0.2 r_x + r_{HAc}) = 6 r_x - 1.5 r_{HAc} \end{aligned} \tag{4}$$

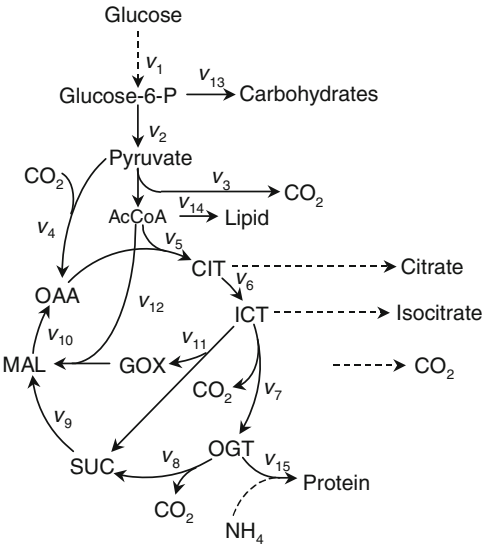

Fig. 5.9 Simplified metabolic network for *Candida lipolytica*. Abbreviations: *AcCoA* acetyl-CoA, *OAA* oxaloacetate, *CIT* citrate, *ICT* isocitrate, *OGT* 2-oxoglutarate, *SUC* succinate, *MAL* malate, *GOX* glyoxylate. *Broken lines* represent reactions where material is transported from/to the cell to/from the environment, whereas *solid lines* represent intracellular reactions

The eigenvalues of the symmetric matrix $\boldsymbol{A}$ in (2) are $\left(12+\sqrt{82}/9\right)$ and $\left(12-\sqrt{82}/9\right)$, and the square root of the ratio between the eigenvalues is $c_2 = 2.67$. This shows that in the presence of experimental errors it is much better to use 4 than 2 measured fluxes to establish the flux vector $\boldsymbol{v}$.

This conclusion always holds: The more measurements included in $\boldsymbol{v}_1$, the better the precision of $\boldsymbol{v}_2$.

Note 5.5 *Linear dependency in reaction stoichiometries.* Because most living cells are capable of utilizing a large variety of compounds as carbon, energy, and nitrogen sources, many complementary pathways exist that would serve similar functions if they operated at the same time. The inclusion of all such pathways may give rise to problems when matrix inversion is applied for flux analysis. This situation usually manifests itself as a matrix singularity, whereby the nonobservable pathways appear as linearly dependent reaction stoichiometries. The fluxes through these different pathways cannot be discerned by extracellular measurements alone. Here, we consider two examples:

- Glyoxylate cycle in prokaryotes.
- Nitrogen assimilation via the GS-GOGAT system.

The glyoxylate cycle is shown in Fig. 5.9. Isocitrate is broken down by reaction v_{11} into glyoxylate and succinate. The glyoxylate reacts with AcCoA to form malate:

$$\underset{\text{Isocitric acid}}{\text{HOOC}-\text{CH}_2-\text{CHCOOH}-\text{CHOH}-\text{COOH}} \rightarrow \underset{\text{glyoxylic acid}}{\text{HOOC}-\text{CHO}} + \underset{\text{succinic acid}}{(\text{CH}_2\text{COOH})_2}$$

$$\text{HOOC}-\text{CHO}+\text{AcCoA} \rightarrow \underset{\text{Malic acid}}{\text{HOOC}-\text{CHOH}-\text{CH}_2-\text{COOH}}+\text{CoA}$$

In prokaryotes, the TCA cycle and all anaplerotic reactions, including the glyoxylate cycle, operate in the cytosol. Often the glyoxylate cycle is considered as a bypass of the TCA cycle

because it shares a number of reactions with this cycle. However, the two pathways serve very different purposes: The TCA cycle has the primary purpose of oxidizing pyruvate to carbon dioxide, whereas the glyoxylate cycle has the purpose of synthesizing precursor metabolites, e.g., oxaloacetate, from acetyl-CoA. Considered individually, the TCA cycle and the glyoxylate shunt are not linearly dependent, but if other anaplerotic pathways, e.g., the pyruvate carboxylase reaction, are included, a singularity arises. This may be illustrated by writing lumped reactions for the three pathways, which all have pyruvate as a substrate.:

$$\textit{TCA cycle} : \text{pyruvate} \rightarrow 3\text{CO}_2 + 4\text{NADH} + \text{FADH}_2 + \text{GTP} \tag{1}$$

$$\textit{Glyoxylate shunt} : 2\text{pyruvate} \rightarrow 2\text{CO}_2 + \text{oxaloacetate} + 4\text{NADH} + \text{FADH}_2 \tag{2}$$

$$\textit{Pyruvate carboxylase} : \text{pyruvate} + \text{ATP} + \text{CO}_2 \rightarrow \text{oxaloacetate} \tag{3}$$

If ATP and GTP are pooled together (which is often done in the analysis of cellular reactions), it is quite obvious that the glyoxylate shunt is a linear combination of the two other pathways, and all three pathways cannot be determined independently by flux analysis. It may be a difficult task to decide which pathway should be eliminated. Fortunately, these pathways rarely operate at the same time since their enzymes are induced differently. Information about induction and regulation of the corresponding enzymatic activities is critical in making a decision as to the exact pathway to be considered at a given set of environmental conditions. For example, expression of isocitrate lyase (the first enzyme of the glyoxylate shunt) is repressed by glucose in many microorganisms, and consequently the glyoxylate shunt is inactive for growth on glucose. In eukaryotes, the presence of the glyoxylate shunt does not give rise to a linear dependency due to compartmentation of the different reactions, i.e., the TCA cycle operates in the mitochondria, and the glyoxylate shunt either in the cytosol or in microbodies. In practice there are many other reactions in the network that involve intermediates of the TCA cycle and the glyoxylate shunt, and these reactions may lead to a removal of the linear dependency between these two pathways. Even in cases where the two pathways are not linearly dependent, the inclusion of both pathways in the model may lead to an ill-conditioned system, i.e., the condition number c_2 may be high.

Another example of linearly dependent reactions is provided by the two ammonia assimilation routes: The glutamate dehydrogenase catalyzed reaction and the GS-GOGAT system (see Sect. 2.3.1). The stoichiometries of these two routes are

$$\textit{GDH} : +\alpha - \text{ketoglutarate} + \text{NH}_3 + \text{NADPH} \rightarrow \text{glutamate} \tag{4}$$

$$\textit{GS}-\textit{GOGAT} : \alpha - \text{ketoglutarate} + \text{NH}_3 + \text{NADPH} + \text{ATP} \rightarrow \text{glutamate} \tag{5}$$

The only difference is that ATP is used in the GS-GOGAT route (which is a high-affinity system), but not in the GDH reaction. The problem here is that an ATP balance is not easy to utilize due to lack of sufficient information about all ATP-consuming reactions. In the absence of an ATP balance to differentiate between them, the two nitrogen assimilation reactions are linearly dependent and, as such, nonobservable. Therefore, the two routes to glutamate are often lumped into a single reaction, and this does not have any significant effect on the stoichiometric model.

If a singularity arises in the stoichiometric matrix, one has the following two options:

(1) Remove the linearly dependent reaction(s) from the model, invoking (or postulating) information about specific enzyme regulation and induction.
(2) Introduce additional information such as the relative flux of the two pathways. Such information may be derived from measurements of enzyme activities, e.g., the relative activity of key enzymes in the two routes. However, this approach is hampered by the fact that in vitro enzyme activity measurements often bear little relationship to actual in vivo flux distributions. A more powerful technique is the use of labeled substrates, e.g., ^{13}C-enriched glucose, followed by measurements of the labeling pattern of intracellular metabolites as discussed in Sect. 5.3.3.

The combination of a metabolic model, based only on reaction stoichiometries, and measurement of a few rates is a very simple method for estimation of intracellular fluxes, and it has been used to study many different fermentation processes (Vallino and Stephanopoulos 1993; Vallino and Stephanopoulos 1994a, b; van Gulik and Heijnen 1995; Sauer et al. 1996; Nissen et al. 1997; Pramanik and Keasling 1997; Pedersen et al. 1999). Clearly, it is valuable to quantify the fluxes through the different branches of the metabolic network considered in the model, and in Sect. 5.3.3 we discuss how information on fluxes may be used to guide genetic modification, resulting in strains with improved properties. The approach may, however, also be used for analysis of the metabolic network, i.e., to estimate which pathways are likely to operate. This will be illustrated in Examples 5.7 and 5.8. It must be emphasized that such analysis must always be followed up with experimental verification, but clearly the simple approach discussed in this section may be used as an efficient guide to the experimental work.

Example 5.7 *Metabolic Flux Analysis of citric acid fermentation by Candida lipolytica.* Aiba and Matsuoka (1979) were probably the first to apply the concept of metabolite balancing to analyze fermentation data. They studied the yeast *C. lipolytica,* a citric acid producer, and the aim of their study was not to quantify the fluxes, but rather to find which pathways were active during citric acid production. For their analysis they employed the simplified metabolic network shown in Fig. 5.9. The network includes the EMP pathway, the TCA cycle, the glyoxylate shunt, pyruvate carboxylation, and formation of the major macromolecular pools, i.e., proteins, carbohydrates, and lipids. At least one of the two anaplerotic routes is obviously necessary to replenish TCA cycle intermediates when citrate and isocitrate are secreted to the extracellular medium.

The network, Fig. 5.9, has ten branch points: G6P (2), PYR (2), AcCoA (3), cit (1), ic (2), OGT (2), SUC (1), MAL (1), OAA (1), GOX (1).

In parenthesis is shown the number of *internal* fluxes *leaving* each branch point. The total is 16.

According to the discussion of Fig. 5.2 all 15 fluxes in Fig. 5.9 are defined if the sum of linearly independent measurements and constraints is 16.

We have eight measurable rates of exchange reactions

$$[r_{\mathrm{glc}}, r_{\mathrm{N}} = r_{\mathrm{NH_3}}, r_{\mathrm{c}}, r_{\mathrm{cit}}, r_{\mathrm{ict}}, r_{\mathrm{prot}}, r_{\mathrm{car}}, r_{\mathrm{lipid}}]$$

r_{N} is proportional to r_{Prot} and given by the moles of NH_3 used to form 1 mol of protein. Hence we need nine constraints.

If, however, the production rate of citrate is measured, this branch point disappears ($v_6 = v_5 - r_{\text{cit}}$). With seven independent exchange rates the required number of constraints is eight.

From the nine remaining branch points, we do not use the mass balance constraint at isocitrate.

Now the network is completely defined with seven measured rates and eight constraints.

$$\begin{aligned}[r_{\text{G6P}}, r_{\text{PYR}}, r_{\text{AcCoA}}, r_{\text{OGT}}, r_{\text{Suc}}, r_{\text{Mal}}, r_{\text{OOA}}, r_{\text{GOX}}] &= 0; \\ [r_{\text{glc}}, r_{\text{c}}, r_{\text{cit}}, r_{\text{ict}}, r_{\text{prot}}, r_{\text{car}}, r_{\text{lipid}}] &\neq 0\end{aligned} \tag{1}$$

Based on the network of Fig. 5.9 we can establish the linear matrix problem (5.10) as exemplified in (5.8). Here *Mole basis* is used for all stoichiometric coefficients. Consequently, in v_2 2 mol PYR is formed for every consumed moles of glucose, and the lipid, protein, and carbohydrate synthesis rates are based on, respectively, the moles of AcCoA, OGT, and G6P consumed.

Notice that neither a redox balance, nor an ATP balance is included. But the TCA cycle, the glyoxylate shunt and the pyruvate carboxylase shunt to OOA are included in the model. Still, the matrix still has full rank. This is due to the reaction from 2-oxoglutarate to protein, which is an additional reaction that imposes a constraint on the flux via the TCA cycle.

In their analysis Aiba and Matsuoka used only six measured reaction rates:

$$[r_{\text{glc}}, r_{\text{c}}, r_{\text{cit}}, r_{\text{ict}}, r_{\text{prot}}, r_{\text{car}}] \neq 0 \tag{2}$$

The rates r_{prot} and r_{car} were found from measurements of the protein and carbohydrate contents of the biomass (from a steady-state chemostat). In addition to the six measurements, Aiba and Matsuoka imposed an extra constraint by setting one of the rates in the network equal to zero.

$$\begin{pmatrix} r_{\text{glc}} \\ r_{\text{N}} \\ r_{\text{c}} \\ r_{\text{cit}} \\ r_{\text{ict}} \\ r_{\text{prot}} \\ r_{\text{car}} \\ r_{\text{lipid}} \\ 0 \\ 0 \\ 0 \\ 0 \\ 0 \\ 0 \\ 0 \\ 0 \end{pmatrix} = \begin{pmatrix} -1 & 0 & 0 & 0 & 0 & 0 & 0 & 0 & 0 & 0 & 0 & 0 & 0 & 0 & 0 \\ 0 & 0 & 0 & 0 & 0 & 0 & 0 & 0 & 0 & 0 & 0 & 0 & 0 & 0 & -\alpha \\ 0 & 0 & 1 & -1 & 0 & 0 & 1 & 1 & 0 & 0 & 0 & 0 & 0 & 0 & 0 \\ 0 & 0 & 0 & 0 & 1 & -1 & 0 & 0 & 0 & 0 & 0 & 0 & 0 & 0 & 0 \\ 0 & 0 & 0 & 0 & 0 & 1 & -1 & 0 & 0 & 0 & -1 & 0 & 0 & 0 & 0 \\ 0 & 0 & 0 & 0 & 0 & 0 & 0 & 0 & 0 & 0 & 0 & 0 & 0 & 0 & 1 \\ 0 & 0 & 0 & 0 & 0 & 0 & 0 & 0 & 0 & 0 & 0 & 0 & 1 & 0 & 0 \\ 0 & 0 & 0 & 0 & 0 & 0 & 0 & 0 & 0 & 0 & 0 & 0 & 0 & 1 & 0 \\ 1 & -1 & 0 & 0 & 0 & 0 & 0 & 0 & 0 & 0 & 0 & 0 & -1 & 0 & 0 \\ 0 & 2 & -1 & -1 & 0 & 0 & 0 & 0 & 0 & 0 & 0 & 0 & 0 & 0 & 0 \\ 0 & 0 & 1 & 0 & -1 & 0 & 0 & 0 & 0 & 0 & 0 & -1 & 0 & -1 & 0 \\ 0 & 0 & 0 & 0 & 0 & 0 & 1 & -1 & 0 & 0 & 0 & 0 & 0 & 0 & -1 \\ 0 & 0 & 0 & 0 & 0 & 0 & 0 & 1 & -1 & 0 & 1 & 0 & 0 & 0 & 0 \\ 0 & 0 & 0 & 0 & 0 & 0 & 0 & 0 & 1 & -1 & 0 & 1 & 0 & 0 & 0 \\ 0 & 0 & 0 & 1 & -1 & 0 & 0 & 0 & 0 & 1 & 0 & 0 & 0 & 0 & 0 \\ 0 & 0 & 0 & 0 & 0 & 0 & 0 & 0 & 0 & 0 & 1 & -1 & 0 & 0 & 0 \end{pmatrix} \begin{pmatrix} v_1 \\ v_2 \\ v_3 \\ v_4 \\ v_5 \\ v_6 \\ v_7 \\ v_8 \\ v_9 \\ v_{10} \\ v_{11} \\ v_{12} \\ v_{13} \\ v_{14} \\ v_{15} \end{pmatrix} \tag{3}$$

Three different cases were examined, reflecting three different modes of operation of the network:

- *Model 1*. The glyoxylate shunt is inactive, i.e., the branch points at GOX and SUC disappear, and $v_{11} = 0$.

- *Model 2*. Pyruvate carboxylase is inactive, i.e., the branch points at PYR and OOA disappear and $v_4 = 0$.
- *Model 3*. The TCA cycle is incomplete, i.e., the branch points at OGT and SUC disappear, and $v_8 = 0$.

With the six listed measured rates, the system of equations is therefore exactly determined for each of the three models, and it can be solved to determine all the intracellular fluxes.

The result for Model 1 is shown in (4) and (5):

$$\begin{pmatrix} v_1 \\ v_2 \\ v_3 \\ v_4 \\ v_5 \\ v_6 \\ v_7 \\ v_8 \\ v_9 \\ v_{10} \\ v_{12} \\ v_{13} \\ v_{14} \\ v_{15} \end{pmatrix} = \begin{pmatrix} -1 & 0 & 0 & 0 & 0 & 0 & 0 & 0 & 0 & 0 & 0 & 0 & 0 & 0 \\ 0 & 1 & 1 & -1 & 0 & 0 & 1 & 1 & 0 & 0 & 0 & 0 & 0 & 0 \\ 0 & 0 & 0 & 0 & 1 & -1 & 0 & 0 & 0 & 0 & 0 & 0 & 0 & 0 \\ 0 & 0 & 0 & 1 & 0 & 1 & -1 & 0 & 0 & 0 & 0 & 0 & 0 & 0 \\ 0 & 0 & 0 & 0 & 0 & 0 & 0 & 0 & 0 & 0 & 0 & 0 & 0 & 1 \\ 0 & 0 & 0 & 0 & 0 & 0 & 0 & 0 & 0 & 0 & 0 & 1 & 0 & 0 \\ 1 & -1 & 0 & 0 & 0 & 0 & 0 & 0 & 0 & 0 & 0 & -1 & 0 & 0 \\ 0 & 2 & -1 & -1 & 0 & 0 & 0 & 0 & 0 & 0 & 0 & 0 & 0 & 0 \\ 0 & 0 & 1 & 0 & -1 & 0 & 0 & 0 & 0 & 0 & -1 & 0 & -1 & 0 \\ 0 & 0 & 0 & 0 & 0 & 0 & 1 & -1 & 0 & 0 & 0 & 0 & 0 & -1 \\ 0 & 0 & 0 & 0 & 0 & 0 & 0 & 1 & -1 & 0 & 0 & 0 & 0 & 0 \\ 0 & 0 & 0 & 0 & 0 & 0 & 0 & 0 & 1 & -1 & 1 & 0 & 0 & 0 \\ 0 & 0 & 0 & 1 & -1 & 0 & 0 & 0 & 0 & 1 & 0 & 0 & 0 & 0 \\ 0 & 0 & 0 & 0 & 0 & 0 & 0 & 0 & 0 & 0 & -1 & 0 & 0 & 0 \end{pmatrix}^{-1} \begin{pmatrix} r_{\mathrm{gkc}} \\ r_{\mathrm{c}} \\ r_{\mathrm{cit}} \\ r_{\mathrm{ici}} \\ r_{\mathrm{prot}} \\ r_{\mathrm{car}} \\ 0 \\ 0 \\ 0 \\ 0 \\ 0 \\ 0 \\ 0 \\ 0 \end{pmatrix} \tag{4}$$

$$\begin{pmatrix} v_1 \\ v_2 \\ v_3 \\ v_4 \\ v_5 \\ v_6 \\ v_7 \\ v_8 \\ v_9 \\ v_{10} \\ v_{12} \\ v_{13} \\ v_{14} \\ v_{15} \end{pmatrix} = \begin{pmatrix} -1 & 0 & 0 & 0 & 0 & 0 \\ -1 & 0 & 0 & 0 & 0 & -1 \\ -2 & 0 & -0.5 & -0.5 & -0.5 & -2 \\ 0 & 0 & 0.5 & 0.5 & 0.5 & 0 \\ 1.5 & 0.5 & 1 & 1 & 0.5 & 1.5 \\ 1.5 & 0.5 & 0 & 1 & 0.5 & 1.5 \\ 1.5 & 0.5 & 0.5 & 0.5 & 1 & 1.5 \\ 1.5 & 0.5 & 0.5 & 0.5 & 0 & 1.5 \\ 1.5 & 0.5 & 0.5 & 0.5 & 0 & 1.5 \\ 1.5 & 0.5 & 0.5 & 0.5 & 0 & 1.5 \\ 0 & 0 & 0 & 0 & 0 & 0 \\ 0 & 0 & 0 & 0 & 0 & 1 \\ -3.5 & 0.5 & -1.5 & -1.5 & -1 & -3.5 \\ 0 & 0 & 0 & 0 & 1 & 0 \end{pmatrix} \begin{pmatrix} r_{\mathrm{glc}} \\ r_{\mathrm{c}} \\ r_{\mathrm{cit}} \\ r_{\mathrm{ici}} \\ r_{\mathrm{prot}} \\ r_{\mathrm{car}} \end{pmatrix} \tag{5}$$

Many of the rows in (5) can be recognized immediately: Obviously $v_1 = (-r_{\mathrm{s}})$, $v_2 = v_1 - r_{\mathrm{car}}$, $v_5 = v_6 + r_{\mathrm{cit}}$, $v_7 = v_8 + r_{\mathrm{prot}}$, $v_{12} = 0$ (since v_{11} has been set to 0), and $v_9 = v_{10}$ (since $v_{12} = 0$).

In fact, the whole of matrix $\boldsymbol{T}_1^{-1} \cdot \boldsymbol{T}_2$ (5.12) can be identified by application of rather simple mass balances. But then, the example is only a very simple application of flux balancing, although at first the network in Fig. 5.9 looks quite formidable.

Aiba and Matsuoka (1979) concluded that Model 1 gives reasonable values for the fluxes. Furthermore, in vitro measurements of the activity of four different enzymes

(pyruvate carboxylase, citrate synthase, isocitrate dehydrogenase, and isocitrate lyase) correlated fairly well with the calculated fluxes. When the two other models were tested, it was found that some of the fluxes were negative, e.g., Model 2 predicts that 2-oxoglutarate is converted to isocitrate. This is not impossible, but most of the reactions are favored thermodynamically in the direction specified by the arrows in Fig. 5.5. Thus, ΔG^0 for the conversion of isocitrate to 2-oxoglutarate is -20.9 kJ $(\text{mol})^{-1}$, and a large concentration ratio of 2-oxoglutarate to isocitrate would be required to allow this reaction to run in the opposite direction. Furthermore, there is better agreement between the measured enzyme activities and flux predictions with Model 1 than with the two other models. Aiba and Matsuoka (1979) therefore concluded that at conditions of citric acid production the glyoxylate shunt is inactive or operates at a very low rate in *C. lipolytica*. In this example, the biomass is built from three components: carbohydrates, lipids, and proteins, and these are assumed to be synthesized from a few precursor metabolites (G6P, PYR, and AcCoA).

In reality, the requirements for precursor metabolites (Table 2.2) are much heavier, and in Note 5.3 a far more complicated way of building the macromolecules of the biomass, namely via building blocks is suggested. This is the way in which genome scale metabolic models are built today, as exemplified for *Clostridium acetobutylicum* by Senger and Papoutsakis (2008) and for *Corynebacterium glutamicum* by Kjeldsen and Nielsen (2009).

The difficult part of network analysis is always the modeling of the biomass synthesis while, as shown in Example 5.4, the distribution of carbon into even a large number of metabolites is not too difficult to analyze.

In the present example it might have led to an equally good description of the network, if the measurement of nitrogen uptake had been used to calculate r_{prot} $(=r_{\text{N}}\ \alpha)$ where α is obtained from an average protein composition (Table 3.1). Afterward, the macromolecular cell composition of the table could be used to find r_{x}, and now a biomass formation equation of the form (5.22), typically used in this chapter, could be set up. Together with r_{cit} and r_{ici} the biomass stoichiometric equation could be used to analyze the network.

Example 5.8 *Analysis of the metabolic network in S. cerevisiae during anaerobic growth.* Nissen et al. (1997) constructed a network model that gives a much more detailed analysis of anaerobic growth of *S. cerevisiae* than the simple model of Example 5.2 (which is still quite adequate to describe the overall growth metabolism of the yeast). The model was based on a comprehensive literature study to find which metabolic pathways are active in *S. cerevisiae*. The model contains 37 reactions and 27 intracellular metabolites. Thus, the degrees of freedom in the system are $F = 10$. In chemostat cultures operating at different dilution rates, the rates of the following 13 compounds were measured: glucose, ammonia, glycerol, pyruvate, carbon dioxide, acetate, ethanol, succinate, carbohydrates, proteins, DNA, RNA, and lipids. The production rate of ethanol and the uptake rate of ammonia were not used for the analysis, but these rates were used to validate the fluxes, which were calculated using the remaining 11 measured rates together with (5.33).

A number of questions were raised concerning certain isoenzymes.

Three isoenzymes of alcohol dehydrogenase (ADH) have been identified in *S. cerevisiae* (after the genome has been sequenced many more putative alcohol dehydrogenases have been identified, but their function is as yet unknown). The cytosolic ADH1 is constitutively expressed during anaerobic growth on glucose, and it is responsible for the formation of ethanol. ADH2, which is also cytosolic, is mainly associated with growth on ethanol, and it is therefore

Table 5.3 Fluxes through key reactions in the metabolic network during anaerobic growth of *S. cerevisiae* and using different models

	Model[a]		
Reaction	Reference model	Including IDP2	Excluding ADH3
Glucose-6P dehydrogenase	7.5	−80	7.9
IDH	1.7	−117	1.3
IDP2	0	176	0
2-Oxoglutarate dehydrogenase	0	22	−0.3
ADH3[b]	1.0	−12	0

[a] All fluxes are normalized with respect to the glucose uptake rate which is set to 100, and the fluxes are given as C-mole (C-mol glucose)$^{-1}$. In all three cases a dilution rate of 0.3 h^{-1} has been used
[b] The flux for ADH3 is given for the direction from acetaldehyde to ethanol where NADH is consumed

not active during anaerobic growth on glucose. The function of the mitochondrial ADH3 is not known, but it has been postulated to be involved in a redox shuttle system between the mitochondria and the cytosol. Using enzyme activity assays Nissen et al. (1997) showed that ADH3 is active during anaerobic growth on glucose, and it was therefore included in the model.

Three isoenzymes of isocitrate dehydrogenase (IDH) have been isolated (IDH, IDP1, and IDP2). The NAD-dependent IDH is localized in the mitochondria, and it is important for the function of the TCA cycle. The function of the two NADP-dependent isoenzymes IDP1 and IDP2 localized in the mitochondria and cytosol, respectively, has not been clearly established. IDP1 is likely to be a major source for NADPH needed in the mitochondria for amino acid biosynthesis that takes place in this compartment. Some results have indicated that IDP2 is not active during growth on glucose, but this has not been clearly established.

To analyze the possible function of ADH3 and IDP2 these reactions were either included or left out of the model, and the fluxes were calculated. Table 5.3 summarizes some key fluxes calculated using the different models. During anaerobic growth on glucose, the major fraction of glucose is shunted toward ethanol, and most other fluxes in the network are therefore low. Some important variations are, however, clearly seen between the different models. In the reference model approximately 8% of the glucose taken up (on a C-mole basis) is shunted through the pentose phosphate pathway in order to supply the cell with ribose-5-phosphate (needed as precursor metabolite) and NADPH needed for biomass synthesis. This flux does not change if ADH3 is excluded from the model, but if IDP2 is included this flux becomes large and negative. This is due to the supply of NADPH via the IDP2 catalyzed reaction, which carries a large flux. With IDP2 it is also seen that the IDH flux becomes large and negative. Negative fluxes in the TCA cycle are not necessarily ruled out They simply imply that the flux is in the opposite direction to that specified in the model. Certain reactions in the network are, however, known to proceed only in one direction due to thermodynamic constraints, and the reaction catalyzed by glucose-6 phosphate dehydrogenase is one of these. It is therefore concluded that IDP2 cannot operate during anaerobic conditions, or its in vivo flux must be tightly controlled at a low level.

When ADH3 is excluded the changes in the fluxes are smaller, and the major difference is that the 2-oxoglutarate dehydrogenase catalyzed reaction carries a negative flux, i.e., succinate is converted back to 2-oxoglutarate. Even though this flux is low, it is quite well determined, and it is a result of a redox problem inside the mitochondria. Apparently, there

are no other reactions that can oxidize NADH, and the TCA cycle reactions therefore start to operate such that they oxidize NADH. The reaction from 2-oxoglutarate to succinate is thermodynamically favored toward succinate formation, and a negative flux in this reaction is unlikely. It is concluded that ADH3 serves a very important function during anaerobic growth on glucose, namely ensuring oxidation of NADH in the mitochondria, and this is done by sending part of the acetaldehyde formed in the cytosol to the mitochondria where it is reduced to ethanol, accompanied by NADH consumption. Since both acetaldehyde and ethanol are easily transported across the mitochondrial membrane it is of no importance for the cell where this reaction is occurring.

The approach of combining a metabolic model and measurement of a few rates is attractive due to its simplicity. The approach does, however, have some pitfalls. Among these are:

- *Linearly dependent reaction stochiometries*. This was discussed in Note 5.5, and it was indicated how the problem could be solved. However, in some cases there is no information available on regulation of the different pathways, and in fact it may be interesting to evaluate the relative activity of two different pathways that have the same overall stoichiometry. As discussed in Example 5.8 one may use enzyme activity measurements as additional constraints, but in vitro determined enzyme activities rarely represent in vivo fluxes.
- *High sensitivity of certain fluxes to certain measured rates*. In some cases the matrix equation is ill-conditioned, and this can result in very high sensitivities of the estimated fluxes to experimental errors in the measured rates. The sensitivity of the calculated fluxes is treated in Note 5.4 where it is shown that the *choice* of measured rates to be used may lead to large differences in the condition number. Typically, we wish c_2 to be smaller than 100.
- *The fluxes are determined by balances for specific cofactors*. As illustrated for the simple metabolic network models in Sect. 5.2, balances for the cofactors NADH, NADPH, and ATP may be very useful for estimation of the fluxes, particularly as these cofactors link different parts of the metabolism together. Basically, it is not a problem to include balances for cofactors in metabolic models, but a requirement for proper use of these balances is that *all* reactions involving these cofactors are included in the model. This may be problematic, since not all parts of the metabolism may be known, and one may inadvertently leave out important reactions that involve these cofactors. This may result in substantial errors in the flux estimation. Estimation of the flux through the pentose phosphate pathway is particularly sensitive to whether *all* reactions involving NADPH are included in the model when the fluxes are estimated from measurable rates alone.

Introducing additional constraints on individual carbon atom transitions, combined with measurements of the labeling patterns of the some metabolites when the cells are growing on specifically labeled substrates, circumvents most of the above-mentioned problems.

This is the topic of the next section.

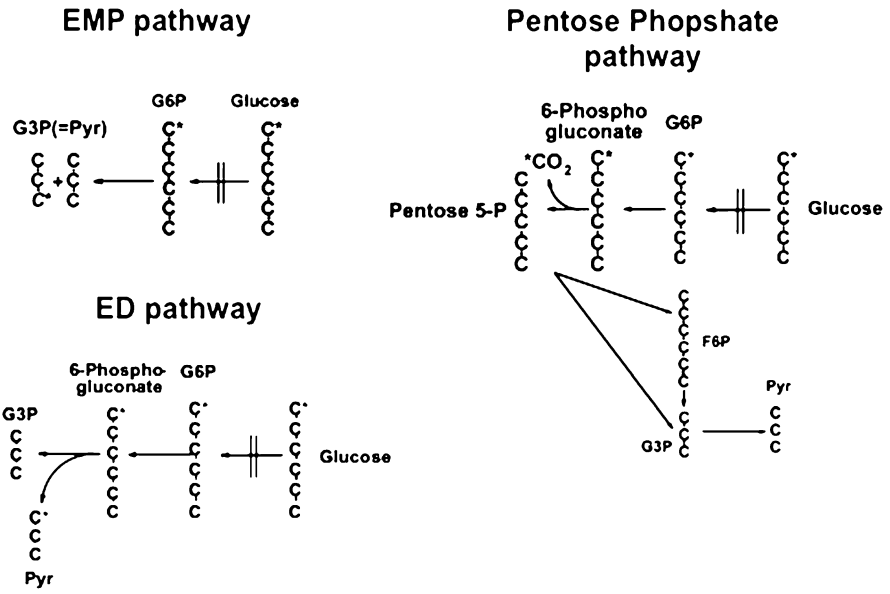

Fig. 5.10 Overview of carbon transitions in three different catabolic pathways: EMP pathway, ED pathway, and pentose phosphate pathway. The ^{13}C-labeled carbon in glucose is marked with *asterisks*. In the EMP pathway the third carbon position of pyruvate is labeled. In the ED pathway the first carbon position of pyruvate is enriched. Carbon that passes through the pentose phosphate pathway will not give any ^{13}C enrichment of pyruvate since the first carbon atom of glucose escapes as carbon dioxide

5.3.3 The Use of Labeled Substrates

If cells are fed with a ^{13}C-labeled substrate, e.g., glucose that is enriched with ^{13}C in the first carbon position, then on catabolism of this substrate some of the carbon atoms present in the different catabolic intermediates will be enriched in ^{13}C. The enrichment of the individual carbon atoms in different metabolic intermediates will depend on the activity of the pathway. As an illustration consider the catabolism of glucose to pyruvate by three different pathways: the Embden Meyerhof Parnas pathway (EMP pathway), the pentose phosphate pathway, and the Entner Doudoroff (ED) pathway. If glucose is labeled specifically in the first position C_1, the pyruvate will be differently labeled depending on the pathway that is used from glucose to pyruvate (see Fig. 5.10).

If one measures the fractional enrichment of pyruvate (see Note 5.6) compared with that of glucose it is possible not only to identify which of the three pathways is operative, but also to calculate the relative activity of the different pathways. Consider a simple case where we feed with 100% [$^{13}C_1$]-labeled glucose (glucose where the first carbon atom is fully labeled and the remaining carbon atoms

are naturally labeled[3]), and we find that 30% of the third position carbons of pyruvate are ^{13}C enriched (specified as PYR(3) = 0.3) and 10% of the first position carbons of pyruvate are ^{13}C enriched (specified as PYR(1) = 0.1). Thus, a set of simple balances gives us:

$$v_{\mathrm{EMP}}0.5 + v_{\mathrm{ED}}0 + v_{\mathrm{PP}}0 = \mathrm{PYR}(3) = 0.3 \tag{5.34}$$

$$v_{\mathrm{EMP}}0 + v_{\mathrm{ED}}0.5 + v_{\mathrm{PP}}0 = \mathrm{PYR}(1) = 0.1 \tag{5.35}$$

Here the sum of the three pathway fluxes is normalized to one and $v_{\mathrm{EMP}} + v_{\mathrm{ED}} + v_{\mathrm{PP}} = 1$. Clearly if the flux through the EMP pathway is 1 (corresponding to no activity of the other pathways), then PYR(3) would be 0.5. Similarly, if the ED pathway is the sole pathway being active PYR(1) should be 0.5. Solving (5.34) and (5.35) together with the normalization equation directly gives: $v_{\mathrm{EMP}} = 0.6$; $v_{\mathrm{ED}} = 0.2$; $v_{\mathrm{PP}} = 0.2$. This simple example clearly illustrates how labeling information can be used both to identify the pathway topology and to quantify the fluxes. The approach is illustrated further in Example 5.9.

Example 5.9 *Identification of lysine biosynthesis.* The biosynthesis of lysine was discussed in Sect. 2.3.1. Lysine is extensively used as a feed additive, and it is produced by fermentation of *C. glutamicum*. It is a relatively low value added product, and it is of utmost importance to ensure a high overall yield of lysine on glucose (the typical carbon source). In bacteria lysine is derived from the precursor metabolites oxaloacetate and pyruvate, which in a series of reactions are converted into tetrahydrodipicolinate (H4D). H4D is converted to *meso*-α,ε-diaminopimelate (*meso*-DAP), and this conversion may proceed via two different routes (see Fig. 5.11). In the last step *meso*-DAP is decarboxylated to lysine. From measurement of the lysine flux v_{lys} (equal to the lysine production rate r_{lys}) it is not possible to discriminate between the activities of the two different pathways. However, the four-step pathway (the pathway on the right hand side of Fig. 5.11) involves a symmetric intermediate, and the epimerase catalyzing the last step in the pathway may therefore lead to formation of *meso*-DAP with two different carbon compositions (see Fig. 5.11). Through analysis of the labeling pattern in the precursor metabolites pyruvate and oxaloacetate and the labeling pattern of lysine, it is therefore possible to estimate the flux through the two different pathways. To illustrate this we set up a simple balance for the first carbon of lysine (LYS(1)):

$$\mathrm{LYS}(1) = \mathrm{Y\ OAA}(1) + (1 - Y)/2\ \mathrm{OAA}(1) + (1 - Y)/2\mathrm{PYR}(1) \tag{1}$$

From measurements of the ^{13}C-enrichment LYS(1), OAA(1), and PYR(1) one can easily calculate Y. Notice that also other balances can be set up to estimate Y, e.g., for the sixth carbon of lysine (LYS(6)):

$$\mathrm{LYS}(6) = Y\ \mathrm{PYR}(2) + (1 - Y)/2\ \mathrm{PYR}(2) + (1 - Y)/2\ \mathrm{OAA}(2) \tag{2}$$

Thus, through measurements of the ^{13}C-enrichment in several different carbon positions one has redundant information and it may be possible to obtain a robust estimate of the flux through

[3]Notice that it is normally necessary to consider natural labeling, which is approximately 1.1% ^{13}C, but for simplicity we will neglect natural labeling here.

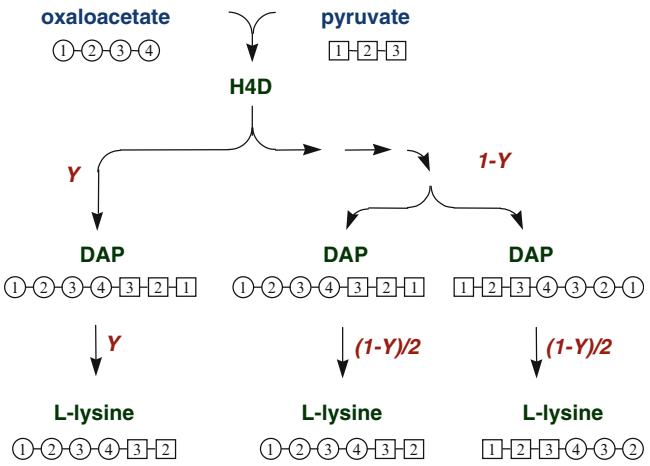

Fig. 5.11 Overview of carbon transitions in two different pathways to lysine from oxaloacetate and pyruvate. The four-step succinylase pathway with the flux $(1-Y)v_{\text{lys}}$ proceeds via diaminopimelate, which is an intermediate in cell wall biosynthesis in certain bacteria. The four-step pathway contains the enzymatic sequence *N*-succinyl-2,6-ketopimelate synthase, *N*-succinylaminoketopimelate:glutamate amino transferase, *N*-succinyldiaminopimelate desuccinylase, and diaminopimelate epimerase. The one-step pathway with the flux Yv_{lys} involves the action of *meso*-DAP dehydrogenase

the two different pathways. It is generally the case that measurement of the ^{13}C-enrichment combined with balances for the individual carbon atoms supplies redundant information, and that robust flux estimates are obtained.

Sonntag et al. (1993) used the approach outlined above for quantification of the fluxes through the two different pathways at different growth conditions. The ^{13}C-enrichment of secreted lysine was measured by NMR, and this information was used to quantify the flux through the two branches at different ammonia concentrations (Fig. 5.12). It was found that the relative flux through the direct pathway increased for increasing ammonia concentration and at the same time the lysine secretion was enhanced. This pointed to an important role of the direct pathway for over-production of lysine.

The approach illustrated above is very simple and straightforward. However, in practice it is difficult to identify the network topology, and the flux quantification is much more complicated. There are many more reactions involved in carbon transitions than those highlighted in Fig. 5.10, and hereby the ^{13}C-enrichment in the different carbon atoms becomes a function of many different pathways. Thus, even though none of the three catabolic pathways shown in Fig. 5.10 should result in ^{13}C-enrichment of the second carbon atom of pyruvate, there is typically some enrichment in this position. This is due to interaction with other pathways, e.g., by an active malic enzyme, but it is also due to scrambling of the labeling via the nonoxidative branch of the pentose phosphate pathway, where the transketolase and transaldolase catalyzed reactions are reversible and may result in many different types of carbon transitions (van Winden et al. 2001).

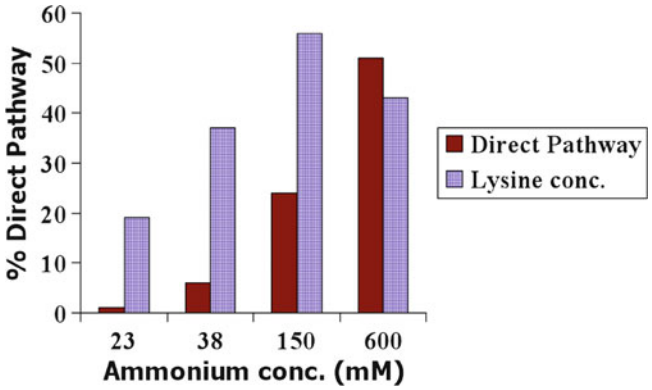

Fig. 5.12 Quantification of the fluxes through the two different pathways leading to lysine shown in Fig. 5.11 for growth at different ammonia concentrations. Lysine concentration is in arbitrary units

It is therefore necessary to obtain relatively detailed information about the ^{13}C-enrichment in the different carbon positions and for this purpose different analytical techniques can be applied (see Note 5.6). Furthermore, it is necessary to set up balances for each individual carbon atom in all the different reactions, as illustrated in Example 5.10.

Note 5.6 *Measurement of ^{13}C-enrichment.* There are different methods for analysis of the ^{13}C-enrichment, but all methods are based on either nuclear magnetic resonance (NMR) spectroscopy or mass spectroscopy (MS). In order to shortly describe the methods it is, however, necessary to look into some definitions concerned with ^{13}C-enrichment. A molecule containing n carbon atoms has 2^n different labeling patterns, or in other words 2^n different isomers of isotopes – often referred to as *isotopomers* (see Fig. 5.13a).

Using ^{13}C-NMR it is possible to identify which of the carbon atoms that are enriched with ^{13}C, and if there are two ^{13}C positioned next to each other this will result in a split of the resonance peak into two peaks in the spectrum. Combining ^{13}C-NMR with proton-NMR it is possible to resolve peaks for many of the carbon atoms, and hereby it is possible to obtain relatively detailed information about the isotopomers. However, in most cases only a fraction of the isotopomers can be identified. With proton-NMR it is possible to identify the specific resonance between protons and ^{13}C, and hereby it can be resolved whether a given carbon is ^{13}C or ^{12}C. It is, however, not possible to tell whether the ^{13}C is connected to a ^{13}C or a ^{12}C. Thus, only information about the so-called *fractional enrichment* can be obtained (see Fig. 5.13b). The fractional enrichment can be used directly in balances for the individual carbon atoms as illustrated in Example 5.9. The fractional enrichment can, however, always be calculated if the distribution of isotopomers is known.

Using MS it is possible to measure the mass of the individual metabolites, since ^{13}C has a higher mass than ^{12}C. Thus, with MS it is possible to measure the so-called *mass isotopomers* (see Fig. 5.13c). It is somewhat more complicated to use this information directly for flux analysis, but as will be shown later, information about ^{13}C enrichments is rarely used directly for flux quantification. Notice that also the mass isotopomers can be calculated if the distribution of isotopomers is known, and this can be used in an iterative process to find the fluxes v_i (see Figure 5.14).

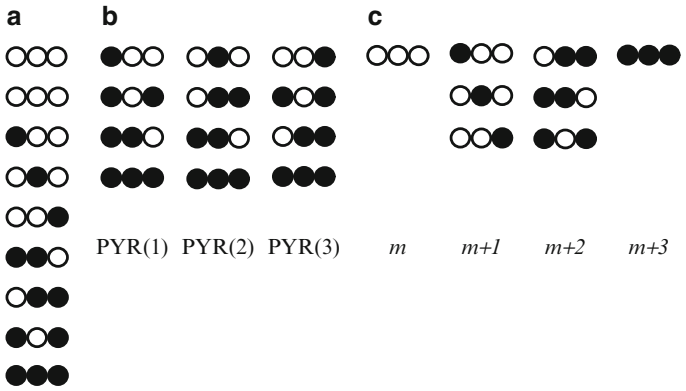

Fig. 5.13 Overview of different labeling patterns possible for a molecule with three carbon atoms, e.g., pyruvate. (**a**) All possible isotopomers. (**b**) Grouping of isotopomers to indicate the different isotopomers that are included when the fractional enrichment is measured. (**c**) Grouping of isotopomers into different mass isotopomers. The mass of the nonlabeled metabolite is *m*

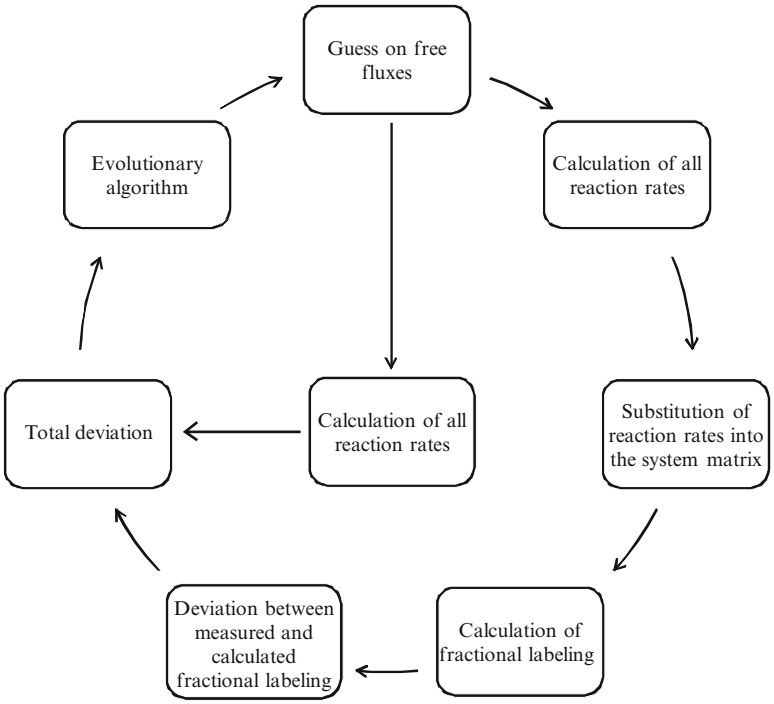

Fig. 5.14 A procedure for estimating metabolic fluxes using ^{13}C-labeled data. The procedure starts with a guess of the free fluxes, and then all the fluxes are calculated using matrix inversion (in analogy with (2) in Example 5.10). The calculated fluxes can be compared directly with measured rates and they can be used to calculate the fractional labeling of all the intracellular metabolites. The calculated fractional labeling can then be compared with experimental data on the fractional labeling, and a total deviation between calculated fluxes and fractional labeling of metabolites can be found. Through the use of an optimization algorithm it is possible to propose a new set of fluxes, and hereby iterate until the total deviation is minimized, resulting in a good estimate of the fluxes

Example 5.10 *Analysis of a simple network.* To illustrate a more formal approach to the use of labeled substrates for flux quantification we will consider the simple network shown below.

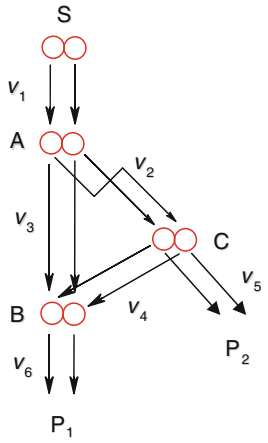

For this network we have the metabolite balance equation:

$$\begin{pmatrix} r_s \\ r_{p_1} \\ r_{p_2} \\ 0 \\ 0 \\ 0 \end{pmatrix} = \begin{pmatrix} -1 & 0 & 0 & 0 & 0 & 0 \\ 0 & 0 & 0 & 0 & 0 & 1 \\ 0 & 0 & 0 & 0 & 1 & 0 \\ 1 & -1 & -1 & 0 & 0 & 0 \\ 0 & 0 & 1 & 1 & 0 & -1 \\ 0 & 1 & 0 & -1 & -1 & 0 \end{pmatrix} \begin{pmatrix} v_1 \\ v_2 \\ v_3 \\ v_4 \\ v_5 \\ v_6 \end{pmatrix} \tag{1}$$

Clearly three fluxes can be measured directly and with three degrees of freedom we can in principle estimate the fluxes using matrix inversion. However, the matrix does not have full rank (addition of the second and fourth column gives the third column), and we therefore need additional information. We now set v_1 to 100 and then express the other fluxes as function of two of the fluxes (v_3 and v_4):

$$\begin{pmatrix} v_1 \\ v_2 \\ v_3 \\ v_4 \\ v_5 \\ v_6 \end{pmatrix} = \begin{pmatrix} 100 \\ 100 - v_3 \\ v_3 \\ v_4 \\ 100 - v_3 - v_4 \\ v_3 + v_4 \end{pmatrix} \tag{2}$$

The two fluxes v_3 and v_4 will be termed free fluxes, and if we can obtain information about these from balances around the individual carbon atoms then all the fluxes in the network can be calculated using (2). With the carbon transitions specified in the network we can set up balances for the individual carbon atoms. Thus, for the first reaction we have:

$$-100S_1 = -(v_2 + v_3)A_1 \tag{3}$$

$$-100S_2 = -(v_2 + v_3)A_2 \tag{4}$$

Here S_1 indicates the enrichment of the first carbon atom in the substrate and S_2 indicates the enrichment of the second carbon atom in the substrate (similarly for A_1 and A_2). The balances simply state that enriched carbon entering the first position in the metabolite pool A balance the enriched carbon in the first position leaving this metabolite pool. Similar to (3) and (4) balances can be written for all metabolites. This is expressed in the matrix formulation (5):

$$\begin{pmatrix} -(v_2+v_3) & 0 & 0 & 0 & 0 & 0 \\ 0 & -(v_2+v_3) & 0 & 0 & 0 & 0 \\ v_3 & 0 & -v_6 & 0 & v_4 & 0 \\ 0 & v_3 & 0 & -v_6 & 0 & v_4 \\ 0 & v_2 & 0 & 0 & -(v_4+v_5) & 0 \\ v_2 & 0 & 0 & 0 & 0 & -(v_4+v_5) \end{pmatrix} \begin{pmatrix} A_1 \\ A_2 \\ B_1 \\ B_2 \\ C_1 \\ C_2 \end{pmatrix} = \begin{pmatrix} -100S_1 \\ -100S_2 \\ 0 \\ 0 \\ 0 \\ 0 \end{pmatrix} \tag{5}$$

Equation (5) can be used to calculate the fluxes, but they cannot be obtained directly from the matrix equation which is nonlinear due to the occurrence of products of fluxes and labeling. However, the matrix has full rank, and if the fluxes are given, the ^{13}C enrichment can be calculated by a simple matrix inversion. This is the basis for the iterative method of Fig. 5.14.

As discussed in Example 5.10, estimation of the fluxes is not straightforward and it requires a robust estimation routine. One approach to estimate the fluxes is illustrated in Fig. 5.14, but other approaches have been described in the literature (see, e.g., Wiechert (2001)). Instead of using the fractional labeling of the metabolites one may also directly calculate the NMR spectra that would arise for a given isotopomer distribution and then compare the calculated NMR spectra with the experimentally determined spectra. Schmidt et al. (1999) used this approach for estimation of the fluxes in *E. coli* based on experimental NMR data. A requirement for any estimation procedure is a mathematical model describing the carbon transitions, and including all relevant biochemical reactions in the network. The carbon transitions for most biochemical reactions are described in biochemical textbooks, and procedures to implement these carbon transitions in a formalized way have been developed (Zupke and Stephanopoulos (1995); Schmidt et al. (1997); Wiechert et al. (1997); Antoniewicz et al. 2007). Although there are good procedures for estimation of the fluxes, it is still important to specify the correct model structure, and in many cases it is necessary to evaluate different model structures in order to identify a proper network that fits the experimental data. In these cases, the network identification and flux quantification goes hand in hand.

When a proper model has been identified it is possible to estimate the fluxes through the different branches of the central carbon metabolism. In the literature one may find several examples of the use of ^{13}C-labeled data to estimate the metabolic fluxes (see, e.g., Christensen and Nielsen 2000). However, the real value of such metabolic flux maps lies in the *flux differences* that are observed when flux maps obtained with different strains or under different conditions are compared with one another. Through such comparisons the impact of genetic and environmental perturbations can be fully assessed, and the importance of specific pathways, or reactions within a given pathway can be accurately described. Hereby, new insight into the function of the different pathways may be obtained, and this can be used to guide metabolic engineering.

Problems

Problem 5.1. *Equation (1) of Example 5.1 relates the four rates* $[r_x, r_{HAc}, r_e, r_{HLac}]$ *by two linear equations*. In the example $\boldsymbol{r_m} = [r_x, r_{HAc}]$ were chosen as the measured quantities and $\boldsymbol{r_c} = [r_e, r_{HLac}]$ were calculated. Any choice of two rates out of the four rates can be used to determine the remaining rates, but when there is an experimental error on the measured quantities the accuracy of the result may depend significantly on the choice of measured rates.

(a) For all six combinations of two rates in the measured rate vector, use the method of Note 5.4 to determine the condition number c_2 for the matrix $\boldsymbol{A}$ in $\boldsymbol{A}\,\boldsymbol{r_c} = \boldsymbol{r_m}$.

Can you explain from the structure of the flux diagram why the choice $[r_e, r_{HAc}]$ as measured rates leads to a particularly poor accuracy for $[r_x, r_{HLac}]$? Compare with the calculations in Note 5.4 based on two measured fluxes $\boldsymbol{v}_1$ out of the six fluxes in $\boldsymbol{v}$.

(b) Also compare the best result obtained in the present problem with that of Note 5.4 when four fluxes out of the 6 were contained in $\boldsymbol{v}_1$. This will illustrate why the method of Example 5.1 has some definite advantages to the method of (5.11)–(5.12).

(c) Your measurement of the components of $\boldsymbol{r_m} = [r_e, r_{HAc}]$ has two digits accuracy. How many digits can you trust in the components of $\boldsymbol{r_c} = [r_x, r_{HLac}]$? As an example you may try $[r_e, r_{HAc}] = [0.60, 0.45]$.

Answer to (a):

$\boldsymbol{r_m}$	$[r_x, r_{HAc}]$	$[r_x, r_e]$	$[r_x, r_{HLac}]$	$[r_e, r_{HLac}]$	$[r_{HAc}, r_{HLac}]$	$[r_e, r_{HAc}]$
c_2	3.37	8.04	1.77	4.56	4.53	123.6

Except for the very small NADH production in the biomass equation the NADH balance closes with the contribution $-1/2$ from ethanol and 1/2 from HAc. Therefore, the choice of $[r_e, r_{HAc}]$ as $\boldsymbol{r_m}$ is unfortunate.

Answer to (c): The measurement accuracy is 0.01, and consequently you can expect errors up to 1.2 in $\boldsymbol{r_c}$. Insert in $0.5 \times 10^{-a} \leq 1.2$ to obtain $a \leq 0.39$. Hardly one digit is correct.

For $[r_e, r_{HAc}] = [0.60, 0.45]$ one obtains an *expected*

$$[r_x, r_{HLac}] = \begin{bmatrix} 0.1 & 0 \\ 2 & -1/3 \end{bmatrix}^{-1} \cdot \begin{bmatrix} 1/2 & -1/2 \\ 1/2 & 1 \end{bmatrix} \cdot \begin{bmatrix} r_e \\ r_{HAc} \end{bmatrix}$$

$$= \begin{bmatrix} 5 & -5 \\ 28.5 & -33 \end{bmatrix} \begin{bmatrix} r_e \\ r_{HAc} \end{bmatrix} = \begin{bmatrix} 0.75 \\ 2.25 \end{bmatrix}$$

If $[r_e, r_{HAc}] = [0.59, 0.46]$ then $[r_x, r_{HLac}] = [0.65, 1.63]$ which fits with the result above.

Problem 5.2 *Determination of stoichiometric coefficients in the biomass pathway reaction for S. cerevisiae.* Assume that the metabolic pathway model corresponding to Example 3.8 can be approximated by the following three pathway reactions:

$$v_1 : -(1+\alpha)\mathrm{CH_2O} + \alpha\ \mathrm{CO_2} + \beta\ \mathrm{NADH} + \mathrm{CH_{1.61}O_{0.52}N_{0.15}} - \gamma\ \mathrm{ATP} = 0$$

$$v_2 : -1.5\ \mathrm{CH_2O} + 0.5\ \mathrm{CO_2} + \mathrm{CH_3O_{0.5}} + 0.5\ \mathrm{ATP} = 0$$

$$v_3 : -\mathrm{CH_2O} + \mathrm{CH_{8/3}O} - 1/3\mathrm{ATP} - 1/3\mathrm{NADH} = 0$$

Determine the value of α, β and γ in the first reaction as functions of Y_{xg} and Y_{sx}. (Answer: $\alpha = (1/6)Y_{\mathrm{xg}} + 0.03$ and $\gamma = (1/3)Y_{\mathrm{xs}} - (13/18)Y_{\mathrm{xg}} - 0.343$).

Consider the set of experimentally obtained yield coefficients in (3.23). Determine numerical values of α and γ for this data set.

The yield coefficients of (3.23) were obtained for a slightly different composition of the biomass. Determine α and γ with the biomass composition used in (3.23) and discuss the sensitivity of the result with respect to changes in κ_{x}. Also relate the present results with the discussion in Example 5.2 in which exactly the same data were used in the end. In Example 5.2 one reached the conclusion that γ is more likely to be 1.8 than the value found here. What is the reason for this different conclusion?

Problem 5.3 *The maximum theoretical yield of lysine on glucose.* In Problem 4.2 it was shown that a growth yield of 6/7 for L-lysine on glucose (Example 3.9) could not be excluded for thermodynamic reasons. In the present problem it will be shown that the explanation for the lower theoretical yield (3/4) – see references to Problem 4.2 – is to be found in the need for NADPH and not NADH in the synthesis of lysine from glucose. This will help you to appreciate that the crude definition of redox equivalents as "H_2" cannot always be used.

(a) Go through the biosynthesis pathway in *C. glutamicum* of L-lysine from 1 mol of pyruvate and 1 mol of phosphoenolpyruvate. For each step write down the chemical formula for the intermediate and the amount of redox units harbored in the compound. Show that the net consumption rate of CO_2 and of 2-oxoglutarate is zero, and that four NADPH is consumed while two NADH is produced for each mole of L-lysine produced from glucose. Prove that this leads to a theoretical yield of 3/4 C-mole lysine (C-mol glucose)$^{-1}$, and that 1/6 O_2 must be used for each C-mole lysine produced.

(b) Can any of the NADPH requiring enzymes in the pathway from glucose to lysine possibly be exchanged with an enzyme that uses NADH as cofactor? Or could an NADH producing enzyme be exchanged with an NADPH producing isoenzyme? What would be the possible thermodynamic consequences of exchanging the glutamate dehydrogenase encoded by GDH1 (using NADPH as cofactor) with the GDH2 encoded isoenzyme (using NADH to produce glutamic acid from 2-oxoglutarate)?

To solve this problem use the following references:

1. "Biochemical Pathways" ed. G. Michal, Spektrum Verlag, Berlin, 1999
2. "ExPASy-Molecular Biology Server, Subsection Biological Pathways"

   This reference is found at: http://www.expasy.ch.

Problem 5.4 *Production of solvents (acetone and butanol) by fermentation.* Reardon et al. (1987) and Papoutsakis (1984) have both studied anaerobic fermentations of butyric acid bacteria using metabolic flux analysis. We shall base our analysis of the primary metabolism of *C. acetobutylicum* on the simplified pathway scheme in Fig. 3 of Reardon et al. (1987), but the corresponding pathway scheme, Fig. 1 of Papoutsakis (1984), differs only in some minor details and could also have been used. Fig. 5.7 shows the branchpoints and reactions.

(a) For each reaction v_1 to v_{13}, write up the stoichiometry and include the ATP/NADH produced or consumed. For all carbon-containing compounds the stoichiometry should be on the basis of one C-mole consumed. Reactions (7)–(9) and (12) do not involve any NADH/NAD^+ conversion. 0.25 ATP is liberated per C-mole converted in reaction (12), and 0.25 ATP is consumed per C-mole converted in reaction (9). Reactions (7), (8), (10), (11), and (13) do not involve ATP/ADP conversion.

   Assume that $r_{pyr} = r_{AcCoA} = r_{AcetoAcCoA} = r_{BuCoA} = r_{NADH} = r_{ATP}$ are all zero. Determine the minimum number of measurements needed to observe the system.

(b) Use the general flux-analysis method (5.11)–(5.12) to solve the problem, assuming that $r_{pyr} = r_{AcCoA} = r_{AcetoAcCoA} = r_{BuCoA} = r_{NADH} = r_{ATP}$ are all zero Show that the system is observable if r_s, r_x, r_e, r_{acn}, r_{HBu}, r_{ac}, and r_b are the measured rates. Calculate the remaining nonzero rates as linear combinations of the measured rates. Compare with the result of Example 5.4.

(c) If v_8 is set to zero, none of the metabolites that are progenies of AcetoAcCoA are formed. If, furthermore, $v_7 = 0$ the whole network is the one considered in Example 5.1. Show that the expressions for r_{HAc}, r_{Hlac}, and r_c are the same as in Example 5.1 if $r_{H_2} = 0$.

(d) Reardon et al. (1987), Fig. 4, gives some results from a batch fermentation carried out at pH = 6. Between 10 and 15 h after the start of the batch the glucose concentration s and the concentrations of HAc, HBu, and cells are all fitted well by linear functions of fermentation time. Virtually no acetoin, lactate, ethanol, acetone, or butanol is produced. CO_2 and H_2 production were not measured. The following concentration changes can be read from the figure (with at least 5% uncertainty) for the 5-h period:

Glucose	-117 mM ($=-21.1$ g L^{-1})
HBu	76 mM ($=6.69$g L^{-1})
HAc	55 mM ($=3.30$g L^{-1})
Biomass	3.3 (g DW) L^{-1}

Calculate from the answer to (b) the amount of HAc that should be produced when the other rates are as stated above. Note that the result fits remarkably well with the experimentally determined r_{HAc}. Next calculate the amounts of H_2 and CO_2 liberated between 10 and 15 h of fermentation time. Check that $r_{\mathrm{HLac}} \approx 0$ to within the accuracy of the data.

(e) Between 15 and 20 h of fermentation time, biomass growth appears to stop [a decrease in x is even indicated in Reardon et al. (1987), Fig. 4]. Reardon et al. obtained the following changes in concentrations:

Glucose	−93 mM
HBu	50 mM
HAc	35 mM
Acetoin	4.5 mM
Acetone	8 mM
Butanol	12 mM
Ethanol	2 mM

Do these data fit the metabolic model of (b)? If not, give a reasonable physiological explanation for the lack of fit of, e.g., the carbon balance. Why is no extra biomass formed?

Reardon et al. (1987) notice a sharp increase in culture fluorescence after 15 h. They tentatively explain this by an increase in NADH concentration in the cells. If this is true, does it point to other flaws in the model of (b) after 15 h?

(f) Papoutsakis (1984) cites some very old (1930) data from van der Lek for a typical "solvent type fermentation" of *C. acetobutylicum*. The biomass production is not stated, but for 100 mol (18 kg) of glucose fermented the following amounts (in moles) of metabolic products are found:

HBu	4.3
HAc	14
H_2	139
CO_2	221
Acetoin	6.3
Acetone	22.4
Butanol	56
Ethanol	9.3

Use the calculated expression in (b) for r_{HAc} to eliminate r_{x} from the expressions for $r_{\mathrm{H_2}}$ and r_{c} in (b) and check whether the model in (b) gives a satisfactory prediction of $r_{\mathrm{H_2}}$ and r_{c}.

(g) In the pathway diagram two reactions used by Reardon et al. (1987) in their Fig. 3 have been left out. These reactions are:

$$-\mathrm{BuCoA} - 0.5\ \mathrm{HAc} + 0.5\ \mathrm{AcCoA} + \mathrm{HBu} = 0 \qquad (v_{14})$$

$$-\mathrm{AcetoAcCoA} - 0.5\,\mathrm{HAc} + 0.5\,\mathrm{AcCoA} + 0.75\ \mathrm{ac}$$

$$-0.25\ \mathrm{CO_2} - 0.25\ \mathrm{ATP} = 0 \quad (v_{15})$$

Reaction (14) is a parallel reaction to reaction (12), but without release of ATP. Reaction (15) is a parallel reaction to reaction (9) where the CoA is transferred to acetate rather than to butyrate. Expand the stoichiometric calculation in b with these two reactions. Obviously, two more rates have to be measured – but can you solve for the remaining rates? Discuss the result, referring to the paper by Reardon et al. to see what they have done. Recalculate the result of b with reaction (15) instead of reaction (9).

Final note: The present problem is very suitable for studies of pathway analysis in real industrial processes. Both Papoutsakis (1984) and Reardon et al. (1987) have many suggestions for further variations of the problem – e.g., abandoning the assumption of $r_{NADH} = 0$ or of $r_{ATP} = 0$. The papers should be consulted for these additional possibilities. In recent years, a number of studies, especially in the group of Terry Papoutsakis has shown that both yield (of solvents) and productivity can be improved by metabolic engineering of the pathway. Hereby it may become economically viable to resurrect the old (First World War) process of making solvents by fermentation of house hold waste.

Problem 5.5 *Production of propane 1,3-diol (3G) by fermentation.* Zeng and Biebl (2002) reviewed the possibilities of making 3G by a fermentation route. The diol can be produced by several chemical routes from either ethylene (Shell) or from acrolein (Degussa), but it may be cheaper to produce it by fermentation using either glycerol or the much cheaper glucose as substrate. An enormous increase in demand for 3G is envisaged, especially since it can condense with terephtalic acid to form an excellent polyester (Sorona™ from DuPont). See also the patent by Emptage et al. (2001).

3G is a natural metabolic product in anaerobic cultivation of *Klebsiella pneumonica* on glycerol:

$$\text{Glycerol} \rightarrow 3 \text{ Hydroxy propanal} \rightarrow 1,3 \text{ Propane diol} \qquad (1)$$

The first step (a dehydration) is catalyzed by glycerol dehydratase that requires vitamin B_{12} as cofactor. Step 2 is catalyzed by 1,3 propane diol dehydrogenase, and NADH is used as cofactor.

When *Klebsiella* grows on glycerol the two steps (see Figure 5.1) from DHAP to glycerol are reversed. One ATP and one NAD^+ are used per glycerol molecule. DHAP enters the EMP pathway and via pyruvate it is metabolized to all the end products shown in Fig. 2.5a (actually a pathway from pyruvate to 2,3 butane diol via α-acetolactate and acetoin can also be followed, but this will not be considered here).

(a) Determine the maximum theoretical yield of 3G on glycerol by anaerobic fermentation with *Klebsiella*. The analysis should be based on the constraints $r_{NADH} = r_{ATP} = 0$. Which end products of the mixed acids from pyruvate metabolism are desirable and which should if possible be avoided?

(b) *Klebsiella* is not the optimal production organism. In a series of brilliant metabolic engineering studies (covered by many patents), DuPont and Genencor have succeeded to insert the pathway from DHAP to glycerol (from *S. cerevisiae*)

and from glycerol to 3G (from *Klebsiella*) into *E. coli*. Hereby, a well-researched organism is used as host for production of 3G and it has been shown that a very high titer of 129 $g\,L^{-1}$ 3G can be obtained by fed-batch fermentation of the engineered *E. coli* (Emptage et al. 2001).

We shall study the DuPont/Genencor process in the following. Three pathways from glucose are considered:

v_1:	Glucose $\rightarrow$ biomass ($CH_{1.8}O_{0.5}N_{0.2}$) by: $-1.1CH_2O + 0.1CO_2 + X + 0.1NADH - 2.42ATP = 0$
v_2:	Glucose $\rightarrow 3G + \alpha NADH + \beta ATP$
v_3:	Glucose $\rightarrow CO_2 + 2NADH + \varepsilon ATP$ (via the EMP pathway and the TCA cycle)
v_4:	$NADH + 12/2O_2 \rightarrow$ P/O ATP

Determine α and β in v_2 when no ATP is produced or consumed from glycerol to 3G

Assume that no glycerol is excreted and that Y_{so} is 0.045 mol O_2 (C-mol glucose)$^{-1}$. Determine the stoichiometry (the "black box" model) for the overall reaction based on the assumption that $r_{NADH} = r_{ATP} = 0$, and P/O = 2. What is the lowest value of P/O for which biomass can be produced?

(c) Assume that (the very small) Y_{sx} can be set to zero. Show that it is now possible to calculate both Y_{sp} and Y_{so} based on knowledge of the P/O ratio. (*Answer*: $Y_{so} = \frac{1}{12P/O+3}$ and $Y_{sp} = \frac{6P/O+1}{8P/O+2}$ for $\varepsilon = Y_{sATP} = !/3$ in v_3).

In this way, the effect of using a more realistic value than 2 for P/O can be studied.

(d) Again assume that $Y_{sx} = 0$ and that some glycerol is excreted from the cells. Glycerol is of course an unwanted byproduct and we wish to study the influence of Y_{sg} on the product yield. Show that

$$Y_{sp} = \text{C - mole 3G (C - mol glucose)}^{-1} = \frac{6P/O + 1 - (2 + 7P/O)Y_{sg}}{8P/O + 2}$$

$$Y_{so} = \frac{1 + 0.5Y_{sg}}{12P/O + 3}$$

Calculate the reduction of Y_{sp} compared with what is found in question (c) when $Y_{sg} = 0.05$ and 0.1.

(e) Return to the stoichiometry of question (b). with P/O = 2 (overall reaction (1)). In parallel with the glucose used to feed this carbon-, redox-, and ATP-balanced set of pathways that determines production of 3G some glucose may be used to produce biomass and CO_2 by pure respiration, and for maintenance of cells by combustion of glucose to CO_2 alone. Write a carbon-, redox-, and ATP-balanced metabolic scheme for purely respiratory biomass production (overall reaction (2)), and a carbon- and redox-balanced stoichiometry for the maintenance reaction (overall reaction (3)).

Show that any experimentally obtained stoichiometry containing only X, 3G, and CO_2 can be written as a linear combination of the three overall stoichiometries.

Use P/O = 2 in overall reaction (2) and determine the contribution of the 3 overall stoichiometries to give the experimentally observed stoichiometry:

$$-\mathrm{CH_2O} + 0.543\mathrm{P} + 0.120\mathrm{X} + 0.337\mathrm{CO_2} - 0.15\mathrm{O_2} = 0$$

(*Answer*: The experimentally observed stoichiometry is obtained by combining overall reactions (1)–(3) in the ratio 0.7714:0.1738:0.0548).

The maintenance demand is significant, but not alarming. There is probably a kinetic bottleneck in the pathway v_2 from glucose to 3G which causes overflow to (useless) biomass formation. This needs to be looked at as a part of the physiological design of the final production strain.

References

Aiba, S., Matsuoka, M. (1979) Identification of metabolic model: Citrate production from glucose by *Candida lipolytica*. *Biotechnology and Bioengineering*., **21**, 1373–1386.

Albers, E., Larsson, C., Liden, G., Niklasson, C., Gustafsson, L. (1996) Influence of the nitrogen source on *Saccharomyces cerevisiae* anaerobic growth and product formation. *Appl. Environ. Microbiol*., **62**, 3187–3195.

Albers, E., Liden, G., Larsson, C., Gustafsson, L. (1998) Anaerobic redox balance and nitrogen metabolism in *Saccharomyces cerevisiae*. *Rec. Res. Devel. Microbiol*., **2**, 253–279.

Antoniewicz, M.C., Kelleher, J.K, and Stephanopoulos, G. (2007). Elementary metabolite units (EMU): A novel framework for modelling isotopic distributions, *Metabolic Eng*., **9**, 68–86.

Bauchop, T., Elsden, S. R. (1960) The growth of microorganisms in relation to their energy supply. *J. Gen. Microb*., **23**, 35–43.

Benthin, S. (1992) Growth and Product Formation of *Lactococcus cremoris,* Ph.D. thesis, Department of Biotechnology, Technical University of Denmark, Lyngby.

Benthin, S., Nielsen, J., Villadsen, J. (1991) Characterization and application of precise and robust flow-injection analysers for on-line measurements during fermentations. *Anal. Chim. Acta*, **247**, 45–50.

Benthin, S., Schulze, U., Nielsen, J., Vlladsen, J. (1994) Growth energetics of *Lactococcus cremoris* FD1 during energy-, carbon- and nitrogen-limitation in steady state and transient cultures. *Chem. Eng. Sci*., **49**, 589–609.

Brown, W. V., Collins, E. B. (1977) End product and fermentation balances for lactis Streptococci grown aerobically on low concentrations of glucose. *Appl. Environ. Microbiol*., **59**, 3206–3211.

Christensen, B., Nielsen, J. (1999) Metabolic network analysis – powerful tool in metabolic engineering. Adv. Biochem. Eng./Biotechnol., **66**, 209–231.

Christensen, B., J. Nielsen, J. (2000) Metabolic network analysis on *Penicillium chrysogenum* using 13C-labelled glucose. *Biotechnol. Bioeng*., **68**, 652–659.

Christiansen, T., Nielsen, J. (2002) Growth energetics of an alkaline serine protease producing strain of *Bacillus clausii* during continuous cultivation. *Bioproc. Biosystems Eng*., **24**, 329–339.

Emptage, M., Haynie, S., Laffend, L., Pucci, J., Whited, G. (2001). Process for the biotechnological production of 1,3 propane diol with high titer. US patent application No. PCT/US 00/22874; cited in WO (World Intellectual Property Organization) 01/12833.

Hempfling, W. P., Mainzer, S. E. (1975) Effects of varying the carbon source limiting growth on yield and maintenance characteristics of *Escherichia coli* in continuous culture. *J. Bacteriol.*, **123**, 1076–1087.

Herbert, D. (1959). Some principles of continuous culture. *Recent Prog. Microb.*, **7**, 381–396.

Ingraham, J. L., Maaløe, O., & Neidhardt, F. C. (1983) Growth of the Bacterial Cell. Sunderland: Sinnauer Associated.

Kjeldsen, K.R and Nielsen, J. (2009) *In silico* genome-scale reconstruction and validation of the *Corynebacterium glutamicum* metabolic network.. *Biotechnol. Bioeng.*, **102**, 583–597.

Lengeler, J.W, Drews, G., and Schlegel, H.O. (1999) Biology of the prokaryotes. Thieme Verlag, Stuttgart.

Major, N. C., Bull, A. T. (1985) Lactic acid productivity of a continuous culture of *Lactobacillus delbrueckii*. *Biotechnol. Letters.*, **7**, 401–405.

Nielsen, J. (1997) Physiological Engineering Aspects of *Penicillium chrysogenum*. Singapore: World Scientific Publishing Co.

Nissen, T.L., Schulze, U., Nielsen, J., Villadsen, J. (1997) Flux distributions in anaerobic, glucose limited continuous cultures of *Saccharomyces cerevisiae*. *Microbiology*, **143**, 203–218.

Otto, R., Sonnenberg, A. S. M., Veldkamp, H., Konings, W. N. (1980) Generation of an electrochemical proton gradient in *Streptococcus cremoris* by lactate efflux. *Proc. Nat. Acad. Sci.*, **77**, 5502–5506.

Oura, E. (1983) Biomass from carbohydrates. In *Biotechnology,* H. Dellweg, ed., Vol. 3, 3-42. VCH Verlag, Weinheim, Germany.

Papoutsakis, E. T. (1984). Equations and calculations for fermentations of butyric acid bacteria. *Biotechnol. Bioeng.*, **26**, 174–187.

Pedersen, H., Carlsen, M., Nielsen, J. (1999) Identification of enzymes and quantification of metabolic fluxes in the wild type and in a recombinant strain of *Aspergillus oryzae* strain. *Appl. Environ. Microbiol.*, **65**, 11–19.

Pirt, S. J. (1965) The maintenance energy of bacteria in growing cultures. *Proc. Royal Soc. London. Series B*, **163**, 224–231.

Pramanik, J., Keasling, J. D. (1997) Stoichiometric model of *Escherichia coli* metabolism: Incorporation of growth-rate dependent biomass composition and mechanistic energy requirements. *Biotechnol. Bioeng.*, **56**, 398–421.

Reardon, K. F., Scheper, T. H., and Bailey, J. E. (1987) Metabolic pathway rates and culture fluorescence in batch fermentations of *Clostridium acetobutylicum*. *Biotechnol. Prog.*, **3**, 153–167.

Sauer, U., Hatzimanikatis, V., Hohmann, H. P., Manneberg, M., van Loon, A. P. G. M., Bailey, J. E. (1996) Physiology and metabolic fluxes of wild-type and riboflavin-producing *Bacillus subtilis*. *Appl. Environ. Microbiol.*, **62**, 3687–3696.

Schmidt, K., Carlsen, M., Nielsen, J., Villadsen, J. (1997) Modelling isotopmer distributions in biochemical networks Using isotopomer mapping matrices. *Biotechnol. Bioeng.*, **55**, 831–840.

Schmidt, K., Nielsen, J., Villadsen, J. (1999). Quantitative analysis of metabolic fluxes in *E. coli*, using 2 dimensional NMR spectroscopy and complete isotopomer models. *J. Biotechnol.*, **71**, 175–190.

Senger, R. S. and Papoutsakis, E. T. (2008) Genome-scale model for *Clostridium acetobutylicum*: Part I Metabolic network resolution and analysis. *Biotechnol. Bioeng.*, **101**, 1036–1052.

Sonntag, K., Eggeling, L., de Graaf, A. A., Sahm, H. (1993) Flux partitioning in the split pathway of lysine synthesis in *Corynebacterium glutamicum* – Quantification by ^{13}C- and ^{1}H-NMR spectroscopy. *Eur. J. Biochem.*, **213**, 1325–1331.

Stouthamer, A. H. (1979) The search for correlation between theoretical and experimental growth yields. In *International Review of Biochemistry*: *Microbial Biochemistry*, Vol. 21, pp. 1–47. Edited by J. R. Quayle. Baltimore: University Park Press.

Stouthamer, A. H., Bettenhaussen, C. (1973) Utilization of energy for growth and maintenance in continuous and batch cultures of microorganisms. *Biochim. Biophys. Acta*, **301**, 53–70.

Vallino, J. J., Stephanopoulos, G. (1993) Metabolic flux distributions in *Corynebacterium glutamicum* during growth and lysine overproduction. *Biotechnol. Bioeng.*, **41**, 633–646.

Vallino, J. J., Stephanopoulos, G. (1994a) Carbon flux distributions at the pyruvate branch point in *Corynebacterium glutamicum* during lysine overproduction. *Biotechnol. Prog*., **10**, 320–326.

Vallino, J. J.; Stephanopoulos, G. (1994b) Carbon flux distributions at the glucose-6-phosphate branch point in *Corynebacterium glutamicum* during lysine overproduction. *Biotechnol. Prog*., **10**, 327–334.

van Gulik, W. M., Heijnen, J. J. (1995) A metabolic network stoichiometry analysis of microbial growth and product formation. *Biotechnol. Bioeng*., **48**, 681–698.

Vanrolleghem P.A., and Heijnen J.J. (1998). A structured approach for selection among candidate metabolic network models and estimation of unknown stoichiometric parameters. *Biotechnol. Bioeng*., **58**, 133–138.

Verduyn, C., Postma, E., Scheffers, W. A., van Dijken, J. P. (1990) Energetics of *Saccharomyces cerevisiae* in anaerobic glucose limited chemostat cultures. *J. Gen. Microbiol*., **136**, 405–412.

de Vries, W., Kapteijn, W. M. C., van der Beek, E. G., Stouthamer, A. H. (1970) Molar growth yields and fermentation balances of *Lactobacillus casei* L3 in batch cultures and in continuous cultures. *J. Gen. Microbiol*., **63**, 333–345.

Wiechert, W. (2001) ^{13}C Metabolic Flux Analysis. Metabolic Eng., **3**, 195–206

Wiechert, W., Siefke, C., de Graaf, A. A., Marx, A. (1997) Bidirectional reaction steps in metabolic networks. Part II: Flux estimation and statistical analysis. *Biotechnol. Bioeng*. **55**:118–135.

van Winden, W., Verheijen, P., Heijnen, S. (2001) Possible pitfalls of flux calculations based on ^{13}C-labeling. *Metabolic Eng*., **3**, 151–162.

Zeng; An-Ping, and Biebl, H. (2002). Bulk chemicals from biotechnology: The case of 1,3 propane diol production and the New Trends. In *Advances in Biochemical Engineering Biotechnology*, **74,** 239**–**259.

Zupke, C., Stephanopoulos, G. (1995) Intracellular flux analysis in hybridomas using mass balances and *in vivo* ^{13}C NMR. *Biotechnol. Bioeng*., **45**, 292–303.

Chapter 6
Enzyme Kinetics and Metabolic Control Analysis

In all probability, the reader of this text has encountered the action of individual enzymes long before becoming aware of the concerted action of the many enzymes that together determine the flow of substrates through metabolic pathways of living cells. It could have been in high school experiments where catalase was used to liberate O_2 from H_2O_2, or by studying how "the enzyme pellets" from a box of a commercial detergent product "dissolved" starch grains.

This chapter will outline the *mechanism* of individual enzyme reactions – for in contrast to microbial reactions, the mechanism can often be derived quite rigorously.

Biocatalysis[1] is concerned with the production of often very complex molecules, using one or a combination of a few enzymes that have been harvested and purified from the medium of microbial fermentations. Although the application of industrial enzymes in biocatalysis is not a core subject of our text, the fundamental mechanism of important enzyme-catalyzed reactions will be discussed, and how the kinetics of one particular enzyme, a carbohydrate oxidase used to oxidize the glucose part of lactose to form lactobionic acid, was derived in the laboratory is shown in an example. Enzyme deactivation is discussed as an important topic in biocatalysis, and it is shown that the influence of physical transport processes may well distort the results of a purely kinetic study. Furthermore, the study of enzyme kinetics will lead to an understanding of the *sensitivity* of pathway enzymes to changes in substrate concentrations and of the concentration, or *activity* of individual pathway enzymes. The *flux* through the pathway and the sensitivities are used in *Metabolic Control Analysis* (MCA) which leads to important results concerning the possibility of enhancing, by genetic engineering, the carbon flux through a pathway, or to redirect the flux to another pathway.

Chemical reactions catalyzed by enzymes are not much different from, e.g., dehydrogenation reactions catalyzed by noble metal catalysts. There is only one reaction to be considered rather than the myriad of reactions that take place in the metabolic network of cells, and the stoichiometry of the reaction is known. As we

[1] The terms *Bioconversion*, *Biotransformation*, or *Enzymatic catalysis* are also used.

J. Villadsen et al., *Bioreaction Engineering Principles*,
DOI 10.1007/978-1-4419-9688-6_6,

have seen in Chaps. 3 and 5, the study of stoichiometry and of the steady-state flux distribution in a metabolic network is a difficult task, and it must necessarily be done before any meaningful investigation of the kinetics of cellular reactions can be started. Enzymes are usually highly specific catalysts that allow only one form of the substrate (reactant) to be treated – e.g., the L- but not the D-form of an enantiomer. Structural studies of the enzymes reveal how the substrate docks on the catalyst, where the cofactor sneaks in, and how the product is detached. *Inhibition* or *deactivation* of enzymes follows the same rules as those developed for inhibition or irreversible poisoning of inorganic catalysts. One can explain why overloading of the enzyme with substrate, or blocking of the enzyme activity by a reaction product or with a foreign molecule can reduce the rate of conversion of the substrate. In short, the enzymatic reaction can, if desired, be treated by mechanistic models to obtain the true kinetics of the reaction. Although enzymes usually are substrate specific, one should be aware that there are several examples where one enzyme in fact catalyzes the same kind of reaction for many chemically similar substances. Different aldehydes may, for instance, be reduced to their corresponding alcohols by the same reductase. This is not necessarily a design flaw by nature, but may provide a "cost-effective" means of removing reactive aldehydes and thereby protect the cell (Jin and Penning 2007).

The treatment of enzyme kinetics in this chapter is, as indicated above, in sharp contrast to the wholly empirical approach that will be used in Chap. 7 to obtain the kinetics of cell reactions. Here, the outcome of the modeling exercise has limited predictive power, and the apparent kinetics may be quite different for steady state and for transient studies.

Quite apart from the pedagogical qualities of studying enzyme reactions which give new insights for readers of classical textbooks on reaction engineering (e.g., Levenspiel (1999) and Scott Fogler (2006)), the subject has, of course, enormous significance for modern biotechnology.

Enzymes (rather than living cells) are used in a multitude of processes, in industry and in the daily household, and enzyme-based processes are replacing many classical processes due to the mild reaction conditions and environmental-friendly outcome. Companies such as Novozymes and Genencor, two dominant players on the enzyme market, are entirely devoted to the production of enzymes by fermentation processes and their application. The market (more than 3.5 billion US $ in 2009) is expanding, and new applications of enzymes, e.g., in second generation bio-ethanol, contribute to the substantial revenues of the enzyme producers.

The main theme of our textbook is the cellular reaction for which the kinetics is treated in Chap. 7. It is impossible to treat the kinetics of cellular reactions solely on the assumption of known kinetics for all the enzyme reactions in the cell – even if the kinetics could be found by in vitro studies. The cell is much more "than a bag of enzymes," and in vitro studies of enzyme kinetics tell nothing about the influence of the control structure of the cell, which is destroyed when the enzymes are investigated outside their natural habitat.

Still, the apparent analogies between enzyme kinetics and cell kinetics have often been used to suggest the right structure of kinetic expressions for the conversion of substrates by a living cell. This alone is a good reason for giving a short treatment of enzyme kinetics. Furthermore, enzyme-based assays are used routinely to study the state of the cell at a certain set of environmental conditions. Some of these assays are not easily understood without prior knowledge of the behavior of the enzymatic reaction on which the assay is based.

Finally, when continuing from the steady-state flux distribution in a metabolic network to an analysis of the *rate* of production supported by the network, one must include a kinetic analysis of the different enzymatic reactions in the network. The outcome of this analysis is a prediction of how genetic manipulations of the network can lead to a change in the flux distribution and perhaps to a higher yield and a higher production rate of the desired product in a given branch of the network. Consequently, enzyme kinetics will be treated with a view to analyze the rates of production in different branches of a metabolic network. The analysis is based on the sensitivity of each enzymatic reaction in a particular pathway to changes in the activity of each of the pathway enzymes and to changes in the metabolite levels at the different steps.

The activity of a given enzyme is a function of a number of environmental factors, e.g., temperature and pH. Many enzyme preparations are sold as particles of immobilized enzymes in a support. Here, mass transport and chemical reaction both play a role in the overall reaction rate, as is well known for conventional chemical reactions. It, therefore, becomes important to analyze when mass transport is likely to influence the bioreaction mediated by the enzyme. This subject is discussed in Sect. 6.3.2. The influence of transport limitation on immobilized *cells* is shortly discussed in Chap. 10 (Problem 10.4) by analogy with the treatment of immobilized enzymes in this chapter. When yeast cells are embedded in an inert matrix, and the biomass concentration is assumed to be constant throughout the matrix, there is, in principle, no difference between the behavior of this system and an immobilized glucose isomerase or penicillin deacylase embedded in a porous polymer matrix. The difference is the continuing growth of more biomass in the matrix, and diffusion resistance may eventually cause the cells to die from lack of nutrients.

6.1 Enzyme Kinetics Derived from the Model of Michaelis–Menten

When the rate r[2] of an enzymatic reaction is pictured as a function of the substrate concentration s, the result is often of the form of Fig. 6.1.

[2] The symbol r will be used for volumetric production rates rather than q, the symbol used for volumetric production rate in cell cultivations. In the context of enzyme reactions with suspended or immobilized enzyme particles, the reactor vessel *is*, in fact, the real reactor.

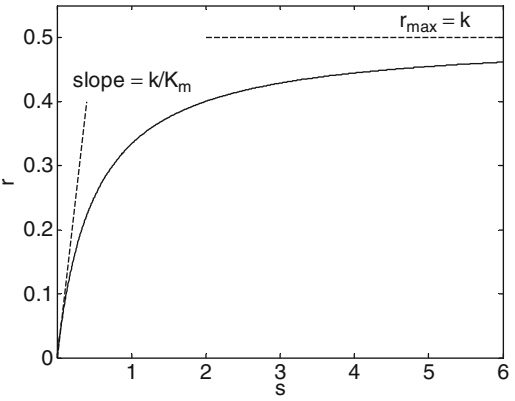

Fig. 6.1 Schematic representation of the rate r of an enzymatic reaction. s is the substrate concentration (typical unit: g substrate (L medium^{-1}) and r is the rate of conversion of s

The shape of Fig. 6.1 with proportionality between r on s for small s, and a final, maximum rate of conversion $r_{\max}$ for large s is well correlated by the following expression:

$$r = \frac{ks}{s + K_m} = \frac{k_0 e_0 s}{s + K_m} \tag{6.1}$$

The substrate concentration s is in units of g (or mole) substrate (L medium)$^{-1}$.

The reaction rate r is as mentioned above specified in units of g substrate converted (L medium h)$^{-1}$. In chemical catalysis the rate is often specified in units of g converted (g catalyst h)$^{-1}$.

Here, r/e_0 with e_0 in units of g enzyme (L medium)$^{-1}$ has the same unit, g (g enzyme h)$^{-1}$, used in heterogeneous catalysis, and it corresponds to the specific rates $-r_s$ elsewhere in the text. But the whole literature on enzyme kinetics is based on conversion of substrate per unit reactor volume, corresponding to the $-q_s$ defined in Chap. 3 of our text. We shall follow this standard nomenclature in biocatalysis. Consequently, k is in units of, e.g., g substrate converted (L medium h)$^{-1}$. e_0 is in units of g enzyme preparation (L medium)$^{-1}$, and finally, k_0 is in units of g substrate converted (g enzyme preparation h)$^{-1}$.

In practical investigations of enzymatic reactions, only k is determined, and it signifies the maximum value of r, or $r_{\max.}$ The rate r actually depends on the *activity* of the enzyme per g of enzyme preparation, and splitting k into two factors k_0 and e_0 indicates that an enzyme with a low activity per unit mass of enzyme will lead to a low rate of conversion of the substrate.

We shall now turn to the derivation of a few classical mechanisms for enzyme reactions.

In 1925 Briggs and Haldane derived the form of (6.1) by mechanistic modeling. They considered that the enzyme could exist in two forms: E = free enzyme, and ES = an enzyme complex with the substrate. The conversion of substrate S to product P proceeds in two steps:

$$E + S \underset{k_{-1}}{\overset{k_1}{\rightleftarrows}} ES \xrightarrow{k_2} E + P \tag{6.2}$$

The first reaction is reversible and the second irreversible. Both reactions are assumed to be elementary reactions with rate proportional to the concentration of reactants. Furthermore, Briggs and Haldane assumed that the concentration (es) of ES was constant in time, i.e., ES is in a "pseudo-steady state."

$$\frac{\mathrm{d}(es)}{\mathrm{d}t} = 0 = k_1 e \times s - k_{-1}(es) - k_2(es) \tag{6.3}$$

The total enzyme "concentration" e_0 was assumed to be constant and representing the "activity" in (6.1)

$$e_0 = e + (es) \tag{6.4}$$

From (6.3),

$$(es) = \frac{k_1 e_0 s}{k_1 s + (k_{-1} + k_2)} = \frac{e_0 s}{s + \frac{k_{-1}+k_2}{k_1}} \tag{6.5}$$

The rate of the reaction is determined by the decomposition of ES (i.e., the first reaction is much faster in both directions than the second), and if ES decomposes by a first-order reaction, then

$$r = k_2(es) = \frac{k_2 e_0 s}{s + \frac{k_{-1}+k_2}{k_1}} = \frac{k_2 e_0 s}{s + K_\mathrm{m}} \tag{6.6}$$

Michaelis and Menten (1913) immediately assumed that the first reaction of (6.2) is infinitely fast and also that the substrate concentration s is much higher than the total enzyme concentration e_0, i.e., that all the catalytic sites on E are occupied. The concentration of the enzyme–substrate complex is

$$(es) = \frac{e \times s}{K_\mathrm{eq}} \tag{6.7}$$

where K_eq is the equilibrium constant for the dissociation of ES to E and S. Inserting (6.4) in (6.7) and again assuming first-order decomposition of ES by the second, rate determining reaction,

$$r = \frac{k_2 e_0 s}{s + K_\mathrm{eq}} \tag{6.8}$$

The derivation of (6.8) by Michaelis and Menten signified the start of quantitative enzymology. A corresponding, fundamental mechanism of heterogeneous catalytic reactions was first derived in 1918 by Langmuir in analogy with the derivation of (6.8). The strict equilibrium assumption for step 1 of (6.2) was relaxed by Briggs and Haldane (1925), who used a similarly speculative hypothesis of pseudo-steady

state for *ES*. Both models – which typically for mechanistically based models can assign a definite physical meaning to the parameters – lead to (6.1), where K_m is called the Michaelis constant in honor of the recognized "father" of enzymology.[3] The picture of K_m as an equilibrium constant for a dissociation reaction according to (6.8) is illustrative: A substrate that is easily captured by the enzyme (the enzyme has a high affinity for the substrate) will have a small K_m value. If k_2 is large – i.e., if the rate of the second reaction in (6.2) is high, then the rate of conversion of the substrate by the enzyme is high, also at low values of s.

Note 6.1 *Assumptions in the mechanistic models for enzyme kinetics.* The simplicity of the derivation of the two mechanistically based models for the rate of an enzyme reaction could lead the reader to believe here that, for once, there is a trustworthy piece of modeling in biotechnology. Indeed, the rate expression (6.1) is very robust – much more so than the apparently equivalent Monod model for cell kinetics discussed in Chap. 7. It allows for a significant extrapolation from the data that are used to determine the two parameters k and K_m, and the parameters are clearly related to stringently defined parameters of elementary reactions. Still, it may be useful to give a few comments to illustrate the effect of the approximations that lurk behind both the Michaelis–Menten and the Briggs–Haldane derivation of (6.1). First of all, the comments given below may help the user to avoid mistakes in an experimental set-up that is aimed to determine the two kinetic parameters.

First, one can easily see that the derivation of (6.6) leads to the same result as that of (6.8) if, indeed the first step of (6.2) is an equilibrium reaction. Then, both k_{-1} and k_1 in (6.2) are infinitely large and the ratio $k_{-1}/k_1 = K_m$ is equal to the equilibrium constant K_{eq} of (6.7) and (6.8). Also, the assumption of (6.3) that (es) is constant is true. The amount of *ES* consumed by the second step of (6.2) is immediately replenished by the fast equilibrium reaction in step 1.

But (6.1) is also derived by (6.2)–(6.6) without the apparently unnecessary assumption of a fast equilibrium – the value of K_m must only be interpreted differently. How trustworthy is the assumption of quasi-steady state of (es)? Clearly, if all three rate constants k_1, k_{-1}, and k_2 are small, it may take a very long time before (es) becomes constant. In fact, (6.3) can easily be integrated by separation of variables for a constant s, and (es), can therefore, be found as a function of time. When $es(t)$ is inserted in the overall rate expression (6.6), one obtains

$$r = \frac{k_2 e_0 s}{s + K_m}\left(1 - \exp[-(k_1 s + k_{-1} + k_2)t]\right) \tag{1}$$

It is well established that k_{-1}, k_2, and $k_1 s$ are very large, 100–1,000 s^{-1} for normal enzymes, and the exponential function vanishes within milliseconds, before s has started to decrease from its initial value.

[3] In the 1920s, both Leonor Michaelis (1875–1949) and Maud Menten (1879–1960) emigrated to USA to take up distinguished academic careers. The Canadian born Maud Menten was among the first female Canadians to take an M.D. (Chicago, 1911) and she took a Ph.D. (1916) with Michaelis in Berlin. The German born Michaelis ran afoul of one of the icons of German physiology by criticizing his (probably fraudulent, but popular during the Third Reich) test for genetically inherited mental syndromes. The German career of Maud Menten might not either have looked very bright when Michaelis left Germany in 1922.

A much more serious criticism of both the Michaelis–Menten and the Briggs–Haldane mechanisms lies in the assumed irreversibility of the step 2 in (6.2). Since enzymes like other catalysts must, in principle, enhance the rate of both the forward and reverse reactions (but certainly not to the same degree – the product might not be able to dock on the enzyme), one must consider

$$E + S \underset{k_{-1}}{\overset{k_1}{\rightleftarrows}} ES \underset{k_{-2}}{\overset{k_2}{\rightleftarrows}} E + P \tag{2}$$

rather than (6.2). Assuming pseudo-steady state for ES yields

$$(es) = \frac{k_1 s + k_{-2} p}{k_{-1} + k_2 + k_1 s + k_{-2} p} e_0 \tag{3}$$

$$r = k_2(es) - k_{-2} p \cdot (e_0 - (es)) = \frac{k_1 k_2 s - k_{-1} k_{-2} p}{k_{-1} + k_2 + k_1 s + k_{-2} p} e_0 \tag{4}$$

Here $p = 0$ yields (6.6).

An enzymatic assay is made with no P initially, and until the product concentration p is built up (6.1) describes the rate of substrate consumption quite accurately. The overall reaction $S \rightarrow P$ may also be thermodynamically favored, which means that almost all S can be converted to P without any influence of the reverse reaction ($k_{-2}k_{-1} \approx 0$), and as we have seen in Chap. 4 an enzymatic reaction in a pathway can convert S to P also when the reaction has a small negative, or even a small positive ΔG^0 when P is sucked away from the equilibrium by further reactions. Consequently, when using models for enzyme kinetics in assays or in the analysis of pathway reactions, the simple form (6.1) is usually adequate.

This is not necessarily so when studying the enzymatic conversion of substrate in an industrial bioreactor. When glucose is converted to fructose in a commercial plug flow reactor using immobilized glucose isomerase, it is desired to come close to the equilibrium conversion (about 50% at 50–60°C) in order to obtain an adequate sweetening of the sugar solution. Calculation of the necessary amount of catalyst will be wildly wrong if (6.1) rather than (4) is used (Gram et al. 1990) – see Problem 6.8.

Finally, one may raise the objection to (6.2) that most enzymatic reactions need a second substrate to proceed. The cooperation of cofactors such as NAD^+/NADPH, $NADP^+$/NADPH, and ATP/ADP is seen in many of the pathway reactions of Chap. 2. It is tacitly assumed that these cofactors are regenerated by other cellular reactions, and that their level is fixed through constraints on redox charge or energy charge. But when planning to use a genetically engineered strain in which the balances between cofactors have been artificially changed (an $NADP^+$-dependent enzyme may have been exchanged with an NAD^+-dependent variant in a high flux pathway), the rate of the enzyme reaction may have changed significantly.

6.2 More Complicated Enzyme Kinetics

Equation (6.1) derived by either (6.3) or (6.7) has an almost exact analogue in Langmuir's treatment (1916) of fast equilibrium adsorption of a gas to a finite number of active sites on the catalytic surface, followed by a reaction in which the

product is formed with a rate proportional to the concentration of occupied sites and finally released by a fast desorption process. The presence of other species that could inhibit the overall reaction either reversibly (the activity of the catalyst returns when the inhibitor is removed from the feed) or irreversibly (it could be the permanent damage caused by sulfides or by sintering of the catalyst during a temperature excursion) has been exhaustively studied both by chemists and by biochemists, each in their own field.

Some of the most common reversible inhibitory effects contributing to reduction of the enzymatic activity through an action on either k or K_m in (6.1) will be discussed in Sect. 6.2.1. In Sect. 6.2.2, we shall discuss certain rate expressions in which the dependence on s is strong in a certain s-interval and small outside this interval. Enzymes exhibiting this type of behavior are important for the regulation of cell metabolism. The kinetics developed in Sects. 6.2.1 and 6.2.2 below both have apparent analogues in expressions for cell kinetics, but there they are used as pure data fitters without any mechanistic foundation at all.

6.2.1 Variants of Michaelis–Menten Kinetics

Although enzymes are usually very specific catalysts, there are important cases of interactions between enzymes and substrate analogues that impede the rate of the desired reaction. The membrane-bound transport enzymes for hexoses are typical examples. A specific example is the membrane-bound mannose–PTS system of lactic bacteria (see Sect. 7.7.2) that can transfer a number of sugars from the medium to the cell, where it arrives in a phosphorylated form. Despite its name, the uptake of mannose by the enzyme is almost completely inhibited by the presence of glucose, and also by the presence of glucose analogues that are not even metabolized by the lactic bacteria (Benthin et al. 1993).

The free enzyme E can be removed from the left hand side of (6.2) by a competing reaction:

$$E + S_1 \underset{k_{-3}}{\overset{k_3}{\rightleftarrows}} ES_1 \tag{6.9}$$

Following the derivation of the Michaelis–Menten expression (6.8) one obtains

$$r = \frac{k_2 e_0 s}{s + K_{eq}\left(1 + \dfrac{s_1}{K_{eq1}}\right)} \tag{6.10}$$

When S_1 is tightly bound to the enzyme form E, i.e., when the dissociation constant for ES_1 in (6.9) is small, the apparent affinity of E for S is small. The result is that r decreases unless s is large enough to make the s_1-dependent denominator term small compared to s. The deposition of active enzyme in a "dead-end" compound ES_1 results in *Competitive inhibition*, which can be alleviated by

increasing the concentration of S. But this may not always be possible, e.g., in an enzymatic assay.

The competing substrate for E could be any foreign chemical or it could be the product P of the reaction. Here, a negative influence of P on the rate is also found when the overall reaction is completely irreversible. When the assay is run at different levels of P, one may detect a possible product inhibition.

If both E and ES can react with the foreign substance S_1 to form inactive complexes ES_1 and ESS_1, respectively, and if also ES_1 can react with S to form ESS_1 then the following reaction network is found:

$$\begin{array}{ccc} & \overset{S}{\leftrightarrows} & \\ E & & ES \longrightarrow E + P \\ S_1 \downuparrows & & \downuparrows S_1 \\ & \overset{S}{\leftrightarrows} & \\ ES_1 & & ESS_1 \end{array} \tag{6.11}$$

Here, "the dead-end complex" ES_1 can be "activated" through conversion to ESS_1, which again can form the active enzyme complex ES. This type of indiscriminate inhibition where S_1 binds randomly to both primary forms of the enzyme does not lower the over all affinity of the enzyme for S, but leads to a general decrease in the rate of the enzymatic reaction through a smaller apparent rate constant.

Assume that ES_1 and ESS_1 have the same dissociation constant K_{eq1} with respect to E and ES and also that the substrate S binds equally well to E and to ES_1. Then, in analogy with (6.7)

$$e = \frac{(es)}{s} K_{eq}; (ess_1) = \frac{(es)s_1}{K_{eq1}}; (es_1) = \frac{(es)s_1 K_{eq}}{K_{eq1}\, s} \tag{6.12}$$

$$(es) = \frac{e_0}{\frac{K_{eq}}{s}\left(1 + \frac{s_1}{K_{eq1}}\right) + \left(1 + \frac{s_1}{K_{eq1}}\right)} \tag{6.13}$$

$$r = \frac{k_2 e_0 s}{K_{eq} + s} \left(1 + \frac{s_1}{K_{eq1}}\right)^{-1} \tag{6.14}$$

(6.14) is the same as (6.8), except for the reduced rate constant. Here, an increase in the concentration of S will not alleviate the inhibitory effect of S_1. If the nature of S_1 is known it is possible to study the inhibition process by repeating the experiment at different S_1 levels, but sadly one does not always know what the inhibitory substance is, and the so-called *non-competitive* enzyme inhibition may be difficult to detect in assays that probably do not contain all the inhibitory substances that are present in the cell.

If the inhibitor attacks ES but not E, the inhibitor is said to be *un-competitive* (for lack of a better word).

With the enzyme balance,

$$e_0 = (es) + \frac{K_{\text{eq}}}{s}(es) + \frac{(es)s_1}{K_{\text{eq1}}} \tag{6.15}$$

$$r = \frac{k_2 e_0 s}{K_{eq} + \left(1 + \frac{s_1}{K_{eq1}}\right)s} \tag{6.16}$$

Now, the Michaelis constant and the rate constant decrease by a factor $\left(1 + \frac{s_1}{K_{\text{eq1}}}\right)$.

In (6.10), (6.14), or (6.16), the inhibitor S_1 could also be the substrate S, in which case we have *substrate inhibition*. Unless the "dead-end" complex ES_1 is interpreted as an enzyme complex between S and another form of E, neither (6.10) nor (6.14) is of much help in interpretation of substrate inhibition. It may, however, well be that S complexes with ES to form ESS which is now the "dead-end" complex. This is the mechanism of (6.16), and this rate expression (with s used instead of s_1) will also appear in Chap. 7 as a typical rate expression for *substrate-inhibited cellular kinetics*.

Figure 6.2 illustrates the difference (and similarity) between the different types of inhibition. In all four cases, $1/r$ is shown as a function of $1/s$, which will give a linear plot of (6.1), (6.10), (6.14), and (6.16). If in (6.16) $s_1 = s$, then $1/r$ is a hyperbolic function of 1/s with a vertical and an inclined asymptote. Plots such as Fig. 6.2 (and similar linear plots found in textbooks on enzyme kinetics) are excellent in a first phase of an experimental investigation of enzyme kinetics. They clearly show what type of inhibition is present (if the nature of S_1 is known!). When the experiment is carried out at different levels of S_1, the parameters of the inhibition and thereafter the "true" Michaelis parameters k and K_{m} of (6.1) can be obtained, possibly by extrapolation to the limit $s_1 = 0$ of data obtained from samples spiked with known concentrations of S_1.

It is, however, not really good to determine kinetic parameters from any type of linear plot based on the variables r and s when the two variables are non-linearly related. In Fig. 6.2, the error bars on $1/r$ would increase dramatically for increasing $1/s$, since it is likely that r is determined experimentally with a given absolute standard deviation, irrespective of the value of s (which can always be determined with a fixed relative standard error).

Once the correct type of inhibition has been found, all parameters in the rate expression should be determined by nonlinear Least-Squares regression. The correlation matrix between the parameters (Sect. 3.6) should be shown together with the estimate of the parameter vector and the standard deviation of the parameters. In general, k and K_{eq} will be strongly correlated, and almost the same value for r will be obtained when both k and K_{m} are multiplied by the same factor, unless experiments in a broad range of s-values are included. If only values of s that are significantly smaller than K_{eq} are used, the correlation between k and K_{m} is almost +1.

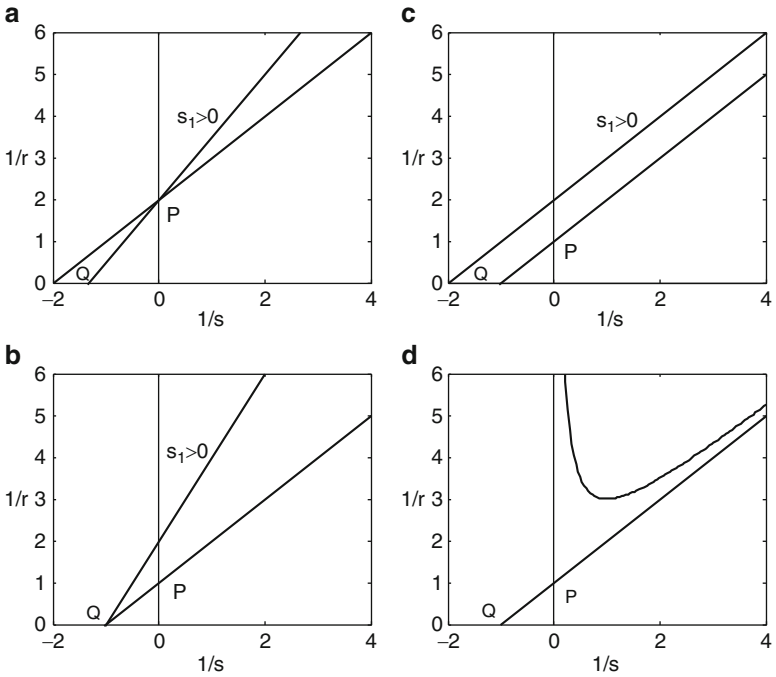

Fig. 6.2 Lineweaver–Burk (double reciprocal plots) of the relation between the rate r and the substrate concentration s. In all four plots, the intersection P with the ordinate axis is k^{-1} in (6.1) for inhibitor concentration $s_1 = 0$, and the apparent value of k^{-1} according to (6.10), (6.14), and (6.16), respectively. $|Q|$ is the corresponding value of K_m^{-1} in (6.1) for $s_1 = 0$, and of the apparent value of K_m^{-1} for s_1 greater than zero. The slope of the lines is equal to $K_{m,apparent}/k_{apparent}$ (**a**) Competitive inhibition by S_1 (6.10). (**b**) Noncompetitive inhibition by S_1 (6.14). (**c**) Uncompetitive inhibition by S_1 (6.16). (**d**) Substrate inhibition by (6.16). Values of k^{-1} and K_m^{-1} are obtained from the ordinate at P and the abscissa at Q. The slope of the inclined asymptote is K_m/k

Needless to say, an increasing degree of correlation between the parameters is obtained when more parameters are included. In Fig. 6.2d, it becomes very difficult to determine k, K_{eq}, and K_{eq1} from a portion of the upward concave part of $1/r$ versus $1/s$. One needs to determine k and K_{eq} separately from experiments conducted at very low values of s. With the two main parameters determined, K_{eq1} can be determined from the shape of the $[1/r, 1/s]$ curve (see Problem 6.1).

The same advice is also valuable when in Chap. 7 parameters in expressions for cell kinetics are determined from (hopefully) a large set of data representing an adequate variation of all the variables of the model.

Example 6.1 *Analysis of enzymatic reaction data.* In an enzymatic reaction, substrate S is converted irreversibly to product P. It is suspected that the product inhibits the reaction, and consequently, the rate r of the reaction is determined for four values of s at each of four levels of the product concentration p. The 16 rate measurements are collected in Table 6.1. s is in g L^{-1} and p in mg L^{-1}.

Table 6.1 Enzymatic rate data r (g substrate converted L^{-1} h^{-1}) at four levels of s and p

	Product concentration (mg/L^{-1})			
s($g\ L^{-1}$)	3	9	27	81
0.1	0.073	0.058	0.036	0.017
0.4	0.128	0.102	0.064	0.032
1.6	0.158	0.126	0.079	0.037
6.4	0.168	0.134	0.084	0.039

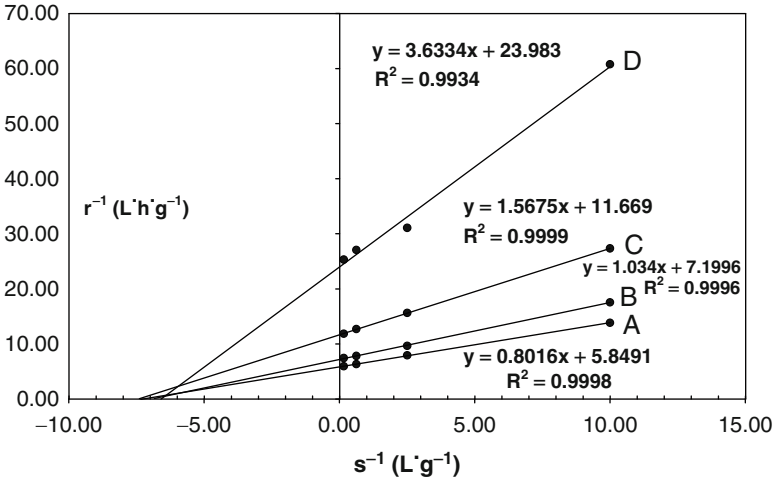

Fig. 6.3 Reciprocal plot of r versus s for a case of noncompetitive inhibition

Figure 6.3 is a Linewaever–Burk plot of the data. For increasing level of product concentration p, the slope of the lines increases (from A to D), and all four lines intersect the abscissa axis at more or less the same point. Clearly, a noncompetitive product inhibition (Fig. 6.2b) is indicated. The value of K_{eq} in Eq. (6.14) is determined from the average of the four intersection abscissas: $K_{eq} = 0.142\ g\,L^{-1}$. Next, the slopes of the four regression lines are plotted against p:

$$\text{Slope} = \frac{K_{eq}}{k}\left(1 + \frac{p}{K_{eq1}}\right) \tag{1}$$

Figure 6.4 is a plot of the slope versus the product concentration. From the slope and the intersection with the ordinate axis, and using the previously determined value for K_{eq}, the following values are determined for $k = k_2 e_0$ in (6.14) and for K_{eq1}:

$$k = 0.212\ \text{g substrate}/L^{-1}/h^{-1} \text{ and } K_{eq1} = 18.45\ mg/L^{-1} \tag{2}$$

The data in Table 6.1 were generated with $K_{eq} = 0.136$, $K_{eq1} = 20.92$, and $k = r_{max} = 0.196$. The data are remarkably accurate with a standard deviation of 1 mg L^{-1} for s and 1 μg L^{-1} for p. Still, the regressed parameters are about 10% from their true values. This is an indication of the difficulties that are encountered in experimental studies of enzyme kinetics: the parameters are strongly correlated and the parameter estimation can easily be distorted by

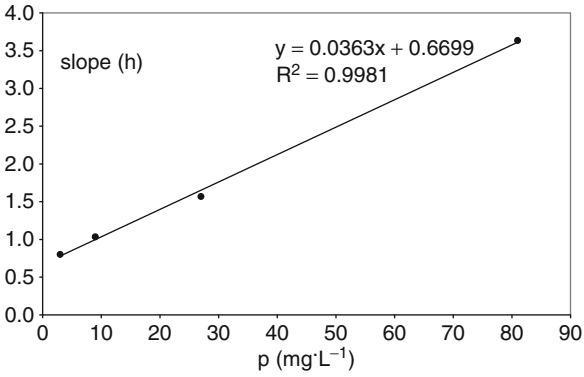

Fig. 6.4 The slope of the lines on Fig. 6.3 as a function of inhibitor concentration

even small experimental errors. In the present case, more data should have been collected at small s values to obtain a better value for K_{eq}, while the values of p were judiciously chosen to obtain a good spread of points on Fig. 6.4.

The piece-wise determination of parameters illustrated in Figs. 6.3 and 6.4 is a nice, intuitive approach, but a full nonlinear regression of the 16 rate data is probably better, once the structure of the model has been revealed by the graphical approach. Using a nonlinear least squares regression, one obtains:

$$K_{eq} = 0.139 \text{ g/L}^{-1}, \quad K_{eq1} = 20.97 \text{ mg/L}^{-1}, \text{ and } \quad r_{max} = 0.197 \text{ g/L}^{-1}/\text{h}^{-1} \tag{3}$$

The correlation matrix is

$$\mathbf{M} = \begin{pmatrix} 1 & 0.4366 & -0.7459 \\ 0.4366 & 1 & -0.0012 \\ -0.7459 & -0.0012 & 1 \end{pmatrix} \tag{4}$$

The parameter values in (3) are, of course, very satisfactory, but the correlation between the parameters is considerable.

6.2.2 Cooperativity and Allosteric Enzymes

We have already seen in Chap. 2 that the living cell is able to control the concentration of metabolic intermediates in the pathways within narrow limits. Enzymatic reactions in a pathway should also be able to react quickly to a sudden environmental change in the input of substrate to the pathway. In particular, the rate of conversion of the substrate by a pathway enzyme should be sensitive to changes in the substrate concentration around the "normal" level that prevails when the cell is operating at a steady state.

The downward convex hyperbolic shape of Fig. 6.1 shows that the Michaelis–Menten kinetics is unable to give a high sensitivity of r to changes in s, except when the "normal" substrate level is much lower than K_m. One might guess that the

saturation constant K (or K_m in (6.1)) of an enzyme in a microorganism has by evolution settled on a value that would give $r/r_{max} = 0.5$ around the s-value that is "normally" offered to the enzyme. If suddenly the enzyme is exposed to a pulse of substrate five times higher than the normal level $s = K$, then the enzyme kinetics given by (6.1) would only increase the rate of the reaction from $r/r_{max} = 1/2$ to 5/6. It would take too long for the enzyme to bring the substrate level back to $s = K$, and meanwhile, other pathway reactions may be induced by the high level of substrate waiting to be consumed by the enzyme. Biological systems have, therefore, evolved to have enzymes that can show different types of kinetics through the use of *cooperativity*.

In 1910, Hill proposed an empirical expression for the uptake of oxygen by the protein hemoglobin. He found that the rate of oxygen uptake when pictured against the oxygen partial pressure had a sigmoidal shape, and the data could be fitted to

$$r = \frac{r_{max}\, s^n}{s^n + K^n} \tag{6.17}$$

The maximum uptake rate $k = r_{max}$ and the denominator constant K (same units as used for s) are similar to the two parameters of the Michaelis–Menten kinetics, and $r/r_{max} = 0.5$ when $s = K$.

For $n > 1$, binding of substrate S to the enzyme increases the affinity of the enzyme to bind more S (a *positively* cooperative reaction), whereas $n < 1$ means that the affinity of the enzyme for S steadily decreases for increasing s (*negatively* cooperative reaction).

For all $n > 1$, $dr/ds = 0$, but $d^2r/ds^2 > 0$ at $s = 0$, and r/r_{max} increases, at first slowly from zero at $s = 0$, but then increasingly fast in a rather narrow s-interval around K.

$$\text{The point } P \text{ of inflexion of } r(s) \text{ is at } s = s_{inflex} = \left(\frac{n-1}{n+1}\right)^{\frac{1}{n}} K \tag{6.18}$$

$$\text{At } s = s_{inflex}, \quad r/r_{max} \text{ is } (n-1)/(2n) \tag{6.19}$$

$$\text{Also, at } s = s_{inflex}, \text{ the slope of } r/r_{max} = \frac{(n-1)\,(n+1)}{4n s_{inflex}} \tag{6.20}$$

For $n < 1$, the slope of r/r_{max} is infinity at $[s, r] = [0, 0]$, and the sensitivity of r to changes in s steadily decreases until the asymptote r/r_{max} is reached for $s \to \infty$.

Figure 6.5 illustrates that the sensitivity of a positively cooperative enzyme to changes in the substrate concentration is very high in an s-interval around $s = K$.

For $n = 4$, and independent of the value of K, an increase in r/r_{max} from 0.5 at $s = K$ to 0.9 will be mediated by a change of s from K to $9^{0.25}K = 1.73K$. For Michaelis–Menten kinetics one would have to change s from K to $9K$ to obtain an increase r/r_{max} from 0.5 to 0.9.

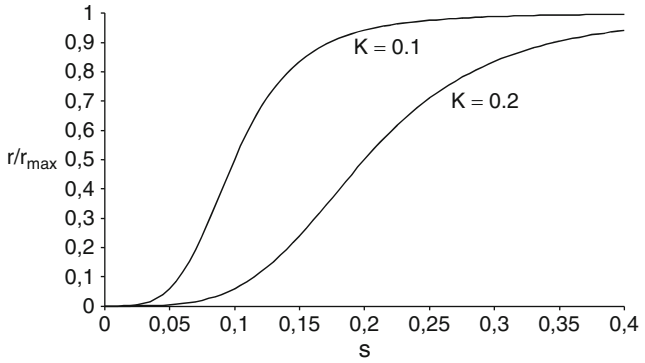

Fig. 6.5 The Hill equation (6.17) for $n = 4$ and $K = 0.1$ and 0.2 (arbitrary units)

If desired, a linear plot can be constructed in which n and K can be determined from experimental data. This is obtained by reordering (6.17):

$$\frac{r_{\max}}{r} - 1 = \frac{s^n + K^n}{s^n} - 1 = \frac{K^n}{s^n} \quad , \quad \text{or} \quad \ln \frac{r}{r_{\max} - r} = n \ln s - n \ln K \tag{6.21}$$

The linearity is most pronounced around $s = K$ and deviations are likely to occur both at very small s-values and when s is much larger than K. The reason is that (6.17) is only an approximation to more complete models of cooperativity, as will be discussed below.

Naturally, a lot of speculation has been devoted to find a mechanistic explanation for the Hill equation. The simplest mechanism was already proposed by Hill himself: The enzyme is thought to consist of n subunits, and each subunit must bind one substrate molecule before the enzyme can function. Later research has shown that hemoglobin is an aggregate of fixed size with four binding sites for oxygen, but Hill's experiments showed that the binding data corresponded to $n = 2.7$. Apparently, the enzyme does not abide by the musketeers oath – "one for all, and all for one" – but the binding of the first substrate molecule facilitates the binding of the next molecule, and so on. This is why the binding is called cooperative. As shown in modern models of cooperativity, both the numerator and the denominator of (6.17) should consist of a sum of powers of s up to s^n, and the approximation (6.17) is only accurate when the dominant power is s^n in both the numerator and the denominator. The derivation of models for cooperativity is fairly complex, and the reader is referred to textbooks on enzymology, e.g., Cornish-Bowden (1995) and Fell (1997) for an adequate treatment of the subject.

As described above, the cooperation may involve only the enzyme and the substrate, or it could involve cooperation between enzyme, substrate, and an *effector* (either an inhibitor or an activator) of the enzyme. This last interaction is of great importance for the regulation of metabolic pathways. Thus, in lactic acid bacteria, fructose 1,6 diphosphate is an effector of both lactate dehydrogenase (LDH) that converts pyruvate to lactic acid and of pyruvate formate lyase (PFL) that directs

pyruvate into the mixed acids pathways (see Fig. 2.5b). A high glucose flux through the EMP pathway gives a high level of fructose 1,6 diphosphate. This activates the LDH and strongly inhibits PFL. At low glucose flux (either because the concentration of glucose in the medium is low or because a less easily fermented sugar such as lactose is used as feed), the inhibition of PFL is immediately lifted (Melchiorsen et al. 2001, see Figure 7.15).

Both in the relatively simple case of substrate cooperativity and in the case of cooperativity between enzyme, substrate, and effector the relationship between r and s (with the concentration s_1 of the effector as a parameter) has the shape of Fig. 6.5. Enzymes that exhibit the property of cooperativity are collectively named *allosteric enzymes*.

Example 6.2 *Competition of two substrates for the same enzyme.* When two substrates S and S_1 are consumed simultaneously on the same site of an enzyme – e.g., when mannose and glucose compete for the same membrane bound PTS transport protein in lactic acid bacteria, it becomes of interest to calculate the relative uptake rate of the two substrates.

Let the rate of conversion of S and S_1 be r and r_1, respectively, and assume a competitive inhibition of r by S_1 and of r_1 by S. In both cases the inhibition is described by (6.10), where the Michaelis constant is denoted by K_m and K_{m1} for r and r_1 respectively.

$$r = \frac{r_{max}\ s}{s + K_m\left(1 + \frac{s_1}{K_{eq}}\right)}; \qquad r_1 = \frac{r_{max\,1}\ s_1}{s_1 + K_{m1}\left(1 + \frac{s}{K_{eq1}}\right)} \tag{1}$$

In r, the equilibrium constant K_{eq} for the capture of E by S_1 to form the "dead-end" complex ES_1 is equal to the Michaelis constant K_{m1} used in r_1 to describe the first step in the conversion of S_1 by the enzymatic reaction. Similarly, in r_1, K_{eq1} is equal to K_m. Consequently, the two expressions in (1) have the same denominator and (1) can be rearranged to:

$$r = \frac{\frac{r_{max}\ s}{K_m}}{\frac{s}{K_m} + 1 + \frac{s_1}{K_{m1}}}, \qquad r_1 = \frac{\frac{r_{max\,1}\ s_1}{K_{m1}}}{\frac{s_1}{K_{m1}} + 1 + \frac{s}{K_m}} \tag{2}$$

The ratio of the two rates of conversion is consequently

$$\frac{r}{r_1} = \frac{\left(\frac{r_{max}}{K_m}\right)}{\left(\frac{r_{max\,1}}{K_{m1}}\right)} \frac{s}{s_1} \tag{3}$$

The value of the *specificity constant* r_{max}/K_m determines the competitive edge of one substrate relative to the other.

Example 6.3 *Determination of NADH in cell extract using a cyclic enzyme assay.* One of the most important applications of enzymes in studies of cell physiology is as a tool to determine the intracellular concentration of metabolites. As has often been pointed out in Chaps. 3 and 5, the intracellular concentrations of NADH and NAD^+, and in particular of the ratio NADH/NAD^+, are of crucial importance for the cellular behavior.

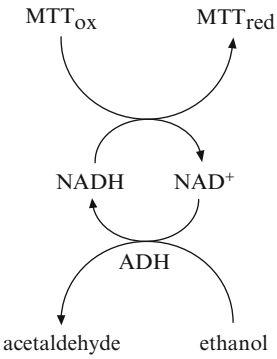

Fig. 6.6 A cyclic assay in which the net reaction is ethanol + MTT$_{ox}$ → acetaldehyde + MTT$_{red}$

In lactic bacteria, the intracellular concentration of NADH is miniscule – of the order of 1 μmol (g DW)$^{-1}$ – and a very large quantity of cell extract must be used to obtain a reasonable accuracy in the assay. Here, cyclic assays come in very handy. Figure 6.6 shows the redox reaction between NADH and NAD$^+$ coupled to two other redox reactions, the oxidation of ethanol to acetaldehyde catalyzed by alcohol dehydrogenase (ADH), and the reduction by NADH of an indicator, MTT, for which the reduced form absorbs light at 570 nm. As long as ethanol and MTT$_{ox}$ are present, the absorbance signal will continue to increase. Since both substrates are available in surplus during the whole experiment, and since NADH is continuously being regenerated by the oxidation of ethanol, its concentration stays constant. As the reaction of NADH with MTT$_{ox}$ is first order in the NADH concentration, the slope of the absorbance versus time curve is proportional to the amount of NADH initially present in the sample.

Applied to a cell extract from a lactic acid bacteria culture where the NAD$^+$ concentration is much higher than the NADH concentration, completely wrong results would be obtained if the NAD$^+$ content of the sample is not quantitatively removed before adding the ADH enzyme to start the experiment. Nordkvist (2001) has shown that treatment for 10 minutes at 56°C and pH = 12.5 of a sample which originally contains 1 μM NADH and 10 μM NAD$^+$ completely destroys the NAD$^+$: The initial slope of the absorbance signal *vs*. time is exactly the same as in a sample with only 1 μM NADH.

The assay must be calibrated by measurements of the initial slope of the absorbance signal with known amounts of NADH added. But the cell extract sample has to undergo a harsh treatment with alkali at 56°C to remove NAD$^+$, and therefore, a number of cell extracts are spiked with known amounts of NADH and incubated at 56°C for 10 min. Ethanol and MTT$_{ox}$ are added in excess, and after addition of a sufficient amount of ADH, the experiment starts.

Figure 6.7 shows that the initial slope of the absorbance *vs*. time signal is a linear function of the added NADH (μM). The intersection with the abscissa represents the amount of NADH in the assay that came from the original cell extract.

From Fig. 6.7, one determines the concentration of NADH in the original cell sample withdrawn from the reactor to be 0.156 μM. The biomass concentration in the reactor was 0.684 L^{-1}, and consequently, the intracellular NADH concentration is 0.228 μmol (g DW)$^{-1}$, or with a cell density of 0.59 g mL^{-1} cell, the molarity of NADH in the cell is calculated to be 0.134 mM. In a series of five experiments based on samples withdrawn from the same exponentially growing anaerobic lactic acid bacteria culture, the mean NADH concentration was found to be 0.172 mM with a standard deviation of 0.029 mM or 17%.

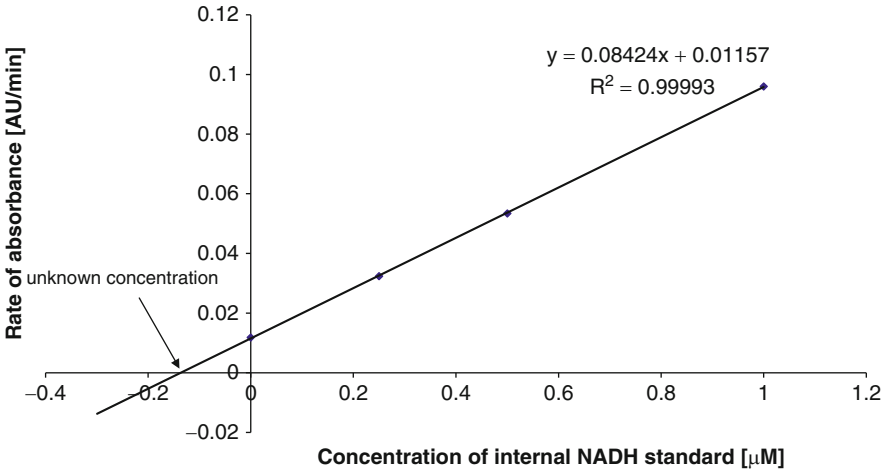

Fig. 6.7 Determination of NADH in a cell extract from cultivation of *Lactococcus lactis*

6.3 Biocatalysis in Practice

In Sects. 6.1 and 6.2, postulated mechanisms of enzymatic reactions were used to derive kinetic expressions for the reactions. For the simple Michaelis–Menten kinetics of Sect. 6.1 and for the variants illustrated in Fig. 6.2, the correctness of the underlying mechanism has been confirmed by numerous experimental studies throughout the twentieth century. Studies of reactions with allosteric enzymes have also proved the correctness of the fundamental concept of enzymes with coordinated action of subunits, action of effectors, and docking patterns on the enzyme. These studies have on several occasions resulted in a Nobel Prize for the discoverers.

Examples 6.1 and 6.2 have illustrated how parameters in the simple kinetic expressions are found from actual experiments, how two substrates compete for the same active sites on an enzyme, and how enzymes are used in analytical chemistry.

This section takes the discussion further, namely to the planning of industrial processes where enzymes are used. There are often several substrates, and the uptake and consumption of these substrates follow more complicated mechanisms and lead to more complicated kinetic expressions. The possibility of irreversible enzyme deactivation, a different phenomenon from the reversible enzyme inhibition shown in Fig. 6.2, must be discussed since it is common in industrial processes, especially for complex substrates. A typical case is the liquefaction and subsequent saccharification of lignocellulosic biomass, where the cost of enzymes is a serious economic problem due to rapid deactivation.

Several important industrial enzymes are sold in immobilized form. The enzyme is embedded in a matrix as pellets that can be recovered and reused after each batch or retained as a fixed bed of immobilized enzyme pellets in a continuous flow reactor.

Hence, transport of substrates from the bulk liquid to the pellet surface and further into the pellet where the bulk mass of enzyme is found become an issue.

Transport of a reactant from a gas phase to a liquid phase where the reaction occurs (i.e., uptake of O_2 from the gas phase in aerobic yeast fermentation) is discussed in Chap. 10. The transport of a dissolved substrate from a liquid phase to a catalytic solid phase is, however, discussed here, since the relatively simple kinetics of enzyme reactions allows a rather stringent quantitative treatment of the combined action of reaction and transport phenomena.

6.3.1 *Laboratory Studies in Preparation for an Industrial Production Process*

All industrial biocatalysis ventures start with extensive laboratory studies.

A molecule is discovered which has interesting properties, as a commodity product or perhaps as a pharmaceutical. Next, the pathways of microorganisms are screened to find which organisms are able to produce the molecule. A small selection of organisms are further screened in search of an organism that produces the enzyme fast and in satisfactory quantity, and preferably also extracellularly (to facilitate the down-stream processes). If the organism is not one of the "preferred" organisms of the company the pathway that contains the enzyme may be transferred to and overexpressed in another organism as described in Sect 2.4.2.

Laboratory experiments are used to optimize the fermentation process that leads to the (hopefully) secreted enzyme, and at the same time, *enzyme engineering* is used to improve the function of the enzyme, e.g., to decrease the value of the Michaelis constant to ensure that practically all the substrate is used up at close to the maximum rate r_{max}, which will considerably reduce the downstream-processing costs.

Thereafter, pilot-plant studies are carried out, partly to produce the enzyme most economically and partly to optimize the biocatalysis process, e.g., to find and to minimize the effect of physical transport processes that did not play any role in the laboratory studies.

The following example, based on Nordkvist et al. (2006), shows how laboratory studies finally led to an understanding of the mechanism for production of a valuable biochemical. A pilot plant study, by Hua et al. (2006), pinpointed the effect of transport resistances and provided the groundwork for a large scale production process.

Example 6.4 *Lactobionic acid from lactose*. Lactobionic acid (4-O-β-D-galactopyranosyl-D-gluconic acid) is produced from lactose, the disaccharide composed of one glucose and one galactose moiety, by oxidation of the glucose ring to gluconic acid, using O_2 as the secondary substrate. The catalyst is a carbohydrate oxidase.

Lactobionic acid has excellent metal-chelating properties. It is currently used in the surgery to preserve organs before transplantation by inhibition of iron-catalyzed production of hydroxyl radicals, as a cheap filler in cheese, and to stabilize supersaturated Ca ion

solutions used for supplementation of Ca in dietary drinks. The Danish company Novozymes became interested in the biomolecule because it effectively prevents precipitation of Ca soaps when washing in "hard" water. Polyphosphates is used to keep calcium in solution, but phosphates in the waste water are definitely undesired, while lactobionic acid is a much stronger chelating agent than polyphosphates, and it is easily biodegradable.

This was the "business idea" behind the Novozyme search for a suitable carbohydrate oxidase to convert the very low value substrate lactose to lactobionic acid.

The carbohydrate oxidase was cloned from *Microdochium nivale* and expressed in *Fusarium venenatum*.

The enzyme is able to catalyze oxidation of several mono-, oligo- and polymeric saccharides, producing an acid + hydrogen peroxide that can be removed by addition of catalase to prevent a possible deactivation of the enzyme. The enzyme is considered safe for use in the food industry.

The Michaelis constant K_m for lactose was determined by Nordkvist et al. (2006) by a spectrophotometric method in which the initial rate of H_2O_2 production was measured for different lactose concentrations. A very low-value $K_m = 0.066$ mM (=22.6 mg lactose L^{-1}) was determined, which means that the enzyme can almost quantitatively convert lactose to lactobionic acid.

The uptake and conversion of the two substrates S (lactose) and O_2 to products P (lactobionic acid) and H_2O_2 follow the "ping-pong" scheme:

$$E_{ox} + S \underset{k_{-1}}{\overset{k_1}{\longleftrightarrow}} E_{ox}S \xrightarrow{k_2} E_{red} + P \tag{1}$$

$$E_{red} + O_2 \xrightarrow{k_3} E_{ox} + H_2O_2 \tag{2}$$

The volumetric rate r of production of P (or H_2O_2) is derived similar to the expressions in Sect. 6.2:

$$r = k_2(E_{ox}S) = k_{cat}(E)\frac{(S)(O_2)}{(S)(O_2) + K_{ms}(O_2) + K_{mO}(S)} \tag{3}$$

From the pseudo-steady- state assumption for the reversible reaction in (1) one obtains

$$K_{ms} = (k_{-1} + k_2)/k_1 = (E_{ox}S)/(E_{ox})(S) \tag{4}$$

Since the rate of production of H_2O_2 equals the rate of production of P,

$$\begin{aligned} k_2(E_{ox}S) = k_3(E_{red})(O_2) \rightarrow (E_{red}) &= (k_2/k_3)(E_{ox}S)/(O_2) \\ &= K_{mO}(E_{ox}S)/(O_2) \end{aligned} \tag{5}$$

When finally a total balance for E is invoked,

$$(E) = (E_{ox}) + (E_{red}) + (E_{ox}S) \tag{6}$$

the rate expression (3) is derived.

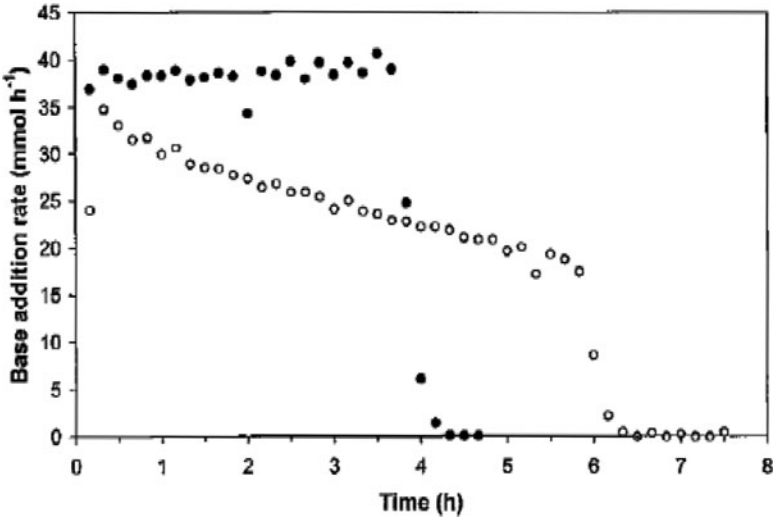

Fig. 6.8 Conversion of lactose to lactobionic acid in a 1-L bioreactor. Temperature = 38°C. Initial lactose concentration 50 g L^{-1} and dissolved oxygen tension 44.1% DOT relative to saturation of water with air at 1 bar. 60 mg pure oxidase and 0.25 g catalase solution were added initially, *Filled circles*: Titration of lactobionic acid to pH 6.4 with 1.8 M NH_3. *Open circles*: Titration with 2 M NaOH (Nordkvist et al. 2006)

The saturation concentration of oxygen c^* in water with a partial pressure of $O_2 = 1$ bar in the gas phase is given by the following expression for $298 < T\,(\mathrm{K}) < 323$:

$$c^*(\mathrm{mmol/L}) = 0.0270 \exp\left(1142/T\right) \tag{7}$$

Batch experiments in a bioreactor with a working volume of 1 L were carried out to find the parameters in (3). The reactor was fitted with two Rushton turbines (see Chap. 11) rotating at 1,000 revolutions per minute (1,000 rpm), and the temperature was controlled to within 0.5°C at 38°C.

The lactobionic acid produced was continuously neutralized to pH 6.4 by titration with either 2 M NaOH or 1.8 M NH_3.

In each batch experiment, the O_2 concentration in the liquid was kept constant using a mixture of air and O_2, with each stream controlled by mass flow controllers. A polarographic oxygen sensor was used to monitor the liquid-phase O_2 concentration relative to the saturation concentration c^* determined by (7) when the partial pressure of O_2 in the gas phase is inserted. Liquid O_2 concentration is measured in units of % dissolved oxygen tension (DOT), relative to saturation with air at 38°C, i.e., DOT = 100% when the oxygen sensor measures $c^* = 0.21 \times 0.0270 \exp(1142/311.2) = 0.222$ mmol L^{-1}.

In all respects, the reactor supposedly operates as "an ideal" laboratory bioreactor.

Figure 6.8 shows the reaction rate r measured from the base addition rate which is equal to the rate of formation of lactobionic acid, since 1 mol base is used to neutralize 1 mol of produced lactobionic acid.

The O_2 concentration in the liquid was kept at 44.1% DOT, i.e., $(O_2) = 0.0979$ mmol L^{-1}.

The initial lactose concentration was 50 g L^{-1} and the coproduced H_2O_2 was quantitatively decomposed by addition of 0.25 g catalase solution to the batch before start of the experiment.

When 1.8 M NH_3 is used to titrate the lactobionic acid, the rate of production is 38 mmol h^{-1} until at about 3.8 h, the rate falls precipitously to zero. This is in accordance with the low value for $K_{ms} = 22.6$ mg L^{-1} determined above: Almost all the lactose is consumed with a constant rate of reaction.

For a very small value of K_{ms}, the rate expression (3) is, indeed, independent of the lactose concentration:

$$r = k_{cat}(E)\frac{(O_2)}{(O_2) + K_{mO}} \tag{8}$$

Unfortunately, titration with NH_3 was not used until after several months of experimentation.

Unsuspectingly, 2 M NaOH was used at first, and now the production rate of lactobionic acid decreases with time until an abrupt drop in r appears when the lactose is used up. Furthermore, when higher initial lactose concentrations (100 or 200 g L^{-1}) were used, the time until all the lactose was used up increased dramatically. The reaction rate could, indeed, decrease to zero before all the lactose was consumed.

Clearly, some "inhibitory" effect was slowing the reaction down.

Several inhibition factors were explored. On the suspicion that H_2O_2 inhibited the reaction, experiments were made with different levels of catalase added. The effect of doubling the catalase addition from 0.25 to 0.5 g L^{-1} was negligible. Consequently, even a small addition of catalase removes the danger of H_2O_2 inhibition. The possible inhibitory effect of lactobionic acid was also investigated by adding large amounts of the acid to the lactose before the start of the experiment. Again no effect of lactobionic acid was found. O_2 could also be an inhibitor or more likely a deactivator of the enzyme, and experiments with different DOT showed that the rate decreased faster when higher DOT were used.

These observations gave rise to a study of enzyme deactivation. Although this study finally proved to be unnecessary – since titration with NH_3 instead of NaOH completely removed the deactivation phenomenon – some elements from the study (Nordkvist et al. 2006) will, however, be discussed here since the approach to find the cause of enzyme deactivation could be useful in other studies where the phenomenon is unavoidable.

For any fixed value of DOT a plot of r against time indicated an exponential decrease in the rate.

This could be explained by *a first-order deactivation* of the enzyme with an exponent that increases with the oxygen concentration:

$$-\frac{d(E)}{dt} = k_d f((O_2))(E) \rightarrow (E) = (E_0)\exp(-k_d f((O_2))t) \tag{9}$$

$$r = k_{cat}(E_0)\frac{(O_2)}{(O_2) + K_{mO}}\exp(-k_d f((O_2))t) \tag{10}$$

A good fit of the data for many values of oxygen concentration gave the following expression for f ((O_2)):

$$f((O_2)) = \frac{(O_2)}{(O_2) + K_d} \tag{11}$$

In (10) and (11), k_d and K_d are determined from the time profiles of r, while k_{cat} and K_{mO} are determined from initial rate experiments (see details in Nordkvist et al. 2006).

When finally titration with NH_3 was tried, and the simple constant rate of lactose consumption was discovered, it became clear that the deactivation was caused be the *alkalinity* of the base.

Although the laboratory reactor is "ideally" stirred, droplets of NaOH apparently deactivate the enzyme before they are dispersed and consumed to pH = 6.4.

The *rate* of base addition determines the exposure of the enzyme to deactivation, and consequently, the deactivation kinetics is determined by (12) rather than by (9):

$$-\frac{d(E)}{dt} = k_d(E)r = k_{cat}k_d(E)^2\frac{(O_2)}{(O_2) + K_{mO}} \tag{12}$$

Integration of (12) and insertion of ($E(t)$) in the rate expression yields:

$$r = \frac{k_{cat}}{k_{cat}k_d\frac{(O_2)}{(O_2)+K_{mO}}t + \frac{1}{E_0}} \times \frac{(O_2)}{(O_2) + K_{mO}} \tag{13}$$

Fitting the data to (13) gave much better results than when (10) is used. When the observation that the deactivation is somewhat slower when large initial lactose concentrations are used – this can be interpreted as a modest "protection" of the enzyme by lactose and lactobionic acid –an excellent fit of all the rate data was obtained.

Deactivation studies are notoriously difficult, and a large amount of accurate rate data obtained over a wide range of the variable values must be at hand, if the correct mechanism for the deactivation process is to be deduced. Intuition – or as shown in this example – and inclusion of another variable (the alkalinity of the base) can assist in the search for the correct mechanism.

The discovery that *inhomogeneities* in a well-stirred liquid phase of a so-called ideal reactor can affect the results is both surprising and potentially valuable in the interpretation of kinetic studies. In larger volume reactors, the effects can, of course, be much more pronounced than here, since the stirring of the liquid phase can never be as intensive as is the case for laboratory reactors (see Chap. 11).

The literature contains a few references to similar observations (see Nordkvist et al. 2006 and Problem 11.4).

From the point of view of designing an industrial process for lactobionic acid production, the most important results are the values of k_{cat} and the two Michaelis constants K_{ms} and K_{mO}.

The investigation shows that K_{ms} is so small that the reaction can safely be regarded as zero-order in the lactose concentration. On the contrary, the value of K_{mO} is substantial, namely, 455% DOT at 38°C.

This means that the rate is virtually *first order* in (O_2) when O_2 is supplied from air.

Saturation with O_2 is only obtained when (technically) pure O_2 is used (DOT = 476%), and it may even be advantageous to use a pressurized reactor.

Further *enzyme engineering* of the oxidase used in this study may yield a variant with a smaller value of K_{mO}, but the value of K_{ms} for the currently used oxidase from *M. nivale* is very small, a great advantage compared with other oxidases for which K_{ms} is in the g L^{-1} range.

6.3.2 Immobilized Enzymes and Diffusion Resistance

Several important industrial enzymes are sold in pellet form where the enzyme is embedded in a solid matrix, e.g., of polymerized glutaraldehyde. The enzyme particles are packed in a fixed bed, and the substrate is converted to product as it trickles or is pressured through the bed.

The enzyme kinetics may not be the same when the enzyme is immobilized in the matrix as it would be in free suspended form. Often, the rate is smaller for the immobilized enzyme, but the stability of the enzyme is usually higher.

Examples of immobilized enzyme products are *glucose isomerase*, the enzyme that converts glucose (mostly from starch-derived glucose syrup) to fructose, and *penicillin deacylase*, which is used to cut off the acid side chain from penicillin to form the 6-APA nucleus, a step in the production of semisynthetic penicillins (see Sect. 2.3.2). Detergent enzymes are immobilized in a solid matrix together with a number of other chemicals that promote the washing process. The product is dust free, it presents no work hazards from allergic reactions, and it has a long shelf-life since unstable chemical components are protected from humidity caused degradation.

The solid matrix is rapidly dissolved in the washing medium when the detergent is used.

Similarly, many enzyme products for the feed industry (e.g., *phytases* used to increase the uptake of phosphorous by the animals and thus reduce the P-content of the manure) are sold in immobilized form. Again a dust-free, easy handling of the product helps to avoid allergenic reactions.

When an enzyme is distributed in the porous, solid matrix that makes up the immobilized enzyme catalyst, the substrates have to be transported not only to the pellet surface from the bulk of the liquid phase, but also into the pellets. Likewise, products must be transported back into the bulk liquid phase. Transport of substrates by convection is normally quite insignificant in the microporous system of the pellet, and the only mechanism that can bring substrate to the enzyme in the pores and the products out of the pellet is *molecular diffusion*. Diffusive transport of substrates into the pellet occurs in the direction of decreasing substrate concentration. When the coordinate system has its origin at the pellet center, then at the distance x from the pellet center, the flux J of mass through the area A towards the center is positive and gives rise to an accumulation of mass in the pellet volume $\mathrm{d}V$ between x and $x+\mathrm{d}x$ from the pellet center:

$$\frac{\partial s_A}{\partial t}\mathrm{d}V = JA = D_{eff}\frac{\partial s_A}{\partial x}A \tag{6.22}$$

s_A is the internal concentration of substrate S_A, and D_{eff} is the *effective diffusion coefficient* of S_A in the porous system of the pellet. D_{eff} is proportional to the

porosity ε_p of the pellet and inversely proportional to the effective distance of travel for a substrate to reach an enzyme molecule through the twisting and perhaps narrowing pore. The *tortuosity* τ_p is a measure of the longer diffusion path.

$$D_{eff} = (\varepsilon/\tau)_p D \tag{6.23}$$

Here, D is the molecular diffusion coefficient of substrate in the liquid medium inside the porous matrix. D can be looked up in tables – e.g., $D = 6 \times 10^{-10}$ m^2 s^{-1} for diffusion of glucose in a liquid solution of about 50 g glucose L^{-1}. ε_p is in the range 0.2–0.5 m^3 pore volume per m^3 pellet, and τ_p is in the range 2–3. Thus, D_{eff} is about a factor 10 smaller than D.

We now include a consumption term $r_A dV$ for S_A. When $dV = A \times dx$ is inserted in (6.22) and $dx \to 0$, one obtains the mass balance (6.24) for the substrate S_A:

$$\frac{\partial s_A}{\partial t} = D_{eff} \nabla^2 s_A - r_A \tag{6.24}$$

In (6.24), ∇^2 is the so-called *Laplacian operator*. Very often, the system is symmetrical, i.e., the concentration is constant at planes equidistant from the center line of a slab, and on a surface at distance x from the center of a spherical particle. For plane-parallel symmetry, the area A is independent of x, and ∇^2 is simply the second derivative of s_A in the direction of x. In spherical coordinates, i.e., for a spherical particle:

$$\nabla^2 = \frac{1}{x^2} \frac{\partial}{\partial x} \left(x^2 \frac{\partial s_A}{\partial x} \right). \tag{6.25}$$

r_A is the rate of consumption of substrate S_A per unit volume *of the pellet* (i.e., the rate per volume *liquid* in the pellet divided by ε_p).

Solution of the unsteady-state mass balance has been a pet subject in chemical reaction engineering, at least for the last 60 years. Numerical solutions have been obtained for all kinds of rate expressions r_A, for coupled reactions and with various deactivation patterns for the catalyst. A standard reference is Aris (1975).

In the present context, we shall only be concerned with the *steady-state solution* of (6.24) ($\frac{\partial s_A}{\partial t} = 0$), and only a few typical rate expressions will be discussed. The aim is to give an impression of how intraparticle diffusion resistance influences the *average* rate of consumption of S_A on an immobilized enzyme particle of, say radius R_p. More complex cases can be studied with the help of the voluminous literature on diffusion and reaction in porous catalysts.

Note 6.2 *The steady-state substrate concentration profile for a spherical particle. The effectiveness factor.* Combination of (6.24) and (6.25) gives the following steady-state mass balance for a spherical particle:

$$D_{eff} R_p^{-2} \frac{1}{\xi^2} \frac{d}{d\xi} \left(\xi^2 \frac{ds_A}{d\xi} \right) = r_A \tag{1}$$

In (1), $\xi = r/R_p$ is the distance from the center of the sphere normalized by the radius R_p of the sphere.

At the pellet surface, $\xi = 1$, the substrate concentration is known. $s_A = s_{A,s}$ (if transport resistance through a liquid film surrounding the pellet is neglected).

At the center of the pellet, $\xi = 0$, both the substrate concentration s_A and $\frac{ds_A}{d\xi}$ are finite.

With these *boundary values*, the second-order *boundary value problem* (1) can be solved for different r_A.

Two different rate expressions r_A will be considered:

(a) Zero-order conversion of S_A: $r_A =$ constant k (unit: g S_A converted (L pellet)$^{-1}$ h^{-1})
(b) First-order conversion of S_A: $r_A = k_1 s_A$ (unit for k_1: h^{-1})

(a) Integration of (1) yields $\frac{d(s_A/s_{A,s})}{d\xi} = \frac{\xi}{3}\Phi_0{}^2 + \frac{C_1}{\xi^2}$, and the arbitrary constant $C_1 = 0$.

On further integration, $s_A/s_{A,s} = \frac{\xi^2}{6}\Phi_0{}^2 + C_2$, where insertion of the second boundary condition yields

$$C_2 = 1 - \frac{1}{6}\Phi_0^2 \quad \text{and} \quad s_A = s_{A,s}\left(1 - \frac{1}{6}\Phi_0^2(1 - \xi^2)\right) \tag{2}$$

$$\Phi_0^2 = \frac{kR_p{}^2}{D_{eff}s_{A,s}} \text{ is the square of the } \textit{Thiele modulus}\ \Phi_n \text{ for a zero order reaction, } n = 0. \tag{3}$$

The Thiele modulus is a dimensionless parameter group for all types of reactions. It is the ratio of the amount of substrate consumed by the reaction when $s_A = s_{A,s}$ and the amount of substrate that enters the pellet by diffusion.

The rate of the zero-order reaction is independent of s_A for all $s_A > 0$. For s_A equal to or smaller than 0, the rate is by definition 0. Hence, for $\Phi_0^2 < 6$, the whole enzyme particle converts substrate with a constant rate k. For $\Phi_0^2 = 6$, both s_A and $ds_A/d\xi$ are 0 for $\xi = 0$, and for $\Phi_0^2 > 6$, that part of the pellet for which $\xi^2 < 1 - 6/\Phi^2$ is empty of substrate and, therefore, completely useless for conversion of S_A.

(b) For the first-order reaction $r_A = k_1\, s_A$,

$$\frac{D_{eff}}{\xi^2}\frac{d}{d\xi}\left(\xi^2\frac{ds_A}{d\xi}\right) = k_1 R_p^2 s_A \tag{4}$$

Equation (1) can be rearranged into

$$\frac{1}{\xi^2}\frac{d}{d\xi}\left(\xi^2\frac{ds_A}{d\xi}\right) = \frac{k_1 R_p^2}{D_{eff}}\xi^2 s_A = \Phi_1{}^2\xi^2 s_A \tag{5}$$

The differential equation (5) can be solved by making the substitution $y = s_A\xi$, whereby (5) becomes

$$\frac{d^2y}{d\xi^2} = \Phi_1{}^2 y, \quad \text{where} \quad \Phi_1{}^2 = \frac{k_1 R_p^2}{D_{eff}} \tag{6}$$

The general solution to (6) is

$$y = s_A\xi = C_1 \sinh(\Phi_1\xi) + C_2 \cosh(\Phi_1\xi) \tag{7}$$

Here, sinh (X) and cosh (X) are the hyperbolic sine = 0.5(exp(X)-exp($-X$)) and the hyperbolic cosine = 0.5(exp(X) + exp($-X$)). cosh(X) = 1 for $X = 0$, while sinh(X) = 0 for $X = 0$. Since s_A is finite at $\xi = 0$, the arbitrary constant $C_2 = 0$. Using the boundary condition at $\xi = 1$ yields the following concentration profile:

$$s_A = s_{A,s}\frac{\sinh(\Phi_1\xi)}{\xi \sinh(\Phi_1)} \tag{8}$$

For $\xi \to 0$, the expression on the right hand side of (8) approaches $s_{A,s}\Phi_1/\sinh(\Phi_1)$.

For both cases *a* and *b*, the Thiele modulus Φ_0 or Φ_1 increases with increasing R_p and rate constant k or k_1, and decreases with increasing effective diffusivity D_{eff}. Hence, the center concentration of substrate is small for large pellets and a fast reaction. This will obviously reduce the *average* rate of reaction $r_{A,av}$ on the pellet, i.e., lead to a less effective utilization of the enzyme in the pellet. Φ_1 is independent of $s_{A,s}$, while Φ_0 decreases for increasing $s_{A,s}$. Therefore, the zero-order reaction is less influenced by diffusion restriction when $s_{A,s}$ is large.

A quantitative determination of the ratio $r_{A,av}/r_{A,s}$ involves the so-called *effectiveness factor* η for the pellet.

Since $r_{A,av}$ is given either by the flux of S_A into the pellet at $r = R_p$ or directly from the integral of r_A over the pellet volume, the effectiveness factor can be calculated in two ways:

$$Vr_{A,s}\eta = D_{eff}\left(\frac{ds_A}{dr}\right)_{r=R_p} 4\pi R_p^2 = \int_{0,or,r(s_A=0)}^{R_p} r_A(4\pi)r^2\,dr \tag{9}$$

In (9), $Vr_{A,s}$ is equal to $k(4/3)\,\pi R_p^3$ for a zero-order reaction and $k_1 s_{A,s}(4/3)\pi R_p^3$ for a first-order reaction.

We shall now calculate $\eta(\Phi)$ for the two cases *a* and *b*.

For the zero-order reaction, case *a*, and $\Phi_0^2//6>1$, the derivative of $s_A/s_{A,s} = y$ is zero, not at $\xi = 0$, but at a value ξ_c where $0 < \xi_c < 1$. Hence, the arbitrary constant C_1 is not 0, but $-1/3\ \Phi_0^2\xi_c^2$.

Further integration and insertion of the boundary condition $y = 0$ at $\xi = \xi_c$ yields

$$s_A/s_{A,s} = z = 1/6\Phi_0^2\xi^2 + 1/3\Phi_0^2\xi_c^3/\xi - 1/2\Phi_0^2\xi_c^2 \tag{10}$$

Finally, the boundary condition $z = 1$ at $\xi = 1$ is applied to give the relation (11) between Φ and ξ_c:

$$6/\Phi_0^2 = 1 + 2\xi_c^3 - 3\xi_c^2 \tag{11}$$

Equation (11) can be solved for ξ_c for any given value of Φ_0. When $\Phi_0^2 = 6$, the value of $\xi_c = 0$, while $\xi_c \to 1$ when $\Phi_0 \to \infty$.

For large values of Φ_0, we can represent ξ_c by $1-a$, where a is close to zero. Insertion in (11) yields

$$a^2(3-2a) = 6/\Phi_0^2 \tag{12}$$

Since a is small, the result for $\Phi_0^2 \to \infty$ is $a = \sqrt{2}/\Phi_0$.

Similarly, the effectiveness factor is written as $\eta = 1 - \xi_c^3 = 1 - (1-a)^3 = a^3 - 3a^2 + 3a \sim 3a$ for $a \to 0$, and the final result (13) is obtained:

$$\eta \to 3\sqrt{2}/\Phi_0 \text{ for } \Phi_0 \to \infty \tag{13}$$

For the first-order reaction, case b, the effectiveness factor η is obtained by differentiation of (8):

$$\left(\frac{\mathrm{d}(s_A/s_{A,s})}{\mathrm{d}\xi}\right)_{\xi=1} = \left(\frac{\mathrm{d}z}{\mathrm{d}\xi}\right)_{\xi=1} = \left(\frac{\xi\Phi_1\cosh(\Phi_1\xi) - \sinh(\Phi_1\xi)}{\xi^2\sinh\Phi_1}\right)_{\xi=1} \tag{14}$$
$$= \Phi_1\coth\Phi_1 - 1$$

$$\eta = \frac{3}{{\Phi_1}^2}\left(\frac{\mathrm{d}z}{\mathrm{d}\xi}\right)_{\xi=1} = 3\frac{\Phi_1\coth\Phi_1 - 1}{{\Phi_1}^2} \tag{15}$$

For $\Phi_1 \to \infty$, $\coth\Phi_1 \to 1$, and consequently $\eta \sim 3/\Phi_1$.

The conclusion for both a and b is *that for large values of the Thiele modulus* Φ_n, η *is inversely proportional to* Φ_n: $\log\eta \sim -\log\Phi_n + \text{constant}$.

For the zero-order reaction, η is exactly 1 for all $\Phi_0 < \sqrt{6}$. For the first-order reaction η slowly decreases from 1 as soon as Φ_1 is greater than 0. Eventually, the two $\eta(\Phi_n)$ profiles meet in parallel asymptotes $\log\eta = -\log\Phi_n + \text{constant}$ in a double logarithmic plot. If the Thiele modulus is based on a length parameter L = catalyst pellet volume/catalyst pellet surface, i.e., $R_p/3$ for a sphere, and if a factor $(n+1)/2$ is included in the Thiele modulus, then the asymptote for all kinetic expressions where r_A is proportional to S_A^n comes together, and a single plot suffices to show η (Φ_{general}). Such plots are seen in all textbooks in Chemical Reaction Engineering. For more general reaction rate expressions, numerical solution of the boundary value problem is necessary to compute $s_A(\xi)$ and thereafter $\eta(\Phi)$. A standard method of finding the numerical solution of the problem is *orthogonal collocation* as described in Villadsen and Michelsen (1978). Kinetic expressions of the Michaelis–Menten type are commonly applicable for enzyme systems, and the solution for the $\eta(\Phi)$ problem lies between the solutions for zero-order and first-order kinetics. Any of these two limiting cases can be used as a good approximation of the desired relation between η and Φ.

Example 6.5 *Kinetics for lactobionic acid synthesis applied to an immobilized enzyme.* Assume that the oxidase of Example 6.3 is used in immobilized form. This may possibly protect the enzyme from deactivation as discussed in Example 6.3. In the following, we shall investigate the resulting reduction in production rate of lactobionic acid compared to the use of freely dispersed enzyme.

Consider the experimental conditions of Fig. 6.8, and use NH_3 to titrate the lactobionic acid.

Since K_{ms} is very small for lactose, and the initial lactose concentration is 50 g L^{-1}, one can safely assume that the lactose concentration inside the pores of an immobilized catalyst particle is far greater than zero.

At 38°C reaction temperature, the O_2 concentration in the bulk liquid is 44.1% DOT $= 0.441 \times 0.210 \times 0.0270 \exp(1142/311.2) = 0.0981$ mmol L^{-1}. Inside the pores, the O_2 concentration is smaller, and depending on the rate constant and the pellet radius the average rate of O_2 consumption in the pellet may well be smaller than that at bulk conditions.

Since the rate of base addition is equal to the rate of lactobionic acid production, and 1 mol of O_2 is used per mole lactose converted, the rate of O_2 consumption is 38 mmol O_2 L^{-1} h^{-1}. The value of DOT is far below the value of $K_{mO} = 455\%$ DOT, and consumption of O_2 can safely be considered to follow first-order kinetics. The bulk concentration of O_2 is 0.0981 mmol L^{-1}, and consequently the rate constant $k_1 = 38/0.0981 = 387\ h^{-1} = 0.108\ s^{-1}$.

The diffusivity of O_2 in water is $D = 2.42 \times 10^{-9}\ m^2\ s^{-1}$ at 25°C (see Table 10.10).

The value ε of the pore space and that of the tortuosity τ (see (6.23)) are taken to be 0.3 and 4, respectively.

Hence, $D_{eff} = 1.87 \times 10^{-10}\ m^2\ s^{-1}$.

Consequently, for a pellet with radius 1 mm, the Thiele modulus Φ_1 is calculated by

$$\Phi_1^2 = \frac{(10^{-3})^2 \times 0.108}{1.82 \times 10^{-10}} = 5.8 \times 10^2$$

This is far into the regime of diffusion limitation and $\eta \sim 3/\sqrt{580} = 0.12$.

The average rate of lactobionic acid production is only 12% of the production rate based on the bulk liquid O_2 concentration. The pellet diameter must be reduced considerably if the use of immobilized enzyme is to be a worthwhile proposition.

6.3.3 *Choice of Reactor Type*

As was mentioned in the introduction to the chapter, enzyme-catalyzed reactions are not different from ordinary homogeneous or inhomogenous catalytic reactions. Hence, the choice of reactor type follows the guidelines discussed in textbooks on *Chemical Reaction Engineering*, e.g., Scott Fogler (2006).

The rate r of the enzymatic reaction increases with the concentration s of the substrate unless the substrate S inhibits the reaction for very high values of s, as seen in (6.16). Consequently the batch reactor is preferred to the continuous stirred tank reactor (CSTR), since for any reaction where the rate increases with s^n ($n > 0$), it is important not to "dilute the feed," i.e., as far as possible, avoid mixing of incoming substrate with reactor medium. The plug flow reactor (the "tubular reactor") is the right choice for continuous operation. If one of the substrates is in the gas phase, the large difference between the dilution rate D (large for the gas phase and small for the liquid phase) often invalidates the assumption of plug flow of the liquid substrate and gives rise to a very unstable flow pattern, unless the enzyme is immobilized on a solid support, "a fixed bed reactor." A series of CSTRs can also approximate plug flow behavior in an aerated enzymatic reaction.

Diffusion restriction can change the true reaction order n to a different value, the apparent reaction order, n_{app}, when the enzyme is immobilized on pellets. In a situation with heavy pellet diffusion resistance, $n_{app} = (n + 1)/2$, as discussed at the end of Note 6.2. For a first-order reaction, the reaction order is not changed, $n = n_{app} = 1$. For a second-order reaction, $n_{app} = 3/2$, while a zero-order reaction changes to half-order kinetics, $n_{app} = 1/2$.

In a plug flow reactor, the change in apparent reaction order is most clearly observed for zero-order kinetics. At the entry, the substrate concentration is high, and the effectiveness factor is 1 throughout the pellets. Further down in the reactor, the substrate concentration at the surface of the pellets is smaller, and finally, the active part of the pellet is so small that the apparent reaction order changes to 1/2.

In the rich harvest of scientific papers on diffusion and chemical reaction, especially from the 1970s, one can learn how the yield of parallel or consecutive reactions with different reaction orders can change due to diffusion limitation (the low-order reaction benefits), and how deactivation kinetics is changed when the catalyst pellet size is increased to give a higher diffusion resistance.

This literature can directly be used to predict the influence of diffusion restriction when the reaction is catalyzed by immobilized enzymes.

6.4 Metabolic Control Analysis

In the previous sections of this chapter, enzymes have been treated in their own right as catalysts for reactions in important industrial processes. Rate expressions for the enzyme-catalyzed process have been derived using quite well-established mechanistic models for the reaction, and it was shown how enzymes can be used in analytical determination of cofactors and other physiologically important cell components. The difficulties encountered in establishing the rate expression for more complicated enzyme catalyzed reactions have been illustrated, and finally, the coupling between enzyme reactions and (mass) transport processes has been discussed in close analogy with similar processes in *Chemical Reaction Engineering*.

Enzyme-catalyzed reactions are the backbone of the analysis of mass flow through the metabolic network of living cells. When the enzyme reactions function optimally, the flux of carbon through the metabolic network is directed toward the right metabolic products, and these products are produced at high rates.

Unfortunately, even a detailed knowledge of how the individual enzyme reactions depend on their substrate and products does not help to construct a metabolic pathway in an optimal way.

The cell is, as stated previously, far more than "a bag of enzymes." It is impossible to deduct by in vitro studies of the individual enzymes how they function in a pathway, since one cannot replicate the right environment of the enzymes. The in vivo rate of a pathway enzyme could depend on metabolite concentrations from anywhere in the metabolic network, and the *control structure* that overlays the mass flow structure is mostly unknown.

This is the important challenge that faces scientists who by genetic engineering try to improve the function of a microbial organism, and this is why both the academic literature and industrial practice, despite many years of intense research effort, can as yet not point to many industrial processes where an undisputed success has been attained, even by clever use of the most modern tools of molecular biology.

Fundamentally, a large flux J (typical unit: mol L^{-1} h^{-1}) of carbon toward a desired product is not determined by the properties of individual enzymes, but by the *combined* action of *all* enzymes in the pathway, and possibly also by the action of enzymes in completely different pathways that can produce *effectors* of the enzymes in the pathway under study.

Therefore, the *sensitivity* of an enzyme to the activities of other pathway enzymes and to effectors from outside the pathway becomes of paramount interest rather than the details of the individual enzyme reactions. The *pathway architecture* which gives a global description of the whole pathway must be considered.

This is the objective of *Metabolic Control Analysis*, and in the following, the sensitivity of a global property, the pathway flux J, to changes in the kinetics of all the individual reactions in the pathway will be discussed.

The flux J of carbon from the substrate S to the end product P is the most important global property of the pathway. J is a function of the activity of all the enzymes in the pathway, and the *Flux control coefficient* C_i^J describes the differential change of J caused by a differential increase in the activity of the ith enzyme in the pathway. In a linear pathway with $N-1$ internal metabolites, there are N pathway enzymes catalyzing the conversion of S to P and, therefore, N flux control coefficients C_i^J. If we know the N enzyme activities e_i and the kinetics of the N enzymatic reactions, $i=1, \ldots, N$, then J can be calculated. The kinetics of each enzyme reaction can be a function of the $N-1$ internal metabolite concentrations s_j, $j=1,\ N-1$, and also of the concentration s of the initial substrate S to the pathway. If the concentration p of the final product P influences any of the N pathway reactions (usually by some kind of product inhibition), p as well as s is an *independent* variable of the pathway architecture, while the s_i is termed *dependent* variables. This means that we can *choose* the value of both s and p, whereas the internal metabolite concentrations s_i are found as functions of s and p (and possibly of effectors, concentrations of metabolites from outside the pathway) when the N kinetic expressions and the N enzyme activities e_i are given.

6.4.1 Definition of Control Coefficients for Linear Pathways

The flux control coefficients are defined by

$$C_i^J = \frac{e_i}{J}\left(\frac{\partial J}{\partial e_i}\right), \quad i = 1, 2, \ldots, N \tag{6.26}$$

The sign ∂ for partial differentiation is used since the activity of all other pathway enzymes is kept constant while the influence of the activity of enzyme E_i on J is being studied.

Two other sets of sensitivities are used in *Metabolic Control Analysis*:

1. The sensitivity of each pathway reaction rate r_i to changes in the concentrations of each internal metabolite concentration s_j (and perhaps to changes in s and p and the concentration c_k of effectors from outside of the pathway) is defined as *elasticity*. If a particular rate r_i changes much when s_j is changed, then the elasticity ε_{ji} is large.

$$\varepsilon_{ji} = \frac{s_j}{r_i}\left(\frac{\partial r_i}{\partial s_j}\right), \quad i = 1, 2, \ldots, N \text{ and } j = 1, 2, \ldots, N-1 \tag{6.27}$$

   If the true rate expression for each of the N rates r_i is known, ε_{ji} can easily be calculated, but unfortunately, this information is not available, and as discussed above, in vitro rate expressions for individual enzyme reactions may not bear much relation to the actual rate expressions for enzymes in a pathway of a living organism, since the control structure of the organism is ignored. Therefore ε_{ji} must be calculated based on approximate rate expressions which, as discussed in Sect. 6.4.4, are constructed from data obtained by kinetic experiments with actual cell cultures.
2. Concentration control coefficients express the sensitivity of each of the $N-1$ internal metabolite concentrations to a differential increase of one of the N enzyme concentrations.

$$C_{ij} = \frac{e_i}{s_j}\left(\frac{\partial s_j}{\partial e_i}\right), \quad i = 1, 2, \ldots, N \text{ and } j = 1, 2, \ldots, N-1 \tag{6.28}$$

   For all three sensitivities listed in (6.26)–(6.28), the partial derivative is scaled by the quantity itself, thereby giving dimensionless sensitivities, albeit the variables have very different units.

The quantities of real importance for pathway engineering are the flux control coefficients since we desire by changing the activity of certain enzymes to improve the flux through the entire pathway from S to P. More specifically, it is desired to increase the activity of the enzyme E_i which has the largest flux control coefficient C_i^J, since this would improve the total flux with the maximum amount. In a next round of experimentation, a second enzyme may come into focus for amplification and so on. We shall later show that the overall maximum amplification of the flux J through the pathway is obtained when all the N flux control coefficients are the same. At this point, amplification of all the enzyme activities by a factor f will lead to an increase in J by the largest amount. In other words, as long as the *control* lies in one particular enzyme, it is not useful to amplify any other enzyme. When all C_i^J have attained the same value, the flux resistance is equally distributed through the pathway, and a concerted amplification of all the enzymes is meaningful.

Since C_i^J are the quantities to be calculated, one might speculate why the other sensitivities are important. However, the reconstruction of an organism by individual amplification of N enzymes calls for an extensive experimental effort, and the result is uncertain. First of all, one cannot change e_i in small increments as is necessary to find the analytical sensitivities, because the change in flux J would be too small to capture amidst experimental errors. It is also difficult to ensure that an effort to increase an enzyme level (concentration) is actually expressed in the organism as an increased activity.

For this reason, the sensitivities ε_{ji} and C_{ij} are important. Especially, the elasticities ε_{ji} will, as shown later, be of help, and these quantities can be determined through transient experiments on the organism *without* changing the enzymatic make-up of the organism.

The rate of an individual pathway reaction r_i has the same units as J. If one knows the values of the elements in the vector $\boldsymbol{s}$ of internal (dependent) metabolite concentrations, of the external (independent) concentrations, collected in vector $\boldsymbol{c}$, and of the elasticity matrices $\boldsymbol{E}_\mathrm{s}$ and $\boldsymbol{E}_\mathrm{c}$ at a reference state denoted by superscript 0, then one can find all elements of the internal rate vector $\boldsymbol{r}$ at a different state where the enzyme levels have changed from $\boldsymbol{e}^0$ to $\boldsymbol{e}$:

$$\boldsymbol{r}/\boldsymbol{r}^0 = (\boldsymbol{e}/\boldsymbol{e}^0)\boldsymbol{f}\left(\boldsymbol{s}/\boldsymbol{s}^0, \boldsymbol{c}/\boldsymbol{c}^0, \boldsymbol{E}_\mathrm{c}^0, \boldsymbol{E}_\mathrm{s}^0\right) \tag{6.29}$$

At the reference *steady* state, all the individual rates r_i are necessarily equal to r_i^0, but if transient experiments are conducted to find the rates, and thereby the elasticities at the reference condition, then individual rates r_i are not equal to r_i^0 until the steady state has again been reached.

When flux control coefficients are determined through elasticities, it is a serious obstacle that the rate expressions, or even the form of these expressions, are unknown. Recent research, e.g., by Hazimanikatis and Bailey (1997) and by Heijnen (2005), has shown that when approximate rate expressions of a certain structure are used instead of the correct expressions, then the transient experiments conducted to obtain the parameters of these approximate expressions are easily interpreted. The resulting approximations for the vector function $\boldsymbol{f}$ in (6.29) can be used to find good approximations for the unfortunately inaccessible exact elasticities.

As a conclusion of this introduction to Metabolic Control Analysis the main theorems that allow flux control coefficients to be calculated without resort to experiments with different levels of enzyme activity will be listed. The theorems hold *for linear pathways*. When pathways with branches are treated more, complicated relations between the sensitivities must be derived.

The proof of the major theorems can be found in textbooks on *Metabolic Engineering* and will not be given here (see, however, Problem 6.4). A good reference is the study by Stephanopolous et al. (1998), which also considers much more complicated networks than the single linear pathway discussed in the present text. The monograph by Fell (1997), one of the original investigators of MCA, also offers many, qualitative insights on the subject.

The most valuable relationships between sensitivities for linear pathways are:

1. Flux Control Summation theorem

$$\sum_{1}^{N} C_i^J = 1\,; \quad C_i^J > 0, \quad \text{for } i = 1, 2, \ldots, N \tag{6.30}$$

The theorem states that the flux control coefficients are positive and sum up to 1. Hence, if N is large, the C_i^J will generally be small, but there will always be one that is largest, and this is the one that belongs to the rate-limiting reaction.

2. Flux Control Connectivity theorem

$$\sum_{1}^{N} C_i^J \varepsilon_{ji} = 0\,; \quad j = 1, 2, \ldots, N-1 \tag{6.31}$$

Since all the C_i^J are positive, some of the ε_{ji} must be negative. Negative ε_{ji} indicates that the metabolite s_j inhibits reaction r_i. Also, the product of a reversible reaction must have a negative influence on the rate of the reaction.

Together the two expressions (6.30) and (6.31) give:

$$\begin{pmatrix} 1 & 1\ldots & 1 & 1 & 1 \\ \varepsilon_{11} & \varepsilon_{12}\ldots & \varepsilon_{1,N-3} & \varepsilon_{1,N-2} & \varepsilon_{1,N-1} \\ \varepsilon_{21} & \varepsilon_{22} & \cdot & \cdot & \varepsilon_{2,N-1} \\ \cdot & \cdot & \cdot & \cdot & \cdot \\ \varepsilon_{N-1,1} & \cdot & \cdot & \cdot & \varepsilon_{N-1,N-1} \end{pmatrix} \cdot \begin{pmatrix} C_1^J \\ C_2^J \\ \cdot \\ \cdot \\ C_N^J \end{pmatrix} = \begin{pmatrix} 1 \\ 0 \\ \cdot \\ \cdot \\ 0 \end{pmatrix} \tag{6.32}$$

The scalar product of the first row of the matrix multiplied with $\boldsymbol{C^J}$ expresses the theorem (6.30), while the scalar products of the following rows with $\boldsymbol{C^J}$ express the $N-1$ sums of (6.31). It is seen that (6.32) is the desired relationship by which the flux control coefficients are found when the $(N-1)\times(N-1)$ elasticities are known.

Westerhoff and Chen (1984) introduced another connectivity theorem:

$$\sum_{1}^{N} C_{ij}\varepsilon_{ki} = -1 \;\text{ where }\; k = j,\;\; j = 1, 2, \ldots, N-1, \;\text{ but} = 0 \;\text{ for }\; k \neq j. \tag{6.33}$$

This last theorem connects the concentration control coefficients (6.28), i.e., the sensitivity of the internal metabolite concentrations to changes in the N enzymes activities, with the elasticities, and if the relations (6.33) are added to (6.32), one obtains a matrix equation:

$$\boldsymbol{EC}^* = \boldsymbol{I} \tag{6.34}$$

E is the matrix on the left hand side of (6.32) and $\boldsymbol{I}$ is an $(N \times N)$ unity matrix. The first column of $\boldsymbol{C}^*$ contains the N flux control coefficients. The next j columns, j = 1, 2, . . . , N−1, contain $-C_{ij}$, i = 1, 2, . . . N, of concentration control coefficients, (6.28). With the help of (6.33) it is easily seen that the matrix equation (6.34) is correct.

Although (6.34) nicely connects all the major sensitivity coefficients used in Metabolic Control Analysis, it is (6.32) which is most important for calculation of the key sensitivities, the flux control coefficients C_i^J.

The calculations involved in Metabolic Control Analysis have now become almost automated after several research groups have developed software to find elasticities and flux control coefficients based on simulated data that have been overlaid by stochastic experimental errors. The programs, e.g., those originating in the group of (Heijnen et al. 2004, Kresnowati et al. 2005), do not assume that the structure of the enzyme reactions is known.

Still, from a pedagogical point of view, it may be helpful to understand, by the use of a simple illustrative example, how C_i^J and ε_{ji} are derived from analytical expressions for the rates r_i. This is the topic of the following Sects. 6.4.2 and 6.4.3.

6.4.2 *Using Connectivity Theorems to Calculate Control Coefficients*

The following linear pathway with only two reactions and one intracellular metabolite concentration s_1 will be used to illustrate the basic concepts of Metabolic Control Analysis

$$S \xrightarrow{r_1} S_1 \xrightarrow{r_2} P \tag{6.35}$$

For simplicity, the reverse reactions are neglected. The concentration p of P is fixed (or the rates do not depend on p), and in Sect. 6.4.2, s is also fixed at a reference value s^0. We wish to calculate the steady-state flux J from S to P via the intracellular species S_1, whose concentration will vary not only with s but also with the architecture of the pathway, i.e., with the parameters of the two enzymatic reactions r_1 and r_2.

Since the steady state is considered, the two rates r_1 and r_2 must be equal and also be equal to the steady-state flux J through the pathway.

We shall consider two different expressions for r_1:

$$r_1 = \frac{k_1 s}{s + K_1} \tag{6.36a}$$

$$r_1 = \frac{k_1 s}{s + K_1\left(1 + \frac{s_1}{K_{eq}}\right)} \tag{6.36b}$$

In (6.36a), the simple Michaelis–Menten kinetics is used, and in (6.36b), the competitive inhibition scheme (6.10). Here, the intermediate S_1 forms a dead-end complex with the free form of the enzyme that catalyzes the first reaction of the pathway.

The second reaction r_2 of (6.35) is assumed to follow simple Michaelis–Menten kinetics:

$$r_2 = \frac{k_2 s_1}{s_1 + K_2} \tag{6.37}$$

The rate constants k_1 and k_2 typically have the dimension mol L^{-1} h^{-1}, and they are assumed to be proportional to the enzyme level e_i used in reaction r_i.

In order to reduce the number of parameters somewhat, the following dimensionless variables and parameters are introduced:

$$\begin{aligned} x &= \frac{k_1}{k_2}, \qquad y = \frac{s_1}{s^0}, \qquad J' = \frac{J}{k_2} \\ a &= \frac{K_{eq}}{s^0}, \qquad b = \frac{K_1}{s^0}, \qquad c = \frac{K_2}{s^0} \end{aligned} \tag{6.38}$$

$$r_1 = \frac{k_1}{1 + b} \tag{6.36a}$$

and with the dimensionless variables (6.36 a, b) are rewritten as:

$$r_1 = \frac{k_1}{1 + b\left(1 + \frac{y}{a}\right)} \tag{6.36b}$$

$$J' = \frac{J}{k_2} = \frac{y}{y + c} \tag{6.39}$$

When r_1 given by (6.36a) is equated with r_2, one obtains:

$$\frac{x}{1 + b} = \frac{y}{y + c} \quad \text{or} \quad y = \frac{cx}{1 + b - x} \tag{6.40}$$

x is the ratio k_1/k_2, which is proportional to the ratio e_1/e_2 between the enzyme dosages of the two reactions. With increasing x, the enzyme dosage of r_1 increases relative to that of r_2. Without loss of generality, e_2 can be set to 1 and e_1 (or $x = e_1/e_2$) is the only independent variable. We note that, as expected,

$$J = k_2 \frac{y}{y + c} = k_2 \frac{x}{1 + b} = \frac{k_1}{1 + b}$$

and J can be calculated both as r_1 and as r_2.

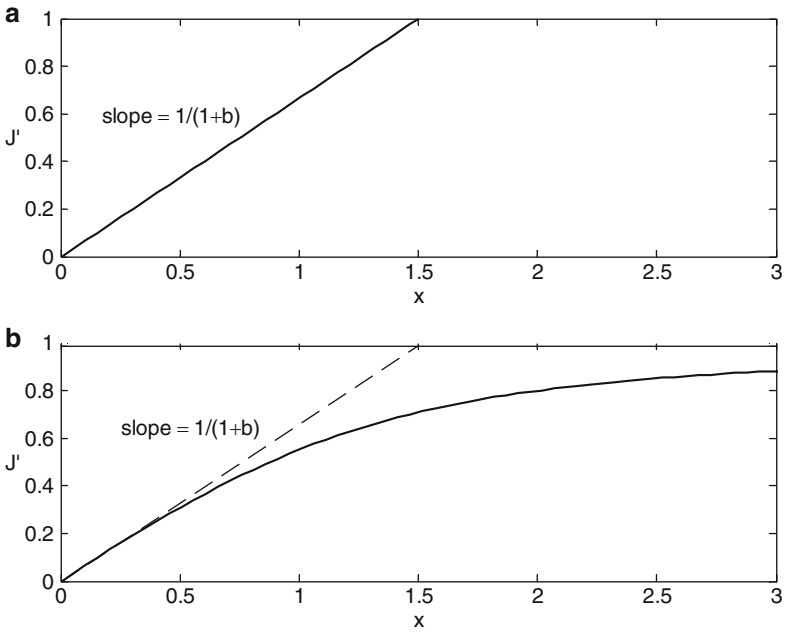

Fig. 6.9 Dimensionless flux $J' = J/k_2$ through a two-step pathway (6.35) as a function of the ratio $r_{\max 1}/r_{\max 2} = k_1/k_2 = x$. In both cases, r_2 is given by (6.37). The parameters of (6.38) are $a = 1$, $b = c = 0.5$. (**a**) r_1 given by (6.36a), and (**b**) r_1 given by (6.36b)

When (6.36b) is used for r_1, y is calculated from either (6.41a) or (6.41b):

$$\frac{k_1}{1 + b\left(1 + \frac{y}{a}\right)} = \frac{k_2 y}{y + c} \rightarrow x = \frac{y}{y + c}\left(1 + b\left(1 + \frac{y}{a}\right)\right) \tag{6.41a}$$

$$2y = -\left(\frac{a}{b} + a - \frac{a}{b}x\right) + \left(\left(\frac{a}{b} + a - \frac{a}{b}x\right)^2 + 4\frac{ac}{b}x\right)^{1/2} \tag{6.41b}$$

The dimensionless pathway flux $J'(x) = J/k_2 = \frac{x}{1+b}$ is shown in Fig. 6.9 for each of the two expressions for r_1, (6.36a) and (6.36b).

There is an important difference between the two expressions (6.36a) and (6.36b).

With (6.23a), J is independent of the parameters of r_2, and J' is proportional to x.

With (6.23b), $J'(x)$ has the typical downward concave shape of the hyperbolic functions which determine the kinetics for individual enzymes. An increase in k_1 for fixed k_2 is profitable for small x (i.e., small k_1), but has little effect for large x.

For small x, a power series expansion of $y(x)$ in (6.41b) yields

$$y \approx \frac{c\,x}{b+1} \quad \text{and} \quad J' \approx \frac{x}{1+b} \tag{6.42}$$

For large x, (6.41b) shows that $y \sim ax/b$ and $J' \rightarrow 1$.

Consequently, for small values of k_1, the flux J depends only on the kinetic parameters k_1 and K_1 of r_1. The value of s_1 is not large enough to give any influence of the denominator term s_1/K_{eq} in (6.36b). For larger k_1 values, the parameters K_2 and K_{eq} start to influence the flux J through the pathway, and for $x \to \infty$, the asymptote $J'(x) = 1$ is approached.

We can conclude the following:

- If both rate constants are multiplied with the same factor f, the flux J through the pathway also increases by a factor f. The shape of J' does not change, since J' depends only on x.
- If s is doubled to $2s^0$, the value of all parameters a, b and c will decrease by a factor 2, and $y(x)$, determined from (6.41b), will have a different shape. $J'(x)$ will increase faster with x since b is smaller but the initial slope $(b+1)^{-1}$ has a maximum of 1 for $s \to \infty$. Hence, J' does not certainly change proportional to a change in s.

These observations originate in the form of r_1. In (6.36a), the parameters of r_2 have no influence at all on the flux. With (6.36b), the control of the flux is distributed between the two reactions, and for a fixed k_2, it moves toward the second reaction when k_1 increases, since a larger value of k_1 leads to a higher value of y in (6.41), and this influences r_1 negatively through the denominator term, which depends on y. The smaller the value of parameter c, the faster is step two of the sequence, and S_1 is removed fast enough to avoid a build-up of S_1, waiting to be processed in step two of the reaction sequence.

The distribution of flux control between step 1 and step 2 depends only on how fast $J'(x)$ increases with x. If the slope of $J'(x)$ is large, the first reaction controls the flux, and as the slope decreases control, it shifts to the second reaction. The flux control is determined by the relative values of the two flux control coefficients (6.43).

$$C_1^J = \frac{\partial J}{\partial e_1}\frac{e_1}{J} \qquad \text{and} \qquad C_2^J = \frac{\partial J}{\partial e_2}\frac{e_2}{J} \tag{6.43}$$

In (6.43), the enzyme concentrations e_1 and e_2 as well as the rate constants k_1 and k_2 can be used if the enzyme activities, and hence the rate constants, are proportional to the enzyme dosages.

For (6.35a), one obtains

$$\begin{aligned} C_1^J &= \frac{\partial J}{\partial k_1}\frac{k_1}{J} = (1+b)^{-1}\frac{k_1}{\left(\frac{k_1}{1+b}\right)} = 1 \\ C_2^J &= \frac{\partial J}{\partial k_2}\frac{k_2}{J} = 0 \end{aligned} \tag{6.44}$$

since k_1 (or x) is an independent variable, while k_2 is a constant.

To obtain the result for (6.35b), the "chain-rule" for differentiation is used:

$$C_1^J = \frac{\partial J}{\partial k_1}\frac{k_1}{J} = \frac{\partial J'}{\partial x}\frac{x}{J'} = \frac{\partial J'}{\partial y}\frac{\mathrm{d}y}{\mathrm{d}x}\frac{x}{J'} \tag{6.45}$$

$$\frac{\mathrm{d}J'}{\mathrm{d}y} = \frac{c}{(c+y)^2} = \frac{cJ'J}{y(c+y)};$$

$$x = \frac{y}{y+c}\left(1+b\left(1+\frac{y}{a}\right)\right) \text{ from (6.41 a), and } \frac{\mathrm{d}y}{\mathrm{d}x} = \frac{1}{\frac{\mathrm{d}x}{\mathrm{d}y}}:$$

$$\frac{\mathrm{d}x}{\mathrm{d}y} = \frac{c}{(c+y)^2}\left(1+b\left(1+\frac{y}{a}\right)\right) + \frac{y}{c+y}\frac{b}{a} = \frac{c}{c+y}\frac{x}{y} + \frac{y}{c+y}\frac{b}{a}$$

$$C_1^J = \frac{x\times c}{y}\frac{1}{\left(c\frac{x}{y}+y\frac{b}{a}\right)} = \frac{1}{1+\frac{by^2}{acx}}; \quad C_1^J = 1 - C_1^J \tag{6.46}$$

For $by^2/acx = 1$, the value of both C_1^J and C_2^J is 1/2. At this point, $y^2 = ac(1+b)/b$ and $x = (1+b)$.

To optimize the architecture of the pathway, the ratio x between k_1 and k_2 should be $(1+b)$. In the case of the numerical example, $k_1/k_2 = x = 1.5$. The flux J can be amplified in an optimal way by increasing both k_1 and k_2, while keeping the ratio between the rate constants at 1.5.

Calculation of C_i^J by means of the *elasticities* is always simpler than by direct application of the definition (6.26) of the flux control coefficients.

The calculation of C_i^J through elasticities and application of the flux connectivity theorem in the form of (6.32) will be illustrated for r_1 given by (6.36b).

With one intracellular concentration s_1 (and fixed values of s and p), there are only two elasticities:

$$\varepsilon_{11} = \frac{\partial r_1}{\partial s_1}\frac{s_1}{r_1} = \frac{\partial r_1}{\partial y}\frac{y}{r_1} = -\frac{\frac{b}{a}y}{\left(1+b\left(1+\frac{y}{a}\right)\right)} \tag{6.47}$$

$$\varepsilon_{12} = \frac{\partial r_2}{\partial s_1}\frac{s_1}{r_2} = \frac{\partial r_2}{\partial y}\frac{y}{r} = \frac{c}{y+c} \tag{6.48}$$

ε_{11} is clearly negative since an increase in s_1 or y must decrease r_1. ε_{12} is positive since an increase in s_1 will increase the rate of conversion of S_1 to P.

If r_1 was given by (6.36a) ε_{11} would be zero since in that case, r_1 will be independent of s_1.

Now (6.32) is used:

$$\begin{pmatrix} C_1^J \\ C_2^J \end{pmatrix} = \begin{pmatrix} 1 & 1 \\ \varepsilon_{11} & \varepsilon_{12} \end{pmatrix}^{-1}\begin{pmatrix} 1 \\ 0 \end{pmatrix} = \frac{1}{\varepsilon_{12}-\varepsilon_{11}}\begin{pmatrix} \varepsilon_{12} \\ -\varepsilon_{11} \end{pmatrix} \tag{6.49}$$

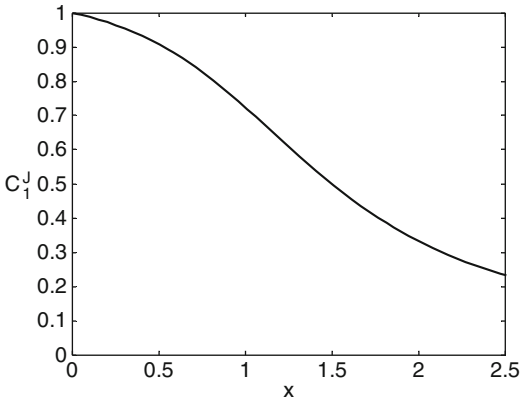

Fig. 6.10 Flux control coefficient C_1^J for the reaction sequence (6.36b), (6.37)

Obviously, $C_1^J + C_2^J = 1$, but more specifically for (6.36b),

$$C_1^J = \frac{\varepsilon_{12}}{\varepsilon_{12} - \varepsilon_{11}} = \frac{1}{1 + \dfrac{\dfrac{b}{ac} y\,(y+c)}{1 + b\left(1 + \dfrac{y}{a}\right)}} = \frac{1}{1 + \dfrac{by^2}{acx}} \tag{6.50}$$

Figure 6.10 shows C_1^J calculated from (6.46) or (6.50) as a function of x. Equation (6.41b) is used to calculate y corresponding to a given value of x. A lot of algebra associated with calculation of C_1^J directly from (6.26) is obviously bypassed.

In general, for a rate expression $r_i = N(\boldsymbol{s})/D(\boldsymbol{s})$, the following relation (6.50) may be useful for calculation of the elasticities ε_{ji}, either manually or by using a symbolic computer software.

$$\varepsilon_{ji} = \frac{\left(D\frac{\partial N}{\partial s_j} - N\frac{\partial D}{\partial s_j}\right)}{D^2} \times \frac{s_j D}{N} = s_j\left(\frac{1}{N}\frac{\partial N}{\partial s_j} - \frac{1}{D}\frac{\partial D}{\partial s_j}\right) \tag{6.51}$$

Example 6.6 *Illustration of Metabolic Control Analysis using analytical expressions for r_i.* We now consider the linear pathway with three intermediates. Consequently, there are four enzymatic reactions, $N = 4$. Feedback inhibition of the second enzyme, e_2, by the last intermediate, s_3, is included. All the reactions are taken to be reversible, and the feedback inhibition is taken to be noncompetitive. Thus, we may write the net rates for the four enzymatic reactions as

$$r_1 = k_1 e_1 \frac{s}{s + K_1\left(1 + \dfrac{s_1}{K_1^*}\right)} \tag{1}$$

$$r_2 = k_2 e_2 \frac{s_1}{s_1 + K_2\left(1 + \dfrac{s_2}{K_2^*}\right)} \frac{1}{1 + \dfrac{s_3}{K_{\text{inhib}}}} \tag{2}$$

$$r_3 = k_3 e_3 \frac{s_2}{s_2 + K_3\left(1 + \dfrac{s_3}{K_3^*}\right)} \tag{3}$$

$$r_4 = k_4 e_4 \frac{s_3}{s_3 + K_4\left(1 + \dfrac{p}{K_4^*}\right)} \tag{4}$$

The rate of the reverse reaction is included in a somewhat unusual fashion, in the inhibition term in the denominator, which increases with increasing conversion. Close to equilibrium, the rate expressions in (1)–(4) cannot possibly be true. For the purpose of illustrating the methodology, the realism of the kinetic expressions is, however, not of overriding importance.

$$\mathbf{E} = \begin{pmatrix} 1 & 1 & 1 & 1 \\ -\frac{s_1 K_1/K_1^*}{a_1} & \frac{K_2(1+s_2/K_2^*)}{a_2} & 0 & 0 \\ 0 & -\frac{s_2 K_2/K_2^*}{a_2} & \frac{K_3(1+s_3/K_3^*)}{a_3} & 0 \\ 0 & -\frac{s_3}{K_{\text{inhib}}+s_3} & -\frac{s_3 K_3/K_3^*}{a_3} & \frac{K_4(1+p/K_4^*)}{a_4} \end{pmatrix} \tag{5}$$

In (5), the parameters combinations $\boldsymbol{a}$ are given by:

$$\begin{pmatrix} a_1 \\ a_2 \\ a_3 \\ a_4 \end{pmatrix}' = \begin{pmatrix} s + K_1(1 + s_1/K_1^*) \\ s_1 + K_2(1 + s_2/K_2^*) \\ s_2 + K_3(1 + s_3/K_3^*) \\ s_3 + K_4(1 + s_4/K_4^*) \end{pmatrix} \tag{6}$$

From (5), it is seen that the elasticity coefficients for the ith enzyme with respect to its substrate – intermediate number $(i-1)$ – is positive, whereas its elasticity coefficient with respect to its product (i.e., the ith intermediate) is negative.

If the kinetic parameters are known together with steady-state levels of the intermediates, the numerical values of the elasticity coefficients can be calculated, but normally it is difficult to obtain in vivo experimental values for the parameters, and it is likely that the in vitro-determined parameters do not represent the true situation. Here we will, however, assume that at a particular steady state [s, p, (s_1, s_2, s_3 (s, p))], we have determined the elasticity coefficients to be given by

$$\mathbf{E} = \begin{pmatrix} 1 & 1 & 1 & 1 \\ -0.9 & 0.5 & 0 & 0 \\ 0 & -0.2 & 0.7 & 0 \\ 0 & -1.0 & -0.5 & 0.5 \end{pmatrix} \tag{7}$$

The control coefficient matrix is obtained from the full equation (6.34) with the concentration control coefficients $-C_{i,j}$, $i = 1, 2, \ldots, N$ filling out the last $N-1$ columns of $\boldsymbol{C}^*$ and the right hand side being an $(N \times N)$ identity matrix.

$$\mathbf{C} = \begin{pmatrix} 0.14 & 0.96 & 0.39 & 0.27 \\ 0.24 & -0.27 & 0.69 & 0.48 \\ 0.07 & -0.08 & -1.23 & 0.14 \\ 0.55 & -0.61 & 0.15 & -0.89 \end{pmatrix} \tag{8}$$

The desired flux-control coefficients C_i^J are found in the first column of $\boldsymbol{C}^*$. The last enzyme in the pathway has a flux-control coefficient significantly higher than $= \frac{1}{N} = \frac{1}{4} = 0.25$, and it is, therefore, the rate-controlling step. The rate of conversion of S_3 is too small. This in itself reduces the total flux through the sequence, and furthermore a buildup of a high level of the metabolite S_3 impedes the second reaction, the conversion of S_1 to S_2. Thus, an increase in the level of the enzyme E_2 that is under feedback control will not necessarily be the best remedial action.

From Eq. (8), it is observed that the concentration-control coefficients for the *i*th metabolite with respect to the *i*th enzyme is positive, but with respect to enzyme $i-1$, it is negative. When the concentration of the *i*th enzyme increases, then the concentration of the *i*th intermediate (product of the reaction) increases. At the same time the concentration of the $(i-1)$ intermediate (the substrate) decreases. The last row of $\boldsymbol{C}^*$ contains in its last three columns the concentration-control coefficients pertinent to the last enzyme. When the activity of this enzyme is increased, the levels of the last intermediate S_3 and of the first intermediate S_1 sharply decrease while the level of the second intermediate increases. This is easily understood; both S_3 and S_1 are substrates that are more rapidly consumed when the level of E_4 increases, and S_3 directly and S_1 indirectly when the inhibition control of E_2 is relieved. Notice that the last three columns of $\boldsymbol{C}^*$ sum to zero, as they should according to (6.33), and that the first row contains only positive control coefficients: The total flux and concentration level of all intermediates increase when the activity of the first enzyme is increased.

The effect of the feedback inhibition can be illustrated by setting $\varepsilon_{32} = 0$ and calculating the control matrix for this situation. The result is given in (9):

$$\mathbf{C} = \begin{pmatrix} 0.27 & 0.82 & 0.75 & 0.52 \\ 0.47 & -0.52 & 1.34 & 0.94 \\ 0.13 & -0.15 & -1.05 & 0.27 \\ 0.13 & -0.15 & -1.04 & -1.73 \end{pmatrix} \tag{9}$$

By comparison of the control coefficients with those in (8), where feedback inhibition is present, it is observed that the rate control is now at the second enzyme in the pathway. This enzyme is now a potential rate-controlling enzyme for the true system with feedback inhibition, since if the inhibition is removed or reduced in strength, the second reaction controls the overall flux. When the feedback inhibition is lifted, all three concentration control coefficients in the last row become negative. Increasing the activity of the last enzyme in a straight sequence lowers the level of all intermediates.

We now consider a microorganism in which the pathway described above (with feedback inhibition) is active. The product of the pathway is a desired product, e.g., an antibiotic, and using MCA, we want to design a new strain in which an increased flux through the pathway is possible. Thus, we want to decrease the rate control, which can be done, e.g., by inserting a gene coding for an enzyme that also catalyzes the conversion of S_1 to S_2 but has different elasticity coefficients, i.e., different kinetic parameters compared with the native enzyme. This could be a higher value of K_{inhib} (less inhibition) and/or a lower ratio of K_2/K_2^*.

Assume that the search leads to a strain that has an enzyme similar to E_4, but with other elasticity coefficients. The gene for this slightly different enzyme is cloned into the chosen production strain. Take the elasticity coefficients for the second pathway reaction to be

$$\begin{pmatrix} \varepsilon_{11} \\ \varepsilon_{12} \\ \varepsilon_{13} \end{pmatrix} = \begin{pmatrix} 1.0 \\ -0.6 \\ -0.3 \end{pmatrix} \tag{10}$$

Now the feedback inhibition by s_3 is weaker, and the ratio K_2/K_2^* is slightly lower. With the slightly different enzyme in the production strain instead of the native enzyme, the control matrix is found to be

$$\mathbf{C} = \begin{pmatrix} 0.25 & 0.83 & 0.72 & 0.50 \\ 0.23 & -0.25 & 0.65 & 0.45 \\ 0.19 & -0.22 & -0.88 & 0.39 \\ 0.33 & -0.36 & -0.49 & -1.34 \end{pmatrix} \tag{11}$$

Thus, with the new enzyme, the flux control of the last enzyme has been reduced, and the control coefficients are all close to $1/N = 0.25$. Consequently, none of the enzymes dominate the flux control in the pathway.

MCA suggests a systematic way of improving the overall performance of a metabolic pathway and points to specific experiments that may assist the protein engineering work. What has not been included in the above discussion is the role of the operating conditions on the performance of the cell. All intracellular metabolite concentrations are calculable once s, p, and the kinetics are given. The elasticity coefficients are complex functions of s_i, and before any enzyme modification (i.e., changes in kinetic parameters) is attempted the current reaction network must be optimized to give the maximum flux by simulations at different s and p values.

When the pathway architecture has been optimized, all the control coefficients are of approximately the same size, but this does not necessarily mean that the flux through the pathway is significantly higher than that in the native strain. This has to be checked separately. However, if one obtains a modified strain in which all the control coefficients have approximately the same value, the flux may be increased by amplifying the level of all the enzymes, e.g. by inserting a stronger promoter upstream of the genes coding for all pathway enzymes.

6.4.3 *The Influence of Effectors*

In the analysis of the two-step linear pathway of Sect. 6.3.2, it was assumed that the feed concentration s of substrate was always equal to the reference concentration s^0 and that the product P did not influence the kinetics. We shall here continue the discussion of the simple example, but include the influence of *effectors* on the pathway architecture. As an example, the influence of s will be discussed. When s is changed from s^0 to another value s, the parameters a, b, and c of (6.38) will change. If, e.g., s is changed from *a reference value* s^0 to a value twice as large the parameters will all be changed by a factor of 1/2, if the *new* S concentration $s = 2\ s^0$ is used to normalize the Michaelis constant. All the calculations leading up to (6.46) are duplicated, and a $C_1^J(x)$ relation similar to that of Fig. 6.9 can be depicted. $C_1^J = 1/2$ when $y^2/x = 1/2$ when the original data for the Michaelis constants are used. Hence, at the point where $C_1^J = 1/2$ the values of (x, y) change from $(1.5, 1.5^{1/2})$ to $(1.25, 0.625^{1/2})$.

In the following, we shall, however, in accordance with (6.29) introduce a new variable $s' = s/s^0$, as a representative of the external variables $\boldsymbol{c}$. s_1/s^0 represents the vector of internal variables.

Consequently, we have the following dimensionless variables

$$x = k_1/k_2, \quad s' = s/s^0, \quad \text{and } y = s_1/s^0 \tag{6.52}$$

The parameters are the same as before

$$a = K_{\text{eq}}/s^0, \quad b = K_1/s^0 \quad \text{and} \quad c = K_2/s^0 \tag{6.53}$$

$$R_1 = r_1/k_2 = \frac{s'x}{s' + b\left(1 + \frac{y}{a}\right)} \quad \text{and} \quad R_2 = r_2/k_2 = \frac{y}{y + c} \tag{6.54}$$

Equating R_1 and R_2 yields

$$\frac{xs'}{s' + b\left(1 + \frac{y}{a}\right)} = \frac{y}{y + c} \rightarrow x = \frac{y}{s'(y + c)}\left(s' + b\left(1 + \frac{y}{a}\right)\right) \tag{6.55}$$

$$2y = -\left(a + \frac{a}{b}s' - \frac{a}{b}s'x\right) + \sqrt{\left(a + \frac{a}{b}s' - \frac{a}{b}s'x\right)^2 + \frac{4ac}{b}s'x} \tag{6.56}$$

The dependent variable y and both dimensionless rates R_1 depend on two (independent) variables, x and s'; in R_1, the dependency is seen directly, but R_2 also depends on s' through y.

The elasticities ε_{1s} and ε_{2s} are given by

$$\varepsilon_{1s} = \frac{\partial R_1}{\partial s'}\frac{s'}{R} = \frac{b(1 + y/a)}{s' + b(1 + y/a)} \quad \text{and} \quad \varepsilon_{2s} = 0 \text{ since } \frac{\partial R_2}{\partial s'} = 0 \tag{6.57}$$

Hence, all the terms in (6.29) are known for the example with two sequential reactions: $r = \begin{pmatrix} r_1 \\ r_2 \end{pmatrix}$, $J^0 = r_1$ or r_2 at the reference state, $\boldsymbol{e} = x$, $\boldsymbol{s} = s_1$, $\boldsymbol{c} = s$, $\boldsymbol{E}_{\text{c}}^0 = (\varepsilon_{11,s}, \varepsilon_{12,s})^0$, $\boldsymbol{E}_{\text{s}}^0 = (\varepsilon_{11,s}, \varepsilon_{12,s})$.

The reference state for $(\boldsymbol{e}, \boldsymbol{s}, \boldsymbol{c})$ is (x^0, s_1^0, s^0).

6.4.4 Approximate Methods for Determination of the C_i^J

As discussed in Sect. 6.4.1, there are two major obstacles in the application of MCA:

1. To find the flux concentration control coefficients at a reference state by (6.26), one needs to measure small changes $J - J^0$ resulting from a small changes in e_i from $(e_i)^0$. The accuracy of $(C_i^J)^0$ will be poor. Also, to find $\boldsymbol{C}^J$ at another value of $\boldsymbol{e}$, N

new strains, each with a different activity level of one enzyme activity (concentration), must be constructed and examined. The change of e_i must not result in a change in the other enzyme activities, and this is difficult to obtain in practice.

2. The rates r_i are not given by analytical functions of $\boldsymbol{s}$ and $\boldsymbol{c}$, as was the case in the illustrative example of (6.54). The rate expressions must be derived by a significant experimental investigation, and there is no chance that the correct form of r_1 and r_2 in (6.54) will be the result of the data-fitting procedure. Hence, C_i^J will be derived by dubious perturbations of rate expressions that are only approximations to the correct ones.

The need for approximate determination of control coefficients is obvious, and an essential point is that the approximate solutions must give reasonably accurate results even for large perturbations in e_i, and that the approximate rate expressions can be extrapolated to values at some distance from the reference values.

Except in a trivial case of irreversible reactions r_i with no feedback control of the pathway flux (the curve on Fig. 6.9a), flux control will always be distributed between the different enzymatic reactions. in the pathway. The hyperbolic curve $J'(x)$ on Fig. 6.9b is much more typical for the relation between flux and enzyme levels. It results whenever an enzymatic reaction is reversible or the metabolic product is an inhibitor of the reaction, as in (6.36b).

In the illustrative example where $\boldsymbol{e}$ is the vector $(x, 1)$ or just x – i.e., only one independent enzyme concentration, the dimensionless flux J' appears to be well approximated by

$$J'(x) = \frac{x}{x+K} \tag{6.58}$$

Using the approximate expression (6.57) for J, the flux control coefficient C_1^J at the reference state $x = x^0$ is given by

$$(C_1^J)^0 = \left(\frac{\partial J'}{\partial x}\frac{x}{J'}\right)^0 = \frac{K}{(x^0+K)^2}\frac{x^0}{J'(x^0)} = KJ'(x^0)/x^0 \tag{6.59}$$

The chord between (x, J') and $(x^0, J'(x^0))$ has a slope $\frac{J'-J'(x^0)}{x-x^0}$, and

$$\frac{x}{J'}\frac{J'-J'(x^0)}{x-x^0} = \frac{x}{J'}\frac{K(x-x^0)}{(x-x^0)(x+K)(x^0+K)} = \frac{KJ'(x^0)}{x^0} \tag{6.60}$$

Consequently, if the approximation (6.58) is acceptable, the flux control coefficient C_1^J at the reference state can be calculated based on two measurements: (x, J') and $(x, J')^0$. The differences $x - x^0$ and $J - J^0$ can be large without affecting the result.

This observation by Small and Kacser (1993) that the flux control coefficient C_i^J can be obtained using *large deviations* from the reference state when the flux $J(e_i)$ is (approximately) a hyperbolic function of e_i has been an important step forward for a practical application of MCA.

Example 6.7 *Calculation of the flux control coefficient at a reference state by large deviations.* At the reference state $[x = x^0 = 1.5,\ s' = 1]$, $(J')^0 = 0.710$; at $x = 1 = \frac{2}{3}x^0$, $J' = 0.553 = 0.779(J')^0$.

Using (6.60), one obtains an approximate value $\left(C_1^J\right)^0_{\text{approx}} = \frac{2/3}{0.779}\frac{0.779-1}{2/3-1} = 0.567$.

The two sets of measurements of $[x, J']$ give a fair assessment of $C_1^J(x = x^0 = 1.5) = 1/2$ that was determined in (6.46) using the analytical expressions for r_1 and r_2 for the sequence of reactions in the illustrative example. One can certainly conclude that the architecture of the pathway is nearly optimal at the reference state.

There are, however, other ways of approximation that give even better results than the hyperbolic approximation proposed by Small and Kacser.

Hatzimanikatis and Bailey (1997) introduced the approximate kinetics of (6.61) for evaluation of flux control in pathways, and they called it log(linear) kinetics. Heijnen (2005) has reviewed different approximate kinetics, and he also found that the approximation (6.61) (which he calls lin-log kinetics) of the function $\boldsymbol{f}$ in (6.29) is in general better than a number of other reasonable approximations.

The rate expressions r_i are approximated by

$$\boldsymbol{r} = \boldsymbol{e}(\alpha + \beta \ln \boldsymbol{s} + \gamma \ln \boldsymbol{c}) \tag{6.61}$$

When all the r_i are equal, one obtains the steady-state flux through the pathway $J = r_i$.

Specifically, when $\boldsymbol{e} = \boldsymbol{e}^{\mathbf{0}}$, the reference values for the N enzyme levels in the pathway, $J = J^0$, the reference flux through the pathway. Thus, for $\boldsymbol{e} = \boldsymbol{e}^{\mathbf{0}}$,

$$\boldsymbol{r}/J^0 = \boldsymbol{i} + \boldsymbol{E}_{\text{s}}^0 \ln(\boldsymbol{s}/\boldsymbol{s}^0) + \boldsymbol{E}_{\text{c}}^0 \ln(\boldsymbol{c}/\boldsymbol{c}^0) \tag{6.62}$$

In (6.62), each element of the vector of dependent variables $\boldsymbol{y}$ and the vector of independent (external) variables $\boldsymbol{c}$ is divided by its value at the reference state. $\boldsymbol{i}$ has N elements $= 1$.

From a computational point of view, the expression (6.61) has the advantage that the elasticities are found by a trivial calculation. Thus, at $\boldsymbol{e} = \boldsymbol{e}^{\mathbf{0}}$,

$$\frac{\partial r_i}{\partial y_j}\frac{y_j}{r_i} = \frac{\partial r_i}{r_i \partial \ln y_j} = \varepsilon_{ji,y} = \beta_{ij}, \quad \text{and} \quad \frac{\partial r_i}{\partial \ln c_k}\frac{1}{r_i} = \varepsilon_{ki,c} = \gamma_{ik}; \qquad j = 1, 2, \ldots, N-1 \ \text{ and } \ k = 1, 2, \ldots, M \tag{6.63}$$

$N - 1$ is the number of intracellular metabolites, and M, the number of effectors.

As indicated above, the major advantage of the so-called *lin-log approximation* of the rates is, however, that (6.61) provides robust approximations – also when extrapolated much beyond the interval $[r_i, (y_j, c_k)]$ used to construct the approximation by linear least squares (LLS) fitting of the data.

To illustrate how the method functions, the illustrative example of Sect. 6.4.2 is again used.

Example 6.8 *Elasticities and flux control coefficients determined by the lin-log method.* A set of 20 y-values, [0.75 (0.05) 1.5] and 20s'-values [1(0.1)2] was fitted by LLS to R_1 and R_2 in (6.54) using the approximation

$$R_1 = \alpha_1 + \beta_1 \ln y + \gamma_1 \ln s'; \quad R_2 = \alpha_2 + \beta_2 \ln y \ln s' \tag{1}$$

The result for $x = 1.5$ is

$$\begin{aligned} R_1 &= 0.74778 - 0.193257 \ \ln \ y + 0.3649 \ \ln \ s', \\ R_2 &= 0.66502 + 0.209124 \ \ln \ y \end{aligned} \tag{2}$$

For $s' = s'^0 = 1$, and equating R_1 to R_2, one obtains $y = y^0 = 1.2283$ (exact value: $\sqrt{1.5} = 1.2247$).

For $s' = 2\,s'^0 = 2$, one obtains $y = 2.3031$ (exact value $(1 + \sqrt{13})/2 = 2.3028$). The exact values are obtained from (6.56).

Obviously, for error-free data, one could have used fewer data points [y, s'] in the fitting procedure. Problem 6.6 reviews the situation for real experiments with random errors in the data.

The elasticities $\varepsilon^0_{ji,y}$ and $\varepsilon_{ji,c}$ are obtained from (1) by division with the flux $J'^0 = 0.708$ (exact value $= 0.710$) at x^0, y^0:

$$\varepsilon_{11,y} = -0.1933/0.708 \quad \text{and} \quad \varepsilon_{12,y} = 0.2953, \ \varepsilon_{ii,s'} = 0.515. \ \varepsilon_{12,s'} = 0.$$

The flux control coefficient C^J_1 is calculated from the approximate $\varepsilon_{1j,y}$ of (3) and using (6.50). One obtains $C^J_1 = 0.515$, in good agreement with the exact value 1/2 at the reference value $x = 1.5$.

The flux control coefficient is, of course, independent of the external variable s'.

The result is, *that the flux control coefficients at the reference state can be obtained without including an experiment with* $x \neq x^0$. Since in a chemostat the rates and the concentration of intracellular metabolites increase with increasing dilution rate a series of steady-state cultivations with increasing D will give a set of [$\boldsymbol{r}$, $\boldsymbol{y}$] values that can be used as described above to obtain the flux control coefficients. This involves much less experimental work than the construction of cells with different levels of $\boldsymbol{e}$.

In a *transient* experiment, a whole set of corresponding values of rates and metabolite concentrations is, however, obtained. The richness of the data obtained by transient experiments is a great advantage compared to the time-consuming experiments needed to obtain steady-state values for different D-values.

Interpretation of transient data with the help of log-lin approximations of the rates will be discussed below.

Let $\boldsymbol{z}$ represent the vector $\left(\frac{s_1}{{s_1}^0}, \frac{s_2}{{s_2}^0}, \cdots, \frac{c_1}{{c_1}^0}, \cdots\right)$, $\boldsymbol{Z}^0$ a diagonal matrix with elements z^0_i, $\boldsymbol{T}$ the stoichiometric matrix for the N reactions of the pathway, and $\boldsymbol{J}^0$ a diagonal matrix that contains the values of r^0_i during the transient.

A transient $\boldsymbol{z}(\theta)$, where θ is dimensionless time from $\theta = 0$ to θ_{final} is obtained by integration of

$$\frac{\mathrm{d}z}{\mathrm{d}\theta} = (Z^0)^{-1} T J^0 \frac{r}{r^0} = (Z^0)^{-1} T J^0 (E_z)^0 \ln z \tag{6.64}$$

Here, (6.62) has been used to express $\boldsymbol{r}/\boldsymbol{j}^0$ in terms of $\ln(\boldsymbol{z})$, and E_z^0 is the matrix of all elasticities originating from $\boldsymbol{s}$ and $\boldsymbol{c}$.

If, in our illustrative example, the reference state is that for which the ratio $k_1/k_2 = x = 1.5$, we obtain the following interpretation of (6.64): $\theta = k_2\, t$; $\boldsymbol{z} = (y, s')$. $\boldsymbol{Z}^0$ is a diagonal matrix with $y^0 = \sqrt{1.5}$ and $s'^0 = 1$ in the diagonal. The two rows of the stoichiometric matrix $\boldsymbol{T}$ are $(1, -1)$ and $(-1, 0)$ for $z_1 = y/y^0$ and $z_2 = s/s^0$, respectively.

In the reference state, the rate of both reactions $r_i^0 = 0.708$ obtained from Example 6.8.

The vector differential equation (6.64) is solved from $\theta = 0$ with the initial conditions $(y, s'') = (z_1, z_{2)} = (\sqrt{1.5}, 2)$. At the end of the pulse experiment, $(z_1, z_{2)}$ has again settled at the steady-state values $(\sqrt{1.5}, 1)$.

$$\frac{\mathrm{d}\begin{pmatrix} z_1 \\ z_2 \end{pmatrix}}{\mathrm{d}\theta} = \begin{pmatrix} (y^0)^{-1} & 0 \\ 0 & (s'^0)^{-1} \end{pmatrix} \begin{pmatrix} 1 & -1 \\ -1 & 0 \end{pmatrix} \begin{pmatrix} 0.708 & 0 \\ 0 & 0.708 \end{pmatrix} \begin{pmatrix} \varepsilon_{11}^{y} & \varepsilon_{12}^{y} \\ \varepsilon_{11}^{s'} & \varepsilon_{12}^{s'} \end{pmatrix}^0 \begin{pmatrix} \ln z_1 \\ \ln z_2 \end{pmatrix} \tag{6.65}$$

If the elasticity matrix $\begin{pmatrix} -0.2729 & 0.2953 \\ 0.515 & 0 \end{pmatrix}$ obtained in Example 6.8 is inserted for $\boldsymbol{E}_z^0$, numerical integration of (6.65) will reproduce the profiles $(z(\theta))$ from $\theta = 0$ until the steady state $\boldsymbol{z}^0 = (\sqrt{1.5}, 1)$ is reached for $\theta \to \infty$.

Instead, we shall simulate an actual perturbation experiment from $z(\theta = 0)$, and use the "experimentally" obtained values of $z(\theta)$ to find approximate values for $\boldsymbol{E}_z^0$.

Example 6.9 *Determination of* E and C^J *from transients in a steady-state chemostat*. The transient experiment sketched above is somewhat unrealistic. At the steady state, there is no flow of S or S_1 out of the reactor, and $(s/s^0, s_1/s^0)$ are kept at their steady-state values by continuously "adding" S and S_1, thus producing a constant steady flux $J'(x) = R_1(x) = R_2(x)$ of the product P until either s or s_1 is perturbed.

A *real* experiment can be set up using a continuous stirred tank. The mass balances for the stirred tank in nonsteady state are discussed at length in Chap. 9, but even using only the introduction to chemostats in Chap. 3, we can establish the mass balances for s and for s_1 during a transient in which the substrate concentration s is changed from its steady-state value by adding a pulse of substrate to the reactor at $t = 0^+$.

For a fixed x, there are two independent variables, the feed concentration $s = s_{\text{feed}}$ to the reactor and the dilution rate D. We shall use a reference value s^0 to normalize s_{feed}, s, and s_1:

$$V\frac{\mathrm{d}s}{\mathrm{d}t} = -Vr_i + v(s_{\text{feed}} - s) = -vk_2R_1 - v(s_{\text{feed}} - s) \to \frac{\mathrm{d}(s/s^0)}{\mathrm{d}(k_2t/s^0)}$$

$$= -R_1 - \frac{v}{V(k_2/s^0)}\left(s_{\text{feed}}/s^0 - s/s^0\right) \tag{1}$$

$$V\frac{ds_1}{dt} = Vk_2R_1 - k_2R_2 - s_1v \rightarrow \frac{d(s_1/s^0)}{d(k_2t/s^0)} = R_1 - R_2 - \frac{v}{V(k_2/s^0)}s_1/s^0 \quad (2)$$

Introducing s' and y, one obtains

$$\frac{ds'}{d\theta} = R_1 - D(1 - s') \text{ (3a)} \quad \text{and} \quad \frac{dy}{d\theta} = R_1 - R_2 - Dy \text{ (3b)}. \quad (3)$$

All quantities in (3a and 3b) are dimensionless. θ is dimensionless time $= k_2t/s^0$, D is a dimensionless dilution rate $= \dfrac{v}{V(k_2/s^0)}$, and R_1 and R_2 are dimensionless reaction rates defined in (6.54).

The steady state considered is that for which $s_{\text{feed}} = s^0$, $D = 1.852$ for $x = 1.5$. For these values of the independent variables, one can calculate the steady-state values of the dependent variables s/s^0 and s_1/s^0 to, respectively, 0.6 and 0.2299 by insertion in (1) and (2), and using the analytical expressions (6.54) for R_1 and R_2. In an actual experiment, $(s', y)_{ss}$ are, of course, measured at the given values of s_{feed} and D for a strain with the given value x for the ratio of enzyme dosage between the first and the second reactions. Thereafter, the steady-state values of R_1 and R_2 can be calculated by inserting the measured $(s', y)_{ss}$ in (1) and (2) together with s_{feed}/s^0 and D.

Thus, for $s'_{ss} = 0.6$ and $D = 1.852$ one obtains $R_1 = 0.7408$ from (3a). When $s = s_{ss} = 0.6s^0$, one obtains $R_2 = R_1 - Dy = 0.7408 - 0.4258 = 0.3150$ at the steady state $s_1 = 0.2299s^0$.

In a reaction sequence with N steps, $\boldsymbol{y}$ is a vector of dimensionless intermediate concentrations, and the N dimensionless rates $R_1, R_2, R_3 \ldots R_N$ at the steady state can be found recursively as shown above for a two-step sequence.

Table 6.2 presents the result of a transient experiment, starting at the steady state determined above and initiated by addition of a pulse of substrate S at $\theta = 0^+$ that increases s' from 0.6 to 2. $s_{\text{feed}} = s^0$ and $D = 1.852$ during the whole experiment.

In columns 2 and 3 of Table 6.2 are values of y and s' generated by integration of (6.54) using a semi-implicit Runge–Kutta differential equation solver (Villadsen and Michelsen (1978)). A total of 25 equal integration steps $\Delta\Theta = 0.1$ are used, followed by one final step to $\Theta = 2.5$. At each point $\Theta = 0.1, 0.2 \ldots 2.4$, and $dy/d\Theta$ and $ds'/d\Theta$ – columns 4 and 5 – are calculated as the average of the slopes of the chords for the adjacent intervals (three-point formula for calculating the derivative). Next R_1 and R_2 are calculated – columns 6 and 7 – using (3a and 3b). Finally, in columns 8 and 9, the true values of R_1 and R_2 obtained by insertion of (y, s') in (6.54) are shown.

Even with the primitive formula for calculation of the derivatives, remarkably accurate values for the rates are obtained. Kresnowati et.al. (2005) use a more complicated, but certainly more accurate numerical algorithm to obtain simulated results for the rates, but the algorithm used above will be accurate enough for a demonstration of the numerical procedure.

The simulated results for y and s' would, of course, in a practical application of the method, be measured values of s_1/s^0 and s/s^0 during the pulse experiment. Based on the "measured" values of s_1 and s during the transient and the corresponding reconstructed reaction rates, approximate expressions for R_1 and R_2 of the same form as (2) of Example 6.7 can be obtained. The result is

Table 6.2 Reconstructing the reaction rates R_1 and R_2 using measurements of (s_1/s^0, s/s^0)

Θ	y	s'	dy/dΘ	ds'/dΘ	R_1	R_2	$(R_1)_{ex}$	$(R_2)_{ex}$
0	0.2299	2.0000						
0.1	0.2632	1.7285	0.272	−2.464	1.115	0.355	1.100	0.345
0.2	0.2844	1.5073	0.167	−2.005	1.065	0.371	1.052	0.363
0.3	0.2966	1.3276	0.0896	−1.626	1.019	0.380	1.008	0.372
0.4	0.3023	1.1821	0.0333	−1.314	0.977	0.383	0.967	0.377
0.5	0.3033	1.0648	−0.0066	−1.058	0.938	0.383	0.931	0.378
0.6	0.3010	0.9705	−0.0335	−0.850	0.905	0.381	0.898	0.376
0.7	0.2966	0.8948	−0.0505	−0.681	0.875	0.377	0.870	0.372
0.8	0.2909	0.8344	−0.0599	−0.544	0.850	0.371	0.846	0.368
0.9	0.2846	0.7861	−0.0636	−0.433	0.829	0.366	0.826	0.363
1	0.2782	0.7478	−0.0634	−0.345	0.812	0.360	0.809	0.357
1.1	0.2719	0.7172	−0.0605	−0.274	0.797	0.354	0.795	0.352
1.2	0.2661	0.6930	−0.0560	−0.217	0.786	0.349	0.784	0.347
1.3	0.2607	0.6738	−0.0506	−0.172	0.777	0.344	0.775	0.343
1.4	0.2560	0.6585	−0.0448	−0.137	0.769	0.340	0.768	0.339
1.5	0.2518	0.6464	−0.0391	−0.108	0.763	0.336	0.762	0.335
1.6	0.2481	0.6369	−0.0337	−0.086	0.758	0.333	0.758	0.332
1.7	0.2450	0.6293	−0.0287	−0.068	0.755	0.330	0.754	0.329
1.8	0.2424	0.6232	−0.0243	−0.054	0.752	0.327	0.751	0.327
1.9	0.2402	0.6185	−0.0204	−0.043	0.749	0.325	0.749	0.324
2	0.2383	0.6147	−0.0170	−0.034	0.748	0.323	0.747	0.323
2.1	0.2368	0.6117	−0.0141	−0.027	0.746	0.322	0.746	0.321
2.2	0.2355	0.6093	−0.0116	−0.021	0.745	0.321	0.745	0.320
2.3	0.2345	0.6074	−0.0095	−0.017	0.744	0.319	0.744	0.319
2.4	0.2336	0.6059	−0.0078	−0.0135	0.743	0.319	0.743	0.318
2.5	0.2329	0.6047						
10	0.2299	0.6000			0.7408	0.3150		

$$\begin{aligned} R_1/R_1^0 &= 1.182 - 0.04381 \ \ln y + 0.4866 \ \ln s' \ \text{ and } \ R_2/R_2^0 \\ &= 2.1628 + 0.7928 \ \ln y \end{aligned} \tag{4}$$

From (1), the flux control coefficient C_1^J at the steady state with $(s', y)_{ss} = (0.6, 0.2299)$ is calculated to $0.7928/(0.7928 - (-0.0438)) = 0.947$. Since the steady state rates $R_1 = 0.7408$ and $R_2 = 0.3150$ are not equal, the x value that belongs to the "measured" $(s', y)_{ss}$ is not $x = 1.5$, but $\boldsymbol{x} = 1.5 \times (0.3150/0.7408) = 0.6378$.

When ($x = 0.6378$, $s' = 0.6$) is inserted in (6.56), one obtains $y = 0.2299$ when $a = 1$ and $b = c = 0.5$.

The exact value of C_1^J is given by (6.50) and it is 0.9235.

The approximate value 0.947 for C_1^J is remarkably close to the exact value, and it is obtained with no information about R_1 and R_2, except the values of Table 6.1, the result of a single transient experiment in a chemostat.

It is not strange that the x value used in the transient experiment is much higher than that needed for obtaining the flux J' through the pathway, since R_1 must also support the flow $D(1 - s') = 0.7408$ of substrate S out of the system besides the product flow $J' = Dy = 1.852 \times 0.2299 = 0.3150$.

With the same enzyme make-up, $x = 1.5$, of the microorganism used in the experiment, one obtains the flux control coefficients at other values of x by changing s_{feed} and D. Thus, by conducting a transient experiment with $D = 0.4871$ and $s_{feed} = 2s^0$, one obtains (s', y, R_1, $R_2)_{ss} = (0.6, 0.4395, 0.6819, 0.4678)$, and the flux control coefficient C_1^J at $x = 1.5 \times 0.4678/0.6819 = 1.029$, $s' = 0.6$ is the result.

A final comment should be made concerning the experimental conditions to be used in the transient experiments on cell cultures.

Typically, the rate constants k_i for metabolic pathway reactions (exemplified with k_2 in Example 6.7) are of the order of 10 μM s^{-1}. With $s^0 = 10$ mM, the time it takes to reach $\Theta = 1$ is 1,000 s in the example. To obtain a dimensionless dilution rate of 1, v/V should be of the order of 0.001 $s^{-1} = 3.6\ h^{-1}$, and the flow rate through the reactor must be high. Measurements must be made at a high frequency to capture the rapid transient after a pulse addition of S. Therefore, it is crucial for practical applications of MCR that methods to be discussed in Sect. 9.3.5 have been developed during the last 15 years to capture fast transients. When the transient is as rapid as indicated here one does, of course, not have to worry about dilution of the metabolites by the growth of biomass during the experiments. Here the time constant is orders of magnitude smaller than that for the transient metabolite experiments, and the biomass concentration can safely be assumed to be constant.

All the results obtained in Sect. 6.4 can of course also be used to study the sensitivity of the enzymatic reactions in Sects. 6.1–6.3 to changes in the enzyme concentrations used in the experiment. Hereby the optimal design of an enzymatic process by which a substrate is converted to a product in a series of consecutive reactions can be determined. For a given value of the enzyme concentration in one of the reactions and a given substrate feed concentration, one can determine the ratio between enzyme concentrations in the different enzymatic steps that will give the highest production rate of the desired end product.

Problems

Problem 6.1 *Kinetic parameters from Lineweaver–Burk plots.* Figure 6.2b–d are drawn using the same values of $K_{eq}(=K_{m,true})$ and k $(=k_2e_0)$.

(a) Determine the values of K_{eq} and k from the figures.
(b) In both Fig. 6.2b, c, a value $s_1 = 1$ was used for the inhibitor. Determine K_{eq1}.
(c) In Fig. 6.2d, you are also required to determine K_{eq1}.

Problem 6.2 *Simulation of an enzyme-catalyzed reaction.* Consider the enzyme kinetics discussed in detail in Sect. 6.4.2. The rate constants of r_1 and r_2 (k_1 and k_2) are, respectively, 0.5 and 1 g substrate S converted (L reactor h)$^{-1}$. s^0 is 1 g L^{-1}. The parameters a, b, and c have the values 1, 0.5, and 0.5 at $s^0 = 1$ g L^{-1}.

A continuous stirred tank reactor is fed with S in a concentration s_{feed}. $p_{\text{f}} = 0$. Make a simulation study in which the productivity of P is determined for different values of dilution rate D and of $s_{\text{f.}}$

Problem 6.3 *Analysis of an enzymatic two-step reaction sequence with a noncompetitive inhibition in the first step.* The two-step reaction sequence with a competitive inhibition of the first step has been exhaustively analyzed in Sect. 6.4. Make the same analysis when the first step is noncompetitively inhibited by the intermediate S_1. Try as far as possible to work with dimensionless groups of parameters in order to make the analysis of more general value. Give the dimensionless parameter groups specific numerical values in order to make a simulation study of the results.

Problem 6.4 *Derivation of the major flux control theorems.*

(a) First consider the Flux Control Summation theorem: In a linear pathway, all the enzyme activities are increased by the same fractional amount $a = \mathrm{d}e_i/e_i$. Show that $\mathrm{d}J/J = a$, where $\mathrm{d}J$ is the sum of all the individual fractional changes of J caused by the fractional changes of each e_i. From here, the theorem can easily be proved.

(b) The proof of the Flux Control Connectivity theorem follows the same lines, but is a little more complicated.
Stephanopolous et al. (1998) give detailed proofs of all the flux control theorems.

Problem 6.5 *Elasticity coefficients for an enzymatic reaction that follows Hill kinetics (6.17).* Derive the elasticity coefficient $\varepsilon_{ji}^{\text{Hill}}$ for reaction i of a linear pathway, where r_i depends on s_j as shown in (6.17), with $n = 4$.

Compare the value of $\varepsilon_{ji}^{\text{Hill}}$, with ε_{ji} obtained for Michaelis–Menten kinetics (where $-1 < \varepsilon_{ji} < 1$).

Consider a two-step sequence where one reaction follows Michaelis–Menten kinetics, and the other Hill kinetics. Which reaction is likely to have the highest flux control coefficient?

Problem 6.6 *Fitting steady-state rates R_i by the lin-log approximation.* In Example 6.8, the rates R_i were calculated from the analytical expressions. This is, of course, not an option when these expressions are unknown.

Describe an experimental set-up in which the values (s, s_1, R_1, and R_2) can actually be obtained. What variables need to be changed in order to obtain the data used in Example 6.8? Specifically: does x need to be varied?

Repeat the calculation of the expressions in (2) of the example when the 20 data points have a random experimental error of 5%. Also, try with ten experimental points.

Problem 6.7 *Determination of flux control coefficients from transient experiments.* Based on the two-step sequence of Example 6.9, you are required to design a pulse experiment that will give you the flux control coefficient for $x = 1.5$ and $s = s^0$.

Follow the numerical method of Example 6.9 and use simulated data based on the analytical expressions for R_1 and R_2. You should use either 20 or 40 steps in the integration of the differential equations.

Next, add a random experimental error of 1 or 5% to all the simulated data for s' and y. Repeat the calculation of C_1^J.

Finally, use the method proposed by Kresnowati et al. (with the same number of time steps $\Delta\Theta$) to see if this method is better, both for the error-free data and for the data with random experimental errors.

Problem 6.8 *Converting glucose to fructose using a glucose isomerase enzyme.*

(a) In Note 6.1, (4), the rate of a first order reversible reaction $S \rightarrow P$ via the substrate–enzyme complex ES is derived. If the substrate contains no product the feed concentration is connected to s and p by

$$s_0 = s + p = s_{eq} + p_{eq} = s_{eq}\left(1 + \frac{p_{eq}}{s_{eq}}\right) = s_{eq}(1 + K_{eq}) \tag{1}$$

In (1), $K_{eq} = \frac{p_{eq}}{s_{eq}} = \frac{k_1 k_2}{k_{-1} k_{-2}}$ is the equilibrium constant which is a function of temperature only.

Insert these expressions in (4) of Note (6.1) and show that $-r_s = \frac{k_{max}(s - s_{eq})}{K_m + (s - s_{eq})}$, where K_m and k_{max} serve the same purpose as in Michaelis–Menten kinetics, but the parameters (K_m, k_{max}) are complicated functions of the four rate constants (see Gram et al.(1990)).

$$\text{For } K_m \gg (s - s_{eq}): \quad -r_s \cong \frac{k_{max}}{K_m}(s - s_{eq}) = k s_0 (x_{eq} - x) \tag{2}$$

In (2), k is a first-order rate constant (unit: h^{-1}) and x is the *conversion* of S. $x = 1 - s/s_0$, and $x_{eq} = \frac{K_{eq}}{1 + K_{eq}}$.

(b) Gram et al. studied conversion of glucose to fructose using the Novo-Industry (now Novozymes) immobilized glucose isomerase product.

They used a reaction temperature of 60°C, at which temperature the equilibrium conversion $x_{eq} = (1 - s/s_0) = 0.51$.

One aspect of the research was to find whether diffusion resistance was significant in catalyst pellets of different pellet radius R_p. Specifically, it was desired to find the diffusion coefficient D_{eff} for the pellet matrix and the rate constant k, which would be applicable if the glucose concentration *inside* the pellet was equal to the glucose concentration in the bulk liquid outside the pellet. For this purpose, steady-state experiments were conducted in a CSTR. The enzyme pellets were homogenously dispersed in the reactor.

In two experiments at 60°C, the following results were obtained for $s_0 = 540$ g glucose L^{-1} and with dilution rate $D = 0.25\ h^{-1}$.

Experiment 1: $R_p = 0.3$ mm, $s = s_{effluent} = 289.0\ g\,L^{-1}$.

Experiment 2: $R_p = 1.0$ mm, $s = 365.2\ g\,L^{-1}$.

Determine the rate of glucose consumption $-(r_s)$ for the two experiments.

(c) What is the significance of the ratio between $r_s(R_p = 0.3)$ and $r_s(R_p = 1.0)$?

Determine an algebraic relation for the ratio between $\Phi(0.3)$ and $\Phi(1.0)$ (see Note 6.2 (15)).

Using this relation, you are required to find a numerical value for $\Phi(0.3)$. Finally, determine k in (2) and the effective diffusion coefficient D_{eff}.

Problem 6.9 *Flux control coefficients derived from real experiments*. Nielsen and Jørgensen (1995) and Delgado et al. (1993) are references to studies of flux control in short pathways. There are other references that you might wish to retrieve by a literature search. For the two references (and for other references that you might find), compare the experimental results with calculations of the kind shown in this chapter. Is the quality of the experiments good enough to merit a quantitative treatment of the results? Are there any other comments to the papers?

References

Aris R, (1975). "The mathematical theory of diffusion and reaction in permeable catalysts" (Volume 1 and 2), Clarendon Press, Oxford.

Benthin, S., Nielsen, J., and Villadsen, J. (1993). Transport of sugars *via* two anomer-specific sites on the mannose-phosphotransferase system in *Lactococcus cremoris*: *in vivo* study of mechanism, kinetics and adaptation. *Biotechnol. Bioeng.* **42,** 440–448.

Briggs G E, and Haldane J B S (1925). A note on the kinetics of enzyme action. *Biochem. J*, **19**, 339–349.

Cornish-Bowden, A. (1995). "Fundamentals of Enzyme Kinetics", Portland Press, London (UK).

Delgado, J.P., Meruane, J., and Liao, J.C. (1993). Experimental determination of flux control distribution in biochemical systems: *In vitro* model to analyze metabolite concentrations. *Biotechnol. Bioeng*., **41**, 1121–1128.

Fell, D. (1997). Understanding the Control of Metabolism. Portland Press, London (UK).

Gram, J., de Bang, M., and Villadsen, J. (1990). An automated glucose-isomerase reactor system with on line flow injection analyzers for monitoring of pH, glucose- and fructose concentrations. *Chem. Eng. Sci*., **45**, 1031–1042.

Hatzimanikatis, V. and Bailey, J.E. (1997). Effect of spatiotemporal variations on metabolic control. Approximate kinetics using log(linear) kinetic models, *Biotechnol. Bioeng*., **54**, 91–104.

Heijnen J J, van Gulik W M, Shimizu H and Stephanopolous G (2004) Metabolic flux control analysis of branch points: An improved approach to obtain flux control coefficients from large perturbation data. *Metabolic* Engineering, **6**, 391–400.

Heijnen J J (2005). Approximative kinetic formats used in metabolic network modeling. *Biotechnol. Bioeng*., **91**, 534–545.

Hua L, Nordkvist M, Nielsen P M, and Villadsen J (2006). Scale-up of enzymatic production of lactobionic acid using the Rotary Jet Head system. *Biotechnol*. Bioeng., **97**, 842–849.

Jin Y, and Penning T M (2007). Aldo-Keto Reductases and Bioactivation/Detoxification (2007), *Ann. Rev. Pharmacol. Toxicol*., **47**, 263–292.

Kresnowati M T A P, van Winden W A and Heijnen J J (2005). Determination of elasticities, concentration and flux control coefficients from transient metabolite data using linlog kinetics. *Metabolic Engineering*, **7**, 142–153.

Langmuir I, (1916). The constitution and fundamental properties of solid and liquid surfaces, *i* solids. *J. Am. Chem. Soc*., **38**, 2221–2295.

Levenspiel, O. (1999). Chemical Reaction Engineering, 3rd edition, Wiley, New York.

Melchiorsen, C.R., Jensen, N.B.S., Christensen, B., Jokumsen, K.V., and Villadsen, J. (2001). Dynamics of pyruvate metabolism in *Lactococcus lactis*. *Biotechnol. Bioeng*., **74**, 271–279.

Michaelis L, and Menten M (1913) Die Kinetik der Invertinwirkung, *Biochem* Z, **49**, 333–369.

Nordkvist, M. (2001). Physiology of Lactic Acid Bacteria. M.Sc. thesis, Biocentrum, DTU, Denmark.

Nordkvist M, Nielsen P M, and Villadsen J (2006), Oxidation of lactose to lactobionic acid by a *Microdochium nivale* carbohydrate oxidase; Kinetics and operational stability. *Biotechnol. Bioeng*., **97**, 694–707.

Nielsen, J., Jørgensen, H. S. (1995) Metabolic control analysis of the penicillin biosynthetic pathway in a high yielding strain of *Penicillium chrysogenum, Biotechnol. Prog*., **11**:299–305

Scott Fogler H (4th Edition, 2006). Elements of Chemical Reaction Engineering. Prentice Hall (Pearson Education International).

Small, J.R. and Kacser, H. (1993). Response of metabolic systems to large changes in enzyme activities and effectors. *Eur. J. Biochem*., **213**, 613–640.

Stephanopolous, G., Aristidou, A.A., and Nielsen, J. (1998). Metabolic Engineering. Academic Press, San Diego (USA).

Villadsen J and Michelsen M L (1978). Solution of differential equation models by polynomial approximation Prentice Hall, Englewood Cliffs, NJ.

Westerhoff, H.V. and Chen, Y.-D., (1984). How do enzyme activities control metabolite concentrations. An additional theorem in the theory of metabolic control. *Eur. J. Biochem.,* **142**, 425–430.

Chapter 7
Growth Kinetics of Cell Cultures

In Chaps. 3 and 5, we have discussed how the two important design parameters for cell cultures, *yield* and *productivity*, can be derived from experimental data, e.g., from measurements of the substrate consumption and the product formation. Furthermore, we have shown how measured steady-state fluxes in and out of the cell, the exchange fluxes, can be used to calculate the fluxes through the different branches of the metabolic network of a given microorganism.

The yield is determined relative to the consumption of a substrate or relative to the production of, e.g., biomass. Units could be kg kg^{-1} or C-mol $(C\text{-mol})^{-1}$.

The productivity P_i is the rate of production or consumption per volume reactor of component i, e.g., kg glucose consumed $(m^3 \text{ reactor } h)^{-1} = -q_s$. Finally, $P_i/x = r_i$ defines the specific rate of production of component i, i.e., the productivity per mass unit of cells X.

All the information obtained by the measurement of exchange fluxes or by the calculation of intracellular fluxes was based on the assumption of *steady state* of all the culture variables. Not only the exchange fluxes, the production rates q_i, but also the composition of the biomass X must be constant in time. For each steady state, e.g., obtained at constant dilution rate D, the vector $\mathbf{q}$ or the vector $\mathbf{r} = \mathbf{q}/x$ defines the stoichiometry of the bioreaction *at the particular value of* D. When the results for a series of D values are collected, one can derive the correlations $\mathbf{r}(D)$ or $\mathbf{q}(D)$, mathematical expressions of the variation of the rates with the variable D. These expressions are descriptors for the state of the cell culture, and if the stoichiometry remains constant for all D as was the case in, e.g., (3.23), then all the components of $\mathbf{r}$ or $\mathbf{q}$ can be determined using just one *key component*, e.g., the specific rate of *net* biomass production r_x, since $|r_i| = Y_{xi} r_x$ and $|q_i| = Y_{xi} q_x$. It will be seen in Sect. 7.3.2 that the *total* substrate consumption $-r_s$ per mass unit biomass is more likely to be a *linear function of* r_x than proportional to r_x. This is due to substrate consumption to keep the already produced cells viable, as already discussed in Sect. 5.2.1. The substrate used for maintenance is converted to metabolic products, and now r_p also becomes a linear function of r_x.

In Chap. 7, the rates $\mathbf{r}$ will be expressed not as a function of D, but as a function of the concentrations $\mathbf{c}$ of all the reactants. This is the normal way to describe the

J. Villadsen et al., *Bioreaction Engineering Principles*,
DOI 10.1007/978-1-4419-9688-6_7, © Springer Science+Business Media, LLC 2011

relationship between the dependent variables **r** (or **q**) and the independent variables **c** in *chemical kinetics*.

In Chap. 6, the rate of an enzymatic reaction was already described as $r(\mathbf{s})$ where **s** is a vector that contains the feed concentration of substrate S and of intermediates in the enzymatic pathway. This could be done with considerable confidence since the reaction mechanism of an enzymatic reaction can be derived either from theory (Sects. 6.1 and 6.2) or by a set of experiments (Example 6.4).

Cell culture kinetics is, however, far more complex than enzymatic kinetics.

As already seen in Chap. 2, the synthesis of new biomass and of the many metabolites encoded by the genome of the organism is the collective result of hundreds of enzymatic reactions. This makes it impossible to derive (and impracticable to use) an overall, global kinetic model for cell cultures expressed through the entire vector of concentrations **c**.

The few components of **c** that we decide to include cannot possibly describe cell culture behavior at all operational conditions. This is why in cell culture models different kinetics are said to determine steady state and dynamic growth, an obvious ad hoc explanation. The truth is that cell kinetics manifests itself at different levels: In steady-state operation, all the intracellular components of **c** are in *quasi steady state* (as was used as an assumption for enzyme kinetics in the Briggs Haldane enzyme model), and the influence of most of the components of **c** is only manifested when *rapid transients* are enforced on the cell culture. Here, reactions with time constants that are orders of magnitude smaller than those relevant for steady-state kinetics suddenly come to life due to the action of the *cell regulatory network*, and these hidden layers of reactions completely dominate the kinetics in a time window of seconds, e.g., leading to an abrupt change of metabolites produced.

Other reactions which have nothing to do with cell mass production, but with a change in morphology of the cell, can play an important role in the production pattern of metabolites. Mutations in the genome of the organism or repression of certain pathway enzymes can lead to permanent cessation of production of a desired metabolite (e.g., loss of productivity of an antibiotic).

Section 7.1 will give a short introduction to model building for cell cultures, and the different model frameworks will be given appropriate names. Typical model structures are discussed in Sect. 7.2, and in the following sections kinetic models, each used for a specific purpose, are introduced.

7.1 Model Structure and Complexity

The first important decision in model building is to decide for what purpose the model is to be used. If the purpose is simply to correlate a set of kinetic data in order to interpolate within the data set, then any expression can be used, but unless some thought is spent on the structure of the data fitting expression it can hardly deserve to be called a "model."

An oral model could well be the first step in scientific model building: "In a series of steady-state chemostat experiments, the specific rate of biomass production r_x is linear in the glucose concentration s for small s, but for large s, r_x is independent of s. This indicates that the rate of the bioreaction is first order in s for $s \to 0$ like any other chemical reaction and that the rate eventually becomes constant because all the metabolic machinery in the cell is fully engaged in converting S." These sentences perfectly express the content of the Monod model for steady-state biomass growth (7.16). The *functionality* of $r_x(s)$ is determined afterwards by data fitting, but the shape of $r_x(s)$ is based on physical arguments, and the model is likely to be generally applicable for steady-state continuous cultures.

In a next step, the observation that formation of a specific metabolic product P gradually reduces r_x leads to inclusion of the concentration p of P in the rate expression, $r_x(s) \to r_x(s, p)$, while the observation that high concentrations of the substrate S has a negative influence on r_x leads to substrate inhibition steady-state kinetics. In this way, the two variants of the Monod kinetics, (7.18)–(7.20), are introduced, and in fact no embellishments are needed on these simple steady-state kinetic expressions. Although they are all entirely empirical in their simple structure, they work well, also for extrapolation, when considering steady-state cultivation in an efficiently stirred tank.

The Monod model is an *unstructured*, *nonsegregated* interpretation of cell kinetics.

Since the biomass concentration x is the only representative of the biomass which is known to have a hugely complex composition, one must assume that the biomass composition stays constant.

In Problem 3.5, it is stated that PHA is a significant part of the biomass for small D where NH_3 is the "limiting" substrate. For this reason, *no* single kinetic expression is able to unify the behavior of *Paracoccus pantotrophus* for small and for large D values. Here a *structured* representation of the biomass, as discussed in Sect. 7.4, is needed.

If the distribution of substrates to cells is different in different parts of the reactor, as is the case in industrial reactors with limited mixing capacity (see Chap. 11), the vector $\mathbf{c}_s$ of substrates offered to cells depends on the mixing pattern, and a *segregated* kinetic model must be used to describe substrate uptake and growth in different regions of the reactor.

The same is the case if the composition of cells, even in the well-stirred reactor, is given by a distribution function as discussed in Chap. 8. This is often the case in plasmid-based production of pharmaceutical products, where different cells have different copy numbers of the plasmid.

The last two examples represent *chemically unstructured* kinetics, but a *segregated population*. A *chemically structured* and probably also a *population segregated* model description should be used to describe penicillin production by a culture of slowly aging filamentous fungi as described in Sect. 7.6.2.

The governing principle is to *keep the model as simple as possible, while including the phenomena that are essential to explain the observed phenomena.* Thus, if the aim is to simulate the biomass concentration in a fermentation process,

an unstructured, but possibly segregated model may be sufficient. Even though these models are completely empirical, they are valuable for design of bioprocesses and for extracting key kinetic parameters. If, on the other hand, the aim is to simulate dynamic growth conditions, one may turn to simple structured models as in Sect. 7.4, e.g., the compartment models, which are in general useful for illustrating the concept of structured modeling.

If the aim is to understand the fundamentals of a given biological process, one must include far more structure in the model, and the best advice is to focus on only a part of the metabolism, e.g., gene transcription from a certain promoter or the mechanism of substrate transport to the cell as is shown in Sects. 7.5 and 7.7. If the aim is to investigate population distributions, which in some cases may have an influence on growth or production kinetics, either a segregated and possibly chemically structured model has to be applied. In Sect. 7.6, we consider simple cellular segregation – here referred to as morphologically structured models, whereas truly population-based models are the topic of Chap. 8.

Note 7.1 *Model complexity.* A simple illustration of difference in model complexity is the quantitative description of the fractional saturation y of a protein for a given ligand concentration c_l. This may be described by either of the two models (1) or (2), where (1) is the Hill equation (6.17):

$$y = \frac{{c_l}^n}{{c_l}^n + K^n}. \tag{1}$$

The model has two parameters, n and K, which are both empirical. The second model (2) was proposed by Monod et al. (1963) in his work on inducers and repressors of enzymatic processes that eventually led to his Nobel Prize in 1965:

$$y = \frac{\left(La\left(1+\frac{ac_l}{K_R}\right)^3 + \left(1+\frac{c_l}{K_R}\right)^3\right)\frac{c_l}{K_R}}{L\left(1+\frac{ac_l}{K_R}\right)^4 + \left(1+\frac{c_l}{K_R}\right)^4}. \tag{2}$$

This model has three parameters, L, a, and K_R. Both equations address the same experimental problem, but whereas (1) is completely empirical with h and K as fitted parameters (2) is taken from a truly mechanistic model for enzymatic reactions, and the parameters have a direct physical interpretation. If the aim of the modeling is to understand the underlying mechanism of the process, (1) can obviously not be applied since the kinetic parameters give no (or little) information about the ligand binding to the protein. In this case, (2) should be applied, since by estimating the kinetic parameter one can obtain valuable information about the system, and the parameters can be directly interpreted. If, on the other hand, the aim of the modeling is to simulate the ligand binding to the protein, (1) may be as good as (2). One may even prefer (1) since it is simpler in structure and has fewer parameters, and it actually often gives a better fit to experimental data than (2). Thus, the answer to which model one should prefer depends on the aim of the modeling exercise. In the list of unstructured models, Table 7.2, the expression (1) appears as "Moser kinetics," but here the mechanistic foundation is completely absent.

7.2 A General Structure for Kinetic Models

In order to describe kinetic growth models, it is useful to apply a general framework that allows uniform presentation of the models. Hereby, the model construction process becomes easier, and different model structures can be compared. In this section, we present such a general framework. Although it may look like a rather theoretical presentation of cellular growth, it will significantly facilitate the subsequent discussion.

7.2.1 Specification of Reaction Stoichiometries

Model construction starts by defining the stoichiometry of the reactions to be considered in the model. In order to start this process, we consider the general model illustrated in Fig. 7.1, where N substrates are taken up by the cells and converted into M metabolic products and Q biomass constituents. The conversions are carried out in J reactions. Since the number of reactions and processes involved in cellular growth is very large, the actual reactions used are typically lumped reactions, e.g., conversion of glucose into cellular protein. Often, the lumped reactions are completely empirical, e.g., conversion of glucose into "active biomass."

In order to describe the stoichiometry of the reactions, we introduce stoichiometric coefficients for all components in the system. These are called α_i for substrate S_i, β_i for metabolic product P_i, and γ_i for the biomass constituent X_i. The numerical value of these coefficients is analogous to the yield coefficients of the black box model introduced in Chap. 3, but since we will use the yield

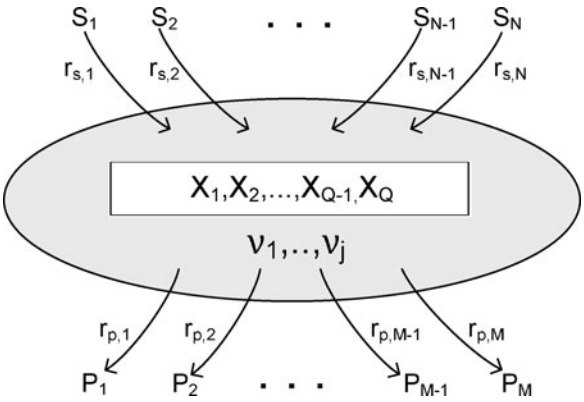

Fig. 7.1 A general representation of reactions involved in cellular growth. N substrates enter the cell and are converted into M metabolic products and Q biomass constituents. The metabolism involves J intracellular reactions for which the rates are given by $v_1 \ldots v_J$. The rates of substrate uptake are $(r_{s,1}, \ldots, r_{s,N})$, while $(r_{p,1}, \ldots, r_{p,M})$ are the rates of the product forming reactions

coefficients to specify overall conversion yields it is necessary to distinguish between the stoichiometric coefficients that appear in individual reactions of the model and the yield coefficients. Clearly, the stoichiometric coefficients would be identical to the yield coefficients if there was only one reaction. Also, when many reactions are lumped together as is done in the black box kinetic models described in Sect. 7.3.1, the stoichiometric coefficients are equal to the yield coefficients Y_{ij}.

Since there are many different compounds involved in many different reactions, it is necessary to use two indices on the stoichiometric coefficients to indicate the reaction number and the compound, e.g., α_{ji} is the stoichiometric coefficient for the ith substrate in the jth reaction. In the general framework for growth models, we introduce stoichiometric coefficients for all substrates, metabolic products, and biomass constituents in each of the J reactions. However, many of the stoichiometric coefficients will be zero, since only a few compounds participate in any given reaction.

For the substrates S_i, the metabolic products P_i and the biomass constituents X_i defined in Fig. 7.1, the stoichiometry for the jth cellular reaction can be specified as

$$\sum_{i=1}^{N} \alpha_{ji} S_i + \sum_{i=1}^{M} \beta_{ji} P_i + \sum_{i=1}^{Q} \gamma_{ji} X_i = 0. \tag{7.1}$$

In a growth model, there will be a stoichiometric equation like (7.1) for each of the J cellular reactions, and it is therefore convenient to write the stoichiometry for all J cellular reactions in a compact form using matrix notation:

$$\mathbf{AS} + \mathbf{BP} + \mathbf{\Gamma X} = \mathbf{0}. \tag{7.2}$$

In (7.2), the stoichiometric matrices $\mathbf{A}$, $\mathbf{B}$, and $\mathbf{\Gamma}$ contain the stoichiometric coefficients in the J reactions for the substrates, metabolic products, and biomass constituents, respectively. In $\mathbf{A}$, $\mathbf{B}$, and $\mathbf{\Gamma}$ rows represent reactions and columns compounds. Thus, the element in the jth row and the ith column of $\mathbf{A}$ specifies the stoichiometric coefficient for the ith substrate in the jth reaction. The stoichiometric coefficients may be positive, negative, or zero. Typically they are negative for substrates (and other compounds consumed in a given reaction) and positive for metabolic products (and compounds formed in a given reaction). With a stoichiometric formulation of the general type of (7.2), a large number of the stoichiometric coefficients become zero, and one may find it cumbersome to specify stoichiometric coefficients for all compounds and all reactions considered in the model. However, the advantage is that the general matrix formulation facilitates much of the subsequent analysis, because it can be done in the compact matrix symbolism that at a later stage may be advantageous for computer simulations. It becomes easy to spot the participation of a given compound in the various reactions by just looking at the column for this compound in the appropriate matrix.

7.2.2 Reaction Rates

The stoichiometry specified above defines the relative amounts of the compounds produced or consumed in each of the J intracellular reactions, but does not allow one to calculate the rates or the relative amounts at which metabolic products are secreted in the medium. This can be done by introducing the rates of the individual reactions and further coupling them to determine the overall rates of product secretion. The rate of a given reaction (or process) considered in the model is defined by the forward reaction rate v, which specifies that a compound with a stoichiometric coefficient β is formed at the rate βv in this particular reaction. Normally, one of the stoichiometric coefficients in each reaction is arbitrarily set to be 1, whereby the forward reaction rate becomes equal to the consumption or production rate of this compound in the particular reaction. For cellular reactions, we use the biomass as reference to define the *specific rates*, usually with the unit g (g DW h)$^{-1}$. We now collect the forward reaction rates of the J reactions considered in the model in the rate vector $\mathbf{v}$. Thus, $\beta_{ji}v_j$ specifies the specific rate of formation of the ith metabolic product in the jth reaction.

With the formulation (7.1) for the stoichiometry, the elements of $\mathbf{A}$ are negative or zero and the specific conversion rate of the ith substrate in the jth reaction is given by $-\alpha_{ji}v_j$. When we want to calculate the overall production or consumption of a compound, we have to sum the contributions from the different reactions. We can therefore write the net specific *consumption* rate for the ith substrate as the sum of its rate of consumption in all J reactions:

$$\left(r_{s,i}\right)_{\text{consumption}} = -\sum_{j=1}^{J} \alpha_{ji} v_j. \tag{7.3}$$

Similarly for the net specific rate of *formation* of the ith metabolic product:

$$r_{\text{p},i} = \sum_{j=1}^{J} \beta_{ji} v_j. \tag{7.4}$$

Equations (7.3) and (7.4) specify important relationships between what can be directly measured, namely, the specific uptake rates of substrates and the specific formation rate of products, and the rates of the reactions considered in the model. In Chap. 5, we used the term *fluxes* for these intracellular reactions, but there we considered well-defined chemical reactions, whereas in growth models the reactions are typically lumped reactions of empirical nature.

Similar to (7.3) and (7.4), we find for the biomass constituents:

$$r_{\text{X},i} = \sum_{j=1}^{J} \gamma_{ji} v_j. \tag{7.5}$$

These rates are not as easy to determine experimentally as the specific substrate consumption rates and the specific product formation rates, but they are related to the specific growth rate of the biomass. Thus, $r_{X,i}$ is the net specific formation rate of the individual biomass constituent i, and the specific growth rate μ is therefore given as the sum of net formation rates of all Q biomass constituents:

$$\mu = r_x = \sum_{i=1}^{Q} r_{X,i}. \tag{7.6}$$

The summed equations (7.3)–(7.5) can be formulated in matrix notation as

$$(\mathbf{r}_s)_{\text{consumption}} = -\mathbf{A}^T\mathbf{v}, \tag{7.7}$$

$$\mathbf{r}_p = \mathbf{B}^T\mathbf{v}, \tag{7.8}$$

$$\mathbf{r}_X = \Gamma^T\mathbf{v}. \tag{7.9}$$

Here, the specific rate vector $(\mathbf{r}_s)_{\text{consumption}}$ contains the N specific substrate uptake rates, $\mathbf{r}_p$ the M specific product formation rates, and $\mathbf{r}_X$ the net specific formation rates of the Q biomass constituents.

7.2.3 Dynamic Mass Balances

In Sect. 3.1, we specified mass balances at steady-state conditions for substrates, metabolic products, and biomass – (3.1)–(3.3). In these mass balances, the specific rates derived above can be inserted and hereby steady-state conditions can be calculated. In many cases, fermentation processes are, however, operated at non-steady-state conditions, i.e., at dynamic growth conditions. At these conditions, the equations are based on the general mass balance which takes the form:

$$\frac{d(\mathbf{c}V)}{dt} = \mathbf{r}(\mathbf{c})xV + v_{\text{feed}}\mathbf{c}_f - v_{\text{exit}}\mathbf{c}_e, \tag{7.10}$$

$\mathbf{c}$ is the vector of medium concentrations of N substrates, M the metabolic products, and Q the biomass components. v_{feed} is the volumetric flow rate to the bioreactor and v_{exit} is the volumetric flow rate out of the reactor. [$\mathbf{c}_f$, $\mathbf{c}_e$] are the inlet and exit concentrations. Different parts of the production rate vector $\mathbf{r}$ are taken from (7.7)–(7.9). In analogy with the steady-state balances presented in Sect. 3.1, transfer of substrates and metabolic products from the gas to the liquid phase can if desired be included in the dynamic mass balance (7.10).

The mass balances for the biomass and the Q biomass constituents X_i that together make up the biomass require special attention. The specific rate of formation

of biomass is the sum of contributions from each of the J reactions as specified in (7.6), which can also be written as:

$$r_{\mathrm{x}} = \mu = \sum_{i=1}^{K} \Gamma_i^{\mathrm{T}} \mathbf{v}. \tag{7.11}$$

$\mathbf{\Gamma}_i$ is the ith column of $\mathbf{\Gamma}$. Consequently, with a sterile feed into a bioreactor, the mass balance for the biomass X is:

$$\frac{\mathrm{d}(xV)}{\mathrm{d}t} = r_{\mathrm{x}} xV - v_{\mathrm{exit}} x = q_{\mathrm{x}} V - v_{\mathrm{exit}} x. \tag{7.12}$$

The concentrations of biomass constituents in the cell are normally expressed in units of g (g DW)$^{-1}$ and consequently the sum of all the concentrations equals 1. Furthermore, a mass balance for component i in a cell of mass m is:

$$\frac{\mathrm{d}(mX_i)}{\mathrm{d}t} = \Gamma_i^{\mathrm{T}} \mathbf{v} m \tag{7.13}$$

or

$$\frac{\mathrm{d}X_i}{\mathrm{d}t} = \Gamma_i^{\mathrm{T}} \mathbf{v} - \frac{1}{m} \frac{\mathrm{d}m}{\mathrm{d}t} X_i = \Gamma_i^{\mathrm{T}} \mathbf{v} - \mu X_i. \tag{7.14}$$

It should be noted that (7.14) is *independent of the type of reactor operation* that is used to produce the biomass. The equation shows that the rate of formation of any biomass component X_i by all the J reactions must at least be μX_i to preserve the same fraction of the component in the biomass. This is a consequence of expansion of the biomass upon growth which results in dilution of all biomass components. As the concentrations of all biomass constituents sum to 1, (7.11) can easily be derived from (7.14).

7.3 Unstructured Growth Kinetics

Unstructured kinetic cell culture models were initially set up to enable prediction of the specific growth rate in a reaction defined by a single black box stoichiometry as a function of one or a few independent variables – most typically one of the substrates. From the relation offered by the stoichiometric coefficients (in this case equal to the yield coefficients), the rates of consumption or production of all other substrates and products could afterwards be found based on the empirical relation between the specific growth rate and the *key-independent variables*. In (3.23), the model would describe the rate of glucose consumption as a function of the concentrations of the glucose concentration s and the concentrations of the metabolic products, ethanol (p_1) and glycerol (p_2). In a more fanciful model, the concentration of biomass x and perhaps even the CO_2 concentration in the medium

would be included. Definitely, pH and temperature T would be included as variables.

$$-r_s = F(sp_1, p_2, \text{pH}, T); \quad r_x = \mu = Y_{sx}(-r_s) = 0.137(-r_s);$$
$$r_{p_1} = 0.510(-r_s); \quad \text{etc.} \tag{7.15}$$

The characteristic feature of the basic unstructured model is that the rates of formation or consumption of all the reactants, except the key reactant (here glucose), are proportional to the key reaction rate. Only this rate, here $(-r_s)$, is expressed as a function of the independent state variables, **c**, pH, and T. All cellular components are pooled into one single representative biomass with concentration x. The kinetic expression F can be used to predict rates at other values of the independent variables as long as the stoichiometry, and hence the yield coefficients stay constant.

Many rate expressions F are proposed in the literature, often based on a fortuitous analogy to the mechanistically derived kinetic models for enzyme reactions. As discussed in Sect. 7.1, one cannot reasonably claim such analogies to be true, and the best model is, as argued previously, that which in a sensible way explains all the observed phenomena. New experiments may make it necessary to revise the model, but the model complexity should always be as low as possible.

In Sect. 7.3.2, the basic concept of unstructured kinetic models will be extended from that of a single stoichiometric equation (7.15) to include cell culture models which contain more than one stoichiometric equation.

7.3.1 The Monod Model

In a seminal communication from 1942, Jacques Monod introduced the following empirical description for the specific rate of biomass growth:
Monod model:

$$r_x = \mu = F(s) = \mu_{\max} \frac{s}{s + K_s}. \tag{7.16}$$

The verbal formulation of the Monod model is discussed in the introduction to Sect. 7.1, and Monod found that for a large number of experiments where *Escherichia coli* grows on different sugars, the shape of the downwards concave function $F(s)$ is best represented by the model shown in (7.16). Figure 7.2 shows the time course of a batch fermentation and a cross plot of μ versus s. After a *lag-phase* of duration about 1 h, there is a long *exponential growth phase* where the biomass concentration increases exponentially with time. When the substrate is nearly used up, growth rapidly stops, and if the culture is retained in this no-growth phase, it will lose viability, cells will start to die, and the biomass concentration decreases.

The lag-phase is a period during which the biomass composition changes and the specific growth rate increases. Here, the Monod model – or any other unstructured model that assumes the growth to be independent of the biomass composition – is

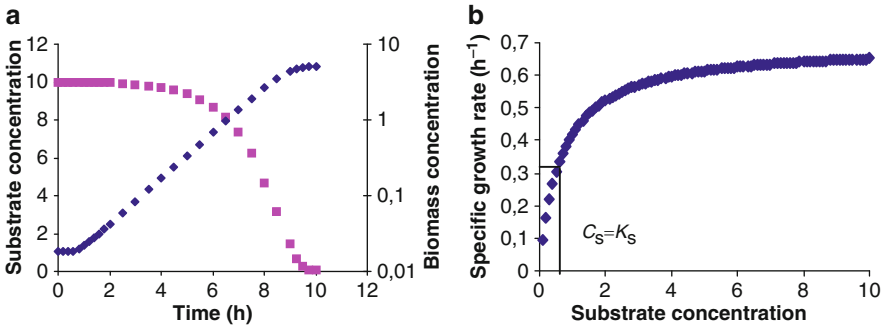

Fig. 7.2 Typical biomass and substrate concentrations profiles during a batch culture. (**a**) The time profile of the biomass concentration (*filled diamond*) and of the limiting substrate concentration (*filled square*). (**b**) A cross plot of the specific growth rate (=d(ln x)/dt) versus the substrate concentration. Corresponding values of μ and s are taken from (**a**). The value of K_s is indicated

not applicable, and a structured model from Sect. 7.4 must be used. Since the batch cultivation starts with an initial substrate concentration $s = s_0$ much higher than K_s, the specific growth rate μ, which is the slope of the curve ln(x) versus time, is almost constant for most of the fermentation period. When finally s becomes comparable in size with K_s, the specific growth rate decreases, and the last bit of substrate is consumed with first-order kinetics in s.

In the Monod model, K_s is the value of the limiting substrate concentration at which the specific growth rate is half its maximum value. Roughly speaking, it divides the plot of μ versus s into a low-substrate-concentration range where the specific growth rate is strongly (almost linearly) dependent on s, and a high-substrate-concentration range where μ is more or less independent of s. This is illustrated in Fig. 7.2b, where μ is plotted against the limiting substrate concentration s for the batch fermentation data. The cross plot of μ versus s has the typical shape of (7.16). Figure 7.2b is of course identical in shape to that of Fig. 6.1.

When glucose is the limiting substrate, the value of K_s is normally in the micromolar range (corresponding to the milligram per liter range). This small value is difficult to determine in a batch experiment, unless the initial sugar concentration is quite low. Normally, K_s and μ_{max} are determined in chemostat experiments: For a series of D values with constant substrate feed concentration s_f, the steady-state effluent concentration s_{exit} (by definition equal to the concentration s in the reactor for a well-stirred "ideal" reactor) is determined. A plot like Fig. 7.2b is directly obtained, since for the steady-state CSTR *with no biomass in the feed* ($x_f = 0$), a substrate balance yields:

$$V\frac{ds}{dt} = 0 = Vq_s + v(s_f - s) \rightarrow -q_s = \frac{q_x}{Y_{sx}} = \frac{xr_x}{Y_{sx}} = D(s_f - s)$$
$$= D\frac{x}{Y_{sx}} \rightarrow r_x = D. \qquad (7.17)$$

Consequently, the ordinate can be either r_x or D.

Table 7.1 Compilation of K_s values for growth of different microbial cells on different sugars

Species	Substrate	K_s (mg L^{-1})
Aerobacter aerogenes	Glucose	8
Escherichia coli	Glucose	4
Klebsiella aerogenes	Glucose	9
	Glycerol	9
Klebsiella oxytoca	Glucose	10
	Arabinose	50
	Fructose	10
Lactococcus cremoris	Glucose	2
	Lactose	10
	Fructose	3
Saccharomyces cerevisiae	Glucose	150
Penicillium chrysogenum	Glucose	4
Aspergillus oryzae	Glucose	5

Some K_s values reported in the literature are compiled in Table 7.1. It should be stressed that the K_s value in the Monod model does not represent the saturation constant for substrate uptake but only an overall saturation constant for the whole growth process. However, since the substrate uptake is often involved in the control of substrate metabolism, the value of K_s is often in the range of the K_m values of the substrate uptake system of the cells (see Sect. 7.7).

Example 7.1 *Steady-state chemostat described by the Monod model with sterile feed.* The relationship (7.17) derived between r_x and D for the steady-state CSTR holds for any functional relation F between r_x and **c**, *if* $x_f = 0$.

Thus, for r_x given by the Monod model (7.16):

$$r_x = D = \frac{\mu_{max} s}{s + K_s}. \tag{1}$$

From (1), one can obtain s as a function of D:

$$s = \frac{DK_s}{\mu_{max} - D}. \tag{2}$$

Finally, the biomass concentration and the concentration of metabolic products in the reactor (and in the effluent) is given by the total mass balances for the bioreactor and using the constant stoichiometric coefficients that are inherent in the black box model:

$$x = Y_{sx}(s_f - s), \tag{3}$$

$$p = Y_{sp}(S_f - s). \tag{4}$$

In (4), it is assumed that $p_f = 0$. Note in (2) that the substrate concentration in the reactor is independent of the substrate feed concentration. This is true for any functional relationship $\mu = \mu(s)$. If μ also depends on the concentration of one of the metabolic products, then

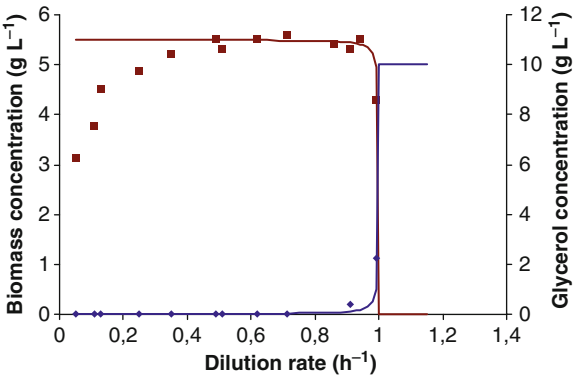

Fig. 7.3 Growth of *Aerobacter aerogenes* in a chemostat with glycerol as the limiting substrate. The lines are model calculations using the simple Monod model, (7.16). The data are taken from Herbert (1959)

s depends also on s_f for a given D. The biomass and product concentrations always depend on the substrate concentration in the feed s_f, and the higher the feed concentration the higher will be their concentrations, at least for simple kinetic models.

The right-hand side of (1) is limited from above by:

$$D_{max} = \mu_{max} \frac{s_f}{s_f + K_s}. \tag{5}$$

If we try to operate the stirred tank continuous reactor with $D > D_{max}$, the rate of removal of biomass will be higher than the maximum volumetric rate of biomass production, q_x. No steady state will be possible except the trivial $x = 0$, $s = s_f$. This subject will be taken up again in Chap. 9.

Since K_s is often in the ppm range (see Table 7.1), the value of s in the reactor is usually orders of magnitude lower than s_f except when D approaches D_{max} and s sharply increases toward s_f. Consequently, x is approximately equal to $Y_{sx}s_f$ until $D \sim D_{max}$, a value only slightly smaller than μ_{max} when $K_s << s_f$.

In Fig. 7.3, experimental data are shown for the growth of *Aerobacter aerogenes* in a chemostat with glycerol as the limiting substrate. The biomass concentration is observed to be approximately constant for dilution rates between 0.4 and 0.95 h^{-1}. The glycerol concentration is very low for $D < 0.95\ h^{-1}$. When D approaches $D_{max} = 1.0\ h^{-1}$, the glycerol concentration increases rapidly to $s = s_f = 10.0\ g\ L^{-1}$. The parameters μ_{max}, K_s, and Y_{sx} of (3) and (5) are obtained from Fig. 7.3.

- $\mu_{max} = 1.0\ h^{-1}$
- $K_s = 0.01$ g glycerol L^{-1}
- $Y_{sx} = 0.53$ g DW (g glycerol)$^{-1}$

The fit between the experimental data and the Monod model is excellent in the D range [0.4, 0.95 h^{-1}]. However, for low dilution rates, the model predicts too high biomass concentrations. This is explained by maintenance metabolism of the glycerol (see Sect. 5.2.1), which is not included in the Monod model. When substrates not used for maintenance processes are limiting, e.g., the nitrogen source, the Monod model normally describes the biomass concentration in the whole dilution range quite well.

Table 7.2 Different unstructured kinetic models with one limiting substrate

Name	Kinetic expression
Tessier	$\mu = \mu_{\max}\left(1 - \mathrm{e}^{-s/K_s}\right)$
Moser	$\mu = \mu_{\max}\dfrac{s^n}{s^n + K_s}$
Contois	$\mu = \mu_{\max}\dfrac{s}{s + K_s x}$
Blackman	$\mu = \begin{cases} \mu_{\max}\dfrac{s}{2K_s}, & s \le 2K_s \\ \mu_{\max}, & s \ge 2K_s \end{cases}$.
Logistic law	$\mu = \mu_{\max}\left(1 - \dfrac{x}{K_x}\right)$

It is not to be expected that the two-parameter Monod model can be used to fit all kinds of fermentation data. Many authors have tried to improve on the original Monod model, and some of these embellished models are listed in Table 7.2. Except for the Moser model, all the models contain two adjustable parameters. The Tessier model (proposed by Monods Ph.D. mentor at Université de Paris) gives the same result as the Monod model for small s since $\exp(-s/K_s) \approx 1 - s/K_s$ for $s \to 0$, but the approach to $\mu_{\max}$ for large s is usually too fast. The logistic law equation contains a constant K_x that obviously depends on the substrate feed concentration since the "maximum x" at which μ is 0 increases with s_f. The use of this model which mimics the result of batch fermentations with a lag-phase, but has no relation to the kinetics of the cell growth, is positively discouraged. The Contois model includes inhibition of the specific growth rate by the biomass. For very high biomass concentration, the biotic phase may take up a substantial part of the total reactor volume, and the uptake of substrates could presumably be hampered just by the presence of the biomass. It is, however, difficult to imagine how cells by their mere presence should inhibit their own growth, and probably the ability of the Contois kinetics to fit experimental data is explained by some unaccounted-for inhibitory effect of the *metabolic products*, since the product concentration in the reactor increases with x.

Perhaps, the most useful extensions unstructured rate expressions for a single rate limiting substrate are those which include inhibition by the substrate (7.18), and inhibition by the product (7.19) or (7.20).

Substrate inhibition:

$$\mu = \mu_{\max}\frac{s}{s^2/K_i + s + K_s}. \tag{7.18}$$

Product inhibition:

$$\mu = \mu_{\max}\frac{s}{s + K_s}\frac{1}{1 + p/K_i} \tag{7.19}$$

or

$$\mu = \mu_{\max}\frac{s}{s + K_s}\left(1 - \frac{p}{p_{\max}}\right). \tag{7.20}$$

Equation(7.18) describes the inhibitory effect of high O_2 concentrations on cell growth, and the model is also well suited to simulate the initial break-down of a recalcitrant toxic compound by anaerobic bioremediation, e.g., of organo-phosphates in the waste water from a pesticide production. The organisms, collected at the site of an earlier, polluted production site, readily degrade small concentrations of the organic P-compound, and the resulting inorganic phosphate is precipitated in the main, aerobic waste water plant, but large concentrations of the toxic compound will either kill the culture or severely inhibit its growth.

The models described by (7.19) or (7.20) can be used to describe inhibition of ethanol in wineries. The best model is probably (7.20) since inhibition sets in rather abruptly, and normal wine yeast stops growing when $p \geq$ about 120 g L^{-1}. A higher ethanol concentration is not desired in wine, but definitely in fuel alcohol production. Strain improvement has pushed p_{max} to above 170 g L^{-1} for yeast strains applied for this purpose.

All the unstructured models presented above assume that there is only one limiting substrate, but often more than one substrate concentration influences the specific growth rate. In these situations, complex interactions can occur, which are difficult to model with unstructured models without using many adjustable parameters. Tsao and Hanson (1975) proposed a general, multiparameter, unstructured model for growth on multiple substrates.

$$\mu = \left(1 + \sum_i \frac{s_{e,i}}{s_{e,i} + K_{e,i}}\right) \prod_j \frac{\mu_{max,j} s_j}{s_j + K_{s,j}}, \tag{7.21}$$

where $s_{e,i}$ are the concentrations of growth-enhancing substrates and s_j are the concentrations of substrates that are essential for growth. The presence of growth-enhancing substrates results in an increased specific growth rate, whereas the essential substrates must be present for growth to take place. Application of (7.21) may be quite successful, but the correlation between the parameters may render the fit of the model to the experimental data somewhat coincidental.

A special case of (7.21) is growth in the presence of two essential substrates:

$$\mu = \frac{\mu_{max,1} \mu_{max,2} s_1 s_2}{(s_1 + K_{s,1})(s_2 + K_{s,2})}. \tag{7.22}$$

Equation (7.22) may, e.g., be used as a model for the growth of methanotrophic bacteria on the two substrates O_2 and CH_4 – an important industrial process leading to single-cell protein as discussed in Example 3.4. If the concentrations of both substrates are at levels where the specific growth rate for each substrate reaches 90% of its maximum value, i.e., $s_i = 9K_i$, then the total rate of growth is limited to 81% of the maximum possible value. This is hardly reasonable, and Roels (1983) has

therefore proposed two alternatives to (7.22), both of which may be generalized for application to more than two limiting substrates:

$$\frac{\mu}{\mu_{\max}} = \min\left(\frac{s_1}{s_1 + K_1}, \frac{s_2}{s_2 + K_2}\right), \tag{7.23}$$

$$\frac{\mu_{\max}}{\mu} = 1 + \frac{1}{2}\left(\frac{K_{s,1}}{s_1} + \frac{K_{s,2}}{s_2}\right). \tag{7.24}$$

Both models will give growth at 90% of the maximum value in the situation mentioned above.

Growth on two or more substrates that may substitute for each other, e.g., glucose and lactose, cannot be described by any of the unstructured models described above. Consider the growth of *E. coli* on glucose and lactose: Glucose is metabolized first since it is the "best" carbon source, and metabolism on lactose will only start after glucose is used up. The bacterium needs one of the sugars to grow, but in the presence of glucose there is not even a growth-enhancing effect of lactose. Application of (7.22) to this example of multiple substrates for glycolysis will clearly not be feasible. To describe this so-called diauxic growth, it is necessary to apply a structured model, as illustrated in Sects. 7.4 and 7.5. Baltzis and Fredrickson (1988) offer a systematic procedure for the treatment of growth limitation by two different substrates that are either complementary (such as O_2 and CH_4 in the SCP process) or substitutable. See also Egli (1991) for some interesting experimental results with dual limitation by C and N.

The discussion of unstructured kinetic models applied to a black box stoichiometry model can be summed up as follows:

1. In the black box stoichiometric model, the yield coefficients Y_{ji} are assumed to be constant. Consequently, only one rate expression, namely, that for the limiting substrate, needs to be set up. All other rates can be derived from total mass balances.
2. For a single limiting substrate, (7.16) or its relatives (7.18)–(7.20) will usually give an adequate representation of the reaction rate. The parameters of the kinetic model are determined from experiments in a continuous steady-state bioreactor.
3. Picking the correct limiting substrate is not easy, since the feed contains many different nutrients, and it is difficult to pinpoint which one is limiting. Typical examples are lactic bacteria cultivations where the feed must contain a cocktail of amino acids. Some nutrients are essential for growth, i.e., growth stops when one of these nutrients is exhausted, whereas others can be synthesized by the cells, but at great cost in ATP (see discussion in Sect. 5.2.2), causing the specific growth rate to diminish. Experiments with different feed levels of each amino acid will help to resolve the question, but the experiments are very time consuming. An indication that a growth-enhancing substrate runs out during a batch fermentation is that the specific growth rate decreases, i.e., in a plot of $\ln(x)$ versus time, the curve bends over, although there is still much left of the substrate that was thought to be limiting. The value of K_s is usually in the ppm range as seen

in Table 7.1, and K_s values in the g L^{-1} range that are sometimes seen in publications may have resulted from misinterpretation of the data as described above. Another reason for a large apparent K_s value can be product inhibition. Here, one has to use models which incorporate the effect of P, e.g., (7.20), and the parameter p_{max} is determined by conducting the experiment at different initial concentrations of P (see, e.g., Problem 7.2).

4. None of the unstructured models gives a sensible description of data resulting from fast transients in a continuous stirred tank reactor. All the models assume that a change in limiting substrate concentration causes an immediate change in rate – such as is the case in simple gas-phase catalytic reactions. With the growth being a result of a large number of biochemical reactions, this is clearly not the case. The slow start up of batch growth – called the lag-phase, is one example. A change in substrate concentration in the reactor can take place within seconds, both in pulse addition of substrate and by changing the feed rate. The catabolic reactions respond very fast, e.g., the change from heterolactic to homolactic fermentation in lactic acid bacteria shown in Fig. 7.15. In contrast, the anabolic reactions have much larger time constants. Thus, a change in biomass composition (see Sect. 7.4.1) resulting from up- or downregulation of genes has a time constant of one to several hours. Consequently, application of simple unstructured kinetic models results in underestimation of time constants for dynamic changes by several orders of magnitude.

Note 7.2 *The genesis of the Monod Model.* Excursions into history should probably not belong in a textbook whose aim is to teach quantitative methods in biotechnology. The story of the discovery by Jacques Monod (1910–1974) of an empirical model for steady-state cell growth does, however, tell also our generation of emerging scholars a lesson of timeless quality in scientific endeavor. Furthermore, the Monod model is used more than any other growth model for cell cultures – unfortunately also in situations where Monod explicitly wrote that it would not work.

Hence, a brief account will be given of the experimental study that led to (7.16). This account is entirely based on Monod (1942), a monograph published during the darkest hour of France while its author, a leading figure of *la Résistance*, was continuously changing address as a fugitive from arrest. Very likely the monograph is based on his thesis (1941, from Université de Paris), and the experimental work was made during the 1930s in cooperation with Georges Tessier – another key member of the *Résistance*.

In the 1930s, the chemostat, in which a constant D can be maintained for many hours until steady state of a continuous culture is reached, did not exist. While in 2010 we would obtain the parameters of (7.16) by automated experiments in a state-of-the-art commercial bioreactor, this option was not available for Monod. His experiments were made in small batch reactors with a reasonable temperature and pH control.

The hypothesis of Monod was that the *E. coli* culture grew exponentially and with constant Y_{sx} on each of the many sugars offered as substrate for the culture:

$$\frac{dx}{dt} = \mu x \text{ and } x = x_0 2^n = x_0 2^{\mu_D t}, \tag{1}$$

where μ_D is the doubling frequency of the culture.

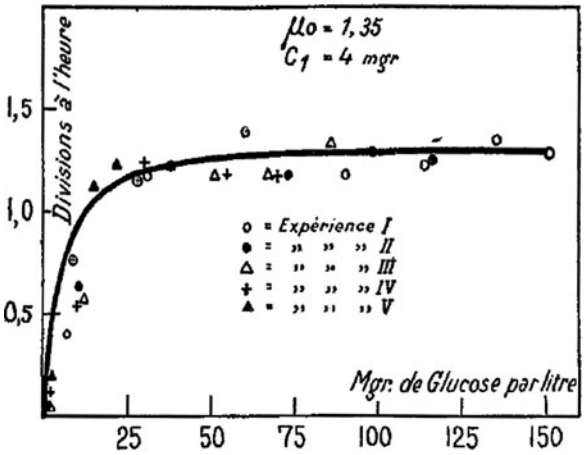

Fig. 7.4 The rate of doubling of the cell culture (h^{-1}) as a function of the glucose concentration (mg L^{-1}) (translation of the original figure text)

Insertion of the expression for x in the differential equation gives:

$$\frac{\mathrm{d}\ln x}{\mathrm{d}t} = \mu_\mathrm{D} \ln 2. \tag{2}$$

At time $t_1, t_2, \ldots, t_{i-1}, t_i, \ldots, t_N$, the biomass concentration x is measured together with the average substrate concentration $\bar{s} = \dfrac{s_{i-1} + s_1}{2}$ in each interval $[t_{i-1}, t_i]$.

$$\mu_\mathrm{D} \cong \frac{\ln x_i - \ln x_{i-1}}{(t_i - t_{i-1}) \ln 2} = \frac{\mu}{\ln 2} \tag{3}$$

and μ_D is plotted against $\bar{s}$ for $t_1 \ldots t_N$.

Figure 7.4 is copied from one of the original figures from Monod (1942).

The initial glucose concentration s_0 is 150 mg L^{-1} and for increasing t (moving from the right to the left on the figure) the glucose concentration decreases to a few milligram per liter while the biomass concentration (measured as OD) increases. There are five experimental series on the figure, and the kinetic parameter K_s (=C_1 on the figure) is determined to 4 mg L^{-1}. The doubling time is $t_\mathrm{doubling} = (\mu_\mathrm{D})^{-1} = 1.35^{-1} = 0.74$ h = 44 min and $\mu = \mu_\mathrm{D} \ln 2 = 0.94\ \mathrm{h}^{-1}$.

The tables of the monograph show the meticulous care with which the experiments on six different sugars were conducted. The yield coefficient Y_sx is determined with about 1% accuracy by measuring the total biomass produced in nine cultivations started with initial substrate concentrations $20 < s_0 < 200$ mg L^{-1}. Even for the lowest $s_0 = 20$ mg L^{-1}, the yield coefficient is no more than 10% off the average value ($\bar{Y}_{\mathrm{sx}=}0.233$ g g^{-1} for glucose as a substrate).

The description of the study which led Monod to formulate the growth kinetics (7.16) is full of illustrative details. The whole monograph gives us a picture of a scientist who worked at the limits of the capability of equipment and analytical methods of his time and who had the imagination to extract a model from his data, a model which is still accepted as satisfactory for interpretation of steady-state bioreactor data. He could well serve as a role model for an emerging generation of natural scientists.

As a final note, we may add that Jacques Monod did not obtain the Nobel Prize for "discovering" the Monod model. The prize was obtained in 1965 (together with André Lwoff and Francois Jacob) in recognition for his discoveries concerning genetic regulation of enzyme and virus synthesis, a subject treated in Sect. 7.5 of the present text.

7.3.2 Multiple Reaction Models

In the black box model, all the yield coefficients are taken to be constant. This implies that all the cellular reactions are lumped into a single overall growth reaction where substrate is converted to biomass. A requirement for this assumption is that there is a constant distribution of fluxes through all the different cellular pathways at different growth conditions. In the present section, we shall start to put some biochemical structure into kinetic models, moving from "unstructured, nonsegregated" toward "structured, nonsegregated." The truly structured models are the topic of Sects. 7.4–7.6, and the models treated below are basically unstructured in the sense that the influence of the biomass is still expressed solely through the biomass concentration x. However, biochemical information will be included in a semiquantitative way, and it will be acknowledged that the overall kinetics is the result of several reactions operating in parallel during cell growth.

The first and obvious example is the substrate consumption for maintenance of Sect. 5.2.1, a process that runs independently of the growth process. From (5.13), we have

$$-r_s = Y_{xs}^{true}\mu + m_s, \tag{7.25}$$

Y_{xs}^{true} is referred to as the *true yield coefficient* and m_s as the *maintenance coefficient*. The extra substrate consumption is accompanied by the synthesis of extra metabolic products and

$$r_p = Y_{xp}^{true}\mu + m_p. \tag{7.26}$$

Equations (7.25) and (7.26) can be used together with any black box model for $\mu(s, p)$ described in Sect. 7.3.1. One simply expands the model with a constant term for substrate consumption and product formation. This may in principle give rise to a conflict since the black box rate expressions are zero for $s = 0$ and in some cases it might be necessary to specify m_s as a function of s.

With the introduction of the linear correlations, the yield coefficients can obviously not be constants. Thus, for the biomass yield on the substrate, the *observed* yield coefficient Y_{sx} is:

$$Y_{sx} = \frac{\mu}{Y_{xs}^{true}\mu + m_s}. \tag{7.27}$$

Table 7.3 "True" yield and maintenance coefficients for different microbial species growing at aerobic growth conditions

Species	Substrate	Y_{xs}^{true} (g (g DW)$^{-1}$)	Y_{xo}^{true} (mmol (g DW)$^{-1}$)	m_s (g (g DW h)$^{-1}$)	m_o (mmol (g DW h)$^{-1}$)
Aspergillus awamori	Glucose	1.92	68	0.016	0.62
Aspergillus nidulans		1.67	111	0.020	0.54
Aspergillus niger					
Aspergillus oryzae					
Bacillus clausii		1.82	24	0.043	1.49
Candida utilis		2	84	0.031	0.87
Escherichia coli		2.27	70	0.057	0.45
Klebsiella aerogenes		2.27	74	0.063	0.99
Penicillium chrysogenum		2.17	70	0.021	0.87
Saccharomyces cerevisiae		1.85	47	0.015	0.62
Aerobacter aerogenes	Glycerol	1.79	63	0.089	2.52
Bacillus megatarium		1.67	90	–	0.70
Klebsiella aerogenes		2.13	58	0.074	2.52

Data are shown for growth on glucose or glycerol. The yield coefficients are all for growth with no formation of metabolic products, except carbon dioxide. The maintenance coefficients are given both for the listed, limiting substrate and for oxygen. The nitrogen source is NH_3

Equation (7.26) shows that for constant m_s, Y_{sx} will decrease to zero for $\mu \to 0$ where all the substrate is used to meet the maintenance requirements of the cell. For large specific growth rates, Y_{sx} approaches $(Y_{xs}^{true})^{-1} = Y_{sx}^{true}$. This corresponds to the situation where the maintenance substrate consumption becomes negligible compared with the substrate consumption for biomass growth, and the model reduces to the black box model described in Sect. 7.3.1. Despite its simple structure, the linear rate equation (7.26) proposed by Pirt (1965) is found to mimic the results of many fermentation processes quite well. Table 7.3 compiles true yield coefficients and maintenance coefficients for various microbial species with glucose and oxygen as substrates. This table complements Table 5.1 that gives values for the corresponding energetic parameters Y_{xATP} and m_{ATP}.

Example 7.2 *Steady-state chemostat described by the Monod model including maintenance.* We now reconsider the experimental data from Example 7.1, but include maintenance requirements. The steady-state balances are

$$\left(Y_{xs}^{true}\mu_{max}\frac{s}{s+K_s}+m_s\right)x = D(s_f - s), \tag{1}$$

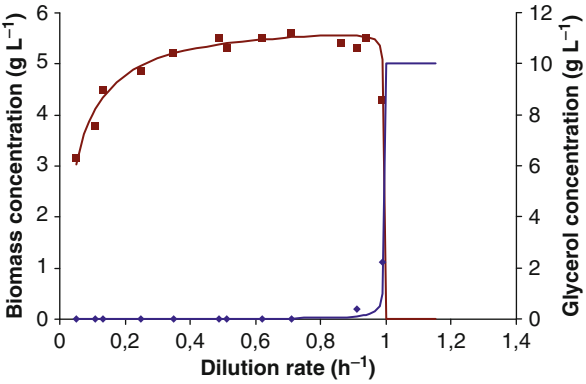

Fig. 7.5 Growth of *Aerobacter aerogenes* in a chemostat with glycerol as the limiting substrate. The lines are calculated using the Monod model, but including maintenance. The data are taken from Herbert (1959)

$$\mu_{\max} \frac{s}{s + K_s} x = Dx. \tag{2}$$

With (2), the steady-state concentration of the limiting substrate is still given by (2) in Example 7.1, since in both cases $\mu = D$ at steady state. However, the steady-state biomass concentration is different from that found when the simple Monod model is used. Combination of the two balances yields

$$x = \frac{D}{Y_{xs}^{\text{true}} D + m_s} (s_f - s). \tag{3}$$

By comparison with (7.27), it is observed that (3) is an analogue of (3) in Example 7.1. At low dilution rates, the term m_s is significant and the biomass concentration becomes smaller than if maintenance is neglected. This is illustrated in Fig. 7.5, where it is observed that the model correctly describes the biomass concentration in the whole dilution-rate range. The model parameters in the revised model are:

- $\mu_{\max} = 1.0\ \text{h}^{-1}$
- $K_s = 0.01$ g glycerol L^{-1}
- $m_s = 0.08$ g glycerol (g DW h)$^{-1}$
- $Y_{sx} = 0.55$ g biomass (g glycerol)$^{-1}$

With these values, the observed yield coefficient Y_{sx} is calculated as 0.50 and 0.53 at D equal to 0.4 and 0.8 h^{-1}, respectively. This is close to the constant value of the yield coefficient for the simple Monod model used in Example 7.1. However, at $D = 0.1\ \text{h}^{-1}$, the yield is calculated as 0.37 which is in much better agreement with the observed biomass yield.

Including maintenance is in principle the same as considering two reactions in the model: A reaction where substrate is converted to biomass and a reaction where substrate is used for cellular maintenance. Extending the number of reactions, but still describing the biomass with a single variable, may allow modeling of more complex phenomena as illustrated in Examples 7.3 and 7.4.

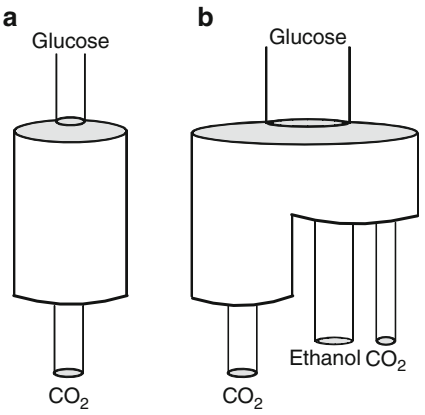

Fig. 7.6 Illustration of the "bottleneck" of the oxidative metabolism in *Saccharomyces cerevisiae*. (**a**) Excess oxidative capacity, and therefore completely oxidative metabolism. (**b**) Limited oxidative capacity. The excess carbon flux is converted to fermentative products

Example 7.3 *An unstructured model describing the growth of Saccharomyces cerevisiae.* *Saccharomyces cerevisiae* is an industrially important microorganism used for the production of baker's yeast and ethanol and today also for the production of recombinant proteins. Sonnleitner and Käppeli (1986) proposed a simple *kinetic model* for the growth of this organism, and in this example we discuss their model. However, before the model is discussed, some fundamental aspects of the fermentation physiology of *S. cerevisiae* will have to be recalled.

As already discussed in Example 3.5 and further in Example 5.3, aerobic growth of *S. cerevisiae* on glucose involves a mixed metabolism, with both respiration and fermentation being active. At high glucose uptake rate, there is some, as yet not quite understood, limitation in the respiratory pathway, which results in an overflow metabolism toward ethanol. The exact location of the limitation has not been identified, but it is probably at the pyruvate node (Pronk et al. 1996). The glucose uptake rate at which fermentative metabolism is initiated is often referred to as the critical glucose uptake rate, and the critical glucose uptake rate is found to depend on the oxygen concentration. Thus, at low dissolved oxygen concentrations, the critical glucose uptake rate is lower than at high dissolved oxygen concentrations (and clearly at anaerobic conditions there is only fermentative metabolism corresponding to the critical glucose uptake rate being zero). The influence of dissolved oxygen concentration on the critical glucose uptake rate is often referred to as the *Pasteur effect*. A simple verbal model for the mixed metabolism is given in Fig. 7.6. When *S. cerevisiae* is grown in an aerobic, glucose-limited chemostat, two distinct growth regimes are observed (see Fig. 7.7): At low dilution rates, all (or most) of the glucose is converted to biomass and carbon dioxide, and at high dilution rates ethanol is formed in addition to biomass and carbon dioxide. As observed in the figure, the shift to ethanol formation is accompanied with a dramatic decrease in the biomass yield from glucose.

In Fig. 7.7, the specific oxygen uptake rate is observed to increase with the dilution rate up to D_{crit}. Hereafter, it is approximately constant, while the specific carbon dioxide formation rapidly increases. Sometimes there is a more distinct decrease in the specific oxygen uptake rate above the critical dilution rate, but this depends on the strain and the operating conditions. The shift in metabolism at D_{crit} is normally referred to as the Crabtree effect, and it is a consequence of a bottleneck in the oxidation of pyruvate and repression of the oxidative system by high glucose concentrations. The bottleneck in the oxidation of pyruvate is illustrated in Fig. 7.6, where the flux through the glycolysis (indicated by the arrow) has to be smaller than

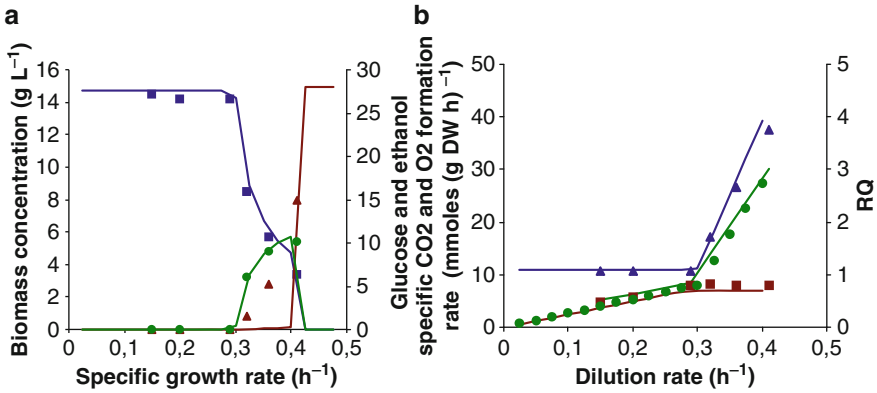

Fig. 7.7 Chemostat culture of *Saccharomyces cerevisiae*. The experimental data are from Rieger et al. (1983). The lines are model simulations with the parameters specified in Table 7.4. (**a**) The concentrations of glucose (*filled triangle*), biomass (*filled square*), and ethanol (*filled circle*) as a function of the dilution rate. All concentrations are given as g L^{-1}. (**b**) The specific carbon dioxide formation rate (*filled circle*) and the specific oxygen uptake rate (*filled square*) are both in mmol (g DW h)$^{-1}$. The respiratory quotient RQ is also shown (*filled triangle*)

the oxidative capacity of the cell (indicated by the bottleneck) if ethanol formation is to be avoided. If the glucose flux is larger than permitted by the bottleneck, the excess glucose is metabolized by the fermentative metabolism, and ethanol is formed.

In the model of Sonnleitner and Käppeli (1986), the verbal model of Fig. 7.6 is applied with two reactions: (1) oxidative glucose metabolism and (2) fermentative glucose metabolism. In the model, two substrates, glucose (S) and oxygen (O_2), and one metabolic product, ethanol (P) together with carbon dioxide (CO_2) are considered. In the original model formulation, ethanol may also serve as a substrate when glucose is not present, but here we will consider a simplified version of the model where ethanol uptake is not considered. The stoichiometry for the two reactions considered in the model is given by (1) and (2) where the general structure of kinetic models of Sects. 7.2.1 and 7.2.2 has been used.

1. *Oxidative glucose metabolism:*

$$\gamma_1 \mathrm{X} + \beta_{11}\mathrm{CO_2} - \mathrm{S} - \alpha_{12}\mathrm{O_2} = 0. \tag{1}$$

2. *Fermentative glucose metabolism:*

$$\gamma_2 \mathrm{X} + \beta_{21}\mathrm{CO_2} + \beta_{22}\mathrm{P} - \mathrm{S} = 0. \tag{2}$$

The nitrogen source (ammonia) and water are not included in the model.

When glucose is consumed solely by the respiratory metabolism, (1) is identical to the black box description of the cell growth, and all stoichiometric coefficients can therefore be interpreted as the yield coefficients Y_{si}. These stoichiometric coefficients can therefore easily be experimentally determined. At anaerobic conditions, the metabolism is exclusively fermentative, and (2) therefore represents a black box description of cell growth at these conditions. The stoichiometric coefficients can therefore be found as shown in Sect. 3.3. Fermentative

metabolism has a much lower ATP yield than respiratory metabolism, and the yield of biomass in the fermentative metabolism is therefore much lower than in the respiratory metabolism.

In order to describe biomass growth when both (1) and (2) contribute to growth, the rates of the two reactions has to be specified. In order to do this, Sonnleitner and Käppeli first specified the total glucose uptake rate (equal to the width of the inlet "funnel" in Fig. 7.6a, b) as:

$$-r_s = k_s \frac{s}{s + K_s}. \tag{3}$$

The maximum possible rate of respiration – or the maximum specific oxygen uptake rate (equal to the opening of the outlet "funnel" in Fig. 7.6a, b) is:

$$-r_{o,max} = k_o \frac{s_o}{s_o + K_o}. \tag{4}$$

The maximum possible rate of respiration is a function of the dissolved oxygen concentration s_o, but normally s_o is much larger than K_o and the maximum rate of respiration becomes equal to k_o. According to the verbal model of Fig. 7.6, the rate of the respiratory metabolism is the minimum of either the glucose uptake rate or the maximum possible rate of respiration, i.e.,

$$v_{res} = \min\left(r_s, \frac{r_{o,max}}{\alpha_{12}}\right). \tag{5}$$

Here, the maximum possible rate of respiration is scaled with the stoichiometric coefficient for oxygen in (1) to give the right comparison of the rates. Thus, at low glucose uptake rate, the rate of the oxidative metabolism is determined by the glucose uptake rate, whereas at high glucose uptake rate, it is determined by the maximum possible rate of respiration. If the glucose uptake rate is larger than $r_{o,max}/\alpha_{12}$, the excess glucose will be metabolized by the fermentative metabolism (2), i.e.,

$$v_{fer} = |-r_s| - \left|\frac{r_{o,max}}{\alpha_{12}}\right|; \quad |-r_s| > \left|\frac{r_{o,max}}{\alpha_{12}}\right|. \tag{6}$$

Clearly reaction (2) acts as a overflow reaction for excess glucose, and it is not active if $r_s < r_{o,max}/\alpha_{12}$.

Biomass is formed by both (1) and (2), and the specific growth rate is:

$$\mu = \gamma_1 v_{res} + \gamma_2 v_{fer}. \tag{7}$$

Hereby, the yield coefficient for biomass on glucose becomes:

$$Y_{sx} = \frac{\mu}{-r_s} = \frac{\gamma_1 v_{res} + \gamma_2 v_{fer}}{v_{res} + v_{fer}}. \tag{8}$$

At low glucose uptake rate where the metabolism is purely respiratory, the yield coefficient is γ_1, whereas with mixed metabolism (high specific glucose uptake rates) the yield coefficient decreases. In Baker's yeast production where the yield of biomass on glucose has

Table 7.4 Model parameters in the Sonnleitner and Käppeli model

Stoichiometric coefficients		Kinetic parameters	
α_{12}	12.4 mmol g^{-1} of glucose	k_s	3.50 g glucose (g DW h)$^{-1}$
β_{11}	13.4 mmol g^{-1} of glucose	k_o	8.00 mmol (g DW h)$^{-1}$
γ_1	0.49 g g^{-1} of glucose	K_s	0.1 g L^{-1}
β_{21}	10.5 mmol g^{-1} of glucose	K_o	0.1 mg L^{-1}
β_{22}	0.48 g g^{-1} of glucose		
γ_2	0.05 g g^{-1} of glucose		

to be maximized, it is obviously desirable to reduce fermentative metabolism by controlling the glucose uptake rate below the critical value (given by $r_{res,max}/\alpha_{12}$).

With the rate of the two reactions specified, it is also possible to find for the specific rate of carbon dioxide production:

$$r_{CO_2} = \beta_{11} v_{res} + \beta_{21} v_{fer} \tag{9}$$

and the specific rate of ethanol production:

$$r_p = \beta_{22} v_{fer}. \tag{10}$$

The respiratory quotient (RQ) is often used to evaluate the metabolic state of baker's yeast, and with the Sonnleitner and Käppeli (1986) model we find:

$$RQ = \left| \frac{r_{CO_2}}{r_{O_2}} \right| = \frac{\beta_{11} v_{res} + \beta_{11} v_{fer}}{\alpha_{12} v_{res}}. \tag{11}$$

If there is no fermentative metabolism, RQ becomes equal to β_{11}/α_{12}, which is close to 1, whereas if there is fermentative metabolism RQ increases above 1. Since it is relatively easy to measure the carbon dioxide production rate and the oxygen uptake rate by head space gas analysis, the RQ can be evaluated almost continuously, and a value above 1 will indicate some fermentative metabolism. This can be used in the control of, e.g., the feed of glucose to the reactor, i.e., if the feed is too fast the glucose uptake rate will be above the critical value and there will be fermentative metabolism. The feed has to be reduced in order to avoid this.

With the specific rates given for all the major substrates, metabolic products, and biomass, it is possible to simulate the concentration of the variables in a bioreactor (see Fig. 7.7) with the model parameters listed in Table 7.4. The model predicts that when the glucose uptake rate increases above the critical value $r_{o,max}/\alpha_{12}$ (corresponding to a certain value of the specific growth rate), ethanol is formed by the cells. In a steady-state chemostat, this is seen as the presence of ethanol in the medium at specific growth rates above this critical value. When the critical value is exceeded and ethanol is produced, the biomass yield drops dramatically, and this results in a rapid decrease in the biomass concentration.

The Sonnleitner and Käppeli (1986) model is an excellent example of how mechanistic concepts can be incorporated into an unstructured model to give a fairly simple and in many situations adequate description of the complex growth of *S. cerevisiae*. With its limited structure, the model does, however, give a poor description of transient operating conditions, e.g., the lag-phase between growth on glucose and the subsequent growth on ethanol in a

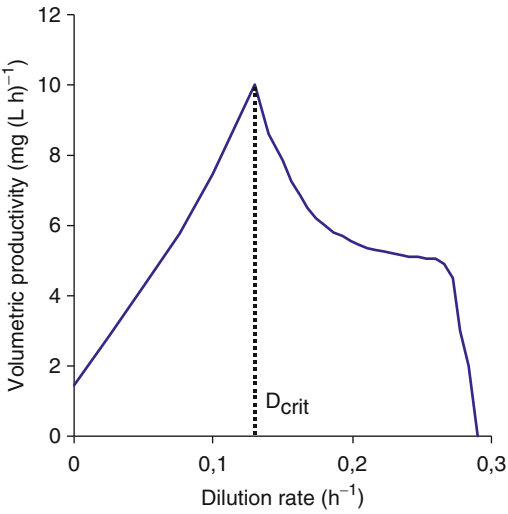

Fig. 7.8 The volumetric production of proteinase A by a recombinant strain of *Saccharomyces cerevisiae* at different dilution rates

batch fermentation cannot be predicted. It would not be difficult to include intracellular structure to describe the level of the oxidative machinery, but this was not the target of Sonnleitner and Käppeli. Any basically sound model can be made to fit new experiments when more structure is added.

Example 7.4 *Extension of the Sonnleitner and Käppeli model to describe protein production.* *Saccharomyces cerevisiae* is also used as a platform for the production of heterologous proteins, and in particular it is used to produce human insulin by the Novo-Nordisk company. Strong glycolytic promoters often drive the production of heterologous proteins, and the productivity of the protein is therefore closely associated with the biomass production. Carlsen et al. (1997) studied the kinetics of proteinase A production by *S. cerevisiae*, and he used a recombinant system very similar to that used for industrial insulin production. From the analysis of the production kinetics in chemostat cultures, Carlsen et al. found that the specific proteinase A production could be described as:

$$r_{\text{prot}} = \beta_{13} v_{\text{res}} + \beta_{23} v_{\text{fer}}, \tag{1}$$

v_{res} and v_{fer} are given by (5) and (6) in Example 7.3, respectively. When this production kinetics was applied, it was found that the model could be fitted quite well to experimental data. Using the model, they predicted the volumetric productivity of proteinase A as a function of the specific growth rate and found the results shown in Fig. 7.8. It is interesting that the volumetric productivity, which is the quantity of interest in connection with heterologous protein production, has a very distinct maximum at the critical dilution rate. Thus, in order to ensure optimal productivity, it is necessary to operate at (or very close to) the critical dilution rate. Even small changes in the dilution rate results in a significant decrease in the volumetric productivity. The reason for the very distinct optimum is that the protein production is related to biomass production, which also decreases drastically around the critical dilution rate.

7.3.3 The Influence of Temperature and pH

The reaction temperature and the pH of the growth medium are other process variables with a bearing on growth kinetics. It is normally desired to keep both of these variables constant (and at their optimal values) throughout the fermentation process – hence they are often called *culture parameters* to distinguish them from other variables such as reactant concentrations, stirring rate, oxygen supply rate, etc., which can change dramatically from the start to the end of a fermentation. The influence of temperature T and pH on individual cell processes can be very different, and since the growth process is the result of many enzymatic processes the influence of both temperature and pH on the overall bioreaction is quite complex.

Large industrial bioreactors present greater control problems than laboratory reactors, and the economic consequences of unscheduled excursions in pH and temperature during a large-scale production process are significant. Hence, the investment in expensive multilevel pH and T control adds substantially to the total reactor investment. The control algorithms are sometimes quite complex since the optimum pH and T may change during the process – e.g., from an initial biomass growth phase to a production phase in which a secondary metabolite is produced.

The influence of temperature on the maximum specific growth rate of a microorganism is similar to that observed for the activity of an enzyme: An increase with increasing temperature up to a certain point where protein denaturation starts, and a rapid decrease beyond this temperature. For temperatures below the onset of protein denaturation, the maximum specific growth rate increases in much the same way as for a normal chemical rate constant:

$$\mu_{\max} = A \exp\left(-\frac{E_g}{RT}\right), \tag{7.28}$$

A is a constant and E_g is the activation energy of the growth process. Assuming that the proteins are temperature-denatured by a reversible chemical reaction with free energy change ΔG_d and that denatured proteins are inactive, one may propose (Roels 1983) an expression for $\mu_{\max}$ that is closely related to the Hougen–Watson expression for catalyst activity in classical reaction engineering:

$$\mu_{\max} = \frac{A \exp(-E_g/RT)}{1 + B \exp(-\Delta G_d/RT)}. \tag{7.29}$$

Figure 7.9 is a typical Arrhenius plot (reciprocal absolute temperature on the abscissa and log μ on the ordinate) for *E. coli*. The linear portion of the curve between approximately 21 and 37.5°C is well represented by (7.28), while the sharp bend and rapid decrease of the specific growth rate for $T > 39$°C shows the influence of the denominator term in (7.29). Table 7.5 lists the parameters found by fitting the model in (7.29) to the data in Fig. 7.9. The results of the model calculations

Table 7.5 Model parameters in μ_{max} (T), (7.29) for *Klebsiella pneumoniae* and for *Escherichia coli* (both for a rich and a for a minimal glucose medium)

Parameter	*K. pneumoniae*	*E. coli* (rich)	*E. coli* (min)	
E_g	86	58	58	kJ mol^{-1}
ΔG_d	288	550	–	kJ mol^{-1}
A	5.7×10^{14}	1.0×10^{10}	6.3×10^{9}	h^{-1}
B	1.4×10^{48}	3.0×10^{90}	–	–

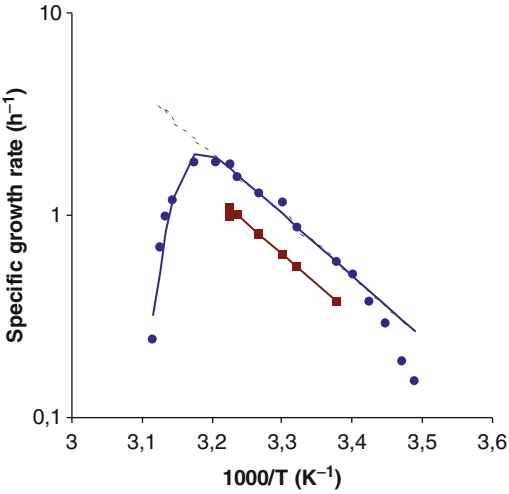

Fig. 7.9 The influence of temperature on the maximum specific growth rate of *Escherichia coli*. The *circles* represent growth on a glucose-rich medium, and the *squares* represent growth on a glucose-minimal medium. The *lines* are calculated using the model in (7.29) with the parameters listed in Table 7.5. The data are taken from Herendeen et al. (1979)

are shown as lines on the figure. Esener et al. (1981a) also applied (7.29) to describe the influence of the temperature on the maximum specific growth rate of *Klebsiella pneumoniae*, and the resulting parameters are also included in Table 7.5. It is observed that in the low temperature range, the influence of the temperature is stronger for *K. pneumoniae* than for *E. coli*, i.e., E_g is larger for *K. pneumoniae* than for *E. coli*. On the other hand, denaturation of the proteins is much more temperature-sensitive in *E. coli* than in *K. pneumoniae*. Figure 7.9 also illustrates the general observation that the maximum specific growth rate is always lower for growth on a minimal medium compared with growth on a complex medium. The parameter A is smaller for growth on the glucose-minimal medium than for growth on the glucose-rich medium, and A is therefore not a characteristic parameter for the individual strain but rather a function of the medium composition. E_g is the same for the two media, and it may therefore be a characteristic parameter for a given strain.

The model presented above for the temperature influence on the maximum specific growth rate has a reasonable physical interpretation, and with some confidence it can also be used to express the temperature dependence of rate constants in structured models for cellular kinetics. One important aspect not considered is the influence of temperature on maintenance processes, which are normally temperature dependent. An expression similar to (7.29) can be used, but the activation

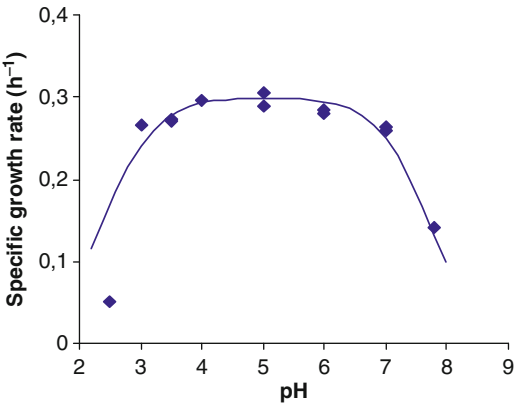

Fig. 7.10 The influence of pH on the maximum specific growth rate of the filamentous fungus *Aspergillus oryzae*. The *line* is simulated using (7.31), $K_1 = 4 \times 10^{-3}$, $K_2 = 2 \times 10^{-8}$, and $ke_{\text{tot}} = 0.3\ \text{h}^{-1}$

energy of the maintenance processes is likely to be different from that of the growth process. Thus, the relative rate of the two processes may vary with the temperature.

The influence of pH on cellular activity is determined by the sensitivity of the individual enzymes to changes in the pH. Enzymes are normally active only within a certain pH interval, and the total enzyme activity of the cell is therefore a complex function of the environmental pH. As an example, we shall consider the influence of pH on a single enzyme which is assumed to represent the cell activity. The enzyme exists in three forms: $e \leftrightarrow e^- + \text{H}^+ \leftrightarrow e^{2-} + 2\text{H}^+ e^-$ is taken to be the active form of the enzyme while the two other forms are assumed to be completely inactive. K_1 and K_2 are the dissociation constants for e and e^-, respectively. The fraction of active enzyme e^- is calculated to be:

$$\frac{e^-}{e_{\text{tot}}} = \frac{1}{1 + [\text{H}^+]/K_1 + K_2/[\text{H}^+]}. \tag{7.30}$$

The enzyme activity is proportional to e^-, $k = k_e e^-$, and if the activity of the cell as such is determined by the activity of this particular enzyme, the maximum specific growth rate is:

$$\mu_{\max} = \frac{ke_{\text{tot}}}{1 + [\text{H}^+]/K_1 + K_2/[\text{H}^+]}. \tag{7.31}$$

Although the dependence of cell activity on pH cannot possibly be explained by this simple model, it is, however, found that (7.31) gives an adequate fit for many microorganisms, as illustrated in Fig. 7.10, where data are shown for *Aspergillus oryzae*. From the profiles of the maximum specific growth rate as a function of pH, it is observed that the optimum is relatively flat. The cell activity does not change much when pH is moved one unit away from the optimum, but larger deviations from the optimum pH leads to drastic reductions in the microbial activity.

The simulation in Fig. 7.10 is based on the naïve assumption that the intracellular pH sensed by the enzymes would be equal to the extracellular pH. However, it is well known that microbial cells have a remarkable ability to maintain the intracellular pH at a constant level even with large variations in the pH of the extracellular medium, but only at the expense of a significant increase in the maintenance demands, since Gibbs free energy has to be used for maintaining the proton gradient across the cell membrane. This ability of the microbial cells to function at suboptimal environmental pH may, however, be compromised by the presence of *uncoupling agents*, e.g., organic acids (see Sect. 7.7). At a low extracellular pH, organic acids present in the medium may be transported by passive diffusion into the cell, where they are dissociated at the higher intracellular pH. The protons have to be pumped back to the extracellular medium, and this requires a considerable amount of ATP, which would otherwise be utilized for growth or for other useful purposes. At high concentrations of the undissociated acids, the cell machinery breaks down with fatal outcome for the cell.

7.4 Simple Structured Models

In Sect. 7.3.2, the first steps were taken to include more biochemistry and biology in the interpretation of cell growth and product formation. It was recognized that maintenance was a separate biological process, different from ab initio cell growth, and that the catabolism of glucose in aerobic yeast growth can lead to different metabolic end products. In Sect. 7.4, we continue to introduce more structure into the kinetics of cell growth. By doing so, the kinetic expressions will become more accurate, but first of all we shall gain more insight into the dynamics of cellular processes. At first, the elements of structure invoked in the modeling will be of a very general character, such as the recognition of a pattern in cell growth which indicates that synthesis of "active" biomass will be the precursor of growth of cell mass as such. This leads to an understanding that catabolism and anabolism work with different time constants, and one can interpret the rapid transients in metabolite production rates that occur right after a shift in the environment of the cell culture. The design of process control equipment for bioreactors is greatly improved by this new insight.

One should harbor no illusion that the simple structured models of this section can explain the really astonishing kinetic processes that, as explained in Sect. 7.5, are involved in the shift from growth on one sugar to growth on another sugar or the mechanism of active transport processes across the cell membrane in Sect. 7.7. To understand these processes, one must rely on far deeper sources of biological insights. But at least the simple structured models open horizons beyond the unstructured models of the Monod type, and they help us to appreciate the rich nature of biological processes.

In simple structured models, biomass components are lumped into a few key variables – the vector $\boldsymbol{X}$ of Sect. 7.2 – that, hopefully, are representative of the cell

behavior. Hereby, the microbial activity becomes not only a function of the abiotic variables, which may change with very small time constants, but also on the much slower change of cellular composition. The microbial activity becomes a function of the *history* of the cell culture, i.e., on the environmental conditions, that it has experienced in the past. The cellular components included in the model represent pools of different enzymes, metabolites, or other cellular components. The cellular reactions of these models are still empirical since they do not represent the conversion between true components. Therefore, the kinetics for the individual "reactions" may be described by empirical expressions, of a form that fits the experimental data with a small number of parameters. Monod-type expressions are often used; since as explained in the verbal models of Sect. 7.1, they summarize some fundamental features of most cellular reactions.

Despite their empirical nature, simple structured models are normally based on well-established cell mechanisms, and they are able to simulate certain features of experiments quite well. In the following, we consider two different types of simple structured models, namely, *compartment models* and *cybernetic models*.

7.4.1 Compartment Models

In compartment models, the biomass is divided into a few compartments or macromolecular pools. These compartments must be chosen with care, and cell components with similar function should be placed in the same compartment. All membrane material and otherwise rather inactive components are placed in one compartment, and all active materials in another compartment. If some thought is put into this crude structuring process, one may regard individual, true cell components, which are not accounted for in the model, as being either in a frozen state or in pseudo-steady-state, i.e., with very long or very short relaxation times compared with the time constants for the change in environment.

With the central role of the protein synthesizing system (the PSS) in cellular metabolism, this is often used as a key component in simple structured models. Besides a few enzymes, the PSS consists of ribosomes (Ingraham et al. 1983), which are made up of 60% ribosomal RNA and 40% ribosomal protein. The ribosomal RNA constitutes more than 80% of the total stable RNA in the cell (see Note 7.3), and the level of the ribosomes is easily identified through measurements of the RNA concentration in the biomass. The RNA content of *E. coli* increases approximately as a linear function of the specific growth rate at steady-state conditions, and a similar observation is made for other microorganisms (see Fig. 7.11). Thus, the level of the PSS is well correlated with the specific growth rate, and there is no doubt that X_{PSS} (or X_{RNA}) is a good representative of the state of activity of the cell. As seen from the chemostat experiments in Fig. 7.12, where the RNA concentration is measured in *Lactococcus cremoris* (*Lactococcus lactis*) together with the biomass concentration during the transient from one steady state to another steady state, a linear correlation between X_{RNA} and μ seems to hold throughout the transient.

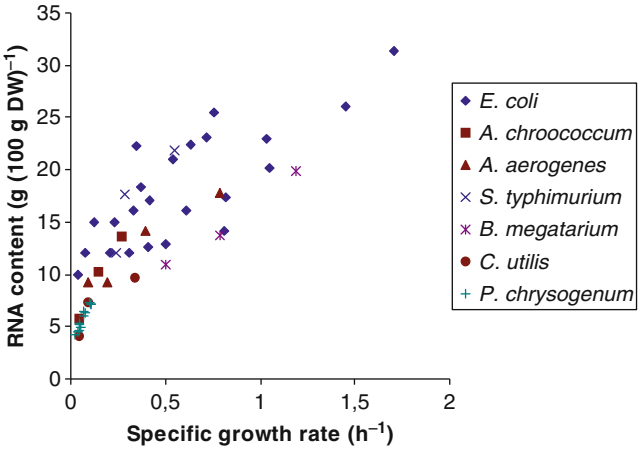

Fig. 7.11 Measurements of steady-state RNA content in various microorganisms as a function of the specific growth rate (equal to the dilution rate). The data are compiled from various literature sources

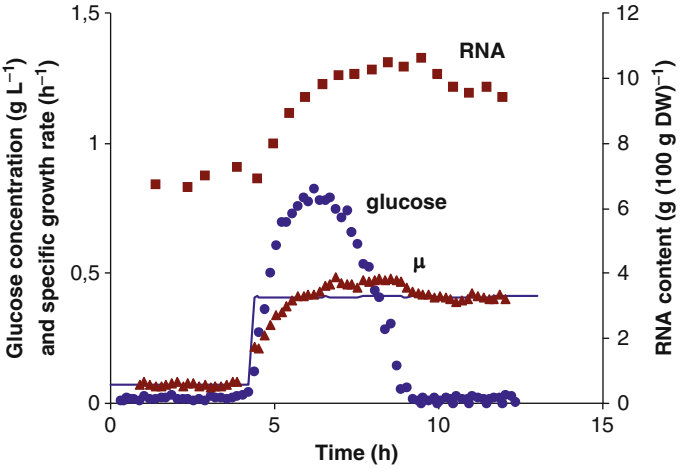

Fig. 7.12 Measurements of the RNA content of *Lactococcus cremoris* and of the specific growth rate in a glucose-limited chemostat. The chemostat is at steady state at the dilution rate of 0.075 h^{-1} during the first 4.3 h of monitoring. Hereafter, D is changed to 0.409 h^{-1}. The specific growth rate μ is calculated from the biomass concentration profile (data not shown), and it is noted that the μ profile closely mimics the RNA profile with an overshoot before it settles down at the new D value. The glucose concentration profile is also shown. At $D = 0.075\ h^{-1}$, $s = 5.5$ mg L^{-1} and after a large excursion (to 0.75 g L^{-1}), the glucose concentration again decreases to a low steady-state value of 10 mg L^{-1} at $D = 0.409\ h^{-1}$. Note the dramatic dependence of the RNA content of cells on glucose concentration in the low concentration range $s \sim 5$–10 mg L^{-1}. The data are taken from Benthin et al. (1991)

Most simple structured models are based on a division of the cell into an active and an inactive part, where the PSS is always included in the active part of the cell (Nielsen and Villadsen 1992). In some models, the DNA content of the cell, X_{DNA}, is also taken to be part of the active cell compartment. Except as a possible determinant for the rate of RNA synthesis, X_{DNA} has little to do with the growth of cells, and as discussed in Note 7.4 the DNA is perhaps better placed in the inactive cell compartment.

Note 7.3 *Stable and unstable RNA.* In microbial cells, there are three types of RNA:

1. Ribosomal RNA (rRNA)
2. Transfer RNA (tRNA)
3. Messenger RNA (mRNA)

Both rRNA and tRNA are fairly stable, whereas mRNA typically has a half-life of 1–2 min [1.3 min is an average value for *E. coli* (Ingraham et al. 1983)]. For an *E. coli* cell at a specific growth rate of 1.04 h^{-1}, the relative content of the three types of RNA is: 5% mRNA, 18% tRNA, and 77% rRNA (see Table 2.3), and the relative content of stable RNA (tRNA plus rRNA) is therefore 95%. With the extremely low half-life of mRNA, this will normally not be included in the RNA measured by standard techniques [see, e.g., Benthin et al. (1991)], and the data specified for RNA measurements therefore represents the sum of tRNA and rRNA. With the values specified above, it is found that rRNA accounts for approximately 80% of the total measured RNA, and measurements of RNA can therefore be considered a good estimate for the ribosome level in the cell.

Whereas the content of stable RNA increases with the specific growth rate (see Fig. 7.11), the tRNA content decreases with the specific growth rate. Thus, the relative content of tRNA is higher than 18% at specific growth rates below 1.04 h^{-1}. However, tRNA is a small fraction of the total RNA and even at very low specific growth rates it constitutes less than 25% of the total RNA (Ingraham et al. 1983). Hence, the stable RNA content of the cell is reasonably taken to be proportional with the ribosome level.

Note 7.4 *What should be positioned in the active compartment of a simple structured model?.* When the cell is divided into an active and an inactive part, it is necessary to define which biomass components should be considered active and which should be considered inactive. Most of the biomass components are involved in the overall growth process, and the only truly inactive components are structural material such as membranes or the cell wall. Thus, for most microorganisms, the inactive part of the cell is small. There are, however, a larger number of components that do not participate directly in the growth process, and furthermore for a number of components their concentration does not influence the overall growth kinetics. An example is DNA, which is of course essential for growth, but it is not an active component since it does not synthesize new material by itself. It is rather the polymerases that synthesize new DNA and mRNA which are active components, but these are present in very low concentrations and do not play a key role in regulation of DNA transcription and gene expression.

The compartment model concept is based on an assumption of a constant composition of the individual macromolecules within each compartment. With only two compartments, one active and the other inactive, one has to make a very rough partition of the components, and this partition cannot be expected to hold under all operating conditions. However,

macromolecules that decrease or increase with. the dilution rate in approximately the same fashion should be put in the same compartment.

A conceptual problem with the division of the cell into two parts is that many active components are placed in the inactive compartment. The tRNA is found to have a constant ratio to DNA at different specific growth rates and should therefore be included in the same compartment as the "inactive" DNA. However, tRNAs are strongly involved in protein synthesis and are therefore active compounds. Similarly, many non-PSS proteins that are involved in the primary metabolism, e.g., enzymes involved in the EMP pathway and TCA cycle, are obviously active even though they are positioned in the inactive compartment. The words *active* and *inactive* should therefore not be interpreted in a strict sense, but rather according to the following verbal rule: *The size of the active compartment increases with and is linearly correlated with the specific growth rate, whereas the size of the inactive compartment decreases with the specific growth rate.*

The first simple compartment models were formulated independently by Ramkrishna et al. (1967) and by Williams (1967). The partition of cell components into two compartments was different in the two studies of which that of Williams (as corrected by Fredrickson (1976)) and of Roels and Kossens (1978) is outlined below.

Williams included small precursors and ribosomes in one compartment designated as the A (or active) compartment. All macromolecules such as protein and DNA were pooled in another compartment, the G compartment. Using the nomenclature introduced in Sects. 7.2.1 and 7.2.2, synthesis of A from S, of G from A, and a first-order decay of G to replenish the precursors and the active parts of A is described, respectively, by the stoichiometry and the production rate of (7.32a)–(7.32c).

$$\gamma_{11} X_A - S = 0; \quad v_1 = k_1 \frac{s}{s + K_s}, \tag{7.32a}$$

$$\gamma_{22} X_G - X_A = 0; \quad v_2 = k_2 X_A X_G, \tag{7.32b}$$

$$X_A - X_G = 0; \quad v_3 = k_3 X_G. \tag{7.32c}$$

With this definition of the compartments, A is certainly an active part of the cell, and the rate of formation of G must depend on the size of A. The role of the G compartment is less clear. Most of the G compartment is probably inactive, but a constant fraction of G may contain enzymes necessary for the growth of G. This must be the reason why Williams postulated that the rate of growth of X_G is proportional to both X_A and X_G, as in (7.32b). In (7.32a), a Monod-type dependence of the substrate concentration s is used for the rate of formation of A.

In analogy with the models of Roels and Kossens (1978), Nielsen et al. (1991a, b) proposed a simple two-compartment model for simulation of the growth of lactic acid bacteria. The LAB model has been used and expanded in many later publications, and a simplified version of the model is discussed in Example 7.6, while the application of (modified) Williams model of (7.32a)–(7.32c) is shown in Example 7.5.

Example 7.5 *Analysis of the model of Williams.* Based on (7.32a)–(7.32c), one can obtain:

$$\mathbf{A} = \begin{pmatrix} -1 \\ 0 \\ 0 \end{pmatrix}; \quad \Gamma = \begin{pmatrix} \gamma_{11} & 0 \\ -1 & \gamma_{22} \\ 1 & -1 \end{pmatrix}. \tag{1}$$

Using (7.11), one can obtain the specific growth rate $r_x = \mu$:

$$\begin{aligned} \mu &= \begin{pmatrix} \gamma_{11} & -1 & 1 \end{pmatrix} \cdot \begin{pmatrix} v_1 \\ v_2 \\ v_3 \end{pmatrix} + \begin{pmatrix} 0 & \gamma_{22} & -1 \end{pmatrix} \cdot \begin{pmatrix} v_1 \\ v_2 \\ v_3 \end{pmatrix} \\ &= \gamma_{11} v_1 - (1 - \gamma_{22}) v_2, \end{aligned} \tag{2}$$

$$\mu = \gamma_{11} k_1 \frac{s}{s + K_s} - (1 - \gamma_{22}) k_2 X_A X_G. \tag{3}$$

The third reaction does not contribute to the specific growth rate since its sole function is to recycle biomass. Using (7.14), we obtain the dynamic mass balance for the active compartment:

$$\frac{dX_A}{dt} = \gamma_{11} k_1 \frac{s}{s + K_s} - k_2 X_A X_G + k_3 X_G - \mu X_A. \tag{4}$$

Since $X_G = 1 - X_A$, the following relation is the final result for steady-state chemostat operation:

$$X_A = \frac{1}{\gamma_{22} k_2} (D + k_3). \tag{5}$$

Clearly, the model predicts that X_A increases with D, as it should according to Fig. 7.11, since the A compartment contains the PSS. If the parameters in the correlation are estimated from the experimental data, k_3 is found to be 0.5 h^{-1}, which as pointed out by Esener et al. (1982) is far too high to be reasonable. The rather arbitrarily postulated kinetics is probably the reason for the inaccurate result. From (5), it follows that if degradation of the G compartment is not included (i.e., $k_3 = 0$), the model predicts $X_A = 0$ when $D = 0$ h^{-1}. This does not correspond with the experimental data of Fig. 7.11 since even resting cells ($\mu = 0$) must have ribosomes on stand-by if they are to develop into actively growing cells. Thus, the degradation of G compartment to active A compartment is taken to be the mechanism that ensures that some A compartment is present at $\mu = 0$. Despite the inconsistencies of the Williams model, it gives a far better description of a fed-batch fermentation with *K. pneumoniae* than a traditional Monod model including maintenance (Esener et al. 1981b, c; Esener et al. 1982), and the number of parameters is not higher than what can be estimated from steady-state growth measurements.

Jöbses et al. (1985) also applied the modified Williams model for the analysis of fermentations with *Zymomonas mobilis*. The experimental data for substrate uptake at different specific growth rates in a steady-state chemostat indicate a nonlinear increase in the volumetric glucose uptake rate q_s (grams of glucose per liter per hour) with D.

This cannot be described by a traditional unstructured model, but the two-compartment model fits the experimental data well.

Example 7.6 *Two-compartment model for lactic acid bacteria.* Nielsen et al. (1991a, b) presented a two-compartment model for the lactic acid bacterium *Lactococcus cremoris* (now renamed *L. lactis*). The model is a progeny of the model of Williams with a similar definition of the two compartments:

- Active (A) compartment contains the PSS and small building blocks
- Structural and genetic (G) compartment contains the rest of the cell material

The model considers both glucose and a complex nitrogen source (peptone and yeast extract), but in the following presentation we discuss the model with only one limiting substrate (glucose). The model includes two reactions for which the stoichiometries are:

$$\gamma_{11} X_{\mathrm{A}} - S = 0, \tag{1}$$

$$\gamma_{22} X_{\mathrm{G}} - X_{\mathrm{A}} = 0. \tag{2}$$

As in the Williams model, the first reaction represents conversion of glucose into small building blocks in A compartment, and these are further converted into ribosomes. The stoichiometric coefficient γ_{11} can be considered as a yield coefficient since metabolic products (lactic acid, carbon dioxide, etc.) are not included in the stoichiometry. In the second reaction, building blocks present in A compartment are converted into macromolecular components of G compartment. In this process, some by-products may be formed, and the stoichiometric coefficient γ_{22} is therefore slightly smaller than 1. It is assumed that the formation of macromolecules is the rate-controlling process in the formation of both the A and G compartments, and the kinetics of the two reactions therefore has the same form, i.e.,

$$v_i = k_i \frac{s}{s + K_{\mathrm{s},i}} X_{\mathrm{A}}; \quad i = 1, 2, \tag{3}$$

v_i is assumed to be a function of the glucose concentration (the carbon and energy source) and proportional to the concentration of the active compartment (the catalyst for the formation of biomass). From (7.11), the specific growth rate for the biomass is found to be:

$$\mu = \begin{pmatrix} \gamma_{11} & -1 \end{pmatrix} \cdot \begin{pmatrix} v_1 \\ v_2 \end{pmatrix} + \begin{pmatrix} 0 & \gamma_{22} \end{pmatrix} \cdot \begin{pmatrix} v_1 \\ v_2 \end{pmatrix} = \gamma_{11} v_1 - (1 - \gamma_{22}) v_2. \tag{4}$$

Inserting the kinetic expressions for v_1 and v_2, one can obtain:

$$\mu = \left(\gamma_{11} k_1 \frac{s}{s + K_{\mathrm{s},1}} - (1 - \gamma_{22}) k_2 \frac{s}{s + K_{\mathrm{s},2}} \right) X_{\mathrm{A}}. \tag{5}$$

The specific growth rate is seen to be proportional to the size of the active compartment. The substrate concentration s influences the specific growth rate both directly and indirectly by also determining the size of the active compartment. The influence of the substrate

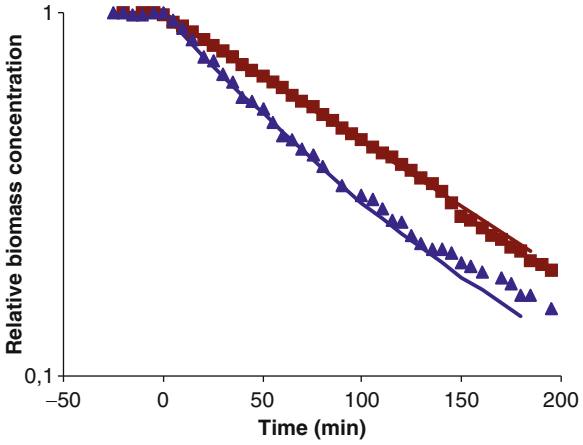

Fig. 7.13 Measurement of the biomass concentration for two transient experiments in a glucose-limited chemostat cultures with *Lactococcus cremoris*. The dilution rate was shifted from an initial value of 0.10 h^{-1} (*filled triangle*) or 0.50 h^{-1} (*filled square*) to 0.99 h^{-1}, respectively. The biomass concentration is normalized by the steady-state biomass concentration before the step change in D at time zero. The lines are model simulations. The data are taken from Nielsen et al. (1991b)

concentration on the synthesis of the active compartment can be evaluated through the ratio v_1/v_2:

$$\frac{v_1}{v_2} = \frac{k_1}{k_2} \frac{s + K_{s,2}}{s + K_{s,1}}. \tag{6}$$

If $K_{s,1}$ is larger than $K_{s,2}$, the formation of X_A is favored at high substrate concentration, and it is hereby possible to explain the increase in the active compartment with the specific growth rate.

Consequently, when the substrate concentration increases rapidly, there are two effects on the specific growth rate:

- A fast increase in the specific growth rate, which results from an increase of $s/(s + K_{s,1})$ with s. The time constant for the increase of s in the medium is small compared to the time constant for the growth process (see Fig. 7.12).
- A slow increase in the specific growth rate, which is a result of a slow build up of the active part of the cell, i.e., additional cellular synthesis machinery has to be formed in order for the cells to grow faster.

This is illustrated in Fig. 7.13 which shows the biomass concentration in two independent wash-out experiments. In both cases, the dilution rate was shifted to a value (0.99 h^{-1}) above the wash-out dilution rate (0.55 h^{-1}), but in one experiment the dilution rate before the shift was low (0.1 h^{-1}) and in the other experiment it was high (0.5 h^{-1}). The wash-out profiles are seen to be very different, with a much faster wash-out when the shift is from a low dilution rate. When the dilution rate is changed to 0.99 h^{-1}, the glucose concentration increases rapidly to a value much higher than $K_{s,1}$ and $K_{s,2}$, and this allows growth at the maximum rate. However, when the cells have been grown at a low dilution rate, the size of the active

compartment is not sufficiently large to allow rapid growth, and X_A therefore has to be built up before the maximum specific growth rate is attained. On the other hand, if the cells have been grown at a high dilution rate, X_A is already near its maximum value and the cells immediately attain their maximum specific growth rate. It is observed that the model is able to correctly describe the two experiments (all parameters were estimated from steady-state experiments), and the model correctly takes account of the previous history of the cells.

The Nielsen et al. model also includes the formation of lactic acid, and the kinetics was described with a rate equation similar to (3). Thus, the rate of lactic acid formation increases when the activity of the cells increases, and hereby it is ensured that there is a close coupling between formation of this primary metabolite and growth of the cells.

It is interesting to note that even though the model does not include a specific maintenance reaction, it can actually describe a decrease in the yield coefficient of biomass on glucose at low specific growth rates. The yield coefficient is given by:

$$Y_{sx} = \gamma_{21}\left(1 - (1 - \gamma_{22})\frac{k_2}{k_1}\frac{s + K_{s,1}}{s + K_{s,2}}\right). \tag{7}$$

Since $K_{s,1}$ is larger than $K_{s,2}$, the last term in the parenthesis decreases for increasing specific growth rate, and the yield coefficient will therefore also increase for increasing substrate concentration.

The presented two-compartment model, which solves some of the conceptual problems with the Williams model, has also been extended for the description of recombinant *E. coli* fermentations (Nielsen et al. 1991c; Strudsholm et al. 1992).

Simple structured models can be set up in many different ways, and if the model reflects some basic tenets of the true physiological response of the culture to changes in the environment, the dynamic behavior of the culture is well described. The LAB model of Example 7.6 is one example. Its main asset is the qualitative insight obtained from the metabolism of the organism.

Duboc et al. (1998), in a study of continuous anaerobic (on glucose) and aerobic (on glucose or ethanol) *S. cerevisiae* cultivation, proposed that after a sudden change in dilution rate, catabolism and anabolism became virtually decoupled. Only after several hours of further cultivation, would the rate of the two basic cell processes again become equal, and a new steady state was reached.

Figure 7.14a shows the result of a sudden change of dilution rate from steady-state anaerobic cultivation at $D = 0.053\,h^{-1}$ to transient cultivation at $D = 0.25\,h^{-1}$. Figure 7.14b shows the net specific rate r_{cat} of catabolism measured by the rate of CO_2 production and of anabolism r_x measured as the rate of biomass formation.

The maximum specific growth rate of the culture was measured to $\mu_{max} = 0.39\,h^{-1}$. Up to the change of D, the culture had grown with only 0.053/0.39 = 14% of its catabolic (and anabolic) machinery active. After the change of D, the active machinery can potentially change to 0.25/0.39 = 64% of full capacity. The striking feature of Fig. 7.14a is that the catabolic machinery has a certain "hidden" activity which immediately comes to life as soon as the glucose level in the chemostat increases. This hidden capacity is almost 35% of the possible activity change between the two steady states.

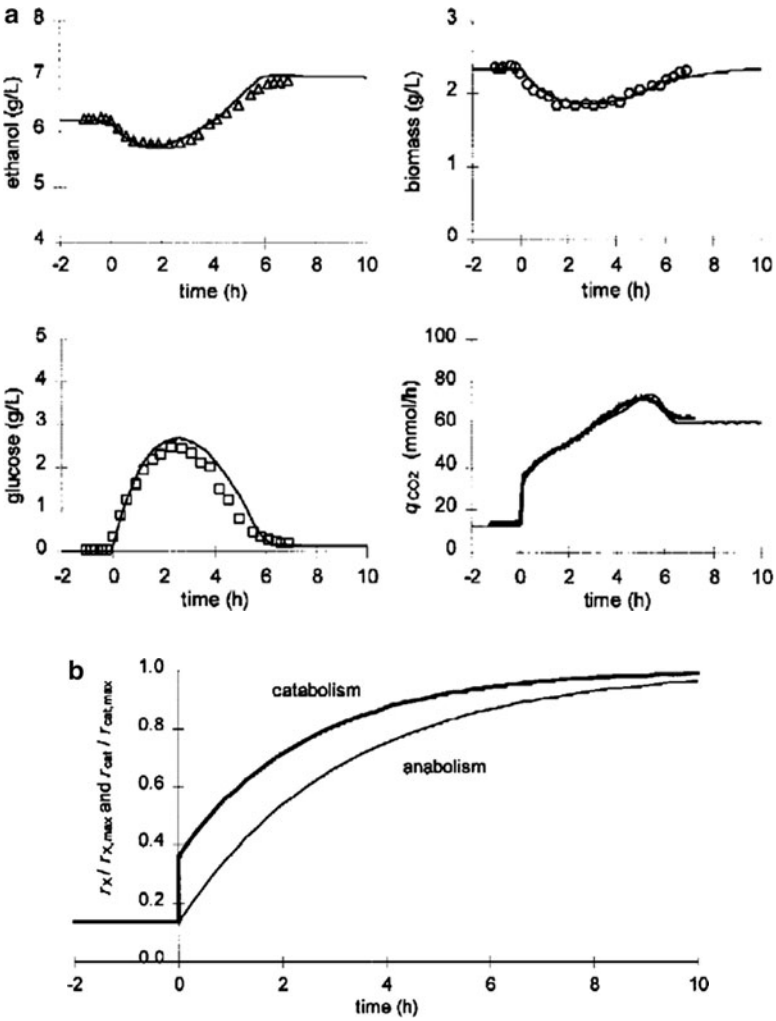

Fig. 7.14 (**a**) Ethanol, biomass, and glucose concentrations, and the rate of CO_2 formation in an anaerobic yeast cultivation where D is changed from 0.053 to 0.25 h^{-1}. *Lines* are model simulations. (**b**) Rates of catabolism and of anabolism after the change of D. The rates are normalized to that obtained at steady state for $D = 0.25\ h^{-1}\tau_{cat} = 2.5\ h^{-1}$ while $\tau_x = 3.2\ h^{-1}$. Data from Duboc et al. (1998) (with permission)

The anabolic reaction rate starts at its value for the steady-state rate at $D = 0.053\ h^{-1}$ and slowly increases (with a considerably larger time constant τ_x) toward the new steady-state value which is equal to that of the catabolic reaction.

The model with only three parameters, the two time constants τ_{cat} and τ_x and the jump in catabolic activity at time zero, is typical of simple structured models. All catabolic and all anabolic reactions are lumped into just two representative reactions, but the dynamic behavior of the yeast culture is simulated quite well, both for anaerobic and aerobic cultivation.

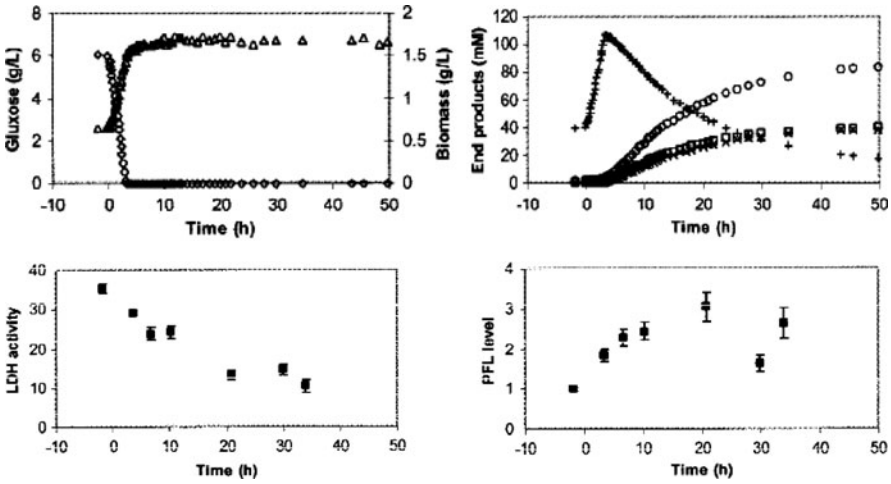

Fig. 7.15 Change from homolactic to heterolactic fermentation. *Upper panel*: The dilution rate is changed from 0.49 to 0.095 h^{-1} at $t = 0$. For $t = 3$ h, the glucose is exhausted, and the HLac concentration (*plus symbol*) in the effluent decreases, while that of formic acid (*open circle*), of HAc (*open square*), and of ethanol (*multiplication symbol*) increases. The biomass concentration (*open triangle*) increases from 0.63 to 1.63 g L^{-1} due to the lower value of $D = \mu$ at the end of the transient. *Lower panel*: During the experiment, the LDH concentration in the cells (=relative activity of LDH) decreases, and that of pyruvate-formate lysase (PFL) increases. (LDH: *filled square*, PFL: *filled circle*). Data from Melchiorsen et al. (2001) (with permission)

The LAB cultivation of Fig. 7.12 can be described by a similar model. Here, the measured increase of the intracellular component RNA is a representative for the rate of the anabolic reactions.

It should finally be emphasized that no embellishment of Monod-type models could ever explain the dynamic responses of Figs. 7.12 and 7.14. The unstructured models are, as explained before, unable to simulate anything but cultivations at a metabolic steady state.

In Fig. 7.15, another simple structured model was used to explain the results of a transient experiment. Here, two enzymes, lactate dehydrogenase (LDH) and pyruvate-formate lyase (PFL) – Fig. 2.5a, b, and Sect. 5.1.1 – were picked out for further study.

The transient experiments of Fig. 7.15 describe what happens after a shift down of D from 0.49 h^{-1} for $t < 0$ to 0.095 h^{-1} for $t > 0$. Before the shift, the glucose concentration in the effluent from the chemostat was 6 g L^{-1} (an amino acid was the limiting substrate) and $x = 0.63$ g L^{-1}. After the shift, the biomass concentration increases to a steady-state value of 1.63 g L^{-1} (since the dilution rate is much smaller) and the lactic acid concentration increases due to the increasing value of x.

The specific growth rate, determined from the slope of ln x versus t for $0 < t < 3$ h, is 0.28 h^{-1}, a value between the two steady state D values. At $t = 3$ h, the glucose concentration has decreased to a value below that where heterolactic

fermentation sets in. The concentrations of formic acid, ethanol, and acetic acid ($p_f = 2p_{HAc}$ and $2p_e$) increase, while the lactate concentration decreases.

New steady-state values of p_{HLac}, p_f, p_{HAc}, and p_e are reached after approximately 40 h.

The figure also shows that during the transient, the LDH activity in the cells decreases by a factor of 3 while that of PFL increases by about the same factor.

It is seen that the cells also had a "hidden capacity" for heterofermentative behavior at $t = 0$ where none of the mixed acid fermentation products were present in the outlet, while the PDF activity (and hence the rate of HLac formation) does not decrease to 0 even after 50 h at the very low value of D.

When a corresponding shift-up experiment (from $D = 0.10$–0.50 h^{-1}) is conducted, the effluent concentration of all the mixed acid metabolic products decrease exponentially from $t = 0$. Here, the PFL is completely inhibited from the start, and the concentration of the inhibited enzyme in the cells decreases through dilution.

The experiment illustrates some basic concepts of enzyme inhibition (the activity of the PFL is 0 for $t < 0$ although the cell contains the enzyme) and of enzyme repression/induction (the rate of PDH production in the cells decreases while the rate of PFL synthesis increases) leading to cells with lower PDH content and higher PFL content in the effluent from the chemostat.

Also, the time profiles for both metabolites and enzymes are well simulated using a model with one time constant, and with the enzyme levels at the two steady states and the jump in activity of PFL as extra parameters.

7.4.2 Cybernetic Models

Most academic fermentation studies are made with only a single carbon source, but sometimes the substrate has several carbon-containing components that can sustain growth. The leavening of bread in the bakery is a well-known example. The dough contains both glucose from hydrolyzed starch and maltose, and there are two distinct phases of the leavening process: First CO_2 is produced due to glucose metabolism, next CO_2 is produced from maltose when all the glucose has been used up.

Modeling the sequential uptake of different substrates that serve the same purpose in the microorganism, e.g., glucose and lactose, is difficult. Very often there are several growth phases separated by lag-phases in which synthesis of enzymes necessary for metabolism of the next substrate takes place. This is referred to as *diauxic growth* with two substrates (triauxic growth with three substrates). The sequential uptake of substrates is a consequence of complex regulatory structures in the cell. The utilization of other carbon sources, galactose, lactose, maltose, sucrose, ethanol, acetate, and carbohydrate polymers is repressed by the presence of glucose (*glucose repression*, or in more general terms *catabolite* repression). The reason is

Table 7.6 Characteristics of microbial growth on truly substitutable substrates (Ramkrishna et al. 1987)

1. Given multiple substrates, microorganisms prefer to utilize the substrate on which they can grow the fastest. This results in sequential utilization of the substrates in a batch culture
2. Sequential utilization may turn into simultaneous utilization when another substrate, e.g., the nitrogen source, becomes limiting
3. Even during simultaneous utilization of multiple substrates, the specific growth rate is never higher than that which can be obtained with growth on any substrate alone
4. If during growth on a "slower" substrate, a "faster" substrate is added to the medium, the growth on the slower substrate quickly stops
5. In continuous cultures, multiple substrates are consumed simultaneously at low dilution rates, while the faster substrate is preferentially consumed at high dilution rates

that glucose is the preferred substrate for most organisms as it supports rapid growth, and the microorganism will therefore attempt to use this carbon and energy source first. Some of the characteristics of microbial growth on sequentially metabolized substrates are compiled in Table 7.6. They capture in a simple fashion the overall consequences for the sequential utilization of carbon and energy sources as a result of the complex regulatory mechanisms behind carbon catabolite repression.

Ramkrishna and coworkers have developed an ingenious modeling concept, originally applied to describe the growth on substitutable carbon and energy sources. Their concept was called *cybernetic modeling* (cybernetic = "guided" (from Greek)), and the hypothesis in cybernetic models is that the organism allocates its resources, i.e., its cellular machinery, to optimize growth (Ramkrishna 1982; Kompala et al. 1984). Since there is no direct way of confirming whether microorganisms really optimize the allocation of their resources toward growth, the cybernetic models should be accepted on the same basis as other simple structured models: They provide a good modeling framework that can be used to simulate growth on multiple substrates and hereby be used for the design of fermentation processes.

The basic idea of the cybernetic model is that one *key enzyme* plays a bottleneck role in the growth of any particular substrate, and this key enzyme must be synthesized before growth can occur on that substrate. In reality, the "key enzyme" may represent several enzymes, e.g., lactose permease and β-galactosidase in case of lactose metabolism.

The reaction scheme for the growth process on each substrate can therefore be summarized by the following three reactions:

$$\gamma_i X - S_i = 0; \quad v_i = r_i^* w_i = k_i \frac{s_i}{s_i + K_i} X_{E_i} w_i, \tag{7.33}$$

$$X_{E_i} - X = 0; \quad v_{E_i} = k_{E,i} \frac{s_i}{s_i + K_i^E} u_i, \tag{7.34}$$

$$X - X_{E_i} = 0; \quad v_{\mathrm{deg},i} = k_{\mathrm{deg},i} X_{E_i}. \tag{7.35}$$

The index i indicates the substrate, and the model may consider N different substrates. The first set of reactions (7.33) is the formation of all biomass components except the enzyme E_i used for uptake of the ith substrate, and the second set of reactions (7.34) is the formation of the particular enzyme. The enzymes are synthesized from the general biomass compartment. Finally, the third set of reactions represents degradation of enzymes. In the model, the "potential" substrate uptake rate is given by r_i^*, i.e., the substrate uptake rate that occurs when there is no limitation in the enzyme system involved in substrate uptake. The kinetics for the potential substrate uptake is described by Monod kinetics. Similarly, the formation of the key enzymes is given by Monod-type expressions with respect to the substrate. Degradation of the enzyme is described by a first-order reaction.

The production of the ith enzyme cannot proceed without some critical cellular resources, which must be suitably allocated for different enzyme synthesis reactions. This feature is included in the kinetics through the *cybernetic variable* u_i, which may be regarded as the fractional allocation of resources for the synthesis of the ith enzyme, and it can be interpreted as a controller of the enzyme production. The kinetics for substrate assimilation (and hereby biomass growth) is determined by another *cybernetic variable* w_i. This variable ensures that the growth takes place primarily on the best-suited substrate, and it may be interpreted as a control mechanism at the enzyme level. It is doubtful whether there are control mechanisms that work directly on the transport enzyme, but with the complex interactions between different intracellular pathways it is reasonable to include this control function in the model.

The definition of the two cybernetic variables u_i and w_i is completely based on empiricism, and the key to success is to make a reasonable choice. Kompala, one of the first to work with Ramkrishna on what was then regarded as a viable way of working around the complexity, or even the lack of knowledge of the cell regulatory system, concluded that the following definitions gave the best fit to experiments (Kompala et al. 1986):

$$u_i = \frac{r_i^*}{\sum_{j=1}^{N} r_j^*}, \tag{7.36}$$

$$w_i = \frac{r_i^*}{\max_j(r_j^*)}. \tag{7.37}$$

The definition of the cybernetic variable u_i in (7.36) is based on the so-called matching law model, which specifies that the total return from the allocation of resources to different alternatives is maximized when the fractional allocation equals the fractional return. Hence in the cybernetic model, the resources are allocated for the synthesis of that enzyme which gives the highest specific growth rate (or highest μ). Originally, the cybernetic variable w_i was also defined according to the matching law model, but the definition in (7.37) is superior to the double

matching law concept – especially for the description of simultaneous metabolism of two equally good substrates where the double matching concept predicts a specific growth rate that is only half of that obtained on each substrate.

Using the definitions (7.33)–(7.37), the cybernetic model can handle both diauxic and triauxic batch fermentations (Kompala et al. 1986). A major strength of the cybernetic models is that all the parameters can be estimated on the basis of experiments with the individual substrates, and thereafter the model does a good job in fitting experiments with mixed substrates. Considering the large amount of experimental data presented by Kompala et al. (1986) and the quantitatively correct description of many experiments, it must be concluded that despite their rather empirical nature cybernetic models are well suited for the description of growth on truly substitutable substrates.

According to the model of Kompala et al. (1986), a biomass which in a chemostat has been fed for a long time with only one carbohydrate should contain transport enzymes only for uptake of this particular substrate. All other enzyme systems would have been degraded or diluted to virtually zero. Thus, a pulse of another carbohydrate added to the chemostat would not be consumed, but this is contradicted by experimental observations. To account for this weakness in the cybernetic model, Turner and Ramkrishna (1988) introduced a term for constitutive enzyme synthesis with the rate $k_{\mathrm{con},i}$ in the Kompala et al. model. The mass balance for the ith enzyme is then given by (7.38):

$$\frac{\mathrm{d}X_{E_i}}{\mathrm{d}t} = k_{E,i}\frac{s_i}{s_i + K_i^E}u_i - k_{\mathrm{deg},i}X_{E_i} + k_{\mathrm{con},i} - \mu X_{E_i}. \tag{7.38}$$

Now the microorganism has a latent capability to metabolize – at least at a low rate – substrate different from that on which it is accustomed to grow.

Since the 1980s, cybernetic models of ever increasing complexity have been proposed to simulate the results of much more complex phenomena than the sequential uptake of two substrates. Young et al. (2008) and Song and Ramkrishna (2010) are recent examples of how cybernetic models are ingeniously used in metabolic pathway analysis to give a systems-level description of metabolic control and to assess metabolic function with very limited data by so-called hybrid cybernetic modeling. These new applications of cybernetic models, and of simple structured models in general, give much insight into cell physiology, but the limit of usefulness of these complex, but basically empirical models must be in sight.

As seen in Sect. 7.5, truly mechanistic models have been developed during the last 30 years for a number of key processes in biology, and the parameters of these models are now being determined by new experimental techniques that can capture the rapid concentration changes of intracellular metabolites.

The future probably lies with these molecular-based models which, as demonstrated, e.g., by Reuss et al. in a series of papers from about 1995, can always be simplified when used in design problems as shown in Note 7.2.

7.5 Derivation of Expression for Fraction of Repressor-free Operators

Many complex regulatory structures operate in the living cell. A large majority of these structures are as yet unknown or are only sketchily described. But some processes, especially those of regulation and gene transcription, have been studied at such depth during the last half of the twentieth century that their functioning on the molecular level is now fully understood. This makes it possible to calculate the rate of these processes based on *mechanistic* mathematical models, just as the rate of enzymatic processes was calculated by stringent mathematical models in Chap. 6. Cell processes that are fully understood on the qualitative, but mechanistical, level are concerned with only small bits of the cell machinery, but a study of these models will give hints on how other processes operate. The ultimate goal of modern biology and its quantitative, model-based arm, systems biology, is to understand enough of the cell processes to permit truly predictive models for the function of the entire cell to be constructed. The so-called *single-cell models* developed in the late 1970s by Shuler and coworkers (Shuler and Domach 1982; Domach et al. 1984) did permit prediction of a great many phenomena during cell growth, but they could not include regulatory mechanisms that were not fully understood 30 years ago. Peretti and Bailey (1986, 1987) and Lee and Bailey (1984a, b, c, d, e) were in particular interested in the effect on the host cell of plasmid insertion, and their models included the quantitative protein synthesis mechanism to be described in Sect. 7.5.1. In the new century, the efforts continue to build complete cell models, or at least to construct models, which in a mechanistic way explain essential cell behavior such as the phases of the cell cycle. The work is supported by the ever increasing fund of knowledge available through bioinformatics and stored in gigantic data banks.

Gene transcription models aim at quantifying gene transcription based on knowledge of the promoter function. Among the best-studied promoters is the so-called lac-promoter of *E. coli*, which takes part in regulating expression of genes that are involved in lactose uptake. Understanding the regulation of this process represented a major breakthrough in molecular biology, and the history of how the mechanisms were unraveled is eloquently described in the Nobel lecture of Jacques Monod (1965).

Since the late 1930s, Monod had studied the phenomenon of diauxie, the sequential uptake of two sugars that both can serve as a substrate for the growth of *E. coli*. Figure 7.16 (from Monod 1942) shows the sequential uptake of glucose and lactose, one of the many systems he studied. Until all the glucose present in the medium was consumed, lactose was neither taken up by the cell, nor hydrolyzed. In the lag-phase between the two parts of the growth curve, the two enzymes β-galactosidase (Lac Z) and β-galactoside-permease (Lac Y), responsible for, respectively, the intracellular cleavage of lactose to one D-glucose and one D-galactose molecule, and the transport of lactose to the cell, were synthesized from a very low initial level, whereafter the second exponential growth phase starts.

During the 1950s, the process of lactose uptake was gradually understood, and essentially the whole truth was revealed in the seminal paper by Jacob and Monod (1961).

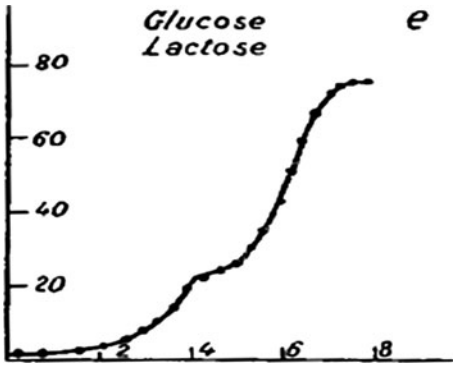

Fig. 7.16 Growth of *Escherichia coli* on a mixture of glucose and lactose (from Monod 1942). Abscissa: hours. Ordinate: mg biomass L^{-1}

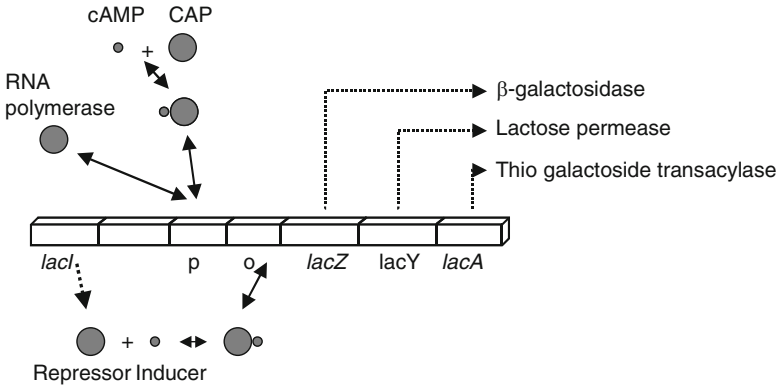

Fig. 7.17 The lac-operon of *Escherichia coli*

Figure 7.17 shows the *lac-operon*[1] and its control elements.

The operon consists of the three proteins Lac Z, Lac Y which are both essential for the uptake of and metabolism of lactose, and a third protein Lac A, thiogalactoside transacylase, which transfers acetyl (CH_2=CO) from AcCoA to β-galactosides. Its function is as yet not quite understood.

Upstream of the operon are the control elements, the operator, and the promoter.

If there is no lactose available, the operon is strongly downregulated by a regulatory protein, the *lactose repressor*. This is encoded by the lacl gene which is located further upstream.

The lactose repressor binds very strongly to the short DNA sequence, the *lac-operator* which is just upstream of the operon. Transcription of the operon occurs

[1] An operon contains a cluster of genes that are all under the control of a single regulatory signal or promoter. They are transcribed together onto a single RNA strand and can be translated together. They also found both in prokaryotes and eukaryotes.

by means of the enzyme RNA polymerase which binds to the promoter in front of the operon, but binding of the polymerase is largely prevented by the blocking of the operator by the lactose repressor. Hence, mRNA for translation of the two enzymes Lac Z and Lac Y (and Lac A) is synthesized in only minute amounts.

When lactose is fed to the medium, the tiny amounts of Lac Z and Lac Y take up a small part of the lactose and convert it to an isomer form allolactose (the two hexoses are connected through a 1,6-O-bridge, whereas in lactose the connection is via a 1,4-O-bridge).

The allolactose binds to the 4-U allosteric lactose repressor and changes its form such that it cannot bind to the operator. Now the RNA polymerase can bind to the promotor and synthesis of the three enzymes starts. Gradually, the cell content of Lac Z and Lac Y increases many fold, and exponential growth on lactose starts.

Another protein, CAP (catabolite activator protein), greatly enhances the binding of RNA polymerase to the promoter *if* it is bound to the DNA at a position somewhat upstream of the lac-promoter. But this binding does not take place unless the protein is bound to cAMP (cyclic adenosine monophosphate), a molecule that signals a low energy level of the cell. cAMP is present in concentrations inversely proportional to the concentration of the preferred sugar, here glucose.

Consequently, the synthesis rates of the enzymes for lactose uptake and metabolism are greatly enhanced by the presence of the cAMP–CAP complex bound close to the operon, but this enhancement is only effective when almost all the glucose is gone.

It is reasonable that the cell does not waste metabolic energy to synthesize Lac Z and Lac Y when there is no lactose present. Somewhat more difficult to understand is the reluctance to synthesize the enzymes when glucose is present. Lactose is, after all, effectively converted to intracellular glucose + galactose (which is excreted to the medium). Thus, lactose would serve the needs of the cell just as well as glucose. Probably, the transport of glucose by means of the transmembrane protein glucose permease is faster (or more efficient) than the transport of lactose through the corresponding lactose permease, and the cell will not start to synthesize Lac Y until all the glucose is used up.

The same preference for glucose relative to other sugars is seen in a vast number of microorganisms. The regulation of the uptake system is different for different organisms, but the regulatory system is well known, e.g., for *S. cerevisiae*.

Quite apart from helping us to understand quantitatively how fast a new transport system for an important substrate is built up after the preferred substrate is used up, the lac-promoter is also of substantial industrial interest as it is often used to drive expression of heterologous genes encoding recombinant proteins in *E. coli*.

In the following, a mechanistic model for the synthesis of the lac-operon will be outlined. The model may contain parameters for which precise values are as yet unknown, but experimental values for all the parameters will eventually be obtained. The model structure is essentially correct and the physical interpretation of the parameters is therefore quite clear.

The model is concerned with a quantitative description of the two key processes:

- Control at the operator by a repressor protein (lactose as inducer)
- Carbon catabolite repression at the promotor (glucose as an inhibitor)

The repressor protein X_r has two binding sites – one site that ensures binding to the operator (X_o) and one which may bind lactose (S_{lac}). When lactose is present its affinity for binding to the operator is significantly reduced, and transcription of the genes by RNA polymerase is allowed. Consequently, lactose serves as an *inducer* of transcription – or as formulated by Monod (1965) "the action of the inducer is to repress the action of the repressor" – of the three genes *lacZ*, *lacY*, and *lacA*.[2] Other inducers are e.g. isopropyl-β-D-thiogalactoside, abbreviated to IPTG.

Binding of the repressor protein to lactose and to the operator is given by (7.39) with $n = 4$ binding sites on the repressor.

The model (7.39) gives a simplified description of the true system since there may be different binding affinities for the repressor protein depending on how much lactose is bound to the protein (see Sect. 6.2.2 and Problem 7.3).

$$X_r + nS_{lac} \overset{K_1}{\leftrightarrow} X_r nS_{lac}, \tag{7.39a}$$

$$X_o + X_r \overset{K_2}{\leftrightarrow} X_o X_r, \tag{7.39b}$$

$$X_o X_r + nS_{lac} \overset{K_3}{\leftrightarrow} X_o X_r nS_{lac}, \tag{7.39c}$$

$$X_o + X_r nS_{lac} \overset{K_4}{\leftrightarrow} X_o X_r nS_{lac}. \tag{7.39d}$$

With the concentration of the species (indicated with squared brackets) being in moles per gram dry weight, the equilibrium constants K_i, $i = 1, 2, 3, 4$ are given by:

$$K_1 = \frac{[X_r nS_{lac}]}{[X_r][S_{lac}]^n}, \tag{7.40}$$

$$K_2 = \frac{[X_o X_r]}{[X_o][X_r]}, \tag{7.41}$$

$$K_3 = \frac{[X_o X_r nS_{lac}]}{[X_o X_r][S_{lac}]^n}, \tag{7.42}$$

$$K_4 = \frac{[X_o X_r nS_{lac}]}{[X_r nS_{lac}][X_o]}. \tag{7.43}$$

[2]The true inducer is allolactose, and some small lactose flux – perhaps by passive diffusion into the cell, is permitted.

The application of equations (7.40)–(7.43) is based on the following assumptions (Harder and Roels 1982):

- A macroscopic description can be used to express the influence of the reacting species on the kinetics, i.e., the concentrations of the different components are used. However, microorganisms only contain a few (1–4) copies of one type of operator per cell, and the number of repressor proteins per cell is also low (10–20). For such small entities, the meaning of concentrations and of thermodynamic equilibrium is disputable, and it may be more correct to apply a stochastic modeling approach.
- As in Michaelis–Menten kinetics for enzymes (Sect. 6.1), all reactions in (7.39) are assumed to be equilibrium reactions. This is reasonable since the relaxation times for the equilibria are much smaller than for most other cellular reactions.

Balances for the repressor, operator, and inducer are

$$[X_r]_t = [X_r] + [X_r n S_{lac}] + [X_o X_r] + [X_o X_r n S_{lac}], \tag{7.44}$$

$$[X_o]_t = [X_o] + [X_o X_r] + [X_o X_r n S_{lac}], \tag{7.45}$$

$$[S_{lac}]_t = [S_{lac}] + n[X_r n S_{lac}] + n[X_o X_r n S_{lac}]. \tag{7.46}$$

Index t refers to the total concentration. In wild-type *E. coli*, there are 10–20 times more repressor molecules than there are operators, and in this case the last two terms in (7.44) can be neglected. Furthermore, with the weak binding of the inducer–repressor complex to the operator, $[X_o X_r n S_{lac}]$ can be neglected in (7.45). Finally, (7.46) can be simplified by assuming that the intracellular concentration of inducer molecules is in sufficient excess over repressor molecules, and consequently that $[X_r n S_{lac}] + n[X_o X_r n S_{lac}] << [S_{lac}]$. With these simplifications, the fraction of repressor-free operators[3] is found (see Note 7.5) to be

$$Q_t = \frac{[X_o]}{[X_o]_t} = \frac{1 + K_1 [S_{lac}]_t^n}{1 + K_1 [S_{lac}]_t^n + K_2 [X_r]_t}. \tag{7.47}$$

Since the transcription of the three genes in the operon is likely to be determined by the fraction of repressor-free operators, (7.47) is valuable for description of the synthesis of the enzymes necessary for lactose metabolism in a structured model that aims at describing diauxic growth on glucose and lactose. The inducer concentration S_{lac} is likely to be correlated with the extracellular lactose concentration, whereas the total content of repressor protein can be assumed to be constant.

[3] Since the total number of operators of a given type in the cell is very small, it does not make much sense to talk about the fraction of repressor-free operators. However, in a description of enzyme synthesis, one may use (7.47) as an expression for the probability that the operator is repressor free.

Note 7.5 *Derivation of expression for fraction of repressor-free operators.* With the assumptions specified for the derivation of (7.47), we have

$$[X_r]_t \approx [X_r] + [X_r n S_{lac}], \tag{1}$$

$$[X_o]_t \approx [X_o] + [X_o X_r], \tag{2}$$

$$[S_{lac}]_t \approx [S_{lac}], \tag{3}$$

Equations (2) and (7.41) give the fraction of repressor-free operator:

$$Q_1 = \frac{[X_o]}{[X_o]_t} = \frac{1}{1 + K_2[X_r]}. \tag{4}$$

After multiplication by $1 + K_1[S_{lac}]^n$ in both the nominator and the denominator, we find

$$Q_1 = \frac{1 + K_1[S_{lac}]^n}{1 + K_1[S_{lac}]^n + K_2([X_r] + K_1[X_r][S_{lac}]^n)}. \tag{5}$$

From (7.40), (1), and (3), we obtain the expression in (7.47) for the fraction of repressor-free operators.

Small molecules that influence the transcription of genes are called *effectors*, and in the lac-operon the effector (lactose) is an *inducer*. In other operons, there may, however, be a negative type of control, and here the effector is called an *antiinducer*. For an inducer, the binding affinity to the operator of the free repressor is much larger than that of the inducer–repressor complex, i.e., $K_2 >> K_4$, whereas for an antiinducer it is the other way round. For an antiinducer, the fraction of repressor-free operators can be found from an expression similar to (7.47) (see Harder and Roels (1982) and Problem 7.3).

The other control mechanism in the lac-operon is the so-called carbon catabolite repression, which ensures that no enzymes necessary for lactose metabolism are synthesized as long as a preferred substrate is available. The mechanisms behind carbon catabolite repression are not completely known, but the binding of the RNA polymerase to the promoter is strongly enhanced when the cAMP–CAP complex is bound to the promoter. When the concentration of glucose (or another energy source) in the extracellular medium is high, the intracellular cAMP level is very low, and hence also the concentration of the cAMP–CAP complex. The site of the binding of the complex has been located in several operons that are under carbon catabolite repression, and binding of the complex to DNA has been found to promote helix destabilization downstream. This in turn facilitates the binding of the RNA polymerase and hereby stimulates gene expression. The carbon catabolite repression can be described by the following equilibria:

$$X_{CAP} + mX_{cAMP} \overset{K_5}{\leftrightarrow} X_{CAP} mX_{cAMP}, \tag{7.48a}$$

$$X_p + X_{CAP} mX_{cAMP} \overset{K_5}{\leftrightarrow} X_p X_{CAP} mX_{cAMP}. \tag{7.48b}$$

In (7.48), m is a stoichiometric coefficient. Equilibrium between CAP and the promoter is not considered, since this binding coefficient must be very small. Again we apply an assumption of pseudo-steady-state and assume that the concentrations of the individual components can be used. Thus, the association constants are

$$K_5 = \frac{[X_{\mathrm{CAP}} m X_{\mathrm{cAMP}}]}{[X_{\mathrm{CAP}}][X_{\mathrm{cAMP}}]^m}, \tag{7.49}$$

$$K_6 = \frac{[X_{\mathrm{p}} X_{\mathrm{CAP}} m X_{\mathrm{cAMP}}]}{[X_{\mathrm{p}}][X_{\mathrm{CAP}} m X_{\mathrm{cAMP}}]}. \tag{7.50}$$

The total balances for CAP and promoter are

$$[X_{\mathrm{CAP}}]_{\mathrm{t}} = [X_{\mathrm{CAP}}] + [X_{\mathrm{CAP}} m X_{\mathrm{cAMP}}] + [X_{\mathrm{p}} X_{\mathrm{CAP}} X_{\mathrm{cAMP}}], \tag{7.51}$$

$$[X_{\mathrm{p}}]_{\mathrm{t}} = [X_{\mathrm{p}}] + [X_{\mathrm{p}} X_{\mathrm{CAP}} m X_{\mathrm{cAMP}}]. \tag{7.52}$$

We can now derive an expression for the fraction of activated promoter:

$$Q_2 = \frac{[X_{\mathrm{p}} X_{\mathrm{CAP}} m X_{\mathrm{cAMP}}]}{[X_{\mathrm{p}}]_{\mathrm{t}}} = \frac{K_5 K_6 [X_{\mathrm{cAMP}}]^m [X_{\mathrm{CAP}}]}{1 + K_5 K_6 [X_{\mathrm{cAMP}}]^m [X_{\mathrm{CAP}}]}. \tag{7.53}$$

The quantity Q_2 of (7.53) is used to model the repression effect of glucose, just as Q_1 in (7.47) is used to describe the induction of lactose on gene expression and hereby synthesis of enzymes necessary for lactose metabolism. However, in order to apply (7.53), one needs to know the intracellular level of CAP (which in a simple model may be assumed to be constant) and also the level of cAMP. Harder and Roels (1982) suggest the following empirical correlation between X_{cAMP} and the extracellular glucose concentration s_{glc}:

$$X_{\mathrm{cAMP}} = \frac{K}{K + s_{\mathrm{glc}}}. \tag{7.54}$$

With (7.54), the genetically structured model is linked up to the glucose concentration in the medium, and the genetically structured model may be used to describe diauxic growth as discussed in Example 7.7. Equation (7.54) is a totally empirical description of all the different processes involved in determining the cAMP level in the cell at different glucose concentrations. This illustrates a general problem when a genetically structured model is combined with overall models for cell function: Certain mechanisms may be described in great detail – in this case the gene expression – whereas other processes are described by completely empirical expressions. Hereby, the performance of the overall model is largely determined by the performance of the empirical expressions in the model, and it may be adequate to apply a simpler model for the gene expression. The real strength of

the genetically structured models is, however, not its linkage to the overall growth model, but rather the possibility offered to analyze the influence of specific model parameters on the process. Thus, using the above model, the importance of the different equilibrium constants which are related to the binding affinities, e.g., of the repressor to the operator, can be studied in detail. This can be done by comparison with experimental data for the mRNA level, preferably at conditions where the overall cell activity is the same in all experiments.

Example 7.7 *A model for diauxic growth.* Based on (7.47) and (7.53), Harder and Roels (1982) developed a structured model for diauxic growth. It describes the synthesis of mRNA encoding for the three enzymes necessary for lactose metabolism and also for translation of the mRNA into proteins (which are collected in one compartment called X_E). The residual biomass, including building blocks for mRNA and enzyme synthesis, is pooled into one compartment X which constitutes almost all of the cell mass, i.e., $X \approx 1$.

Synthesis of mRNA is described by

$$-X + X_{mRNA} = 0; \quad v_1 = k_1 f(\mu) Q_1 Q_2, \tag{1}$$

$f(\mu)$ is a linear function of the specific growth rate which is used to describe the way the activity of the cell (e.g., expression of genes) increases with the specific growth rate. The expression is completely empirical, but one could combine the Harder and Roels model with one of the two-compartment models of Sect. 7.4.1, replacing $f(\mu)$ with the concentration of the active compartment. In (1), the functions Q_1 and Q_2 of (7.47) and (7.53) both appear as factors. The fraction of repressor-free operators and the fraction of activated promoters must both be high to obtain a rapid mRNA synthesis.

The rate of synthesis of enzymes necessary for lactose metabolism is assumed to be first order in the mRNA concentration as expressed in (2):

$$-X + X_E = 0; \quad v_2 = k_2 X_{mRNA}. \tag{2}$$

The half-life of mRNA is short due to rapid degradation by an assumed first-order process:

$$-X_{mRNA} + X = 0; \quad v_3 = k_3 X_{mRNA}. \tag{3}$$

Similarly, degradation of the lactose-metabolizing enzymes is included as one first-order process:

$$-X_E + X = 0; \quad v_4 = k_4 X_E. \tag{4}$$

With these four reactions, the mass balances for X_{mRNA} and X_E are

$$\frac{dX_{mRNA}}{dt} = k_1 Q_1 Q_2 f(\mu) - k_3 X_{mRNA} - \mu X_{mRNA}, \tag{5}$$

$$\frac{dX_E}{dt} = k_2 X_{mRNA} - k_4 X_E - \mu X_E. \tag{6}$$

The formation of residual biomass from either glucose or lactose is described with Monod-type kinetics, but for the metabolism of lactose a dependence of X_E is included. Thus,

$$-s_{glc} + \gamma_{glc} X = 0; \quad r_{glc} = k_{glc} \frac{s_{glc}}{s_{glc} + K_{glc}}, \tag{7}$$

$$-s_{lac} + \gamma_{lac} X = 0; \quad r_{lac} = k_{lac} \frac{s_{lac}}{s_{lac} + K_{lac}} X_E. \tag{8}$$

Since the reactions in (1)–(4) do not contribute to a net formation of new biomass, the specific growth rate is found to be

$$\mu = \gamma_{glc} r_{glc} + \gamma_{lac} r_{lac}. \tag{9}$$

For a batch fermentation where the glucose and the lactose concentrations are both initially high, $[S_{lac}]_t$ is high and, according to (7.47), Q_1 is therefore high. However, since the glucose concentration is also high, X_{cAMP} is low according to (7.54), and Q_2 is therefore low. Thus, the rate of synthesis of mRNA is small, and with the rapid turnover of mRNA (k_3 high) the intracellular concentration of mRNA tends to be very low. This again results in a low level of X_E, and consequently the last term in (9) is negligible, i.e., only the metabolism of glucose contributes to the formation of cell mass. When later in the batch fermentation, the glucose concentration decreases, X_{cAMP} and thus Q_2 increases, and as a result the rate of formation of mRNA becomes sufficiently high to ensure an increasing level of mRNA. The result is de novo synthesis of enzymes, and this will lead to a larger and larger contribution of lactose metabolism to the total formation of residual biomass. Finally, when the glucose concentration is zero, the cells grow only on lactose. Since some time is needed for synthesis of the enzymes needed for metabolism of lactose, the specific growth rate may be low in a period where both s_{glc} and X_E are low. Thus, the model correctly predicts a lag-phase between growth on glucose and on lactose.

Equations (7.47) and (7.53) are true mechanistic elements of the model. Unfortunately, the number of adjustable parameters is quite large, and the model is still empirical due to (7.54). It is, however, an excellent example of how known mechanisms can be included in structured models, and it may be possible to find values for some of the binding coefficients in the literature (see Note 7.6).

As mentioned earlier, the lac-promoter is often applied as a tool for expression of heterologous genes in connection with industrial production of recombinant proteins. Most industrial enzymes exhibit a complex regulation with induction and carbon catabolite repression, and also here genetically structured models can be used to gain insight into the expression of the gene encoding the enzyme of interest. A more general expression for the synthesis of mRNA encoding a given protein than that used in Example 7.7 is:

$$r_{mRNA} = k_m \eta_{tr} X_g = k_m Q_1 Q_2 Q_3 X_g, \tag{7.55}$$

k_m is the overall transcription rate constant, η_{tr} is the overall transcription efficiency, and X_g is the copy number of the gene to be transcribed (could be

given as a number of genes per g DW). The overall transcription efficiency is given as the product of Q_1, Q_2, and Q_3. The factors Q_1 and Q_2 represent, respectively, the fraction of repressor-free operators and the fraction of activated promoters, i.e., those that may bind RNA polymerase. These factors are not necessarily identical with those derived for the lac-operon above. If the control mechanism involves an antiinducer, Q_2 is not given by (7.53) (see Problem 7.3). The factor Q_3 is the fraction of promoters that form complexes with the RNA polymerase, i.e., it is a function of the cellular content of RNA polymerases.

The overall transcription rate constant k_m is a function of the environmental conditions, and Lee and Bailey (1984c) specified it as a function of the specific growth rate (see Note 7.6). With mRNA being very unstable, it is necessary to include degradation of mRNA in the model. This is normally done as a first-order process as illustrated in Example 7.7:

$$r_{mRNA,deg} = k_{m,deg} X_{mRNA}. \tag{7.56}$$

Translation of the mRNA to form the desired protein is generally described by (7.57).

$$r_p = k_p \xi X_{mRNA}, \tag{7.57}$$

k_p is the overall translation rate constant (see Note 7.6) and ξ is the translation efficiency which is often set to 1. Similar to the degradation of mRNA, a turnover of protein can be included as a first-order process:

$$r_{p,deg} = k_{p,deg} X_p. \tag{7.58}$$

The above model for protein synthesis is generally applicable, and the parameter values have been identified for many different systems (see Note 7.6). The model is, however, often simplified in order to keep its complexity at a reasonably low level.

Note 7.6 *Mechanistic parameters in the protein synthesis model.* Lee and Bailey (1984c) used the above model for the analysis of the influence of the specific growth rate on the productivity of a recombinant *E. coli*. Because of the mechanistic nature of the model, each of the parameters has a physical meaning. We illustrate how Lee and Bailey calculated the model parameters.

The overall transcription rate constant and the overall translation rate constant are given by:

$$k_m = a_m k_{me} N_p, \tag{1}$$

$$k_p = a_p k_{pe} N_r, \tag{2}$$

where a_m and a_p are conversion factors, k_{me} and k_{pe} represent the mRNA chain elongation rate per active RNA polymerase and the polypeptide chain elongation rate per active

ribosome, respectively. N_p and N_r are the number of active RNA polymerase molecules per gene and the number of active ribosomes per mRNA, respectively. The rate of elongation of mRNA chains per active RNA polymerase (k_{me}) is about 2,400 nucleotides per minute, and this value does not vary significantly with the specific growth rate. The polypeptide chain elongation rate per active ribosome (k_{pe}) is about 1,200 amino acids per minute when $\mu >> \ln(2)$, whereas it is proportional to μ for $\mu << \ln(2)$. Thus,

$$k_{pe} = 1,200a, \tag{3}$$

where

$$a = \begin{cases} 1, & \mu > \ln(2), \\ \mu/\ln(2), & \mu < \ln(2). \end{cases} \tag{4}$$

N_p is estimated from the size of the gene and the intermolecular distances between transcribing RNA polymerase molecules (d_p). Similarly, N_r is found from the size of the mRNA and the intermolecular distance between translating ribosomes (d_r). The intermolecular distances depend on the cellular activity, and they are correlated with the specific growth rate (in h^{-1}):

$$d_p = 233\mu^{-2} + 78\text{nucleotides}, \tag{5}$$

$$d_r = 82.5\mu^{-1} + 145 \text{ nucleotides}. \tag{6}$$

The intermolecular distances are specified as, respectively, the number of nucleotides between two transcribing RNA polymerase and between two translating ribosomes.

Assume that there are z deoxyribonucleotides in the gene. These are transcribed into z ribonucleotides, and at a specific growth rate $\mu = \ln(2)\ h^{-1}$ (corresponding to a doubling time of 1 h) we obtain

$$k_m = \left(\frac{1 \text{ mRNA molecule}}{z \text{ ribonucleotides}}\right)\left(\frac{2,400 \text{ ribonucleotides}}{\text{Active RNA polymerase min}}\right)\left(\frac{1 \text{ active RNA polymerase}}{563 \text{ deoxyribonucleotides}}\right) \left(\frac{z \text{ deoxyribonucleotides}}{\text{gene}}\right) = 4.26 \text{ mRNA molecules per gene per min}. \tag{7}$$

Similarly, if y amino acid molecules are used to synthesize one protein molecule, the overall protein translation rate constant is determined by

$$k_p = \left(\frac{1 \text{ protein molecule}}{y \text{ ribonucleotides}}\right)\left(\frac{1,200 \text{ amino acids}}{\text{Active ribosomes min}}\right)\left(\frac{1 \text{ active ribosome}}{264 \text{ ribonucleotides}}\right) \left(\frac{3y \text{ deoxyribonucleotides}}{\text{mRNA}}\right) = 13.8 \text{ proteins per mRNA per min}. \tag{8}$$

In (8), for each amino acid incorporated in the protein, three ribonucleotides on the mRNA have to be translated. The transcription and translation constants calculated above can be used to estimate reasonable values of the parameters in other, less mechanistic models.

Furthermore, it is illustrated how the parameters in a very mechanistic model can be calculated from information in the biochemistry literature.

The rate of degradation of mRNA, $k_{m,deg}$ is on the order of 0.53 min^{-1} and fairly constant for different mRNAs. The rate of degradation of protein, $k_{p,deg}$ is different from protein to protein but degradation is a much slower process – for most proteins the rate constant is below 0.1 h^{-1}.

For recombinant microorganisms, the cellular content of the gene to be expressed (normally called the *gene dosage*) is not necessarily constant. If the gene is inserted directly in the chromosome, the gene dosage is approximately independent of the operating conditions. However, in bacteria and yeast, the inserted gene is often present in so-called plasmids, which are circular, nonchromosomal DNA. The plasmids are replicated independently of the chromosomal DNA, and the ratio of the plasmid number to the chromosome number (often called the *plasmid copy number*) may therefore vary with the operating conditions. The concentration of the gene X_g in (7.55) should therefore be replaced with the concentration of plasmid copy number when recombinant bacteria are considered. The plasmid is normally designed with a certain replication control mechanism, and in some cases one uses a replication control mechanism that permits induction of rapid plasmid replication, e.g., by addition of chemical components or by changing the temperature.

With the detailed knowledge of recombinant *E. coli*, it has been possible to set up truly mechanistic models for this organism. The largest contribution to the modeling of recombinant *E. coli* has been made in a series of papers from the group of Jay Bailey. Thus, Lee and Bailey (1984a, b, c, d, e) describe very detailed modeling of both plasmid replication and protein synthesis. In Lee and Bailey (1984a, b, c), a mechanistic model for replication of the plasmid in *E. coli* is discussed. The plasmid copy number was found to vary with the specific growth rate. Replication control of the plasmid involves both a repressor and an initiator (which are both proteins). In their model, formation of the repressor and the initiator is described by transcription of the genes followed by translation of the mRNA using kinetic expressions similar to (7.55) and (7.57). The repressor affects the transcription efficiency of the genes coding for both the repressor and the initiator, whereas the initiator is necessary for formation of a so-called replication complex. The plasmid replication is initiated when the replication complex increases above a certain threshold value, and once plasmid replication is initiated it is assumed that the replication is almost instantaneous, a reasonable assumption considering the small size of the plasmid. The influence of the specific growth rate is included through the overall transcription and translation constants, as discussed in Note 7.6. The model correctly describes a decreasing plasmid content with increasing specific growth rate, and model simulations reveal that the primary reason for the higher copy number at the lower specific growth rate is reduced by the synthesis of the repressor protein. In Lee and Bailey (1984d, e), the gene transcription efficiency η is examined for the recombinant protein when the lac-promoter is included in the plasmids. Quite often the promoters of operons for which the control mechanisms

are well known are used in plasmids, since thereby the transcription of the gene can be controlled. A similar model describes the lac-operon in the chromosome, but the binding of RNA polymerase to the promoter is included. This is important since in the recombinant strain the promoters in the plasmids and in the chromosome compete for the available RNA polymerases. The overall transcription efficiency is given as the product of Q_1, Q_2, and Q_3 (see (7.55)). In a study of the effects of multicopy plasmids containing the lac-promoter, Lee and Bailey (1984d, e) found that Q_1 increases with the plasmid copy number and that both Q_2 and Q_3 decrease with the plasmid copy number. The overall effect is decreasing gene-expression efficiency with increasing plasmid copy number, and the overall transcription rate of the cloned gene is therefore not increasing linearly with the plasmid copy number, as has also been experimentally verified (Seo and Bailey 1985). The decrease in Q_3 with the plasmid copy number is explained by an increasing competition for the available RNA polymerases. Lee and Bailey (1984e) suggest that the empirical expression (7.59) may be used in simple structured models to account for this effect:

$$Q_3 = \left(1 - \frac{X_\mathrm{p}}{X_{\mathrm{p.\,max}}}\right)^n. \tag{7.59}$$

The modeling work of Lee and Bailey has been used to study host–plasmid interactions and to explain experimental observations, which are seldom obvious due to the many interactions present in recombinant microorganisms.

7.6 Morphologically Structured Models

In Sects. 7.3–7.5, we specified the growth kinetics, assuming that all the cells in a culture have the same metabolism; i.e., the cell population is assumed to be completely homogeneous, and a nonsegregated model for cellular performance resulted. For some microbial systems, differentiation of the cells in the culture does, however, play an important role in the overall performance of the culture, and both growth kinetics and productivity are affected by the presence of more than one cell type in the culture. In Chap. 8, complete segregation is considered, and instead of postulating a finite number of distinguishable cell types the culture is characterized by a continuous distribution of an important cell property, e.g., the cell age. Obviously, the model for a culture with only a few distinguishable cell types (e.g., cells that produce a desired protein and cells that have lost this property) is much simpler than a model that has to take a continuous distribution of a property into account. We shall refer to the crudely segregated models as *morphologically structured models*. These models are particularly relevant for description of the growth of filamentous fungi, where cellular differentiation takes place in connection with hyphal extension, but they find application for description of other cellular systems, e.g., cultures with

bacteria containing unstable plasmids, and also they are used to explain why yeast cultures sometimes exhibit oscillatory behavior in several variables.

In morphologically structured models, the cells are divided into a finite number Q of cell states $\mathbf{Z}$ (or morphological forms), and conversion between the different cell states is determined by a sequence of empirical *metamorphosis reactions*. Ideally, these metamorphosis reactions can be described as a set of intracellular reactions, but the mechanisms behind most morphological conversions are largely unknown. Thus, it is not known why filamentous fungi differentiate into cells with a completely different phenotype than that of their origin. It is therefore not possible to set up detailed mechanistic models describing these changes in morphology, and empirical metamorphosis reactions have to be used. The stoichiometry of the metamorphosis reaction where the jth form is converted to the ith form is given by very simple relations:

$$Z_i - Z_j = 0, \tag{7.60}$$

Z_q will be used in the following to describe both the qth morphological form itself and the fraction of cell mass that is Z_q (g (qth morphological form) (g DW)$^{-1}$). In the metamorphosis reaction, one morphological form is spontaneously converted to another form. This is of course an extreme simplification since the conversion between morphological forms is the sum of many small changes in the intracellular composition of the cell. Clearly there may be many different metamorphosis reactions, and the stoichiometry for these reactions can be summarized in analogy with the matrix equation (7.2) for intracellular reactions:

$$\Delta\mathbf{Z} = 0. \tag{7.61}$$

$\mathbf{\Delta}$ is a stoichiometric matrix. *It is assumed that the metamorphosis reactions do not involve any change in the total mass,* and the sum of all stoichiometric coefficients in each reaction is therefore equal to zero.

To describe the rate of the metamorphosis reactions, a forward reaction rate u_i is introduced for the ith reaction, and the rates of all the metamorphosis reactions are collected in the rate vector $\mathbf{u}$. Besides formation from other morphological forms, a given morphological form may also be synthesized from substrate through intracellular reactions (and different metabolic products may also be formed by different morphological forms). A structured intracellular model may describe these reactions, but in order to reduce the model complexity one will normally use a simple unstructured model for description of the growth and product formation of each cell type, e.g., the Monod model describes the specific growth rate of the qth morphological form. When the specific growth rate has been specified for each morphological form, the specific growth rate of the total biomass is given as a weighted sum of the specific growth rates of the different morphological forms:

$$\mu = \sum_{i=1}^{Q} \mu_i Z_i. \tag{7.62}$$

The rate of formation of each morphological form is determined both by the metamorphosis reactions and by the growth associated reactions for each form, and the mass balance for the qth morphological form can be derived in analogy with (7.14) (see Nielsen and Villadsen (1992) for details):

$$\frac{\mathrm{d}Z_q}{\mathrm{d}t} = \Delta_q^{\mathrm{T}}\mathbf{u} + \left(\mu_q - \mu\right)Z_q. \tag{7.63}$$

The first term accounts for the net formation of the qth morphological form by the metamorphosis reactions (the vector $\mathbf{\Delta}_q$ specifies the stoichiometric coefficients for the qth morphological form in all the metamorphosis reactions). The second term accounts for growth of the qth morphological form and the last term accounts for dilution due to growth of the biomass (this is a consequence of the normalization of the concentrations of the morphological forms). The use of morphologically structured models is illustrated in Example 7.8.

Example 7.8 *A simple morphologically structured model describing plasmid instability.* A potential obstacle to commercial application of recombinant bacteria and yeasts is plasmid instability. Sometimes a daughter cell that does not contain plasmids is formed upon cell division, and since the metabolic burden is higher for plasmid-containing cells, the plasmid-free cell will grow faster than the plasmid-containing cells. Even a small tendency to plasmid instability will therefore ultimately result in the appearance of a large fraction of non-protein-producing cells. Plasmid stability can be improved by increasing the plasmid copy number or by designing the host–plasmid system in a way that ensures that plasmid-free cells cannot survive.

Modeling of plasmid instability can be done using the concept of morphologically structured models. Thus, we assume that when plasmid-containing cells Z_p are dividing, a certain fraction δ of the cells are converted to plasmid-free cells Z_h, whereas the remaining fraction of the cells maintains the plasmid. This is described by the metamorphosis reactions for Z_p and Z_h before and after division:

$$Z_{\mathrm{p,after}} = Z_{\mathrm{p,before}} - \delta Z_\mathrm{p} \quad \text{and} \quad Z_{\mathrm{h,after}} = Z_{\mathrm{h,before}} + \delta Z_\mathrm{h}. \tag{1}$$

The stoichiometric coefficient δ (often called the *segregation parameter*) is equal to the probability of formation of a plasmid-free cell upon growth of plasmid-containing cells. The stoichiometry in (1) is illustrative since it shows that when one unit of recombinant cells divides, a fraction δ of plasmid-free cells is formed. However, since no new cell mass is formed by the metamorphosis reaction $\delta Z_\mathrm{p} = \delta Z_\mathrm{h}$ and in terms of stoichiometry one can obtain the following simplification:

$$\left(Z_\mathrm{p} + Z_\mathrm{h}\right)_{\mathrm{before}} = \left(Z_\mathrm{p} + Z_\mathrm{h}\right)_{\mathrm{after}} = 1. \tag{2}$$

However, the rate of the overall reaction (2) is different from that of reaction (1). Since the metamorphosis reaction (1) specifies growth of the plasmid-containing cells, the forward rate of this reaction is equal to $\mu_\mathrm{p}Z_\mathrm{p}$, whereas the rate of the metamorphosis reaction is equal to $\delta\mu_\mathrm{p}Z_\mathrm{p}$.

In order to apply the general mass balance for the two morphological forms, we first specify the stoichiometric matrix Δ:

$$\Delta = \begin{pmatrix} -1 & 1 \end{pmatrix}. \tag{3}$$

Now we set up the mass balance for the plasmid-containing cells:

$$\frac{dZ_p}{dt} = -\delta\mu_p Z_p + (\mu_p - \mu)Z_p = [(1-\delta)\mu_p - \mu]Z_p. \tag{4}$$

For the plasmid-free cells, the mass balance is:

$$\frac{dZ_h}{dt} = \delta\mu_p Z_p + (\mu_h - \mu)Z_h. \tag{5}$$

For each morphological form, there is a contribution from the metamorphosis reaction, a contribution from growth of the form, and finally a contribution accounting for dilution due to the expansion of the total biomass. The term for the dilution is analogous to the dilution term in models with intracellular structure, whereas the term accounting for formation of intracellular components in intracellular structured models is replaced by two terms in the morphologically structured models, one for exchange between forms and one for growth.

The specific growth rate for the total biomass is given by:

$$\mu = \mu_p Z_p + \mu_h Z_h. \tag{6}$$

Normally, the specific growth rate for plasmid-containing cells is lower than that of plasmid-free cells, and the specific growth rate for the total biomass will therefore also be smaller than μ_h. Consequently, both terms on the right-hand side in the mass balance (5) are positive, and the fraction of plasmid-free cells will continuously increase due to two factors: There is a constant formation of plasmid-free cells from plasmid-containing cells, and as $\mu_h > \mu_p$ the plasmid-free cells will outgrow the plasmid-containing cells.

With the formation of plasmid-free cells, a culture with two different strains develops. These are the recombinant strain and the parental (or "wild-type") strain. Thus, the culture is *mixed*, with two different strains of the same species.

The metamorphosis reaction (2) may also be used to describe the spontaneous occurrence of mutants during cellular growth, but here the forward reaction rate is not necessarily similar to the specific growth rate of the original strain. Occurrence of spontaneous mutants is a phenomenon often observed for filamentous fungi, especially when they are grown in continuous cultures for long periods, and the resulting mutants are normally referred to as *colonial mutants*.

When growth of individual morphological forms is described by an intracellularly structured model, the complexity of morphologically structured models increases substantially. It is possible to derive a general mass balance for the concentration of the intracellular variables in different morphological forms (Nielsen and Villadsen 1994), but as these equations have limited practical use we will not elaborate on this topic. Instead we will focus on two different

applications of morphologically structured models: quantitative description of oscillating yeast cultures and growth of filamentous microorganisms.

7.6.1 Oscillating Yeast Cultures

Whereas the division of unicellular bacteria is symmetric, with the formation of two almost identical cells, the cell division of yeast is asymmetric, with formation of a so-called mother and a so-called daughter cell (see Fig. 7.18). The daughter cell is converted to a mother cell within the time t_d. After a period of maturation (t_m), a new bud emerges on the mother cell, and after a further time period t_b the bud has obtained a critical size, resulting in cell division. At cell division, a *bud scar* is formed on the cell envelope of the mother cell, and it is believed that the cell cannot form a new bud at this position. t_d, t_m, and t_b are functions of the cellular composition, and therefore also of the environmental conditions.

The cellular metabolism of the daughter cells (or *unbudded cells*) and the mother cells (or *budded cells*) is very different, and to give a correct description of the overall growth kinetics of yeast cultures it is therefore necessary to apply a morphologically structured model. In many cases, one may, however, describe the average metabolism of the culture with an intracellularly structured model, i.e., assume that the population is homogeneous, and still get a satisfactory description of many experimental data (see Example 7.3).

These models cannot, however, describe a fascinating phenomenon observed in a glucose-limited chemostat with *S. cerevisiae*: Spontaneous oscillations of many easily measured process variables such as the dissolved oxygen, ethanol, and glucose concentrations; oxygen uptake rate; and carbon dioxide evolution rate as well as intracellular variables (e.g., NADH and DNA). Figure 7.19 shows some typical results. Spontaneous oscillations in (always aerobic) yeast cultures, with glucose or with other substrates such as ethanol and acetate have been described in a large number of academic papers from the last 40 years, mostly giving accounts of experimental observations, but modeling of the phenomenon is also discussed. The oscillations can be maintained for many generations, especially when one uses high-performance bioreactors, in which the environment is practically homogeneous throughout the reactor (Strässle et al. 1988, 1989; Keulers et al. 1996a, b; Duboc and von Stockar 2000; Beuse et al. 1999).

Spontaneous oscillations can only be maintained if the growth of the culture is *synchronous*, since after completion of one cycle the fraction of each morphological form in the cell mass must be the same as it was at $t - T_{osc}$, where T_{osc} is the length of the oscillation period. With the asymmetric cell division of *S. cerevisiae*, it is not immediately clear how the synchrony can be maintained for many generations. If, however, the population can be divided into a discrete number of subpopulations (e.g., mother cells *m* and daughter cells *d*), and if the generation time of one subpopulation is an integer multiple of the generation time of the other, then synchrony can be obtained. Thus, if the creation of a mother cell from a new born

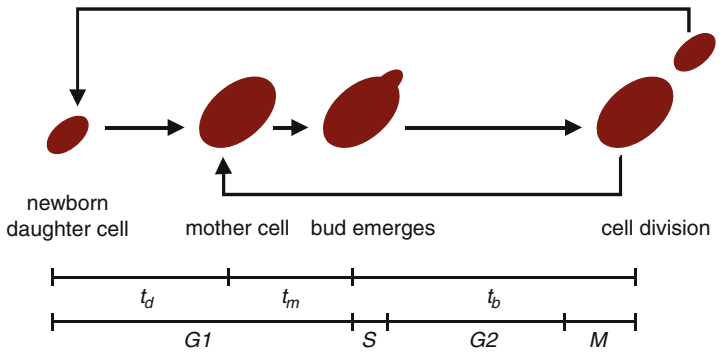

Fig. 7.18 The cell cycle of budding yeast. The period of maturation (i.e., $t_d + t_m$ for a daughter cell and t_m for a mother cell) is called the *G1-phase*, and in this phase the cells prepare for budding (e.g., carbohydrate storage is built up). The budding itself (lasting t_b) consists of three phases. First the chromosomes are duplicated in the *S-phase*. Thereafter, the cells prepared for cell division (the *G2-phase*), and finally they enter the *M-phase* (M for mitosis), where cell division occurs

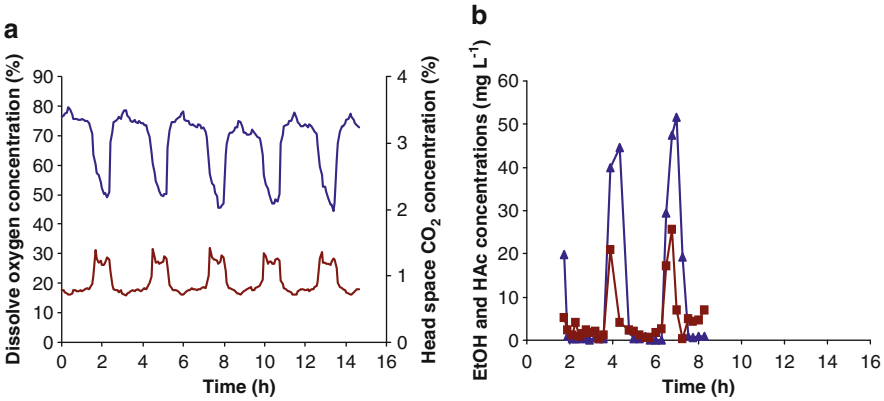

Fig. 7.19 Spontaneous oscillation of *Saccharomyces cerevisiae*. (**a**) Measurements of carbon dioxide in the exhaust gas and the dissolved oxygen concentration (DOT) in % of the equilibrium value. (**b**) Measurements of the concentrations of ethanol (*filled square*) and acetate (*filled triangle*). The data are taken from Frandsen (1993)

daughter cell takes exactly $T = 2(t_b + t_m)$, then the ratio of mother cells to daughter cells in the population will be constant and equal to $(1 + \sqrt{5})/2$ as shown by Hjortso and Nielsen (1994).

There is, however, no reason why the oscillation period should be given as simply as in the Hjortso and Nielsen model, and an observed variation of T_{osc} with the dilution rate D is modeled by both Duboc and Beuse as discussed in Note 7.7.

More papers on the subject have appeared since 2000. The experimental techniques used to measure the time profiles of metabolites have greatly improved,

but the theoretical explanation for the oscillations is still uncertain, and this weakness is not overcome with the increasingly complicated models used.

A good review of the state of the art in yeast oscillations is Patnaik (2003), and despite the fact that the oscillation fingerprint ought to reveal features of the deep-level regulatory structure of *S. cerevisiae*, it is doubtful if this issue will be pursued, mostly because the subject of yeast oscillations seems to have lost academic interest during the last few years.

The fact that spontaneous oscillations are never seen in industrial size tanks of, e.g., 80 m^3 volume for insulin production by aerobic fermentation of *S. cerevisiae* has obviously not induced industry to show a prolonged interest in the subject, although as discussed in Chap. 11 the inhomogeneous environment in even a well-stirred industrial bioreactors leads to all sorts of process upsets, including loss of yield and loss of product quality.

Note 7.7 *Relation between T_{osc} and the dilution rate in continuous culture.* The result of Hjortso and Nielsen (1994) is a special case of the following:

Let m be the population of mother cells and d the population of daughter cells. New mother-and daughter-cells are born in each generation. Thus, at $t = (n + 1)T_{osc}$:

$$m_{n+1} = m_n + d_n (\text{or } m_{n+2} = m_{n+1} + d_{n+1}), \tag{1}$$

$$d_{n+1} = pm_n. \tag{2}$$

p is the probability that a mother cell develops a new daughter cell exactly at $t = (n + 1)$ T_{osc}. Eliminating d_{n+1} between (1) and (2) yields a second-order difference equation:

$$m_{n+2} - m_{n+1} - pm_n = 0. \tag{3}$$

But the whole culture grows exponentially with time, and consequently after one cycle, time T_{osc} is in a continuous culture:

$$m_{n+1} = m_n \exp(\mu\ T_{osc}). \tag{4}$$

When (4) is inserted in the difference equation (3), one can obtain the following algebraic equation for $\rho = \exp(D\ T_{osc})$:

$$\rho^2 - \rho - p = 0 \quad \text{or} \quad \rho = \frac{1}{2}\left(1 + (1 + 4p)^{1/2}\right). \tag{5}$$

From (5), a relation between D and T_{osc} is derived:

$$T_{osc} = \ln\rho / D. \tag{6}$$

For $p = 1$ (i.e., all mother cells start to make daughter cells immediately after they have lost a bud), the result is identical to what is found in the Hjortso and Nielsen (1994) model.

With the extra parameter p, Duboc and von Stockar (2000) could fit experimental data better. For $p = 1/2$, the value of ρ decreases from 1.618 to 1.366 and at a given D a smaller oscillation time T_{osc} is predicted. In both cases, the oscillation time is, however, predicted to decrease inversely proportional to D. This last feature is confirmed by experiments, but the experiments also show that different values of p between 2 and 1/2 should be used at different D values (see Fig. 7 of Duboc and von Stockar (2000)). The value $p = 2$ is of course not allowed in the Duboc and von Stockar hypothesis, but the resulting relation $T_{osc} = \ln 2/D$ corresponds to the cell cycle of prokaryotes where daughter cells start to develop into mother cells immediately after cell division has taken place. For the reasons outlined below, stable oscillations are not likely to develop for these organisms.

Finally, it should be mentioned that Beuse et al. (1999) explained synchrony in the culture by a hypothesis that it is a mirror image of the Duboc-von Stockar hypothesis. Beuse *et al.* propose that some daughter cells may take more than $2(t_b + t_m)$ to develop into a mother cell while all mother cells can give birth to daughter cells after $t_b + t_m$.

Both hypotheses do however suffer from the weakness that it is difficult to understand why a fixed proportion of the mother cells (or daughter cells) should choose to take "an extra day off" and that they should do so, generation after generation.

If the population does not consist of a finite number of subpopulations with stringently kept rules for the generation time, then the whole concept of synchrony falls apart. In a real culture of cells, there must be a statistical distribution of, e.g., generation times for the cells, and if synchrony should prevail in the real culture there must be some mechanism by which "slow" cells catch up with faster proliferating cells. In mathematical terms, there must exist an *attractor*, and in the case of bioreactions the nature of the attractor must be biochemical. Sohn and Kuriyama (2001) discuss an example where H_2S is the attractor.

7.6.2 Growth of Filamentous Microorganisms

Filamentous microorganisms constitute a large and a very important part of the microbial world. In Sect. 2.3.2, we have seen how both eukaryotes (*Penicillin sp.*, *Cephalosporin. sp.*) and prokaryotes (soil bacteria like *Streptomyces sp.*) are used to produce antibiotics. Due to their efficient expression systems, filamentous fungi are used as producers of industrial enzymes. The role of filamentous fungi in the food industry is well known, both to produce high-quality end products, but also as infamous food spoilers.

Mechanisms for the growth of filamentous microorganisms are very different from those of unicellular microorganisms. The cells are connected in a so-called *hyphal element* (a "*hypha*" or "*mycelium*," where the latter term is also used for the clumps of entangled hyphae seen on Fig. 7.20b). While all cells in a hyphal element may contribute to the growth process, i.e., production of protoplasm, extension of the element occurs only at the tips. The number of tips in a mycelium is therefore a characteristic morphological variable. Even though the linear rate of tip extension has an upper limit, the total length of a mycelium may increase exponentially due to

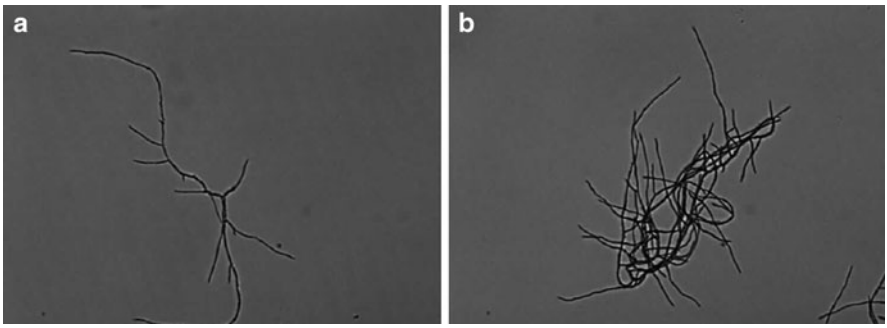

Fig. 7.20 Some typical pictures of hyphal element of filamentous fungi. (**a**) Single hyphal element of *Aspergillus nidulans*. (**b**) Agglomerate of several hyphal elements of *Aspergillus nidulans*

the formation of new tips. The frequency of formation of new tips is determined by the rate of production of protoplasm within the mycelium and the number of tips to which the material is distributed. The ratio between the size of the mycelium and the number of tips is therefore another characteristic morphological variable, which Caldwell and Trinci (1973) called the *hyphal growth unit*. They originally defined it as the total mycelium length divided by the number of tips (called the *hyphal growth unit length* l_{hgu}), but it may also be defined on the basis of total mycelium mass (called *hyphal growth unit mass*). At conditions that support rapid growth, a densely branched mycelium with a large hyphal diameter is observed, while at poor growth conditions the mycelium is less branched, and the diameter of the hypha (or rather of the "central" string of the hypha where growth started) is small (Nielsen 1992). With a long, slim hyphal element, where substrate is not used to form branches, the organism hopes to reach an environment where the growth conditions are better.

In a hyphal element, several cells behind the tip are involved in the tip extension process. They supply the necessary cellular material for tip extension, e.g., cytoplasmic material and building blocks for wall synthesis. These cells are not separated by a *septum* (a partition between the individual cells), and they therefore share a common cytoplasm in which the nuclei of all the cells are found. The part of the hyphal element between the tip (*apex*) and the first septum is called the *apical compartment*. The cells just behind the apical compartment have an intracellular composition very similar to that of the apical cells, and this part of the hyphal element is called the *subapical compartment*. Despite the presence of a septum between the apical and subapical cells, there may be an exchange of protoplasm since the septa are often perforated. When moving further away from the tip, one finds cells containing large vacuoles. These cells do not participate directly in the tip extension process, but they are believed to be of importance in creating an intracellular pressure sufficient to ensure transport of protoplasm toward the tip section. This part of the hyphal element is referred to as the *hyphal compartment*.

In filamentous fungi, there is a substantial accumulation of small vesicles at the apex, and the vesicles are likely to play an important role in the tip extension. They are believed to contain wall subunits, lytic enzymes, and synthetic enzymes

that are transported with the vesicles to specialized regions of the endomembrane system in the apical and subapical compartments (McIntyre et al. 2001). The vesicles, each carrying its load of enzymes and/or wall precursors, are transported by unknown mechanisms through the cytoplasm to the tip section of the apical cell, normally referred to as the *extension zone*. When a vesicle comes into contact with the cell membrane at the apex, it fuses with the membrane, and the vesicle content is released into the wall region. The excreted lytic enzymes attack the microfibrillar skeleton in the cell wall, resulting in plastification of the wall structure, which thereby becomes unable to withstand the inner pressure from the cytoplasm. The microfibrils become stretched, and the surface area of the wall increases. In filamentous prokaryotes (typically *Streptomyces* species), the wall material is soluble in the cytoplasm and is probably transported to the apex by molecular diffusion. It has been found that the wall section at the apex is more susceptible to compounds affecting wall synthesis and assembly than other sections. This indicates that the lytic enzymes in filamentous prokaryotes are positioned in the wall section at the apex (Prosser and Tough 1991).

When a new tip is formed, its initial growth phase corresponds to an increase in the size of the apical compartment. When the apical compartment has reached a certain size, a septum is formed behind the tip, and some of the old apical cell mass becomes new subapical cell mass. Under constant environmental conditions, the size of the apical compartment remains constant, and the net result of tip extension is therefore formation of subapical cells. The control of septum formation has been studied in filamentous fungi, and Fiddy and Trinci (1976) introduced the term *duplication cycle* to describe the events that lead to the net formation of a whole new apical compartment. For *Aspergillus nidulans*, the duration of the duplication cycle has been found to be identical with the doubling time of the biomass.

Branching is the mechanism by which new apical compartments are formed, and it occurs at certain preferred "branching points" on a hyphal element. It has been suggested that in eukaryotes branching occurs at locations where for one reason or another there is an accumulation of vesicles, whereas branch formation in filamentous prokaryotes does not result from accumulation of material (Prosser and Tough 1991). Since vesicles are synthesized both in the subapical and in the apical compartment in hyphae of filamentous fungi, it seems reasonable that at positions where the protoplasmic flow is reduced, e.g., at the position of a septum, there is an accumulation of vesicles. Branching may therefore be associated with septum formation, and for the filamentous fungus *Geotrichum candidum* more than 70% of the observed branch points in a subapical compartment are positioned close to the septum separating this compartment from the apical compartment (Trinci 1984). For other species of filamentous fungi, there is, however, a more equal distribution of the branch points throughout the subapical compartment. Branching is observed mainly in the subapical compartment, but in some filamentous species apical branching may occur.

Originally, the growth mechanisms of filamentous microorganisms was studied using surface cultures, but here the morphology is completely different from that found in a submerged culture. Through the use of automated image analysis it

has, however, become possible to analyze a large number of hyphal elements in submerged cultures, and hereby information on the hyphal morphology may be obtained (Cox et al. 1998). Furthermore, through the use of flow-through cells that are positioned directly under a microscope equipped with an automated image analysis system it is possible to follow the outgrowth of single hyphal elements and hereby study the growth kinetics in great detail (Spohr et al. 1998; Christiansen et al. 1999).

Not many models specifically address the growth mechanism of filamentous microorganisms (Krabben and Nielsen (1998) is a review of the subject). Normally, the focus is on the primary metabolism, where it is not necessary to consider the hyphal structure explicitly; i.e., many of the intracellularly structured models described in Sects. 7.3–7.4 may also be used to describe the primary metabolism of filamentous microorganisms. To model the formation of secondary metabolites, which may be determined by the cellular differentiation, it is, however, often necessary to consider morphological structure. Furthermore, when a description of the morphology of the hyphal elements is the objective, one must of course include morphological structure in the model.

Megee et al. (1970) described the first morphologically structured model for filamentous fungi. The model was used to describe growth and production formation of *Aspergillus awamori*.

Five separate morphological forms are considered in the model:

Z_A – Apical compartment in actively growing hyphae
Z_H – Subapical compartment in actively growing hyphae
Z_C – Conidiophore[4] developing hyphae
Z_B – Black spores
Z_M – Matured spores

With these five morphological forms, it was possible to describe the complete life cycle of so-called *imperfect fungi* (fungi with no sexual reproduction). The model includes product formation as a result of the differentiation processes, a reasonable hypothesis for many secondary metabolites. The model describes several general observations concerning the growth of *A. awamori*. There are many parameters, but one may neglect spore formation and consider only actively growing hyphae, i.e., the morphological forms Z_A and Z_H. Thereby, the original model is substantially simplified, as illustrated in Example 7.9.

Example 7.9 *A simple morphologically structured model for the growth of filamentous microorganisms.* Based on the growth mechanisms described above, Nielsen (1993) derived a simple structured model including the three morphological forms shown in Fig. 7.21.

- Apical cells (Z_A)
- Subapical cells (Z_S)
- Hyphal cells (Z_H)

[4]Conidiphores are modified hyphae on which the asexual spores are formed.

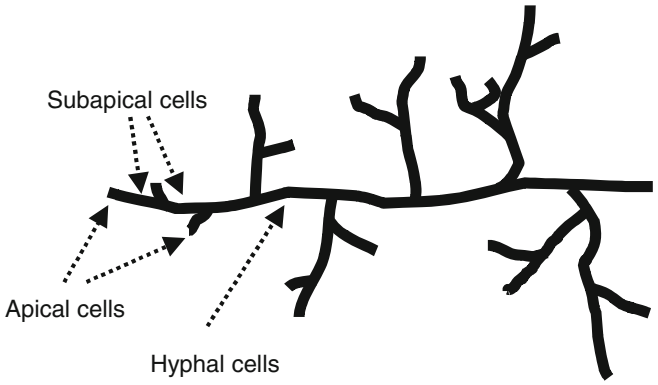

Fig. 7.21 Structure of a densely branched hyphal element with indication of apical, subapical, and hyphal cells

The model is a progeny of the Megee et al. model. The verbal formulation of the model is:

> Active growth, i.e., uptake of substrates and formation of biomass, occurs only in apical and subapical cells. When the tip extends, an apical cell is converted to a subapical cell, whereas a new apical cell is produced from subapical cell material when a branch point is formed in the subapical compartment. When the subapical cells become more and more vacuolated, they change into inactive hyphal cells.

The mathematical formulation is given in (1) and (2). Three metamorphosis reactions, described in matrix form in (1), are considered. They represent branching, tip growth, and differentiation, respectively. The kinetics of all three metamorphosis reactions is taken to be first order in the morphological form which disappears. Furthermore, formation of inactive hyphae is assumed to be inhibited by high substrate concentrations. The Monod model describes growth of both the apical and subapical cells, where s is the extracellular glucose concentration.

$$\begin{pmatrix} 1 & -1 & 0 \\ -1 & 1 & 0 \\ 0 & -1 & 1 \end{pmatrix} \begin{pmatrix} Z_A \\ Z_S \\ Z_H \end{pmatrix} = \begin{pmatrix} 0 \\ 0 \\ 0 \end{pmatrix}; \quad \begin{pmatrix} u_1 \\ u_2 \\ u_3 \end{pmatrix} = \begin{pmatrix} k_1 Z_S \\ k_2 Z_A \\ k_3 Z_S/(sK_3+1) \end{pmatrix}, \tag{1}$$

$$\begin{pmatrix} -\alpha_A \\ -\alpha_S \\ 0 \end{pmatrix} s + \begin{pmatrix} 1 & 0 & 0 \\ 0 & 1 & 0 \\ 0 & 0 & 0 \end{pmatrix} \begin{pmatrix} Z_A \\ Z_S \\ Z_H \end{pmatrix} = \begin{pmatrix} 0 \\ 0 \\ 0 \end{pmatrix}; \quad \begin{pmatrix} \mu_A \\ \mu_S \\ \mu_H \end{pmatrix} = \begin{pmatrix} k_A s/(s+K_s) \\ k_S s/(s+K_s) \\ 0 \end{pmatrix}. \tag{2}$$

Inserting (1) and (2) in (7.62) and (7.63), one can obtain the specific growth rate of the total biomass and the mass balances for the three morphological forms:

$$\mu = (k_A Z_A + k_S Z_S) \frac{s}{s+K_s}, \tag{3}$$

$$\frac{d}{dt} \begin{pmatrix} Z_A \\ Z_S \\ Z_H \end{pmatrix} = \begin{pmatrix} u_1 - u_2 + (\mu_A - \mu) Z_A \\ -u_1 + u_2 - u_3 + (\mu_S - \mu) Z_S \\ u_3 - \mu Z_H \end{pmatrix}. \tag{4}$$

The rates of the metamorphosis reactions and the morphological variables have been shown to correlate with specific measures of the hyphae (Nielsen 1993). Thus, the hyphal diameter is given by:

$$d_{\text{hyphae}} = a_1 \frac{\mu}{Z_{\text{A}}}, \tag{5}$$

a_1 in (5) is a physiological constant determined by the water content and the density of the hyphae. Equation (5) is based on the assumption that only precursors synthesized in the apical compartment contribute to tip growth. For some species of filamentous microorganisms, precursor synthesized in the subapical compartment may also be transported to the apex and incorporated in the hyphal wall, but the contribution from the subapical compartment to the total precursor synthesis is assumed to be small and is neglected in the model. The hyphal growth unit length may also be derived from the model:

$$l_{\text{hgu}} = \frac{\mu}{a_2 u_1}, \tag{6}$$

a_2 in (6) is physiological constant determined by the mass of apical compartment per tip. Finally, the tip extension rate q_{tip} can be derived from the hyphal growth unit length and the specific growth rate:

$$q_{\text{tip}} = \mu l_{\text{hgu}}. \tag{7}$$

With the morphologically structured model, the fraction of the morphological forms can be calculated, and using (5)–(7) it is then possible to calculate the development of directly measurable morphological variables.

The model was compared with experimental data for *G. candidum*, *Streptomyces hygroscopicus*, and *Penicillium chrysogenum*, and in Figs. 7.22 and 7.23 the results of the comparison with data for *G. candidum* are shown.

In Fig. 7.22, measurements of the hyphal diameter, the hyphal growth unit volume, and the hyphal growth unit length in a steady-state chemostat are shown as functions of the dilution rate D. The hyphal diameter increases with D, and since the hyphal growth unit volume is approximately constant, l_{hgu} decreases with the dilution rate. Thus, when the glucose concentration decreases, the hyphal elements become less branched and form long hyphae.

In Fig. 7.23, measurements of the total hyphal length, the number of tips, and the hyphal growth unit length during outgrowth of a single spore on a solid medium are shown, together with model simulations.

The total hyphal length is observed to increase exponentially, whereas there is a lag-phase before the first branch point is formed, i.e., the number of tips increases from one to two. Due to the sudden formation of new tips, the hyphal growth unit length oscillates until the number of tips becomes large and an almost constant value for l_{hgu} is obtained. The modeling concept illustrated here has been applied for simulation of many other systems, e.g., for enzyme production by *Aspergillus oryzae* (Agger et al. 1998). Reviews on modeling of filamentous fungi are given by Nielsen (1996) and Krabben and Nielsen (1998).

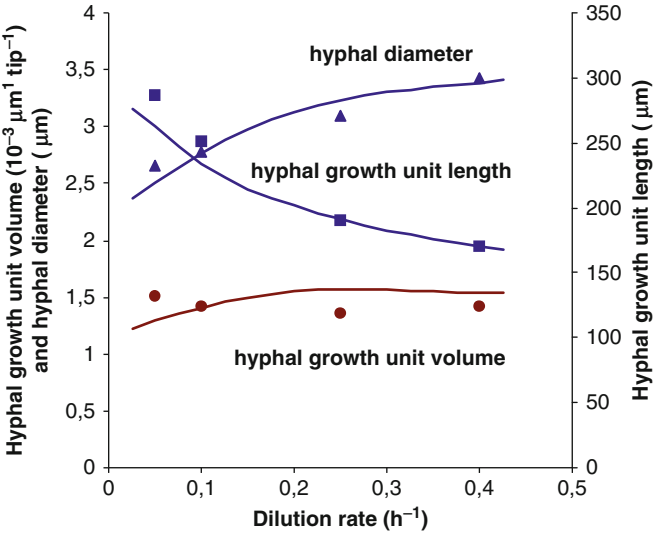

Fig. 7.22 Morphology of *Geotrichum candidum* as a function of the specific growth rate in a submerged culture. Hyphal growth length, hyphal growth unit volume, and hyphal diameter are shown as a function of the dilution rate in a chemostat. Experimental data from Robinson and Smith (1979), and *lines* are model simulations from Nielsen (1993)

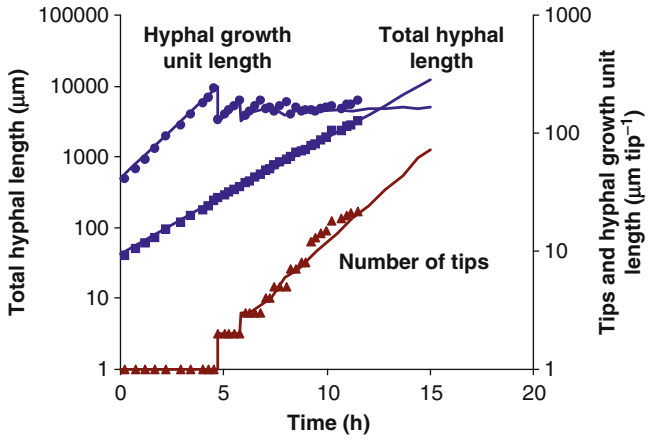

Fig. 7.23 The morphology of *Geotrichum candidum* during outgrowth from a single spore. Total hyphal length (l_t in µm), the number of tips, and the hyphal growth unit length (l_{hgu} in µm per tip). Data from Trinci (1974) and model simulations from Nielsen (1993)

7.7 Transport Through the Cell Membrane

The rate of *intracellular* reactions has until now been the subject of Chap. 7. None of these reactions will, however, occur unless the substrates are transported to the cytoplasm from the medium, and likewise the metabolic products, small metabolites as well as secreted proteins, must be transported the other way.

Two structures surround the cytoplasm of most microbial cells, the *cell wall* and the *cytoplasmic membrane*. The cell wall has a rigid structure of cross-linked disaccharides and peptides (peptidoglycans), and its major function is to prevent the cell from rupturing, either because of a high intracellular osmotic pressure or because an external force acts on the cell. Actually, the cell wall resists very high external forces, and often extreme shear forces have to be applied to recover, e.g., proteins that are not secreted from a microorganism, such is the case for many proteins when *E. coli* is used as production organism.

It is, however, the extremely thin (6–10 nm) cytoplasmic membrane that serves a crucial role for the living cell, and the following discussion is restricted to this barrier between the medium and the cell interior. The cytoplasmic membrane of bacteria and eukaryotes is an extended double layer, typically made up of phospholipids that contain a glycerol scaffold onto which two fatty acids (on C-1 and C-2 of the glycerol) and one alcohol are bound. The fatty acids generally have 16–20 carbon units, and the alcohol (e.g., choline and trimethyl-ethanolammonium) is connected to the C-3 of the glycerol scaffold via a phosphate ester.

Phospholipids have one very hydrophilic end, the alcohol, and one very hydrophobic end, the long C-chain of the fatty acids. The double layer of the membrane exposes the hydrophilic (polar) ends to the outside of the membrane.

Substances can cross the cytoplasmic membrane by *passive diffusion*, the mechanism discussed in Sect. 6.3.2. The stationary flux J is proportional to the concentration difference between the outside and the inside of the membrane:

$$J = \frac{D_{\text{mem}}}{d_{\text{mem}}} K_{\text{par}} (c_{\text{a}} - c_{\text{b}}) \left(\text{unit: mass transported } \left(\text{m}^2 \text{ membrane unit time} \right)^{-1} \right), \quad (7.64)$$

K_{par} is the partition coefficient of the substance between the aqueous phase on either side of the membrane and the hydrophobic interior of the membrane, d_{mem} the thickness of the membrane (6–10 nm), and D_{mem} is the diffusivity of the solute in the membrane. The three parameters multiplying the concentration difference are combined to form one parameter, the *permeability coefficient*, P (unit: e.g., m s^{-1}).

A small molecule can easily transverse the membrane *if it is solvable in the hydrophobic lipid double layer*, *i.e., if it is nonpolar or is able to shed its solvation shell of water* (K_{par} high) *and retrieve it on the other side of the membrane*. Thus, O_2 and CO_2 can easily pass the membrane. In *undissociated* form, fatty acids have large values of K_{par} (0.03 for HAc, 0.44 for HBu, and increasing with the molar weight), and they as well as HLac also pass quite easily through the membrane.

Ethanol passes through the membrane unless its concentration is so high that it changes the fluidity of the phospholipids, but hexoses have a very low K_{par}, and consequently the permeability coefficient P is 4–5 orders of magnitude smaller than for even low Mw carboxylic acids. Ions such as H^+, K^+, and Na^+ are unable to pass the membrane by passive diffusion.

Macromolecules cannot pass the membrane by passive diffusion, partly because their diffusivity D_{mem} is so small.

The reason sugars, amino acids, and other substrates can be transported into the cell, and that products of the cell reactions, e.g., proteins can be secreted is, that other transport mechanisms allow the barrier to be breached. The mechanisms by which fast transmembrane transport is permitted are *membrane channels, pumps, and carrier proteins*.

Most of these mechanisms depend on the action of proteins, and a large number of proteins with different transport functions stick through the thin endoplasmic membrane. Some proteins have a receptor "head" in the fluid outside the membrane onto which the substance to be transported is attached before it is transported to the other side of the membrane. The proteins can generally move slowly along the membrane, but they are unable to rotate.

Not only the cytoplasmic membrane has high protein content, but in eukaryotes different organelles are separated from the cytoplasm by membranes, each with its particular set of transport proteins. The cytoplasmic membrane typically has a protein content of 50 wt%, while the membrane that surrounds the energy transduction organelle, the mitochondria, has a composition with 75 wt% proteins.

The action of the transport proteins can be driven solely by the concentration difference of the substrate between the two sides of the membrane. This is called *facilitated transport*. Sometimes, the concentration-driven transport is supported or counteracted by an electrochemical gradient across the membrane.

In other cases, metabolic energy has to be expended to transport the substance, especially when the transport is against a concentration gradient. This is called *active* transport. Again the transport can be influenced by an electrochemical gradient as was seen (Sect. 4.3.2) in the pumping out of protons from the mitochondria through the inner mitochondrial membrane.

7.7.1 Facilitated Transport, Exemplified by Eukaryotic Glucoside Permeases

An important example of facilitated transport is the uptake of glucose and other sugars by yeast and filamentous fungi. There are no similar sugar transporters in prokaryotes.

The carrier protein (glucose permease) has one configuration E_1 outside the membrane and another E_2 on the inner, cytosol side of the membrane. Glucose in the medium binds to E_1, and the protein–sugar complex diffuses through the membrane and releases the glucose while taking on the E_2 configuration. Finally, the free

protein diffuses back to the medium side where it reverts to the E_1 configuration. In all important aspects, the action of the eukaryote sugar transporter resembles that of an enzyme: It displays saturation kinetics like the Michaelis–Menten mechanism, it can be inhibited by the presence of other sugars (in the presence of glucose, mannose permease is inhibited), and most important, the speed of transport is many orders of magnitude faster than the nonfacilitated transport.

Example 7.10 *Transport of glucose to a yeast cell by facilitated diffusion.* Glucose is transported across the cytosolic membrane by a carrier molecule C, which is present in the membrane either in free form (concentration c) or bound to glucose (concentration sc). On the medium side, $z = 0+$, the concentration of the glucose is Ks_a, and at the other side of the membrane, $z = d-$, the glucose concentration is Ks_b. K is the very small partition coefficient K_{par} of (7.64).

At every point z within the membrane, $0+ < z < d-$ the following reversible chemical reaction occurs with the net rate r_m:

$$S + C \overset{r_m}{\longleftrightarrow} SC. \tag{1}$$

All three components, S, C, and SC are transported by steady-state diffusion across the membrane.

This gives rise to the following mass balances written for the positive z direction:

$$D\frac{d^2s}{dz^2} - r_m = 0, \tag{2}$$

$$D\frac{d^2c}{dz^2} - r_m = 0, \tag{3}$$

$$D\frac{d^2sc}{dz^2} - r_m = 0. \tag{4}$$

The diffusivities of S, C, and SC have been set equal to a common constant D.

The first differential equation (2) is subject to the boundary conditions

$$s = Ks_a \text{ at } z = 0 \quad \text{and} \quad s = Ks_b \text{ at } z = d. \tag{5}$$

Here, the partition coefficient at the two sides of the membrane has been set to the same constant K.

This assumption is also implicitly made in the derivation of (7.64).

The assumption of a common diffusivity D and of constant partition coefficient K at the two sides of the membrane may not be accurate, but the assumptions greatly simplify the analysis, and a qualitatively correct result is obtained.

Also the total carrier concentration c_t in the membrane is

$$c_t = \frac{1}{d}\int_0^d (c + sc)\mathrm{dz}. \tag{6}$$

Further analysis depends on the assumptions made concerning the net rate r_m of reaction (1).

One would presume that the chemical reaction is much faster than the diffusion process, i.e., that the reaction is at equilibrium at every point in the membrane.

$$sc = K_{eq} sc, \tag{7}$$

where K_{eq} is the *association* constant for the *SC* complex (see (6.7))

Equations (2) and (3) are added and integrated to give:

$$D\left(\frac{dc}{dz} + \frac{dsc}{dz}\right) = k_1. \tag{8}$$

When the chemical reaction is assumed to be infinitely fast, the sum of the fluxes of *C* and *SC* must be zero at both boundaries, and the arbitrary constant k_1 of (8) is zero.

A consequence of this is that on further integration of (8), one can obtain for any $z \subset [0, d]$:

$$c + sc = k_2, \tag{9}$$

where the arbitrary constant is equal to c_t.

Using the equilibrium assumption (7) and the result (9) that $c_t = c + sc$ throughout the film, one can eliminate *sc* from the sum of (2) and (4), whereafter the linear differential equation is integrated:

$$-J = D\left(\frac{ds}{dz} + \frac{d}{dz}\left(\frac{e_t s}{1/K_{eq} + s}\right)\right). \tag{10}$$

Separation of variables and integration from $z = 0$ to $z = d$ yields

$$J = \frac{D}{d} K\left[(s_a - s_b) + \frac{c_t(s_a - s_b)/K_{eq}}{(1/K_{eq} + Ks_a)(1/K_{eq} + Ks_b)}\right]. \tag{11}$$

The first term on the right-hand side of (11) is obviously the free diffusion term corresponding to (7.64). This term may safely be neglected compared to the second term.

If $s_b << s_a$, then the flux through the membrane is

$$J = \frac{D}{d} \frac{c_t s_a}{K'_{eq}/K + s_a}. \tag{12}$$

Equation (12) is a complete analogue to the rate expression obtained for an enzyme reaction that follows Michaelis–Menten kinetics (Chap. 6, (6.8)) with K'_{eq} equal to the *dissociation* constant for the enzyme–substrate complex *ES*. Since *K* is likely to be substantially smaller than K'_{eq} even when *S* is tightly bound to *C* (and K'_{eq} is small), the flux through the membrane is proportional to s_a unless s_a is very large and the carrier protein becomes

saturated with S. In any case, the ratio $K/K'_{eq} >> K$, and this explains why facilitated transport is much faster than the simple passive diffusion.[5]

Clearly, the efficiency of the carrier mechanism decreases if the carrier can also bind to other substrates at $z = 0$ by any of the mechanisms described in Sect. 6.2. This is one reason why a mannose transport system is inhibited by glucose, and even worse, synthesis of the mannose transporter is repressed when there is glucose in the medium. A lag-phase is to be expected between exhaustion of glucose and efficient uptake of mannose.

7.7.2 *Active Transport*

Lactose permease, the Lac Y membrane bound enzyme discussed in Sect. 7.5.1, operates by a more complex mechanism than the hexose transporters in yeast and filamentous fungi.

The lactose binds to the transmembrane transporter protein *together with a proton*, and the complex between lactose, H^+, and the protein is released in the cytoplasm.

The transport of H^+ from the generally more acidic medium phase to the cytoplasm would upset the pH in the organism which it assiduously tries to keep constant at about 7.

Hence the protons have to be pumped out from the cell, and this is done at the expense of ATP. Together with the H^+, the lactate is pumped out of the cell.

Since the transport of the substrates (H^+ and lactose) occurs in the same direction, this type of active (i.e., not driven solely by the concentration gradient of the substrate, but also at the expense of ATP) is named *symport* active transport. The flow of one species can also be supported by flow of another species in the opposite direction (*antiport*).

The uptake of glucose by yeast which is driven solely by the free energy ($-\Delta G = -\Delta G^0 - RT \ln\left(\frac{s_a}{s_b}\right)$) is called transport by *uniport*. The complex mechanism of the respiration-driven regeneration of ATP by "F type ATP synthases" is the subject of Sect. 4.3.2. Finally, the transport of Na^+ and K^+ in eukaryotes (and of K^+ in prokaryotes) is mediated by transport proteins that are phosphorylated at the expense of ATP before the ion-transport can take place. These are called "P-type ATP synthases."

The subject of membrane transport mechanism is of course much too complex to review in a text which is focused on the cellular reactions. Whole books are devoted to cellular membrane transport, e.g., Stein (1990). Only what we find to be

[5]The assumption of an infinitely fast reaction is a bit shaky. It means that C has to diffuse at a constant rate up to the boundary $z = 0$, react instantly with S, and move away toward $z = d$ at the same rate. This is unrealistic as shown by Schultz et al. (1974), unless the following relation is true: $Q = kd^2/D >> 1$. For a rate constant $k = 10^7\ s^{-1}$, $d = 10$ nm, and $D = 10^{-12}\ m^2\ s^{-1}$, $Q = 10$ which can be shown to give an overestimation of the flux by about 10%. An error of this magnitude does, however, not invalidate the results obtained above.

absolutely relevant to understand the discrimination between substrates that leads to diauxie, and to evaluate (in a semiquantitative manner) the influence of the rate of substrate transport on the overall metabolism of the organism, has been included.

As an important example of active membrane transport mechanisms, we shall briefly discuss the "group-translocation" systems that play a key role for substrate uptake in prokaryotes at low-substrate concentration:

In *E. coli*, *L. lactis,* and in many other bacteria, it is possible to convert substrate (glucose, lactose, etc.) in the medium to phosphorylate sugars in the cytoplasm. Thus, glucose is converted to G6P and lactose to G6P (+galactose which is secreted to the medium and may be reabsorbed when the glucose has been metabolized (Benthin et al. 1994)). The energy required for the process comes from hydrolysis of the high-energy compound phospho-enol-pyruvate (PEP) to pyruvate.

Since the G6P synthesizes 4 ATP − 1 ATP (G6P → 1,6 FDP), the net ATP yield is still 2 ATP per glucose, when the ATP that would normally result from hydrolysis of PEP is taken into account.

The mechanism of this highly efficient substrate system, the phospho(ryl) transferase system (*PTS-system*) of *E. coli* is described in Lengeler et al. (1999).

It has a high affinity for the sugar, i.e., the maximum rate of transport is obtained even for very small sugar concentrations, and since the phosphorylated sugar cannot be transported back through the membrane, leak of substrate from the cell is effectively prevented.

In a final example, the passive diffusion of organic acids through the cell membrane will be used to illustrate how the formation of metabolic products can effectively hurt the organism and lead to cessation of growth even when there is sufficient availability of the energy-rich substrate.

Example 7.11 *Free diffusion of organic acids across the cell membrane.* When lactic bacteria are cultivated in batch, the metabolic product lactic acid accumulates in the medium. The cultivation is clearly product inhibited, and the specific growth rate is well described by (7.20). When the lactic acid concentration exceeds about 42 g L^{-1}, the growth stops.

In the following, we shall seek the explanation of this phenomenon, observed in many other systems where a carboxylic acid is a metabolic product, in the membrane transport reactions.

As described in Sect. 7.7.2, transport of lactose into the lactic bacteria cell occurs by co-transport of H^+, and the protons are subsequently pumped out of the cell (together with the lactate ion) by an ATP-driven process. Hereby, the cell maintains its internal pH, a crucial factor for the health of the organism. It has been found that the increase in medium concentration of lactic acid which occurs in batch cultivations, or the constant, high lactic acid concentration in a continuous cultivation with high feed concentration of lactose, severely upsets the ATP balance of the cell. This typically happens when the pH is not controlled, but also with pH control growth slows down and may eventually stop, and this indicates an effect not only of H^+, but also of lactate.

The effect is observed not only for prokaryotes, but also in, e.g., yeast cultivation. Verduyn et al. (1992) analyzed the influence of benzoic acid (C_6H_5COOH) on the respiration of *S. cerevisiae*. They found that the biomass yield on glucose decreased with increasing concentration of the acid. At the same time, the specific uptake rates of glucose and oxygen increased. Thus, the yield of biomass on glucose or O_2 decreases, while the rate of the

catabolic reactions in which ATP is formed increases. In another study, Schulze (1995) analyzed the influence of benzoic acid on the ATP costs for biomass synthesis in anaerobic cultures of *S. cerevisiae*. He found that the ATP costs for biomass synthesis increased linearly with the benzoic acid concentration, also a consequence of the increased proton influx when this acid is present in the medium.

Henriksen et al. (1998) derived a set of equations that allows quantification of the ATP costs resulting from uncoupling of the proton gradient by organic acids. The aim of the study was to quantify the uncoupling effect of phenoxyacetic acid, a precursor for penicillin V production, on the proton gradient in *P. chrysogenum*. Both forms of this acid may diffuse passively across the plasma membrane, but the undissociated acid has a much larger solubility, i.e., a larger partition coefficient, and is therefore transported much faster. To describe the mass flux of the two forms across the plasma membrane, Henriksen et al. (1998) applied (7.64).

The specific cell area is about 2.5 m^2 $(g\ DW)^{-1}$ for *P. chrysogenum,* and the permeability coefficients for the undissociated and dissociated forms of phenoxyacetic acid have been estimated to be 3.2×10^{-6} and 2.6×10^{-10} m s^{-1}, respectively (Nielsen 1997).

Because the undissociated and dissociated forms of the acid are in equilibrium on each side of the cytoplasmic membrane ($HA \leftrightarrow H^+ + A^-$) with equilibrium constant K_a, (1) which correlates the two forms with the total acid concentration can be written as

$$c_{\text{undiss}} = c_{\text{diss}} 10^{\text{p}K_a - \text{pH}} = \frac{c_{\text{total}}}{1 + 10^{\text{pH} - \text{p}K_a}}. \tag{1}$$

In (1), the pK_a for phenoxyacetic acid is 3.1. At pseudo-steady-state conditions, the net influx of undissociated acid will equal the net outflux of the dissociated form of the acid:

$$\begin{aligned} r_{\text{undiss,in}} &= r_{\text{diss,out}} \text{ or } P_{\text{undiss}} a_{\text{cell}} \left(c_{\text{undiss,a}} - c_{\text{undiss,b}}\right) \\ &= P_{\text{diss}} a_{\text{cell}} \left(c_{\text{diss,b}} - c_{\text{diss,a}}\right). \end{aligned} \tag{2}$$

Subscripts a and b indicate the abiotic and biotic (cytosolic) side of the membrane, respectively. By substituting from (1) for the undissociated and dissociated acid concentrations on the abiotic and cytosolic sides of the membrane in terms of the total concentrations on the abiotic and cytosolic sides and rearranging, we obtain the following equation for the ratio of the total concentrations on the two sides of the membrane:

$$\frac{c_{\text{b,tot}}}{c_{\text{a,tot}}} = \frac{P_{\text{undiss}} \dfrac{1 + 10^{\text{pH}_b - \text{p}K_a}}{1 + 10^{\text{pH}_a - \text{p}K_a}} + P_{\text{diss}} \dfrac{1 + 10^{\text{pH}_b - \text{p}K_a}}{1 + 10^{\text{p}K_a - \text{pH}_a}}}{P_{\text{diss}} 10^{\text{pH}_b - \text{p}K_a} + P_{\text{undiss}}}. \tag{3}$$

Because the permeability coefficient for the undissociated form of the acid is orders of magnitude greater than that of the dissociated form, this equation can be reduced to

$$\frac{c_{\text{b,tot}}}{c_{\text{a,tot}}} = \frac{1 + 10^{\text{pH}_b - \text{p}K_a}}{1 + 10^{\text{pH}_a - \text{p}K_a}}. \tag{4}$$

Now, the intracellular pH is usually greater than the typical pH of the medium in penicillin cultivations. Equation (4) then indicates that there is a higher total concentration of the acid inside the cells than in the extracellular medium. Using this equation, Henriksen et al. (1998) calculated the concentration ratio at different extracellular pH values and

an intracellular pH of 7.2. For an extracellular pH of 6.5, the accumulation is low (about 2.3-fold), whereas at an extracellular pH of 5.0 the accumulation is high (about 100-fold).

For a given total extracellular acid[6] concentration, the concentrations of both forms of the acid on each side of the cytoplasmic membrane can be calculated using (1). Next the mass flux of acid across the membrane can be calculated using (7.64). Because the net outflux of dissociated acid equals the net influx of undissociated acid, the result of acid transport is a net influx of protons, which have to be re-exported by the cytoplasma membrane-bound ATPase in order to maintain a constant intracellular pH. If it is assumed that the export of each proton requires the expenditure of one ATP by the ATPase reaction, Henriksen et al. (1998) calculated that the ATP consumption resulting from this futile cycle amounts to 0.15 mmol of ATP (g DW)$^{-1}$ h^{-1} at an extracellular pH of 6.5 and an intracellular pH of 7.2. This is a low value compared with other non-growth-associated processes that also consume ATP (see Sect. 5.2). However, at an extracellular pH of 5.0, the ATP loss is about 7 mmol of ATP (g DW)$^{-1}$ h^{-1} (again with an intracellular pH of 7.2), which is a significant drain of cellular free energy. It is thus seen how the maintenance of acid concentration gradients across the plasma membrane contributes to the decoupling of ATP generation and ATP consumption used strictly for biosynthetic demands.

Problems

Problem 7.1 *Estimation of parameters in the Monod model.* From measurements of the residual glucose concentration in a steady-state chemostat at various dilution rates, you can find the following results:

D (h^{-1})	s (mg L^{-1})
0.13	11
0.19	14
0.23	18
0.36	38
0.67	85
0.73	513

Calculate by linear regression the parameters in the Monod model. Are any of the data points suspect?

If you want to check the value of μ_{max} determined above, increase the dilution rate in the chemostat to $D = 1.1$ h^{-1}. This results in a rapid increase of the glucose concentration in the medium. After a while, $s >> K_s$. The result of the change in

[6]Benzoic acid as well as citric acid and lactic acid are used to preserve food, exactly because of their inhibition of microbial growth. In acidified food (it could be a soft drink or a fruit juice, or the pH may start to decrease through incipient growth of spoilage bacteria) much of the benzoic acid is on the undissociated form ($pK_a = 4.1$), and the undissociated acid freely diffuses into the cell. In anaerobic yeast cultivation, growth of the yeast almost stops when pH reaches 5, but the ethanol yield increases in a frantic effort of the yeast cell to acquire enough ATP to expulse the protons after the acid has dissociated at the intracellular pH of close to 7. Lactic acid ($pK_a = 3.88$) has the same effect.

dilution rate is a decrease in the biomass concentration, and during the wash-out you measure the biomass concentration as a function of time, and obtain the following results:

Time (h)	x (g L^{-1})
0	5.1
0.5	4.5
1.0	3.7
2.0	2.8
3.0	2.1
4.0	1.4

Determine μ_{max} from this experiment. Discuss the applied method [see also Esener et al. (1981c)].

Problem 7.2 *Inhibitory effect of lactic acid.* Bibal et al. (1988, 1989) studied the inhibition of lactic acid on *Streptococcus cremoris*, and in this exercise we will analyze their data.

(a) The influence of lactic acid on the growth of *S. cremoris* was examined by measuring the maximum specific growth rate during batch growth of the bacterium in media containing various concentrations of lactic acid (p). The results are summarized below:

p (g L^{-1})	μ (h^{-1})
0	0.90
12.0	0.68
39.0	0.52
55.0	0.13

As discussed in Example 7.11, it is mainly the undissociated form of lactic acid that passes through the cellular membrane, and we will therefore assume that it is only the undissociated acid that has a toxic effect on the cells. Plot the relative specific growth rate, i.e., $\mu_{max}(p)/\mu_{max}(p = 0)$, versus the concentration of the undissociated acid concentration (in mM). pH = 6.3 was used and pK_a for lactic acid is 3.88. Assume that the inhibition model given by (7.19) holds. Find the inhibition constant K_i. Plot the model together with the experiments.

(b) From the results in (**a**) you conclude that (7.19) is not well suited for description of the experimental data, since the inhibition by lactic acid seems to be stronger, especially at high values of undissociated lactic acid concentrations (p_u). There seems to be a certain maximum concentration of undissociated acid above which growth stops. Next try the model (7.20) to find the influence of p_u on μ, and estimate the model parameter. At what concentration of lactic acid will growth stop?

(c) Plot the maximum specific growth rate as a function of the pH in a medium containing 1 and 10 g L^{-1} of lactic acid (total concentration), using the model found in (**b**).

(d) Measuring the yield coefficient on lactose in a steady-state chemostat at different concentrations of lactic acid, Bibal et al. (1988, 1989) found the data below:

p (g L^{-1})	Y_{sx} (g DW g^{-1})
0	0.16
7.5	0.16
13.0	0.14
18.5	0.14
21.0	0.14
32.0	0.12
38.5	0.11
45.0	0.10
48.5	0.09

How can you explain the decrease in the yield coefficient with increasing lactic acid concentration?

(e) Assume that the maintenance coefficient m_s is 0.05 h^{-1}. Calculate the true yield coefficient in (7.27) for $p = 0$. Using the model derived in (**b**), calculate the maintenance coefficient as a function of p_u. Explain the results.

Problem 7.3 *Modeling of the lac-operon in E. coli.* We will now revisit the model for the lac-operon described in Sect. 7.5.1.

(a) The repressor has four binding sites for the inducer (lactose), but in the derivation of (7.47) only the repressor–inducer complex where all four sites are occupied is considered. We now consider binding at all four sites. Specify all the equilibria and the definitions of the association constants. The association constant for formation of X_rS_i is termed K_{1i}, and that for formation of $X_OX_rS_i$ is termed K_{4i}. Binding of the inducer to the repressor operator complex can be neglected (i.e., the equilibrium in (7.39c) is not considered).

Assume that the affinity for the binding of the repressor to the operator is approximately the same whether no, one, two, or three inducers are bound to the repressor, i.e., $K_{41} = K_{42} = K_{43} = K_{44}$. This assumption is reasonable since the repressor probably changes its conformation only when the last inducer is bound to it. With this assumption show that the fraction of repressor-free operators is given by

$$Q_1 = \frac{[X_O]}{[X_O]_t} = \frac{1 + K_1[S_{lac}]_t^4}{1 + K_1[S_{lac}]_t^4 + K_2[X_r]_t + K_S K_{11}[X_r S_{lac}][S_{lac}]_t \left(1 + K_{12}[S_{lac}]_t + K_{12}K_{13}[S_{lac}]_t^2\right)}. \quad (1)$$

In (1), $K_1 = K_{41}K_{42}K_{43}K_{44}$.

We now assume that the $K_{11} \approx K_{12} \approx K_{13} \approx K_{14}$, i.e., the association constant for the fourth inducer is much stronger than the corresponding constants for the first three sites. This assumption follows from our assumption above that the conformation of the repressor changes only when the fourth inducer is bound and when the conformation changes the repressor–inducer complex becomes very stable. What other assumptions are required for reducing (1) to (7.47)?

(b) Lee and Bailey (1984d) also modeled the lac-operon, but they included binding of the repressor to a nonspecific binding site in the chromosome (X_d). Again we neglect binding of inducer to the repressor–operator complex, and the equilibria are therefore

$$X_r + nS_{lac} \overset{K_1}{\leftrightarrow} X_r nS_{lac}, \tag{2a}$$

$$X_o + X_r \overset{K_2}{\leftrightarrow} X_o X_r, \tag{2b}$$

$$X_o + X_r S_{lac} \overset{K_4}{\leftrightarrow} X_o X_r S_{lac}, \tag{2c}$$

$$X_d + X_r \overset{K_5}{\leftrightarrow} X_d X_r, \tag{2d}$$

$$X_d + X_r S_{lac} \overset{K_6}{\leftrightarrow} X_d X_r S_{lac}. \tag{2e}$$

By assuming that $[X_d]_t \approx [X_d]$, show that

$$Q_1 = \frac{[X_O]}{[X_O]_t} = \frac{1 + K_5[X_d]_t + K_1[S_{lac}]_t^n\left(1 + K_6[X_d]_t\right)}{1 + K_5[X_d]_t + K_1[S_{lac}]_t^n\left(1 + K_6[X_d]_t\right) + K_2[X_r]_t}, \tag{3}$$

(c) Lee and Bailey (1984d) specified the parameters in (3) to be

$$K_1 = 10^7\ \mathrm{M}^{-1}, \quad K_2 = 2 \times 10^{12}\ \mathrm{M}^{-1}, \quad K_4 = 2 \times 10^9\ \mathrm{M}^{-1}$$
$$K_5 = 10^3\ \mathrm{M}^{-1}, \quad K_6 = 1.5 \times 10^9\ \mathrm{M}^{-1}.$$

Furthermore, they state that

$$[X_d]_t = 4 \times 10^{-2}\ \mathrm{M} \text{ and } [X_r]_t = 2 \times 10^{-8}\ \mathrm{M}.$$

Plot the value of Q_1 using both (3) and (7.47) as a function of the inducer concentration $[S_{lac}]_t$. Comment on the result.

The parameters given by Lee and Bailey are for IPTG (isopropyl-β-D-thiogalactosidase), a frequently used inducer in studies of the lac-operon. Assume that the parameters are the same for lactose as inducer and calculate the concentration of lactose (in mg L^{-1}) to give $Q_1 = 0.5$. Discuss why even this low concentration of lactose leads to induction of the lac-operon.

(d) Show that for an antiinducer (neglect binding of the repressor to nonspecific sites)

$$Q_1 = \frac{[X_O]}{[X_O]_t} = \frac{1 + K_1[S_{lac}]_t^m}{1 + K_1[S]_t^n + K_1K_4[S]_t^n[X_r]_t}. \tag{4}$$

Problem 7.4 *Facilitated transport through membranes.*

(a) In Example 7.10, (2) [$s_a >> s_b$] and negligible contribution from the non-carrier- associated transport, the total *volumetric* flux v through the membrane area A is

$$JA = \frac{DA}{d}\frac{c_t s_a}{K_m + s_a} = \frac{v_{max} s_a}{K_m + s_a} \text{ where } K_m = \frac{K'_{eq}}{K} \text{ and } v_{max} = \frac{DAc_t}{d}. \tag{1}$$

For uptake of glucose in human erythrocytes (red blood cells), the following data are found experimentally:

Glucose concentration (mmol L^{-1})	Glucose flux (mmol min^{-1})
1.0	0.09
1.5	0.12
2.0	0.14
3.0	0.20
4.3	0.25
5.0	0.28

Make a double reciprocal plot of $(JA)^{-1} = v^{-1}$ versus s_a and determine the parameters v_{max} and K_m.

(b) In the example, an infinitely fast equilibrium for the reversible reaction $S + Cr_m \longleftrightarrow SC$ is postulated.

Consider the other extreme: an infinitely fast diffusion of C and SC across the membrane, and a slow reaction.

Now c and sc are both constant and have the values $\bar{c}$ and $\overline{sc}$ while the solute concentration must vary across the membrane according to

$$D\frac{d^2 s}{dz^2} - k_1 s\bar{c} - k_2\overline{sc} = 0. \tag{2}$$

with boundary conditions given by (5) of the example.

Solve the differential equation (2), and determine the values of the two constant carrier concentrations in terms of c_t, the two rate constants, and $\bar{s} = K\frac{s_a + s_b}{2}$.

[You may consult Note 6.2 since the mathematics involved in this problem is essentially the same as that used in the note, except that plane-parallel symmetry is used here and spherical symmetry in the note]

Problem 7.5 *Phosphotransferase-based membrane transport systems.* Many interesting physiological phenomena can be observed due to the complexity of sugar transport systems.

(a) In Benthin et al. (1993a), stable oscillations are observed in both μ and r_p because fructose can be taken up by two PTS systems.
Describe the oscillatory phenomenon, and discuss the mechanism proposed by the authors to explain the complex behavior of the cultivation.
(b) In Benthin et al. (1993b), the uptake of glucose and mannose through two specific sites on the transmembrane Mannose-PTS transporter is discussed. It turns out that the transporter is able to distinguish between α glucose and β glucose, an astonishing specificity of the protein.

What is the difference between α and β glucose?

Describe the set of experiments used by the authors to arrive at the conclusion that there must be two different and specific sites on the medium side for uptake of nearly identical sugars.

Discuss the mathematical model used to explain the widely different uptake profiles for α and β glucose after a pulse addition of a mixture of two different sugars.

Finally, discuss the adaptation of the transport system for a chemostat cultivation with constant dilution rate when the medium is changed from mannose limitation to glucose limitation.

References

Agger, T., Spohr, A. B., Carlsen, M., Nielsen, J. (1998). Growth and product formation of *Aspergillus oryzae* during submerged cultivations: Verification of a morphologically structured model using fluorescent probes. *Biotechnol. Bioeng.* **57**, 321–329.

Baltzis, B. C., Fredrickson, A. G. (1988). Limitation of growth by two complementary nutrients: Some elementary, but neglected considerations. *Biotechnol. Bioeng.* **31**, 75–86.

Benthin, S., Nielsen, J., Villadsen, J. (1991). A simple and reliable method for the determination of cellular RNA content. *Biotechnol. Techniques* **5**, 39-42.

Benthin, S., Nielsen, J., Villadsen, J. (1993a). Two uptake systems for fructose in *Lactococcus lactis* subsp. *cremoris* FD1 produce glycolytic and gluconogenic fructose phosphates and induce oscillations in the growth and lactic acid formation. *Appl. Environ. Microbiology*, **59**, 3206–3211.

Benthin, S., Nielsen, J., Villadsen, J. (1993b). Transport of sugars via two anomer-specific sites on mannose.phophotransferase system in *Lactococcus cremoris*: In vivo study of mechanism, kinetics, and adaptation. *Biotechnol. Bioeng.* **42**, 440–448.

Benthin, S., Nielsen, J., Villadsen, J. (1994). Galactose expulsion during lactose metabolism in *Lactococcus lactis* due to dephosphorylation of intracellular galactose 6-phosphate. *Appl. Envir. Microbiol.* **60**, 1254–1259.

Beuse, M., Kopmann, A., Diekmann, H., Thoma, M. (1999). Oxygen, pH value and carbon source induced changes in the mode of oscillation in synchronous continuous culture of *Saccharomyces cerevisiae*. *Biotechnol. Bioeng.* **63**, 410–417.

Bibal, B., Goma, G., Vayssier, Y., Pareilleux, A. (1988). Influence of pH, lactose and lactic acid on the growth of *Streptococcus cremoris*: A kinetic study. *Appl. Microbiol. Biotechnol.* **28**, 340–344.

Bibal, B., Kapp, C., Goma, G., Pareilleux, A. (1989). Continuous culture of *Streptococcus cremoris* on lactose using various medium conditions. *Appl. Microbiol. Biotechnol.* **32**, 155–159.

Caldwell, I. Y., Trinci, A. P. J. (1973). The growth unit of the mould *Geotrichum candidum*. *Arch. Microbiol.* **88**, 1–10.

Carlsen, M., Jocumsen, K. V., Emborg, C., Nielsen, J. (1997) Modelling the growth and Proteinase A production in continuous cultures of recombinant *Saccharomyces cerevisiae*. *Biotechnol. Bioeng.* **55**, 447–454

Christiansen, T., Spohr, A., Nielsen, J. (1999) On-line study of growth kinetics of single hyphae of *Aspergillus oryzae* in a flow-through cell. *Biotechnol. Bioeng.* **63**, 147–153

Cox, P. W., Paul, G. C., Thomas, C. R. (1998) Image analysis of the morphology of filamentous micro-organisms. *Microbiol.* **144**, 817–827.

Domach, M. M., Leung, S. K., Cahn, R. E., Cocks, G. G., Shuler, M. L. (1984). Computer model for glucose-limited growth of a single cell of *Escherichia coli* B/r-A, *Biotechnol. Bioeng.* **26**, 203–216.

Duboc, P., von Stockar, U., and Villadsen, J.(1998). Simple generic model for dynamic experiments with *Saccharomyces cerevisiae* in continuous culture. *Biotechnol. Bioeng.* **60**, 180–189.

Duboc, P., von Stockar, U. (2000). Modeling of oscillating cultivations of *Saccharomyces cerevisiae*: Identification of population structure and expansion kinetics based on on-line measurements. *Chem. Eng. Sci.* **55**, 149–160.

Egli, T. (1991). On multiple nutrient limited growth of microorganisms with special reference to dual limitation by carbon and nitrogen substrates. *Antonie van Leeuwenhoek* **60**, 2257–234.

Esener, A. A., Roels, J. A., Kossen, N. W. F. (1981a). The influence of temperature on the maximum specific growth rate of *Klebsiella pneumoniae*. *Biotechnol. Bioeng.* **23**, 1401–1405.

Esener, A. A., Roels, J. A., Kossen, N. W. F. (1981b). Fed-batch culture: Modeling and applications in the study of microbial energies. *Biotechnol. Bioeng.* **27**, 1851–1871.

Esener, A. A., Roels, J. A., Kossen, N. W. F., Roozenburg, J. W. H. (1981c). Description of microbial growth behaviour during the wash-out phase; determination of the maximum specific growth rate. *Eur. J. Appl. Microbiol. Biotechnol.* **13**, 141–144.

Esener, A. A., Veerman, T., Roels, J. A., Kossen, N. W. F. (1982). Modeling of bacterial growth; Formulation and evaluation of a structured model. *Biotechnol. Bioeng.* **29**, 1749–1764.

Fiddy, C. and Trinci, A. P. J. (1976). Mitosis, septation, branching and the duplication cycle in *Aspergillus nidulans*. *J. Gen. Microbiol.* **97**, 169–184.

Frandsen, S. (1993). Dynamics of *Saccharomyces cerevisiae* in Continuous culture, Ph.D. thesis, Technical University of Denmark, Lyngby.

Fredrickson, A. G. (1976). Formulation of structured growth models. *Biotechnol. Bioeng.* **18**, 1481–1486.

Harder, A., Roels, J. A. (1982). Application of simple structured models in bioengineering. *Adv. Biochem. Eng.* **21**, 55–107.

Henriksen, C. M., Nielsen, J., Villadsen, J. (1998). Modelling of the protonophoric uncoupling by phenoxyacetic acid of the plasma membrane of *Penicillium chrysogenum*. *Biotechnol. Bioeng.* **60**, 761–767.

Herbert, D. (1959). Some principles of continuous culture. *Recent Prog. Microbiol.* **7**, 381–396.

Herendeen, S. L., van Bogelen, R. A., Neidhardt, F. C. (1979). Levels of major proteins of *Escherichia coli* during growth at different temperatures. *J. Bacteriol.* **139**, 185–194.

Hjortso, M. A. and Nielsen, J. (1994). A conceptual model of autonomous oscillations in microbial cultures. *Chem. Eng. Sci.* **49**, 1083–1095.

Ingraham, J. L., Maalöe, O., Neidhardt, F. C. (1983). *Growth of the Bacterial Cell*, Sinauer Associates, Inc., Sunderland.

Jacob, F., Monod, J. (1961). Genetic regulatory processes in the synthesis of proteins. *J. Mol. Biol.* **3**, 318–356.

Jöbses, I. M. L., Egberts, G. T. C., van Baalen, A., Roels, J. A. (1985). Mathematical modeling of growth and substrate conversion of *Zymomonas mobilis* at 30 and 35°C, *Biotechnol. Bioeng.* **27**, 984–995.

Keulers, M., Satroutdinov, A. D., Suszuki, T., Kuriyama, H. (1996a). Synchronization affector of autonomous short period sustained oscillation of *Saccharomyces cerevisiae*. *Yeast* **12**, 673–682.

Keulers, M., Suzuki, T., Satroutdinov, A. D., Kuriyama, H. (1996b). Autonomous metabolic oscillation in continuous culture of *Saccharomyces cerevisiae* grown on ethanol. *FEMS Microbiol. Letters* **142**, 253–258.

Kompala, D. S., Ramkrishna, D., Tsao, G. T. (1984). Cybernetic modeling of microbial growth on multiple substrates. *Biotechnol. Bioeng.* **26**, 1272–1281.

Kompala, D. S., Ramkrishna, D., Jansen, N. B., Tsao, G. T. (1986). Investigation of bacterial growth on mixed substrates: Experimental evaluation of cybernetic models. *Biotechnol. Bioeng.* **28**, 1044–1055.

Krabben, P., Nielsen, J. (1998) Modeling the mycelium morphology of *Penicillium* species in submerged cultures. *Adv. Biochem. Eng./Biotechnol.* **60**, 125–152.

Lee, S. B., Bailey, J. E. (1984a). A mathematical model for λ*dv* plasmid replication: Analysis of wild-type plasmid, *Plasmid* **11**, 151–165.

Lee, S. B., Bailey, J. E. (1984b). A mathematical model for λ*dv* plasmid replication: Analysis of copy number mutants. *Plasmid* **11**, 166–177.

Lee, S. B., Bailey, J. E. (1984c). Analysis of growth rate effects on productivity of recombinant *Escherichia coli* populations using molecular mechanism models. *Biotechnol. Bioeng.* **26**, 66–73.

Lee, S. B., Bailey, J. E. (1984d). Genetically structured models for lac promoter-operator function in the *Escherichia coli* chromosome and in multicopy plasmids: lac operator function. *Biotechnol. Bioeng.* **26**, 1372–1382.

Lee, S. B., Bailey, J. E. (1984e). Genetically structured models for lac promoter-operator function in the *Escherichia coli* chromosome and in multicopy plasmids: lac promoter function. *Biotechnol. Bioeng.* **26**, 1381–1389.

Lengeler, J. W., Drews, G., Schegel, H. G. (1999). *Biology of the Prokaryotes*. Thieme Verlag, Stuttgart.

McIntyre, M., Müller, C., Dynesen, J., Nielsen, J. (2001). Metabolic engineering of the morphology of *Aspergillus*. *Adv. Biochem. Eng./Biotechnol.* **73**, 103–128.

Megee, R. D., Kinishita, S., Fredrickson, A. G., Tsuchiya, H. M. (1970). Differentiation and product formation in molds. *Biotechnol. Bioeng.* **12**, 771–801.

Melchiorsen, C. R., Jensen, N. B. S., Christensen, B., Jochumsen, K. V., Villadsen, J. (2001). Dynamics of pyruvate metabolism in *Lactococcus lactis*. *Biotechnol. Bioeng.* **74**, 271–279.

Monod, J. (1942). *Recherches sur la croissance des cultures bacteriennes*, Hermann et Cie, Paris.

Monod, J. (1965). From enzymatic adaption to allosteric transitions. Nobel lecture December 11, 1965 (in "Nobel lectures, Physiology and Medicine 1963-1970", Elsevier, 1972).

Monod, J., Wyman, J., Changeux, J.-P. (1963). Allosteric proteins and cellular control systems. *J. Mol. Biol.* **6**, 306–329.

Nielsen, J. (1992). Modelling the growth of filamentous fungi. *Adv. Biochem. Eng. Biotechnol.* **46**, 187–223.

Nielsen, J. (1993). A simple morphologically structured model describing the growth of filamentous microorganisms. *Biotechnol. Bioeng.* **41**, 715–727.

Nielsen, J. (1996). Modelling the morphology of filamentous microorganisms. *TIBTECH* **14**, 438–443.

Nielsen, J. (1997). *Physiological engineering aspects of* Penicillium chrysogenum. World Scientific Publishing Co., Singapore.

Nielsen, J., Villadsen, J. (1992). Modeling of microbial kinetics, *Chem. Eng. Sci.* **47**, 4225–4270.

Nielsen, J., Villadsen, J. (1994). *Bioreaction Engineering Principles*. 1st edition, Plenum Press, New York.

Nielsen, J., Nikolajsen, K., Villadsen, J. (1991a). Structured modeling of a microbial system 1. A theoretical study of the lactic acid fermentation. *Biotechnol. Bioeng.* **38**, 1–10.

Nielsen, J., Nikolajsen, K., Villadsen, J. (1991b). Structured modeling of a microbial system 2. Verification of a structured lactic acid fermentation model. *Biotechnol. Bioeng.* **38**, 11–23.

Nielsen, J., Pedersen, A. G., Strudsholm, K., Villadsen, J. (1991c). Modeling fermentations with recombinant microorganisms: Formulation of a structured model. *Biotechnol. Bioeng.* **37**, 802–808.

Patnaik, P. R. (2003). Oscillatory metabolism of *Saccharomyces cerevisiae*: An overview of mechanisms and models. *Biotechnology Advances*, **21**, 183–192.

Peretti, S. W., Bailey, J. E. (1986). Mechanistically detailed model of cellular metabolism for glucose-limited growth of *Escherichia coli* B/r-A. *Biotechnol. Bioeng.* **28**, 1672–1689.

Peretti, S. W., Bailey, J. E. (1987). Simulations of host–plasmid interactions in *Escherichia coli*: Copy number, promoter strength, and ribosome binding site strength effects on metabolic activity and plasmid gene expression. *Biotechnol. Bioeng.* **29**, 316–328.

Pirt, S. J. (1965). The maintenance energy of bacteria in growing cultures. *Proc. Royal Soc. London Ser. B.* **163**, 224-231.

Pronk, J. T., Steensma, H. Y., van Dijken, J. P. (1996). Pyruvate metabolism in *Saccharomyces cerevisiae*. Yeast **12**, 1607–1633.

Prosser, J. I., Tough, A. J. (1991). Growth mechanisms and growth kinetics of filamentous microorganisms, *Crit. Rev. Biotechnol.* **10**, 253–274.

Ramkrishna, D. (1982). A cybernetic perspective of microbial growth, in *Foundations of Biochemical Engineering: Kinetics and Thermodynamics in Biological Systems*, American Chemical Society, 161–178.

Ramkrishna, D., Fredrickson, A. G., Tsuchiya, H. M. (1967). Dynamics of microbial propagation: Models considering inhibitors and variable cell composition. *Biotechnol. Bioeng.* **9**, 129–170.

Ramkrishna, D., Kompala, D. S., Tsao, G. T. (1987). Are microbes optimal strategists? *Biotechnol. Prog.* **3**, 121–126.

Rieger, M., Käppeli, O., Fiechter, A. (1983). The role of limited respiration in the incomplete oxidation of glucose by *Saccharomyces cerevisiae*. *J. Gen. Microbiol.* **129**, 653–661.

Robinson, P. M. and Smith, J. M. (1979). Development of cells and hyphae of *Geotrichum candidum* in chemostat and batch culture. *Proc. Br. Mycol. Soc.* **72**, 39–47.

Roels, J. A. (1983). *Energetics and Kinetics in Biotechnology*. Elsevier Biomedical Press, Amsterdam.

Roels, J. A., Kossen, N. W. F. (1978). On the modeling of microbial metabolism, *Prog. Ind. Microbiol.* **14**, 95–204.

Schultz, J. S., Goddard, J. D., Suchdeo, S. R. (1974). Facilitated transport via carrier mediated diffusion in membranes, Part I and II. *AIChE J*, **20**, 417–445 and 625–645.

Schulze, U. (1995). Anaerobic physiology of *Saccharomyces cerevisiae*. Ph.D. Thesis, Technical University of Denmark.

Seo, J.-H., Bailey, J. E. (1985). Effects of recombinant plasmid content on growth properties and cloned gene product formation in *Escherichia coli*. *Biotechnol. Bioeng.* **27**, 1668–1674.

Shuler, M. L., Domach, M. M. (1982). Mathematical models of the growth of individual cells, in *Foundations of Biochemical Engineering: Kinetics and Thermodynamics in Biological Systems*, American Chemical Society Publications, 93–133.

Sohn, H. Y., Kuriyama, H. (2001). Ultradian metabolic oscillation of *Saccharomyces cerevisiae* during aerobic continuous culture: Hydrogen sulphide, a population synchronizer, is produced by sulphite reductase. *Yeast* **18**, 125–135.

Song, H. S., Ramkrishna, D. (2010). Prediction of metabolic function from limited data: Lumped Hybrid Cybernetic Modeling (L-HCM). *Biotechnol. Bioeng.* **106**, 271–284.

Sonnleitner, B., Käppeli, O. (1986). Growth of *Saccharomyces cerevisiae* is controlled by its limited respiratory capacity: Formulation and verification of a hypothesis. *Biotechnol. Bioeng.* **28**, 927–937.

Spohr, A. B., Mikkelsen, C. D., Carlsen, M., Nielsen, J., Villadsen, J. (1998) On-line study of fungal morphology during submerged growth in a small flow-through cell. *Biotechnol. Bioeng.* **58**, 541–553.

Stein, W. D. (1990). Channels, Carriers and Pumps. An Introduction to Membrane Transport. Academic Press, San Diego.

Strässle, C., Sonnleitner, B., Fiechter, A. (1988). A predictive model for the spontaneous synchronization of *Saccharomyces cerevisiae* grown in continuous culture I. Concept, *J. Biotechnol.* **7**, 299–318.

Strässle, C., Sonnleitner, B., Fiechter, A. (1989). A predictive model for the spontaneous synchronization of *Saccharomyces cerevisiae* grown in continuous culture II. Experimental verification. *J. Biotechnol.* **9**, 191–208.

Strudsholm, K., Nielsen, J., Emborg, C. (1992). Product formation during hatch fermentation with recombinant *E. coli* containing a runaway plasmid, *Bioproc. Eng.* **8**, 173–181.

Trinci, A. P. J. (1974). A study of the kinetics of hyphal extension and branch initiation of fungal mycelia. *J. Gen. Microbiol.* **81**, 225–236.

Trinci, A. P. J. (1984). Regulation of hyphal branching and hyphal orientation. In *The Ecology and Physiology of the Fungal Mycelium,* D. H. Jennings and A. D. M. Rayner, eds., Cambridge University Press, Cambridge, UK.

Tsao, G. T., Hanson, T. P. (1975). Extended Monod equation for batch cultures with multiple exponential phases. *Biotechnol. Bioeng.* **17**, 1591–1598.

Turner, B. G., Ramkrishna, D. (1988). Revised enzyme synthesis rate expression in cybernetic models of bacterial growth. *Biotechnol. Bioeng.* **31**, 41–43.

Verduyn, C., Postma, E., Scheffers, W. A., van Dijken, J. P. (1992). Effect of benzoic acid on metabolic fluxes in yeast. A continuous culture study on the regulation of respiration and alcoholic fermentation. *Yeast* **8**, 501–517.

Williams, F. M. (1967). A model of cell growth dynamics. *J. Theoret. Biol.* **15**, 190–207.

Young, J. D., Henne, K. L., Morgan, A. E., Konopka, A. E., Ramkrishna, D. (2008). Integrating cybernetic modeling with pathway analysis provides a dynamic, systems-level description of metabolic control. *Biotechnol. Bioeng.* **100**, 543–559.

Chapter 8
Population Balance Equations

In Chap. 7, cell population balances are written in terms of a distribution of mass fractions of the total biomass. This allows a direct combination of intracellularly structured models and population models. However, the population balances based on mass fractions do not permit the incorporation into the model of specific events in the cell cycle. Since there are numerous examples that show a direct influence of certain specific events in the cell cycle on the overall culture performance, e.g., the distribution of plasmids to daughter cells on cell division in recombinant cultures, we need to derive a population balance based on cell number to obtain a correct description of these processes.

In a population balance based on cell number, the basis is the individual cells. Thus, the cellular content of the intracellular components has the unit grams per cell, and we can therefore not use the composition vector $\mathbf{X}$ (unit: grams per gram dry weight). Instead the properties of the cell are described by the vector $\mathbf{y}$, which may also contain information about the cell's age, size, etc. The distribution of cells in the population is given by $f(\mathbf{y},t)$, where $f(\mathbf{y},t)\mathrm{d}\mathbf{y}$ represents the number of cells per unit volume within the property space $\mathbf{y}$ to $\mathbf{y} + \mathrm{d}\mathbf{y}$ at time t. Thus the total number of cells per unit volume in the population is given by

$$n(t) = \int_{V_\mathbf{y}} f(\mathbf{y}, t)\ \mathrm{d}\mathbf{y} \tag{8.1}$$

$V_\mathbf{y}$ is the total property space. In general, n is determined from a mass balance for the limiting substrate, as illustrated in Note 8.1.

Note 8.1 *Determination of the total number of cells from a substrate balance.* For a distribution of cells with different substrate uptake kinetics, the volumetric rate of substrate consumption $q_\mathrm{s}(t)$ for a single limiting substrate is given by,

$$q_\mathrm{s}(t) = -\int_{V_\mathbf{y}} r_\mathrm{s}(\mathbf{y}, s) f(\mathbf{y}, t)\ \mathrm{d}\mathbf{y} \tag{1}$$

J. Villadsen et al., *Bioreaction Engineering Principles*,
DOI 10.1007/978-1-4419-9688-6_8,

where $r_s(\mathbf{y}, s)$ is the rate of substrate consumption per cell per time. The mass balance for the limiting substrate is therefore

$$\frac{ds}{dt} = D(s_f - s) - \int_{V_y} r_s(\mathbf{y}, s) f(\mathbf{y}, t)\, d\mathbf{y} \tag{2}$$

If $r_s(\mathbf{y}, s) \lim_{x \to \infty}$ is taken to be independent of the cellular state, the steady-state solution to the mass balance gives

$$n = \frac{D(s_f - s)}{r_s(s)} \tag{3}$$

Thus if the substrate concentration is known, the total number of cells can be calculated. If the single-cell kinetics is described as a function of the limiting substrate concentration, s can be calculated from the parameters in the single-kinetic model (see Problem 8.1).

For a homogeneous system (or for a given homogeneous volume element), the dynamic balance for the distribution function is (8.2):

$$\frac{\partial f(\mathbf{y}, t)}{\partial t} + \nabla_{\mathbf{y}}[\mathbf{r}(\mathbf{y}, t) f(\mathbf{y}, t)] = h(\mathbf{y}, t) - Df(\mathbf{y}, t) \tag{8.2}$$

$\mathbf{r}(\mathbf{y}, t)$ is the rate of change of properties, i.e., r_i is the rate along the ith property axis in the total property space $V_{\mathbf{y}}$. $h(\mathbf{y}, t)$ is the net rate of formation of cells with the property $\mathbf{y}$ due to cell division and D is the dilution rate in the bioreactor. It is assumed that there are no cells in the liquid stream entering the bioreactor (or the considered volume element), i.e., $f_{in}(\mathbf{y}, t) = 0$. The first term is the accumulation term. The second term accounts for the formation and removal of elements with the given properties due to cellular processes, e.g., growth. The first term on the right hand side accounts for net formation of elements/cells with the property $\mathbf{y}$, e.g., upon cell division there is a net formation of new cells. The last term on the right hand side accounts for washout of elements/cells from the bioreactor.

The population balance (8.2) holds only for a homogeneous bioreactor; i.e., the distribution function is the same in each volume element in the bioreactor. This assumption is reasonable for laboratory-scale bioreactors, whereas it is doubtful for large-scale bioreactors. In Note 8.2, the population balance is generalized to consider variations in the distribution function throughout the three-dimensional physical space.

Note 8.2 *General form of the population balance.* With a nonhomogeneous physical space, the distribution function also becomes a function of position in the space (i.e., $f(\mathbf{z}, \mathbf{y}, t)$, where $\mathbf{z}$ is the physical state space). $f(\mathbf{z}, \mathbf{y}, t)d\mathbf{z}d\mathbf{y}$ is the number of cells within the physical space between $\mathbf{z}$ and $\mathbf{z} + d\mathbf{z}$ and within the property space between $\mathbf{y}$ and $\mathbf{y} + d\mathbf{y}$, and the total number of cells per unit volume in the population is therefore given by

$$n(t) = \int_{V_y} \int_{V_z} f(\mathbf{z}, \mathbf{y}, t) d\mathbf{z}d\mathbf{y} \tag{1}$$

The generalized form of the population balance is given by (2) where $\mathbf{v}(\mathbf{z},t)$ is the rate of liquid flow at position $\mathbf{z}$ in the physical space:

$$\frac{\partial f(\mathbf{z},\mathbf{y},t)}{\partial t}+\frac{1}{V}\frac{\mathrm{d}V}{\mathrm{d}t}f(\mathbf{z},\mathbf{y},t)+\frac{1}{V}\nabla_{\mathbf{z}}[\mathbf{v}(\mathbf{z},t)f(\mathbf{z},\mathbf{y},t)] + \nabla_{\mathbf{y}}[\mathbf{r}(\mathbf{z},\mathbf{y},t)f(\mathbf{z},\mathbf{y},t)]=h(\mathbf{z},\mathbf{y},t) \tag{2}$$

For a homogeneous system, the distribution function is the same throughout the physical space:

$$f(\mathbf{z},\mathbf{y},t)=f_{\mathrm{h}}(\mathbf{y},t)=\int_{V_{\mathbf{z}}} f(\mathbf{z},\mathbf{y},t)\mathrm{d}\mathbf{z} \tag{3}$$

Consequently,

$$\frac{\partial f_{\mathrm{h}}(\mathbf{y},t)}{\partial t}+\frac{1}{V}\frac{\mathrm{d}V}{\mathrm{d}t}f_{\mathrm{h}}(\mathbf{y},t)+\frac{1}{V}f_{\mathrm{h}}(\mathbf{y},t)\int_{V_{\mathbf{z}}}\nabla_{\mathbf{z}}\mathbf{v}(\mathbf{z},t)\,\mathrm{d}\mathbf{z} + \nabla_{\mathbf{y}}[\mathbf{r}(\mathbf{y},t)f_{\mathrm{h}}(\mathbf{y},t)]=h(\mathbf{y},t) \tag{4}$$

Now, applying the divergence theorem of Gauss [see, e.g., Kreyszig (1988)]

$$\int_{V_{\mathbf{z}}}\nabla_{\mathbf{z}}\mathbf{v}(\mathbf{z},t)\mathrm{d}\mathbf{z}=\int_{s}\mathbf{n}(\mathbf{z},t)\mathbf{v}(\mathbf{z},t)\mathrm{d}S \tag{5}$$

where $\mathbf{n}(\mathbf{z},t)$ is the outward normal on the system's surface S. Normally the transport across the surface of the system is characterized by two flows, one ingoing flow v_{in} and the other outgoing flow v_{out}. We therefore have

$$\int_{V_{\mathbf{z}}}\nabla_{\mathbf{z}}\mathbf{v}(\mathbf{z},t)\mathrm{d}\mathbf{z}=v_{\mathrm{in}}f_{\mathrm{in}}(\mathbf{y},t)-v_{\mathrm{out}}f_{\mathrm{h}}(\mathbf{y},t) \tag{6}$$

Inserting (6) in (4) we find

$$\frac{\partial f_{\mathrm{h}}(\mathbf{y},t)}{\partial t}+\nabla_{\mathbf{y}}[\mathbf{r}(\mathbf{y},t)f_{\mathrm{h}}(\mathbf{y},t)]=h(\mathbf{y},t)+\frac{1}{V}\left[v_{\mathrm{in}}f_{\mathrm{in}}(\mathbf{y},t)-\left(v_{\mathrm{out}}+\frac{\mathrm{d}V}{\mathrm{d}t}\right)f_{\mathrm{h}}(\mathbf{y},t)\right] \tag{7}$$

For a chemostat and a batch reactor the volume is constant, i.e., $\mathrm{d}V/\mathrm{d}t=0$, and $v_{\mathrm{out}}/V=D$ for the chemostat. For a fed-batch reactor (see Chap. 9), $v_{\mathrm{out}}=0$ and $(1/V)\,\mathrm{d}V/\mathrm{d}t=D$. With no cells in the ingoing stream, i.e., $f_{\mathrm{in}}(\mathbf{y},t)=0$, (7) therefore reduces to (8.2).

As mentioned above the formation of cells with property $\mathbf{y}$ is described by the function $h(\mathbf{y},t)$ in the population balance of (8.2). Thus, the population balance equations allow description of discrete events that occur, for example, at cell division through the function h which is often split into two terms:

$$h(\mathbf{y},t)=h^{+}(\mathbf{y},t)-h^{-}(\mathbf{y},t) \tag{8.3}$$

The function $h^+(\mathbf{y},t)$ represents the rate of formation of cells with property $\mathbf{y}$, and similarly $h^-(\mathbf{y},t)$ represents the rate of disappearance of these cells as they divide. Cell division is normally a singular event, which occurs quite independent of what happens to the other cells in the population. Let $b(\mathbf{y},t)$ represent the division frequency (or *breakage frequency*), i.e., $b(\mathbf{y},t)\mathrm{d}t$ is the probability that a cell with property $\mathbf{y}$ at time t divides in the interval t to $t+\mathrm{d}t$. Thus,

$$h^-(\mathbf{y},t) = b(\mathbf{y},t)f(\mathbf{y},t) \tag{8.4}$$

To identify the function $h^+(\mathbf{y},t)$, we must consider the (average) number of cells arising from division of a cell with property $\mathbf{y}$. This is normally 2, independent of the cellular properties and the environmental conditions, i.e., two new cells are formed upon cell division.[1] Next we define the function $p(\mathbf{y},\mathbf{y}^*,t)$ to represent the probability of the formation of cells with properties $\mathbf{y}$, and $\mathbf{y}^*-\mathbf{y}$, respectively, upon division of a cell with property $\mathbf{y}^*$.[2] The rate of formation of cells with property $\mathbf{y}$ is then given by

$$h^+(\mathbf{y},t) = 2\int_{V_y} b(\mathbf{y}^*,t)p(\mathbf{y},\mathbf{y}^*,t)f(\mathbf{y}^*,t)\mathrm{d}\mathbf{y}^* \tag{8.5}$$

The function $p(\mathbf{y},\mathbf{y}^*,t)$ is called the *partitioning function*. It satisfies the constraints $p(\mathbf{y},\mathbf{y}^*,t)=0$ whenever one of the elements y_i in the property vector $\mathbf{y}$ is larger than y_i^*, and it is scaled by

$$\int_{V_y} p(\mathbf{y},\mathbf{y}^*,t)\mathrm{d}\mathbf{y} = 1 \tag{8.6}$$

Combination of (8.3)–(8.5) gives:

$$h(\mathbf{y},t) = 2\int_{V_y} b(\mathbf{y}^*,t)p(\mathbf{y},\mathbf{y}^*,t)f(\mathbf{y}^*,t)\,\mathrm{d}\mathbf{y}^* - b(\mathbf{y},t)f(\mathbf{y},t) \tag{8.7}$$

No direct influence of the environmental conditions is included in (8.7). However, both r and h are normally functions of the concentrations of substrate and metabolic products in the surrounding medium. Application of the population balance with an example of the breakage frequency and the partitioning function is illustrated in Example 8.1.

[1] For the meiosis of eukaryotes, four cells are formed in a cell cycle, but this special situation will not be considered here.

[2] This holds only when the cell properties are conserved upon cell division. There are many cell properties for which this is not the case, e.g., cell age and surface area. However, here the h function can often be described explicitly, for example by a Dirac delta function as illustrated in Example 8.2.

Example 8.1 *Specification of the partitioning function and the breakage frequency*. Kothari et al. (1972) applied a population model originally derived by Eakman et al. (1966) for description of the size distribution of the yeast *Schizosaccharomyces pombe* at steady state in a chemostat. They used a one-dimensional distribution function $f(m, t)$, which at steady state is given by

$$\frac{d[f(m)r(m,s)]}{\mathrm{d}m} = 2\int_m^\infty b(m^*,s)p(m^*,m)f(m^*)\,\mathrm{d}m^* - b(m,s)f(m) - Df(m) \tag{1}$$

or

$$\frac{\mathrm{d}f(m)}{\mathrm{d}m} = \frac{2}{r(m,s)}\int_m^\infty b(m^*,s)p(m^*,m)f(m^*)\,\mathrm{d}m^* - \frac{1}{r(m,s)}\left[b(m,s) + \frac{\mathrm{d}r(m,s)}{\mathrm{d}m} + D\right]f(m) \tag{2}$$

$r(m, s)$ is the growth rate for cells with mass m (grams per cell per hour). Both the growth rate and the breakage function are taken to be functions of the substrate concentration s in the surrounding medium. In the model it is assumed that the distribution of division masses around the mean division mass m_d is of a Gaussian type, and the breakage function is therefore given by

$$b(m,s) = \frac{2\mathrm{e}^{-[(m-m_\mathrm{d})/\varepsilon]^2}r(m,s)}{\varepsilon\sqrt{\pi}erfc[(m-m_\mathrm{d})/\varepsilon]} \tag{3}$$

For the partitioning function, it is furthermore assumed that the distribution of daughter cell mass m is also of the Gaussian type, with a median of half the mass of the parent cell at division, m^*. Thus,

$$p(m^*,m) = \frac{\mathrm{e}^{-[(m-0.5m^*)/\xi]^2}}{\xi\sqrt{\pi}erf(m^*/2\xi)} \tag{4}$$

These definitions of the breakage and partitioning functions give the right trends. It is, of course, not biologically reasonable that $b(0, s) \neq 0$ and $p(m^*, m) \neq 0$, but this does not influence the conclusions drawn by Kothari et al. (see below).

By comparing model calculations with experimental data for the mass distribution (obtained using a Coulter counter), Kothari et al. estimated the parameters in the model, i.e., the average mass at division m_d and the standard deviations (ε and ξ) for the functions in (3) and (4). Furthermore, they examined different models for $r(m)$ (s is constant at a given dilution rate in the chemostat), and found that a model where $r(m)$ is constant and independent of m, i.e., $r(m) = k$ corresponding to zero-order growth kinetics for the cell mass, gave the best fit to the experimental data obtained at different dilution rates (see Fig. 8.1). With a model where $r(m)$ is first order in m, $r(m) = km$, corresponding to exponential growth of the single-cell mass, the calculated distribution function could not be fitted to the measured profile.

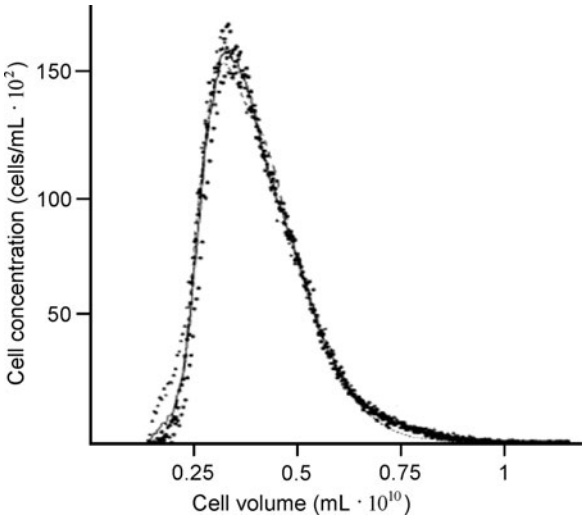

Fig. 8.1 Cell size distribution for *Schizosaccharomyces pombe*. The data points are measurements obtained using a Coulter counter, and the line reflects model simulations [Reprinted with permission from I. R. Kothari et al. (1972)]

Thus, the application of the population model based on number revealed that *the growth rate of individual cells is not proportional to their mass*. This does not contradict the dictum that the growth rate of a microbial culture is proportional to the *total* biomass concentration, since

$$q_x = \int_0^\infty kf(m)\,\mathrm{d}m = kn = \frac{k}{\langle m \rangle} x \tag{5}$$

$\langle m \rangle$ is the average cell mass for the population (equal to x/n). Since $k/\langle m \rangle$ is equal to the specific growth rate for the population, (5) is equal to the standard expression for q_x, and when r is independent of m, the specific growth rate for the culture is a function of the average cell mass. This would not be the situation with exponential growth of the individual cells, since here we find

$$q_x = \int_0^\infty kmf(m)\,\mathrm{d}m = k\langle m \rangle n = kx \tag{6}$$

The integral is evaluated as shown in (8.10).

Example 8.1 illustrates how the population balance can be used to examine the behavior of the single cells in a culture: By comparison of the calculated distribution function with an experimentally determined distribution function, different models for the behavior of the individual cells can be evaluated. In their analysis, Kothari et al. (1972) used the cell mass distribution function obtained using a Coulter counter. Today, it is also possible to obtain distribution functions for

many other cellular properties by *flow cytometry*.[3] With this technique one may measure the single-cell content of macromolecules such as proteins, chromosomal DNA, carbohydrates, and plasmid DNA by applying specific fluorescent dyes that label the macromolecular pool of interest. Furthermore, by measuring the accumulation of an intracellular fluorescent product formed by the action of a certain enzyme, it is possible to quantify the cellular content of a specific enzyme. In addition to measurement of the cellular content by fluorescent techniques, it is also possible to measure the cell size by light scattering, and most modern flow cytometers are equipped with both light-scattering and fluorescent-measurement facilities whereby a two-dimensional distribution function for a population can be obtained.

With measurements of both cell size and cell composition it is possible to calculate the distribution function, based on mass fractions $\psi(X)$ from the two-dimensional distribution function $f(y,m)$ (y is the content of the measured component in grams per cell). Cells with the composition X (grams per gram dry weight) are found on the curve $y = Xm$ in the y–m plane, and the total concentration of cells with a composition X is therefore given by

$$\psi(X)x = \int_0^\infty mf(m, Xm)\ \mathrm{d}m \tag{8.8}$$

Thus, flow cytometry measurements may also be used to obtain the distribution function based on mass fraction.

The population balance in (8.2) must satisfy an initial condition describing the state of the population, i.e., $f(\mathbf{y},0)$ should be known. Generally, this is sufficient since the model normally satisfies consistency criteria, i.e., the flux is zero at the boundaries of the property space. On some occasions, boundary conditions do enter the analysis, but this depends on how the problem is formulated. The solution to the dynamic balance (8.2) can be found by one of several weighted residual methods, as has been illustrated for a one-dimensional distribution function by Subramanian and Ramkrishna (1971) [see also Ramkrishna (1985) for a discussion of various solution methods for the dynamic population balance].

In many situations it is, however, sufficient to obtain qualities pertaining to the average composition and the standard deviation for the population. These can be calculated from the moments of the distribution functions, where the nth moment of a one-dimensional distribution function is defined by

$$M_n(t) = \int_{V_y} y^n f(y,t)\ \mathrm{d}y \tag{8.9}$$

[3]The flow cytometer was also invented (1953) by the famous American business man and inventor Wallace Coulter (1913–1998). The first commercial version (1968) of this instrument which has now found widespread use in industry, in academia and in the clinic is by Wolfgang Göhde at Universität Münster. A good reference to the many applications of flow cytometry is Ormerod (2000).

The zero-order moment is equal to the total number of cells per unit volume [see (8.1)], and from the first moment the average cell composition can be calculated:

$$\langle y(t)\rangle = \frac{M_1(t)}{M_0(t)} = \frac{\int_{V_y} yf(y,t)\ \mathrm{d}y}{n(t)} \tag{8.10}$$

From the definition of the variance σ^2 of the distribution function,

$$\sigma(t)^2 = \int_{V_y} [y - \langle y(t)\rangle]^2 f(y,t)\ \mathrm{d}y \tag{8.11}$$

We find a relationship between the variance and the second moment of the distribution function:

$$\sigma(t)^2 = \frac{M_2(t)}{n(t)} - \langle y\rangle^2 = \frac{\int_{V_y} y^2 f(y,t)\ \mathrm{d}y}{n(t)} - \langle y\rangle^2 \tag{8.12}$$

The definitions of the moments can easily be extended to the case of a multi-dimensional distribution function. Thus, for a two-dimensional property space (see Example 8.4),

$$M_{ij}(t) = \int_{V_{y_1}} \int_{V_{y_2}} y_1^i y_2^j f(y_1, y_2, t)\ \mathrm{d}y_1\ \mathrm{d}y_2 \tag{8.13}$$

Besides its application to single-cell populations, the population balance of (8.2) may also be used for many other systems [again Ramkrishna (1979) who has worked with population balances for a life-time gives a good review]. Typical applications in connection with bioprocesses are

1. Single-cell populations (illustrated in Examples 8.1–8.3).
2. Populations of hyphal elements in connection with cultures of filamentous microorganisms (Example 8.4).
3. Populations of pellets in cultures of filamentous microorganisms and immobilized cells.
4. Description of the bubble-size distribution in the liquid during aerated fermentation processes.

For processes where agglomeration is involved instead of breakage (or cell division), the function $h(\mathbf{y},t)$ is not given by (8.7) [see Ramkrishna (1985) for details]. In the following, we illustrate the application of the population balance (8.2) for some microbial systems.

Example 8.2 *Population balance for recombinant Escherichia coli*. Seo and Bailey (1985) examined the distribution of plasmid content in recombinant *E. coli* cultures by means of a population balance. They first considered the steady-state age distribution of the cells:

$$\frac{\mathrm{d}[r(a)f(a)]}{\mathrm{d}a} = h(a) - Df(a) \tag{1}$$

With age being the considered cell property, we have (by definition) that $r(a) = 1$ and

$$h(a) = 0\,; \quad a < t_\mathrm{d} \tag{2}$$

t_d is the length of the cell cycle (assumed to be constant in the model). The balance (1) therefore reduces to

$$\frac{\mathrm{d}f(a)}{\mathrm{d}a} = -Df(a) \tag{3}$$

At cell division it is assumed that there is a certain probability θ for the formation of a plasmid-free cell (the *segregation-parameter*), and a cell balance relating newborn cells to the dividing cells (the so-called renewal equation) therefore gives

$$f(0) = (2 - \theta)f(t_\mathrm{d}) \tag{4}$$

The solution to the differential equation (3), subject to (4) and (8.1) is

$$f(a) = \frac{2 - \theta}{1 - \theta} D \times n\,\mathrm{e}^{-Da} \tag{5}$$

Equation (5) gives the steady-state age distribution for plasmid-containing cells. The distribution is observed to be a function of the specific growth rate and the segregation parameter θ (see Fig. 8.2). The doubling time t_D is also a function of the segregation parameter:

$$t_\mathrm{D} = \frac{\ln(2 - \theta)}{\mu} \tag{6}$$

Thus, for a given specific growth rate μ of the culture it is seen that the cell cycle time decreases when the segregation parameter increases, i.e., the cells have to speed up their growth rate in order to compensate for the loss of a certain category of cells at cell division.

In order to find the distribution of plasmid content in the population of recombinant cells, it is necessary to specify the distribution of plasmids to the two daughter cells upon cell division and the rate of plasmid synthesis in the cells. First, the age distribution of cells with p_b plasmids at birth has a form (7), similar to (5), i.e.,

$$f_\mathrm{b}(a) = c_\mathrm{b} n\,\mathrm{e}^{-Da} \tag{7}$$

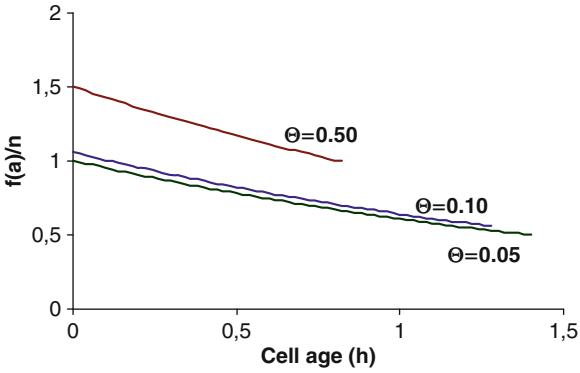

Fig. 8.2 Age distribution for recombinant cells at $D = 0.5\ \mathrm{h}^{-1}$ and for different values of the parameter θ

where c_b is determined by the applied model for the distribution of plasmids to the daughter cells. Three models for c_b were examined by Seo and Bailey:

- *Model 1*. In this model, it is assumed that plasmids are randomly distributed to daughter cells at cell division and that all cells contain N plasmids at cell division.
- *Model 2*. The assumptions underlying this model are similar to those for Model 1, but here it is furthermore assumed that $2M$ plasmids are evenly distributed to the daughter cells, whereas the rest are distributed at random.
- *Model 3*. In this model, it is assumed that all the plasmids are distributed randomly and that K plasmids are synthesized for each cell cycle.

Obviously, Model 2 does not result in instability of the recombinant culture, since each daughter cell always receives M plasmids from the dividing cell. From the age distribution specified for each subpopulation of cells with p_b plasmids at birth, it is possible to find the distribution of plasmid content p in cells with p_b plasmids at birth:

$$f_\mathrm{b}(p) = f_\mathrm{b}(a)\left|\frac{da}{dp}\right| \tag{8}$$

By assuming zero-order kinetics for the plasmid replication within each cell, the relationship between the plasmid content and the cell age is given by

$$p = p_\mathrm{b} + ca \tag{9}$$

Here c is the plasmid replication rate constant. Combination of (7)–(9) gives:

$$f_\mathrm{b}(p) = f_\mathrm{b}(a)\frac{1}{c} = c_\mathrm{b}\frac{1}{c}\exp\left(-D\frac{p - p_\mathrm{b}}{c}\right) \tag{10}$$

Finally, the distribution function for all plasmid-containing cells is found from summation of all the subpopulations:

$$f(p) = \sum_i f_i(p) \tag{11}$$

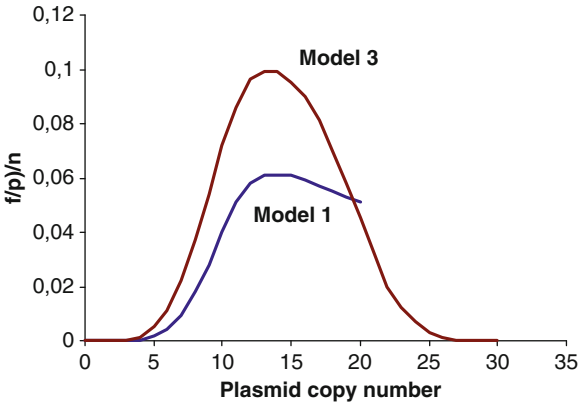

Fig. 8.3 Calculated distribution of cells with varying plasmid copy number for Model 1 and Model 3

With this model Seo and Bailey calculated the plasmid content distribution for the population of recombinant cells using Models 1 and 3. The results are shown in Fig. 8.3. For Model 1, there is a distinct maximum plasmid copy number of $N = 20$, whereas for Model 3 there is broad distribution of plasmid copy number in the population.

Using the plasmid copy number distribution found from the model, Seo and Bailey calculated the productivity of the recombinant culture, i.e., the rate of formation of the recombinant product. For the individual cells the product formation kinetics was taken to be

$$r_e(p) = k_e p\left(1 - \frac{p}{p_{max}}\right) \tag{12}$$

This is an analogue of (7.59). The total productivity for the culture is

$$q_e = \int_0^\infty f(p) r_e(p)\, dp \tag{13}$$

With the plasmid copy number distribution in Fig. 8.3, q_e was found to have a maximum when it is specified as a function of the average plasmid copy number (calculated as the first moment of the distribution function). Thus, for production of a recombinant protein there is an optimal *average* plasmid copy number for the population.

Finally, Seo and Bailey examined the instability of the recombinant population by using the dynamic age distribution for two subpopulations: (1) plasmid-containing cells and (2) plasmid-free cells. Depending on the parameters N and K in Models 1 and 3, the stability of the recombinant culture was studied. Obviously the stability increases for increasing values of both parameters.

The Seo and Bailey model represents a detailed analysis of recombinant cultures, and it has served as a useful guide for setting up simple models where homogeneity in the cell population is assumed.

Example 8.3 *Age distribution model for Saccharomyces cerevisiae.* The asymmetric cell division of budding yeast (see Fig. 7.18) has been modeled by Hjortso and Bailey (1982). Their model is based on an age distribution. Cells having an age less than $a_1 = t_d$ are defined

as daughter cells, and cells with an age more than a_1 are called mother cells. Since cell division occurs only at $a = a_1 + a_2$ (where $a_2 = t_m + t_b$), a balance similar to that of (3) of Example 8.2 holds for the steady-state age distribution:

$$\frac{df(a)}{da} = -Df(a) \tag{1}$$

Hjortso and Bailey used a normalized distribution function

$$\phi(a) = \frac{f(a)}{n} \tag{2}$$

The zero moment of this distribution function is equal to 1, and the first moment is the average cell age for the population. The balance for the normalized distribution function is similar to (1):

$$\frac{d\phi(a)}{da} = -D\phi(a) \tag{3}$$

The cell balances relating to cell division, i.e., the renewal equations, are

$$\phi(0) = \phi(a_1 + a_2) \tag{4}$$

$$\phi(a_1^+) = \phi(a_1^-) + \phi(a_1 + a_2) \tag{5}$$

The solution to the differential equation (3) with the boundary conditions (4) and (5) is given by:

$$\phi(a) = \begin{cases} D(e^{Da_2} - 1)\, e^{-Da}\,; & 0<a<a_1 \\ D\, e^{D(a_2 - a)}\,; & a_1<a<a_1 + a_2 \end{cases} \tag{6}$$

In (6) the parameter a_1 is given by:

$$a_1 = -\frac{1}{D} \ln(e^{Da_2} - 1) \tag{7}$$

From the age distribution function it is possible to calculate other distribution functions by using (8). This equation is a generalization of (8) in Example 8.2:

$$\phi(w) = \phi(a(w)) \left| \frac{da(w)}{dw} \right| \tag{8}$$

$$\phi(a) = \begin{cases} \dfrac{D}{r(w)} \exp\left(-D \displaystyle\int_{w_0}^{w} \frac{dy}{r(y)} \right); & w_0<w<w_1 \\ \dfrac{D\, e^{Dt_2}}{r(w)} \exp\left(-D \displaystyle\int_{w_1}^{w} \frac{dy}{r(y)} \right); & w_1<w<w_2 \end{cases} \tag{9}$$

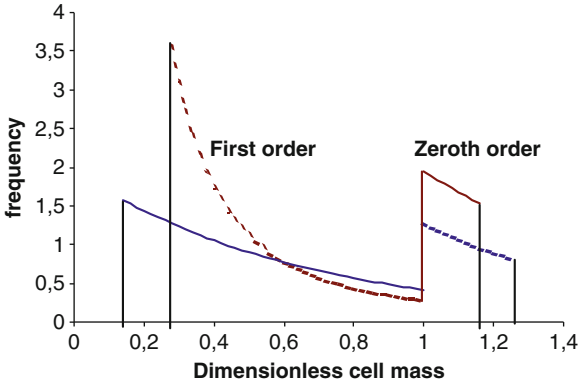

Fig. 8.4 Cell mass distribution function with, respectively, first- and zero-order growth kinetics of the individual cells. The model parameters are $D = 0.2\ \mathrm{h}^{-1}$; k (zero-order) $= 0.13$ and k (first-order) $= 0.2$. The cell mass has been rendered dimensionless by w_1, which is set to 1

Here $\phi(w)$ is a distribution function for another characteristic cellular variable w, e.g., cell mass. If w is synthesized at a rate $r(w)$ which is independent of cell age one finds that $\phi(w)$ is given by (9). w_0, w_1, and w_2 are values of w for cells with an age of respectively 0, a_1, and $a_1 + a_2$.

When w is the mass m of the individual cell, $r(w)$ is given by (10) and (11) for, respectively, first- and zero-order growth kinetics for the single cell.

$$r(m) = km \tag{10}$$

$$r(m) = k \tag{11}$$

With these two models for the single-cell growth rate, the steady-state distribution function $\phi(w)$ can be determined, and the results are shown in Fig. 8.4. It is observed that the distribution function is completely different in the two models, and with measurements of the cell size distribution (e.g., by flow cytometry), it should be possible to distinguish between the two models.

For the distribution function in (9), one can calculate the number fraction of daughter and mother cells, respectively (here termed Z^* in order to avoid confusion with the mass fraction Z used in Sect. 7.6):

$$Z_{\mathrm{d}}^{*} = \int_{0}^{a_1} \Phi(a)\mathrm{d}a = 2 - \mathrm{e}^{\mu a_2} \tag{12}$$

$$Z_{\mathrm{b}}^{*} = \int_{a_1}^{a_1+a_2} \Phi(a)\mathrm{d}a = \mathrm{e}^{\mu a_2} - 1 \tag{13}$$

The length t_{b} of the budding phase is often considered to be independent of the specific growth rate ($t_{\mathrm{b}} \approx 1.8$ h), even though it decreases slightly with μ (see Fig. 8.5). If the same holds for the time for maturation, i.e., t_{m} approximately constant, then it is concluded that a_2 is independent of the specific growth rate. Thus from (13) the fraction of mother cells in the

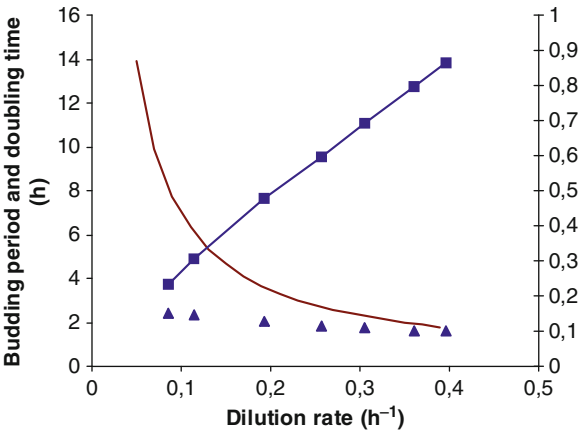

Fig. 8.5 Measurements of the length of the budding period t_d (*filled square*) and the fraction of budded cells Z_b* (*filled triangle*) as functions of the dilution rate in a steady-state chemostat. Assuming that $a_2 \approx t_b$, the fraction of budded cells is calculated using (13) (shown as *line*). Also shown is $t_D = \ln 2/D$. The data are from Lievense and Lim (1982)

culture increases with the specific growth rate. This corresponds well with experimental data given by Lievense and Lim (1982), who found that the budding index, i.e., the fraction of budded cells, increases with D in a steady-state chemostat (Fig. 8.5).

From Fig. 8.5, it is observed that the doubling time approaches the length of the budding period for high specific growth rates. Consequently, t_d decreases for increasing μ – showing that the size of the daughter cells resulting from the cell division increases with increasing μ, and for high specific growth rates the cell division becomes almost symmetric (two cells of almost equal size are formed).

Due to the formation of a bud scar on the cell envelope of the mother cell upon cell division it is expected that mother cells would have a maximum age. Hjortso and Bailey (1982) introduced the concept of the genealogical age of mother cells and calculated the distribution of cells with varying numbers of bud scars. Thereby, the effect of various hypotheses concerning the growth ability of mother cells with many bud scars could be examined. Hjortso and Bailey (1983) also carried out transient experiments modeled by the dynamic balance (14), which is derived from (8.2) with $h(a) = 0$ for all $a \neq a_1 + a_2$, and $r(a) = 1$.

$$\frac{\partial \phi(a)}{\partial t} + \frac{\partial \phi(a)}{\partial a} = -D\phi(a) \tag{14}$$

The dynamic balance was solved by the method of characteristics and again the influence of changing the single-cell kinetics from zero to first order was examined.

Hjortso and Bailey (1984a) extended their segregated population model to predict plasmid stability at steady-state growth. They assumed that the culture is under selection pressure, whereby only plasmid-containing cells can survive in the environment. The population balance (3) still holds, but the cell balances relating to cell division in (4) and (5) are modified to those of (15) and (16) in order to account for plasmid loss. θ_m and θ_d (the segregation parameters) are the probabilities of formation of, respectively, a plasmid-free mother and a plasmid-free daughter cell at cell division.

$$\Phi(0) = (1 - \theta_d)\Phi(a_1 + a_2) \tag{15}$$

$$\Phi(a_1^+) = \Phi(a_1^-) + (1 - \theta_m)\Phi(a_1 + a_2) \tag{16}$$

With these boundary conditions, the steady-state solution of the population balance becomes

$$\phi(a) = \begin{cases} D\dfrac{e^{D(a_1+a_2)} - 1 + \theta_m}{1 - \theta_d - \theta_m} e^{-Da}; & 0<a<a_1 \\ D\dfrac{e^{D(a_1+a_2)}}{1 - \theta_d - \theta_m} e^{-Da}; & a_1<a<a_1 + a_2 \end{cases} \tag{17}$$

The parameter a_1 is given by (18):

$$a_1 = \frac{1}{D} \ln\left(\frac{1 - \theta_d}{e^{Da_2} - 1 + \theta_m}\right) \tag{18}$$

It is observed that the length of the unbudded period decreases with increasing values of θ_m and θ_d. The reason for this is, that when a large portion of the cells lose their plasmid at cell division (and thereby die due to selection pressure from the environment), the culture has to speed up its specific growth rate at the cellular level. This is observed as formation of larger daughter cells during the budding period, and the length of the unbudded period for the daughter cells is therefore shortened. The decrease in a_1 results in a narrower age distribution, with a larger fraction of the cells being mother cells.

In the model above, only the age distribution for the plasmid containing cells is considered. However, for prediction of productivity of a recombinant product one needs information on the plasmid copy number distribution, and Hjortso and Bailey therefore extended their model to describe the plasmid copy number distribution (by an approach similar to that illustrated in Example 8.2). Two models for plasmid replication during the cell cycle were examined: (a) sufficient plasmids are synthesized during the cell cycle to ensure that the copy number is always N at cell division and (b) N plasmids are synthesized during the cell cycle. The plasmid copy number distribution was calculated, and the distribution is quite different for the two models (one being bimodal and the other looking qualitatively like an exponential decay).

Finally, Hjortso and Bailey (1984b) extended their model for the recombinant yeast to dynamic conditions and examined a shift to a nonselective medium. In a chemostat, the fraction of the population that contains plasmids approaches zero asymptotically as growth proceeds. The decrease in the fraction of plasmid-containing cells depends on the value of a_1, which is a function of the specific growth rate. For any $a_1 > 0$, asymmetric division results in a faster decrease in the fraction of plasmid-containing cells than does binary fission. This shows that the asymmetric division of budding yeast results in a different behavior than that observed for recombinant bacteria.

Example 8.4 *Population model for hyphal elements.* In submerged cultures of filamentous fungi, there is a population of hyphal elements, which may be characterized by many different properties (e.g., their length and the number of tips), but the relative content of different cell types may also be important (see Sect. 7.6.2). We now assume that each hyphal element is characterized completely by its total length (l) and the number of actively growing tips (n); i.e., $f(l,n) \times dl \times dn$ is the number of hyphal elements with length l and n actively growing tips. The hyphal diameter is normally constant (at least for certain environmental conditions), and this also holds for the hyphal density. The hyphal length is therefore proportional with the hyphal mass, and the total tip extension rate for the hyphae is therefore

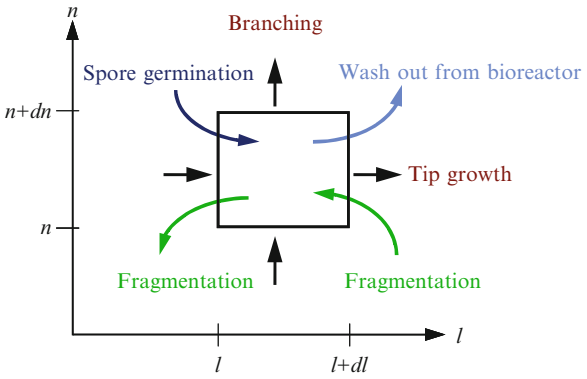

Fig. 8.6 Illustration of the different elements in the population balance equation for individual hyphal elements in a filamentous fungal culture

given by $\mu(l,n,t)l$. n is in reality an integer, but it is here taken to be a real number. The length of the hyphal element increases due to growth with the specific rate $\mu(l,n,t)$, and new actively growing tips are formed due to branching with the frequency $\phi(l,n,t)$. It is now assumed that both the specific growth rate of the hyphal element and the branching frequency are independent of the hyphal element properties, i.e., they are not functions of l and n. Consequently, the rate of change of length is $\mu(t)l$, and the rate of change of actively growing tips is $\phi(t)$. The dynamic mass balance for the distribution function $f(m,n)$ is therefore given by

$$\frac{\partial f(l,n,t)}{\partial t} + \frac{\partial}{\partial l}[\mu(t)lf(l,n,t)] + \frac{\partial}{\partial n}[\phi(t)f(l,n,t)] = h(l,n,t) - Df(l,n,t) \tag{1}$$

The dynamic mass balance is illustrated in Fig. 8.6 which shows that for a given control volume in the $[l,n]$ plane, there are inputs and outputs due to tip extension and branching. Furthermore, there are inputs due to formation of new hyphal elements by fragmentation and spore germination. Finally, there are hyphal elements leaving the control volume due to hyphal fragmentation and washout.

We now consider growth of a mycelium in an agitated tank where shear stress causes the hyphae to break up (hyphal fragmentation). With binary fission of hyphal elements, the net rate of formation of hyphal elements with property $\{l,n\}$ formed upon fragmentation is given by (8.7):

$$h(l,n,t) = 2\int_{V_m}\int_{V_n} b(l^*,n^*,t)p(\{l^*,n^*\},\{l,n\})f(l^*,n^*,t)\mathrm{d}n^*\mathrm{d}l^* - b(l,n,t)f(l,n,t) \tag{2}$$

$b(l,n,t)$ is the breakage function, which describes the rate of fragmentation of hyphal elements with property $\{l,n\}$, and $p(\{l^*,n^*\},\{l,n\})$ is the partitioning function.

Within the population of hyphal elements there will be more or less fragmentation at different positions in the individual hyphal elements. This fragmentation occurs when the local shearing forces become larger than the tensile strength of the hyphal wall (van Suijdam and Metz 1981). The tensile strength of the hyphal wall depends on the morphological state of the individual cell in the hyphal element, e.g., the tensile strength of the hyphal cells could

be smaller than that of apical cells, but here it is assumed that it is constant and independent of the state of the hyphae. The breakage function and the partitioning function are therefore both taken to be independent of the morphological state of the individual cells.

In a culture with a very large number of hyphal elements, the average ratio of hyphal length to the number of actively growing tips in the two "daughter" fragments is identical, i.e., $\langle l\rangle/\langle n\rangle = \langle l^* - l\rangle/\langle n^* - n\rangle$, if fragmentation occurs with equal probability at any position on the hyphal elements. It is therefore assumed that $l/n = (l^* - l)/(n^* - n)$ (or $l/n = l^*/n^*$), whereby the partitioning function can be stated as a function of l^* and l only. Furthermore, since the tensile strength of the hyphal wall is assumed to be constant, there is an equal probability of fragmentation at any position in the hyphal element. The partitioning function is therefore given by

$$p(\{l^*, n^*\}, \{l, n\}) = p^*(l^*, l) = \begin{cases} 1/l^* & \text{if } l^* > l \text{ and } l/n = l^*/n^* \\ 0 & \text{in all other cases} \end{cases} \tag{3}$$

The breakage function specifies the rate of fragmentation, and this is taken to be a linear function of the total length of the hyphal element:

$$b(l, n, t) = \psi(t) l \tag{4}$$

$\psi(t)$ is the specific rate of fragmentation, which is here taken to be a function of the environmental conditions only. $\psi(t)$ is determined by the number of times the hyphal elements enter the zones where the local shearing forces are larger than the tensile strength of the hyphal element, e.g., the impeller zone, and it is therefore determined both by the circulation pattern and the shear force distribution in the bioreactor. However, in a simple model describing growth in a stirred tank reactor, one can assume that $\psi(t)$ is a function only of the energy input which can be calculated from the stirring speed, i.e., it is constant for constant stirring speed (van Suijdam and Metz 1981).

By inserting the partitioning function of (3) and the breakage function of (4) in (2) we get

$$h(l, n, t) = 2\psi(t) \int_l^\infty f(l^*, n^*, t) \mathrm{d}l^* - \psi(t) l f(l, n, t) \tag{5}$$

In order to solve the dynamic balance (1) for the distribution function, it is necessary to specify proper boundary conditions, and these are given in (6)–(8). Fragmentation never results in the formation of hyphal elements with zero length or no actively growing tips, and the boundary conditions in (6) therefore hold. Since the breakage function is linearly dependent on the length of the hyphal element, no hyphal elements have infinite length. Furthermore, due to the assumption $l^*/n^* = l/n$ there are also no hyphal elements with an infinite number of tips. Finally, $f_0(m, n)$ specifies the distribution function at time $t = 0$:

$$f(0, n, t) = 0\ ; \qquad f(m, 0, t) = 0 \tag{6}$$

$$\lim_{l\to\infty} f(l, n, t) = 0\ ; \qquad \lim_{n\to\infty} f(l, n, t) = 0 \tag{7}$$

$$f(m, n, 0) = f_0(m, n) \tag{8}$$

Solving the dynamic balance for the distribution function is complicated, since the property space is two dimensional and an integration step is involved in the calculation of $h(l,n,t)$. For comparison of the population model with measurements obtained in a continuous bioreactor at steady state, it is, however, sufficient to find the steady-state solution of the population balance. For a population balance with a one-dimensional property space Singh and Ramkrishna (1977) used the method of weighted residuals to find the steady-state solution. This method could probably be extended to find the steady-state solution for the population balance derived here. Alternatively one may introduce discrete variables and then solve differential equations for each discrete variable (Krabben et al. 1997). However, an intuitively simpler approach is to apply Monte-Carlo simulations where a large number of individual hyphal elements are simulated, and the elements may then together form the distribution function. Krabben et al. (1997) applied this approach to simulate the distribution function for different fragmentation kinetics, i.e., different partitioning functions and different breakage functions. It is practically impossible to obtain sufficient experimental data – even with fully automated image analysis, on the distribution function in two dimensions to validate different models. Krabben et al. (1997) therefore took a different approach. Based on the simulated distribution functions they generated contour plots for the function. These contour plots were then statistically used to evaluate experimentally obtained data for the hyphal element properties. Hereby it was possible to evaluate the different models, and based on this it was concluded that hyphal fragmentation only takes place for hyphal elements above a certain size, and then follows second-order kinetics. It was, however, not possible to discriminate between two models for the partitioning function, i.e., whether there is largest probability for fragmentation at the center of the hyphae or whether there is equal probability for fragmentation along the hyphae.

Even though the Monte Carlo simulations offer a simple method for simulation of even complex models, it is often sufficient to look at the average properties of the hyphal elements, as these may be directly compared with measured data. Using the balance for the distribution function discussed above Nielsen (1993) derived dynamic balances for the average hyphal length and the average number of tips. These balances are given by

$$\frac{\mathrm{d}e}{\mathrm{d}t} = (\psi - D)e \tag{9}$$

$$\frac{\mathrm{d}\langle l\rangle}{\mathrm{d}t} = (\mu - \psi)\langle l\rangle = \varphi\langle n\rangle - \psi\langle l\rangle \tag{10}$$

$$\frac{\mathrm{d}\langle n\rangle}{\mathrm{d}t} = \phi - \psi\langle n\rangle \tag{11}$$

φ is the average tip extension rate for all the hyphal tips in the population. Using these balances it is possible to obtain information about the growth kinetics, i.e., the branching frequency and the tip extension rate from measurements of the average total hyphal length and the average number of tips. The total biomass concentration x is given by $x = \langle l\rangle e$, and combining the dynamic balances of (9) and (10), the well-known mass balance for biomass is found:

$$\frac{\mathrm{d}x}{\mathrm{d}t} = (\mu - D)x \tag{12}$$

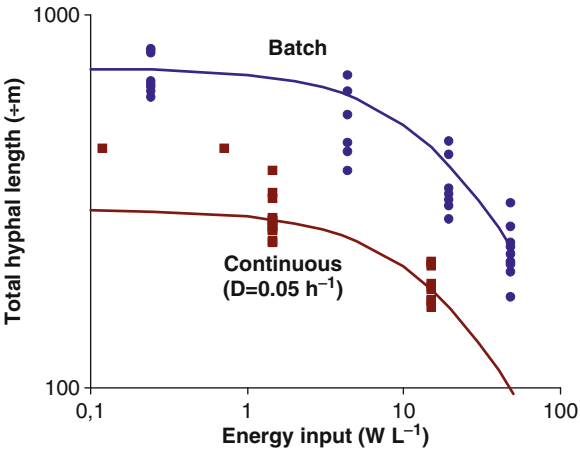

Fig. 8.7 Effect of energy input (W L^{-1}) on the total hyphal in μm of *Pencillium chrysogenum* in a submerged culture. The two data sets (Metz 1976) are from a series of batch fermentations (batch) and from a series of chemostat experiments (continuous, $D = 0.05\ h^{-1}$). The lines are model simulations

With the technique of image analysis, it is possible to determine experimentally the average properties of the hyphal elements, and the simple model based on average properties may be valuable for extracting the growth kinetics of hyphal elements. The variance of the properties of the hyphal element is, however, normally quite large, i.e., the relative standard deviation of the hyphal length is often 50% or more of the average values. The estimation of the average properties should therefore be based on a large number of single estimations. Thus many individual hyphal elements have to be measured. The variance of the distribution function can be calculated from (8.11), and if an explicit expression for the variance could be derived the model predicted variance could be compared with the experimentally determined variance. It is, however, not possible to derive simple expressions to be used in the calculation of the variances, and the model is therefore evaluated only by comparison with experimental data for the average properties. It should, however, be noted that the kinetics derived from the above model is based on average properties, and it may therefore not necessarily specify much about the kinetics of individual hyphal elements. Here it is necessary to study the growth kinetics of individual hyphal elements in a growth chamber positioned under a microscope equipped with an image analysis system. Using such a system the growth kinetics of *Aspergillus oryzae* has been studied in great detail (Spohr et al. 1998; Christiansen et al. 1999).

Nielsen (1993) compared the population model derived above with experimental data for the total hyphal length and the number of tips obtained during fermentations with *Pencillium chrysogenum*. The model was also used to examine the influence of the energy input on the morphology of *P. chrysogenum* by comparing model simulations with experimental data given by Metz et al. (1981) and van Suijdam and Metz (1981) [the data were obtained both during a batch fermentation and in a steady-state chemostat ($D = 0.05\ h^{-1}$)]. In Fig. 8.7, data for the total hyphal length are shown as a function of the energy input for the two cases. The data for the batch fermentation are the measurements obtained in the exponential growth phase, where $\mu = 0.12\ h^{-1}$. The energy input E (units of W L^{-1}) was calculated from the stirrer speed as specified by van Suijdam and Metz (1981). By assuming the linear relation in (13) between the specific rate of fragmentation and the energy input, the total hyphal length was calculated from the steady-state form of the balance for $\langle l \rangle$ in (10) and a hyphal diameter of 3.6 μm (Metz et al. 1981).

The data for the batch fermentation are the measurements obtained in the exponential growth phase, where $\mu = 0.12\ \mathrm{h}^{-1}$. The energy input E (units of $\mathrm{W\ L}^{-1}$) was calculated from the stirrer speed as specified by van Suijdam and Metz (1981). By assuming the linear relation in (13) between the specific rate of fragmentation and the energy input, the total hyphal length was calculated from the steady-state form of the balance for $\langle l \rangle$ in (10) and a hyphal diameter of 3.6 μm (Metz et al. 1981).

$$\psi = 2.1 \times 10^6 \times E + 50.0 \times 10^6 \tag{13}$$

The model is observed to correspond well with the experimental data, except for the two measurements at very low energy input in the chemostat. Considering the data scatter, and the presence of only two measurements in this range, it is reasonable to conclude that the rate of fragmentation is linearly correlated to the energy input (note that the same correlation holds for the two sets of independent experimental data).

Problems

Problem 8.1 *Derivation of single-cell mass distribution functions.* Consider an organism for which division occurs at the cell mass M, birth at the cell mass $M/2$, and the single-cell mass growth rate follows first-order kinetics, i.e., $r(m) = km$.

(a) Find the normalized, steady-state cell mass distribution $\phi(m)$ for this organism in a chemostat with dilution rate D.
(b) Find the relation between D and k, and use it to eliminate k from the expression for $\phi(m)$.
(c) Find the distribution function for zeroth-order kinetics (i.e., $r(m) = k$), and compare the distribution functions for, respectively, zero and first-order kinetics.
(d) Assuming a constant yield Y_{sx} of mass per individual cell from the substrate, write a steady-state substrate balance and simplify this to obtain an equation among D, k, and n (the total cell number).
(e) Assume that the substrate dependence of k follows a Monod-type expression. Find the substrate and cell number concentrations as functions of the dilution rate.

Problem 8.2 *Linear single-cell kinetics.* Consider an organism for which division occurs at cell mass M, birth at cell mass $M/2$, and the single-cell mass growth rate follows $r(m) = k_1 m + k_2$.

(a) Find the normalized, steady-state cell mass distribution $\phi(m)$ for this organism in a chemostat with dilution rate D.
(b) Find the relation among D, k_1, and k_2.
(c) Because there is more than one parameter in the rate expression for the single-cell kinetics, it is not possible to use the last result to simplify the expression for the distribution of states and write it solely as a function of the dilution rate in the chemostat. There are simply not enough equations

to solve for k_1 and k_2 in terms of D. This problem can be resolved if one postulates kinetic expressions for both parameters in terms of the concentration of the limiting substrate. From these equations one can eliminate the substrate concentration and obtain one of the parameters in terms of the other. This result can then be used with the expression obtained in (a) to find all the parameters in terms of the dilution rate. Demonstrate this procedure for the model, above assuming that

$$k_1 = \frac{k_{1,\max} s}{s + K} \tag{1}$$

$$k_2 = \frac{k_{2,\max} s}{s + K} \tag{2}$$

s is the concentration of the growth-limiting substrate and the parameters $k_{i,\max}$ and K must be determined from experiments. Express k_2 as a function of k_1, and substitute the result into the expression obtained in (b), solve for k_1 as a function of D, and eliminate k_2 and k_1 from the expression for $\phi(m)$.

Problem 8.3 *Continuous plant cell cultures.* For plant cell cultures it has been found experimentally that the cell concentration in the outlet stream from a chemostat is less than the concentration in the vessel. This is caused by the large size of plant cells, which occasion them to sediment out of the outlet stream and back into the vessel. Of course, this effect is more pronounced for large cells than for small cells, and the phenomenon can therefore be expected to affect the cell mass distribution.

We can model this by assuming that the cell mass distribution in the outlet stream can be calculated from the distribution in the vessel by the following expression:

$$\phi_{\text{outlet}}(m) = \phi_{\text{vessel}}(m) \frac{a}{m + a} \tag{1}$$

where a is a constant parameter.

Derive a population balance equation for this situation, and find the normalized steady-state cell mass distribution in the vessel, assuming that cells divide when they reach the cell mass M, cells are born with cell mass $M/2$, and the cell mass growth rate follows zero-order kinetics.

Problem 8.4 *Cell death.* Consider an organism which, when it attains the age a_{d} either dies (with a probability θ) or divides.

(a) Write the cell balance over dividing cells and solve for the normalized, steady-state age distribution, $\phi(a)$, in a chemostat with dilution rate D.
(b) Show that the doubling time, defined as the duration of the cell cycle a_{d}, does not equal the doubling time defined on the basis of the specified growth rate of the population.

Problem 8.5 *Derivation of conversion rates in a yeast model.* Cazzador (1991) evaluated the parameter k_u and k_b in a morphologically structured model and in this evaluation he assumed that

- The critical mass for budding is assumed to be constant and equal to 1, i.e., $m = 1$.
- The critical mass for cell division is assumed to be a known function of the substrate concentration $m_{div}(s) \lim_{x\to\infty}$ such that $1<m_{div}<2$.
- The size of the mother cells after division is assumed to be $m = 1$ and that of newborn daughters $m = m_{div} - 1$.
- The specific growth rate of the single cell is assumed to be μ_u in the first (unbudded) phase and μ_b in the second (budded) phase of the cell cycle.

(a) Write the steady-state balances for the distribution function of cell mass for cells in the two phases. Specify the renewal equations.
(b) Solve the balances for the distribution functions.
(c) The transfer rates between the two morphological forms can be expressed as

$$k_u x Z_u = \mu_u f_u(1) \tag{1}$$

$$k_b x Z_b = (m_{div} - 1)\mu_b m_{div} f_b(m_{div}) \tag{2}$$

(d) Use these equations to derive expressions for k_u and k_b as functions of m_{div} (which again is a function of the limiting substrate concentration) in the two cases

i. $\mu_u = \mu_b = \mu$
ii. $\mu_u \neq \mu_b$

(d) Let m_{div} and μ be given as

$$m_{div} = 1.2 + 0.5\frac{s^8}{s^8 + 10^8} \tag{3}$$

$$\mu = 0.3\frac{s}{s+4} \tag{4}$$

Plot k_u and k_b as functions of the limiting substrate concentration s. Simulate using a PC the dynamic equations for Z_u, Z_b, s, and x in a chemostat operated with $D = 0.2\ h^{-1}$, $s_f = 400\ g\ L^{-1}$, $a_u = 10$, and $a_b = 2$. Show that a stable limit cycle is obtained.

References

Cazzador, L. (1991). Analysis of oscillations in yeast continuous cultures by a new simplified model, *Bull Math. Biol.* **5**, 685–700.

Christiansen, T., Spohr, A., Nielsen, J. (1999). On-line study of growth kinetics of single hyphae of *Aspergillus oryzae* in a flow-through cell. *Biotechnol. Bioeng.* **63**, 147–153.

Hjortso, M. A. and Bailey, J. E. (1982). Steady-state growth of budding yeast populations in well-mixed continuous-flow microbial reactors, *Math. Biosci.* **60**, 235–263.

Hjortso, M. A. and Bailey, J. E. (1983). Transient responses of budding yeast populations, *Math. Biosci.* **63**, 121–148.

Hjortso, M. A. and Bailey, J. E. (1984a). Plasmid stability in budding yeast populations: Steady state growth with selection pressure. *Biotechnol. Bioeng.* **26**, 528–536.

Hjortso, M. A. and Bailey, J. E. (1984b). Plasmid stability in budding yeast populations: Dynamics following a shift to nonselective medium. *Biotechnol. Bioeng.* **26**, 814–819.

Kothari, I. R., Martin, G. C., Reilly, P. J., Martin, P. J., and Eakman, J. M. (1972). Estimation of parameters in population models for *Schizosaccharomyces pombe* from chemostat data. *Biotechnol. Bioeng.* **14**, 915–938.

Eakman, J. M., Fredrickson, A. C., and Tsuchiya, H. M. (1966). Statistics and dynamics of microbial cell populations. *Chem. Eng. Prog. Symp. Ser.* **62**, 37–49.

Krabben, P., Nielsen, J., Michelsen, M. L. (1997). Analysis of single hyphal growth and fragmentation in submerged cultures using a population model. *Chem. Eng. Sci.* **52**, 2641–2652.

Kreyszig, E. (1988). *Advanced Engineering Mathematics,* 6th ed., John Wiley & Sons, New York.

Lievense, J. C. and Lim, H. C. (1982). The growth and dynamics of *Saccharomyces cerevisiae*, *Ann. Report Ferm. Proc.* **5**, 211–262.

Metz, B. (1976). *From Pulp to Pellet,* Ph.D. thesis. Technical University of Delft, Delft.

Metz, B., Bruijn, E. W., and van Suijdam, J. C. (1981). Method for quantitative representation of the morphology of molds. *Biotechnol. Bioeng.* **23**, 149–162.

Nielsen, J. (1993). A simple morphologically structured model describing the growth of filamentous microorganisms. *Biotechnol. Bioeng.* **41**, 715–727.

Ormerod, M. G. (ed.), 2000 (3rd edition). Flow cytometry. BIOS Scientific Publishers, Oxford University Press.

Ramkrishna, D. (1979). Statistical models for cell populations. *Adv. Biochem. Eng.* **11**, 1–48.

Ramkrishna, D. (1985). The status of population balances. *Rev. Chem. Eng.* **3**, 49–95.

Seo, J. H. and Bailey, J. E. (1985). A segregated model for plasmid content on growth properties and cloned gene product formation in *Escherichia coli* . *Biotechnol. Bioeng.* **27**, 156–166.

Singh, P. N. and Ramkrishna, D. (1977). Solution of population balance equations by MWR. *Comp. Chem. Eng.* **1**, 23–31.

Spohr, A. B., Mikkelsen, C. D., Carlsen, M., Nielsen, J., Villadsen, J. (1998). On-line study of fungal morphology during submerged growth in a small flow-through cell. *Biotechnol. Bioeng.* **58**, 541–553.

Subramanian, G. and Ramkrishna, D. (1971). On the solution of statistical models of cell populations. *Math. Biosci.* **10**, 1–23.

van Suijdam, J. C. and Metz, B. (1981). Influence of engineering variables upon the morphology of filamentous molds. *Biotechnol. Bioeng.* **23**, 111–148.

Chapter 9
Design of Fermentation Processes

In previous chapters, the stoichiometry of bioreactions has been investigated, and it was shown that how *steady-state rates* could be measured for many reaction components. In Chaps. 3 and 4, the *extent* of the bioreaction was determined as a function of the reaction conditions, in particular, the feed composition, the redox level, and pH. In Chap. 5, the black box model for a bioreaction was greatly expanded to include a sub-set of the almost infinite number of reactions in the metabolic network. Finally, in Chaps. 6 and 7, the chemical reaction, first in enzyme reactions and then in cell cultivations, was treated by the same tools as are used in "ordinary" chemical reactions: The reaction rate was described as a function of the concentrations of reactants and afterwards included in mass balances. A large number of rate models were explored. Most of the rate models for cell reactions were of empirical nature, but biological knowledge was included to choose a *structure* of the rate expression that is suitable for the situation to be studied. The structure could extend from a consciously simplified picture of the culture as homogenous in space as well as in the biology that determines the cell reaction(s) to both biologically and spatially structured population balance based models in Chap. 8.

Transport phenomena were included right from the start where the influence of gas-to-liquid transfer was introduced (Example 3.4), and in Sect. 6.3.2 the influence of diffusion resistance on the rate of the bioreaction was discussed in some detail.

A serious discussion of reaction rates would not have been possible without introducing the equipment in which the reaction takes place, the *bioreactor*. Consequently, the steady state, flow through reactor, the CSTR (continuous stirred tank reactor) was introduced at the very start of Chap. 3, and the name used there, the *chemostat*, referred to the way the dilution rate was controlled. In Sect. 6.3.2, the *fixed-bed tubular reactor* was introduced as a means of conducting reactions on immobilized enzymes.

In Chap. 9, the focus is *on deciding the best possible conditions for conducting a bioreaction*.

Productivity in a reactor of a given volume is of considerable importance for the commercial value of a bioprocess, sometimes more important than the yield and

J. Villadsen et al., *Bioreaction Engineering Principles*,
DOI 10.1007/978-1-4419-9688-6_9,

the final titer of the desired product. Thus, we shall discuss the optimal combination of equipment (the bioreactor) and the environmental conditions, e.g., the dilution rate D, with the purpose of *designing* the best possible overall process (highest yield, productivity, and final titer), while considering the variable and the fixed production costs of the process.

This survey of the *practical* feasibility of bioproduction is to be done by involving the material of all the preceding chapters *together with an engineering approach* to the subject.

Table 9.1 is an overview of the reactors used in the bioindustry where, in very general terms, the application areas as well as advantages/disadvantages of the reactors are stated.

By far the most commonly used bioreactor is the *stirred tank reactor* (STR).

Steady-state operation is the preferred mode of operation of the STR since the CSTR can be designed to give either maximum productivity or maximum yield of

Table 9.1 Advantages and disadvantages of different reactor types and of different operating modes of the reactors

Reactor type/mode of operation	Advantages	Disadvantages
Stirred tank reactors		
1. Steady state (CSTR)	(a) Large-scale production of cheap products STR, *especially CSTR*, is by far the best due to low capital and labor costs (b) CSTR (or fed-batch) needed when production of the desired product is catabolite repressed (c) Due to autocatalytic nature of microbial reactions, *productivity* is high (d) Product quality is constant	(a) Infection is a risk, e.g., caused by a short stop of the continuous feed sterilization by steam (b) The strain may mutate to a nonproducing strain after long production time (c) Downstream equipment can be difficult to operate in the continuous mode (d) Very inflexible
2. Batch operation	(a) Easily switched between different production duties with low retrofitting costs (b) Can be properly sterilized. Small risk of infection and mutation (short production time)	(a) High labor costs (b) Much idle time for sterilization, outgrowth of inoculum, and cleaning (c) Safety problems when filling and emptying reactor
3. Fed-batch operation	(a) Same advantages as CSTR (a and b) (b) The production time is limited with smaller risk of mutations	(a) More labor cost than CSTR (b) Large volume to be downstream processed between runs. Holding tanks used
Plug flow reactor		
1. Steady state	(a) Very high conversion of the substrate can be obtained (b) Fixed-bed operation (immobilized enzymes or cells). Film reactors (c) High conversion of gas-phase substrates (loop-reactors)	(a) Requires cells in feed and it can only be used *after* another reactor (b) The large difference in holding time between gas and liquid prevents the use of a single-pass PFR

the desired product, and the operating conditions can be kept at the set-point for very long times with the use of state-of-the-art process control equipment which is now obligatory in the bioindustry. A case in point is the continuous production of insulin by Novo-Nordisk where the strict FDA regulations concerning constant product quality are met in "campaigns" of 3–4 weeks of continuous operation. Also, virtually all bioremediation plants operate as STR in the continuous mode, and a clever design of several CSTRs in parallel or in sequence can be used to prevent wash-out after sudden up-sets of the process.

The batch reactor and the fed-batch reactor both operate in non-steady state, but it is important to realize that *the culture is nearly in metabolic steady state* during cultivation in these reactors: The changes in the environment during the process are often sufficiently slow to justify that, in terms of the metabolic state of the cells, the non-steady-state operating STR is not different from the CSTR.

True dynamic behavior of the culture is only experienced after sudden changes in the substrate concentration level in the reactor or after sudden changes in culture parameters, such as the pH. The discussion in Chap. 6, Figs. 7.12, 7.14, and 7.15 is concerned with *truly* transient behavior. Here, kinetics that are applicable in the design of processes where the culture is in metabolic steady state cannot be used, and as pointed out in Chap. 7 it is impossible to set up a general model that would predict the cell-level changes of metabolism after a large upset of the steady state.

Hence, true transients are combated with the help of efficient process control equipment, and the effect of large transients which may have disastrous effects on the process are only seen after a failure in the process control system (or as a result of human errors).

When the sensitivity of the enzymatic reactions in a metabolic network is studied, an important experimental tool is, however, as discussed in Sect. 6.4.4, to introduce step changes in D or a pulse change in the substrate level. Here, violent and rapid changes in the metabolite concentrations occur, and we shall discuss recently developed experimental methods to measure fast changes in metabolite levels. This is not because these transients are normally experienced in industrial production, but because the results of the transient STR experiments can be used to construct better production strains.

Finally it should be mentioned that the CSTR is applied in many different fields of bioprocessing, and different names are used. A CSTR with cell retention to improve the productivity (see Sect. 9.1.4) is sometimes called a *membrane bioreactor*, and when used to produce the fragile animal or plant cells the names *perfusion bioreactor* and hollow fiber cell culture reactor are used.

As indicated in Table 9.1, the *plug flow reactor* (PFR) is rarely used in bioprocessing. If, however, a valuable gaseous substrate (e.g., technically pure (95–97%) O_2) is used in a continuous cultivation, too much of the gaseous substrate is lost when the gas is simply sparged to the bottom of a STR. The solution is to keep the liquid-phase substrates and products in (almost) completely mixed state, e.g., with a typical holding time of 4–5 h, while consuming the gas-phase substrates in plug flow mode where a satisfactory conversion can be obtained, also with a holding time of only 20–40 s. The equipment used is called a *loop-reactor*, and modeling of the loop reactor is discussed in Sect. 9.4.2.

The PFR is also used to "mop up" the remainder of the substrate in the effluent from a CSTR cultivation – see Sect. 9.4.1. The kinetics of the reaction will always become first order in the limiting substrate concentration s when $s \to 0$, and here the CSTR fails while the PFR easily converts the last bits of the substrate. This can be important in the complete removal of toxic compounds in, e.g., waste water.

In enzymatic reactions, a continuous PFR operation (either using a fixed bed of immobilized pellets or a fluid ("expanded") bed of immobilized enzyme particles) can also be better than CSTR operation, giving higher conversion of the substrate or even a higher selectivity if several reactions compete for the substrate.

Film reactors, where a film of, e.g., bacteria can be made to grow on the walls of a pipe or on an inert support material, are used in waste water biomediation. These are also examples of steady-state PFR operation.

In Sects. 9.1–9.3, the design of STR processes is discussed, starting with the CSTR, followed by batch and fed batch, and finally by a treatment of true transients applied in the STRs.

In Sect. 9.4, the steady-state continuous PFR is the subject. The application of the PFR after a CSTR and the loop reactor will be given special attention.

This ordering of the vast literature on bioreactors, from academia, but most importantly from industry, follows the relative use of the reactor types in practice.

As a final note: *In Chap. 9, only ideally mixed reactors are treated. Reactors with spatial inhomogeneities due to incomplete mixing are treated in Chap. 11.*

9.1 Steady-State Operation of the STR

A *general* mass balance for a STR is

$$\frac{\mathrm{d}(V\mathbf{c})}{\mathrm{d}t} = V(\mathbf{q}^{\mathrm{t}} + \mathbf{q}) + v_{\mathrm{f}}\mathbf{c}_{\mathrm{f}} - v_{\mathrm{e}}\mathbf{c}_{\mathrm{e}}. \tag{9.1}$$

On the right-hand side of (9.1), we find the rate of transport $\mathbf{q}^{\mathrm{t}}$ of substrates (or products) from the gas phase to the liquid medium and the rate of production of substrates (or products) by the bioreaction. Both are in units of, e.g., kg (m^3 reactor)$^{-1}$ h^{-1}. When multiplied by V, we obtain the sum of contributions of reaction components transported *from* the gas to the medium and the reactants *produced* in the reactor (kg h^{-1}). Also on the right-hand side of (9.1), we have the difference between the inlet flow $v_{\mathrm{f}}\mathbf{c}_{\mathrm{f}}$ and effluent flow $v_{\mathrm{e}}\mathbf{c}_{\mathrm{e}}$ of reaction components (kg h^{-1}). On the left-hand side of (9.1) is the *accumulation* of reactants in the reactor (kg h^{-1}).

Figure 9.1 is a schematic representation of the STR showing inputs and outputs.

Both in the CSTR and in the batch reactor, V is constant. In the batch reactor, both flow terms on the right-hand side of (9.1) are zero, and in the fed-batch reactor $v_{\mathrm{e}}\mathbf{c}_{\mathrm{e}}$ is zero, but V is a function of time t, and most of the variables in $\mathbf{c}$ change with time, although we often desire to use a fed-batch strategy where s is constant.

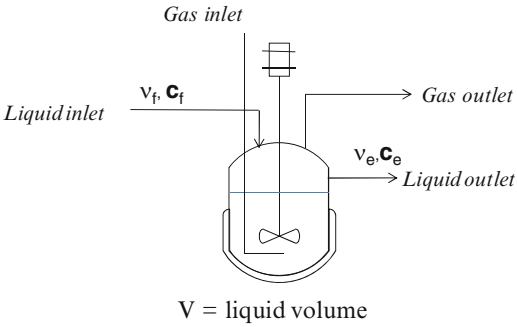

Fig. 9.1 Schematic representation of the stirred tank reactor

In a CSTR with cell retention x_e is different from x, the cell concentration in the reactor, while the other components of $\mathbf{c}_e$ have the same values of $\mathbf{c}$ as in the reactor.

In Sect. 9.1, we study (9.1) when $\dfrac{d(V\mathbf{c})}{dt} = 0$, i.e., the steady state.

9.1.1 The Standard CSTR with $\mathbf{v}_f = \mathbf{v}_e = \mathbf{v}$

This is the reactor and the operation modes which have so often been used in the examples of the previous chapters to obtain the rate data. The control strategy to obtain steady-state conditions in the continuous flow reactor has usually been to maintain the dilution rate D at a constant value by manipulating the flow rate v to keep V or the weight of the medium in the reactor as constant, i.e., chemostat operation.

$$\mathbf{q}^t + \mathbf{q} + D(c_f - \mathbf{c}_e) = 0. \tag{9.2}$$

In steady-state calculations, the reaction rates $\mathbf{q}$ can certainly be represented by the unstructured kinetic models of the Monod type, (7.16), (7.18)–(7.20), perhaps with the addition of a maintenance term as discussed in Sect. 7.3.2, (7.25)–(7.26). In Sects. 9.1.1–9.1.3, $\mathbf{c}_e$ will be equal to the values of $\mathbf{c}$ which are used in the calculation of $\mathbf{q}$, and when D and the parameters of $\mathbf{q}$ and $\mathbf{q}^t$ are fixed, the only dependent variables in (9.2) are the components of $\mathbf{c}$.

In Sect. 9.1.4, the condition $\mathbf{c} = \mathbf{c}_e$ will be relaxed, and a new design problem appears.

For $x_f = p_f = 0$, the design model for the CSTR with maintenance included is:

$$q_x = \mu\, x = \mu_{max} \frac{s}{s + K_s} x = Dx, \tag{9.3}$$

$$q_s = -Y_{xs}\mu x = -D(s_f - s) = -(Y_{xs}^{true} D + m_s)x, \tag{9.4}$$

$$q_p = Y_{xp}\mu x = Dp = (Y_{xp}^{true} D + m_p)x, \tag{9.5}$$

$$D = \mu = \mu_{\max}\frac{s}{s + K_s}, \quad X = \frac{S(1-S)}{S + b(S+a)}, \quad P = \frac{S + b_1(S+a)}{S + b(S+a)}(1-S). \quad (9.6)$$

The dimensionless variables are:

$$X = \frac{x}{s_f Y_{sx}^{true}}, \quad P = \frac{p}{s_f Y_{sp}^{true}}, \quad \text{and} \quad S = \frac{s}{s_f}. \quad (9.7)$$

The dimensionless parameters are:

$$a = \frac{K_s}{s_f}, \quad b = \frac{m_s Y_{sx}^{true}}{\mu_{\max}}, \quad b_1 = \frac{m_p Y_{px}^{true}}{\mu_{\max}}. \quad (9.8)$$

The middle of the three equations in (9.6) is the same as (3) in Example 7.2, but x is made dimensionless as defined in the first equation of (9.7). The equation for the dimensionless product concentration P in the effluent (and in the reactor) is derived by insertion the explicit expression of $X(S)$ into (9.5).

The dimensionless variables X and P have good physical interpretations: If there is no maintenance consumption of substrate leading to an added production of P, then X is the fraction of the inlet substrate converted to biomass and P is the fraction converted to product. Increasing maintenance substrate consumption corresponds to a smaller value for the *observed* yield Y_{sx} and a larger value for Y_{sp}.

The value of P decreases for increasing S when $b > 0$, and due to the factors S and $(1 - S)$ in the expression for X, the biomass concentration is 0 both for $S = 0$ and for $S = 1$. At some S between $S = 0$ and 1, X passes through a maximum. This is quite different from what happens when m_s (and hence b) is zero. Here both X and P have the value of 1 at $S = 0$ and decrease with increasing S.

Example 9.1 *Biomass and product concentrations for Monod kinetics with maintenance.* We shall return to Example 7.2 and reproduce Fig. 7.5, using the dimensionless variables X and S of (9.7). This time, the dimensionless product concentration will also be included. The kinetic and stoichiometric parameters are taken from the previously discussed example.

We assume that the (single) metabolic product obtained in Example 7.2 is CO_2. In the example, the *true* biomass yield coefficient is found to be 0.549 g biomass/g glycerol, and with the biomass composition $CH_{1.8}O_{0.5}N_{0.2}$, this converts to $Y_{sx} = 0.6842$ C-mol X/C-mol S.

The stoichiometry of the main ("true") reaction is obtained using the procedure in Chap. 3:

$$CH_{8/3}O + 0.4483\ O_2 + 0.1368\ NH_3 \rightarrow 0.6842\ CH_{1.8}O_{0.5}N_{0.2} + 0.3158\ CO_2 + 0.923\ H_2O. \quad (1)$$

Maintenance is supplied by oxidation of glycerol to CO_2:

$$CH_{8/3}O + 1.1667\ O_2 \rightarrow CO_2 + 1.3333\ H_2O, \quad (2)$$

$$\begin{aligned} Y_{sx}^{true} &= 0.6842 \times (24.6/30.67) = 0.549 \text{ g biomass/g glycerol}, \\ Y_{sp}^{true} &= 0.3158 \times (44/30.67) = 0.4531 \text{ g } CO_2\text{/g glycerol}, \\ Y_{px}^{true} &= Y_{sx}^{true}/Y_{sp}^{true} = 1.212 \text{ g biomass/g } CO_2, \end{aligned} \tag{3}$$

$$b = \frac{0.08 \times 0.549}{1} = 0.04392 \text{ g glycerol (g biomass h)}. \tag{4}$$

According to (2), consumption of 1 C-mol glycerol produces 1 mol CO_2.
Hence, $m_p = 0.08 \times 44/30.67 = 0.1147$ g CO_2/(g biomass h),

$$b_1 = 0.1147 \times 1.212/1 = 0.1390 \text{ g } CO_2\text{/(g biomass h)}. \tag{5}$$

For $D \to 0$,

$$[X, P] \to [0, b_1/b] = [0, 3.16 \text{ g } CO_2\text{/g glycerol }]. \tag{6}$$

Since $3.16\ Y_{sp}^{true} = 3.16 \times 0.3158 = 1$, we observe that the "main" reaction (1) degenerates to the maintenance reaction (2) when $D \to 0$.

Differentiation of the expression for X gives the maximum value of $X_{max}(S)$ for X:

$$X_{max} = \frac{\left(\sqrt{1+a^*} + \sqrt{a^*}\right)^2}{1+b} \quad \text{for } S = -a^* + \sqrt{a^{*2} + a^*} \text{ where } a^* = \frac{a \times b}{1+b}. \tag{7}$$

For the parameters of the example, $a^* = 0.4207 \times 10^{-4}$ and one can obtain the following:

$X_{max} = 0.964$ at $S = 64.4 \times 10^{-4}$, where $D = 0.866\ h^{-1}$.

At $S = 64.4 \times 10^{-4}$, insertion in the formula for P gives $P = 1.1045$ and $P/X = 1.146$.

Now from (9.7), $P/X = \left(Y_{sx}/Y_{sp}\right)^{true} \times (p/x) = Y_{px}^{true} \times (Dp/Dx) = Y_{px}^{true} \times Y_{xp}$.

The product of the two yield coefficients should indeed be 1 if $Y_{xp} = Y_{xp}^{true}$ which is easily confirmed when the units for the yield coefficients are harmonized:

$$P/X = (0.3158/0.6842) \times 1.212 \times (44/24.6) = 1.0006.$$

Since the ratio of P/X is 1.146 at the D value of 0.866 h^{-1}, the influence of maintenance is still observed, even at a D value which is close to $D_{max} = 1/(1 + a) = 0.999\ h^{-1}$.

Figure 9.2 shows S (~0 until $D \sim 1\ h^{-1}$), X, and P as a function of D.

The calculations done above are confirmed by the profiles shown on the figure.

When maintenance substrate consumption can be ignored, m_s (and m_p) = 0, $Y_{ij}^{true} = Y_{ij}$, and the formulas (9.6) simplify to

$$D = \mu = \mu_{max} \frac{S}{S+a}\ ;\ \ X = 1 - S\ ;\quad P = 1 - S. \tag{9.9}$$

Here, both X and P are linear functions of S, a very different behavior than that of Fig. 9.1.

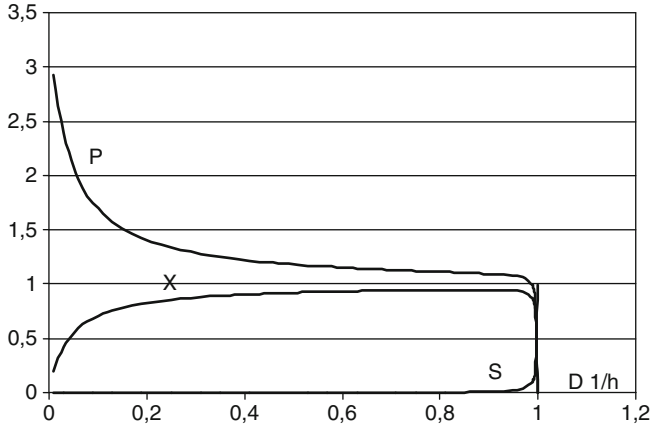

Fig. 9.2 Dimensionless substrate, biomass, and product concentrations as a function of the dilution rate. Data for biomass yield Y_{sx}^{true}, μ_{max}, K_s, s_f, and m_s are taken from Example 7.2

Again, it must be emphasized that (9.9) only holds when the feed to the STR contains neither biomass nor product. If x_f and p_f are different from 0, then instead of (9.9):

$$D(x - x_f) = \mathbf{r}_x x \text{ (where } \mathbf{r}_x = \mu_{max} \frac{s}{s + K_s} \text{ for simple Monod kinetics)}, \quad (9.10)$$

$$x - x_f = Y_{sx}(s_f - s) \text{(or } X = X_f + (1 - S) \text{ with dimensionless variables)}, \quad (9.11)$$

$$p - p_f = Y_{sp}(s_f - s) = Y_{xp}(x - x_f). \quad (9.12)$$

9.1.2 Productivity in the Standard CSTR

The productivity of the bioreactor is an important design consideration.

The productivity, i.e., the amount of a product that can be obtained per volume reactor and per unit time, q_x, q_p (or $-q_s$ when the purpose of the reaction is to get rid of an undesired substrate), determine how well the capital invested in the reactor is utilized.

From the mass balance for the steady-state continuous stirred tank:

$$-q_s = D(s_f - s), \quad q_x = D(x - x_f), \quad \text{and} \quad q_p = D(p - p_f). \quad (9.13)$$

The maximum productivity can be found by differentiating the q_i of one of the expressions in (9.13), and thereafter calculating the s value, s_{opt}, for which the derivative is zero. This s-value is either inserted in q_i to determine $(q_i)_{max}$ or it can be inserted on the right-hand side of the expressions.

It does not matter which of the q_i that is used to find s_{opt} since all the volumetric rates are connected via the constant yield coefficients Y_{si}.

Differentiation of q_i and finding zero(s) of dq_i/ds work well for simple rate expressions, i.e., when the function $f_i(s)$ in $q_i = xf_i(s)$ is not too complicated.

A direct numerical calculation of $xf_i(s)$ – where $x = x_f + Y_{sx}(s_f - s)$ – is, however, always an option. With a modern pocket calculator equipped with graphic facilities, the optimum value of $s = s_{opt}$ can be pinpointed after a few minutes work, although an exact expression for s_{opt} has inherent qualities that are not appreciated when s_{opt} is found by tabulation.

In the following, a number of analytical expressions for s_{opt} will be derived.

As a final comment to the above, it should be mentioned that optimal production is not (or almost never) obtained at (1) the smallest s value, (2) the highest value of x or p, or (3) the value where the yield coefficient Y_{sp} is highest.

At $s = 0, f(s)$ is usually 0, at $s = s_f$ the other factor, x, is zero, and although r_x or r_p, the specific productivities can be at a maximum at this point the volumetric rate is zero. For substrate-inhibited kinetics, (7.18) $r_x = \mu$ can have a maximum for some $s < s_f$, but operation near this point is a poor choice since the culture is likely to wash out.

These features will be quite clearly exposed in the following examples.

For Monod kinetics with no maintenance included and $x_f = 0$:

$$q_x = Dx = \frac{\mu_{max} S}{S + a} Y_{sx} s_f (1 - S), \tag{9.14}$$

$$\frac{q_x}{\mu_{max} Y_{sx} s_f} = \frac{S(1 - S)}{S + a}. \tag{9.15}$$

By differentiation of (9.15), one can obtain the maximum value of q_x:

$$Q = \left(\frac{q_x}{\mu_{max} Y_{sx} s_f} \right)_{max} = \left(\sqrt{1 + a} - \sqrt{a} \right)^2 \quad \text{for} \quad S_{opt} = -a + \sqrt{a^2 + a}. \tag{9.16}$$

The corresponding D value is

$$D_{opt} = \mu_{max} \frac{-a + \sqrt{a^2 + a}}{\sqrt{a^2 + a}} = \mu_{max} \left(1 - \frac{1}{\sqrt{1 + 1/a}} \right). \tag{9.17}$$

For substrate-inhibited kinetics, (7.18):

$$Q = \frac{q_x}{\mu_{max} Y_{sx} s_f} = \frac{S(1 - S)}{S + a + bS^2}; \quad b = s_f K_i^{-1}, \tag{9.18}$$

$$S_{opt} = -c + \left(c^2 + c \right)^{1/2}, \quad \text{where } c = a/(1 + b). \tag{9.19}$$

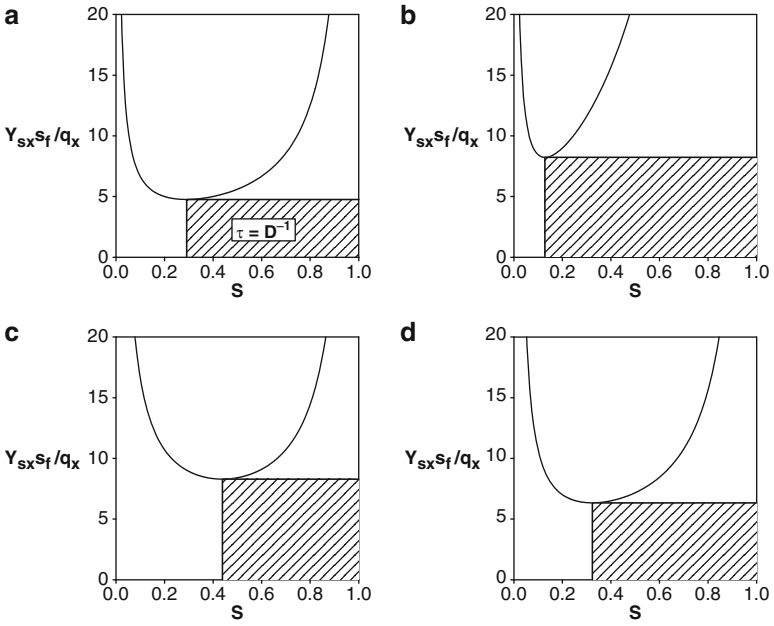

Fig. 9.3 Productivity of a steady-state stirred tank reactor. (**a**) Monod kinetics: $\mu_{max} = 0.5\ h^{-1}$, $K_s = 0.4\ g\ L^{-1}$, $s_f = 2\ g\ L^{-1}$, and $Y_{sx} = 0.5\ g\ g^{-1}$. (**b**) Substrate inhibition: as in (**a**), and $K_i = 0.25\ g\ L^{-1}$, i.e., $b = 8$ in (9.18). (**c**) Product inhibition (7.20): as in (**a**), and $s_f Y_{sp}/p_{max} = 2/3$. (**d**) Maintenance [(9.4) and (9.5)]: as in (**a**), and with $b = 0.2$ in (9.8). Hatched area: holding time τ to achieve maximum productivity. (**a**) 3.37 h; (**b**) 7.17 h; (**c**) 4.69 h; (**d**) 4.29 h

For product inhibition with the kinetics (7.20):

$$Q = \frac{S(1-S)\ (1-d\ (1-S))}{S+a}\,, \quad \text{where } d = Y_{sp}s_f/p_{max}. \tag{9.20}$$

And finally for simple *Monod kinetics with maintenance* included as in Example 9.1:

$$Q = \frac{S^2(1-S)}{(S+a)\ (S+b(S+a))}\,. \tag{9.21}$$

Analytical solutions for S_{opt} are stated for both the simple Monod kinetics and for Monod kinetics with substrate inhibition, but in Fig. 9.3 a graphical representation of the optimization problem for q_x is given for all four kinetic expressions listed above.

The values for μ_{max}, K_s, s_f, and Y_{sx}^{true} are the same [$0.5\ h^{-1}$, $0.4\ g\ L^{-1}$, $2\ g\ L^{-1}$, and $0.5\ g\ X\ (g\ S)^{-1}$]. The extra parameters for cases b, c and d are given in the figure caption. K_s is much higher than the values stated in Table 7.1, but for a much smaller s_f, say $s_f = 0.15\ g\ L^{-1}$, the same value for $a = K_s/s_f$ as used on Fig. 9.3 would be obtained for a reasonable K_s.

For the values of s_f used in practical cultivations, say $s_f = 50$ g L^{-1}, the value of $(q_x)_{max}$ is found at a value of S that is very close to 0 (see (9.16)) and one probably needs to consider the influence of maintenance, i.e. (9.21) rather than (9.15).

In baker's yeast production or in production of a growth-associated protein such as insulin from yeast (see Example 7.4) one needs to work at a D value close to D_{crit} (=0.25 h^{-1} in Example 3.5) to have the highest q_x and yet avoid ethanol formation. Severe process control problems are associated with this choice (Andersen et al. 1997).

In Fig. 9.3, $Y_{sx}s_f/q_x$ has been plotted against S, and the minimum of the curve corresponds to the maximum productivity. Thus, in Fig. 9.3a, the minimum of the curve is obtained from (9.14), (9.15): $S = -0.2 + \sqrt{0.24} = 0.29$, and $(q_x)_{max}/(\mu_{max}s_fY_{sx}) = 0.29 \times 0.71/0.49 = 0.42$, i.e., $s_fY_{sx}/(q_x)_{max} = (0.42\ \mu_{max})^{-1} = 4.76$ h as also seen in the figure.

The reason why μ_{max} is separated out is that the hatched rectangles on the figures will now have an area equal to D^{-1} = the holding time τ, to obtain a certain value of S, as indicated on the abscissa:

$$q_x = DY_{sx}(s_f - s) \rightarrow D^{-1} = \tau = (1 - S) \times (s_fY_{sx}/q_x)^{-1}. \tag{9.22}$$

To obtain the maximum productivity the rectangle which touches the curve at S_{opt} is obviously that for which τ is smallest. In this way, the optimization problem has a nice graphical solution using the choice of plotting in Fig. 9.3.

Any solution in which S_{opt} is reached by the application of several sequentially coupled CSTR will obviously have a higher total holding time τ, and hence a lower productivity than the single CSTR designed as described above.

If a final substrate concentration S_{final}, smaller than S_{opt} is desired, the one-CSTR solution is not the best. As discussed in Sect. 9.4, the highest overall productivity is obtained if a PFR is used downstream of a CSTR which brings S down from 1 to S_{opt}. In the PFR, the substrate concentration is further reduced from S_{opt} to S_{final}.

The futility of trying to obtain a high productivity at an S value where $r_x = \mu$ is maximum is illustrated by the substrate-inhibited kinetics

$$\mu = \frac{\mu_{max}s}{s^2/K_i + s + K_s} = \frac{\mu_{max}S}{bS^2 + S + a}. \tag{9.23}$$

$$a = \frac{K_s}{s_f}\ ; \quad b = \frac{s_f}{K_i}.$$

$\mu(S)$ has an extremum:

$$\mu_{extr} = \frac{\mu_{max}}{2\sqrt{ab} + 1} = \frac{\mu_{max}}{2\sqrt{K_s/K_i} + 1} \quad \text{at} \quad S_{extr} = \sqrt{\frac{a}{b}} = \frac{\sqrt{K_iK_s}}{s_f}. \tag{9.24}$$

Since μ is an increasing function of S for $0 < S < S_{\text{extr}}$, the maximum dilution rate is obtained from one of the two expressions in (9.25):

$$D_{\max} = \begin{cases} \mu_{\text{extr}}, & \text{when } a/b \leq 1, \\ \mu_{\max}/(b+1+a), & \text{when } a/b \geq 1. \end{cases} \tag{9.25}$$

For $a/b < 1$ and $\mu_{\text{extr}} < D$ ($S = 1$), operation near $D = \mu_{\text{extr}}$ is extremely dangerous since, as we shall see in Sect. 9.3.3, any perturbation that increases S to a value $> S_{\text{extr}}$ eventually leads to wash-out of the culture. The maximum productivity is found for an S value between 0 and S_{extr} given by (9.24). The correct S_{opt} is stated in (9.19).

The value of μ_{extr} is independent of s_{f}, while for any given value of the kinetic parameters K_i and K_{s}, it is seen that S_{extr} is inversely proportional to s_{f} (whereas, of course, s_{extr} is independent of s_{f}).

When $a/b > 1$, $D_{\max}$ is at $S = 1$, and operation at $D_{\max}$ leads to wash-out, irrespective of the kinetic expression for the specific growth rate μ.

9.1.3 *Productivity in a Set of Coupled, Standard CSTR's*

The standard CSTR is, as argued in previous Sect. 9.1.2, the best choice of reactor if high productivity is desired. The production strain must be stable, and the sterilization of the feed must be strictly controlled to avoid infection over the desired, very long continuous operation period – otherwise enormous losses will be incurred, not only by the loss of perhaps 400 m^3 cultivation, but also by the clean up of the discarded reactor content in a waste water treatment plant.

The good properties of the standard CSTR are explained by the nature of bioreaction kinetics: For $S > S_{\text{crit}}$, the reaction is of negative order in the substrate concentration, i.e., the volumetric reaction rates $\mathbf{q}$ increase with decreasing s. In this situation, a standard CSTR is superior to *any* other type of reactor, and the extensive use of, e.g., fed-batch cultivation is due to worries about long-time stability of the cultivation as discussed above.

When the substrate level has to be reduced to below S_{opt}, a set of sequentially coupled CSTR will do a fine job. Sequential or parallel coupled CSTR can, in general, improve the productivity when the feed input varies in time, and especially this design option provides a good insurance against wash-out after a process upset. This is the only inherent weakness of the CSTR compared to batch operation.

In the following example (Example 9.2), it is shown that how optimal solutions can be obtained by diligent use of the almost infinite variations that are offered by CSTR combinations.

Example 9.2 *Design of a robust waste water treatment plant.* Assume that a substrate with an undesirable (limiting) component S is treated in a waste water pond.

The kinetics of the reaction is:

$$r_x = \mu = \frac{4}{3}(\mathrm{h}^{-1})\frac{s}{s + 4(\mathrm{mg\ L}^{-1})}, \tag{1}$$

$Y_{sx} = 0.1$ g biomass (g substrate)$^{-1}$ and $s_f = 60$ mg L^{-1}.

If the design objective is to remove as much as possible of the substrate S per m^3 reactor, the effluent concentration s is calculated from (9.16):

$$S_{opt} = -\frac{1}{15} + \sqrt{\left(\frac{1}{225} + \frac{1}{15}\right)} = \frac{1}{5} \text{ or } s = 12 \text{ mg L}^{-1}. \tag{2}$$

$$(q_x)_{max} = (4/3) \times 0.1 \times 60 \times \frac{0.2 \times 0.8}{0.2 + 1/15} = 4.8 \text{ mg L}^{-1}\text{h}^{-1} \text{ and}$$
$$(-q_s)_{max} = 48 \text{ mg L}^{-1}\text{h}^{-1}, \tag{3}$$

$$D_{opt} = \frac{4}{3}\left(1 - \frac{1}{\sqrt{(1 + 15)}}\right) = 1\mathrm{h}^{-1}. \tag{4}$$

Thus, if the waste water plant receives a constant feed $v = 1$ m^3 h^{-1} with $s_f = 60$ mg L^{-1} and it is permitted to send treated water with 12 mg L^{-1} to the environment, the reactor should be designed with a volume $V = 1$ m^3.

If s_f fluctuates around 60 mg L^{-1}, one may sometimes emit treated water with more than 12 mg L^{-1} of the pollutant, but the plant will never fail in a catastrophic way. Thus, if the inlet pollution level increases to $s_f = 100$ mg L^{-1}, the effluent concentration will at first increase above 12 mg L^{-1}, but now the biomass concentration increases from 4.8 mg L^{-1} until it reaches a level of $0.1 \times (100 - 12) = 8.8$ mg L^{-1}. At the same time, the effluent S concentration slowly reverts to 12 mg L^{-1}.

The reason is, as pointed out in Sect. 7.3.1, that the simple Monod kinetics (7.16) does *not* depend on the feed concentration s_f, and an increase of s_f does not lead to a new value for s, but only to a new value for x. The transient is illustrated in Fig. 9.8.

Substrate inhibition kinetics (7.18) is also independent on s_f, but product inhibition kinetics [(7.19) or (7.20)] depends on s_f through the product concentration p which increases with x.

The disaster happens if, due to a sudden process upset, e.g., caused by a rainstorm, the feed volume v increases for some period of time to more than 1.25 m^3 h^{-1}. Now, in the 1 m^3 reactor, $D > D_{max} = (4/3) \times (60/(60 + 4)) = 1.25$ h^{-1}, and the biomass sludge starts to wash out exponentially as shown in Fig. 7.13. Since rebuilding biomass in a waste water plant is a slow process, the productivity of the plant will remain low for quite some time, even if the culture is not completely washed out.

One precautionary measure is to install a stand-by CSTR besides the 1 m^3 reactor.

Assume that the *highest* possible inlet flow anticipated is 2.5 m^3 h.

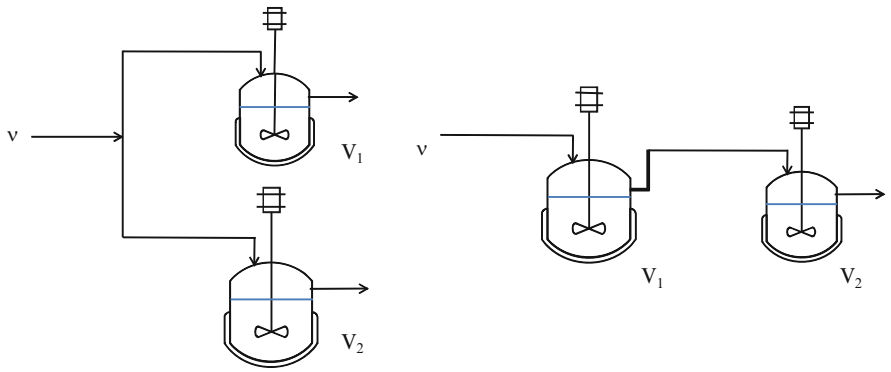

Fig. 9.4 Two different ways of coupling two STR

How should the new tank with volume V_1 be operated together with the original tank of volume $V = V_2 = 1\ \mathrm{m}^3$, and what should be the value of V_1 to safeguard against the event that $v = 2.5\ \mathrm{m}^3\mathrm{h}^{-1}$?

There are two immediate options: The tanks could be operated in parallel or in series as shown on Fig. 9.4.

(a) If the two reactors operate in parallel, the new tank should have the volume $V_1 = 1.5\ \mathrm{m}^3$, and the flow to V_1 and V_2 should be distributed in the ratio 1.5:1. Now both tanks operate optimally, and 48 mg L^{-1} h^{-1} S is removed in both tanks, i.e., 120 mg pollutant is removed per hour.

For $1 < v < 2.5\ \mathrm{m}^3\ \mathrm{h}^{-1}$, one may still distribute the feed to the two tanks and thereby achieve a smaller s, but the combination of tanks does not work with optimum productivity, and the cost of operating two tanks may exceed the benefit of obtaining a smaller s.

(b) The two tanks may also be installed in series. Which tank should be first, and what should be the volume of V_1 to obtain maximum productivity?

Clearly V_1 should be the first tank since the 1 m^3 tank could never work with $v = 2.5\ \mathrm{m}^3\ \mathrm{h}^{-1}$.

The design of the system must be done iteratively. Thus, one may guess the value of V_1, and a mass balance for tank 1 will give the concentrations $[s_1, x_1]$ between the tanks. Now x_2 is calculated based on a mass balance for the second tank V_2 of known volume 1 m^3. Alternatively, one may start by guessing x_2 and working backwards to find V_1.

The second design method is the easiest and it consists of the following steps:

1. Assume that the outlet biomass concentration x_2 from the 1 m^3 tank is 5.5 mg L^{-1} (any value below 6 mg $\mathrm{L}^{-1} = 0.1 s_\mathrm{f}$ could be chosen). The effluent substrate concentration is $s_2 = 60 - 55 = 5$ mg L^{-1}.
2. Now the biomass concentration x_1 in the inlet to the 1 m^3 tank can be calculated:

$$(4/3) \times (5/(5+4)) \times 5.5 = 2.5 \times (5.5 - x_1) \rightarrow x_1 = 3.87\ \mathrm{mg\ L}^{-1}. \quad (5)$$

In (5), we have used (9.10) instead of (9.3), since x_f to the 1 m^3 tank is different from zero.

Knowing x_1, the corresponding value $s = s_1$ is calculated as $60 - 38.7 = 21.3$ mg L^{-1}.

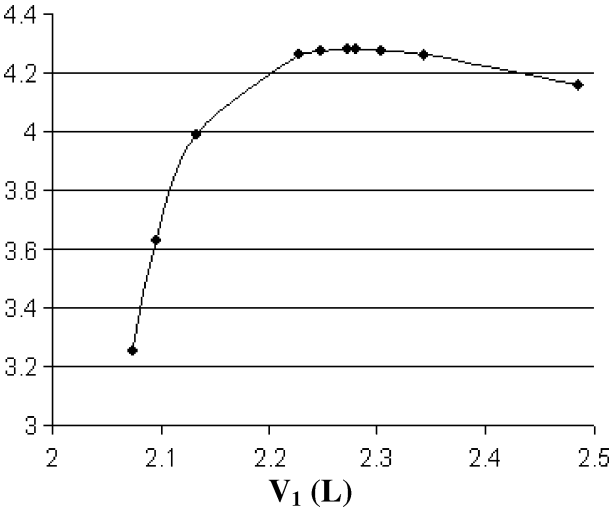

Fig. 9.5 Optimal design of the first tank V_1 in a two-tank sequence

3. The dilution rate D_1 for the first tank is calculated from (9.6) since $x_f = 0$ for the first tank.

   $D = 2.5/V_1 = (4/3) \times 21.3/25.3 = 1.1225\ \mathrm{h}^{-1}$, and one finally obtains $V_1 = 2.5/1.1225 = 2.23\ \mathrm{m}^3$.

   The design procedure, (1)–(3), is repeated for other values of x_2 until the smallest value is found for the objective function.

$$\Omega = 2.5\ x_2 \left(V_{\text{total}} = V_1 + 1\mathrm{m}^3\right)^{-1}. \tag{6}$$

   There is no need to extend the search for the best value of V_1 outside the interval $[2, 2.5]\ \mathrm{m}^3$.

   If V_1 is smaller than $2\ \mathrm{m}^3$, the first tank will also wash out, and if $V_1 > 2.5$ the first tank works at suboptimal productivity.

   If the design process starts by guessing V_1, one ends up by calculating x_2 and $\Omega = 2.5\ x_2/(V_1 + 1)$.

   Since q_x is not monotonous in s, but allows two different s values to give the same q_x (see Fig. 9.5), one has to solve a quadratic to find $[s_1, x_1]$. The work is harder, and one must choose the right s_1.

   The highest productivity reached by the sequential reactor design is $43\ \mathrm{mg\ L}^{-1}\ \mathrm{h}^{-1}$ substrate removed, and this is smaller than the $48\ \mathrm{mg\ L}^{-1}\ \mathrm{h}^{-1}$ removed with the parallel reactor design (**a**).

   But the $43\ \mathrm{mg\ L}^{-1}$ is a result of a suboptimal design applied for the sequential reactor system where *another* design variable, *the feed split f*, between the reactors has not yet been implemented.

(c) Split the $2.5\ \mathrm{m}^3\ \mathrm{h}^{-1}$ feed stream in the ratio 1:1.5, and let $1\ \mathrm{m}^3\ \mathrm{h}^{-1}$ pass through the $1\ \mathrm{m}^3$ reactor, while the remaining $1.5\ \mathrm{m}^3\ \mathrm{h}^{-1}$ rejoins the flow between the two reactors.

Just before entering V_1, the biomass composition $[x_1, s_1]$ is given by:

$$x_1 = (1 \times 4.8 + 1.5 \times 0)/2.5 = 1.92 \text{ mg L}^{-1} \quad \text{and}$$
$$s_1 = (1 \times 12 + 1.5 \times 60)/2.5 = 40.8 \text{ mg L}^{-1}. \tag{7}$$

If we demand that the composition after the second tank is $[x_2, s_2] = [4.8, 12]$ mg L^{-1}, the volume V_1 of the second reactor can be calculated from (9.10):

$$(4/3) \times 12 \times 4.8/(12 + 4)V_1 = 2.5(4.8 - 1.92) \rightarrow V_1 = 1.5 \text{ m}^3. \tag{8}$$

Obviously, the sequential reactor system with split feed gives the same optimal productivity as the parallel arrangement of the two reactors in (**a**). The same result is, of course, obtained if the 1.5 m^3 is first and is fed with 1.5 m^3 h^{-1} of the total feed to the system.

The sequential reactor system with $V_1 = 1.5$ m^3 has the added advantage that it also works when the feed flow increases above 2.5 m^3 h^{-1}. The *overloaded* system will now be analyzed.

Intuitively, one would like to choose the split f such that the first reactor operates at maximum productivity, and also one would think that it does not matter which reactor is first.

Assume that $v = 3$ m^3 h^{-1}.

With $V_1 = 1.5$ m^3 placed first and fed with 1.5 m^3 h^{-1}, the composition of the stream entering the 1 m^3 reactor is $[x_1, s_1] = [2.4, 36]$ mg L^{-1}. The effluent from the 1 m^3 reactor has the composition $[x_2, s_2]$ calculated as follows:

$$\frac{x(60 - 10x)}{60 - 10x + 4} \times \frac{4}{3} \times 1 = 3(x - 2.4) \rightarrow x$$
$$= 3.84 \text{ mg L}^{-1} \big(\text{and the infeasible solution } x = 7.2 \text{ mg L}^{-1}\big).$$

$$\text{Hence } [x_2, s_2] = [3.84, 21.6] \text{ mg L}^{-1} \tag{9}$$

Next the 1 m^3 tank is placed first, and 2 m^3 h^{-1} of $v = 3$ m^3 h^{-1} is fed between the two reactors.

$$[x_1, s_1] = [1.6, 44] \text{ mg L}^{-1} \text{ and } [x_2, s_2] = [3.70, 23] \text{ mg L}^{-1}.$$

We conclude that intuition failed us. Except if both reactors work at maximum productivity, it does matter which reactor is first, when the "maximum productivity in the first reactor" strategy is followed. Apparently, it is best to have the large reactor first to give much biomass to the seriously overloaded small reactor which is placed last.

One may fiddle further with the optimization problem, and perhaps send slightly more feed through the first, large reactor to help the small, second reactor to perform better – see Problem 9.1.

But the main message is that *the combination of two smaller reactors in series is able to handle a serious overload situation that one large reactor with the combined volume of the two reactors could not handle*.

In the opposite situation in which the load on the reactor system is smaller than the design value, a similar optimization problem appears. It certainly looks advantageous to have the small reactor first in which case one may bring the substrate concentration in the effluent much below the design value.

In a situation where v fluctuates significantly around the design value, one may contemplate to switch the entry point to the system from the large reactor ($v > v_{\text{design}}$) to the small reactor ($v < v_{\text{design}}$), a strategy that reduces the surge in effluent S in an overload situation and gives a fine performance of the system in the under-load situation.

Example 9.2 illustrates that an imaginative combination of CSTRs can lead to optimization of design problems of considerable economic value, both in terms of quality of the process and in terms of low operating costs.

The design may aim to optimize production of a particular metabolite, to minimize fluctuations in product quality, or to minimize the risk of strain mutation. Different strategies will have to be used for different kinetic expressions (product inhibition and substrate inhibition, or a change of kinetics for a certain D – as experienced in aerobic yeast fermentation), and the basic tank reactors can be combined with biomass recirculation or with the removal of an inhibitory product by membrane filtration.

In any situation, the optimization problems introduced here and in the previous and following sections illustrate that engineering intuition and engineering tools play an independent role in bioengineering when it comes to reaping the fruits of biology.

9.1.4 Biomass Recirculation

We have seen that for the given fermentation kinetics (with or without maintenance) and for a given feed composition, it is possible to calculate the complete effluent composition based on a single measured quantity. This may be either the dilution rate or the concentration of substrate, biomass, or product in the effluent. If in (9.2) an extra degree of freedom is introduced by relaxation of the assumption that the biomass concentration x_e in the effluent is equal to the biomass concentration x in the reactor, then a new set of design problems arises. For all other reactants and products, the assumption of ideal homogeneity of the STR is maintained, but the value of D that corresponds to the given feed and effluent concentrations will now depend also on x_e. When $x > x_e$, the reactor is able to process more feed than in the basic situation with $x = x_e$ since the rate of biomass formation is proportional to x.

Enrichment of the reactor medium relative to the effluent stream can be achieved by means of a cell centrifuge installed after the reactor and *recirculation of cells* to the inlet of the reactor through an exterior loop. The same effect can also be obtained by means of a filter installed in parallel with the reactor – typical online probes for the removal of cell-free medium to analysis are extreme cases of complete cell-medium separation.

The cells may undergo a partial sedimentation in the reactor. Cells immobilized on granules of inactive carrier material such as sand particles or flocs of microorganisms are typical examples. Finally, a more-or-less loose wall growth of cells leads to enrichment of cells in the reactor, but cells growing on the walls or on granules may exhibit different kinetic behavior than that determined with freely suspended cells.

With maintenance-free Monod type kinetics and $x_f = p_f = 0$, (9.3)–(9.5) are modified to:

$$Dx_e = \mu x, \tag{9.26}$$

$$D(s_f - s) = Y_{xs}\mu x, \tag{9.27}$$

$$Dp = Y_{xp}\mu x. \tag{9.28}$$

Equation (9.26) is a total biomass balance for the reactor: Biomass produced is removed in the effluent. s and p have the same values in the reactor and in the effluent.

Define $f = x_e/x$. $f < 1$ since $x_e < x$ when some cells are recirculated as in Fig. 9.4.

$$Df = \mu. \tag{9.29}$$

The substrate and product balances are:

$$D(s_f - s) = Y_{xs}Df\frac{x_e}{f} \quad \text{or} \quad x_e = Y_{sx}(s_f - s) = Y_{sx}(s_f - s_e). \tag{9.30}$$

$$Dp = Y_{xp}Df\frac{x_e}{f} \quad \text{or} \quad p_e = p = Y_{sp}(s_f - s_e). \tag{9.31}$$

Equations (9.30) and (9.31) show that the overall mass balances for x_e and $p = p_e$ are identical with those of (9.4)–(9.5). The cell-enrichment model differs from the basic model in one respect only: For a given value of D, it is possible to obtain *any* specified value of μ or effluent composition $(s_e,\ x_e, p_e)$ by a suitable choice of f in (9.29).

We shall now relate f to the operating variables of a cell-recirculation design. In Fig. 9.6a, a hydro-cyclone separates the effluent from the reactor into a product stream v and a recirculation stream Rv, where R is the *recirculation factor*. The cell concentration is x_R in the recirculation stream, and $x_R = x\beta$, where $\beta > 1$. Neither product concentration nor substrate concentration is affected by the hydro-cyclone.

A mass balance for cells at the hydro-cyclone gives

$$v(1 + R)x = vx_e + Rvx_R \tag{9.32}$$

or

$$1 + R = f + R\beta \quad \text{or} \quad f = 1 - R(\beta - 1). \tag{9.33}$$

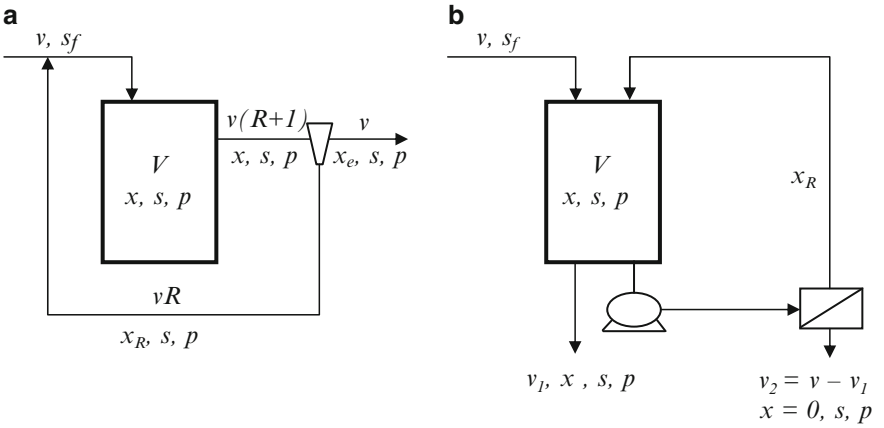

Fig. 9.6 Biomass recirculation using a hydro-cyclone (**a**), and an ultrafilter (**b**). In (**b**), the permeate $v_2 = v - v_1$ is cell free. The bleed stream v_1 is taken from the reactor

The fraction of cells sent back to the reactor is

$$\alpha = \frac{Rvx_R}{v(1+R)x} = \frac{R\beta}{1+R}. \tag{9.34}$$

The cell concentration in the reactor is

$$x = \frac{x_e}{1 - R(\beta - 1)}. \tag{9.35}$$

Next, consider the ultrafiltration version in Fig. 9.6b:
A mass balance for biomass is

$$V\mu(s)x = v_1 x \quad \text{or} \quad \mu = v_1/V = (v - v_2)/V = D(1 - \Omega). \tag{9.36}$$

Ω is the filter separation factor defined as v_2/v, and $D = v/V$ as usual.

It is seen that unit B can work at a dilution rate $(1 - \Omega)^{-1}$ higher than the ordinary continuous stirred reactor for which $D(\Omega = 0) = \mu$. Since μ is usually the same with or without recycling of biomass, the biomass productivity is increased by a factor $(1 - \Omega)^{-1}$. The biomass appears in a small stream $v_1 = (1 - \Omega)\, v$, and with a much higher concentration $x = x(\Omega = 0) \times (1 - \Omega)^{-1}$ than without recycling. A metabolic product is in a cell-free stream v_2, ready for downstream processing. Also here the productivity has increased by a factor $(1 - \Omega)^{-1}$ if the biomass and product from v_1 can be retrieved. If the stream v_1 is regarded as waste, the productivity of P is increased by a factor $\Omega(1 - \Omega)^{-1}$.

We can shortly describe the functioning of the cell-recirculation set-up as follows:

μ and consequently the effluent concentrations of substrate and product, which are both functions of μ alone, are chosen by the designer of the reactor at values

which are optimal by some criterion – it may be that a low effluent s-value is needed or the yield of product may be small if s is too high. To obtain a satisfactory volumetric production, rate recirculation by either scheme A or scheme B is chosen. The two design parameters (f in A and Ω in B) are chosen such that the value of D (chosen to satisfy a given production criterion) matches the desired value of μ. In both schemes, the higher productivity is due to the higher cell density in the reactor. This result is at least in theory independent of whether there is a loss of substrate due to maintenance. Certainly more substrate is "lost" due to maintenance, but at the same time a much larger feed stream has been treated in the system. Relatively speaking the same percentage of substrate is "lost" (the maintenance loss depends only on μ).

The stress on the cells caused by rapid pumping of medium through the recirculation loop and the filter may, however, give an independent contribution to the maintenance demand of the cell. In that case, the recirculation solution may be at a disadvantage. Otherwise, the only negative aspect of cell recirculation is that the pumping costs may outweigh the savings in capital investment for the reactor. This situation is illustrated in Example 9.5.

Cell recirculation is a standard feature of aerobic waste water plants. The sludge is pumped back from settling tanks to the bioreactor. Also anaerobic water treatment units can benefit greatly from cell recirculation. Often the cell density is small (the culture does not thrive unless the feed concentration of, especially a toxic, substrate is low).

In cultivations with heavy product inhibition, cells may be sent back to the reactor from the effluent – possibly after removing the product by membrane separation (pervaporation if the product is volatile), by vacuum distillation, or by some other means.

Low cell density suspended plant- or animal-cell cultures can greatly profit by cell recirculation. Very mild processes must, however, be used to protect the fragile cells.

Cell retention mammalian cell cultures using *Perfusion bioreactors* were developed in the 1980s. The products, e.g., monoclonal antibodies or complex glycoproteins, are excreted to the medium. To the perfusion reactor, a more or less constant stream of sterile filtered substrate is fed, e.g., through a pressure-supported hollow fiber membrane module, and an equal volume of medium is sucked out in another hollow fiber module. The effluent containing the product is downstreamed in batches.

The early industrial-scale perfusion reactors had a high failure rate due to insufficient control of the feed quality and inability to avoid strain deterioration due to mutations and loss of viability in the long production campaign (often 6–8 weeks) promised by the continuous cultivation concept. Therefore, fed-batch cultivation (Sect. 9.2.2) came to dominate the industry. Now much better process control algorithms are available, and intensive research is being done to increase the stability of the production strains. This has brought back large-scale perfusion cultivation as a good alternative to fed-batch cultivation in the production of pharmaceutical proteins (see, e.g., http://www.cmcbio.com).

In perfusion cultures, the cells are well protected from toxic metabolic products. These will remain in the fed-batch cultivation throughout the 15 days of cultivation, whereas they are continuously removed from the perfusion reactor.

The full advantage of high productivity due to the constant operation at optimal process conditions and to the high cell density permitted in perfusion cultures can now be obtained.

Example 9.3 *Design of cell recirculation system.* It is desired to process 1 $m^3\ h^{-1}$ of a feed with $s_f = 4$ g L^{-1} of the growth-limiting substrate. Assume Monod kinetics with $K_s = 1$ g L^{-1} and $\mu_{max} = 1\ h^{-1}$. $Y_{sx} = 0.5$ g g^{-1} of substrate. The reactor volume is 500 L. What is the maximum cell productivity with and without cell recirculation?

1. $x = x_e$: $D = 1/0.5 = 2\ h^{-1}$, and since $a = K_s/s_f = 0.25$ and $\mu_{max} = 1\ h^{-1}$, the productivity is zero because $D > \mu_{max}/(a + 1) = 0.8\ h^{-1}$.
2. $x > x_e$: To avoid wash-out, Df must be smaller than 0.8 h^{-1} and, consequently,

$$f = 1 - R\ (\beta - 1) < \frac{0.8}{2} = 0.4. \tag{1}$$

The maximum productivity is, of course, obtained when $S = 0$, i.e., when $x_e = s_f \times Y_{sx} = 2$ g L^{-1} and $(q_x)_{max} = Dx_e = 2 \times 2 = 4$ g L^{-1} or 2 kg h^{-1} in a 500-L reactor. When $S \to 0$, the specific growth rate tends to zero, and from (9.29) with a given $D = 2\ h^{-1}$, one can obtain $f \to 0$, which means that the reactor cell concentration $x \to \infty$. This is not a feasible solution.

To illustrate the remaining calculations, choose $S = 0.309$, for which $\mu = 0.553\ h^{-1}$ and, consequently,

$$f = 1 - R\ (\beta - 1) = \frac{\mu}{D} = 0.276. \tag{2}$$

The biomass concentration in the effluent is

$$x_e = 4 \times 0.5\ (1 - 0.309) = 1.382\ \text{g}\ L^{-1}, \tag{3}$$

$$q_x = Dx_e = 2.764\ \text{g}\ L^{-1}h^{-1} \text{ or } 1.38\ \text{kg}\ h^{-1}. \tag{4}$$

The cell concentration in the reactor is

$$x = \frac{x_e}{f} = 5.01\ \text{g}\ L^{-1}. \tag{5}$$

The fraction of cells that are recirculated depends on the effectiveness of the cell separator. Thus, for $R = 2$, one can obtain $\beta = 1.36$ and $\alpha = 90.8\%$. The cell concentration in the recycle loop is $x_R = \beta x = 6.81$ g L^{-1}. For a less efficient operation of the centrifuge, $R = 3$, one can obtain $\beta = 1.24$, $\alpha = 93.1\%$, and $x_R = 6.21$ g L^{-1}.

Example 9.4 *Design of a recirculation system – with maintenance requirement.* Here, the influence of maintenance on the solution of the optimal productivity problem is studied. Take $m_s = m_p = 0.1\ h^{-1}$ and $Y_{sp}^{true} = Y_{sx}^{true} = 0.5$. All other kinetic and operational parameters are as in Example 9.3. The maximum cell density X_{max} is calculated as in Example 9.1

$$X_{max} = \frac{1}{b+1}\left(\sqrt{1+a^*} - \sqrt{a^*}\right)^2 = 0.7660, \tag{1}$$

$$S_{max,x} = -a^* + \sqrt{a^{*2} + a^*} = 0.09785. \tag{2}$$

Since D is given ($= 2\ h^{-1}$), the maximum productivity is obtained for $X = X_{max}$.

$$(q_x)_{max} = DX_{max}s_f Y_{sx}^{true} = 2 \times 0.7660 \times 4 \times 0.5 = 3.06\ g\ L^{-1}\ h^{-1}, \tag{3}$$

$(q_x)_{max}$ is obtained for $\mu = 0.2813\ h^{-1}$, $f = 0.1406$, and $x = 0.7660 \times 0.5 \times 4/0.1406 = 10.90\ g\ L^{-1}$. For $R = 2$, the value of β is calculated from (9.33). $\beta = 1.43$ and $x_R = 15.58\ g\ L^{-1}$. $\alpha = 95.3\%$ of the cells that are recycled. The recycle stream is much thicker than is the case for the corresponding maintenance-free example.

Example 9.5 *Design of an integrated lactic acid production unit.* A total of 4.5 wt% lactose in a waste stream from a large cheese factory is to be converted to lactic acid in a stirred tank continuous reactor. The feed stream is 15 $m^3\ h^{-1}$ to which enzymatically hydrolyzed whey protein is added as nitrogen source. A high yield of lactic acid on lactose is not a requirement per se, but the product is going to be used as the monomer for the production of polylactate, and to avoid prohibitory downstream costs it is necessary to convert almost all the sugar, and at the same time to work with a high enough D value to avoid the formation of byproducts (the "mixed acids" of Example 5.1). The choice of a continuous process is obligatory. Otherwise the value of the product (88 wt% polymer grade lactic acid) will not match the cost of raw materials, labor, and energy.

The feed is sterile, and in a conventional CSTR, the effluent product concentration is p. The reactor volume is 10 m^3.

In an ultrafilter cell-recirculation system, the separation factor Ω is chosen to be 0.9, and v_1 and v_2 are 1.5 and 13.5 $m^3\ h^{-1}$, respectively.

A conservatively designed ultrafilter supports a flux $J = 10\ L\ m^{-2}\ h^{-1}$, and consequently the required filter area is 1,350 m^2.

From an ultrafilter brochure, one can obtain the information that the necessary volumetric flow to the filter in order to sustain a flux $J = 10\ L\ m^{-2}\ h^{-1}$ through the filter is 0.74 m^3 $(m^2\ filter)^{-1}$. Hence, a recirculation flow of $0.74 \times 1{,}350 = 1{,}000\ m^3\ h^{-1}$ is needed.

Assume that a pressure drop of 4 bar $= 4 \times 10^5$ Pascal across the filter is needed to support the flux and that the pump has a mechanical efficiency of 65%. Then the energy input is

$$4 \times 10^5 (0.65 \times 3{,}600)^{-1} \times 1{,}000\ W = 171\ kW.$$

The reactor capacity has been increased by a factor of 10 by cell recirculation, but at the cost of a considerable energy input.[1] A filter must be installed anyhow in order to separate the product stream from the biomass and remaining proteins, but a conventional drum filter working on only 15 $m^3\ h^{-1}$ is bound to be cheaper than an ultrafilter treating 1,350 $m^3\ h^{-1}$.

9.1.5 *Steady-State CSTR with Substrates Extracted from a Gas Phase*

Having discussed many variations of steady-state cultivation of a single organism in a CSTR, we finally need to study the influence of transport of one or several reactants from a gas phase to the medium.

This means that the term $\mathbf{q}^t$ in (9.2) must be included.

Mass transfer from the gas phase to the liquid reaction medium was introduced already in the introduction (3.1.1) of Chap. 3, and the rate constant $k_l a$ for mass transport (same unit as the specific growth rate) was found from experiments as discussed in Example 3.4.

With the very low solubility of gases like O_2 and CH_4, the rate of transport of these reactants from the gas phase is slow, and since the rate of the bioreaction $\mathbf{q}$ would soon drop to zero if the gas-phase reactions were not transported to the liquid *at a rate equal to* $\mathbf{q}$ it may well be that the limiting substrate is one supplied from the gas phase.

We shall here discuss the design of cultivations with gas-phase substrates while the measurement of the rate constant for $\mathbf{q}^t$ or its calculation from empirical formulas is postponed to Chap. 10.

If transport process of a gas-phase substrate S_1 is rate limiting, then from (9.2):

$$\mathbf{q}^t(S_1) + \mathbf{q}(S_1) = k_l a(s_1{}^* - s_1) - Y_{xs_1}\,\mu(s_1)x = D(s_1 - s_{1f}). \tag{9.37}$$

s_1 is the liquid-phase concentration of S_1 and $\mu(s_1)$ is the specific growth rate, expressed as a function of the limiting substrate concentration s_1. As usual for steady-state continuous reactors, $D = \mu(s_1)$.

Both s_1 and s_{1f} can be set equal to zero compared with s_1^*, and (9.37) degenerates to

$$q_x = Dx = Y_{s_1 x}\, s_1{}^* k_l a. \tag{9.38}$$

If on the other hand a substrate S_2, introduced to the reactor through the liquid feed, is rate limiting, then:

$$x = Y_{s_2 x}\,(s_{2f} - s_2) \text{ and } q_x = Dx. \tag{9.39}$$

[1] In 2003, a corn-based lactic acid plant was commissioned near Omaha, Nebraska, in a Dow – Cargill cooperation (presently: NatureWorks LLC, a Cargill owned company). The plant has a yearly capacity of 190,000 ton lactic acid. Economic considerations of the kind illustrated in Example 9.5 are typical for the design of large, integrated production plants.

One should operate the reactor at conditions where q_x calculated from either (9.38) or (9.39) is the same.

This can be used to calculate the optimal, i.e., the minimum required value of the operating variable $k_l a$ for the given D and s_{2f}. For Monod kinetics in substrate S_2:

$$(k_l a)_{opt} = D \frac{Y_{s_2 x}}{Y_{s_1 x}} \frac{s_{2f}}{s_1^*} \left(1 - \frac{K_2 D / s_{2f}}{\mu_{max} - D}\right). \tag{9.40}$$

Example 9.6 *Optimal design of a single cell production.* Let S_1 be methane which is fed to the STR as natural gas (90% methane) mixed with oxygen in the volumetric ratio 1:1.31. The total pressure is 1 atm and the cultivation temperature is 45°C.

At these conditions:

$s_1^* = 4.67$ mg L^{-1} and $Y_{s_1 x} = 0.8$ g biomass (g methane in the liquid phase)$^{-1}$.

The second substrate is ammonia. $\mu_{max} = 0.35$ h^{-1}, $K_s = 50$ mg L^{-1} in a Monod rate expression.

The biomass composition is $CH_{1.8}O_{0.5}N_{0.2}$.

Let the dilution rate be $D = 0.2$ h^{-1}, while $s_{2f} = 200$ mg L^{-1}.

From (9.40), one can obtain

$$(k_l a)_{opt} = 0.2 \frac{24.6/(0.2 \times 17)}{0.8} \frac{200}{4.67} \left(1 - \frac{50 \times 0.2/200}{0.35 - 0.20}\right) = 51.6 \text{ h}^{-1},$$

$$x = \frac{0.8 \times 4.67 \times 51.6}{0.2} = 965 \text{ mg L}^{-1}. \tag{1}$$

It would serve no purpose to increase $k_l a$ above 51.6 h^{-1} since the liquid-phase reaction would then become rate limiting.

If the biomass concentration calculated in (1) is considered to be too low to obtain a reasonable volumetric production rate, it becomes interesting to redesign the process, e.-g., $x = 10$ g L^{-1} From (9.38), the required mass transfer coefficient is calculated to be $k_l a = 51.6 \times (10/0.965) = 535$ h^{-1}. But at the same time the ammonia feed concentration must be increased; otherwise the higher rate of methane consumption cannot be sustained.

Solution of (9.40) with $k_l = 535$ h^{-1} for s_{2f} gives us $s_{2f} = 1{,}449$ mg L^{-1}.

The conclusion is clear that if one feed stream is "improved," then the other feed stream must also be "improved."

An overall maximum productivity is found when the volumetric rate of the bioreaction is maximized according to (9.16) and (9.17) and the matching $k_l a$ value is calculated.

With the given data for the liquid-phase reaction and with $s_{2f} = 1{,}449$ mg NH_3 L^{-1}, one can obtain

$$D_{opt} = 0.2861 \text{h}^{-1}, \quad x = Y_{s_2 x}(s_{2f} - s_2) = 8{,}865 \text{ mg L}^{-1},$$
$$q_x = D_{opt} x = 2.54 \text{ g L}^{-1} \text{ h}^{-1}. \tag{2}$$

Finally from (9.38):

$$k_l a = 2,540/(0.8 \times 4.67) = 679 \mathrm{h}^{-1}. \tag{3}$$

A mass transfer coefficient of 679 h^{-1} can be obtained, also in an industrial reactor designed for good mass transfer.

Consequently, a maximum productivity improvement of 27% compared with $D = 0.2$ h^{-1}, $x = 10$ g L^{-1} can be obtained by simultaneous optimization of the bioreaction and the mass transfer process.

When the liquid-phase concentration of one of the reactants is constrained by a mass transfer balance, one should be wary of using one of the popular rate expressions in which the specific growth rate is given as the product of two Monod expressions, one for each of the substrates.

Let S_2 be the liquid-phase substrate and S_1 the substrate transferred from the gas phase.

The yield coefficients are Y_{s_1x} and Y_{s_2x}, respectively. The mass transfer coefficient has a known value $k_l a$.

The amount of S_1 transferred from the gas phase is $q_1^t = k_l a(s_1^* - s_1)$ while the rate of the bioreaction is $q_x = q_1^t Y_{s_1x}$.

Consequently, q_x can be calculated in two ways:

$$q_x = Y_{s_1x} k_l a\left(s_1^* - s_1\right) = \mu_{\max} Y_{s_2x} \frac{s_2}{s_2 + K_2} \frac{s_1}{s_1 + K_1} (s_{2f} - s_2). \tag{9.41}$$

Equation (9.41) looks like an equation, from which s_2 can be found when the value of s_1 is given.

But this cannot be true for all values of s_1 since the right-hand side of the equation is zero for $s_1 = 0$. There is clearly a lower value for s_1 below which no solutions for s_2 can be found. The right-hand side of (9.41) has a maximum value determined from (9.16), and consequently we must look for the lowest value of s_1 at which the left-hand side of (9.41) is smaller than or equal to this maximum value. If s_1^* increases (e.g., by increasing the total pressure), then the lowest permissible s_1 value also increases. If $\mu_{\max}$ increases, then $(s_1)_{\min}$ decreases toward zero, and the process is controlled by mass transfer alone. The two values obtained for s_2 when s_1 is above its minimum value are no surprise. The same value for q_x can be obtained both for a small $s \rightarrow a$ large x and for a large $s \rightarrow a$ small x.

9.2 The STR Operated as a Batch or as a Fed-Batch Reactor

In the whole of Sect. 9.1, we have considered the STR, the CSTR, operating in steady state. In Sect. 9.4, another continuous reactor type, the PFR is discussed, and again only steady-state operation is considered.

In Sects. 9.2.1 and 9.2.2, the STR operating in batch mode or in fed-batch mode is discussed, and in Sect. 9.3 we revert to the CSTR, but discuss what happens during transients in this important bioreactor type.

The reason for separating the discussion of the two non-steady-state operating STRs, the batch reactor and the fed-batch reactor, from that of the CSTR operating in non-steady state is twofold:

First, the batch reactor and especially the fed-batch reactor are very important examples of bioreactors, and many features of fed-batch operation need to be described in detail.

Secondly, both the batch and the fed-batch reactor essentially operate in metabolic steady state, although time is an independent process variable, and both **c** and (in fed-batch) V change during the cultivation. Since the culture is essentially in metabolic steady state, one may use Monod-type rate expressions to design the reactors.

The reason for studying the CSTR in true non-steady state operation is also twofold:

1. Deeper layers of the control structure come alive when the CSTR is subjected to drastic process upsets such as the injection of a pulse of substrate or by an instantaneous change of s_f or D. The effect of these large disturbances can best be studied from a given steady state in a CSTR where the intracellular variables have well-established values. Methods for obtaining metabolic data during fast kinetics are outlined in Sect. 9.3.5, and the theoretical basis for analysis of the data was already given in Sect. 6.4.4.
2. The steady-state CSTR is supposed to run according to the stated operating conditions for a very long time, otherwise the whole idea of continuous STR operation is lost. Hence, robust process control algorithms are especially important for this type of cultivation, and since the results of process upsets to the CSTR can have disastrous effects, one may need to study the *stability* of the steady-state operation. This topic is emphasized in Sect. 9.3.3.

9.2.1 The Batch Reactor

Design of batch cultivations is quite easy. There are not nearly as many operation variables and very few optimization possibilities, compared to the steady-state CSTR.

The use of unstructured kinetic models such as (7.16) and (7.18)–(7.20), perhaps including maintenance in a simple fashion, will generally give an acceptable result.

The batch cultivation is initiated by injection into the STR of inoculum to give an initial biomass concentration x_0. The initial substrate concentration $\mathbf{s}$ ($t = 0$) has a given value s_0, $\mathbf{p}(t = 0) = 0$, and the flow in and out of the reactor is zero.

Solution of the following initial-value problem will give **c** as a function of time t:

$$\frac{d\mathbf{c}}{dt} = \boldsymbol{q}(\mathbf{c}), \quad x(0) = x_0, \quad \boldsymbol{s}(0) = \boldsymbol{s_0}, \quad \text{and} \quad \boldsymbol{p}(0) = 0. \tag{9.42}$$

Assume that (9.42) is based on a single black box stoichiometry with no maintenance substrate consumption. Then for s (substrate), p (product), and x (biomass):

$$\frac{\mathrm{d}x}{\mathrm{d}t} = \mu x \text{ and } \frac{\mathrm{d}s}{\mathrm{d}t} = -Y_{xs}\mu x \rightarrow \frac{\mathrm{d}(x + Y_{sx}s)}{\mathrm{d}t} = 0 \rightarrow s - s_0 = -Y_{\mathrm{xs}}(x - x_0),$$

$$\frac{\mathrm{d}p}{\mathrm{d}t} = Y_{\mathrm{xp}}\mu x \rightarrow p = Y_{\mathrm{xp}}(x - x_0). \tag{9.43}$$

Equation (9.43) has been used many times before in the text (in stoichiometric balances), but it is now seen that the "key-reaction component" concept also holds during a transient.

Consequently, if the biomass concentration is known throughout the transient, the concentrations of the limiting substrate S, of all other substrates, and of all the products are given in (9.43).

The linear relation is correct for any kinetic expression μ, but the assumption is that Y_{jx} stays constant through the cultivation.

When the Monod expression (7.16) is inserted for μ in $\mathrm{d}x/\mathrm{d}t = \mu(s)\ x$ and $s = s_0 + Y_{\mathrm{xs}}\,x$ is inserted from (9.43), the following explicit solution for $\theta = \mu_{\max}t$ as a function of x is obtained after integration of the differential equation by the separation of variables:

$$\theta = \left(1 + \frac{a}{1 + X_0}\right)\ln\left(\frac{X}{X_0}\right) - \frac{a}{1 + X_0}\ln\,(1 + X_0 - X). \tag{9.44}$$

$X = \dfrac{x}{Y_{\mathrm{sx}}s_0}$, $a = \dfrac{K_{\mathrm{s}}}{s_0}$, and $X_0 = \dfrac{x_0}{Y_{\mathrm{sx}}s_0}$ in analogy with the nomenclature used in (9.7).

For small values of time, $X \sim X_0$ and the second term in (9.44) can be neglected. This is the exponential phase of the batch cultivation where $\dfrac{X}{X_0} = \dfrac{x}{x_0} \cong \exp(\mu_{\max}\mathrm{t})$ since $X_0 << 1$ and furthermore $a << 1$, unless s_0 is very small.

For $t \rightarrow \infty$, $x \cong x_0 + Y_{\mathrm{sx}}s_0$ and $X \cong X_0 + 1$. Here, the first term tends to zero and the second term dominates (9.44).

For very small values of a, one will hardly notice the break in the curve that predicts $\ln(x/x_0)$ as a function of time from a straight line of slope $\mu_{\max}$ to a horizontal line, but if s_0 is small as was the case in Monod's experiments, Note 7.2, there will be plenty of measurements $[x, t]$ to find both $\mu_{\max}$ from the experiments for small t and K_{s} from the intermediate time interval between the two asymptotes. The batch experiment may consequently be an option to the time-consuming determinations of $[D = \mu, s]$ which today is regarded as the recommended method of obtaining the kinetic parameters of the Monod kinetics.

For other kinetic expressions, one may also analytically integrate the differential equation for $x(t)$. Thus, for the substrate-inhibited and the product-inhibited Monod-type expressions (7.18) and (7.20), one can obtain, respectively, (9.45) and (9.46):

$$\theta = b(1+X_0)\ln\left(\frac{X}{X_0}\right) - b(X-X_0) + \left(1+\frac{a}{1+X_0}\right) \ln\left(\frac{X}{X_0}\right) - \frac{a}{1+X_0}\ln\,(1+X_0-X), \tag{9.45}$$

$$\theta = (P_0 + X_{\max} - X_0)\left[\frac{1+X_0+a}{X_{\max}(1+X_0)}\ln\left(\frac{X}{X_0}\right) - \frac{a}{(1+X_0)\,(X_{\max}-1-X_0)}\right.$$

$$\left.\ln(\,X_0+1-X) - \frac{X_{\max}-1-X_0-a}{X_{\max}\,(X_{\max}-1-X_0)}\ln\left(\frac{(X_{\max}-X)}{(X_{\max}-X_0)}\right)\right]. \tag{9.46}$$

In both cases, separation of the variables t and x has been used to integrate the differential equation.

Although numerical integration of the mass balance can easily be obtained for any given set of parameters in the mass balance – and analytical integration leads to any number of algebraic errors for the nontrained practitioner – the analytical expression, complicated as they may be, do give some qualitative feeling for the influence of the parameters.

In (9.45), the parameter b is the ratio between s_0 and K_i in (7.18). The parameter b is large for large s_0 and small K_i (see the analogous derivation of the enzyme kinetics, (6.16), although in the present context any mechanistic interpretation of K_i is fictitious).

For $b \to 0$, (9.45) degenerates to (9.44), but for large b, linearization of the first term in (9.45) from $X = X_0$ (i.e., for small t) leads to

$$b(1+X_0)\left(\frac{X}{X_0}-1\right) - b(X-X_0) = b\left(\frac{X}{X_0}-1\right). \tag{9.47}$$

Since it takes a long time before x moves away from x_0, (9.45) can erroneously be interpreted as expressing a lag-time before cells start to grow. The result clearly shows that batch cultivation of an organism which grows with substrate-inhibited kinetics is inferior to cultivation in a steady-state CSTR where the substrate concentration in the reactor is far below s_f as long as D is appreciably below $D_{\max}$. Since, as mentioned in Sect. 7.3.1, the organisms used to degrade toxic compounds by anaerobic digestion typically show substrate-inhibited kinetics, one will definitely recommend that steady-state CSTR operation is used in these processes.

In (9.46), the parameters are:

$$P_0 = \frac{p_0}{Y_{sp}s} \quad \text{and} \quad X_{\max} = \frac{p_{\max}-p_o}{Y_{sp}s_0} + X_0. \tag{9.48}$$

For $p_0 = 0$ and $p_{max} >> Y_{sp}s_0$, (9.46) also degenerates to (9.44), but this is obviously is not the case in wine fermentation using the sugar-rich grapes of warm climates. Equation (9.46) may be instructive when studying the influence of the growth parameters (Y_{sx} and Y_{sp}) on a wine fermentation that starts with a juice of concentration s_0. Note that the kinetic parameter μ_{max} only occurs as a scaling factor on t, and the issue of "stuck-fermentation," cessation of fermentation while there is still many grams of sugar left in the medium, can be studied with (9.46) as a guideline. With s_0 in the range of 200–250 g sugar L^{-1}, the parameter $a = K_s/s_0$ can safely be set to zero.

9.2.2 The Fed-Batch Reactor

As indicated in Table 9.1, the operation of bioreactors in semibatch mode is very popular in the fermentation industry.

The fed-batch process was developed around 1920, both in Denmark and Germany, as a way to increase the biomass yield in production in Baker's yeast. By a slow addition of sugar, overflow metabolism can be avoided (see Example 9.7). Today, fed-batch operation is frequently used in recombinant protein production by many organisms for partly the same reasons, i.e., the presence of an overflow metabolism which diverts the carbon flow to undesired by-products. This applies, e.g., for *Escherichia coli*, in which acetate formation occurs at high carbon fluxes. Furthermore, substrate inhibition, either of the biomass formation itself or of a desired product, may occur.

In a typical fed-batch process for protein synthesis, the reactor is started as a batch, and a suitably large biomass concentration is obtained by consumption of the initial substrate. The rate of product formation is typically zero during the batch cultivation, since P is only synthesized when an *inducer* is added.

When the biomass concentration has increased to a desired level x_0 and correspondingly the substrate level has decreased to a low level, a feed of (usually very concentrated) substrate is started. At the same time, the inducer is added to switch on the metabolic pathways that lead to the desired product.

During the whole fed-batch period, no product is withdrawn from the reactor and the medium volume keeps increasing. At the end of the fed-batch period, the whole or a portion of the medium is harvested and sent to downstream processing. New substrate is added, and (possibly after a batch period) a second fed-batch period is started. This is *repeated fed-batch* operation. It will work quite well unless the remainder of biomass which is used to grow up a new culture is different from that of the inoculum, and therefore produces the desired product at a low yield.

Two objections have been raised to the fed-batch process:

1. Why would one wish to use a somewhat complicated process rather than batch operation where good process control of pH, O_2 supply, and temperature will

lead to total consumption of the substrate and production of a high titer of biomass and the desired product?
2. Why not use a steady-state CSTR where product or biomass production will continue indefinitely at optimal process conditions which can be calculated beforehand?

The answer to the first objection is: The right product may not be produced when the substrate concentration is high: A high sugar concentration in a baker's yeast production will lead to an initial production of substantial amounts of ethanol, and with a low initial sugar concentration the productivity is too low. Also, in, e.g., heterologous protein production, synthesis of the protein may be catabolite repressed.

The difficulty of getting a substrate-inhibited cultivation started in the batch mode is discussed in Sect. 9.2.2.

The answer to the second objection lies in the limited time horizon of the fed-batch culture. When continuous feed of substrate has increased the medium volume to a maximum $V_{\max}$, the process is stopped, the product is harvested, and a new fed-batch period may start, perhaps with 1/4 of the final medium left in the reactor to avoid the slow outgrowth of an entirely new biomass culture in batch cultivation.

The steady-state CSTR operation with its promise of an indefinite production period has traditionally suffered from the disadvantages listed in Table 9.1: Strain mutation after a long time on stream, a difficult control situation, and perhaps an unsatisfactory flexibility of the equipment.

This criticism of steady-state CSTR operation is now slowly subsiding. Industry wants to capitalize on the superior productivity of the CSTR, and better medium control and a stringent monitoring and control of the cultivation process have led to such great performance improvements of the continuous STR mode of operation that this is now accepted in many places. Still, fed-batch cultivation is widely used even where CSTR operation is known to give higher productivity, e.g., in baker's yeast production (and in production of compounds expressed in yeast), and in production of industrial enzymes, of antibiotics, and of many other final products.

When a time-varying feed stream $v(t)$ containing one or more of the substrates at a constant concentration $\mathbf{c}_\mathrm{f}$ is admitted to a STR without withdrawal of a corresponding effluent stream, the mass balances become

$$\frac{\mathrm{d}(\mathbf{c}V)}{\mathrm{d}t} = V\frac{\mathrm{d}\mathbf{c}}{\mathrm{d}t} + \mathbf{c}\frac{\mathrm{d}V}{\mathrm{d}t} = V\frac{\mathrm{d}\mathbf{c}}{\mathrm{d}t} + \mathbf{c}v(t) = V\mathbf{q}(\mathbf{c}) + \mathbf{c}_\mathrm{f}v(t). \tag{9.49}$$

The mass balances for the fed-batch operational mode therefore become

$$\frac{\mathrm{d}\mathbf{c}}{\mathrm{d}t} = \mathbf{q}(\mathbf{c}) + \frac{v(t)}{V(t)}(\mathbf{c}_\mathrm{f} - \mathbf{c}). \tag{9.50}$$

There is a striking similarity between (9.50) and the mass balances for a STR. In (9.50), the dilution rate $D = v(t)/\ V(t)$ is, of course, a function of time, and fed-batch is in principle a purely transient mode of operation, although the process can safely be analyzed assuming that the culture is in steady-state metabolic balance.

One may visualize the fed-batch as a control problem: Subject to certain constraints, it is possible to choose the control function $v(t)$ such that a given goal is reached. This goal may be defined at the end of the fermentation process where $V(t)$ has reached a specified value. This end-point control problem is a classical problem of control theory: e.g., to choose $v(t)$ and $[s_f, s_0, x_0]$ that characterize the initial state and the feed policy, so that a given state (x, s) is reached in the shortest possible time. The chemical engineering literature abounds with solutions of this kind of problem. Menawat et al. (1987) and Palanki et al. (1993) are typical references.

We shall, however, choose to study two simpler problems where the control action is applied with the purpose of achieving optimal metabolic conditions for the cell culture at every instant during the fermentation. The concept of an instantaneous control action is illustrated in sufficient generality with only one growth-limiting substrate and the biomass as the state vector. To simplify the discussion, maintenance-free kinetics will be used.

The two most obvious feed policies are

- Choose $v(t)$ so that $s = s_0$ throughout the fermentation.
- Choose $v(t)$ so that $q_x = q_x^0$ throughout the fermentation.

The two policies correspond to fermentation at *constant specific growth rate* and at *constant volumetric rate* of biomass production, respectively. Both policies have obvious practical applications.

When s is kept at a constant value, just below that, at which part of the added substrate is converted to undesired products, a large amount of biomass (together with any growth-associated metabolic product or a valuable protein) is produced at a reasonably high rate, and high final biomass and product titer can be obtained.

The constant volumetric rate policy is important if removal of the heat of reaction is a problem or if the capability to supply another substrate, e.g., oxygen, is exceeded when $q_x > q_x^0$.

Calculation of $v(t)$ for the constant specific growth rate policy (where s is constant since μ is a function of s alone) is quite easy. From (9.49), and with $x_f = 0$:

$$\frac{d(xV)}{dt} = \mu_0 xV \quad \Rightarrow \quad xV = x_0 V_0 \exp(\mu_0 t). \tag{9.51}$$

The substrate balance is obtained from (9.50):

$$\frac{ds}{dt} = 0 = -Y_{xs}\mu_0 x + \frac{v(t)}{V(t)}(s_f - s). \tag{9.52}$$

Solution of (9.52) for $v(t)$ yields:

$$v(t) = \frac{Y_{xs}\mu_0}{s_f - s_0} xV = \frac{Y_{xs}\mu_0}{s_f - s_0} x_0 V_0 \exp(\mu_0 t). \tag{9.53}$$

$V(t)$ is found by integration of (9.53) from $t = 0$, and $x(t)$ by inserting $V(t)$ in (9.51).

$$\frac{V}{V_0} = 1 - bx_0 + bx_0 \exp(\mu_0 t)\,; \quad b = Y_{xs}/\,(s_f - s_0), \tag{9.54}$$

$$\frac{x}{x_0} = \frac{\exp(\mu_0 t)}{1 - bx_0 + bx_0 \exp(\mu_0 t)} = \frac{y}{1 - bx_0 + bx_0 y} = \frac{V_0}{V} y. \tag{9.55}$$

Equations (9.53)–(9.55) constitute the complete, explicit solution to the constant specific growth rate problem.

v is seen to increase exponentially with time according to (9.53).

The value of x for a specified V/V_0 is calculated from (9.55), using the value of t obtained by the solution of (9.54).

According to (9.55), x will at first increase exponentially with t, but eventually it approaches an upper value equal to $b^{-1} = Y_{sx}(s_f - s_0)$ which is proportional to $s_f - s_0$. Since $q_x = \mu_0 x$, the volumetric biomass production rate can reach a very high value for large s_f.

The design of the fed batch by the above procedure is based on the assumption of a single black box stoichiometry with constant Y_{ij}. Hence $(-q_0) = Y_{xo}\, q_x$ can reach a value where, according to the discussion of Sect. 9.1.5, not enough O_2 can be supplied by physical mass transfer from the gas phase.

At this point, one should switch to the second of the two operation policies mentioned above, namely, the constant volumetric productivity policy. This policy is adapted, not because it gives advantages in terms of productivity, but because the constant μ policy breaks down due to the interplay between the bioreaction and physical processes.

The best one can do after the process has become limited by mass transfer from the gas phase is to work at the value q_x^0 where $(-q_0)_{max} = Y_{xo} q_x^0$.

It will be shown below that the "constant q_x feed policy" is, in fact, easily designed. It turns out that an exponential feed policy can be maintained, although the exponent is smaller than μ_0, and therefore that the cultivation process slows down.

The value of $(-q_0)_{max}$ primarily depends on $k_l\, a$ and on the partial pressure π_0 of O_2 in the gas phase, (3.9). π_0 is proportional both to the gas mole fraction of O_2 and to the total pressure.

The relation between $k_l a$ and the power input used to disperse the gas in the liquid phase is discussed in Chaps. 10 and 11. It turns out that an unacceptable power input must be used to increase $k_l a$ above ~ 1,000 h^{-1}. Using "technical quality O_2 – about 95% pure" is a relatively cheap way to increase $(-\,q_0)_{max}$, but

bioreactors working at moderate hyperbaric conditions, e.g., a reactor pressure of 2–3 bar, are a promising option.

In any case $(-q_0)$ has a maximum value $(-q_0)_{\max}$, and at the starting point of the "constant q_x feed period," the variables have the following values:

$$q_x^0 = Y_{ox}(-q_0)_{\max}; \quad x^0 = q_x^0/\mu_0; \quad y = \exp(\mu_0 t^0) \rightarrow t^0 = \ln y/\mu_0,$$

as determined from (9.55).

Finally, V^0/V_0 is found from (9.54) and $v(t^0)$ from (9.53).

Just before $t = t^0$, the reactor volume V increases exponentially with slope.

$$\left(\frac{dV}{dt}\right)^0 = v^0 = b\mu_0 x_0 V_0 \exp(\mu_0 t^0). \tag{9.56}$$

It is *postulated* that exponential feed can be continued for $t > t^0$, and that

$$v(t') = kV^0 \exp(kt') \rightarrow V = V^0 \exp(kt'), \qquad \text{where } t' = t - t^0. \tag{9.57}$$

Villadsen and Patil (2007) show that (9.56) can, indeed, be used to calculate $V(t')$ with a high accuracy, and they also find the value for the exponent k.

The mass balance for S after $t = t^0$ is again satisfy (9.52), but s is not constant for $t > t^0$.

$$\frac{ds}{dt'} = -Y_{xs}\mu x + \frac{v(t')}{V(t')}(s_f - s) = -Y_{xs}\mu_0 x^0 + k(s_f - s). \tag{9.58}$$

The corresponding mass balance for the biomass is integrated from $t' = 0$ to give

$$\frac{dx}{dt'} = q^0 - kx = \mu_0^0 x^0 - kx \rightarrow x = \left(x^0 - \frac{q^0}{k}\right)\exp(-kt') + \frac{q^0}{k}. \tag{9.59}$$

When the substrate balance multiplied by Y_{sx} and the biomass balance are added and integrated from $t' = 0$, one can obtain:

$$x + Y_{sx}s = \left(x^0 + Y_{sx}(s_0 - s_f)\right)\exp(-kt') + Y_{sx}s_f. \tag{9.60}$$

In (9.60), $x >> Y_{sx}s$ and $s_0 << s_f$. When these small terms are neglected, (9.60) becomes identical to (9.59), *if* $Y_{sx}s_f = q^0/k$.

Consequently, a value for k has been determined for which exponential feed can be used, also when O_2 mass transfer has becomes limiting.

$$k = \frac{q^0}{Y_{sx} s_f} = \frac{\mu_0 x^0}{Y_{sx} s_f}. \tag{9.61}$$

k is equal to μ_0 scaled by the ratio between the biomass concentration obtained when mass transfer limitation sets in, and that which would be obtained if the substrate admitted since the start of the batch fermentation period is completely converted to biomass.

Example 9.7 *Design of a fed-batch process for baker's yeast production.* A typical industrial strain of *Saccharomyces cerevisiae* converts glucose to biomass according to:

$$\begin{aligned} CH_2O \; + 0.3944\, O_2 + 0.115\; NH_3 \rightarrow & 0.5768\; X\; (CH_{1.8}O_{0.5}N_{0.2}) \\ & + 0.4232\; CO_2 + 0.65\, H_2O. \end{aligned} \tag{1}$$

The specific growth rate is given by the Monod expression:

$$\mu = \frac{0.4(h^{-1})s}{s + 150\ (mg\ L^{-1})}. \tag{2}$$

Ethanol is produced when $\mu > 0.25\ h^{-1}$, and since ethanol is an undesired byproduct, the process should be operated at $\mu = \mu_0 = 0.25\ h^{-1}$ to obtain the highest possible productivity of biomass without losing glucose to ethanol. For $\mu = 0.25\ h^{-1}$, solution of (2) for s gives $s = s_0 = 250\ mg\ L^{-1}$.

Fed-batch cultivation is started at the end of a batch where x has reached the value $x_0 = 1\ g\ L^{-1}$.

The glucose concentration in the reactor is adjusted to $s_0 = 0.25\ g\ L^{-1}$ to give $\mu_0 = 0.25\ h^{-1}$.

The glucose feed concentration is $s_f = 100\ g\ L^{-1}$

The fed-batch cultivation is to be continued until $V = 4V_0$.

Using good Rushton turbines (see Chap. 11), a value of $k_l a = 650\ h^{-1}$ can be obtained.

From the stoichiometry (1), $Y_{xo} = 0.3944/0.5768 = 0.684$ mol O_2/C-mol X.

If the reactor is sparged with air, and $[P, T] = [1\ bar, 30°C]$, $s^*(O_2) = 0.244$ mM (Table 10.8).

It is assumed that the O_2 concentration in the reactor must be at least 10% of the saturation concentration $s^*(O_2)$. Therefore:

$$(-q_0)_{max} = 650 \times 0.244 \times (1 - 0.1) = 142.5\ mmol\ L^{-1}\ h^{-1},$$

$$q_x^0 = 142.5 \times 10^{-3} \times 24.6(g/C\text{ - }mol)/0.684 = 5.12\ g\ X\ L^{-1}\ h^{-1} \quad \text{and}$$
$$x^0 = 5.12/0.25 = 20.47\ g\ L^{-1}.$$

The parameter $b = Y_{xs}/(s_f - s_0) = (0.5768 \times 24.6/30)^{-1}/(100 - 0.25) = 0.0212$ L (g biomass)$^{-1}$.

The design of the operation can now be carried out:

1. The fed-batch cultivation is operated at $\mu_0 = 0.25\ \mathrm{h}^{-1}$ until $x/x_0 = 20.47$.
   From (9.55), one can obtain $y = \exp(\mu_0 t) = 35.4$ and $t = t^0 = \ln(35.4)/0.25 = 14.26$ h.
   From the second part of (9.55), one can obtain $V^0/V_0 = 1.73$ at $t = t^0$.
2. The remainder of the fed batch until $V/V_0 = 4$ is carried out with exponential feed, $v(t') = v(t' = 0)\exp(kt')$, where from (9.61), $k = 5.12 \times 2.12/100 = 0.108\ \mathrm{h}^{-1}$.
   The value $V/V_0 = 4$ is reached for $t' = 7.73$ h, and the total cultivation time is 22 h.

If the cultivation had continued to $V/V_0 = 4$ with $\mu = 0.25\ \mathrm{h}^{-1}$ (which would not be possible, because the culture is O_2 limited for $t > 14.26$ h), the total cultivation time would be 19.84 h.

The final biomass concentration x_{final} depends only on V_{final}/V_0 and will reach the value of $35.6\ \mathrm{g\ L}^{-1}$, irrespective of the feed policy used to reach V_{final}.

Figure 9.7, obtained by numerical integration of the mass balances, shows the time course of the biomass concentration and also the value of $s(t)$. From $t = t^0$, the substrate concentration must decrease since with exponential feed after t^0, $\mu = q^0/x$, and x increases by a factor of $35.6/20.47 = 1.74$ from t^0 to t_{final}.

A constant feed policy after $t = t_0$, i.e., keeping v at the value v^0 of (9.57), is definitely not a good idea. The total cultivation time to reach V_{final} is 26.4 h, and both μ and s reach much smaller values than would be obtained by the exponential feed policy advocated above.

The low substrate concentration (and hence the small μ) obtained during the last part of the cultivation is definitely undesirable. Svensson et al.(2005) point out that the stress response caused by the low substrate concentration at the end of a "constant v feed policy" used after $t = t^0$ leads to a massive synthesis of endotoxins in a protein production process using *E. coli*. This causes severe downstream problems when the heterologous protein is purified. Svensson et al. propose a somewhat different solution to avoid the low values of s, namely, a gradual decrease of the cultivation temperature while the feed rate v is controlled to give a constant $s(O_2)$. The exponential feed policy described above is likely to be an easier way to reach the same objective.

In the derivation of (9.51)–(9.55), we have focused on the biomass production, and in Example 9.7, no mention was made of a metabolic product.

The design can, as illustrated in Problem 9.8, equally well be based on product specifications at the end of the fed batch. As long as the yield coefficients are constant, $q_p = Y_{xp}q_x$, and the feed v does not contain P, the derivation of the design formulas given above can be repeated for p (which is usually 0 at $t = 0$), and one can calculate V, x, and the cultivation time to reach a certain final titer for P.

The feed concentration of a compound that needs to be present at constant concentration throughout the cultivation can also be calculated (see Problem 9.8).

In Example 9.7, simple Monod kinetics was used, but any kinetic expression $\mu(s)$ can be inserted, and the substrate concentration s_0 during the constant μ period can be calculated.

Maintenance can be included if in (9.52) and in the following equations, $Y_{xs}\mu_0$ is replaced by $Y_{xs}^{\mathrm{true}}\mu_0 + m_s$. Numerical integration of the mass balances must always be used to find $s(t')$ and $\mu(t')$ after the switch to operation at constant q_x.

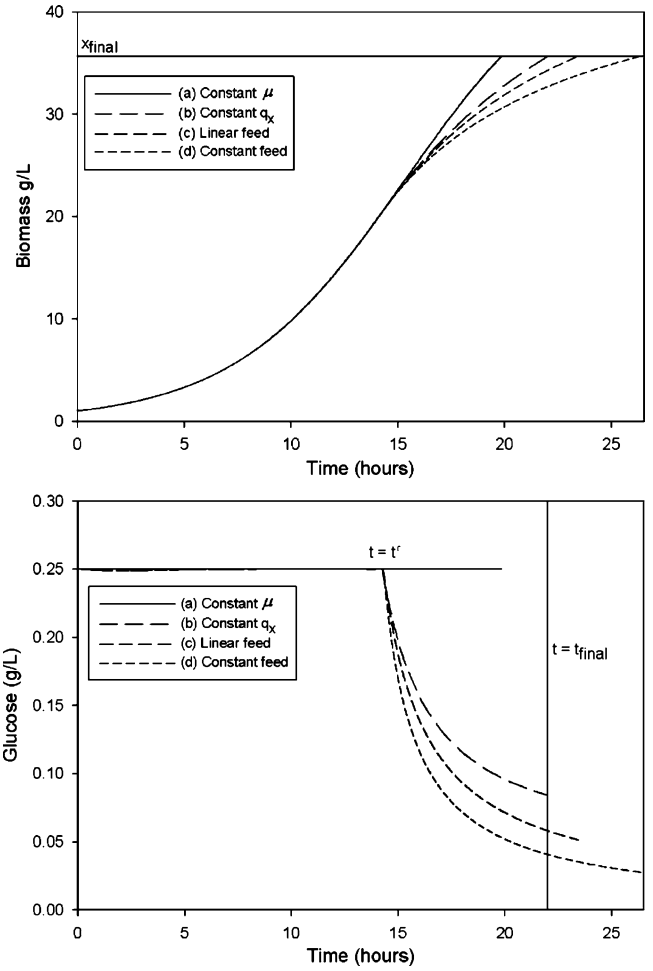

Fig. 9.7 Biomass concentration and substrate concentration in a fed-batch cultivation using four different feed policies after transport limitation sets in at $t = t^0 = 14.26$ h

It follows from our discussion of fed-batch cultivation that the design of these processes offers no great calculation problems.

What is, however, important to emphasize is that *fed-batch operation does not give as high a productivity as CSTR operation*, see Note 9.1.

Note 9.1 *Comparison of the productivity of a fed-batch and a continuous baker's yeast process.* Assume in Example 9.7 that the whole reactor volume $V = 4V_0$ was used for continuous production of biomass at the final concentration $x = 35.6$ g L^{-1} obtained in the example. From previous examples, e.g., Example 3.5, we know that at $D = \mu = 0.25$ h^{-1} the effluent sugar concentration from the CSTR is practically 0.

Consequently, $s_f = 35.6 \times 2.12 = 75.5$ g L^{-1} and the volumetric rate of biomass formation is $q_x = 0.25 \times 35.6 = 8.9$ g L^{-1} h^{-1}.

According to the calculation in Example 9.7, this rate cannot be obtained with the assumed mass transfer rate used in the example. To obtain $-q_0 = 5.12\text{gL}^{-1}\text{h}^{-1}$, D must be reduced to $D = 0.25 \times (5.12/8.9) = 0.144\ \text{h}^{-1}$.

The total production of biomass over a fermentation period of $t = 22$ h in a CSTR of volume $4V_0$, operated at $D = 0.144\ \text{h}^{-1}$ and $x = 35.6\ \text{g L}^{-1}$, is $(4V_0) \times 22 \times 0.144 \times 35.6 = 3.17$ $(4 \times V_0 \times 35.6)$. This is a total production and it is 3.17 times higher than that would be obtained in the fed batch operated with the best possible feed strategy.

There is no doubt that industrial bioprocesses will increasingly be carried out in steady-state CSTRs. The economic incentives are sufficiently high to merit a considerable research effort to find the causes of strain instability and to run the continuous process with the help of most advanced process control equipment.

9.3 Non-steady-State Operation of the CSTR

The CSTR is, as discussed in Note 9.1 the ideal bioreactor for most industrial processes, and because of its low operating costs it is essential to consider CSTR operation for all processes where a low value product is obtained in large volumetric scale. The CSTR is also the ideal reactor for scientific studies since the effect of all process variables can be studied at high precision and at steady state.

In the present section, non-steady-state operation of the CSTR is considered. Start-up of a CSTR is necessarily a non-steady-state operation, as is the deliberate change of dilution rates in CSTR experiments. It is essential to understand the dynamics of these processes to allow sufficient time for the process to adjust to a new steady-state. Furthermore, the effect of instabilities arising from process disturbances, which may completely ruin what is designed to be a steady-state CSTR process, must be understood. Also another specific topic of non-steady-state CSTR operation, the case of the simultaneous growth of more than one organism on the same substrate, is discussed. Finally, the design of CSTRs that permits the dynamic response of very fast bioreactions to be captured will be reviewed.

9.3.1 Relations Between Cultivation Variables During Transients

The non-steady-state mass balances for the CSTR are:

$$\begin{aligned} \frac{\mathrm{d}x}{\mathrm{d}t} &= \mu x - Dx, \\ \frac{\mathrm{d}s}{\mathrm{d}t} &= -Y_{\text{xs}}\mu x + D(s_{\text{f}} - s), \\ \frac{\mathrm{d}p}{\mathrm{d}t} &= Y_{\text{xp}}\mu x - Dp. \end{aligned} \tag{9.62}$$

The specific growth rate can depend on both s and p, and it is assumed that the yield coefficients are constant.

For maintenance-free kinetics, linear combinations of the mass balances reduce (9.62) to

$$\begin{aligned}\frac{\mathrm{d}(x + Y_{\mathrm{sx}}s)}{\mathrm{d}t} &= -D(x + Y_{\mathrm{sx}}s) + DY_{\mathrm{sx}}s_{\mathrm{f}},\\ \frac{\mathrm{d}(x - Y_{\mathrm{px}}p)}{\mathrm{d}t} &= -D(x - Y_{\mathrm{px}}p).\end{aligned} \tag{9.63}$$

The linear differential equations (9.63) have the solution:

$$\begin{aligned}x + Y_{\mathrm{sx}}s &= A\,\exp(-Dt) + Y_{\mathrm{sx}}s_{\mathrm{f}},\\ x - Y_{\mathrm{px}}p &= B\,\exp(-Dt).\end{aligned} \tag{9.64}$$

Equation (9.64) is a general relation between x, s, and p during the transient. The relation is true for any maintenance-free specific growth expression $\mu(x, s, p)$ – if Y_{xs} is different from $Y_{\mathrm{xs}}^{\mathrm{true}}$, the variables x and s, and x and p in the two equations of (9.63) cannot be collected into a single dependent variable.

In the following, we derive a relation between x, p, and s during the transient, but first the arbitrary constants A and B must be determined. Their values depend on how the transient from the initial condition $[x_0, p_0, s_0]$ is started at $t = 0^+$, and three types of transients are considered in (**a**)–(**c**) below:

(a) *D is changed from D_0 to D at $t = 0^+$ while s_{f} is unchanged.*
The arbitrary constants A and B *i*n (9.64) are:

$$\begin{aligned}&A = x_0 + Y_{\mathrm{sx}}s_0 - Y_{\mathrm{sx}}s_{\mathrm{f}} = 0;\\ &B = x_0 - Y_{\mathrm{px}}p_0 = x_0 - Y_{\mathrm{px}}Y_{\mathrm{sp}}(s_{\mathrm{f}} - s_0) = x_0 - Y_{\mathrm{sx}}(s_{\mathrm{f}} - s_0) = 0.\end{aligned} \tag{9.65}$$

(b) *s_{f} is changed from s_{f}^0 to s_{f} at $t = 0^+$ while D is unchanged.*

$$\begin{aligned}&x_0 + Y_{\mathrm{sx}}s_0 = A + Y_{\mathrm{sx}}s_{\mathrm{f}}^0 + Y_{\mathrm{sx}}(s_{\mathrm{f}} - s_{\mathrm{f}}^0) \quad \text{or} \quad A = -Y_{\mathrm{sx}}(s_{\mathrm{f}} - s_{\mathrm{f}}^0),\\ &x_0 - Y_{\mathrm{px}}p_0 = x_0 - Y_{\mathrm{sx}}(s_{\mathrm{f}}^0 - s_0) = 0 = B.\end{aligned} \tag{9.66}$$

(c) *A pulse of substrate is added at $t = 0^+$ while D and s_{f} are unchanged.*

$$\begin{aligned}&x_0 + Y_{\mathrm{sx}}s_0 + \Delta s = A + Y_{\mathrm{sx}}s_{\mathrm{f}} \quad \text{or} \quad A = \Delta s.\\ &x_0 - Y_{\mathrm{px}}p_0 = x_0 - Y_{\mathrm{sx}}(s_{\mathrm{f}} - s_0) = 0 = B.\end{aligned} \tag{9.67}$$

In all three transients $B = 0$, and $p = Y_{\mathrm{xp}}x$ when the yield coefficients are constant. The substrate and the biomass balances are also uncoupled:
In case (**a**), x and s are linearly related, $s = s_0 - Y_{\mathrm{xs}}\,x$, throughout the transient. In cases (**b**) and (**c**), the linear relation holds only after an initial transient:

$$\begin{aligned}(\mathbf{b}) \quad &x + Y_{\mathrm{sx}}s = Y_{\mathrm{sx}}s_{\mathrm{f}} - (s_{\mathrm{f}} - s_{\mathrm{f}}^0)Y_{\mathrm{sx}}\exp(-Dt),\\ (\mathbf{c}) \quad &x + Y_{\mathrm{sx}}s = \Delta s\,\exp(-Dt) + Y_{\mathrm{sx}}s_{\mathrm{f}}.\end{aligned} \tag{9.68}$$

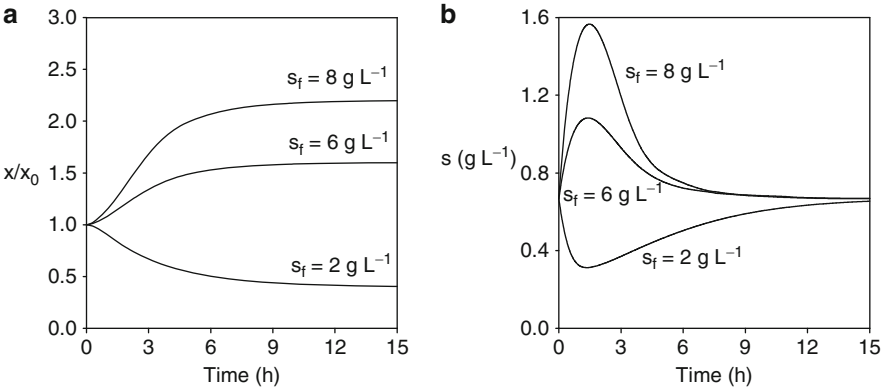

Fig. 9.8 Transients in a CSTR following a shift in the substrate concentration s_f at constant D

When $s_f > s_f^0$ in (**b**), $x + Y_{sx}s < Y_{sx}s_f$, until the new steady state has been reached and the sum of x and $Y_{sx}s$ has reached a new and higher value $Y_{sx}s_f$. If μ is independent of s_f, then for the constant D s will return to s_0 in case (**b**), and after the transient $x = Y_{sx}(s_f - s_0) = x_0 + Y_{sx}(s_f - s_f^0)$, while $p = Y_{xp}x = p_0 + Y_{sp}(s_f - s_f^0)$.

Figure 9.8 illustrates the time course of a transient when s_f is increased or decreased from s_f^0, and μ is given by the simple Monod expression (7.16) which is independent of p.

When μ depends on s_f, the final s value is different from s_0. This is illustrated in Example 9.8. s_f is increased from 2 to 4 g L^{-1}, and s increases from 0.8 to 2.4 g L^{-1}. Consequently, neither x nor p increase nearly as much as predicted by the above equations.

In the pulse experiment (**c**), return to the original steady state will, as discussed in Sect. 9.3.2, only happen *if this steady state is stable*, and *if the pulse* Δs *is not too large*.

Monod kinetics with $\mu_{max} = 1$ h^{-1} and $K_s = 1$ g L^{-1}. The dilution rate is $D = 0.4$ h^{-1}.

At $s_f = s_f^0 = 4 g L^{-1}$, and for $x_f = 0$, one can obtain $[s, x] = [2/3, 5/3]$ when $Y_{sx} = 1/2$.

When s_f is increased to 8 g L^{-1} for $t > 0$, s returns to 2/3 g L^{-1} after an overshoot that lasts about 12 h (~5 times D^{-1}), while x has increased to $x_0 + Y_{sx}(s_f - s_f^0) = 11/3$.

Example 9.8 *A step change of* s_f *for constant* D. Consider the product-inhibited kinetics (7.20). In the steady state, D is given by:

$$D = \frac{\mu_{max} s}{s + K_s}\left(1 - \frac{Y_{sp}(s_f - s)}{p_{max}}\right). \tag{1}$$

The parameters chosen are those of Fig. 9.3c:
$\mu_{max} = 0.5$ h^{-1}, $K_s = 0.4$ g L^{-1}, $Y_{sx} = Y_{sp} = 0.5$, and $p_{max} = 3/2$ g L^{-1}.

For $s_f = 2$ g L^{-1}, the parameter $a = K_s/s_f = 0.2$ and the parameter $s_f Y_{sp}/p_{max} = 2/3$.

For $s_f = 4$ g L^{-1}, $a = 0.1$, and $s_f Y_{sp}/p_{max} = 4/3$.

For $D = 0.2$ h^{-1}, one can determine $[s_f, s]$ equal to [2, 0.8] and [4, 2.4] by the solution of (1).

$[s_f, x]$ is equal to [2, 0.6] and [4, 0.8], and these are also the values of $[s_f, p]$ since $x_f = p_f = 0$ and $Y_{sp} = Y_{sx}$.

According to (9.64) with A and B determined from (9.66), any steady-state solution satisfies:

$$x + Y_{sx}s = Y_{sx}s_f \quad \text{and} \quad x - Y_{px}p = 0. \tag{2}$$

The solutions for $s_f = 2$ and 4 g L^{-1} are both seen to satisfy the relations in (2).

Note the large increase of s when s_f increases from 2 to 4 g L^{-1} and p approaches p_{max}.

9.3.2 *The State Vector [s, x, p] in a Transient CSTR Experiment*

Although the relations (9.64) can tell us what happens to the linear combinations of s and x and of x and p for maintenance-free kinetics, the time profiles $s(t)$, $x(t)$, and $p(t)$ have not yet been derived.

In the particularly simple case (**a**), where the dilution rate is changed from D_0 to D at time $t = 0^+$, $x + Y_{sx}s$ is constant and equal to $Y_{sx}s_f = x_0 + Y_{sx}s_0$ during the transient. Here, one can derive the following relation (9.69) between t and x when μ is given by the simple Monod equation (7.16). The differential mass balance equation for x in (9.62) is solved after the insertion of $s = s_f - Y_{xs}x$, in the same way as (9.44) was obtained in the design of the batch reactor:

$$t = \frac{1}{D_{max} - D}\left(\ln z - \left(\frac{\mu_{max} - D_{max}}{\mu_{max} - D}\right) \ln\left(\frac{|z - z_\infty|}{|1 - z_\infty|}\right)\right). \tag{9.69}$$

In (9.69), D is the dilution rate *after* $t = 0$, $D_{max} = \dfrac{\mu_{max}}{1 + a}$ where $a = \dfrac{K_s}{s_f}$ and $z = \dfrac{x}{x_0}$.

$$z_\infty = \frac{D_{max} - D}{D_{max} - D_0}\,\frac{\mu_{max} - D_0}{\mu_{max} - D}. \tag{9.70}$$

For $D < D_{max}$, the transient ends in a new steady state $(x/x_0)_{t\to\infty} > 0$.

$$\left(\frac{x}{x_0}\right)_{final} = \frac{Y_{sx}(s_f - s)}{Y_{sx}(s_f - s)} = \frac{s_f(\mu_{max} - D) - DK_s}{s_f(\mu_{max} - D_0) - D_0K_s} \times \frac{\mu_{max} - D_0}{\mu_{max} - D}$$
$$= \frac{D_{max} - D}{D_{max} - D_0}\,\frac{\mu_{max} - D_0}{\mu_{max} - D} = z_\infty.$$

For $D > D_{max}$, the culture washes out, and z_∞ is a parameter which is not equal to zero with no physical interpretation.

Finally, for $D = D_{max}$, the culture also washes out following:

$$D_{max}t = \frac{1}{a}\ln z + \frac{Y_{sx}s_f}{x_0} \times \frac{1+a}{a} \times \frac{1-z}{z}. \tag{9.71}$$

In the last term of (9.69), the numerical value of both nominator and denominator is used, since for $D < D_0$ one can obtain $z_\infty > z > 1$ for all $t > 0$, while for $D_{max} > D > D_0$ one can obtain $z_\infty < z < 1$ for all $t > 0$.

For $D > D_{max}$, $z(t \to \infty) = 0$, but the parameter z_∞ is different from 0. As seen from (9.70), z_∞ is either negative, namely, for $D_{max} < D < \mu_\infty$, or positive when $D > \mu_{max}$.

Consequently, for large t, the first term dominates on the right-hand side of (9.69).

This means that in the wash-out case, $D > D_{max}$, the relation between t and (x/x_0) in (9.69) approaches an asymptote:

$$\ln\left(\frac{x}{x_0}\right) = \ln z = (D_{max} - D)t + \text{ constant}. \tag{9.72}$$

Equation (9.72) can be used in an accurate determination of D_{max}, by a transient experiment where a steady state at D_0 is subjected to a sudden change of dilution rate to a value $D > D_{max}$.

The method is applied in Problem 7.1, and from the linear ($\ln z$ vs. t) plot in Fig. 7.13, one can determine $D - D_{max}$ to $60 \times 2.303/320 = 0.43\ h^{-1}$.

The method can *only* be used when the culture is in metabolic steady state through the transient – which is probably the case in Fig. 7.13 for $D_0 = 0.5\ h^{-1}$, but *not* when D_0 is $0.10\ h^{-1}$.

Example 9.9 *Transients obtained after a change of dilution rate from D_0 to D.* Consider the kinetics of Example 9.8 and the operating conditions $[s_f, D] = [4\ g\ L^{-1}, 0.4\ h^{-1}]$ before the feed concentration s_f was changed. $[s_0, x_0]$ was determined to $[2/3, 5/3]\ g\ L^{-1}$.

In the present example, s_f remains at $4\ g\ L^{-1}$, while D is changed to 0.6, 0.8, and $4/3\ h^{-1}$ in three experiments.

(a) $D = 0.6\ h^{-1}$.

Using $s = \dfrac{K_s D}{\mu_{max} - D} = \dfrac{1 \times 0.6}{1 - 0.6} = \dfrac{3}{2}$ and $(x_{final}/x_0) = z_\infty = 3/4$.

$$t = 5\left\{\ln\left(\frac{x}{x_0}\right) - \frac{1}{2}\ln\left[4\left(\frac{x}{x_0} - \frac{3}{4}\right)\right]\right\}. \tag{1}$$

(b) $D = 0.8\ h^{-1} = D_{max}$, and from (9.71):

$$t = \frac{6}{5} \times \frac{25}{4}\left(\frac{x_0}{x} - 1\right) + 5\ \ln\left(\frac{x}{x_0}\right) = 7.5\left(\frac{x_0}{x} - 1\right) + 5\ \ln\left(\frac{x}{x_0}\right). \tag{2}$$

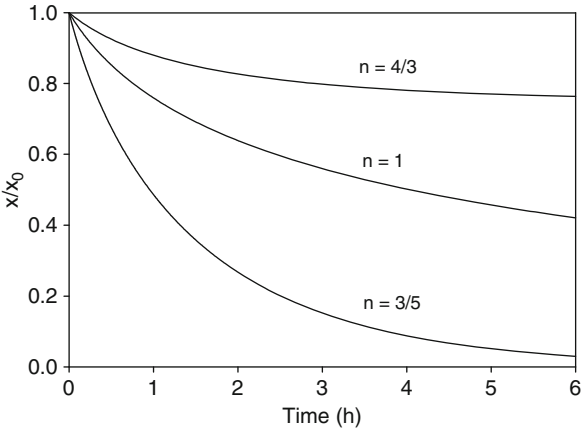

Fig. 9.9 Transients when the dilution rate is changed from $D_0 = 0.4\ h^{-1}$ to $0.6\ h^{-1}$, and to $0.8\ h^{-1}$ or $4/3\ h^{-1}$, corresponding to $n = D_{max}/D = 0.8/0.6 = 4/3$, $n = 1$, and $n = 3/5$. Kinetic and other data for the system are given in the text

(c) $D = 4/3\ h^{-1}$, and $n = 3/5$.

The culture washes out according to (9.69). $z_\infty = 12/5$ and:

$$t = -\frac{15}{8}\left(\ln\frac{x}{x_0} - \frac{3}{5}\ln\left(\frac{x/x_0 - 12/5}{-7/5}\right)\right). \tag{3}$$

The three transients are shown in Fig. 9.9.

Note the very slow approach of z to its final value of 0 when $D \approx D_{max}$.

Typically, the experience is that the final approach to a new steady state is very slow when one works near the wash-out dilution rate D_{max}. This is a result of the asymptotic behavior (9.72).

The analytical expressions for the change in x after a change in D are complicated, and yet this is the only case where an analytical expression can be established. Even for the case of a step change in s_f, Fig. 9.8, the inhomogeneous differential equations (9.62) cannot be solved analytically due to the occurrence of the exponential term in (9.68). Numerical integration was used to find the solution in Fig. 9.8.

The analytical solution obtained in Example 9.9 gives a certain amount of insight into how the parameters influence the solution, but virtually all other transient experiments must be compared with computer-generated model simulations. This is, of course, not at all an obstacle since PC-based software for this purpose is universally available.

The real difficulty is to set up a model which, after the model parameters have been fitted by a suitable number of well-planned experiments, can also be used outside the region of the available data.

Thus, none of the transient experiments of Figs. 7.12, 7.14, and 7.15 could ever be fitted to a Monod-type model. Unfortunately, this fact is as yet not appreciated by all engineers and biologists who use quite impossible models to analyze transient data from cultivations in bioreactors.

9.3.3 Pulse Addition of Substrate to a CSTR. Stability of the Steady State

When a pulse of substrate is added to a steady-state CSTR at constant dilution rate, the substrate concentration s immediately jumps to $s_0 + \Delta s$. Extra biomass is eventually produced from the substrate pulse, and since the feed $v \times s_f$ remains constant this biomass should eventually reduce s to its value before the addition of the pulse. If in another experiment, a pulse of biomass is added to the steady-state CSTR, this pulse of biomass will consume extra substrate, and when s decreases below its steady-state value the pulse of biomass will slowly wash out. According to (9.68c), the sum $x + Y_{sx}\, s$ decreases exponentially toward $Y_{sx}s_f$ with a time constant D^{-1}. One will intuitively assume that the original steady state is the final state which is approached both after a pulse of S and after a pulse of X has been added.

Whereas it is always true that addition of a pulse Δx to steady-state CSTR will bring the state back to the original $[s, x]$, this is only true in the experiment with pulse substrate addition, if the original steady state is *stable*. $[s, x, p] = [s_f, 0, 0]$ is always a steady-state solution to (9.62) when $[x_f, p_f] = [0, 0]$. When $\mu(s)$ attains the same value for two different s values in the interval $[s_f, 0]$ as was illustrated in the substrate-inhibited kinetics (9.23), the transient might end in (two) different steady states with nonzero values of x and p. In the mathematical language introduced in the discussion of a steady oscillation of a culture in Sect. 7.6.1, there are two *attractors*, i.e., stable end points of the transient. This subject is of great interest in the study of bioreactions, as well as in any other physical system governed by nonlinear dynamics.

Generally speaking, we have to analyze the *stability* of a given steady state to perturbations in the state variables, here x, s, and p.

In our discussion, perturbations in s are of specific interest. When biomass is added, the rate of biomass wash-out is always greater than its rate of production from the (initially) decreasing substrate concentration in the reactor, and the system returns to the original steady state $[s_0, x_0]$.

Likewise, addition of a product pulse, will either not affect μ or, if the product inhibits the reaction, μ will decrease, and the pulse of P will be washed out.

This verbal description of the stability of a steady state to perturbations in the state variables can be translated to a rigorous mathematical analysis by standard methods from mathematical physics.

To illustrate the concepts of this analysis, the stability of a steady-state solution to the substrate and biomass mass balances in (9.62) is discussed.

Including a mass balance for the product or substrate consumption for maintenance, is, however, possible without much extra work – see Problem 9.6.

Thus, if we define the *state vector* $\mathbf{c}$ as (x, s) and a vector function $\mathbf{F}$ of the vector variable $\mathbf{c}$ as the right-hand side of (9.62): $F_1 = \mu x - Dx$; $F_2 = -Y_{xs}\mu x + D(s_f - s)$, then by a linear perturbation from the steady state $F_0 = F_0\,(x_0, s_0) = (0, 0)$:

$$\mathbf{F} \approx \mathbf{F}_0 + \left(\frac{\partial \mathbf{F}}{\partial \mathbf{c}}\right)_{\mathbf{c}_0} \mathrm{d}\mathbf{c}. \tag{9.73}$$

$\left(\frac{\partial \mathbf{F}}{\partial \mathbf{c}}\right)_{\mathbf{c}_0}$ is a matrix with four elements, defined as

$$\mathbf{J} = \begin{pmatrix} \frac{\partial F_1}{\partial x} & \frac{\partial F_1}{\partial s} \\ \frac{\partial F_2}{\partial x} & \frac{\partial F_2}{\partial s} \end{pmatrix}_{x_0, s_0} . \tag{9.74}$$

Consequently, we obtain the following *linear* differential equations in the *deviation variable* $\mathbf{y} = \mathbf{c} - \mathbf{c}_0$:

$$\frac{\mathrm{d}\mathbf{y}}{\mathrm{d}t} = \mathbf{J} \cdot \mathbf{y}. \tag{9.75}$$

This was of course just what was illustrated in Sect. 6.4.4 in the linearization of $\mathbf{r}$ from a given state $\mathbf{r}^0$ by a perturbation of $\mathbf{c}$ from its "standard" value $\mathbf{c}^0$.

The solution of the N linear differential equations with constant coefficients is, in general, a weighted sum of exponentials. If all exponentials have negative exponents, then the perturbation will die out, and the steady state will be exponentially approached.

The *eigenvalues* λ_i of the *Jacobian matrix* $\mathbf{J}$ determine the exponents.

Matrix $\mathbf{J}$ of dimension $(N \times N)$ has N eigenvalues. These are determined as the N zeros of the polynomial obtained by calculating the determinant of the matrix $\mathbf{J} - \lambda \mathbf{I}$.

For our case of $N = 2$, the determinant (9.76) is a polynomial of degree 2 in λ.

$$\mathrm{Det} \begin{pmatrix} \mu - D - \lambda & \mu_\mathrm{s} x \\ -Y_\mathrm{xs}\mu & -Y_\mathrm{xs}\mu_\mathrm{s} x - D - \lambda \end{pmatrix}_{x_0, s_0} . \tag{9.76}$$

μ_s is defined as $\left(\frac{\partial \mu}{\partial s}\right)_\mathrm{ss}$, and the subscript ss stands for the investigated steady state.

In the steady state $\mu = D$, while during the transient μ must be different from D since s is different from s_0. When $\mu = D$ is inserted in (9.76), one can obtain λ by the solution of (9.77):

$$\begin{aligned} \lambda(Y_\mathrm{xs}\mu_\mathrm{s} x + D + \lambda) + Y_\mathrm{xs} x D \mu_\mathrm{s} = 0, \\ \lambda = \begin{cases} -D, \\ -Y_\mathrm{xs} x \mu_\mathrm{s}. \end{cases} \end{aligned} \tag{9.77}$$

There is always one negative eigenvalue, namely $-D$, and if μ_s is positive for the steady state the other eigenvalue is also negative.

For *Monod kinetics*, μ increases monotonically with s, and μ_s is positive for any steady state. For substrate inhibition kinetics, (9.23), all steady states to the left

of the maximum of $\mu(s)$ at $s = (K_i K_s)^{1/2}$ have $\mu_s > 0$, while $\mu_s < 0$ to the right of the maximum.

The stability of the steady state is determined by the following rules:

- If all eigenvalues have a negative real part, then the steady state is *asymptotically stable*. This means that the state is stable, at least for infinitely small perturbations of the state variables.
- If just one eigenvalue has a positive real part, then the steady state is unstable.
- If the imaginary part b_i of all eigenvalues $\lambda_i = a_i \pm ib_i$ is zero, then the deviation variable $\mathbf{y}$ either increases exponentially away from $\mathbf{y}_0$ ($a_i > 0$), or decreases exponentially to 0 ($a_i < 0$). If any $b_i \neq 0$, then the movement away from or back to $\mathbf{y}_0$ or toward 0 is oscillatory.

By these rules, all steady states are asymptotically stable for Monod kinetics while steady states with $s > (K_i K_s)^{1/2}$ are unstable for the substrate inhibition kinetics. Oscillations will not be found, neither for Monod kinetics nor for substrate inhibition kinetics.

The asymptotic stability analysis gives no clue as to the final goal of the transient away from an asymptotically unstable steady state. It does not either tell what happens if an asymptotically stable steady state is submitted to a perturbation of finite magnitude.

Figure 9.10 gives the time profiles of $S = s/s_f$, after perturbation of an unstable steady state with substrate inhibition kinetics. S tends to either $S = 1$ (for a positive perturbation of S) or (for a "negative perturbation of S," i.e., addition of a pulse of X) to the asymptotically stable steady state which has the same D value as the unstable steady state, but it is to the left of the maximum in $\mu(S)$ in (9.23).

These two stable steady states are the *attractors* for the solution of the dynamic mass balances. In Fig. 9.11, a much more general representation of the dynamics is given in terms of a phase diagram for the same example as discussed in Fig. 9.10. Here, the trace of (S, X) is followed from any starting point (S_0, X_0), and the diagram clearly shows which initial conditions will lead to a transient that ends up in each of the two attractors.

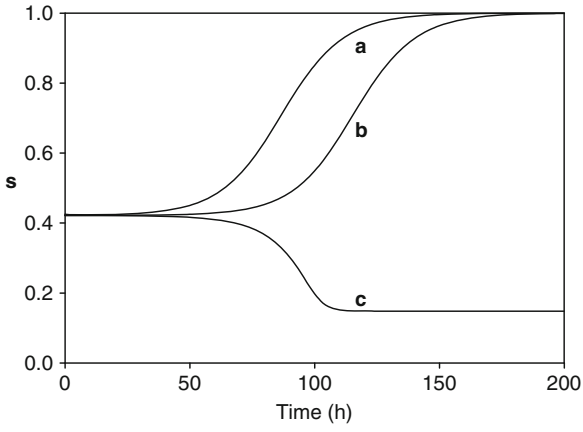

Fig. 9.10 Time profiles of the response of a continuous stirred tank reactor which is disturbed by applying a pulse ΔS to an unstable steady state. Substrate inhibition kinetics (9.23) with $\mu = 0.5S/(S^2 + S + 0.0625)$; $S = s/s_f = 0.42162$ at the steady state $D = 0.3185\ h^{-1}$. $\Delta S = 0.00338$ (a), 0.00038 (b), and −0.00062 (c)

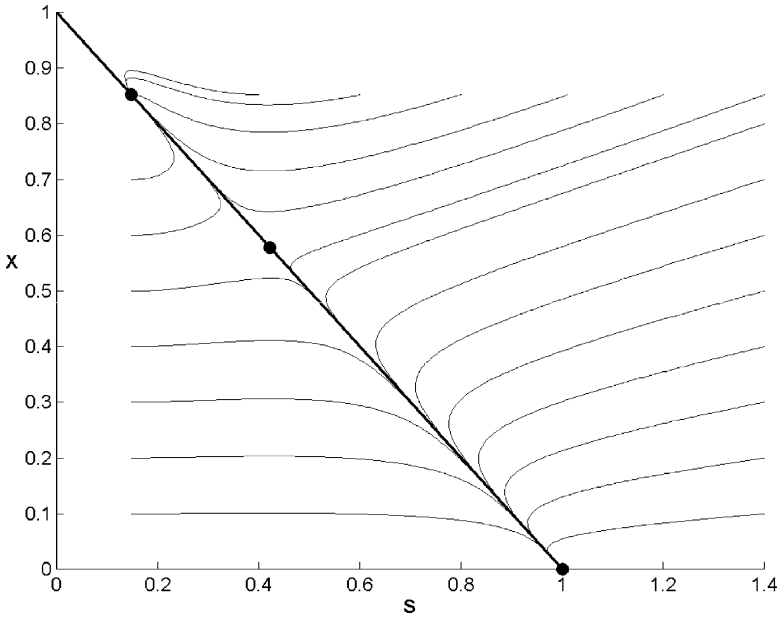

Fig. 9.11 Phase diagram showing $X = x/(s_f Y_{sx})$ vs. $S = s/s_f$ for the substrate-inhibited kinetics of Fig. 9.10. The straight line shows steady-state values of $[S, X]$ obtained for $x_f = 0$ and different D in a CSTR, or the progress of a batch reaction started with $x_f \approx 0$. On the line are marked the two steady-state solutions $[S, X]$ to the mass balances for $D = 0.3185\ h^{-1}$ ([0.1483, 0.8517] and [0.42162, 0.5784]), and the trivial steady-state solution [1,0]. The curves are trajectories followed when continuous operation is started from different initial values $[S_0, X_0]$. The trajectories always bend away from the saddle-point at the unstable steady state at $S = 0.42162$. When the batch reaction is started with larger inoculum (X_0 finite), or $X_f > 0$, the straight line is shifted to the right. Note that the upper steady state [0.1483, 0.8517] is also reached when $S_0 > 0.42162$, but only if X_0 is sufficiently high.

When the batch reaction is started with larger inoculum (X_0 finite), or $X_f > 0$, the straight line moves to the right.

Note that the upper steady state [0.1483, 0.8517] is also reached when $S_0 > 0.42162$, but only if X_0 is sufficiently high.

If maintenance substrate consumption is included as in (9.3) and (9.4), one can obtain, in complete analogy with the derivation of (9.77), that

$$2\lambda = -(Y_{xs}^{true}\mu_s x + D) \pm \sqrt{(Y_{xs}^{true}\mu_s x - D)^2 - 4\mu_s x m_s} = -\left(Y_{xs}^{true}\mu_s x + D\right) \pm \delta, \quad (9.78)$$

$$\lambda = \begin{cases} -D - \delta \\ -Y_{xs}^{true}\mu_s x + \delta \end{cases} \quad \text{for} \quad \mu_s > 0 \text{ at } (x_0, s_0), \quad (9.79a)$$

$$\lambda = \begin{cases} -D + \delta \\ -Y_{xs}^{true}\mu_s x - \delta \end{cases} \quad \text{for} \quad \mu_s < 0 \text{ at } (x_0, s_0), \quad (9.79b)$$

Maintenance appears to destabilize the nontrivial steady state where $\mu_s > 0$ while an unstable steady state μ_s is somewhat stabilized.

Very few rate expressions will lead to an analytical evaluation of (9.78), but the simple Monod kinetics is an exception. Here, one can obtain:

$$\mu_s = \frac{1}{s_f}\frac{d\mu}{dS} = \frac{1}{s_f}\frac{a}{S(S+a)}D, \tag{9.80}$$

$$2\lambda = D\left\{-\left[X\frac{a}{S(S+a)}+1\right] \pm \sqrt{\left[X\frac{a}{S(S+a)}-1\right]^2 - \frac{4abX}{S^2}}\right\}. \tag{9.81}$$

For all steady-state values (S, D), a real eigenvalue is always negative. There may be complex eigenvalues, but their real part is always negative. Consequently, all the steady states are stable, but oscillations may occur in the transient if for a given steady state

$$\left[X\frac{a}{S(S+a)}-1\right]^2 < \frac{4abX}{S^2}. \tag{9.82}$$

9.3.4 Several Microorganisms Coinhabit the CSTR

When several microbial species live together in a CSTR, a rich variety of dynamic problems emerge, and the solution of many of these problems is of great practical interest.

The following are the examples of the situations which might arise:

- The organisms compete for the same limiting substrate S.
- A product from one organism poisons the organisms that live on the same substrate.
- A product from an organism that lives on S serves as a substrate for another organism.
- One organism X_1 lives on S while another organism X_2 lives on X_1, but not on S.

The concepts are illustrated in the following by a population of two microbial species X_1 and X_2 that live on the same limiting substrate. The other cases are exemplified by organisms that excrete antibiotics to kill competitors for S, by different species of lactic bacteria that grow in coculture because one species uses a metabolic product of another species as substrate and finally by organisms that devour other organisms as substrate, or to proliferate.

Since product formation is a simple function of the concentrations of the two species, we shall not consider the product mass balance. Consequently, the mass

balances for maintenance-free kinetics and two species competing for the same limiting substrate S are:

$$\frac{\mathrm{d}x_1}{\mathrm{d}t} = \mu_1 x_1 - q_{12} + q_{21} - Dx_1, \tag{9.83a}$$

$$\frac{\mathrm{d}x_2}{\mathrm{d}t} = \mu_2 x_2 - q_{21} + q_{12} - Dx_2, \tag{9.83b}$$

$$\frac{\mathrm{d}s}{\mathrm{d}t} = -(Y_{x_1 s}\mu_1 x_1 + Y_{x_2 s}\mu_2 x_2) + D(s_\mathrm{f} - s). \tag{9.83c}$$

Here, both species grow on the same limiting substrate S. An interconversion between the two species – by the metamorphosis reactions of Sect. 7.6 or perhaps by the loss of plasmids – is included. q_{12} is the volumetric rate of conversion of species 1 to species 2, while q_{21} is the volumetric rate of conversion of species 2 to species 1.

A number of widely different situations are described by a suitable interpretation of the interspecies reaction rates, and a few examples will be considered. But first the simplest case of $q_{12} = q_{21} = 0$ will be treated. This case is extremely important since it describes what happens after an *infection* of the continuous stirred tank reactor. Dimensionless mass balances for the case of an infection and Monod kinetics are:

$$\frac{\mathrm{d}X_1}{\mathrm{d}\theta} = \frac{\mu_{\max,1}}{D}\,\frac{SX_1}{S + a_1} - X_1, \tag{9.84a}$$

$$\frac{\mathrm{d}X_2}{\mathrm{d}\theta} = \frac{\mu_{\max,2}}{D}\,\frac{SX_2}{S + a_2} - X_2, \tag{9.84b}$$

$$\frac{\mathrm{d}S}{\mathrm{d}\theta} = -\left(\frac{\mu_{\max,1}}{D}\,\frac{SX_1}{S + a_1} + \frac{\mu_{\max,2}}{D}\,\frac{SX_2}{S + a_2}\right) + (1 - S). \tag{9.84c}$$

θ is defined as Dt, since D^{-1} is a common scale factor in the three equations. S and (X_1, X_2) are defined as in (9.7). Local asymptotic stability of a given steady state (S_0, X_{10}, X_{20}) is examined by the same method used in (9.75). The analysis turns out to be remarkably simple since the only nontrivial steady state with both species coexisting is that for which

$$\begin{aligned} &\frac{\mu_{\max,1} S_0}{S_0 + a_1} = \frac{\mu_{\max,2} S_0}{S_0 + a_2} = D \\ &\Downarrow \\ &S_0 = \frac{\mu_{\max,1} a_2 - \mu_{\max,2} a_1}{\mu_{\max,2} - \mu_{\max,1}}\ ; \quad D = \frac{\mu_{\max,1} a_2 - \mu_{\max,2} a_1}{a_2 - a_1}. \end{aligned} \tag{9.85}$$

The sum $X_{10} + X_{20} = 1 - S_0$, but the distribution between X_{10} and X_{20} is unknown. The Jacobian for the system described by (9.84a–c) is

$$\mathbf{J} = \begin{pmatrix} \dfrac{\beta_1 S_0}{S_0 + a_1} - 1 & 0 & \dfrac{a_1 \beta_1 X_{10}}{(S_0 + a_1)^2} \\ 0 & \dfrac{\beta_2 S_0}{S_0 + a_2} - 1 & \dfrac{a_2 \beta_2 X_{20}}{(S_0 + a_2)^2} \\ \dfrac{-\beta_1 S_0}{S_0 + a_1} & \dfrac{-\beta_2 S_0}{S_0 + a_2} & -\left(\dfrac{a_1 \beta_1 X_{10}}{(S_0 + a_1)^2} + \dfrac{a_2 \beta_2 X_{20}}{(S_0 + a_2)^2} + 1 \right) \end{pmatrix}. \quad (9.86)$$

$\beta_1 = \mu_{\max,1}/D$ and $\beta_2 = \mu_{\max,2}/D$. From (9.85), one can obtain

$$\beta_1 \frac{S_0}{S_0 + a_1} = \beta_2 \frac{S_0}{S_0 + a_2} = 1. \quad (9.87)$$

Consequently, the eigenvalues of matrix $\mathbf{J}$ in (9.86) are zeros of

$$F(\lambda) = \lambda \left\{ \lambda^2 + \left[\left(\frac{a_1 X_{10}}{\beta_1} + \frac{a_2 X_{20}}{\beta_2} \right) \frac{1}{S_0^2} + 1 \right] \lambda + \left(\frac{a_1 X_{10}}{\beta_1} + \frac{a_2 X_{20}}{\beta_2} \right) \frac{1}{S_0^2} \right\}. \quad (9.88)$$

The zeros of the third-degree polynomial are:

$$\lambda = \begin{cases} 0 \\ -1 \\ -\left(\dfrac{a_1 X_{10}}{\beta_1} + \dfrac{a_2 X_{20}}{\beta_2} \right) \dfrac{1}{S_0^2} \cdot \end{cases} \quad (9.89)$$

The eigenvalue -1 is related to the time it takes before an added mass pulse of S, X_1, or X_2 has been washed out of the continuous stirred tank reactor. This is seen by adding the three equations in 9.84 and integrating as in (9.68c), i.e.,

$$S + X_1 + X_2 = (\Delta S + \Delta X_1 + \Delta X_2) \ \exp(-Dt) + 1. \quad (9.90)$$

Here ΔS, ΔX_1, and ΔX_2 are the excess concentrations of substrate and of the two biomass components at the start of the transient $t = 0^+$. One of the remaining eigenvalues associated with the steady state where both X_1 and X_2 coexist is clearly negative, but the eigenvalue of zero tells us that this steady state is only *conditionally stable*, as discussed in Example 9.9.

Example 9.10 *Competing microbial species.* Let $s_f = 100$ mg L^{-1} and

$$\mu_1 = \frac{0.4s}{s + 10} \ ; \quad \mu_2 = \frac{0.5s}{s + 20} \qquad (s \text{ in mg L}^{-1} \ ; \ \mu_1, \mu_2 \text{ in h}^{-1}). \quad (1)$$

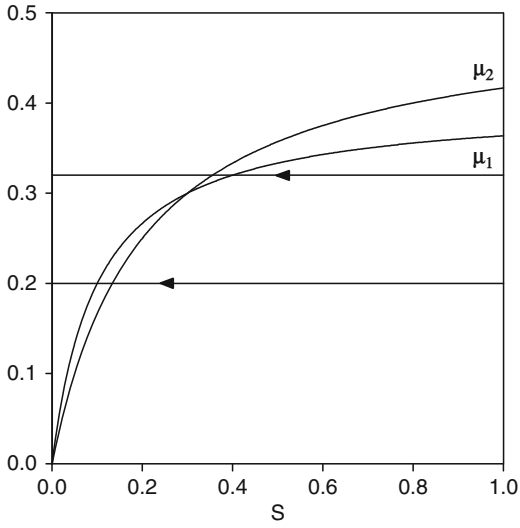

Fig. 9.12 Competition of two microbial species X_1 and X_2 that coexist at $\mu = D = 0.3\ \mathrm{h}^{-1}$. The specific growth rates μ_1 and μ_2 are given in (1). Arrows indicate what happens after an infection of a monoculture at $D = 0.32$ and $0.2\ \mathrm{h}^{-1}$, respectively. A steady state on the right-hand curve is changed to a steady state on the left-hand curve after a perturbation in S

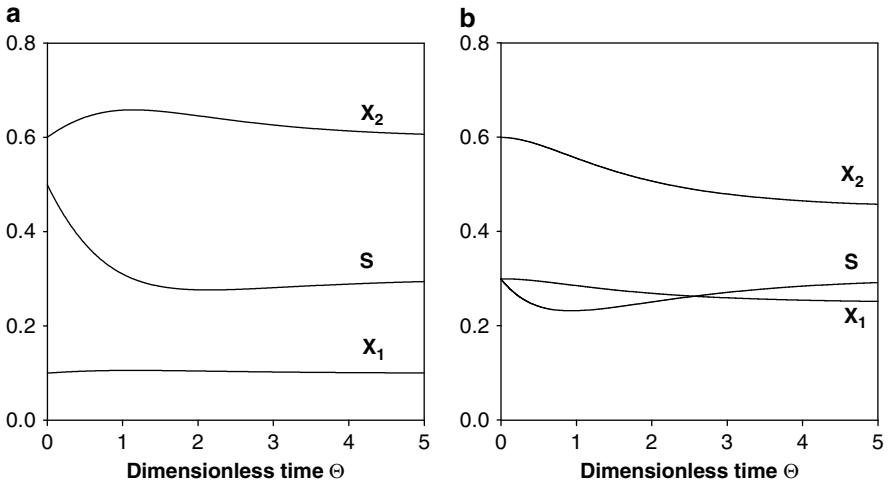

Fig. 9.13 Disturbance of the *common* steady state on Fig. 9.12 for which $\mu = D = 0.3\ \mathrm{h}^{-1}$ (**a**) $\Delta S = 0.2$ and (**b**) $\Delta X_1 = 0.2$

The steady state where x_1 and x_2 coexist is determined by (9.85):

$$S_0 = \frac{0.4 \times 0.2 - 0.5 \times 0.1}{0.5 - 0.4} = 0.3; \quad X_{10} + X_{20} = 0.7; \quad D = 0.3\ \mathrm{h}^{-1}, \tag{2}$$

$\mu_1(S)$ and $\mu_2(S)$ are shown in Fig. 9.12.

Figure 9.13a, b and 9.14a, b shows the transients after perturbation of the common steady state $S_0 = 0.3$.

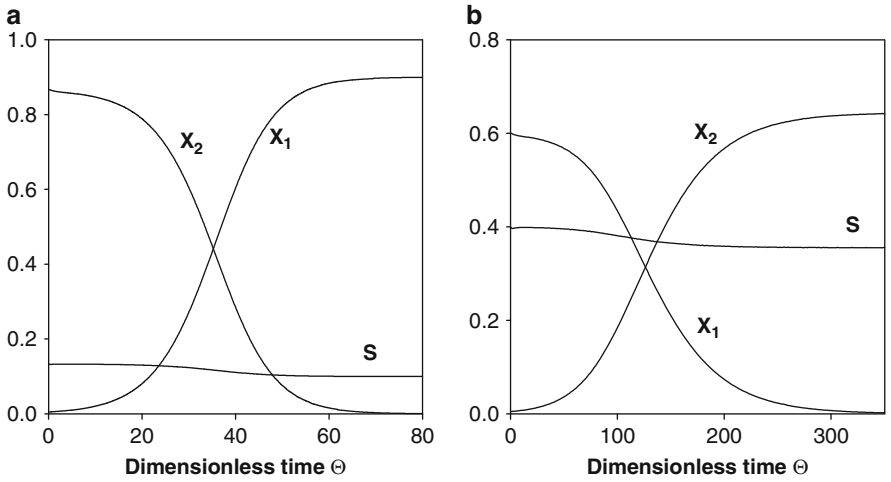

Fig. 9.14 Wash-out of the slowest-growing species. In (**a**), $D < 0.3\ \mathrm{h}^{-1}$ and X_2 is washed out. In (**b**), $D > 0.3\ \mathrm{h}^{-1}$ and X_1 is washed out. In both (**a**) and (**b**), a pulse $\Delta X_i = 0.005$ is added to simulate an infection. $D = 0.20\ \mathrm{h}^{-1}$ in (**a**) and $0.32\ \mathrm{h}^{-1}$ in (**b**)

In Fig. 9.13a, a pulse of substrate $\Delta S = 0.2$ is added to a CSTR with $X_{10} = 0.1$ and $X_{20} = 0.6$, causes an initial increase in both X_1 and X_2. Both concentrations return to their initial steady-state values after the pulse has been washed out. S undershoots its steady-state value 0.3 exactly one time.

In Fig. 9.13b, the effect of a pulse $\Delta X_1 = 0.2$ (i.e., $X_1 = 0.3$ and $X_2 = 0.6$ at $t = 0^+$) is examined. After S has returned to 0.3, the biomass composition has *changed* to $X_1 = 0.25$, $X_2 = 0.45$.

Whereas the pulse addition of substrate gives an equal advantage to the two competing species and leaves the final biomass composition unchanged, the addition of a pulse of one of the species selectivity favors this species, and one ends up with a biomass richer in the favored species. This is an implication of the zero eigenvalue of the Jacobian: Only S is fixed at the steady state, while the partition of the remaining mass $1 - S$ is arbitrary.

Figure 9.14a, b shows what happens after infection of the reactor with the growth-favored microbial species. For $D < 0.3$, the specific growth rate of X_1 is higher than that of X_2. A stable steady-state cultivation of X_2 can only be maintained when X_1 is absent, in which case (9.84 a) is automatically satisfied. Even a minute infection of the reactor by X_1 leads to wash-out of X_2, and S decreases from 2/15 to the lower steady-state value 1/10 associated with the growth of X_1 alone at the specified $D = 0.2\ \mathrm{h}^{-1}$. For $D > 0.3\ \mathrm{h}^{-1}$, infection of a monoculture of X_1 will correspondingly lead to a takeover by X_2, as illustrated in Fig. 9.12 for $D = 0.32\ \mathrm{h}^{-1}$.

The situation illustrated in Example 9.10 is encountered in the operation of waste water treatment plants. The biomass (which may be a consortium of several organisms which in some way lend support to each other) is subjected to a change in dilution rate. Hereafter a large part of the biomass is washed out, and slowly a new consortium of organisms takes over.

Reversion of a producing strain to a nonproducing wild-type strain of the same microorganism is a well-known cause of disappointment in the industrial application of microorganisms. The reversion may occur by mutation or a valuable plasmid may be lost from a recombinant microorganism. Kirpekar et al. (1985) give an example of a Cephamycin-C producing strain which reverts to a nonproducing strain, and their analysis of experimental data from a CSTR culture to find a kinetic model for the metamorphosis reaction is discussed in Example 9.11. A similar case study is discussed in Problem 9.7, and Problem 9.11 reports how laboratory data can be misinterpreted with catastrophic results for an industrial production process.

For growth kinetics of the monotonic Monod type and a dilution rate where species X_2 is growth favored, even a small net rate of conversion of X_1 to X_2 by metamorphosis reactions will lead to wash-out of X_1, even when the culture was initially free of X_2. Conversely, a metamorphosis reaction in the other direction may help to stabilize the growth-handicapped species in the continuous culture.

The most frequent outcome of competition or parasitism in a stirred tank continuous reactor is that one of the microbial species is washed out except at a certain value of the dilution rate. The transient of a perturbation usually follows a straight (exponentially damped) path toward the final steady state, but oscillations can occur, and if the model has suitably complex growth kinetics the oscillations may even become chaotic. In ecological models, this phenomenon is well known, e.g., when prey-animals feed on grass (substrate) and predators which cannot eat grass scavenge the prey animals.

Example 9.11 *Reversion of a desired mutant to the wild type.* Let X_1 be the mutant (or plasmid-containing microorganism) that decays to the wild-type variant X_2 of the microorganism by a metamorphosis reaction. Both X_1 and X_2 grow on the same substrate, but with different specific growth rates.

Using dimensionless concentrations $[X_1, X_2]$ of the two species, the mass balances for the CSTR are:

$$\frac{\mathrm{d}X_1}{\mathrm{d}\theta} = \frac{\mu_1}{D}X_1 - \frac{q_{12}}{D} - X_1, \tag{1}$$

$$\frac{\mathrm{d}X_2}{\mathrm{d}\theta} = \frac{\mu_2}{D}X_2 + \frac{q_{12}}{D} - X_2, \tag{2}$$

$$\frac{\mathrm{d}S}{\mathrm{d}\theta} = -\frac{1}{D}(\mu_1 X_1 + \mu_2 X_2) + 1 - S. \tag{3}$$

$\theta = Dt$, $X_1 = x_1/(s_f Y_{sx})$, and $X_2 = x_2/(s_f Y_{sx})$. For simplicity, Y_{sx_1} has been set equal to $Y_{sx_2} = Y_{sx}$.

q_{12} is the rate of the irreversible metamorphosis reaction by which X_1 is converted to X_2. Addition of the three equations and integration shows that at the end of any transient, $S + X_1 + X_2$ is still $= 1$.

Following Kirpekar et al. (1985), we shall assume that the growth kinetics is studied at conditions of high substrate concentration where $\mu_1 = \mu_{max,1}$ and $\mu_2 = \mu_{max,2}$. In this way, we can focus on the influence of the metamorphosis reaction. Thus,

$$\mu_1/D = \beta_1; \quad \mu_2/D = \beta_2; \quad \text{and} \quad \beta_2/\beta_1 = c > 1.$$

The metamorphosis reaction is usually very slow compared to the reactor dynamics (time constant $t(q_{12}) >> 1/D$), and it is not a bad assumption that the total biomass concentration $x_1 + x_2$ in the effluent is constant in a reactor operated at constant D and s_f. What happens is that $f = x_2/(x_1 + x_2)$ slowly increases toward 1, because both the growth kinetics and the metamorphosis reaction favor x_2.

Consequently, by the addition of (1) and (2):

$$\frac{d(X_1 + X_2)}{d\theta} = 0 = \beta_1 X_1 + \beta_2 X_2 - (X_1 + X_2). \tag{4}$$

Insert $f = x_2/(x_1 + x_2)$ to obtain:

$$\beta_1(1-f) + \beta_2 f = 1 \rightarrow \beta_2 = \frac{c}{1 - f + fc}. \tag{5}$$

Furthermore,

$$\frac{df}{d\theta} = \frac{d[X_2/(X_1 + X_2)]}{d\theta} = \frac{1}{X_1 + X_2}\frac{dX_2}{d\theta} + 0 = \frac{f}{X_2}\frac{dX_2}{d\theta} \tag{6}$$

or

$$\begin{aligned}\frac{df}{d\theta} &= \frac{f}{X_2}\left(\frac{cX_2}{1 - f + fc} + \frac{q_{12}}{D} - X_2\right) = \frac{fc}{1 - f + fc} + \frac{fq_{12}}{X_2 D} - f, \\ &= \frac{fc}{1 - f + fc} + \frac{q_{12}}{X_1 D} f\frac{1-f}{f} - f = \frac{f(1-f)(c-1)}{1 - f + fc} + \frac{q_{12}(1-f)}{X_1 D}.\end{aligned} \tag{7}$$

The most reasonable metamorphosis kinetics is $q_{12} = kX_1$, i.e., the rate by which species X_1 is converted to X_2 is proportional to the concentration x_1 of the reactant. With this kinetic expression,

$$\frac{df}{d\theta} = \frac{f(1-f)(c-1)}{1 - f + fc} + \frac{k}{D}(1-f). \tag{8}$$

For $k = 0$, and integration by separation of variables,

$$\theta = \frac{1}{c-1}\left[\ln\left(\frac{f}{f_0}\right) - c\ln\left(\frac{1-f}{1-f_0}\right)\right], \tag{9}$$

f_0 is the fraction of X_2 in the biomass for $\theta = 0$, and $c = \mu_{max,2}/\mu_{max,1}$.

f approaches 1 (i,e., $x_1 \rightarrow 0$) when $\theta \rightarrow \infty$, and the transient is independent of the dilution rate.

For $k \neq 0$ and $k' = k/D$, i.e., the rate constant of the reversion reaction is inversely proportional to D:

$$\theta = -\frac{c}{c-1+ck'} \ln\left(\frac{1-f}{1-f_0}\right) + \frac{1}{(c-1+ck')\,(1+k')} \ln\left[\frac{(c-1)\,(1+k')\,f+k'}{(c-1)\,(1+k')\,f_0+k'}\right]. \tag{10}$$

Again, f approaches 1 when $\theta \rightarrow \infty$, but now the transient depends on the value of D.

Kirpekar et al. (1985) simulate the progress of f for experimental runs with various values of D. For the given $c(=1.25)$, they can fit the value of k to the experiments.

An acceptable fit of the f versus θ transient (10) for the three D values 0.025, 0.036, and 0.045 h^{-1} is obtained with $k = 0.0035\ h^{-1}$ (note that $k/D << 1$).

They also investigate various other models for the metamorphosis reaction:

$$\text{Model 1}: \quad q_{12} = k\mu_{\max,1}X_1 \quad (k \text{ dimensionless}), \tag{11}$$

$$\text{Model 2}: \quad q_{12} = kfX_1 = k\frac{X_1X_2}{X_1+X_2} \quad (k \text{ in } h^{-1}), \tag{12}$$

$$\text{Model 3}: \quad q_{12} = kf\mu_{\max,1}X_1 = k\mu_{\max,1}\frac{X_1X_2}{X_1+X_2}. \tag{13}$$

In all three cases, analytical integration is possible. The authors believe that the kinetics of (13) is the most reasonable, but their data do not allow them to discriminate between the metamorphosis reaction models of (12) and (13).

9.3.5 *The CSTR Used to Study Fast Transients*

In Sect. 6.4, metabolic control analysis was introduced as a tool for improving the flux of carbon in the metabolic network toward a desired product.

A pulse of, e.g., glucose, suitably labeled if necessary, was introduced to a CSTR and the change in concentrations of internal metabolites as well as of final products was followed as a function of time. Hereby, data were obtained for the determination in Sect. 6.4.4 of flux control coefficients in the investigated pathway or section of the metabolic network.

Most of the pathway reactions are very fast compared to the specific growth rate of the culture which is equal to D in steady-state CSTR cultivation.

It would be impossible to take out samples and quench them fast enough to even get a glimpse of the rapid transients if "conventional" sampling methods, e.g., removing a sample with a pipette, were used. With time constants in the order of at

most seconds for a pulse of substrate to move through a pathway, none of the concentration–time profiles needed in Example 6.7 would be obtained.

Since sampling methods that are fast enough to capture the fast transients are needed to support the calculation of flux control by means of transient experiments, new reactor constructions have been invented. In the following, we shall introduce some of these constructions, in particular, from TU Stuttgart and TU Delft, the two institutions which have been leaders in developing methods for capturing fast metabolic transients.

It must be emphasized that these measurement techniques are not developed for studies of simple cultivation experiments, modeled by unstructured models. In the study of the dynamics of specific pathways, all the reactions can be modeled by expressions that are based on mechanistic reaction rate models, although as discussed in Sect. 6.4.4 the reaction rates are intentionally approximated, e.g., by Lin-Log kinetics, to simplify the retrieval of rate parameters for the determination of the flux control coefficients.

In the previous sections of Chap. 9, the discussion was mostly based on an assumption of metabolic steady state in the organism, and as stated in Sects. 9.3.1–9.3.3 there is no chance that simple kinetic models will ever be able to give a full quantitative understanding of how rapid transients, applied to a cell culture, will influence the over-all behavior of the metabolic network in the cell.

During the 1990s, the Stuttgart group (Theobald et al. 1993, 1997) developed fast sampling and quenching methods where 10–20 measurements could be made in 1950s. By 2002, a fully automated sampling technique had been developed, and the rate of sampling had been increased to about 10 samples per second (Buziol et al. 2002). Figure 9.15 is a schematic representation of the system, and Fig. 9.16 shows

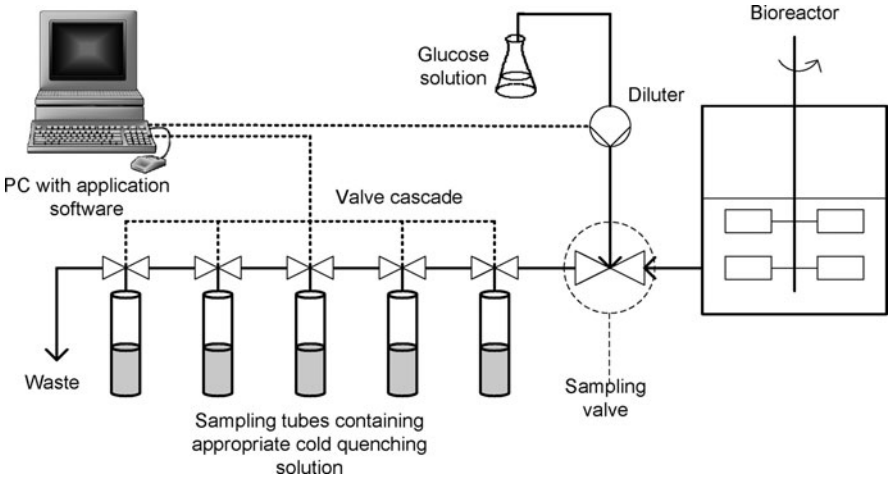

Fig. 9.15 A system for measuring the rate of fast metabolic reactions. Adapted from Buziol et al. (2002)

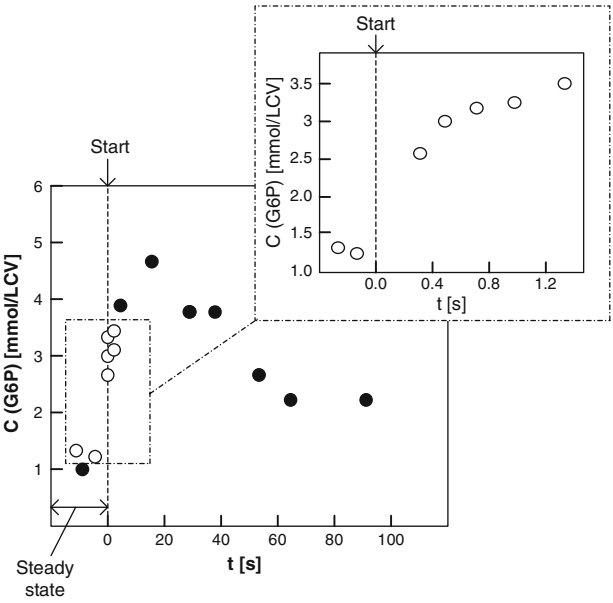

Fig. 9.16 The concentration of glucose-6-phosphate (G6P) in *Saccharomyces cerevisiae* after a pulse of glucose is injected at $t = 0$. Results are shown both from the measurement system of Fig. 9.15 (*open circle*) and from an earlier experimental system, Theobald et al. (1993, 1997) (*filled circle*). The *insert* shows data from the first second after injection, and an extremely small time constant for the production of G6P from extracellular glucose (~0.4 s) is obtained. The experiment confirms that neither glucose permease (see Sect. 7.7.1) nor hexokinase is the bottleneck in the EMP pathway, and it takes more than 100 s before the reactions downstream of hexokinase have consumed the G6P peak. The unit "CV" refers to cell volume and mmol $(\text{LCV})^{-1}$ equals mmol $(420\ \text{g DW})^{-1}$. Adapted from Buziol et al. (2002)

some results obtained by perturbing steady-state CSTR cultures of *S. cerevisiae* by injecting a pulse of glucose. The almost instantaneous increase in [G6P] could not have been captured by the techniques used only a few years earlier.

At the heart of the system is the sampling valve. When the valve is opened, a jet of medium and cells is injected into the valve. Immediately the valve on the reactor is opened, concentrated glucose solution flows in a jet to a mixing chamber in the valve where it meets the sample jet, and the two streams are intimately mixed. The combined stream flows to a rack of sampling tubes, and depending on the position of the valves on the rack it ends up in a particular sampling tube where all cell activity is quenched in $-196°\text{C}$ liquid N_2. After flushing the capillary in the rack, a sample is directed to another tube. Knowing the exact passage time to each sampling tube, and the exact time in which the valve on the rack is opened, permits samples to be collected where the time of exposure of the cell suspension to the glucose solution is known with high precision. Note 9.2 gives a few details on the procedure.

Note 9.2 *Sampling in the Buziol et al. system and extraction of metabolites*. The system is an example of so-called stopped flow sampling systems that were introduced in the 1960s by Chance et al., and perfectioned at the end of the twentieth century using robotics and computer-activated valves (see references in Buziol et al. 2002).

Before the sampling sequence, the capillary is flushed with the cell suspension + glucose mixture which is collected in the waste recipient. The first sample taken is that for which the contact time is smallest, and this is collected by opening the first, computer controlled valve on the capillary. When the first valve is closed, the capillary is again flushed, and thereafter the second valve is opened to receive a sample. The first valve is 261 mm from the mixing chamber, the fifth 686 mm. The flow rate is measured by weighing the sample tube + quenching liquid before and after a sample has been received. The Reynolds number *Re* (see Chaps. 10 and 11) is about 2,500 in the sampling capillary to ensure plug flow.

During the sampling, the culture in the CSTR is unaffected since addition of the glucose pulse is in the mixing chamber which is outside the reactor. The sampling time and the reaction time is decoupled by a suitable operation of the computer-activated valves on the sampling line, and the sample size can be different for the different samples (more sample in the first tube where the reaction time is smallest).

Finally, other stimuli such as a pulse of $[H^+]$ can be applied in the same equipment in order to study other effectors of the metabolic rates.

If an aerobic cultivation is studied, one must be sure that the liquid reaching the last sampling point still has an oxygen concentration above the saturation level, since otherwise the rate would be influenced by $[O_2]$. Experiments in the system have shown that this is the case for all holding times <20 s which is far above the time interval studied in the equipment.

The metabolites under study are extracted from liquid-N_2 quenched samples of ~3 mL. The samples are treated with perchloric acid to open up the cell membrane and extract the metabolites. After neutralization of the acid, the perchloric salts are removed by precipitation, and the metabolite solution is analyzed by, e.g., HPLC. The whole procedure has been subjected to several checks with known concentrations of the metabolites in order to ensure that the metabolites are not degraded during the rather long sample preparation and extraction process.

The *BioScope* rapid sampling system developed at TU Delft is based on the same construction principles as the TU Stuttgart system: The culture is not disturbed by the sampling, sampling ports are located in sequence along a sampling line, and the time of exposure of the cell suspension to the added substrate is calculated with precision. The sampling frequency is not as high as in the Buziol et al. system, but many samples are taken in a time-window from 1 to 50 s.

The first report of the BioScope system is by Visser (2002), and a large number of subsequent papers referred to in Mashego et al. (2007) document that the equipment has been of great importance for the metabolic studies in the group of J.J. Heijnen at TU Delft.

9.4 The Plug Flow Reactor

The basic model for the tubular reactor is the so-called plug flow reactor (PFR) model in which no concentration or temperature gradients in the radial coordinate are considered. Hence there is only one spatial dimension, the distance z along the reactor axis.

A mass balance for reaction component i in a volume element $A\mathrm{d}z$ where A is the constant cross-sectional area of the reactor yields

$$\frac{\partial c_i}{\partial t} = -v_z \frac{\partial c_i}{\partial z} + q_i(c), \tag{9.91}$$

v_z is the linear velocity in the z direction.

The transient mass balance for the PFR is a hyperbolic partial differential equation which can be solved using the method of characteristics, as described in Aris and Amundson (1973). The initial condition $c_i(z, t = 0)$ as well as a boundary condition $c_i(z = 0, t)$ must be known in order to solve (9.91). If $c_i(z = 0, t)$ is constant in time, a steady-state profile $c_i(z)$ will gradually develop. An inlet disturbance, e.g., a substrate pulse, travels along the reactor axis as a pulse of diminishing amplitude if c_i is being consumed. With these few comments on the transient equation, (9.91), we shall devote the remainder of this section to the steady-state solution of the equation.

If, as assumed in the plug flow model, v_z is constant in the cross-section, the steady-state model becomes

$$\frac{\mathrm{d}\mathbf{c}}{\mathrm{d}\tau} = \mathbf{q}(\mathbf{c}). \tag{9.92}$$

In (9.92) $\tau = z/v_z$, which is the *holding time* in the reactor. It is the time it takes for a fluid with linear velocity v_z to travel the distance z from the reactor inlet. τ has dimension time^{-1}. Unless v_z or the inlet condition $\mathbf{c}(z = 0)$ changes with time the profile $\mathbf{c}(z)$ is independent of time, and the PFR is a steady-state continuous reactor.

The value of τ for $z = L$, the length of the reactor, is the important design variable for the PFR.

Equation (9.92) is mathematically identical to (9.42) with τ replacing t. The two reactors do, of course, operate quite differently. The batch reactor is inoculated at time $t = 0$, and the composition of the reactant mixture in the ideally mixed tank changes as a function of time. The PFR is studied at steady state, it operates in a continuous mode, and no mixing, even between neighboring fluid elements, is admitted.

The weak point in a PFR design is that cells must be continuously injected in concentration x_0 at $z = 0$. This would definitely lead to infection of the system and continuous operation could not be maintained. The problem of infection can be handled by admitting a small initial amount of biomass into the PFR and recirculating some of the effluent back to the inlet. This introduces some degree of mixing in the PFTdesign, but a CSTR with some recirculation of cells will almost certainly be preferable. Consequently, the PFR is always used downstream from a continuous stirred tank. Hereby, as explained in Sect. 9.4.1, an efficient reactor system for almost complete conversion of substrate is obtained.

An added difficulty of the PFR is that transfer of gaseous substrates to the liquid medium along the reactor axis becomes very difficult. Inevitably the sparging of the liquid with gas will lead to axial mixing, and since the volume of the gas phase is so much bigger than the liquid phase, it is extremely difficult to feed gas at the rate

required by the stoichiometry of the liquid-phase reaction. The PFR is best for anaerobic cultivations, and as mentioned above, it should be placed after a CSTR.

The *loop reactor* discussed in Sect. 9.4.2 is, however, a useful combination of a CSTR (for the liquid-phase reactants) and a PFR (for the reactants transferred from the gas phase).

9.4.1 A CSTR Followed by a PFR

The integrated form of (9.92) is exactly the same as the integrated expressions for the batch reactor in Sect. 9.2.1, except that time t is replaced by V/v, the holding time τ in a PFR of volume V which is fed at a constant volumetric rate v. Thus, for maintenance-free Monod kinetics, (9.44) is used to calculate the effluent concentration from the PFR.

$$\theta = \mu_{\max}\frac{V}{v} = \left(1 + \frac{a}{1+X_0}\right)\ \ln\left(\frac{X}{X_0}\right) - \frac{a}{1+X_0}\ln\left(1 + X_0 - X\right). \tag{9.93}$$

As explained in connection with (9.44), the scaling factor used in a, and X_0 is the substrate concentration s_0 at the start of the batch. Here s_0 is the inlet substrate concentration to the PFR. When the PFR is installed downstream from a STR, it is more practical to use the inlet substrate concentration s_f of the sterile feed *to the stirred tank* as the scaling factor. Thus, for maintenance-free kinetics

$$x_0 = Y_{\mathrm{sx}}(s_\mathrm{f} - s_0)\ ; \quad X_0 = \frac{x_0}{Y_{\mathrm{sx}}s_0} = \frac{s_\mathrm{f}}{s_0} - 1. \tag{9.94}$$

There are two dimensionless parameters, a to be is used in (9.93), and a_f:

$$a = \frac{K_\mathrm{s}}{s_0}\ ; \qquad \frac{a}{1+X_0} = \frac{K_\mathrm{s}}{s_\mathrm{f}} = a_\mathrm{f}. \tag{9.95}$$

Furthermore,

$$1 + X_0 - X = \frac{s_\mathrm{f}}{s_0} - \frac{x_0 + Y_{\mathrm{sx}}(s_0 - s)}{Y_{\mathrm{sx}}s_0} = \frac{s_\mathrm{f}}{s_0} - \frac{s_\mathrm{f} - s_0 + s_0 - s}{s_0} = \frac{s}{s_0}. \tag{9.96}$$

Consequently, (9.93) can be written in a more convenient form

$$\mu_{\max}\tau = (1 + a_\mathrm{f})\ \ln\left(\frac{x}{x_0}\right) - a_\mathrm{f}\ \ln\left(\frac{s}{s_0}\right). \tag{9.97}$$

Equation (9.97) is correct for an *unbroken chain of reactors*. If side streams are admitted, the simplifications of (9.97) cannot be applied, but (9.93) still holds.

Example 9.12 *A steady-state CSTR followed by a PFR.* It is desired to reduce the concentration of substrate in a sterile stream with $s_f = 60$–3 mg L^{-1}. This is to be done in a combination of two reactors, a CSTR followed by a PFR. The kinetics is given in Example 9.2:

$$q_x = \frac{4}{3}\frac{s}{s+4}x \text{ mg } L^{-1}h^{-1}, \tag{1}$$

i.e., the Monod constant is 4 mg L^{-1}, while $\mu_{max} = 4/3$ h^{-1}. Furthermore,

$$q_s = -10 \text{ g } g^{-1} \times q_x \quad \text{and} \quad v = 2.5 \text{ m}^3 \text{ h}^{-1}. \tag{2}$$

With two bioreactors in series, it is possible to minimize the total reactor volume necessary to reduce s from 60 to 3 g m^{-3}. The CSTR should be operated at an S value for which q_x is maximum, i.e.,

$$S = -a_f + \sqrt{a_f^2 + a_f} = -\frac{4}{60} + \sqrt{\left(\frac{4}{60}\right)^2 + \frac{4}{60}} = 0.2. \tag{3}$$

$$\begin{aligned} &s_0 = 0.2 \times 60 = 12 \text{mgL}^{-1}; \quad x_0 = 0.1 \times (60 - 12) = 4.8 \text{ mgL}^{-1}; \\ &D = \frac{4}{3} \times \frac{4}{4+12} = 1 \text{ h}^{-1}, \end{aligned} \tag{4}$$

i.e., $V_1 = 2.5$ m^3, the same result as was obtained in Example 9.2. Since the PFR is fed with biomass at a concentration of 4.8 mg L^{-1}, the PFR operates perfectly well, and it can reduce s to any desired level below 12 mg L^{-1}. It takes over exactly at the point wherein a CSTR q_x starts to decrease with decreasing s, i.e., at the minimum on the curves in Fig. 9.2. It is known from any textbook on reaction engineering that a PFR is the best reaction vessel whenever the rate of conversion is a monotonically increasing function of the reactant concentration.

From (9.97),

$$\frac{4}{3}\tau = \left(1 + \frac{1}{15}\right) \ln\left(\frac{0.1 \times (60-3)}{4.8}\right) - \frac{1}{15} \ln\left(\frac{3}{12}\right) \Rightarrow \tau = 0.2068 \text{ h}, \tag{5}$$

i.e., $V_2 = 0.2068 \times 2.5 = 0.517$ m^3.

No other CSTR-plus-PFR combination could give a smaller total reactor volume than $V_1 + V_2 = 3.017$ m^3 if the substrate level of a feed stream 2.5 m^3 h^{-1} is to be reduced from 60 to 3 mg L^{-1}.

We shall now assume that another stream $v_1 = 0.5$ m^3 h^{-1} of $s = 30$ mg L^{-1} and $x = 0$ is introduced after the CSTR. The combined streams are to be treated in the PFR to give an effluent of $s = 3$ mg L^{-1}. The CSTR is still operated so that the effluent is $(x, s) = (4.8, 12)$ mg L^{-1}, i.e., at its maximum production rate. Conditions at the inlet to the PFR are:

$$\begin{aligned} &x_0 = 4.8 \times 2.5/3 = 4 \text{ mg } L^{-1}; \\ &s_0 = \frac{12 \times 2.5 + 30 \times 0.5}{3} = 15 \text{ mg } L^{-1}. \end{aligned} \tag{6}$$

The exit conditions are $s = 3$ mg L^{-1}, i.e., $x = x_0 + 0.1(15 - 3) = 5.2$ g m^{-3}. Thus,

$$\frac{4}{3}\frac{V}{v} = \left[1 + \frac{4/15}{1 + 4/(0.1 \times 15)}\right] \ln\left(\frac{5.2}{4}\right) - \frac{4}{55} \ln\left(1 + \frac{40}{15} - \frac{52}{15}\right)$$
$$= \frac{59}{55} \ln\left(\frac{5.2}{4}\right) - \frac{4}{55} \ln\left(\frac{1}{5}\right) = 0.4 \text{ h},$$

i.e., $V_2 = 3/4 \times 0.40 \times 3 = 0.90$ m^3 or $V_1 + V_2 = 3.4$ m^3. With an extra stream, the minimum of $V_1 + V_2$ is not quite at the point where the CSTR operation is optimized. The cell-free side stream requires a few more cells delivered from the CSTR to operate the PFR better. Just as in Example 9.2, one may manipulate the reactor design parameters. For the present case, the true optimum is obtained for $(x, s) = (4.87, 11.3)$ mg L^{-1} from the CSTR and $(V_1 + V_2)_{\min} = 3.3939$ m^3.

9.4.2 Loop Reactors

Reactors in which the biomass and the medium are subjected to a given circulation pattern have been used, at least since the 1950s, for a number of different bioproductions. The circulation can be established either with the help of the gas which is sparged to the reactor, or liquid and gas can be forced round the reactor by the action of a pump.

The *airlift reactor* consists of an inner (or outer) tube through which the gas rises through the medium. At the top of the reactor, the gas is separated from the medium which descends by gravity flow to the bottom of the reactor where it is again moved to the top of the reactor in the low-density air-medium stream. This reactor type is widely used, in citric acid fermentation, in the growth of algae in photo bioreactors, in the biofuels industry, and in aerobic treatment of waste water. Natural circulation of the medium including biomass gives quite low mass transfer coefficients, and it is only used when the demand for gas to liquid-phase transfer is modest (Fig. 9.17).

In a *forced flow loop reactor*, Fig. 9.18, circulation is accomplished by means of a pump, and much higher mass transfer can be obtained. The medium velocity in the tube is high (0.6–1.1 m s^{-1}) which requires a considerable power input, since the gas to liquid mass transfer is accomplished by forcing the gas–liquid dispersion through static mixers, packings of, e.g., corrugated steel sheets. The loop can either be outside the reactor (and used for a very efficient mass transfer of gases to the liquid), or it can be internal like in the jet-air lift reactor. Cooling of the reactor medium is easily achieved when the loop is outside the reactor since, as discussed in Problem 9.4 and further in Chap. 11, any amount of (efficient) heat-exchanger area can be mounted in connection with the outside loop.

The loop reactor has its obvious place in strongly aerobic bioreactions or in general if low soluble gases are to be transferred to the medium. The reason is that the holding time for the gaseous substrate in the reactor is very small compared to the holding time for the liquid-phase reactants. One needs to transfer the gaseous reactants in plug flow to counter the rapid decrease of the overall reaction with

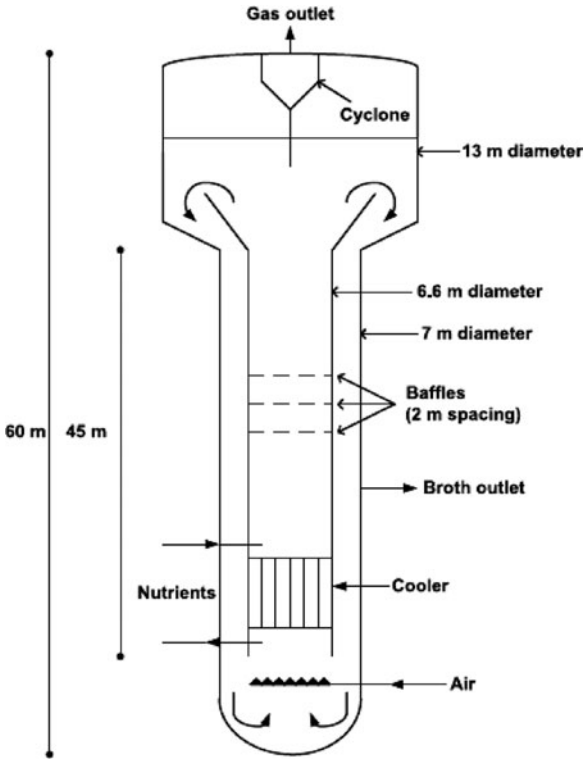

Fig. 9.17 Probably the largest air lift reactor ever constructed with a volume of 1,900 m^3 and a height of 60 m. The reactor was commissioned around 1970 and used for the production of SCP from methanol by the ICI company at Billingham, UK

decreasing concentration of the gas-phase reactant when the reaction becomes gas transfer limited. The advantages of the loop reactor relative to a CSTR are illustrated in Example 9.13, which also shows that a CSTR cannot satisfy fundamental design criteria for the process.

Example 9.13 *Design of a loop reactor for single cell production.* Certain microorganisms can grow aerobically on methanol as the sole source of carbon and energy, even at 55°C. These microorganisms are well suited for the production of single cell protein (SCP) in a hot climate such as that in Trinidad, Brunei or Qatar where the cooling-water temperature is rarely below 30°C. All three countries have a huge methanol production (in Trinidad 2×10^4 t day^{-1}) and it is profitable to convert a small portion of the methanol to the much higher priced protein.

Laboratory tests show that the biomass composition is $CH_{1.8}O_{0.5}N_{0.2}$ and that biomass yield on methanol Y_{sx} is 9/16 kg kg^{-1}, approximately independent of the growth rate. NH_3 is the nitrogen source, and only CO_2 and H_2O are produced besides the biomass.

One literature source states the following cell growth kinetics at 45°C:

$$q_x = \frac{\mu_{max} s}{s + K_s} \frac{s_1}{s_1 + K_1} x \text{ (kg of cells m}^{-3} \text{ h}^{-1}\text{)}, \quad (1)$$

s is the methanol concentration (kg m^{-3}), s_1 is the oxygen concentration (μM), $K_s = 0.0832$ kg m^{-3}, $K_1 = 2\,\mu M = 2 \times 10^{-3}$ moles of O_2/m^3, and $\mu_{max} = 0.9\ h^{-1}$. The organism

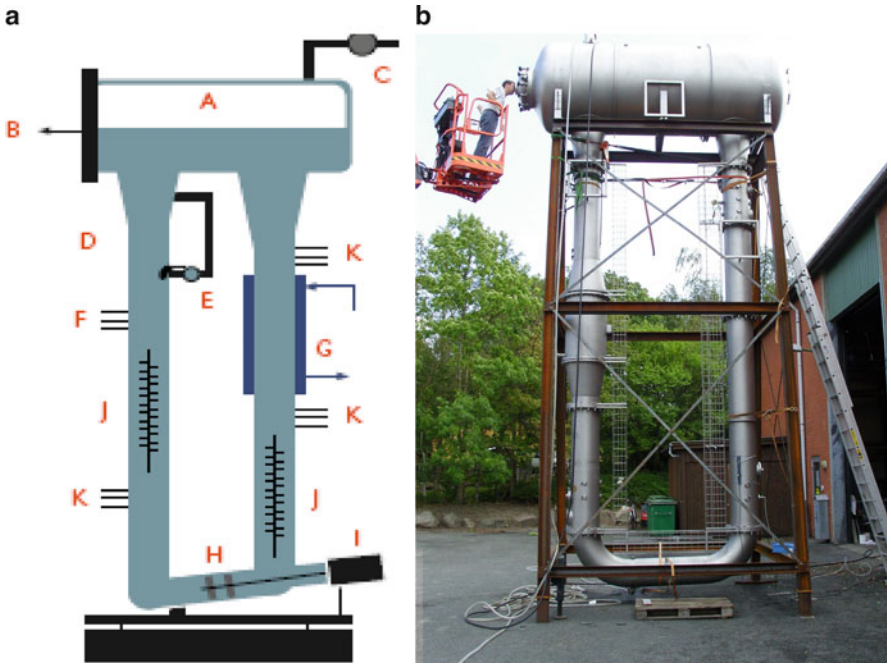

Fig. 9.18 The forced flow loop-bioreactor. (**a**) Schematic representation: A, degassing unit; B, harvest point for biomass and medium; C, outlet for CO_2 and unconverted gas-phase reactants; D, two-phase nozzle in which gas is injected with medium as propellant, and using pump E; F, feed port for medium; G, heat exchanger for cooling of medium; H and I, propeller pump for moving medium + biomass anticlockwise through the reactor; J, Sulzer static mixers; K, probes. The 500 L reactor was constructed in 2002 at DTU. (**b**) A 1-m^3 working volume loop reactor for pilot plant production of 90–100 kg SCP/24 h. The reactor is constructed by Unibio A/S (http://www.Unibio.com) and installed with downstream processing facility and analytical laboratory at the University of Trinidad and Tobago, Point Lisas Campus, Trinidad

needs an oxygen concentration of $s_1 = 20$ μM in the medium to stay healthy. The saturation concentration of O_2 (1 bar, 45°C) is $s_1^* = 910$ μM.

We wish to design a SCP plant for the production of 50,000 ton biomass (with about 70 wt% protein). The feed contains $s_f = 50$ kg m^{-3} methanol, and the reactor is sparged with technically pure O_2. The mass transfer coefficient k_la in a well-stirred CSTR is here taken to be 0.2 s^{-1} = 720 h^{-1}.

The very efficient static mixers of a loop reactor might give a k_la value as high as 0.45 s^{-1} = 1,620 h^{-1}.

In order to utilize the most expensive substrate, O_2, efficiently, 95% conversion of the O_2, is required.

Based on the yield coefficient of biomass on methanol, the stoichiometry of the bioreaction is:

$$\begin{aligned} CH_3OH + 0.7317\,O_2 + 0.1463\,NH_3 \rightarrow & 0.7317\,X\,(CH_{1..8}O_{0.5}N_{0.2}) \\ & + 0.268\,CO_2 + 1.56\,H_2O. \end{aligned} \quad (2)$$

(a) First a STR is considered.

It is desired to produce 50,000 ton biomass per year or 16.67 ton h^{-1} based on 3,000 h of continuous operation per year.

The optimum methanol concentration in the CSTR is given by (9.16), and the corresponding value of D by (9.17) if the rate limiting step is the bioreaction (1):

$$\begin{aligned} S = 0.03916 \rightarrow s = 1.958 \text{ kg m}^{-3}, &\text{corresponding to } x \\ = (9/16) \times (50 - 1.96) = 27.02 \text{ kg m}^{-3}, & \end{aligned} \tag{3}$$

$$D_{\text{opt}} = 0.8633\text{h}^{-1} \quad \text{and} \quad (q_x)_{\max} = Dx = 23.33 \text{ kg m}^{-3}\text{h}^{-1}. \tag{4}$$

The reactor volume needs to be $V = 16{,}667/23.33 = 714 \text{ m}^3$.

$Y_{so} = (0.7317/0.7317)/24.6 = 0.04065 \text{ kmol } O_2 \text{ (kg X)}^{-1} = 0.9484 \text{ kmol m}^{-3} \text{ h}^{-1} = 677.5 \text{ kmol h}^{-1} = 21.68 \text{ t h}^{-1}$ for a bioreactor of volume 714 m^{-1}.

Clearly, the consumption of O_2 represents a very large operational cost.

With an oxygen consumption of $q_0 = 0.948$ kmol m^{-3} h^{-1}, one would require a k_la determined by:

$$0.948 = k_la(910 - 20) \times 10^{-6} \times 10^3 \rightarrow k_la = 1{,}065\text{h}^{-1},$$

which is higher than the previously stated value of $(k_la)_{\max} = 720 \text{ h}^{-1}$.

Even the estimated requirement of $k_la = 1{,}065 \text{ h}^{-1}$ is likely to be too low. According to the discussion in Example 3.4, it is not correct to use an s^* based on the inlet O_2 pressure. If, in accordance with the problem specification, it is required to utilize 95% of the injected O_2, a lower limit of $s^* = 46$ μM should be used for the gas leaving the reactor.

The conclusion is that due to mass transfer limitation a CSTR is unsuited for the process.

(b) Next the design of a loop reactor is considered.

The concentration of all substrates (methanol, NH_3, and minerals) and of biomass is considered to be constant throughout the loop. From the point of injection, the O_2 partial pressure in the gas phase decreases from 1 bar to a much lower value. The gas-phase volume decreases somewhat (see the stoichiometry (2)), but besides CO_2 it may also contain H_2O vapor if the inlet gas is dry.

The methanol concentration in the reactor is assumed to be 1 kg m^{-3} (and the NH_3 concentration as low as 10–20 g m^{-3} to avoid a parallel oxidation of NH_3 to NH_2OH or ${NO_2}^{-1}$ which will inhibit the bioreaction). Consequently, the biomass concentration in the reactor is $0.7317 \times (24.6/32) \times (50 - 1) = 27.56 \text{ kg m}^{-3}$. When this value is inserted in (1), one can obtain $q_x = 20.82$ kg m^{-3} h^{-1} *when the rate of biomass formation is based on the bioreaction.*

At the gas injection point, q_x *based on the* O_2 *transfer* is given by:

$$\begin{aligned} q_x = 1{,}620(910 - 20) \times 10^{-6} &\left(\text{mol } O_2\text{m}^{-3}\text{h}^{-1}\right) \times (0.7317/0.7317) \\ \times 24.6 &\left(\text{kg X mol } {O_2}^{-1}\right) = 35.47 \text{ kg m}^{-3}\text{h}^{-1}. \end{aligned}$$

At the point of O_2 injection, there is enough O_2 mass transfer to make the overall reaction limited by the rate of the bioreaction. This situation prevails until $s^* = 542$ μM where q_x determined by the mass transfer equation is also 20.82 kg m^{-3} h^{-1}. Consequently, in the first part of the reactor from the point of injection of O_2, the reaction rate is constant and equal to 20.82 kg m^{-3} h^{-1} at $s^* = 542$ μM.

From this point on, the rate is determined by mass transfer and the rate is proportional to $(s^* - 20)$, i.e., the overall rate is first order in the remaining O_2 driving force. The arguments given above exactly follow the "balancing of rates" discussion in Sect. 9.1.5.

Let z be the O_2 volume left from 1 m^3 injected O_2. $1 - z$ is *the degree of conversion of* O_2.

Let y be the ratio between s^* for an O_2 conversion of $(1 - z)$ and s^* when the conversion is 0.

Since s^* is proportional to the partial pressure of O_2 in the gas phase, one can obtain:

$$y = \frac{O_2}{O_2 + CO_2} = \frac{z}{z + (1 - z)(0.2863/0.7317)}. \tag{5}$$

For $s^* = 542$ μM, one can obtain $y = 542/910 = 0.5956$ and from (5) one can obtain $z = 0.3507$.

Almost 65% of the injected O_2 has been converted when the production rate changes from zero-order in O_2 to first order in the remaining O_2.

In the first part of the reactor $-q_0 = 20.82 \times (1{,}000/24.6) = 846$ mol O_2 m^{-3} h^{-1} = 0.235 mol O_2 m^{-3} s^{-1}.

Let the inlet feed of O_2 be G_0 mol s^{-1}, and let the total reactor volume be V.

The reactor volume V_1 in which the biomass production rate is constant is $V_1 = G_0(1 - z)/0.235$ m^3.

The choice of reactor volume V is a design parameter, and we shall choose $V = 30$ m^3.

If a constant production rate could be maintained through the whole reactor, i.e., $V_1 = V$, and if oxygen was completely converted ($z = 0$ at the reactor outlet) then $G_0 = 30 \times 0.235 = 7.05$ mol s^{-1}.

Let us use $G_0 = 7.05$ mol s^{-1} and calculate the conversion $1 - z$ at the outlet from a 30 m^3 reactor.

Now $V_1 = 7.05 \times (1 - 0.3507)/0.235 = 19.48$ m^3. In the remainder of the reactor, $V_2 = 10.52$ m^3, the rate of conversion of oxygen follows the design equation (9.92) for a PFR if plug flow of the gas phase through the last 10.52 m^3 can be assumed.

$$G_0 \frac{dz}{dV} = q_0 = -0.45 \times (910y - 20) \times 10^3 \text{mol } O_2 m^{-3} s^{-1}, \tag{6}$$

$y(z)$ is inserted from (5), and with $G_0 = 7.05$ mol s^{-1}, the differential equation is reorganized to:

$$\frac{z + 0.5790}{z - 0.008173} dz = \left(1 + \frac{0.5872}{z - 0.008173}\right) dz = -0.09041 dV_2; \quad V_2 = 0 \text{ for } z = 0.3507. \tag{7}$$

The solution of (7) gives z as a function of V_2, and for $V_2 = 10.52\ \mathrm{m}^3$, z is the solution of:

$$(0.3507 - z) + 0.5872\ \ln\left(\frac{0.3507 - 0.008173}{z - 0.008173}\right) = 0.09041 V_2 = 0.9511. \tag{8}$$

The solution to (8) is $z = 0.11$ which is higher than the required 0.05. Consequently, the 30 m^3 reactor can only handle a smaller quantity G_0 of oxygen than 7.05 mol s^{-1} if 95% conversion is demanded.

Iteration on (6)–(8) gives the solution $G_0 = 5.8\ mol\ s^{-1}$ for $z = 0.05$ at the reactor exit.

The O_2 consumed is $5.8 \times (1 - 0.05) = 5.51$ mol O_2 s^{-1}, and this corresponds to a biomass production of $5.51 \times 24.6 \times 10^{-3} \times 3{,}600 = 488$ kg biomass h^{-1} in a 30 m^3 loop reactor.

The total number of 30 m^3 reactors to be used is 16,667/488 = 34 to 35 reactors.

A number of other design problems can easily be solved, e.g., that of increasing the total pressure in the reactor to 2 bar. In all cases, the requirement of 95% conversion of O_2 is satisfied.

Problems

Problem 9.1. In Example 9.2, two sequentially coupled CSTR were studied for a particular Monod rate expression. The present problem is based on Example 9.2, but explores other variants.

(a) Can the two reactors with intermittent feed of substrate be further optimized for productivity?
(b) Repeat the optimization of the two-reactor system for

1. Monod type kinetics with maintenance. Use the data of Example 9.1.
2. Substrate-inhibited Monod. Use the data of Fig. 9.8.

Problem 9.2 *Lactic acid production.* As an employee in the R&D division of an agro-industrial company, you are entrusted with the solution of the following problem: "The effluent from one of our cheese factories contains 45 kg of lactose per cubic meter. There is 4,000 m^3 per annum of effluent (production time 7,200 h), and the effluent is an environmental burden. Can this effluent be used to produce lactic acid? The market for lactic acid is weak and minimum investment cost of the reactor per kilogram produced of lactic acid is desirable."

Your preliminary research confirms that the lactose substrate is sterile and contains no lactic acid. From a literature search, you come upon the following rate expressions:

$$\begin{aligned} q_x &= \mu_{max}\left(1 - \frac{p}{p_{max}}\right)\frac{sx}{K_s + s}\ , \quad \mu_{max} = 0.5\ \mathrm{h}^{-1}\ , \\ p_{max} &= 50\ \mathrm{kg\ m}^{-3}, \quad K_s = 0.3\ \mathrm{kg\ m}^{-3}, \end{aligned} \tag{1}$$

$$q_s = -Y_{xs} q_x; \qquad Y_{sx} = \frac{1}{Y_{xs}} = 0.11 \text{ kg DW per kilogram of lactose,} \tag{2}$$

$$\begin{aligned} q_p &= bq_x + cx \ ; \ b = Y_{xp} = 8 \ \text{ kg of lactic acid per kilogram dry weight;} \\ c &= 0.1 \text{ kg of lactic acid per kilogram dry weight per hour.} \end{aligned} \tag{3}$$

On the basis of these pieces of information, you decide to go ahead with the design of a CSTR in which the productivity q_p in kilograms of lactic acid per cubic meter per hour is maximized.

(a) Your first inspiration is to neglect the complications of the kinetics, i.e., to assume that $p << p_{max}$, and $cx << bq_x$. With these assumptions, calculate the reactor volume for which maximum q_p is obtained. Also calculate the effluent concentrations of lactic acid, biomass, and lactose from the CSTR, and determine the maximum productivity $q_{p,max}$ of lactic acid. Comment on the validity of the two assumptions.

(b) With the slight suspicion that the assumption $p << p_{max}$ may not be realistic, you repeat the calculation of the effluent concentrations and of q_p for the reactor volume determined in (**a**), but now using the correct kinetic expression in (1). The assumption $cx << bq_x$ is still assumed to hold. You are allowed to be relieved that you did not build the reactor based on your approximate design.

(c) With the approximate model of (**b**), you decide to calculate the reactor size which gives maximum productivity q_p. Analytical optimization is difficult, but tabulation is easy: For $s/s_f = 0.9, 0.8, \ldots, 0.1$, calculate D, x, p, and $q_p = Dp$. For the three entries closest to the maximum in q_p, find the optimal S by quadratic interpolation. Calculate V(opt). Does the assumption $cx << bq_x$ appear to be reasonable?

(d) You decide to base your design on a reactor of volume $V = 2.40$ m^3. The effluent from the reactor must, however, not contain more than 3 kg of lactose per cubic meter. Hence, a centrifuge is installed at the outlet, and 0.2 m^3 of solution plus cells per hour is returned to the inlet. For $s = s_e = 3$ kg m^3, calculate the corresponding values of x and p, using the whole of (1), but $cx << bq_x$. Determine the separation factor β for the centrifuge and the cell concentration x in the reactor.

(e) The rather high value of x calculated in (**d**) reawakens your suspicion that the assumption $cx << bq_x$ may be invalid. Therefore, you decide to redo the calculations of part (**d**), but now with the full model of (1)–(3). You are in for several surprises:

1. It may be difficult to find a solution to (**d**).
2. This should prompt you to redo the calculations in (**c**), but using the full model.
3. Doing so may give you more solutions than you desire for some S and disappointingly few for other S values.

Do these calculations give you any reason to criticize the kinetic model in (1)–(3)? What could be wrong with the model?

Problem 9.3 *Lactic acid batch fermentation.* On a certain yeast extract-casein peptone medium, it has been reported that the growth-associated ATP consumption for lactic acid fermentation is

$$r_{\mathrm{ATP}} = 31 \left(\frac{\text{mmoles of ATP}}{\text{gram dry weight}}\right) \mu(\mathrm{h}^{-1}) + 17 \left(\frac{\text{mmoles of ATP}}{\text{gram dry weight} \times \text{hour}}\right). \quad (1)$$

The process is anaerobic, and lactic acid is the only metabolite formed. You are required to check the validity of this expression, and for this purpose you set up a fermentation experiment. The initial medium volume is $V_0 = 750$ mL, and the glucose concentration is $13 \times 1/3$ g L^{-1}. The medium is inoculated with $x_0 = 10$ mg of cells per liter, and exponential growth with $\mu = \mu_{\max} = 0.6\,\mathrm{h}^{-1}$ starts immediately after inoculation. To keep pH constant at 6.80, the lactic acid produced by conversion of glucose has to be continuously titrated. 1-M NaOH solution is used, and since the medium volume is consequently a function of time it becomes a little difficult to check the validity of the kinetics [i.e., (1) and the assumption $\mu = 0.6\,\mathrm{h}^{-1}$] by comparison of experimentally determined concentrations of biomass x (g L^{-1}) and lactic acid p (g L^{-1}), and the simulated results.

(a) Assuming that (1) is valid and that $\mu = 0.6\,\mathrm{h}^{-1}$, derive an expression for $x(t)$ that can be used for comparison with the experimentally determined biomass concentration time profile. Also derive an expression for $V(t)$. Hint: It is easy to find xV, and $v(t)$ can be found from (1).
(b) Derive an expression for $p(t)$, assuming that $p(t = 0) = 0$.
(c) Determine the time t_{end} at which all sugar is depleted, assuming that the glucose is quantitatively converted to lactic acid. What are x, p, and V when $T = T_{\mathrm{end}}$? What is the relation between the apparent specific growth rate μ_{obs} and μ for large t_{end}?

Problem 9.4 *Heat transfer limitation in SCP production.*

(a) In an SCP production, $2.5N$ m^3 $\mathrm{CH_4}$ ($N = 273$ K, 1 atm) is used to produce 1 kg of biomass $\mathrm{X} = \mathrm{CH_{1.8}O_{0.5}N_{0.2}}$ by continuous fermentation in a stirred tank. Determine Y_{so} and thereafter the total stoichiometry of the reaction, assuming that biomass, $\mathrm{CO_2}$, and $\mathrm{H_2O}$ are the only products and that $\mathrm{NH_3}$ is used as nitrogen source. Calculate the heat of reaction Q in kJ (kg biomass)$^{-1}$.
(b) The bioreactor is cylindrical with diameter d and height h. $h = 3d$. The inner cylinder area A (m^2), but not the bottom of the reactor, is covered with heat exchange surface The effective temperature driving force is $\Delta T = 30°\mathrm{C}$, and the heat transfer coefficient h_{T} is 300 kJ (m^2 h K)$^{-1}$. The heat transferred is consequently $Q^{\mathrm{t}} = h_{\mathrm{T}}\,\Delta T A$ kJ h^{-1}. Show that – due to heat transfer limitation – the maximum productivity of biomass is:

$$(q_{\mathrm{x}})_{\max} = 0.60\mathrm{V}^{-1/3}\ \text{kg}\ \mathrm{m}^{-3}\mathrm{h}^{-1}, \quad (1)$$

where V is the reactor volume.

For a sterile feed and $x = 20$ g L^{-1}, determine the maximum possible dilution rate, $D_{\max}$, for $V = 1$ L and for $V = 50$ m^3.

(c) Laboratory experiments are conducted in a small reactor where heat transfer is not a problem. The liquid feed is sterile and contains 5 g L^{-1} NH_3 and a sufficient supply of minerals. The gas feed is $1N$ m^3 per m^3 reactor volume and per min. The composition is 25 vol% CH_4 and 75 vol% O_2. With this much O_2 in the feed, the reaction is always limited by CH_4. At steady state, one can obtain the following data:

D (h^{-1})	CH_4 (vol% in exit gas)	Biomass in effluent: x g L^{-1}
0.05	20.53	36.17
0.1	14.16	36.17
0.2	13.18	19.20
0.3	9.63	15.20
0.5	25.00	0

Assume that no water is transferred from gas to liquid phase or vice versa.

(a) Show that $-q_{CH_4}$ in mol CH_4 consumed (L reactor min)$^{-1}$ and the gas-phase concentrations in the second column of the table are related by:

$$\frac{\text{vol }\%}{100} = \frac{0.25 \times 0.044642 + q_{CH_4}}{0.044642 + (1 + Y_{so})q_{CH_4} - Y_{sc}q_{CH_4}}. \tag{2}$$

Add a column ($-q_{CH_4}$) to the table.

For $D = 0.2$ and 0.3 h^{-1}, show that the yield coefficient Y_{sx} calculated in (**a**) is also found from the data of the table. Calculate the effluent NH_3 concentration. No NH_3 is stripped to the gas phase.

Finally, explain the data for $D = 0.05$ and 0.1 h^{-1}. What happens at $D = 0.5$ h^{-1}?

Problem 9.5 *Start-up of a CSTR.* A waste water treatment plant is going to be operated in steady state in a CSTR.

The specific growth rate is determined by the following expression in the limiting substrate S:

$$\mu = r_x = \frac{0.5(h^{-1})S}{S^2 + S + 1/16}, \quad \text{where } S = s/s_f \text{ and } X = \frac{x}{Y_{sx}s_f}. \tag{1}$$

(a) Determine the value of S for which $(-r_s)$ attains its maximum value, and find X and D for $S = S_{opt}$.

(b) It is decided to operate the reactor at the point $S = S_{opt}$. To get to this optimal operating point, the STR is started as a batch reactor with $S = s/s_0 = 1$ and $X = X_0$. The batch operation is monitored, and when S has decreased to S_{opt} continuous feeding of the reactor is started with $s = s_f$, and $x_f = 0$. For simplicity, assume that $s_f = s_0$. After a while, the continuous operation of the STR with $D = D_{opt}$ determined in (**a**) is assumed to settle at the optimal steady state determined in (**a**).

Determine the time t^0 of the batch reaction to reach $S = S_{opt}$. What is X at this point if $X_0 = 0.05$?

(c) By numerical integration of the mass balances, determine the time $t' = t - t^0$ it takes for $[S, X]$ to approach the desired steady-state operation point to within 1%.

(d) Due to an operational error, the batch-period is stopped after 9 h.

Determine $[S, X]$ at $t^0 = 9$ h, and thereafter trace the transient as in (**c**) by numerical integration of the mass balances.

What has happened compared with (**c**)? Would you have obtained the same result, if the batch process had been started with $X_0 = 0.10$ or 0.15?

Note: Since the rate expression used here is the same as that used in Fig. 9.11, it is quite instructive to compare the results of (**c**) and (**d**) with this figure.

Problem 9.6 *Stability analysis with product inhibition, maintenance, and cell recirculation.* If, in the dynamic mass balances for the stirred tank continuous reactor, the separation factor Ω of the cell recirculation system with an ultrafilter (9.36) is introduced together with maintenance according to (9.4)–(9.5), the following balances are obtained:

$$\frac{dx}{dt} = \mu x - (1 - \Omega) D x = 0, \tag{1}$$

$$\frac{ds}{dt} = D(s_f - s) - (Y_{xs}^{true}\mu + m_s)\, x, \tag{2}$$

$$\frac{dp}{dt} = -Dp + (Y_{xp}^{true}\mu + m_p)\, x. \tag{3}$$

Introduce in (1) to (3) dimensionless variables $S = s/s_f$, $X = x(1-\Omega)/\left(Y_{sx}^{true} s_f\right)$, and $P = p/\left(Y_{sp}^{true} s_f\right)$. Also let $\beta_s = Y_{sx}^{true} m_s$ and $\beta_p = Y_{px}^{true}$.

Consider a steady-state solution $\mathbf{C}_0 = (X_0, S_0, P_0)$ and introduce the deviation variable $\mathbf{y} = \mathbf{C} - \mathbf{C}_0$, the solution of the linear differential equation (9.75).

$$\begin{aligned} \text{Show that : } \mathrm{Det}(\mathbf{J} - \lambda \mathbf{I}) = &-\lambda\Delta_1 + (\mu + \beta_s)\Delta_2/(1-\Omega) \\ &+ (\mu + \beta_p)\Delta_3/(1-\Omega), \end{aligned} \tag{4}$$

$$\Delta_1 = (D+\lambda)^2 - (D+\lambda)(\mu_p - \mu_s)X/(1-\Omega),$$

$$\Delta_2 = -(D+\lambda)\mu_s X, \tag{5}$$

$$\Delta_3 = (D+\lambda)\mu_p X.$$

As in Sect. 9.3.3, μ_p and μ_s are the partial derivatives of μ with respect to p and s. Continue the simplification to obtain the following equation forλ:

$$(D+\lambda)(-\lambda^2 + \lambda(-D+a) + D(1-\Omega)a + b) = 0. \tag{6}$$

In (6):

$$a = (\mu_p - \mu_s)X/(1 - \Omega) \text{ and } b = (\beta_p\mu_p - \beta_s\mu_s)X/(1 - \Omega).$$

Make an analysis of the stability of a steady state $\mathbf{C}_0$ with different rate expressions $\mu(S, P)$.

What is the general effect of a product inhibition? The effect of cell recirculation?

You should make several simulation studies as part of your answer to this problem.

Note that the range of application of the text in Sect. 9.3.3 has been greatly expanded by means of the results of this problem.

Problem 9.7 *Providing an experimental foundation for the design of a fermentation process.* Vara et al. (2002) made an experimental study of teicoplanin production by *Actinoplanes teichomyceticus* in order to obtain design data for an industrial production of the last-resort antibiotic teicoplanin in continuous culture.

(a) You are required to make a short review of their experimental plan and to compare it with the experimental plan used in Example 6.1. The kinetic parameters used to construct Table 6.1 were in fact extracted from the results of the above reference, thus illustrating the resemblance between mechanistically based kinetic expressions for enzymatic reactions and empirical rate expressions for cellular reactions. Which experimental plan is likely to lead to the best values for the kinetic parameters?

(b) Figure 6 of Vara et al. (2002) shows simulations of the concentrations of substrate (glucose $= s$), biomass (x), and product (teicoplanin $= p$) as a function of dilution rate in a continuous cultivation. You are required to check the simulations using the kinetic model (including maintenance). Why does $x(D)$ decrease for small D while $p(D)$ continues to increase?

(c) Table 1 of Vara et al. (2002) shows results of continuous experiments in a stirred tank with recirculation according to Fig. 9.6.b. Find the connection between the parameter c in the reference and Ω used in (9.36). Why are the data in the last column of the table almost independent of D? Confirm the conclusion of the paper that continuous operation with cell recirculation is the best mode of operation, and that an increase of productivity by a factor of 3 compared to straight continuous operation is achieved.

(d) The microorganism gradually looses the ability to produce teicoplanin. Compare the deactivation model (10) and (11) used by the authors with that used in Example 9.10, and confirm that the model simulates the data in Fig. 8 of Vara et al. (2002) with a high accuracy. Why could a simpler model taken from Example 9.10 not be applied?

Problem 9.8 *Design of a fed-batch process to obtain a desired product titer.* Propane-1,3 diol (P) is to be produced by fed-batch fermentation from glucose.

The stoichiometry is supposed to be:

$$-\mathrm{CH_2O} - 0.150\ \mathrm{O_2} - 0.024\mathrm{NH_3} + 0.120\mathrm{X} + 0.543\mathrm{P} + 0.337\,\mathrm{CO_2} + 0.204\,\mathrm{H_2O} = 0. \quad (1)$$

Before $t = 0$ when the fed-batch process starts, biomass $\mathrm{X} = \mathrm{CH_{1.8}O_{0.5}N_{0.2}}$ has been grown (in a batch fermentation with $V = V_0$) to a concentration $x_0 = 1$ g $\mathrm{L^{-1}}$, and a glucose concentration of $s_0 = 1$ g $\mathrm{L^{-1}}$.

For $t > 0$, s is to be kept at 1 g $\mathrm{L^{-1}}$ by feeding a glucose solution with $s_\mathrm{f} =$ 400 g $\mathrm{L^{-1}}$ and rate v_f.

At $t = 0$, the production of P is initiated by the addition of the cofactor B_{12} (needed to convert glycerol to 3-hydroxy-propanal, the substrate for the last reaction to P). No glycerol is formed, and the above stoichiometry holds for all $t > 0$.

It is desirable to use a constant B_{12} concentration of 0.01 g $\mathrm{L^{-1}}$ for all $t > 0$. This is a compromise between a really low concentration where glycerol will accumulate, and a higher concentration that would lead to accumulation of 3-hydroxy-propanal which would harm the *E. coli* used as production organism.

At the constant $\mathrm{B_{12}}$ level $= 0.01$ g $\mathrm{L^{-1}}$, the specific production rate r_p of the diol is constant:

$$r_\mathrm{p} = 2.4 s_{\mathrm{B12}} / \left(s_{\mathrm{B12}} + 0.005\ \left(\mathrm{g\ L^{-1}}\right)\right) = 1.6\ \mathrm{g}P\ (\mathrm{gbiomass})^{-1}\mathrm{h^{-1}}. \quad (2)$$

(a) Determine the specific rates $r_\mathrm{x} = \mu$, $(-r_\mathrm{s})$ (g (g X)$^{-1}$ h^{-1}), and $(-r_0)$ (mol $\mathrm{O_2}$ (g X)$^{-1}$ h^{-1}). What is the value of Y_{xs} (g glucose(g biomass)$^{-1}$)?
Write expressions for $x \times V$, v_f, and V/V_0 as functions of t, s_f, x_0, and V_0.

(b) It is desired to stop the fed-batch cultivation when $p = 120$ g $\mathrm{L^{-1}}$.
From a mass balance for p derive an expression for p as a function of t and V/V_0.
Determine the time t when $p = 120$ g $\mathrm{L^{-1}}$, and thereafter V/V_0 at this time.

(c) The medium is sparged with air (partial pressure of $\mathrm{O_2} = 0.21$) at a temperature of 30°C. The oxygen concentration in the medium must be 20% of the saturation concentration.
Determine the minimum value of $k_\mathrm{l}a$ (h^{-1}) required to satisfy the demand for $\mathrm{O_2}$ at the end of the fermentation when $p = 120$ g $\mathrm{L^{-1}}$. Can this $k_\mathrm{l}a$ value be obtained with commercially available mass transfer equipment?

(d) Unfortunately B_{12} is slowly metabolized by the *E. coli* cells. The rate of degradation of B_{12} is $(-r_{\mathrm{B12}}) = 0.0001 r_\mathrm{p}$, i.e., it is proportional to the rate of product formation.
Consequently, to keep a constant level of B_{12} ($s_{\mathrm{B12}} = 0.01$ g $\mathrm{L^{-1}}$), the feed must contain B_{12}.
Determine the concentration s_f (B_{12}) in v_f necessary to keep s_{B12} at 0.01 g $\mathrm{L^{-1}}$.

Note: The rate expressions given for propane-diol production and for B_{12} consumption are not those used by the DuPont company in their production of the diol, but they have a reasonable structure.

Problem 9.9 *Production of a protein that is degraded by the action of proteases.* A valuable protein is produced by a growth-associated process using a microorganism for which the volumetric growth rate is given by

$$q_x = \frac{0.2\ s}{s+1} x \text{ g biomass}(\text{L medium h})^{-1}. \tag{1}$$

In (1), the concentration of the growth-limiting substrate is s g L^{-1}. x is the biomass concentration in g L^{-1}. The yield of biomass on the substrate is $Y_{sx} = 0.5$ g g^{-1}.

Production of the protein is severely catabolite repressed and the volumetric production rate is

$$q_p = \frac{1}{1+10s} q_x \text{ g protein}(\text{L medium h})^{-1}. \tag{2}$$

Production of the protein is to take place in a continuous, steady-state stirred tank, and the glucose feed concentration is $s_f = 10$ g L^{-1}.

(a) Determine the largest value of D for which the steady-state process will work. Thereafter, determine the yield coefficient Y_{sp}. For which value of D (or s) is Y_{sp} at its maximum? Is that the same value for which q_p is at its maximum? Why is the continuous stirred tank process better than a batch reactor process?

(b) Make a sketch of q_p as a function of s for $0 < s < 10$ g L^{-1}. Calculate the largest productivity $(q_p)_{max}$ which can be obtained and determine the corresponding value of D.

(c) Equation (2) is an idealization of the real situation. The microorganism also produces proteases that to a considerable degree destroy the desired protein. The correct expression for q_p is:

$$q_p = \frac{1}{1+10s} q_x - kx \tag{3}$$

Determine the maximum value of k above which no net production of the protein will be obtained for any operating condition. Derive an approximate relation between k and the maximum protein productivity. You should not attempt to obtain an algebraic solution, but use a graphical representation in which q_p given by (2) is plotted together with kx. Make your approximate solution based on this graph.

(d) It is contemplated to install a cell separator at the exit of the reactor and recirculate cells to the inlet.

Discuss whether an increase of productivity (given by (3)) can be obtained in this way. Is there any difference between the two cases: (A) The protein product is secreted 100% to the medium and (B) The protein product remains quantitatively inside the cells? What is the potential increase in maximum productivity if a recirculation ratio $R = 0.5$ and a cell separation factor $\beta = 1.5$ (9.33) is used?

Problem 9.10 *Protein production in fed-batch operation.* The protein in Problem 9.9 is P = $CH_{1.3}O_{0.31}N_{0.27}$ (the elementary composition is not quite that shown in Table 3.1 in the book). Biomass X = $CH_{1.8}O_{0.5}N_{0.2}$.

In the present problem, a fed-batch process for production of the protein is studied.

We use the kinetics of problem 9.9, both for q_x and for q_p, and we use $Y_{sx} = 0.5$ g g^{-1}.

In reality, one would have to multiply q_p with a small factor, e.g., 0.05, in order to scale the productivity of P to "normal" protein production, but this does not change the structure of the problem, and the discussion in Problem 9.9 concerning "the best choice of s" still applies here.

(a) Write the yield coefficients Y_{sj} of the stoichiometry (1) as a function of s.

$$CH_2O + Y_{so}O_2 + Y_{sn}NH_3 \rightarrow Y_{sx}X + Y_{sp}P + Y_{sc}CO_2 + Y_{sw}H_2O. \qquad (1)$$

(Y_{sw} H_2O is included in order that you may check that no algebraic errors are made. You should convince yourself that both the H and the O balance close).

(b) At which value of s would you prefer to operate a "constant s fed-batch fermentation" for the reaction (1)? You should try to give a plausible reason for your choice, but as will be discussed in (**e**) the choice also depends on certain economic factors.

(c) Write the stoichiometry (1) for your choice of s.

Determine the yield coefficients Y_{xn} (g NH_3/g X), Y_{xp} (g P/g X), and Y_{xo} (mol O_2/g X).

Calculate the value of r_x at which you will work for the given choice of s.

(d) The fed batch is induced (for the production of P) at $t = 0$ where $V = V_0 = 100$ m^3 and $x = 5$ g L^{-1}. It is to be stopped when $x = 80$ g L^{-1}.

The glucose concentration in the feed is $s_f = 400$ g L^{-1}.

Determine $t = t_{final}$ at which $x = 80$ g L^{-1}. Thereafter determine the corresponding value of V, the final concentration of P, and the required feed concentration of NH_3 if it is desired to have a constant ammonia concentration of $s_{NH3} = 1$ g L^{-1} during the fermentation.

Assume that the fermentation temperature is 30°C. The reactor is sparged with air, and that DOT has to be 20% of the saturation concentration of O_2. Will you be able, also at t_{final}, to meet the O_2 demand with a reasonable value of k_la?

(e) We would like to examine the sensitivity of the design for choices of s that are different from the choice in (**b**).

Repeat the calculations of (**c**) and (**d**) for $s = 2$ g L^{-1} and $s = 0.2$ g L^{-1}, and discuss the results compared with "the base case." You should especially consider the total production of P, the productivity of P in kg h^{-1}, and the yield of P (g P obtained per g glucose spent) until t_{final}.

Problem 9.11 *Adhesion of cells can lead to serious under-design of an industrial reactor.* In a continuous stirred tank reactor operating at a given dilution rate D and with sterile feed, the concentration of biomass in the medium (the suspended culture) is x g L^{-1}. Some biomass adheres to the inner surface of the reactor. The concentration of adhering biomass (converted from a more "natural" unit of g (m^2 reactor surface)$^{-1}$) is x_1 g L^{-1}. Suspended and adhering biomass grow with the same yield coefficient Y_{sx} and the same specific growth rate μ. Suspended and adhering biomass are exchanged by first-order rate processes: $k_1 x$ (adhesion) and $k_2 x_1$ (attrition of biofilm).

(a) Write mass balances for the suspended and for the adhering biomass. Add a substrate balance to the model. Derive the following relation between the steady-state value of D and the corresponding value of μ:

$$D = \frac{k_1 + k_2 - \mu}{k_2 - \mu}\mu. \tag{1}$$

Show that D is always larger than μ for realistic values of k_1 and k_2.

Assume that $s_f = 10$ g L^{-1}, $Y_{sx} = 0.5$ g g^{-1}, $k_1 = 2$ h^{-1} and $k_2 = 1.5$ h^{-1}, $D = 0.2$ h^{-1}, and that:

$$\mu = \frac{0.5(h^{-1})s}{s + 2}. \tag{2}$$

Calculate s, x, and x_1 and compare with the corresponding values for $k_1 = 0$.

Assume that the above data were obtained with a small laboratory reactor of volume $V = 1$ L, height $h = 1.3 \times$ diameter d. The inner surface of the reactor is 550 cm^2.

For a film density $\rho = 1$ g cm^{-3}, calculate the film thickness Δ.

(Answer: 123 μm. This is a film thickness unlikely to be detected in the experiments)

Make a simulation of x g L^{-1} as a function of D, both in the case of biomass adhesion and for $k_1 = 0$ (no adhesion).

(b) Consider a 50 m^3 industrial reactor with $h = 3d$ for the same process. The internal surface, including baffles, heat exchangers etc., is 100 m^2.

What would the film thickness be if k_1 and k_2 have the same values as in (**b**)?

In reality, a film of this thickness would never be stable. It is more likely that the film thickness Δ is also 123 μm in the industrial reactor. The adhesion mechanism is probably the same in both scales ($k_1 = 2$ h^{-1}), but k_2 is much larger for the industrial reactor.

Determine the "effective" large scale value of k_2 and the relation between x and D. You will conclude that a serious under-design of the large scale operation would result if the laboratory data were used uncritically as the design basis.

The data were taken from a real process, the production of lipases by a microorganism that hydrolyzes linseed oil in an aqueous emulsion of the vegetable oil. Some oil sticks to the reactor surface and part of the culture adheres to this film.

References

Andersen, M.Y., Pedersen, N., Brabrand, H., Hallager, L., and Jørgensen, S.B. (1997). Regulation of continuous yeast fermentation near the critical dilution rate using a productostat, *J.Biotechnol.*, **54**, 1–14.

Aris, R. and Amundson, N. R. (1973). *First-Order Partial Differential Equations with Applications*, Prentice-Hall, Englewood Cliffs, NJ.

Buziol, S., Bashir, I., Baumeister, A., Classen, W., Rizzi, N.N., Mallinger, W., and Reuss, M. (2002). New bioreactor-coupled rapid stopped-flow technique for measurement of metabolite dynamics on a subsecond time scale, *Biotechnol. Bioeng.*, **80**, 632–638.

Kirpekar, A.C., Kirwan, D.J., and Stieber, R.W. (1985). Modeling the stability of Cephamycin C producing *N. lactamdurans* during continuous culture, *Biotech. Prog.*, **1**, 231–236.

Mashego, M.R., van Gulik, W.M., and Heijnen, J.J. (2007). Metabolome dynamic responses of *Saccharomyces cerevisiae* to simultaneous rapid perturbations in external electron acceptor and electron donor, *FEMS Yeast Research*, **7**, 48–66.

Menawat, A., Muthurasan, R., and Coughanowr, D.R. (1987). Singular control strategy for a fed-batch bioreactor: numerical approach, *AlChE J.*, **33**, 776–783.

Palanki, S., Kravaris, C., and Wang, H.Y. (1993). Synthesis of state feedback laws for end-point optimization in batch processes, *Chem. Eng. Sci.*, **48**, 135–152.

Svensson, M., Silfwersparre, G., Häggström, L., and Enfors, S.O. (2005). Control of endotoxin release in *E. coli* fed batch cultures, *Bioprocess Biosyst. Eng.*, **27**, 91–97.

Theobald, U., Mailinger, W., Reuss, M., and Rizzi, M. (1993) In vivo analysis of glucose induced fast changes in yeast adenine nucleotide pool applying a rapid sampling technique, *Anal. Biochem.*, **214**, 31–37.

Theobald, U., Mailinger, W., Rizzi, M., and Reuss, M. (1997). In vivo analysis of metabolic dynamics in *S. cerevisiae*. I Experimental observations, *Biotechnol. Bioeng.*, **55**, 305–316.

Vara, A.G., Hochkoepple, A., Nielsen, J., and Villadsen, J. (2002). Production of Teicoplanin by *Actinoplanes teichomyceticus* in continuous culture, *Biotechnol. Bioeng.*, **77**, 589–598.

Villadsen, J. and Patil, K.R. (2007). Optimal fed-batch cultivation when mass transfer becomes limiting, *Biotechnol. Bioeng.*, **98**, 706–710.

Visser, D. (2002). Measuring and modelling *in vivo* kinetics of primary metabolism. PhD thesis, TU Delft, March 2002.

Chapter 10
Gas–Liquid Mass Transfer

The first requirement for any chemical reaction to take place is that the reactants are present at the site of reaction. In multiphase systems, rates of transport processes are often smaller than the intrinsic maximum reaction rates. The result is that the actual reaction rate is smaller than what would be anticipated from kinetics alone. For the unprepared mind this may come as both a surprise and a disappointment. Transport phenomena played a role for diffusion in immobilized enzyme systems in Sect. 6.3.2, where the basic mathematical models for analysis of combined mass transfer and kinetics were introduced. In biological multiphase systems, mass transfer takes place between two liquid phases, between a liquid and a solid phase, or between a gas and a liquid phase.

Most large-scale fermentation processes – bioethanol and lactic acid production excluded – are aerobic, and typically conducted in aerated gas–liquid bioreactors. In these systems, the transfer of oxygen from the gas phase to the liquid phase (where its solubility is low) is vital for the success of bioprocess. Understanding gas–liquid mass transfer is therefore very important for the design of bioprocesses. The development of large-scale production of penicillin in the 1940s – which in a sense constitutes the birth of industrial biotechnology outside the food sector – was closely coupled to the development of efficient submerged cultivation, where the supply of a large amount of sterile air was of significant importance.

We have already touched upon gas–liquid mass transfer in previous chapters, notably in Chap. 3 where the basic mass balances were first formulated but also in Chap. 9 in the design of processes. We will now in more detail study the origin of the "rate constant" for mass transfer, the $k_l a$ value: How is it defined, how is it measured, and how can it be calculated from empirical expressions? The discussion of mass transport will be limited to the transfer of reactants between a gas phase and a liquid phase. However, one should keep in mind that other multiphase mass transfer processes are also important:

- *In downstream processing*. This will often involve transfer of a product from an aqueous phase to an organic phase.

J. Villadsen et al., *Bioreaction Engineering Principles*,
DOI 10.1007/978-1-4419-9688-6_10, © Springer Science+Business Media, LLC 2011

- In conversion of natural fats to biodiesel, where the action of lipases depends on transfer of reactants to the interface between an organic and an aqueous phase.
- In solid-state fermentations (important in many food production processes), which depend on the rate at which a substrate can be transported to the surface of the solid and further into the interior of the solid.
- In the utilization of enzymes for the liquefaction of lignocellulosic biomass, i.e., the first step of a second generation bio-ethanol production, where enzymes must be transferred to the carbohydrate polymer matrix and the oligosaccharides must be transported out of the matrix.

A single problem (Problem 10.4) will suffice to illustrate solid-phase diffusion processes, but, as stated above, the theory for their analysis has been outlined in Chap. 6.

10.1 The Physical Processes Involved in Gas to Liquid Mass Transfer

The fundamental physical physical principles that determine mass transfer are, as eloquently described by Bird et al. (2002), the same as those for heat transfer and transfer of momentum. Mass transfer takes place by two basic processes; convection and diffusion. Molecular diffusion and convective transport in mass transfer is mimicked by similar processes in diffusive or turbulent momentum transport processes to be treated in Chap. 11 in connection with the design of mixing equipment. A detailed treatment of mass transfer requires that the flow field is completely known, and computational fluid dynamics (CFD) is used to construct at least an approximation to the flow field in a stirred tank reactor. In our text we shall resort to the simplified classical treatment in which the overall mass transfer is schematically divided into a few distinct transfer steps. This approach has for many years proven useful for quantification of gas–liquid mass transfer.

Oxygen gas–liquid transport in aerobic bioprocesses is the most important gas–liquid process to consider in bioprocess design. The solubility of oxygen in aqueous media is low, i.e., the "storing capacity" for oxygen in water is low. The saturation concentration of oxygen is about 7–8 mg L^{-1} in a typical aerated process, and a continued transfer of oxygen from the gas phase to the liquid phase is therefore essential to maintain a fully oxidative cellular metabolism (see Example 10.1). A few minutes without aeration of the medium will, e.g., have a serious impact on the ability of a culture of the mold *Penicillium chrysogenum* to produce the desired penicillin, whereas facultatively aerobic organisms, such as the yeast *Saccharomyces cerevisiae* or the bacterium *Escherichia coli*, will drastically change their product formation when deprived of oxygen.

Example 10.1 *The oxygen requirement of a rapidly respiring yeast culture.* To illustrate the requirement for a high gas-liquid mass transfer of oxygen, we consider the experimental data

for *S. cerevisiae* in Example 3.5. For dilution rates smaller than ~0.25 h^{-1} the metabolism is still purely respiratory, and the oxygen yield coefficient is

$$Y_{so} = 0.425 \text{ mol } O_2(\text{C-mol glucose})^{-1} \tag{1}$$

For a dilution rate of 0.2 h^{-1} there is virtually no glucose in the reactor outlet, and the volumetric glucose uptake rate is therefore

$$q_s = 0.2\ h^{-1} 28\ g\ L^{-1} = 5.6\ g\ L^{-1}h^{-1} = 0.1867\ \text{C-mol}\ L^{-1}h^{-1} \tag{2}$$

Thus, the volumetric oxygen uptake rate is

$$q^t = -q_O = 0.425 \times 0.1867\ \text{C-mol}\ L^{-1}h^{-1} = 79.3\ \text{mmol}\ O_2\ L^{-1}h^{-1} \tag{3}$$

If the dissolved oxygen concentration c_O^* is at its maximum (approximately 0.26 mmol O_2 L^{-1} when sparging with air, see Table 10.8. Oxygen will be depleted within 12 s, if the supply of oxygen is stopped. In Example 10.2, we quantify the rate of mass transfer which is necessary to keep the dissolved oxygen concentration in the liquid constant.

The transport of oxygen from a bulk gas phase to the interior of a cell occurs in several sequential steps:

1. Diffusion of O_2 from the bulk gas phase to the gas–liquid interface.
2. Transport across the gas–liquid interface.
3. Diffusion of O_2 through a relatively stagnant liquid region adjacent to the gas bubble, i.e., from the gas–liquid interface to the well-mixed bulk liquid.
4. Transport of dissolved oxygen to the cell, to a clump of cells, or to a pellet of immobilized cells.
5. Diffusion through the stagnant film to the cell surface, into cell aggregates, or into a support pellet.
6. Transport across the cell membrane (see Sect. 7.7).
7. Transport of dissolved O_2 inside the cell to the intracellular reaction site, e.g., the mitochondria.

Many of the steps 1–7 are in pseudosteady state. Step 2 is a fast equilibrium process. For sparingly soluble gases, step 1 is much faster than step 3, and step 4 is much faster than step 3 when the bulk liquid is effectively stirred. Due to the small size of the cells, transport to the surface of a freely suspended cell is likewise much faster than the transport through the liquid film surrounding the gas bubbles (see Note 10.2). When the cells agglomerate, the O_2 transport into the interior of the clump can be so poor that cells in the interior of the clump die from oxygen starvation, a phenomenon that is also encountered when the cells are immobilized on pellets. Consequently, for cultivation with freely suspended cells, step 3 is usually the rate-limiting step in the overall transport process.

Oxygen gas–liquid mass transfer is not the only important gas–liquid transfer process. Carbon dioxide is formed during respiration, as well as in most

fermentative processes. A too high concentration of carbon dioxide may inhibit the metabolism of the microorganism, and a continuous removal of the carbon dioxide formed is therefore needed. Methane is, together with carbon dioxide, a product gas in an aerobic waste water treatment processes, and also here gas–liquid transfer is from the liquid to the gas phase.

10.1.1 Description of Mass Transfer Using $\mathbf{k_l a}$

The volumetric mass transfer rate of a compound A, q_A^t can be quantitatively described as the product of a volumetric mass transfer coefficient, $k_l a$, and a driving force, the difference between the saturation concentration of the compound, c_A^*, and the actual concentration of the compound in the liquid phase, c_A.

$$q_A^t = k_l a(c_A^* - c_A) \tag{10.1}$$

The volumetric mass transfer coefficient, the $k_l a$, is normally treated as one coefficient, but it really consists of two parts; namely the mass transfer coefficient, k_l, which is connected to the mass flux (i.e. the transfer rate per unit area), and the specific surface area, a, which is the transfer area per volume of liquid.

Example 10.2 *Requirements for $k_l a$ in a laboratory bioreactor*. Again we use the data of Example 3.5. We want to calculate the minimum value of $k_l a$ needed to maintain the dissolved oxygen concentration in the medium above a desired value. Since the dissolved oxygen concentration in aqueous solutions is very low, the oxygen consumption approximately equals the mass transfer of oxygen at steady state (see Sect. 3.1.1 and Example 3.4).

$$q_O = q_O^t = k_l a(c_O^* - c_O) \tag{1}$$

$$k_l a = \frac{q_o^t}{(c_O^* - c_O)} \tag{2}$$

If the dissolved oxygen concentration is to be kept at 60% of the saturation value obtained by sparging with air containing 20.95% oxygen, we find

$$(c_O^* - c_O) = c_O^*(1 - 0.6) \tag{3}$$

When the bioreactor is operated at 1 atm, we find from Table 10.1

$$c_O^* = \frac{0.2095}{790.6} = 0.265 \times 10^{-3}\,\text{mol L}^{-1} \tag{4}$$

Inserting this value in (3) and using the calculated value of $-q_O$ in Example 10.1, we find from (2):

$$k_l a = 748\,\text{h}^{-1} = 0.208\,\text{s}^{-1} \tag{5}$$

Table 10.1 Henry's constant for some gases in water at 25°C

Compound A	H_A (atm L mol^{-1})
Ammonia[a]	17.1×10^{-3}
Methane	745.5
Ethane	545.1
Carbon dioxide	29.7
Oxygen	790.6
Hydrogen	1,270.0

[a]At a concentration of 0.2 g L^{-1} in the aqueous phase

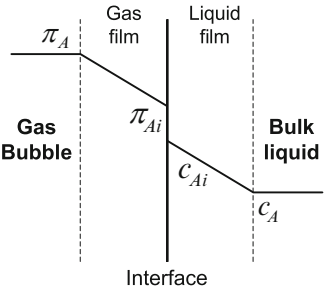

Fig. 10.1 Concentration profiles in gas and liquid films for the transfer of a gaseous compound A into the liquid phase. The gas and liquid phase bulk concentrations are assumed to be constant

This $k_l a$ value can normally be obtained in a well-stirred laboratory bioreactor. For larger stirred tank bioreactors, it requires a considerable power input to obtain a $k_l a$ value above 500 h^{-1}.

Gas–liquid mass transfer is normally modeled by the two-film theory (see Fig. 10.1), which was introduced by Whitman (1923). The flux J_A of compound A through each of the two films is described as the product of the concentration difference across the film layer, i.e., a linear driving force, and a mass transfer coefficient, k_g. Thus the flux across the gas film is given by

$$J_{A,g} = k_g(\pi_A - \pi_{A,i}) \tag{10.2}$$

π_A is the partial pressure of compound A in the gas bubble, and $\pi_{A,i}$ is the corresponding partial pressure in the bulk gas bubble that corresponds to the equilibrium concentration $c_{A,i}$, of A at the gas–liquid interface.

Similarly, for the flux across the liquid film

$$J_{A,l} = k_l(c_{A,i} - c_A) \tag{10.3}$$

In dilute aqueous cultivation media, the equilibrium concentrations on each side of the gas–liquid interface can be related to each other by *Henry's law*:

$$\pi_{A,i} = H_A c_{A,i} \tag{10.4}$$

H_A is Henry's constant for compound A in units of, e.g., atm L mol^{-1}. Table 10.1 lists the values of Henry's constant for a few important gases. Note that ammonia and to some extent CO_2 are far more soluble than the other gases.

Since the interfacial concentrations are not directly measurable, we specify the overall flux of the considered component from the gas bubble to the bulk of the liquid phase as an overall mass transfer coefficient multiplied by the driving force in the liquid phase:

$$J_A = K_l(c_A^* - c_A) \tag{10.5}$$

c_A^* is the saturation concentration in the *bulk* liquid corresponding to the *bulk* gas phase:

$$c_A^* = \frac{\pi_A}{H_A} \tag{10.6}$$

In previous chapters, we have used s_O^* and s_O for the bulk liquid phase oxygen concentrations.

At steady state, $J_{A,g} = J_{A,l} = J_A$ and by inserting (10.4) and (10.6) in (10.2), we find

$$\frac{1}{K_l} = \frac{1}{H_A k_g} + \frac{1}{k_l} \tag{10.7}$$

With the large value of the Henry's law constant H_A for oxygen and the other sparingly soluble gases, the first term on the right hand side of (10.7) can be neglected The measureable transport coefficient K_l is therefore approximately equal to the liquid-side transport coefficient k_l, and both have, e.g., the unit m s^{-1}.

k_l is the first factor in the *volumetric mass transfer coefficient* $k_l a$ (s^{-1}). To find the rate of mass transfer of compound A per unit of reactor volume, i.e., the volumetric mass transfer rate q_A^t, we multiply the overall flux J_A by the gas–liquid *interfacial area* per unit liquid volume a (unit: $m^2\ m^{-3} = m^{-1}$). Thus

$$q_A^t = J_A a = k_l a(c_A^* - c_A) \tag{10.8}$$

From (10.8), $k_l a$ can be calculated based on the measured q_A^t, and the driving force $(c_A^* - c_A)$. The influence of the operating conditions on the value of $k_l a$ is discussed in the following sections.

In a well-mixed tank, c_A has the same value at any position in the tank, whereas the value of c_A^* depends on the gas-phase concentration. Due to consumption or production in the bioreaction, the inlet and outlet mole fraction of A will be different. An approximation for the average driving force is the so-called *logarithmic mean driving force*, in which the known saturation concentrations at the inlet and exit from the tank are used in place of the true position-dependent variable c_A^*.

$$(c_A^* - c_A) = \frac{(c_{A,\text{inlet}}^* - c_A) - (c_{A,\text{outlet}}^* - c_A)}{\ln(c_{A,\text{inlet}}^* - c_A) - \ln(c_{A,\text{outlet}}^* - c_A)} \tag{10.9}$$

Equation (10.9) is, strictly speaking, based on plug flow of the gas through a thoroughly mixed liquid phase, an assumption that can rarely be true. Still the application of the formula does, as seen already in Example 3.4, give a reasonable value for the mean driving force.

10.1.2 Models for $\mathbf{k}_l$

The idea of expressing the mass transfer across surfaces by an overall mass transfer coefficient multiplied by a concentration difference is clearly a simplification of a complicated physical reality. A vast amount of experimental studies have been made in an effort to find the individual values of the two factors k_l and a in $k_\mathrm{l}a$, since these may, in fact, be changed individually.

The first model of this kind was due to Nernst (1904), who assumed that mass transfer occurred by diffusion through a stagnant film. Whitman (1923) took this a step further in his two-film theory, in which it was assumed that mass transfer from a gas bubble could be described by molecular diffusion through the two stagnant films. From Fick's first law (6.22) with a constant concentration gradient through the film, we obtain:

$$k_\mathrm{l} = \frac{D_\mathrm{A}}{\delta_\mathrm{f}} \tag{10.10}$$

D_A is the diffusion coefficient for component A and δ_f is the thickness of the liquid film. The film theory gives a simple relation between the diffusivity and the mass transfer coefficient. However, it is not possible to calculate k_l from D_A, since the film thickness is normally not known. Strictly speaking, there is no stagnant film surrounding the bubbles, although the liquid velocity relative to the surface is low very close to the bubble. Furthermore, the assumption of a constant concentration gradient may be wrong, e.g., if the diffusing species A is consumed by a chemical reaction within the film. Despite these shortcomings, the film model is probably the most widely used model to illustrate the concept of mass transfer.

Not all models for mass transfer make use of a stagnant film. In the so-called surface renewal theory of Denbigh (see Danckwerts 1970), discrete liquid elements close to the gas–liquid interface are thought to be interchanged with a well-mixed bulk liquid. Each element stays close to the surface for a certain time, during which it is considered to be stagnant. The transfer of compound A from the gas phase to the element is determined from the exposure time of the liquid element by solving the partial differential equation (6.24) without the reaction rate term. The mean residence time, τ_ren, at the surface for $r_\mathrm{A} = 0$ is introduced in the model, and one finds that k_l is related to D_A through

$$k_l = \sqrt{D_\mathrm{A}/\tau_\mathrm{ren}} \tag{10.11}$$

Equation (10.11) gives a slightly different relation between k_l and D_A than that predicted from the film theory. The dependence of k_l on D_A is experimentally found to be between the value predicted by the film theory and that predicted by the surface-renewal theory. Again, a calculation of k_l is not possible from the model, since it is difficult to obtain a reasonably accurate value for the mean residence time at the surface.

A more rigorous approach is to connect the mass transfer coefficient to a solution of the flow field close to a surface. This can be done using boundary-layer theory, see, e.g., Cussler (1997). The mass transfer coefficient, averaged over a length L for transfer of a compound present in the solid phase of a sharp-edged plate, is given (in SI units[1]) by:

$$\frac{k_l L}{D_A} = 0.646 \left(\frac{Lu\rho}{\eta}\right) \left(\frac{\eta}{\rho D_A}\right)^{\frac{1}{3}} \tag{10.12}$$

u is the linear flow velocity for the bulk phase (m s^{-1}).

This results in the following relation between k_l and the diffusion coefficient:

$$k_l \propto D_A^{2/3} \tag{10.13}$$

The equation contains a proportionality factor which is a function of the physical properties of the liquid and of the liquid flow rate.

None of these theoretically based models are of much use for calculating the value of k_l in a real system, e.g., in an agitated and sparged liquid. They do, however, tell us something about how the physical properties of the liquid influence the liquid mass transfer coefficient. Furthermore, the relative values of k_l for various compounds may be compared, even if the diffusivities of the compounds are unknown (see Sect. 10.3.5).

10.1.3 Models for the Interfacial Area, and for Bubble Size

In (10.8), the *specific interfacial area a* is based on the liquid volume, V_l, i.e.,

$$a = \frac{A}{V_l} \tag{10.14}$$

[1]In both Chaps. 10 and 11 there will occur expressions like (10.12) which empirically correlate variables such as L and u in (10.12). A number of physical properties such as ρ (density, kg m^3), η (viscosity, kg m^{-1} s^{-1}) and D_A (molecular diffusivity, m^2 s^{-1}) are incorporated in an attempt to make the expression applicable for many compounds with different properties. One must be careful with the numerical parameter (0.646 in (10.12)). *If* the expression consists of only dimensionless combinations of variables and parameters, *any* set of consistent units can be used. This is the case for (10.12) where $\eta/\rho = \nu$ (kinematic viscosity, m^2 s^{-1}), but otherwise *the reference must state which units to use*.

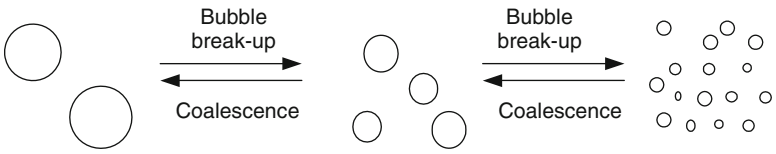

Fig. 10.2 Factors influencing the dynamic bubble-size distribution in a bioreactor

A is the total interfacial area in the gas liquid dispersion. This definition of the specific interfacial area is most convenient when the volumetric rate of the mass transfer process is to be used together with mass balances for dissolved components, e.g., for dissolved oxygen. However, in empirical correlations for the volumetric mass transfer coefficient (see Sect. 10.2), one often uses the specific interfacial area based on the total volume V_d of the gas–liquid dispersion:

$$a_\mathrm{d} = \frac{A}{V_\mathrm{d}} = \frac{A}{V_\mathrm{l} + V_\mathrm{g}} \tag{10.15}$$

The two definitions of the specific interfacial area are related by

$$a_\mathrm{d} = (1 - \varepsilon)a \tag{10.16}$$

In (10.16) *the gas holdup* ε is introduced:

$$\varepsilon = \frac{V_\mathrm{g}}{V_\mathrm{d}} \tag{10.17}$$

The specific interfacial area is a function of the bubble size distribution in the gas liquid dispersion, and a is obtained from

$$a = \frac{6\varepsilon}{(1 - \varepsilon)d_\mathrm{mean}} \tag{10.18}$$

d_mean is the average bubble diameter, which may be calculated as the first moment of the bubble size distribution function. A surface-averaged diameter, the so-called *mean Sauter diameter*, is, however, often used:

$$d_\mathrm{Sauter} = \frac{\sum n_i d_{\mathrm{b},i}^3}{\sum n_i d_{\mathrm{b},i}^2} \tag{10.19}$$

Three main processes interact to determine the bubble size distribution (Fig. 10.2):

1. *Bubble formation*, determined by the breakup into discrete bubbles of the gas stream as it is sparged into the liquid phase.

2. *Bubble breakup*, determined by the competition between the stabilizing effect of the surface tension and the destabilizing effect of inertial forces.
3. *Bubble coalescence*, i.e., fusion of bubbles, determined by the properties of the gas–liquid interface.

Bubbles are formed at the orifices of the sparger when the *buoyancy force* on the bubble exceeds the surface tension acting on the periphery of an orifice. Thus, the initial bubble diameter $d_{b,i}$ is determined from a force balance:

$$\pi d_o \sigma = \frac{\pi}{6} d_{b,i}^3 g(\rho_l - \rho_g) \rightarrow d_{b,i} = \left[\frac{6\sigma d_o}{g(\rho_l - \rho_g)}\right]^{\frac{1}{3}} \tag{10.20}$$

σ is the surface tension of the liquid phase (unit: N m^{-1}), d_o is the orifice diameter (m), and g is the acceleration of gravity (m s^{-2}). Equation (10.20) holds up to a certain gas flow rate V_g. At higher rates the diameter of the bubbles starts to increase with gas flow rate, V_g. For much higher gas flow rates, swarms of bubbles and finally an almost continuous jet flow will be formed. In a viscous medium, liquid viscosity rather than bubble surface tension provides the predominant resistance to bubble formation. For such systems an empirical correlation for the initial bubble diameter can be used.

When the bubbles have been formed at the orifices of the sparger, they circulate in the gas liquid dispersion until finally leaving the dispersion for the *head space*. The gas liquid dispersion is normally vigorously agitated, resulting in the formation of a *turbulent flow field*, in which there is a maximum bubble size $d_{b,max}$ determined by the balance of opposing forces:

1. Shear forces acting on the bubble tend to distort the bubble into an unstable shape, and the bubble breaks up into smaller bubbles.
2. The surface tension force acting on the bubble tends to stabilize the spherical shape of the bubble.
3. In the dispersed phase, there is a viscous resistance to deformation of the bubble.

In gas liquid dispersions, the viscous resistance on the gas side is negligible compared to the surface tension contribution, and at equilibrium we therefore have:

$$\tau_s = k_1 \frac{\sigma}{d_{b,max}} \tag{10.21}$$

τ_s is the *shear stress*, i.e., the force per unit area acting parallel to the surface (N m^{-2} = kg m^{-1} s^{-2}), and k_1 is a dimensionless constant. If $d_b > d_{b,max}$ the shear force acting on the bubble is larger than the surface tension forces, and the result is bubble breakup. In order to calculate $d_{b,max}$ we need to determine a value for the shear stress. According to the statistical theory of turbulence, the dynamic shear

stress acting on bubbles with diameter d_b is given by (10.22) for a turbulent flow field (see Note 10.1):

$$\tau_s = k_2 \rho_l^{\frac{1}{3}} \left(\frac{P_g}{V_l} \right)^{\frac{2}{3}} d_b^{\frac{2}{3}} \tag{10.22}$$

P_g/V_l is the *power dissipation to the gas per unit volume liquid*, or just P/V_l (W m^{-3} = N m^{-2} s^{-1}), and k_2 is a dimensionless constant. In a low viscosity medium like water, the dynamic shear stress given by (10.22) is much larger than the viscous shear stress. For this case, a combination of (10.21) and (10.22) will give the empirical, expression (10.23) for the maximum stable bubble diameter:

$$d_{b,max} = k \frac{\sigma^{0.6}}{(P_g/V_l)^{0.4} \rho_l^{0.2}} \tag{10.23}$$

$d_{b,max}$ decreases (giving a higher specific interfacial area) for increasing power input. Based on theoretical predictions in the turbulent regime, Lehrer (1971) states $k = 1.93(m)$ – which is also the unit of $d_{b,max}$ since the rest of the expression is dimensionless. Other researchers specify k as a function of the gas hold-up ε. For water Lee and Meyrick (1970) suggest the following for k:

$$k(m) = 4.25\varepsilon^{\frac{1}{2}} \tag{10.24}$$

In the case of highly viscous media, also the viscous resistance needs to be taken into account and (10.23) is therefore less accurate.

Coalescence of bubbles can be considered as a three-step process (Moo-Young and Blanch 1981).

1. Bubbles occasionally come into contact with each other within the liquid phase. This contact is characterized by a flattening of the contact surfaces, leaving a thin liquid film separating them.
2. The thickness of the separating liquid continuously decreases to a thickness of approximately 10^{-6} cm Tse et al. (1998).
3. Finally, the film ruptures, and this completes the coalescence process.

Note 10.1 *Calculation of maximum stable bubble diameter using the statistical theory of turbulence*. A turbulent flow field is normally described by the statistical theory of turbulence, and the flow field is regarded as a distribution of superimposed *eddies* or velocity fluctuations characterized by their direction and magnitude. According to this theory, large *primary eddies* emerge due to the impeller action. The scale of these primary eddies is on the order of magnitude of the impeller diameter. These primary eddies are unstable and disintegrate into smaller eddies (called *intermediate eddies*), which are again unstable and therefore disintegrate further into even smaller eddies (called *terminal eddies*). The terminal eddies have completely lost their unidirectional nature and are therefore isotropic. Thus, kinetic energy flows through the cascade of eddies until ultimately the energy is dissipated as heat

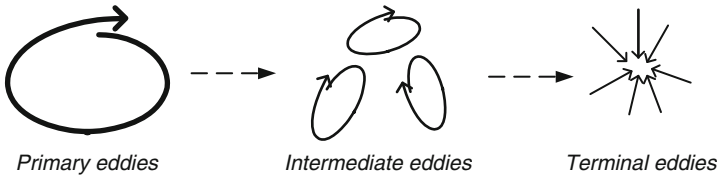

Fig. 10.3 Energy transfer from primary eddies to terminal eddies

(see Fig. 10.3). The size of the terminal eddies is (see, e.g., Moo-Young and Blanch 1981) is given by the dimensionless expression:

$$l_{\min} = \frac{\eta_l^{\frac{3}{4}}}{\rho_l^{\frac{1}{2}}} \left(\frac{P_g}{V_l}\right)^{-\frac{1}{4}} = \left(\frac{{v_l}^3}{P_g/M}\right)^{1/4} \tag{1}$$

In the simpler parameter, combination of the last expression the kinematic viscosity $v_l = \eta_l/\rho_l$ has been introduced, and P_g/M is the power input to the gas per unit mass of the liquid.

Any given location will be passed by eddies of widely different velocities, and it is appropriate to introduce time-averaged values of the eddy velocity. For eddies of scale much smaller than the primary eddies, but larger than the terminal eddies (of scale $l_{\min}$), the time-averaged velocity of the eddies is given by

$$u(L) = c_2^{\frac{1}{2}} \left(\frac{P_g}{V_l}\right)^{\frac{1}{3}} \left(\frac{L}{\rho_l}\right)^{\frac{1}{3}} \tag{2}$$

In (2) c_2 is dimensionless. If SI units are used $u(L)$, the velocity for length scale L, is in m s^{-1}.

The shear stress acting on a bubble is largely determined by the velocity of eddies of about the same size as the bubble diameter. The shear stress τ_s is therefore represented by:

$$\tau_s = \rho_l u(L = d_b)^2 \tag{3}$$

Inserting (2) in (3), we obtain (10.22) with $k_2 = c_2$ (both dimensionless).

Description of energy input to a process by the theory of isotropic turbulence is valuable for understanding bubble behavior in a bioreactor. The theory may also be used to predict the influence of energy input on the fragmentation of hyphal elements and mycelial pellets. Local isotropic turbulence is, however, an idealization not always realized in practice. Furthermore, in the derivation of (2), the energy dissipated per unit liquid volume is used regardless of the means by which that energy is delivered (mechanical agitation or injection of compressed gas). This is an idealization, but an acceptable approximation for many systems.

The entire process of bubble coalescence occurs in the milliseconds range, and the last step is practically instantaneous. Coalescence will happen when the time constant of the second step is smaller than the contact time of the bubbles. The rate of the second step is controlled by the properties of the liquid film. In a multicomponent liquid phase, interaction between molecules of different species leads to an

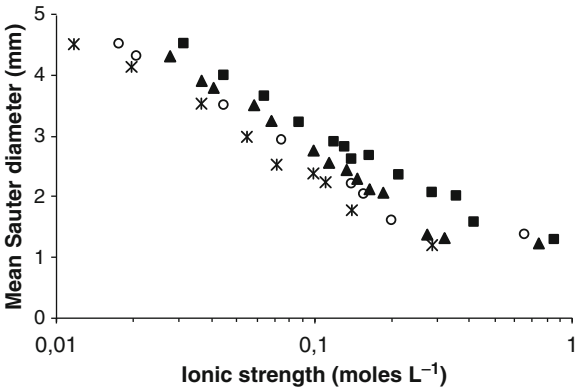

Fig. 10.4 Mean Sauter bubble diameter as a function of ionic strength for aqueous solutions of the salts: $Al_2(SO_4)_3$ (*filled square*), Na_2SO_4 (*filled triangle*), NaCl (*open circle*), NaOH (*asterisks*). The data are from an air–water system in a bubble column (Keitel and Onken (1982))

enhanced concentration in the film layer of one or more of the species in solution. The result is an increased repulsion between two bubbles and therefore a reduced tendency to coalesce. Especially with surface-active compounds, the enrichment in the film layer is considerable, even for very small concentrations in the bulk liquid. The influence of inorganic ions on the coalescence is illustrated in Fig. 10.4, where the mean Sauter diameter is shown as a function of the ionic strength of the electrolyte solution. Alcohols and other organic compounds have a similar influence on the coalescence. Small alcohols are less efficient as coalescence reducers than larger alcohols, e.g., methanol has less influence on the mean bubble diameter than octanol at the same concentration (Keitel and Onken 1982). Surface-active compounds also strongly influence the coalescence. Foam-stabilizing compounds, such as proteins, reduce the coalescence, whereas antifoam agents, such as fatty acids, increase the coalescence.

Normally, surface-active materials reduce the mass transfer coefficient k_l for the liquid film, and therefore the overall effect of surface-active materials on the volumetric mass transfer coefficient $k_l a$ is quite complex.

However, for foam-stabilizing compounds the increase in the specific interfacial area a (due to a smaller average bubble diameter) is normally larger than the decrease in k_l. In most cultivation media, the tendency for coalescence is smaller than for pure water. Water is therefore often called a *coalescing medium*, whereas many cultivation media are *noncoalescing*.

It is quite clear that the mechanism of coalescence is not yet fully understood (Craig et al. 1993). Whereas the presence of some ions in an aqueous medium reduces the coalescence, other ions seem to have no influence at all.

The combined effect of bubble breakup and coalescence on the average bubble diameter is determined by the relative rate of the two processes. If coalescence is very slow compared to bubble breakup, the average bubble diameter is determined by the breakup process, i.e., by (10.22). However, if the bubbles formed at the orifice are smaller than the maximum stable bubble diameter (i.e., $d_o < d_{b,max}$) the average bubble diameter is determined by the bubble formation process,

Table 10.2 Parameter values for power law correlation of specific interfacial area a, (10.26)

	Coalescing	Noncoalescing
k	55	15
α	0.5	0.3
β	0.4	0.7

i.e., by (10.20). On the other hand, if coalescence occurs rapidly, bubbles formed at the orifices coalesce and grow larger until they exceed the maximum stable bubble size, after which bubble breakup occurs. Since bubble breakup depends on the local eddy-velocity, there are is a local coalescence-breakup equilibrium, resulting in variation of bubble size throughout the bioreactor.

Assuming that the average bubble diameter is given by (10.23), we may obtain a correlation for the specific interfacial area by using (10.16) and (10.18):

$$a_\mathrm{d} = \frac{6\varepsilon}{k}\frac{\rho_\mathrm{l}^{0.2}}{\sigma^{0.6}}\left(\frac{P_\mathrm{g}}{V_\mathrm{l}}\right)^{0.4} \tag{10.25}$$

In this correlation (with a_d having the same unit as k^{-1}, e.g. m^{-1}) the gas holdup ε, appears, and not necessarily as a proportionality factor, since k may be a function of ε, according to (10.24). The gas holdup depends on the operating conditions, e.g., the dissipated energy and the gas flow rate, and normally an empirical correlation is applied for the gas holdup resulting in a completely empirical correlation such as (10.26) for the specific interfacial area (Moo-Young and Blanch 1981).

$$a_\mathrm{d} = k u_\mathrm{s}^{\alpha}\left(\frac{P_\mathrm{g}}{V_\mathrm{l}}\right)^{\beta} \tag{10.26}$$

u_s is the *superficial gas velocity* (unit: m s^{-1}) obtained from the gas flow rate (m^3 s^{-1}) divided by the cross-sectional area of the tank (m^2). The parameters for this correlation are listed in Table 10.2 for both a coalescing and a noncoalescing medium. k is a dimensionless constant, and all the variables must be inserted in SI-units – see also Eq. (10.27).

Example 10.3 *Bubble size and specific interfacial area in an agitated vessel.* Consider aeration of a small pilot-plant bioreactor (total volume 41 L) by mechanical agitation (Pedersen et al. 1994). Some of the data for the tank are summarized in Table 10.3.

We first consider a system with water and air at 25°C:

$\rho_\mathrm{l} = 997\ \mathrm{kg\ m^{-3}}$
$\rho_\mathrm{g} = 1.285\ \mathrm{kg\ m^{-3}}$
$\sigma = 71.97 \times 10^{-3}\ \mathrm{N\ m^{-1}}$
$\eta = 1.00 \times 10^{-3}\ \mathrm{kg\ m^{-1}\ s^{-1}}$

First, we calculate the initial bubble diameter using (10.20):

$$d_{\mathrm{b},i} = \left[\frac{6 \times 71.97 \times 10^{-3} \times 10^{-3}}{9.82 \times (997 - 1.285)}\right]^{1/3} = 3.53 \times 10^{-3}\,\mathrm{m} \tag{1}$$

Table 10.3 Data for a sparged, mechanically mixed pilot plant bioreactor

Symbol	Parameter	Value
d_o	Orifice diameter[a]	10^{-3} m
d_T	Tank diameter	0.267 m
V_l	Liquid volume	25 L
v_g	Gas flow rate	25 L min^{-1}
P_g	Power input	75 W

[a] The sparger is equipped with ten orifices

From visual inspection of the system, however, we observe that a jet stream is formed at the orifices. We therefore search in the literature for a correlation for the initial bubble diameter, which may be more suitable for the high gas flow rate applied in the system. Bhavaraju et al. (1978) states that the correlation in (2) holds for gas flow rates up to 2×10^{-4} m^3 s^{-1} (which is close to the value 4.2×10^{-4} m^3 s^{-1} which is used for the present system). Re_o is the Reynolds number for the gas stream at the orifice [given by (3)] and Fr_o is the *Froude number* for the gas stream at the orifice [given by (4)]:

$$d_{b,i} = 3.23 d_o Re_o^{-0.1} Fr_o^{0.21} \tag{2}$$

$$Re_o = \frac{4\rho_l v_g}{\pi \eta d_o} \tag{3}$$

$$Fr_o = \frac{v_g^2}{d_o^5 g} \tag{4}$$

With the operational values specified in Table 10.3, we find $Re_o = 5.3 \times 10^4$ and $Fr_o = 1.8 \times 10^5$ (the total gas flow is equally distributed to the ten orifices in the sparger), and therefore

$$d_{b,i} = (3.23 \times 10^{-3})(5.3 \times 10^4)^{-0.1}(1.8 \times 10^5)^{0.21} = 13.8 \times 10^{-3}\,\text{m} \tag{5}$$

This is a larger initial bubble diameter than that found by using (10.20), and it corresponds better with the bubble size observed in the bioreactor when there is no agitation. Note that the correlation in (2) is insensitive to even large variations in the orifice diameter, and a change of the hole size of the sparger therefore has little effect on the initial bubble diameter. The two completely different values obtained tell us that correlations (both empirical and theoretically derived) should always be used with some caution, i.e., one should always check the range of validity for the correlation.

With the specified power input, we calculate the maximum stable bubble diameter, using (10.23). First we take k to be 1.93 m.

$$d_{b,i} = 1.93(\text{m})\frac{(71.97 \times 10^{-3})^{0.6}}{(75/25 \times 10^{-3})^{0.4}(997)^{0.2}} = 4.07 \times 10^{-3}\,\text{m} \tag{6}$$

Next we assume that the gas holdup is 0.1 (as is reasonable for the examined system) and use (10.24) to find $k = 1.34$(m). Thus from (10.24) we now find

$$d_{b,\max} = 2.83 \times 10^{-3}\,\text{m} \tag{7}$$

Again we find some deviation among the various correlations. The order of magnitude is, however, the same, and this is often sufficient for design purposes because of the large uncertainties of all the calculations. If the initial bubble diameter really is 13.8 mm as found in (5), the breakup process results in a rapid disintegration of the bubbles formed at the orifice, and we therefore do not observe the large bubbles formed right at the orifice when the dispersion is agitated.

10.2 Empirical Correlations for k_la

In Sect. 10.1, we have examined models for predicting each of the two factors in k_la. These models can all claim to have some sort of mechanistic foundation, but apart from pointing to variables which influence the values of the factors, a mechanistic approach does not bring us far in terms of a quantitative determination of k_la. The volumetric mass transfer coefficient is, however, determined by relatively simple experimental methods to be discussed in Sect. 10.2, and understandably the literature on quantitative determination of k_la by compilation of data from many experimental systems is quite rich (see, e.g., the review of Moo-Young and Blanch 1981). Most of these correlations can be written in the form

$$k_la_d = ku_s^{\alpha}\left(\frac{P_g}{V_l}\right)^{\beta} \tag{10.27}$$

Equation (10.25) has a great similarity to (10.26), the expression for the specific interfacial area. The parameters tend to depend on the considered system, i.e., on the bioreactor design. Thus, for different stirrers (see Chap. 11) and different tank geometry the parameter values may change significantly, and a certain set of parameters can only be safely used when studying a system, which resembles that from which the parameters were originally derived. Some parameter values reported in the literature for stirred tanks are listed in Table 10.4.

Normally, the correlation (10.27) holds independently of whether mixing is performed mechanically in stirred tanks or pneumatically in bubble columns. Thus for the same power input per liquid volume, the magnitude of k_la is approximately the same in a stirred-tank reactor and in a bubble column. It is, however, possible to obtain much higher power input in stirred-tank reactors than in bubble columns, and stirred tanks are therefore traditionally used in aerobic fermentation processes when there is a high oxygen demand, e.g., in the production of antibiotics. In the Loop-bioreactor of Sect. 9.3.2 very high values of k_la can be obtained compared to a stirred tank, but as discussed earlier this comes at the cost of a high energy input to pump the medium at quite high linear velocity through the static mixers of the loop reactor. The Rotary Jet Head reactor discussed both in this chapter and in Chap. 11 can also give quite high k_la values, and the reactor is particularly advantageous at small power inputs.

Table 10.4 Parameter values for the empirical correlation (10.27)

Medium	k	α	β	Agitator	Reference
Coalescing	0.025	0.5	0.4	Six-bladed Rushton turbine	Moo-Young and Blanch (1981)
	0.00495	0.4	0.593	Six-bladed Rushton turbine	Linek et al. (1987)
	0.01	0.4	0.475	Various agitators	Moo-Young and Blanch (1981)
	0.026	0.5	0.4	Not specified	van't Riet (1979)
Noncoalescing	0.0018	0.3	0.7	Six-bladed Rushton turbine	Moo-Young and Blanch (1981)
	0.02	0.4	0.475	Various agitators	Moo-Young and Blanch (1981)
	0.002	0.2	0.7	Not specified	van't Riet (1979)

SI units must be used, e.g., W m^{-3} for the power input per volume medium, P_g/V, m s^{-1} for the superficial gas flow $u_{s,}$ and s^{-1} for $k_l a$

When the range of process variables for which the correlation (10.27) holds is studied in more detail, it is observed that the mass transfer coefficient $k_l a$ in a noncoalescing medium is greater by about a factor of 2 than that for a coalescing medium under the same operating conditions. These overall correlations are, however, very rough simplifications since they are constructed to fit data obtained in many different bioreactors. For a specific agitator system, e.g., a six-bladed Rushton turbine (see Fig. 11.1), the situation is more complex. Here, it is found that the influence of the power input is larger in the noncoalescing medium, whereas the influence of the superficial gas velocity is smaller compared with a coalescing medium, e.g., pure water (see Table 10.4).

In the derivation of (10.23), it was assumed that the dynamic shear stress caused by eddies was much larger than the viscous stress. This will not be true for highly viscous media, and very simple correlations of the type given by (10.27) will therefore not be valid. In general, $k_l a$ decreases with increasing liquid viscosity, but the effect is small until $\eta > 50 \times 10^{-3}$ kg m^{-1} s^{-1} (50 times the viscosity of water). A detailed review of mass transfer in highly viscous media is given by Schugerl (1981). The influence of viscosity on mixing in general is discussed in Chap. 11.

Example 10.4 *Derivation of empirical correlations for $k_l a$ in a laboratory bioreactor.* Pedersen (1992) examined the gas–liquid mass transfer in a stirred laboratory bioreactor. The value of the volumetric mass transfer coefficient $k_l a$ was determined by the sulfite method (see Sect. 10.3.3), and the influence of aeration rate and stirring speed on $k_l a$ was examined. Data for the bioreactor and the operating conditions are summarized in Table 10.5.

The results using the sulfite method are shown as double logarithmic plots in Figs. 10.5 and 10.6.

Table 10.5 Data for a standard laboratory bioreactor with two Rushton turbines

Variable	Value	Meaning
V_t	15 L	Tank volume
V_l	10 L	Liquid volume
d_t	0.20 m	Tank diameter
d_i	0.07 m	Stirrer diameter
N	4–25 s^{-1}	Stirring speed
v_g	2.2–25 × 10^{-5} m^3 s^{-1}	Gas flow rate

The range of operating conditions for N and v_g is shown (Pedersen 1992)

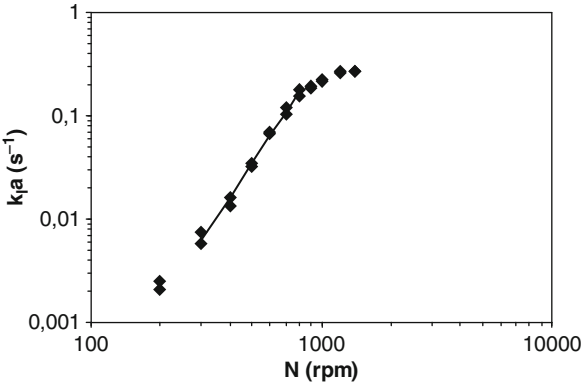

Fig. 10.5 Double-logarithmic plot of the influence of the stirring speed N (s^{-1}) on the volumetric mass transfer coefficient k_la (s^{-1}). The aeration rate is $v_g = 10^{-4}$ m^3 s^{-1}. The *line* is the regression line for the correlation in (1)

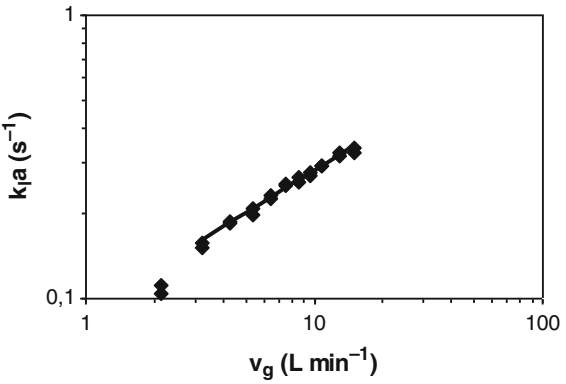

Fig. 10.6 Double-logarithmic plot showing the influence of the aeration rate v_g on the volumetric mass transfer coefficient k_la. The stirring speed is 16.7 s^{-1}. The *line* is the regression line for the correlation in (2)

The volumetric mass transfer coefficient increases with increasing gas aeration rate v_g and with increasing stirring speed N, but there is an upper limit to k_la. From each of the two series we find the correlations

$$k_la = 4.5 \times 10^{-5} N^{3.146} \tag{1}$$

$$k_la = 27.0 v_g^{0.523} \tag{2}$$

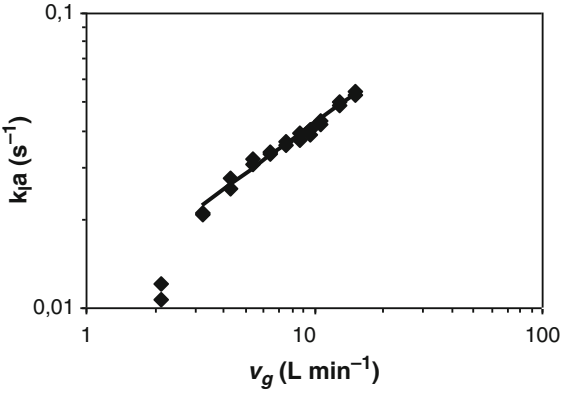

Fig. 10.7 Double-logarithmic plot showing the influence of the aeration rate v_g (L min^{-1}) on the volumetric mass transfer coefficient $k_l a$ (s^{-1}). The stirring speed is 8.33 s^{-1}. The *line* is the regression line for the correlation in (5)

From the correlation for the influence of the aeration rate, we find

$$k_l a = 27.0\left(\frac{\pi d_t^2}{4}\right)^{0.523}\left(\frac{4v_g}{\pi d_t^2}\right)^{0.523} = 4.42u_s^{0.523} \tag{3}$$

$$k_l a = 4.42u_s^{0.523}\left(\frac{N}{16.7}\right)^{3.146} = 6.3 \times 10^{-4}u_s^{0.523}N^{3.146} \tag{4}$$

Similarly, we find from the correlation for the influence of the stirring speed

$$k_l a = 4.5 \times 10^{-5}\left(\frac{u_s \pi d_t^2}{4 \times 10^{-4}}\right)^{0.523} \times N^{3.146} = 9.1 \times 10^{-4}u_s^{0.523}N^{3.146} \tag{5}$$

Thus, the value of the numerical constant found for each of the two sets of experiments is slightly different. The correlation in (1) holds only for $N < 15$ s^{-1}, whereas the correlation in (2) is based on $N = 16.7$ s^{-1}. From Fig. 10.5 it is observed that for $N = 16.7$ s^{-1} the measured $k_l a$ value is lower than predicted by the correlation in (1), and this may explain the lower value for the constant in (4) compared with (5). Thus the correlation in (5) is probably the best, and to test the correlation another series of experiments was performed, with varying v_g at $N = 8.33$ s^{-1}. The results of this comparison are shown in Fig. 10.7.

If we compare the correlation derived in this example with (10.27), we see that the structure is the same since the power input is correlated to the stirring speed. For the examined bioreactor, it was found that the power input (measured as the power drawn by the motor) correlates with the stirring speed to the power 3:

$$P \propto N^3 \tag{6}$$

Equation (6) indicates that the influence of the power input is stronger in the present system than that reported in the literature (see Table 10.4). The influence of the superficial gas flow rate is also larger than that reported in the literature (see value of α for noncoalescing

medium in Table 10.4). The correlation derived here is based on measurement of $k_l a$ using the sulfite method, and since the sulfite concentration must be quite high (around 0.5 M) to obtain accurate measurements of the rate of sulfite consumption, the medium is strongly noncoalescent. This may explain the deviation between the correlation of the present example and similar correlations based on other measurement methods

Linek et al. (1987) also applied the sulfite method to determine $k_l a$ in a stirred-tank reactor and found the correlation

$$k_l a = 0.00135 u_s^{0.4} \left(\frac{P_g}{V_l} \right)^{0.946} \tag{7}$$

In (7) the influence of power input is much higher than that indicated in Table 10.4. Thus, application of the sulfite method may result in a correlation that is not valid for normal fermentation media (even when these are noncoalescing). The sulfite method is discussed further in Sect. 10.2.

In the experiments on which the present example is based, the power input was not measured directly, but calculated from the measured stirring speed and the correlation in (6). This correlation is, however, not generally valid, and it should be used only for preliminary calculations. Since determination of the power input requires measurement of the torque on the impeller shaft inside the bioreactor, it is convenient to use the stirring speed rather than the power input in empirical correlations for $k_l a$.

There is a tradition in the chemical engineering literature to express correlations for various transport coefficients in terms of dimensionless groups named after prominent members of the engineering community. Unfortunately, these dimensionless groups have come to work as filters, which tend to separate the treatment of transport phenomena by chemical engineers from that of their colleagues active in the fields of biology or chemistry. Also, the dimensionless correlations are all too frequently based on measurements with only a few chemical species (e.g., water and glycerol) and in a very restricted region of variation for the operation variables.

Hence one must regard the correlations with some caution, but still there are several advantages to be gained from using dimensionless groups. Most importantly, these groups show *in what way physical variables interact* in their effect on the interesting property, e.g., $k_l a$. This is helpful when designing experiments to derive empirical correlations, and also for obtaining a qualitative understanding of how transport phenomena may be influenced by operating conditions. A practical advantage is, furthermore, that dimensionless equations can be used in any consistent frame of units and with a minimum risk of unit conversion errors. Equations of the type given in 10.27, on the other hand, carry dimensions, which is sometimes not realized or clearly stated in the reference.

Dimensionless groups may be derived by two principally different routes. If known, the fundamental mechanism of the phenomenon of interest can relatively easily be transformed into a dimensionless form. In the transformed equation dimensionless groups will appear as coefficients. Well-known examples are, e.g., the *Reynolds number* and *Froude number,* which appear in the dimensionless form of the Navier–Stokes equation (see Bird et al. (2002)).

Table 10.6 Some important dimensionless groups for mass transfer correlations

Definition	Name	Significance
$Sh = \left[\frac{k_l d}{D_A}\right]$	Sherwood number	Mass transfer velocity relative to diffusion velocity
$Sc = \left[\frac{\eta}{D_A \rho_l}\right]$	Schmidt number	Momentum diffusivity relative to mass diffusivity
$Re = \left[\frac{ud\rho_l}{\eta}\right]$	Reynolds number	Inertial forces relative to viscous forces
$Gr = \left[\frac{d^3 g \rho_l (\rho_l - \rho_g)}{\eta^2}\right]$	Grashof number	Bouyancy forces relative to viscous forces
$Pe = \left[\frac{du}{D_A}\right]$	Peclet number	Flow velocity relative to diffusion velocity

d is a length scale characteristic of the system which is studied, i.e., bubble, cell, or cell aggregate. D_A is the diffusion coefficient for the considered species in the continuous phase; u is the linear velocity of the bubble, the cell, or the cell aggregate relative to the continuous phase

Also, in the absence of a known fundamental mechanism, it is possible to derive dimensionless variables upon which empirical correlations can be based. This can be done by *dimensional analysis*, i.e., by checking that the correlations are dimensionally correct. The basis for this analysis is the Buckingham π-theorem, which is explained in detail in many chemical engineering textbooks (see, e.g., Geankoplis 1993).

Some well-known dimensionless groups used in mass transfer correlations are listed in Table 10.6.

Reported correlations for the Sherwood number are often of the kind

$$Sh = 2 + \text{const} \times Sc^{\alpha} Re^{\beta} \tag{10.28}$$

If the exponents α and β have the same value, the Schmidt and Reynolds number can be multiplied together to form the *Peclet number*, *Pe*. In cases where free convection dominates, the Grashof number appears instead of the Reynolds number.

It is seen from (10.28) that as the Reynolds number approaches 0, i.e., for a bubble which is stagnant relative to the surrounding liquid, the Sherwood number will approach 2. This is in accordance with the analytical steady-state solution of the diffusion equation for a sphere in stagnant medium (see Note 10.2). For high values of *Re* the first term may be neglected compared to the second term.

A key question is whether the bubble behaves as a rigid surface or not (see Table 10.7). For a rigid bubble, with an immobile interface, the boundary conditions at the surface will state a zero relative velocity between the liquid and the bubble surface. For a mobile interface, however, this boundary condition does not apply, and the mass transfer characteristics will be different, as discussed, e.g., by Blanch and Clark 1997.

Table 10.7 Literature correlations for the Sherwood number, *Sh*

Correlation	Conditions	Remarks	Source
$Sh = 2 + 0.55\,Re^{\frac{1}{2}}Sc^{\frac{1}{3}}$	$2 < Re < 1{,}300$	Immobile gas–liquid interface	Froessling (1938)
$Sh = 0.82\,Re^{\frac{1}{2}}Sc^{\frac{1}{3}}$	$200 < Re < 4{,}000$	Immobile gas–liquid interface	Rowe et al. (1965)
$Sh = \left(4 + 1.21\,Pe^{\frac{2}{3}}\right)^{\frac{1}{2}}$	$Re < 1$; $Pe < 10^4$	Immobile gas–liquid interface	Brian and Hales (1969)
$Sh = 0.42\,Gr^{\frac{1}{3}}Sc^{\frac{1}{2}}$	Free convection	Mobile interface, large bubbles	Calderbank and Moo-Young (1961)
$Sh = 0.65\,Pe^{\frac{1}{2}}$	$Re < 1$	Mobile gas–liquid interface	Blanch and Clark (1997)
$Sh = 0.65\left(1 + \frac{Re}{2}\right)^{\frac{1}{2}}Pe^{\frac{1}{2}}$	$1 < Re < 10$	Mobile gas–liquid interface	Blanch and Clark (1997)
$Sh = 1.13\,Pe^{\frac{1}{2}}$	$Re >> 1$	Mobile gas–liquid interface	Blanch and Clark (1997)

Note 10.2 *Derivation of and use of the relation Sh = 2 for a sphere in stagnant medium.* For the case of steady-state mass transfer from a spherical particle with radius, $R_p = d_p/2$, in a stagnant medium, it is possible to derive an analytical value for the Sherwood number. The diffusion equation for species A at steady state is given by

$$\nabla^2 c_A = 0 \tag{1}$$

Due to the symmetry of the problem, it is convenient to use spherical coordinates, and with the radial distance denoted ξ, (1) can be expressed

$$\frac{1}{\xi^2}\frac{\partial}{\partial \xi}\left(\xi^2 \frac{\partial c_A}{\partial \xi}\right) = 0 \tag{2}$$

The boundary conditions are

$$c_A = c_{A,s} \quad \text{for } \xi{=}R_p, \quad \text{and } c_A \to 0 \text{ for } \xi \to \infty \tag{3}$$

Integrating (2) twice gives the solution (4) for c_A:

$$c_A = c_{A,s}\frac{R_p}{\xi} \quad \text{for } \xi \geq R_p \tag{4}$$

The mass flux of A at $\xi = R_p$, expressed either by Fick's law or using the mass transfer coefficient must be equal, i.e.,

$$k_l(c_{A,s} - 0) = -D_A \frac{\partial c_A}{\partial \xi} \tag{5}$$

The derivative is obtained by differentiation of c_A in (4), and one obtains:

$$k_l c_{A,s} = D c_{A,s}\frac{R_p}{R_p^2} \;\rightarrow\; \frac{k_l d_p}{D_A} = 2 \tag{6}$$

Table 10.8 Solubility of oxygen in pure water at an *oxygen* pressure $\pi_O = 1$ atm

Temperature (°C)	Solubility of O_2 (mmol L^{-1})
0	2.18
10	1.70
15	1.54
20	1.38
25	1.26
30	1.16
40	1.03

This result, i.e., $Sh = 2$, is correct for steady-state mass transfer between a single sphere of diameter $d_p = 2\,R_p$ and a stagnant medium.

The following example illustrates how (6) is used to calculate the rate of oxygen transport from the bulk liquid to a spherical cell of diameter 2 μm. The diffusivity of O_2 is taken from Table 10.10:

$$k_l = \frac{2 \times 2.42 \times 10^{-9}\ \mathrm{m^2 s^{-1}}}{2 \times 10^{-6}\ \mathrm{m}} = 2.42 \times 10^{-3}\ \mathrm{m\ s^{-1}} \tag{7}$$

The specific interfacial area per unit biomass is

$$a_{cell} = \frac{6}{d_{cell}(1-w)\rho_{cell}} \tag{8}$$

In (8) w is the fractional water content. With $w = 0.7$ and a density of the cell of $10^6\ \mathrm{g\,m^{-3}}$, the volumetric mass transfer coefficient for the cell is

$$k_l a_{cell} = \frac{6k_l}{d_{cell}(1-w)\rho_{cell}} = \frac{6 \times 2.42 \times 10^{-3}\mathrm{m\ s^{-1}}}{2 \times 10^{-6}\mathrm{m}(1-0.7)10^6\ \mathrm{g\ DW\ m^{-3}}} = 0.024\ \mathrm{m^3\,g^{-1}\,s^{-1}} \tag{9}$$

With a bulk phase oxygen concentration equal to 60% of the saturation value at 25°C (Table 10.8), the maximum specific oxygen transport rate when sparging the reactor with air can be calculated when we assume that $c_{O,surface} \sim 0$:

$$k_l a_{cell} c_{O,bulk} = 0.024 \times 0.6 \times 0.2095 \times 1.26 \times 10^{-3} = 3.8 \times 10^{-3}\,\mathrm{mol\,O_2\,(g\ DW)^{-1}\,s^{-1}} \tag{10}$$

Thus, mass transfer to the cells from the bulk liquid is very rapid compared with the O_2 requirement inside the cell (see Example 10.1), and it is therefore not necessary to consider the process in the model. Even with a mass transfer coefficient much lower than that calculated in (7), the maximum mass transfer rate from the bulk liquid to the cell is still very rapid compared to the cellular oxygen requirements.

10.3 Experimental Techniques for Measurement of O_2 Transfer

Due to the importance of aerobic fermentation processes, gas–liquid mass transfer is almost synonymous with oxygen transfer from gas bubbles to the liquid medium. In this section, some of the many methods that have been used to measure O_2 transfer are reviewed.

Since the volumetric rate of mass transfer is proportional to the difference between the equilibrium (saturation) concentration c_O^* and the actual value of the dissolved oxygen concentration in the medium c_O^* , we shall first state some tabular values for $c_O^* = (s_O^*$ in previous chapters). Table 10.8 shows that c_O^* decreases with increasing temperature, and Table 10.9 shows that the presence of various dissolved substances in the water also tends to decrease c_O^*. In (10.29), a formula for O_2 solubility in water supplements Table 10.8. The formula was first used and is explained in equation (3) of Example 3.4.

When using the tables or (10.29) one must always remember that it is the *partial* pressure of O_2 in the gas phase that is to be used, and this is proportional to the total pressure P.

$$c_O^* = s_O^* = 0.0270 \exp\left(\frac{1,142}{T(\mathrm{K})}\right) \text{ mmol } O_2 \text{ L}^{-1} \quad \text{for} \quad 298 < T < 324 \text{ K} \qquad (10.29)$$

Example 10.2 shows that a high $k_l a$ value is required to maintain the dissolved oxygen concentration at 60% of the saturation value in a rapidly respiring culture of *S. cerevisiae*. This high $k_l a$ value for oxygen can be obtained in a laboratory bioreactor (and perhaps in small-scale pilot-plant bioreactors), but will be difficult to obtain in a large bioreactor. However, a substantially lower dissolved oxygen concentration than 60% is normally acceptable in industrial applications of *S. cerevisiae*. The simplest way to describe oxygen uptake kinetics is through a Monod expression. The saturation constant, K_o, is in the range 1–10 μM, which corresponds to approximately 0.4–4.0% of the saturation concentration (at 25°C and 1 atm of air). As long as the dissolved oxygen concentration is maintained well above this value, the oxygen consumption rate will therefore be zero order with respect to the dissolved oxygen concentration, i.e., oxygen limitation does not occur.

Among the many methods for experimental determination of $k_l a$, we shall discuss two methods which are directly tied to the oxygen consumption by the bioreaction and two methods where another chemical species is added. A fifth method relates $(k_l a)_A$ to the volumetric mass transfer coefficient $k_l a$ of a standard substance which is conveniently chosen to be O_2.

10.3.1 The Direct Method

Most bioreactors used for aerobic fermentation processes are equipped with exhaust gas analysis for oxygen and probes for measuring the dissolved oxygen

Table 10.9 Solubility of oxygen at 25°C and $\pi_O = 1$ atm in various aqueous solutions

Component	Concentration (g L^{-1})	Solubility of O_2 (mmol L^{-1})
Glucose	20	1.233
	50	1.194
	90	1.133
	180	0.990
Citric acid	25	1.242
	100	1.137
	200	0.983
Gluconic acid	25	1.210
	100	1.121
	200	0.991
Corn steep liquor	10	1.205
	50	1.189
	100	1.154
Yeast extract	5	1.255
	10	1.228
Xanthan	1	1.250
	5	1.251
Pullulan	1	1.266
	10	1.241
	20	1.240

The data are taken from Popovic et al. (1979)

concenration. From the measurement of oxygen content in the inlet and exhaust gases together with measurement of the gas flow rate, it is possible, as already discussed in Sect. 3.1, to determine the steady-state volumetric oxygen transfer rate, q_O^t. At steady state q_O^t is equal to the volumetric oxygen consumption rate, $-q_O$, and from (3.10):

$$q_O^t = \frac{1}{V_l}\left(\frac{\pi_O^{in} v_g^{in}}{RT^{in}} - \frac{\pi_O^{out} v_g^{out}}{RT^{out}}\right) \tag{10.30}$$

R is the gas constant (=8.314 J(mol K)$^{-1}$ = 0.08206 L atm (mol K)$^{-1}$), T is the temperature (K), π_O is the partial pressure of oxygen, and v_g is the gas flow rate.

Most gas analyzers will give the result in terms of mole fraction of oxygen in the gas. When normal air is used, it is sufficient to analyze only the outlet gas composition. However, for large bioreactors it is important to take the pressure difference over the reactor into account. If simultaneously the dissolved oxygen concentration, c_O, is measured in the medium, it is possible to calculate the volumetric mass transfer coefficient from:

$$k_l a = \frac{q_O^t}{(c_O^* - c_O)} \tag{10.31}$$

Equation (10.31) assumes that the saturation concentration, c_O^*, is the same throughout the reactor, i.e., that the pressure difference is small and that the decrease in partial pressure of oxygen in the gas phase is small. A small difference between π_O^{in} and π_O^{out} gives a large relative error in (10.30), and a large difference between the two partial pressures necessitates that a model for the gas flow through the reactor is available (see Example 3.4). A compromise is to use (10.9) to calculate the concentration driving force. The direct method is simple to apply, and first of all it can be applied during a real fermentation. However, accurate measurements of the oxygen content as well as of the gas flow rates are necessary and, as stated above, the solubility of oxygen during the passage of gas bubbles through the medium must be known. Finally note, that possibly, $v_g^{in} \neq v_g^{out}$, e.g., due to evaporation of water during the passage of the gas through the medium.

10.3.2 The Dynamic Method

The dynamic method is also based on measurement of the dissolved oxygen concentration in the medium. However, it does not require measurement of the gas composition and is therefore cheaper to establish. The dynamic mass balance for the dissolved oxygen concentration is

$$\frac{dc_O}{dt} = k_l a(c_O^* - c_O) + q_O \tag{10.32}$$

If the gas supply to the bioreactor is turned off, q_O^t is zero and the first term on the right hand side of the equation immediately drops to zero. The dissolved oxygen concentration decreases at a rate equal to the oxygen consumption rate, $-q_O$, which can therefore be determined from measurement of the dissolved oxygen concentration $c_O(t)$. If q_O is independent of c_O the dissolved oxygen concentration decreases as a linear function of time. When the gas supply is turned on again, the dissolved oxygen concentration increases back to the initial level, and by using the estimated (average) value for q_O, the value of $k_l a$ can be determined from the measured profile of dissolved oxygen.

This method is simple, and it can be applied during a real fermentation. It is, however, restricted to situations in which q_O can be determined correctly when the gas supply is turned off. Most available probes for measuring the dissolved oxygen concentration do, unfortunately, have a response time close to the characteristic time for the mass transfer process, and the measured concentrations are therefore influenced by the dynamics of the measurement device, e.g., an oxygen electrode.

The dynamic method can also be applied at conditions where there is no reaction, i.e., $q_O = 0$. This is interesting when studying the influence of operating parameters, e.g., the stirring speed and the gas flow rate, on the volumetric mass transfer coefficient in model media. After a step change in the concentration in the inlet gas, there are dynamic changes both in the dissolved oxygen concentration and

in the oxygen concentration of the exhaust gas. Because of the slow dynamics of oxygen electrodes, it is preferable to apply the exhaust gas measurements and a mass balance for O_2 in the gas phase to determine the mass transfer coefficient. However, before this approach is applied, it is important to make a careful check of the dynamics of the gas analyzer.

10.3.3 The Sulfite Method

It is possible to determine the oxygen transfer rate by using an oxygen consuming chemical reaction. The traditional sulfite method is based on the oxidation of sulfite to sulfate by oxygen:

$$SO_4{}^{-2} - SO_3{}^{-2} - \frac{1}{2}O_2 = 0 \tag{10.33}$$

This reaction is catalyzed by a number of metal ions, which may occur as impurities. However, one normally adds a known amount of a copper (e.g., 10^{-3} M Cu^{+2}) or a cobalt salt to the medium in order to make the reaction almost instantaneous. Now the rate of sulfite consumption is determined solely by the rate at which oxygen is transferred from the gas phase. Since, from (10.33):

$$q_{SO_3{}^{-2}} = 2q_O \tag{10.34}$$

Consequently,

$$k_l a = -\frac{q_O}{c_O^* - c_O} = -\frac{q_{SO_3}}{2(c_O^* - c_O)} \tag{10.35}$$

The dissolved oxygen concentration, c_O, is virtually zero due to the very rapid reaction with sulfite. The reaction rate is determined by measuring the concentration of sulfite in samples taken at a set of time values after the start of the experiment. The sulfite concentration in the samples can be determined by adding an excess amount of iodine, and thereafter back-titrate with thiosulfate, using starch as an indicator. The reactions are given by (10.36) and (10.37):

$$SO_4{}^{-2} + 2H^+ + 2I^- - SO_3{}^{-2} - I_2 - H_2O = 0 \tag{10.36}$$

$$S_4O_6{}^{-2} + 2I^- - I_2 - 2S_2O_3{}^{-2} = 0 \tag{10.37}$$

To apply the method, it is necessary to know the saturation concentration of oxygen in the strong sulfite solution. Since (for obvious reasons) this is not known, one may use the solubility of oxygen in sulfate solutions, which is 1.02 mM at 25°C for 0.25 M $SO_4{}^{2-}$ (Linek and Vacek 1981). The sulfite method was often used in

earlier days, since it is relatively easy to implement. However, it has a number of drawbacks. The sulfite oxidation may enhance the oxygen absorption, since the rapid chemical reaction may occur not only in the bulk liquid, but also in the liquid film. The assumption of a linear concentration profile in the film is therefore questionable. Another complication is the significant coalescence-reducing effects of sulfite on the bulk liquid, which results in a higher specific interfacial area. Both the enhancement of mass transfer due to reaction in the film, and the coalescence-reducing effect of sulfite, may lead to an overestimation of $k_l a$ compared to what is found in a normal fermentation media. This is a significant drawback of the method. A further practical disadvantage is that the sulfite method cannot be applied at all during a real fermentation, since the microorganisms would most likely be killed.

10.3.4 The Hydrogen Peroxide Method

This method due to Hickman (1988) is, like the sulfite method, a chemical method. However, it has several advantages compared with the sulfite method. In the hydrogen peroxide method, the transfer of oxygen from the liquid to the gas phase is measured. Oxygen is generated by the enzyme-catalyzed decomposition of hydrogen peroxide:

$$2H_2O_2 \xrightarrow{\text{catalase}} 2H_2O + O_2 \tag{10.38}$$

The reaction is first order with respect to both H_2O_2 and the enzyme, catalase. A constant volumetric flow of air passes the reactor with liquid volume V_l, and after addition of a known amount of catalase, a continuous feed of H_2O_2 is applied to the reactor. Initially, hydrogen peroxide will accumulate in the reactor medium, but a steady state will soon be established. At steady state the rate of decomposition of hydrogen peroxide, $-q_{H_2O_2}$, equals half the rate of oxygen transfer from the liquid phase to the gas phase:

$$k_l a(c_O^* - c_O) = \frac{q_{H_2O_2}}{2} \tag{10.39}$$

The volumetric decomposition rate of hydrogen peroxide is calculated from the volumetric addition rate and the concentration of hydrogen peroxide in the added liquid according to

$$q_{H_2O_2} = -\frac{v_{H_2O_2}^f c_{H_2O_2}^f}{V_l} \tag{10.40}$$

The interfacial concentration of oxygen is calculated from the gas phase partial pressure of oxygen. (Note that both terms in (10.39) are negative, since oxygen

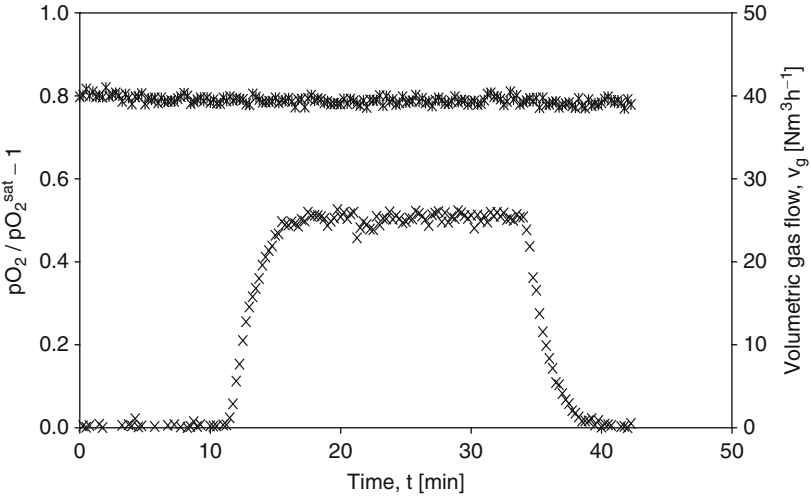

Fig. 10.8 Typical oxygen mass transfer experiment using the H_2O_2 method at 25°C. During the steady-state period of $15 < t < 35$ min the steady-state O_2 tension is 50% higher than when no peroxide is added (data from Nordkvist 2005)

is generated in the liquid and thus dissolved oxygen tension (DOT) $= c_O/c_O^* > 1$). An assumption concerning the mixing of the gas phase is necessary to determine the interfacial concentration of oxygen. Hickman used the assumption of complete back-mixing of both the liquid and the gas phase, which gives

$$c_O^* = \frac{p_O^{exit}}{H_O} \quad \text{and} \quad k_l a = \frac{v^f_{H_2O_2} c^f_{H_2O_2}}{2V_l(c_O - c_O^*)} \tag{10.41}$$

The hydrogen peroxide method is easy to implement. All that is needed to estimate the $k_l a$ value is to measure the addition rate of hydrogen peroxide and the oxygen concentration in the liquid phase. An independent, but much less accurate measurement-see Problem 10.5-of q_O^t is obtained from the difference in oxygen content between v_g^{in} and v_g^{out} as in the "direct method." Compared with the sulfite method, a significant advantage of the hydrogen peroxide method is that the $k_l a$ value is not enhanced by the catalase concentration over a rather wide range (Hickman 1988). The risk of enhancing the mass transfer by reaction in the liquid film is smaller, and the effect of the small added amount of catalase on the coalescence of the medium is negligible. The method has been applied with good results for $k_l a$ measurements in large industrial reactors, also with viscous, non-Newtonian media (Pedersen 1997).

Figure 10.8 shows the results of a typical measurement of $k_l a$ by the H_2O_2 method. The experiment was carried out in a tank with $V_l = 3.4$ m^3 tap water, and air was sparged to the tank using a Rotary Jet Head (RJH) with nozzle diameter $d = 10$ mm (see Chap. 11 for a description of the RJH system). O_2 tension is measured with an Ingold O_2-electrode placed 0.3 m below the liquid surface.

The volumetric air flow was constant at $39.5 \pm 0.2\ \mathrm{Nm^3\,h^{-1}}$. At time 11.5 min, a constant flow of 93.2 mol $\mathrm{h^{-1}}$ of H_2O_2 was fed to the recirculation loop of the tank, and it is assumed that the H_2O_2 is dispensed homogenously to the tank volume due to the efficient mixing of the RJH. After about 4.5 min the rate of O_2 production from the H_2O_2 that is fed to the reactor and split to O_2 and H_2O by the added catalase equals the rate of stripping O_2 from the tank by the air. For the next 18 min the DOT is 50% higher than before H_2O_2 was added. Finally, at 35 min the flow of H_2O_2 is stopped and the dissolved oxygen concentration c_O settles to its stationary value of $c_O^* = 0.21 \times 1.26 \times 1.10$ mM for contact between water and air at 25°C. The factor 1.10 accounts for the production of O_2 which increases the O_2 content of the gas, and hence c_O^*.

$$k_l a = \frac{93.2}{2 \times 3.4 \times (0.5 \times 0.21 \times 1.26 \times 1.10)} = 93.6\,\mathrm{h^{-1}} \tag{10.42}$$

At the end of the experiment all H_2O_2 that has been added has been consumed, and a new experiment can immediately be started. This is really an enormous advantage compared to the sulfite method where one needs to fill in new water in the tank between each experiment, since otherwise the increasing ionic strength of the water would influence the measurement of $k_l a$. Also, of course, a considerable amount of sulfate waste is produced in each experiment.

Nordkvist obtained the following relation between $k_l a$, and the operating variables P/V and u_g in the range $248 < P/V < 2{,}023\ \mathrm{W\,m^{-3}}$ and $0.0052 < u_g < 0.043\ \mathrm{m\,s^{-1}}$:

$$k_l a\,(\mathrm{s^{-1}}) = 0.0772\,(P/V)^{0.27} u_g^{0.63}\ (\text{SI units}) \tag{10.43}$$

for tap water and the RJH mentioned above. The results $k_l a$ determined as in Fig. 10.8 for different P/V and u_g are quite accurate since the steady-state period of measuring c_O contains at least 50 measurements on an O_2 electrode that can be placed in different positions in the tank to study a possible influence of inadequate mixing.

The correlation (10.43) shows that the RJH is favorable compared to sparging air in the region near a Rushton turbine, especially at low P/V, as can be seen from the rather low exponent β of P/V compared to the values in Table 10.4

10.3.5 $k_l a$ Obtained by Comparison with the Mass Transfer Coefficient of Other Gases

The $k_l a$ values for other gases for which it is less easy to measure the mass transfer than it is by one of the above discussed methods for O_2 can be obtained by the following relation:

$$\frac{(k_l a)_{O_2}}{(k_l a)_A} = \left(\frac{D_{O_2}}{D_A}\right)^{\frac{2}{3}} \tag{10.44}$$

Table 10.10 Molecular diffusivity D_A of solutes in dilute aqueous solution at 25°C

Component	D_A (10^{-9} m^2 s^{-1})
Oxygen	2.42
Carbon dioxide	1.91
Hydrogen	5.11
Methane	1.84
Krypton	1.84
Ethanol	1.4
Lactose	0.60
Glucose	0.85
Sucrose	0.73

Data from Handbook of Chemistry and Physics (6–199), 83rd ed. (2002)

Equation (10.44) is based on the assumption that a is independent of the gas transferred, and that k_l is proportional to ${D_A}^{2/3}$ according to (10.13).

Table 10.10 shows values of D_A for different solutes in dilute aqueous solutions.

Even the measurement of oxygen transfer can be standardized using (10.44):

^{85}Kr is a volatile isotope emitting beta and gamma radiation. By injecting the isotope into the medium and then by measuring the radioactivity in the exhaust gas, it is possible to determine the volumetric mass transfer coefficient for Kr (see Problem 10.3).

$$\frac{(k_l a)_{Kr}}{(k_l a)_{O_2}} = \left(\frac{D_{Kr}}{D_{O_2}}\right)^{\frac{2}{3}} \cong 0.83 \tag{10.45}$$

This method is easy to implement, and it is well suited for measurement both in model media and under real fermentation conditions [see, e.g., Pedersen et al. (1994)]. The main drawback is the radioactivity, which obviously limits the application in an industrial environment. However, the isotope is very volatile and the radiation has normally returned to the background level a few minutes after the injection. Kr is of course completely inert in connection with fermentations.

One of the more interesting gases to be transported between the gas and the liquid phase is CO_2, which according to Table 10.10 must have a somewhat lower mass transfer coefficient than O_2. In contrast to O_2 the rate of mass transfer of CO_2 strongly depends on the pH of the medium. This is due to the dissociation of H_2CO_3 which is formed by a slow reaction between $(CO_2)_{aq}$ and water.

The equilibrium constants for the two dissociation steps are K_1 and K_2, and one obtains the total carbon dioxide concentration in the medium from

$$CO_{2,aq} + H_2O \leftrightarrow H^+ + HCO_3^-; \quad K_1 = \frac{[H^+][HCO_3^-]}{[CO_2]_{aq}} \tag{10.46}$$

$$HCO_3^- \leftrightarrow H^+ + CO_3^{-2}; \quad K_2 = \frac{[CO_3^{-2}][H^+]}{[HCO_3^-]} \tag{10.47}$$

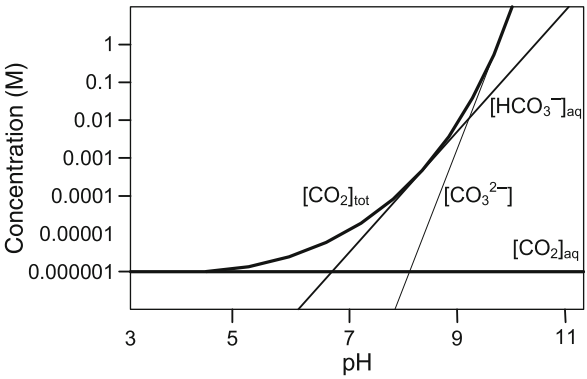

Fig. 10.9 Equilibrium concentrations of $(CO_2)_{aq}$, HCO_3^-, and CO_3^{-2} at 25°C. The *full line* shows $[CO_2]_{tot}$ calculated from (10.48), and the *horizontal line* shows $[CO_2]_{aq}$

$$[CO_2]_{tot} = [CO_2]_{aq}\left(1 + \frac{K_1}{[H^+]} + \frac{K_1 K_2}{[H^+]^2}\right) \tag{10.48}$$

At 25°C the value of $K_1 = 10^{-6.3}$ and $K_2 = 10^{-10.25}$. For pH < 5 nearly all CO_2 is present as $(CO_2)_{aq}$. For $7 <$ pH < 9, HCO_3^- dominates, while virtually all dissolved CO_2 is present as CO_3^{-2} when pH > 12. The total solubility of CO_2 increases dramatically with increasing pH as shown in Fig. 10.9.

CO_2 is commonly regarded as a metabolic product which has to be stripped from the medium, but it is also a substrate in anabolic reactions, e.g., in the synthesis of long-chained fatty acids. A large CO_2 tension in the medium is harmful to cell growth, and this may counteract the positive effect of a high oxygen partial pressure, achieved either by using O_2 rather than air or by using hyperbaric cultivation conditions. Normally, an upper limit of 2 bar for π_{O_2} can be safely used in strongly aerobic processes such as single cell production where mass transfer limitation is a severe problem. The effect of an insufficient CO_2 tension is seen in anaerobic processes conducted at rather low pH. Thus, the growth of lactic bacteria may stop completely if the small amounts of CO_2 produced in catabolism are driven out by an injudicious use of sparged N_2 to ensure anaerobicity.

Problems

Problem 10.1 *Determination of k_la in a pilot bioreactor.* Christensen (1992) and Pedersen (1992) studied penicillin production in *P. chrysogenum* with the aim to set up models for the microbial and reactor dynamics. A major purpose of the studies was to see how mass transfer affects the overall performance of the process. A series of experiments was therefore designed for this purpose. The bioreactor was assumed to be ideal, i.e., with no concentration gradients in the medium. The reactor was sparged with air of composition 20.95% O_2, 0.030% CO_2, and

79.02% N_2. The total volume of the bioreactor was $V = 15$ L. The equilibrium concentration of O_2 in solutions of sulfite or sulfate is given by the following eqaution:

$$c_O^* = 5.909 \times 10^{-6} \exp\left(\frac{1602.1}{T} - \frac{0.9407 c_s}{1 + 0.1933 c_s}\right) \text{M atm}^{-1} \quad (1)$$

c_s is the molarity of the salt solution and T is in K (Linek and Vacek 1981). All experiments were carried out at 25°C, with 1 atm head space pressure and constant stirrer speed.

(a) *Determination of $k_l a$ by the sulfite method.*
The bioreactor was filled with 10 L of water, and sulfite was added to give a concentration of 0.26 mol L^{-1} at $t = 0$. The gas was turned on, and liquid samples were analyzed for sulfite concentration. The experimental results are shown in the table below. During the experiment the dissolved oxygen concentration can be assumed to be zero because of fast reaction. Calculate $k_l a$ in the bioreactor and discuss the sulfite method.

t (min)	Sulfite concentration (mM)
0	260
3	241
9	209
15	178
22	146
28	112
34	80

(b) *Determination of $k_l a$ by the direct method.*
We now want to determine $k_l a$ during a fermentation experiment, and we therefore implement an exhaust-gas analyzer for measuring O_2 and CO_2. The O_2 analyzer is based on paramagnetic resonance, and the CO_s analyzer is based on infrared detection. Since the analyzers measure the partial pressures, it is essential to dry the gas by letting it pass through a column containing Drierite (anhydrous $CaSO_4$). During penicillin fermentation, the gas-flow rate is 1 vvm (volume per volume per minute), and the working volume is 10 L. At a certain time the O_2 content in the exhaust gas is 20.63%, and the dissolved O_2 concentration is measured to be constant at 69% of the equilibrium concentration, which is about 90% of that in water. The gas constant is $R = 0.082045$ L atm mol^{-1} K^{-1}. Calculate $k_l a$ during the fermentation, and discuss the difference from the value determined by the sulfite method.

Problem 10.2 *Mass transfer during fermentations with mammalian cells.*
Mammalian cells are shear-sensitive, and aeration is often carried out by diffusion of O_2 across the wall of silicone tubing placed inside the bioreactor. The inlet gas (often pure O_2) normally has a higher pressure than the head space pressure, which ensures a pressure drop across the wall of the silicone tubing. $k_l a$ for this system

depends on the pressure difference across the silicone tube wall, the temperature, and the porosity of the silicone tubing. The flux of O_2 across the silicone tube to the medium is assumed to be very small, and the O_2 concentration is almost constant along the length of the tube. It is the aim to quantify these effects in a bioreactor of volume of $V = 1$ L.

(a) Show that

$$k_l = \frac{D_{O,g}}{\delta_l} \frac{p_g - H_O c_O}{c_O^* - c_O} \tag{1}$$

$D_{O,g}$ is the diffusion coefficient of O_2 in the inlet gas, p_g is the concentration of O_2 in the inlet gas, c_O^* is the equilibrium concentration of O_2 in the medium, and δ_l, is the wall thickness of the silicone tubing.

(b) Plot k_l vs. c_O in a system where $\delta_l = 0.35$ mm, the head space pressure is 1 atm, and the pressure in the inlet gas is 2 atm. The temperature is 30°C. $D_{O,g} = 0.2\ 10^{-4}$ m^2 s^{-1} and c_O^* (1 atm, 30°C) = 1.16 mmol L^{-1}.

(c) State k_l as a function of the inlet gas pressure and the temperature, when the head space pressure is 1 atm.

(d) For a given length l and inner diameter d_i, of the tube, calculate the effect of the wall thickness on the volumetric surface area a. The porosity of the tubing is ε.

(e) For $l = 1$ m, $d_i = 1$ mm, and $\varepsilon = 0.40$, calculate $k_l a$ for a bioreactor in which the inlet gas is pure O_2 with a pressure of 2 atm and a temperature of 30°C. The head space pressure is kept constant at 1 atm, and the dissolved O_2 concentration is measured to be 0.6 mmol L^{-1}.

(f) From experiments at different agitation speeds, you observe that $k_l a$ increases with the agitation speed. How do you explain this observation?

Problem 10.3 *Mass transfer in a pilot plant bioreactor*. Data for the determination of $k_l a$ by the ^{85}Kr method are given in the following table:

v_g (vvm)	P_g (W)	$k_l a$ (h^{-1})
1.0	3,000	951
0.2	3,000	688
0.1	3,000	598
0.05	3,000	525
1.0	5,000	1,358
1.0	1,000	440
1.0	500	268

A pilot plant bioreactor with a height-to-diameter ratio of 3:1 is equipped with two standard Rushton turbines. The bioreactor is filled with 1 m^3 of sterile medium. The aeration rate is 1 vvm, and with a total power dissipation of 3,000 W, the degree of filling is 69.5%, and the gas holdup is measured to be 10%. The temperature is 30°C, and the head space pressure is 1 atm.

(a) Calculate the superficial gas velocity u_s, the mean bubble rise velocity u_b, and the average residence time of gas bubbles t_b (units: m s^{-1} and s).

(b) Under the assumption that the medium is coalescing, calculate k_la using the correlation of (10.27) with $k = 0.026$, $\alpha = 0.5$, and $\beta = 0.4$. From measurements in the exhaust gas and the dissolved oxygen concentration during a fermentation experiment, you suspect that the calculated k_la value is too low. You therefore decide to examine the system more carefully.

(c) Using the ^{85}Kr method to determine k_la, you observe the effect of variations in v_g and P_g when the bioreactor is filled with sterile medium. The results of the study are listed in the table above.

Estimate the parameters for the correlation in (10.27) using these data. How do you explain that the measured k_la is significantly higher than the value calculated from the literature correlation?

(d) With the estimated k_la value, find the largest possible oxygen consumption rate when $v_g = 1$ vvm and $P_g = 3{,}000$ W. During penicillin fermentations, it is found that the dissolved oxygen concentration should be above 30% of the saturation value if the penicillin production is not to be inhibited. Assume that the oxygen uptake rate can be described by Monod kinetics with $K_O = 0.015$ mmol L^{-1} and $r_{O,max} = 0.65$ mmol (kg DW)$^{-1}$ s^{-1}. Calculate the maximum biomass concentration that can be sustained without inhibition of the penicillin production.

Problem 10.4 *Mass transport into pellets.* In Sect. 6.3.2, the mass balance for a substrate A which is transported into a porous spherical pellet where it is consumed by an enzymatic reaction is set up and solved. Exactly the same mass balance can be set up when the substrate is consumed at a rate $q_A'(s_A)$ (mol (m^3 pellet)$^{-1}$s^{-1}) of a cell reaction:

$$\frac{1}{\chi^2}\frac{\mathrm{d}}{\mathrm{d}\chi}\left(\chi^2\frac{\mathrm{d}S_A}{\mathrm{d}\chi}\right) = 9\Phi^2\frac{q'_A(s_A)}{q'_A(s_A = s_{A,s})} \tag{1}$$

The dimensionless concentration, S_A, and the dimensionless radial coordinate, χ, are given by

$$S_A = \frac{s_A}{s_{A,s}} \quad \text{and} \quad \chi = \frac{\xi}{R} \tag{2}$$

The Thiele modulus, Φ, is given by (3)

$$\Phi^2 = \frac{q(s_{A,s})R^2}{9D_{\mathrm{eff}}s_{A,s}} \tag{3}$$

R is the pellet radius, and D_{eff} is the effective diffusion coefficient in the pellet for the species being considered. c_b is the bulk concentration of the species. For zero-order kinetics the pellet size that gives a zero concentration precisely at the center of the pellet is given by (see Note 6.2)

$$R_{\mathrm{crit}} = \sqrt{\frac{6D_{\mathrm{eff}}s_{A,s}}{-q'_A(s_{A,s})}} \tag{4}$$

We now consider oxygen diffusion into a pellet of *P. chrysogenum*. For this microorganism, the oxygen uptake rate can be approximated by

$$-q_O(s_O) = k\frac{s_O}{s_O + K_O}x \tag{5}$$

$k = 4.0$ mmol O_2 (g DW)$^{-1}$ h^{-1} and $K_O = 58$ μmol O_2 L^{-1}. The biomass concentration in the pellet is approximately 99 kg DW m^{-3} of pellet (this corresponds to a void volume of around 70% and a water content of 67% in the cells), and the concentration of oxygen in the bulk medium is 17.4 μmol L^{-1}. Calculate the critical pellet radius when it is assumed that (4) can be used. Discuss the application of (4). Calculate the effectiveness factor using the generalized Thiele modulus (3) as a function of the pellet radius (25 μm $< R <$ 500 μm).

Problem 10.5 *Measuring k_la by the hydrogen peroxide method.* As described in Sect. 10.2, one method to measure k_la is based on the consumption of hydrogen peroxide in a catalase containing medium (see reaction below).

$$2H_2O_2 \xrightarrow{\text{catalase}} 2H_2O + O_2$$

After the addition of a known amount of catalase to the reactor, a continuous feed of H_2O_2 is applied to the reactor. Initially, hydrogen peroxide will accumulate in the reactor medium, but a steady state will soon be established at which the rate of decomposition of hydrogen peroxide equals the addition rate of hydrogen peroxide. By measuring the dissolved oxygen concentration, as well as the inlet and outlet oxygen mole fractions in the gas, it is possible to calculate the value of k_la.

In the original work by Hickman (1988), the values given in the table below can be found:

Hydrogen peroxide addition rate·10^5 (mol s^{-1})	Dissolved oxygen concentration (% of saturation)	Measured exit oxygen concentration (mol%)	Stirrer rate (rpm)
1.6	111.5	21.14	500
3.2	123.8	21.36	500
6.4	147.2	21.78	500
12.8	195.8	22.6	500
3.2	110.6	21.35	900
6.4	121.7	21.77	900
12.8	143.4	22.60	900

Measured dissolved oxygen tension in liquid phase and oxygen concentrations in inlet and exit gas streams for determination of k_la by the hydrogen peroxide method. Note that, as explained in the text, $c_O > c_O^*$ since oxygen is generated and transferred to the gas phase.

The following additional information is given: reactor (medium) volume: $V_l = 0.005$ m^3

Gas flow rate: $v_{gas} = 9.2 \times 10^{-5}\ m^3\ s^{-1}$ of air with 21% O_2 (i.e., approximately 1 vvm)

(a) Calculate the value of $k_l a$ for the two stirrer rates given in Table 10.1. Assume that $T = 20°C$. Assume that the gas analyzer has an absolute error of 0.1% of the measured value. How big is (in the worst case) the error in the calculated $k_l a$-value? Under what conditions do you expect to get the most accurate measurements.

References

Bhavaraju, S. M., Russell, T. W. F., and Blanch, H. W. (1978). The design of gas sparged devices for viscous liquid systems. *AIChE. J.* **24**, 454–465.

Bird, R. B., Stewart, W. E., and Lightfoot, E. N. (2002). Transport phenomena, 2nd ed., John Wiley&Sons, New York.

Blanch, H. W., and Clark, D. S. (1997). Biochemical Engineering. Marcel Dekker, New York.

Brian, P. L. T., and Hales, H. B. (1969). *AIChE J.* **15**, 419–425.

Calderbank, P. H., and Moo-Young, M. M. (1961). *Chem. Eng. Sci.* **16**, 39–54.

Christensen, L. H. (1992). Modelling of the Penicillin Fermentation. PhD. thesis, DTU, Lyngby, DK.

Craig, V. S. J., Ninham, B. W., and Pashley, R. M. (1993). Effect of electrolytes on bubble coalescence. *Nature* **364**, 317–319.

Cussler, E. L. (1997). Diffusion – Mass transfer in fluid systems, 2nd ed. Cambridge University Press, Cambridge, U.K.

Danckwerts, P. V. (1970). Gas Liquid Reactions. McGraw-Hill, New York.

Froessling, N. (1938). *Gerlands Beitr. Geophys.* **32**, 170–215.

Hickman, A. D. (1988). Gas-liquid oxygen transfer. A novel experimental technique with results for mass transfer in aerated agitated vessels. Proc. 6th Eur. Conf. Mixing, Pavia, 369–374.

Geankoplis, C. J. (1993). Transport processes and unit operations, 3rd ed., Prentice Hall, Englewood Cliffs, New Jersey.

Keitel, G., and Onken, U. (1982). The effect of solutes on bubble size in air-water dispersions. *Chem. Eng. Commun.* **17**, 85–98.

Lee, Y. H., and Meyrick, D. L. (1970). Gas-liquid interfacial areas in salt solutions in an agitated tank. *Trans. Inst. Chem. Eng.* **48**, T37–T45.

Lehrer, I. H. (1971). Gas hold-up and interfacial area in sparged vessels. *Ind Eng. Chem. Des. Dev.* **10**, 37–40.

Linek, V., and Vacek, V. (1981). Chemical engineering use of catalyzed sulphite oxidation kinetics for the determination of mass transfer characteristics of gas liquid contractors. *Chem. Eng. Sci.* **36**, 1747–1768.

Linek, V., Vacek, V., and Benes, P. (1987). A critical review and experimental verification of the correct use of the dynamic method for the determination of oxygen transfer in aerated agitated vessels to water, electrolyte solutions and viscous liquids. *Chem. Eng. J.* **34**, 11–34.

Nernst, W. (1904) *Zeitschrift für Physikalische Chemie* **47**, 52–55.

Moo-Young, M. and Blanch, H. W. (1981). Design of biochemical reactors. Mass transfer criteria for simple and complex systems. *Adv. Biochem. Eng.* **19**, 1–69.

Nordkvist, M. (2005). Mixing and mass transfer by rotating jets: Fundamentals and applications. PhD thesis, DTU, Lyngby, DK.

Pedersen, A. G. (1992). Characterization and Modelling of Bioreactors. PhD. thesis, DTU, Lyngby, DK.

Pedersen, A. G. (1997). $k_l a$ characterization of industrial fermentors. Proc. 4th Int. Conf. Bioreactor Bioprocess Fluid Dynamics, BHRG, 263–276.

Pedersen, A. G., Andersen, H., Nielsen, J., and Villadsen, J. (1994). A novel technique based on ^{85}Kr for quantification of gas liquid mass transfer in bioreactors. *Chem. Eng. Sci.* **49,** 803–810.

Popovic, M., Niebelschutz, H., and Reuss, M. (1979). Oxygen solubilities in fermentation fluids. *Eur. J. Appl. Microb. Biotechnol.* **8**, 1–15.

Rowe, P. N., Claxton, K. T., and Lewis, J. B. (1965). *Trans. Inst. Chem. Eng.* **43**, 14–31.

Tse, K., Martin, T., McFarlane, C. M., and Nienow, A. W. (1998). Visualisation of bubble coalescence in a coalescence cell, a stirred tank and a bubble column. *Chem. Eng. Sci.* **53**, 4031–4036.

van't Riet, K. (1979). Review of measuring methods and results in non-viscous gas liquid mass transfer in stirred vessels. Ind. Eng. Chem. Process Dev. **18**, 357–364.

Schugerl, K. (1981). Oxygen transfer into highly viscous media. *Adv. Biochem. Eng.* **19**, 71–174.

Whitman, W. G. (1923). A preliminary experimental confirmation of the two-film theory of gas absorption. *Chem. Metal. Eng.* **29**, 146–148.

Chapter 11
Scale-Up of Bioprocesses

The previous chapters in this book have dealt with stoichiometric, thermodynamic and kinetic analysis of bioreactions, as well as the operation of small-scale, "ideal," bioreactors. These subjects constitute the basis for exploitation of microorganisms in fermentation processes. The ultimate goal for process development is, however, the realization of large-scale commercial production. The basis for a successful scale-up is to follow the advice of H. Baekeland, the inventor of Bakelite: *"Commit your blunders on a small scale and make your profits on a large scale."* This is, however, not always easy. Many different engineering tools need to be applied (Leib et al. 2001), and the final scaled-up process will necessarily be a delicate compromise between inherently conflicting desirable options. Furthermore, even if the best engineering judgment is used, there are sometimes surprises in the final process which were difficult to anticipate from the lab-scale experiments.

The purpose of the present chapter is to give an understanding of the fundamental problems that arise when a process is scaled-up, and to provide some useful tools for analysis of critical scale-up factors.

We have seen in Chaps. 6 and 9 how the microbial kinetics and mass transfer suffice to understand the behavior of small, so-called ideal reactors where no spatial variation in the reactant concentrations $\boldsymbol{c}$ or in other process variables such as temperature and pH influence the design. Spatial homogeneity can never be attained in large reactors, and sometimes, such as in Example 6.4, it was shown that even in a well-stirred laboratory bioreactor the time constant of side-reactions (in the example it was the deactivation of the enzyme due to insufficient pH homogeneity, when NaOH was used to titrate lactobionic acid) severely influence the process design.

Mixing is clearly the key unit process in scale-up, and the concept of mixing will therefore be defined and discussed in this chapter. Mixing is achieved by *mechanical energy input* to the reactor, and we shall derive expressions for the *mixing time*, t_{mix}, and show that t_{mix} depends on the scale of the reactor. It also depends on the choice of *mixing equipment*, as well as on a number of physical properties of the medium, in particular the medium viscosity. Experimental methods for determination of mixing time will be outlined.

J. Villadsen et al., *Bioreaction Engineering Principles*,
DOI 10.1007/978-1-4419-9688-6_11,

With these theoretical and experimental methods in hand, one starts to understand how other design variables, such as the mass- and heat transfer coefficients, depend on the mixing time and hence on the operating variables that influence mixing time. This will facilitate the design of well-functioning, perhaps close to optimal, industrial bioreactors.

11.1 Mixing in Bioreactors

Mixing is the process of achieving uniformity, i.e., it is a process by which substrates, from the liquid feed or from a gaseous phase, are intimately dispersed throughout the reactor to present cells that move through the reactor volume with, as far as possible, the same environment at every point. Mixing is a simple physical process in which mechanical energy is used to achieve the goal of homogeneity in the reactor. Yet, mixing is one of the least understood processes, both in classical chemical engineering and in biochemical engineering, and it has a large influence on the process and on the product quality. It is claimed (Villadsen 1997) by industry that "Inadequate mixing is the cause of more than 60% of the problems associated with industrial processes." The quotation (from Unilever) refers in particular to mixing of liquids, of liquids and gases, of liquids and solids, and of solids.

In bioreactions mixing problems give rise to reduction in both product yield and product quality as witnessed by numerous, but mostly empirical studies from the past 50 years.

Most of the studies have dealt with cultivations of either bakers' yeast (*Saccharomyces cerevisiae*) or *Escherichia coli*. The general result is that the yield of the desired product, the yeast or bacterial biomass and of a product, usually a protein associated with biomass growth, decreases when the power input to mixing is insufficient. This is, unfortunately, a typical situation for large-scale cultivations.

George et al. (1998), studied production of bakers yeast in an industrial scale (120 m^3) bubble column and in a 10-L stirred tank laboratory reactor. They observed that the biomass yield was 6.8% lower in the industrial reactor. Other publications from the same group concern the production of recombinant proteins with *E. coli* as host organism (Bylund et al. 2000, and Schweder et al. 1999). When a 12 m^3 reactor (working volume 8–9 m^3) was fed from the top, one could measure a glucose concentration near the top of the reactor that was a factor 4 different from the average concentration. The average biomass yield was 20% lower than in a lab-scale reactor while the acetate yield was much higher. This shows that one should definitely not feed large bioreactors from the top, but inject the feed near the stirrer. The large differences in biomass yield may not directly be caused by the inhomogeneous glucose distribution, but may be due to O_2 limitation in regions of high glucose concentration. Schweder et al. (1999) observed an increased expression of stress-related genes that respond to O_2 limitation or glucose excess. Enfors (2001) published results from an EU joint research program on the influence of mixing in large reactors. The response of *E. coli* to inadequate homogeneity was again that

production of acetate and re-assimilation of acetate in regions of low glucose concentration contributed to a low biomass yield.

The effect of insufficient pH homogeneity is also reported in a few papers. Amanullah et al. (2001) show that, due to insufficient mixing in a lab-scale reactor, the metabolism of a pH-sensitive strain of *Bacillus subtilis* changes from acetoin + butane 2,3-diol production to acetate production when pH is titrated to 6.5 with 5 M NaOH (see Problem 11.4). Parente and Ricciardi (1999) produced the baceriocin *nisin* using *Lactococcus lactis* at the optimum pH of 5.5, but when the local pH varied in the reactor by 1 to 2 units the yield of nisin decreased appreciably. Both of these studies observe the same unfortunate consequence of inadequate mixing in pH-controlled laboratory reactors as was found by Nordkvist et al. (2006) for lactobionic acid production and was discussed in Example 6.4.

11.1.1 Characterization of Mixing Efficiency

In order to compare different mixing aggregates or mixing in different scales one needs a characteristic *metric* for mixing effectiveness. The mixing time t_{mix} is a useful metric, and one can determine t_{mix} as a function of the power input P/V to the reactor. Thereafter, other quantities, for example the value of $k_{\text{l}}a$, can be correlated with t_{mix} or directly with the independent operational variable, the power input.

Mixing efficiency E at a given point is defined by:

$$E = \frac{c(t) - c_0}{c_{\text{final}} - c_0}, \tag{11.1}$$

where $c(t)$ is the concentration of a tracer at time t after start of a mixing experiment, c_0 and c_{final} are initial and final tracer concentrations.

The tracer concentration $c(t)$ is likely to be dependent, not only on time, but also on the position of the probe in the medium. Hence, probes should be placed at strategic positions in the reactor (guided by visual inspection of mixing patterns), and the average reading of the probes gives a measure of the average value for $E(t)$. Also, the point of injection of the tracer at $t = 0$ has a significant influence on $E(t)$ since tracer fed to the surface of a mixed liquid volume is likely to give an $E(t)$ which at any finite t is lower than when the tracer is fed close to the mixing aggregate.

For any feed position or mixing equipment one observes that E approaches 1. The approach can be a damped oscillation, but very often the signal is well represented by a single time constant k_{mix}, named the *mixing constant*:

$$1 - E = \left| \frac{c(t) - c_{\text{final}}}{c_{\text{final}} - c_0} \right| \cong \exp(-k_{\text{mix}} t), \tag{11.2}$$

where ${k_{\text{mix}}}^{-1}$ is the time it takes to achieve a degree of mixing equal to $1 - \text{e}^{-1} = 0.632$ of complete mixing of the tracer.

In both laboratory experiments and in industrial practice the time to reach 95% complete mixing is used for comparison between different mixing modes:

$$t_{\mathrm{mix.E}} = -\frac{1}{k_{\mathrm{mix}}}\ln(1-E)[E=0.95]. \tag{11.3}$$

When $\ln(1-E)$ is plotted against t one can determine $k_{\mathrm{mix},0.95}$ as the reciprocal of the time it takes to reach $\ln(1-E) = \ln 0.05 = -3.00$. Near the endpoint of the mixing experiment the amplitude of the signal is small compared to the fluctuations, and Brown et al. (2004) suggests that the data should be plotted as the log of variance σ^2 as a function of time:

$$\log\left(\sigma^2\right) = \log((1-E))^2. \tag{11.4}$$

Now the time to achieve 95% complete mixing is obtained when $\log\ (\sigma^2) = -\dfrac{2\times 3.00}{\ln 10} = -2.61$. With several probes the responses are pooled and weighed toward the probe that has the largest deviation from equilibrium. Equation (11.4) is also applicable for a damped oscillation of $E(t)$ toward $E = 1$.

At this point, some empirical observations can already be compiled:

1. In a stirred tank equipped with baffles the mixing time is approximately proportional to the reciprocal of the stirrer speed N which is frequently given in units of rotations per second (rps) (s^{-1}) or rpm (min^{-1}):

$$t_{\mathrm{mix,E}} \propto \frac{1}{N}. \tag{11.5}$$

   In (11.5) the proportionality constant depends on the mixer, e.g., on the impeller type.
2. Rotation of the impeller transports a liquid volume v_{pump} from the mixer into the bulk liquid volume. v_{pump} is proportional both to N and to the cube of the impeller diameter d_{s}. The proportionality constant N_{f}, the *flow number*, depends on the impeller type.

$$v_{\mathrm{pump}} = N_{\mathrm{f}}\left(N{d_{\mathrm{s}}}^3\right) \tag{11.6}$$

   For a Rushton turbine and a low viscosity medium the flow number $N_{\mathrm{f}} \approx 0.72$.
3. Finally the *circulation time* t_{c} is defined as the ratio between total medium volume V and the *pumping capacity* v_{pump} defined by (11.6):

$$t_c = \frac{V}{v_{\mathrm{pump}}} = \frac{V}{N_{\mathrm{f}}{d_{\mathrm{s}}}^3}\frac{1}{N} \tag{11.7}$$

   Equation (11.7) gives an approximate value for the proportionality constant in (11.5). Furthermore, for fully turbulent flow in a baffled tank reactor, mixing is often complete for $t \approx 4t_{\mathrm{c}}$.

Example 11.1 *Mixing time in a baffled tank reactor*. A tank reactor with medium volume $V_l = 600$ L is equipped with one six-bladed Rushton turbine that rotates with $N = 2\ \mathrm{s}^{-1}$.

The blades of the turbine have a diameter of $d_s = 0.10$ m.

$v_{\mathrm{pump}} = 0.72 \times 2 \times 0.1^3 = 0.00144 \mathrm{m}^3\mathrm{s}^{-1} \rightarrow t_c = 0.6/0.00144 = 417\,\mathrm{s}$. "Full mixing" is obtained within $\approx 4 \times 417 = 1{,}668$ s $= 0.46$ h.

A tracer experiment is carried out, and the average of three probes shows that after 720 s $E = 0.7$. What degree of mixing can be estimated to have been achieved after 1,668 s?

$k_{\mathrm{mix,E}} = -\ln(0.3)/720 = 0.00167\ \mathrm{s}^{-1}$, and (using 11.3): $1 - E = \exp(-0.00167 \times 1{,}668) = 0.0615$.

Consequently, "full mixing" according to (11.7) means about 93.8 % completion for the mixer investigated above. Mixing to 95% would require $t_{\mathrm{mix}} = 3.00/0.00167 = 1{,}796$ s.

This is a long mixing time, and mixing is improved either by increasing N or d_s. To increase d_s is – as clearly seen from (11.6) – by far the best option. Example 11.4 is a continuation of the present example, and both the design of the reactor and of the stirrer is criticized.

Mixing in the turbulent region by any mechanical means produces eddies, and mixing improves until these eddies have decreased to a limiting size, the so-called Kolmogorov characteristic length, l_{min} given by (11.8).[1] Any further turbulent mixing action will not increase the homogeneity of the mechanical mixing process. The Kolmogorov characteristic length was already introduced in Note 10.1 in connection with calculation of the minimal stable bubble size that can be achieved by turbulent mixing, and the direct relation between the maximal interfacial area for mass transfer and dispersion of a liquid is clearly seen.

$$l_{\mathrm{min}} = \left(\frac{{v_l}^3}{P/M}\right)^{1/4} \tag{11.8}$$

Any further homogenization of the liquid can only occur by molecular diffusion, and the time constant t_D for the diffusion is much larger than the time constant $t_{\mathrm{mix,m}}$ for mixing the liquid to its smallest entities by means of mechanical energy.

Example 11.2 *Macro- and micro-mixing of a liquid*. For an aqueous medium with kinematic viscosity $v_l = 10^{-3}$ (kg m^{-1} s^{-1})/1,000 (kg m^{-3}) $= 10^{-6}$ m^2 s^{-1}:

$$l_{\mathrm{min}} = 3.16 \times 10^{-5} (P/M)^{-1/4} (\mathrm{m}), \tag{1}$$

where P/M is the power input (W) per kg medium.

For a laboratory bioreactor with 1 kg medium and a power input of 10 W (using an impeller of diameter 47 mm)

$$l_{\mathrm{min}} = 3.16 \times 10^{-5} \times 0.56\ \mathrm{m}\ = 1.8 \times 10^{-2} \mathrm{mm}\ = 18\,\mu\mathrm{m}.$$

[1] Andrei N. Kolmogorov (1903–1987) was a famous Russian mathematician who contributed significantly to statistical mechanics, stochastic processes, fluid mechanics, and nonlinear dynamics. His papers from 1941 on turbulent flow have been of fundamental importance for the development of this scientific field.

This is probably enough to ensure that cells of diameter 1–2 μm are presented to a medium with a virtually homogenous glucose concentration.

In (1) the large influence of liquid viscosity η is clearly seen. In a cultivation of filamentous fungi η can easily be 500 times larger than for water, and this will increase l_{min} by a factor $500^{0.75} = 106$. Now the size of the smallest possible liquid element reached by mechanical mixing increases to 3.35 $(P/M)^{-0.25}$ (mm), or 1.9 mm for the laboratory reactor, and transport of glucose into the micro-elements of the liquid may well lead to glucose limitation.

The time constant t_D for transport by diffusion is obtained by solution of the non-steady-state mass balance (6.22), and for a spherical micro-element (Crank 1956, (6.20)):

$$t_D = {l_{min}}^2/\left(4\pi^2 D_A\right) \tag{2}$$

With $l_{min} = 1.9 \times 10^{-3}$ m and D_A (glucose) $= 0.85 \times 10^{-9}$ m^2 s^{-1} from Table 10.10 one obtains

$$t_D = 107\,\text{s}. \tag{3}$$

Final mixing of the medium with respect to complete homogeneity of the glucose concentration is far slower than the macro-mixing process.

In larger scale, a power input of 10 W kg^{-1} cannot at all be obtained, and the danger of inadequate mixing becomes much greater. This subject will be taken up in Sect. 11.2.

11.1.2 Experimental Determination of Mixing Time

The time needed to achieve a certain degree of uniformity in miscible liquids is generally determined by injecting a pulse of tracer and monitoring the response. A simple, and often quite illustrative monitoring method is *visual inspection*, e.g., of the change of the color of a pH indicator after a pulse of acid or base has been injected to the transparent reactor system. Figure 11.9b illustrates the immediate appeal of the method.

It is advisable to use both a colorization and a de-colorization method: In the first experiment the regions of poor mixing will eventually be hidden by dark, colored regions where mixing has already taken place, and in the second experiment the regions of least mixing will remain colored after regions of good mixing have become transparent.

Good pH-based indicators are bromo-phenol blue (color change from blue to yellow), methyl red (red to yellow) and phenolphthalein (pink to colorless), while the redox indicator iodine-thiosulfate has an easily observable color change from colorless to dark blue. But whichever indicator is used it is difficult to obtain more than a qualitative impression of when the last wisps of color disappear. The visualization experiments are easy to set up (see Brown et al. (2004)), and they indicate where sensors are to be placed to give a good description of the whole tank volume by quantitative methods.

In recent years, quantitative colorimetric methods have also appeared, e.g., Melton et al. (2002) who by an appropriate choice of the pH change could obtain a yellow colorization only in regions where a certain degree of mixing was achieved. Delaplace et al. (2004) quantified the colorization pattern from digital images captured on a video taken during the mixing process, and he determined $t_{mix,0.90}$ based on the quantified images.

The most important *quantitative* methods for determination of t_{mix} are the *conductivity method* and the *pH method*. These will be discussed below together with three other, less popular, but promising methods.

Conductivity Method

When a pulse of a concentrated salt solution is added to the tank a conductivity probe will monitor the increase in conductivity of the medium as a function of time.

The response time of the electrodes is very fast, and this is a definite advantage of the method.

On the negative side is that gas bubbles entering the space between the electrodes severely upset the measurement due to their low conductivity, but when the electrodes are protected by a fine-meshed net the noise level is reduced significantly (Otomo et al. 2003).

Another limitation of conductivity probes is that after a few measurement rounds on the same medium in the tank the conductivity level has increased substantially, and the sensitivity of the measurement decreases. Since cultivation media generally contain significant amounts of inorganic salts, the sensitivity of the method for these media is poor right from the start.

pH Method

Gas bubbles do not disturb the measurement by pH probes, and the amount of salts formed is so small that the measurements can be carried out during a cultivation process. When an acid is produced in the cultivation process it might influence the result, but it is probably safe to assume that the mixing time experiment takes much less time than the time constant for acid production. The large buffer capacity of most cultivation media does, however, imply that rather large pulses of acid or base have to be used in each experiment to avoid that the sensitivity becomes too small.

A major disadvantage of the pH method is that pH probes have a long response time compared to conductivity probes. They are therefore unsuited for mixing time experiments in laboratory scale since the response time of the probe (up to 1–3 s) could well be of the order of the whole mixing experiment. This is, however, not a problem in large reactors where t_{mix} can be of the order of minutes.

Thermal Method

A liquid pulse of temperature different from the medium is added, and the medium temperature is monitored by thermocouples, e.g., Masiuk (2000).

Very large pulses are needed for large-tank experiments, and since the viscosity of the medium is sensitive to temperature one may introduce systematic errors in the experiment.

Isotope-Based Method

A radioactive isotope is used as a tracer, and the radioactivity is measured on one or several scintillation counters placed outside the reactor wall. The method is clearly noninvasive. It is insensitive to gas bubbles, but its use in an industrial environment is not advisable.

In small reactors a large fraction of the medium volume is exposed to the measurement by the scintillation counter, and this leads to blurring of the results with little detail obtained concerning the mixing pattern. Pedersen et al.(1994) and Dominguez et al.(1999) are examples where isotopes are used to determine t_{mix}, but despite the simplicity of the method it may not become popular due to above-mentioned excessive averaging of the signal over the reactor volume.

Fluorophore Method

Fluorophores can also be used as tracers. An early study is by Einsele et al. (1978) who used injection of a pulse of quinine to a culture of *Saccharomyces cerevisiae*.

The response time is fast, but as in the conductivity method the presence of bubbles will give rise to noise, and the sensitivity will decrease if several experiments are carried out on the same volume of liquid. Many fermentation media are fluorescent and this will also give rise to a high background level which decreases the sensitivity of the method.

These comments to different experimental methods to determine t_{mix} point to the following characteristics for a good method:

- The probe should have a small response time and measure on only a small volume of liquid to avoid averaging effects.
- The probe should be applicable, also when gas is sparged through the liquid.
- The addition of the tracer should not alter the properties of the liquid measured, since repeated preparations of a new medium is both costly and labor intensive.
- Probes and probe supports should not influence the flow pattern in the tank.
- The physical properties of the medium (e.g., its viscosity) should not change when tracer is added.

Example 11.3 *Measuring a pulse response using the pH rather than [H$^+$].* In the pH method one determines the mixing efficiency by the expression:

$$E = \left| \frac{\mathrm{pH}(t) - \mathrm{pH}_{\mathrm{final}}}{\mathrm{pH}_{\mathrm{final}} - \mathrm{pH}_0} \right|. \tag{1}$$

In (11.1) E is determined based on concentrations (here on [H$^+$]) and the nonlinear dependence of the quantities in (1) on [H$^+$] will, in principle, give rise to a systematic error.

In Nordkvist et al.(2003) a model was set up to quantify the error on t_{mix} that will result from using (1) instead of (11.1).

A simulated step-up experiment (pH 3.50 → pH 3.80) gave $t_{\mathrm{mix},0.95} = 64$ s, while a simulated step-down experiment (pH 3.80 → 3.50) gave $t_{\mathrm{mix},0.95} = 57$ s. The average between the two mixing times, $t_{\mathrm{mix},0.95} = 60.5$ s was almost the same as the result of a concentration-based experiment where [H$^+$] was changed from, respectively, $10^{-3.50}$ to $10^{-3.80}$ or the other way round.

Consequently, when the average of step-up experiments and step-down experiments based on pH changes is used, the pH method gives the same result as when the experiment is based on concentration measurements if the change in pH is relatively small.

11.1.3 Mixing Systems and Their Power Consumption

The two classical impeller types are the propeller and the Rushton turbine (Fig. 11.1). The propeller mainly gives an axial flow pattern and is most suited for long, slim tanks while the latter gives a mainly radial flow pattern.

Figure 11.2a is a schematic representation (adapted from Nienow (2010) of a typical stirred tank bioreactor equipped with four 6-bladed Rushton turbines (Rushton et al. 1950a, b). The motor is connected via bearings to the shaft through a sterile seal, and the shaft is supported by the bearing at the bottom of the reactor. The motor necessary to deliver sufficient power to a large-scale bioreactor is (also physically) very large – a 75 m^3 tank may easily require a 500 kW motor. Hence, the support of the shaft at the bottom is essential to avoid mechanical stresses on the shaft and on the bearings at the top.

The reactor is equipped with baffles (B). Without these the liquid in any mechanically stirred cylindrical reactor would form a vortex, and the liquid elements would move in concentric circles without any appreciable radial mixing, even when the speed of the agitator N increases. The vortex would simply become deeper with a shape that depends on the Froude number $\mathrm{Fr} = N^2 \times d_s/g$ (d_s = stirrer diameter, g = acceleration of gravity).

Each Rushton turbine typically has six 90$^{\mathrm{o}}$ wedged-shaped blades, a mechanically very simple construction. The turbine shown on the figure rotates clock-wise with a tip speed $v_{\mathrm{tip}} = \pi N d_s$. Four Rushton turbines are shown on the figure, and the distance between the turbines ΔC is related to the tank diameter T. The lowest turbine is at a height C over the bottom of the reactor.

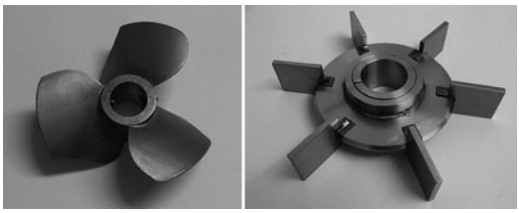

Fig. 11.1 Two typical mixers: The propeller and the Rushton turbine (courtesy of Novozymes A/S)

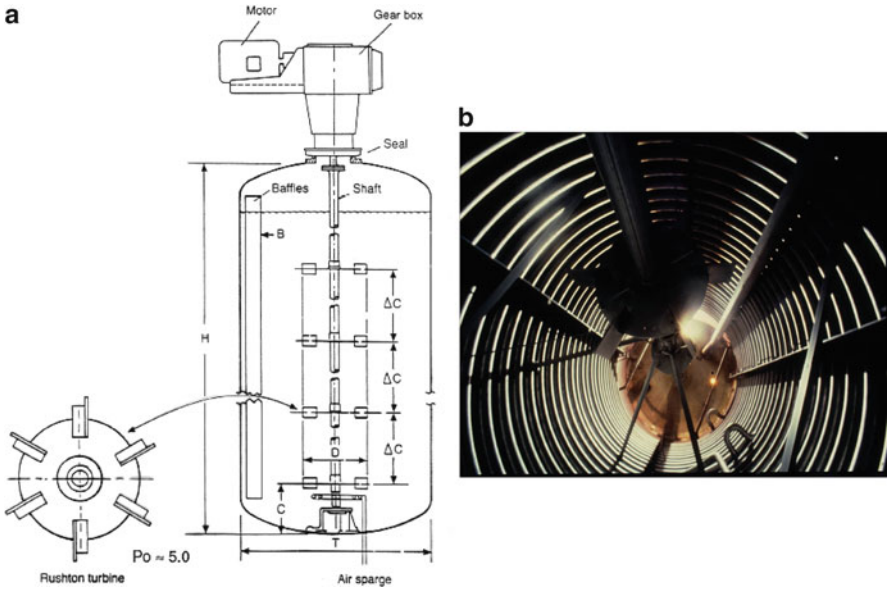

Fig. 11.2 (**a**) Typical stirred tank bioreactor equipped with four Rushton turbines. "Po" is the *Power number* N_p for a six-bladed Rushton turbine (see Fig. 11.3). (**b**) View from the top of an industrial STR (courtesy of Novozymes A/S)

Gas feed is through a sparger placed a short distance below the bottom turbine, and liquid feed should preferably be into the Rushton turbines (if this is possible from a construction point of view – and due to sterility concerns industry still prefers top-feeding in spite of the well documented increase of mixing time, unless an axial mixing aggregate is used). Finally, heat-exchange surface is mounted as vertically or horizontally spaced coils.

The photograph on Fig. 11.2b is a look from the top of an industrial bioreactor, and it shows the (horizontally coiled) heat transfer tubes, the shaft, and one (of two) Rushton turbines. For strongly aerobic reactions one might have to use an exterior heat exchanger to give sufficient heat transfer area. Internal coils are difficult to CIP (Cleaning In Place). Much higher heat transfer can be obtained in an optimally engineered external heat exchanger than by internal heat transfer where a part of the heat transfer area is only little affected by the mechanical agitation.

The following relative dimensions are proposed by the Mixing Equipment Company:

$$\text{Height } H/\text{ Diameter } T = 3.3;\ d_s/T = 0.35;\ C/T = 0.25;\ \Delta C/T = 0.5;\ B/T = 0.10$$

Obviously, these numbers depend on the properties of the system.

For *any* stirred tank reactor (STR) the power drawn for the mixing process is given by either (11.9) or (11.10):

$$P = 2\pi NTo, \tag{11.9}$$

$$P = N_p \rho_l N^3 {d_s}^5. \tag{11.10}$$

In (11.9), *To* (N m) is the torque. *To* is the force acting on the shaft to rotate an impeller of diameter d_s at N revs s^{-1}, and to a large extent *To* determines the choice of shaft diameter, the bearings and the motor. Hence (11.9) determines the capital cost of the mixing aggregate.

(11.10) determines the operating cost for given N and d_s. ρ_l is the liquid density (close to 1,000 kg m^{-3}) and N_p is the (dimensionless) *power number*. A large value of N_p means that the power cost is high for given $[d_s, N]$, but unfortunately a high power cost P does not imply that mixing is good. The quality of mixing depends to a significant degree on the *choice* of mixer, although a higher power input will give better mixing for all liquids (and mixtures of liquids and gases). In tables, N_p is stated as a dimensionless number, but this requires that consistent units (e.g., SI units) are used.

For a constant power input P_c the speed of rotation N can be reduced by a factor 2 by increasing d_s by a factor $2^{3/5}$, but according to (11.9) this implies that the torque *To* increases by a factor 2 which leads to a higher capital cost of the mixing aggregate. In the discussion of power input needed to disperse a gas phase effectively in the liquid and hence obtain a high $k_l a$ it will be shown that the most efficient impeller is that for which a given P_c is obtained with a large value of d_s, but the efficiency is only obtained at the price of a higher capital investment.

The Rushton turbine has a power number N_p of about 5.2 at fully turbulent conditions. This is high compared to several of the more modern impellers shown in Fig. 11.3. Hence, if two impellers with power numbers $N_{p,1}$ and $N_{p,2} < N_{p,1}$ are compared, one can, indeed, increase d_s without changing N, P, or *To*:

$$d_{s,2} = d_{s,1}\left(N_{p,1}/N_{p,2}\right)^{1/5}. \tag{11.11}$$

This is an important sales argument for impellers more modern than Rushton turbines.

The *Solidity ratio (SR)* mentioned in the text to Fig. 11.3 is defined by (McFarlane and Nienow (1995)):

$$\text{SR} = \frac{4nA_p}{\pi {d_s}^2}, \tag{11.12}$$

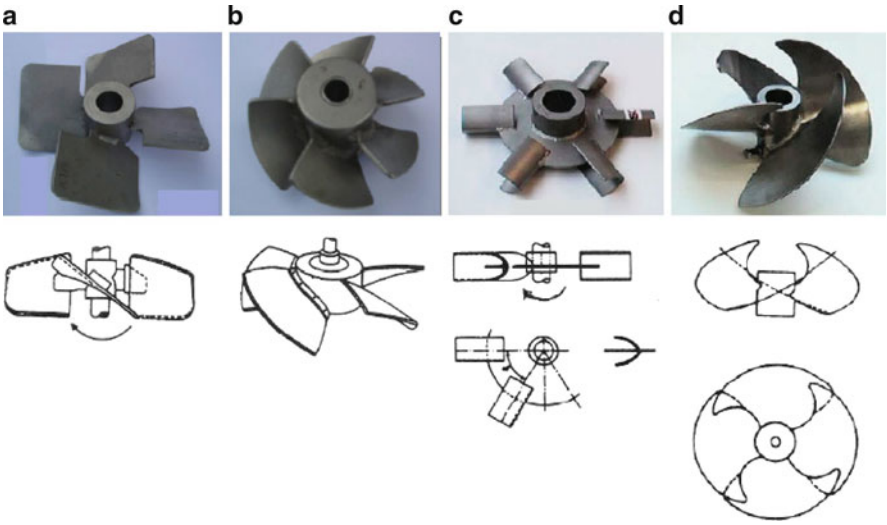

Fig. 11.3 Examples of impellers with smaller power number than Rushton turbines ($N_p \approx 5.2$). (**a**, **b**) Down-pumping hydrofoils (which can also be used for up-pumping). (**a**) Four-bladed Lightnin A 315, $N_p \approx 0.8$; Solidity ratio ≈ 0.9. (**b**) Six-bladed Prochem Maxflow *T*, $N_p \approx 1.5$; Solidity ratio ≈ 0.9. (**c**) Six-bladed Scaba 6SRGT, $N_p \approx 1.5$; Solidity ratio ≈ 0.4. (**d**) Four-bladed APV B-2, $N_p \approx 0.8$–0.9; Solidity ratio ≈ 1 (used for up-pumping – and also good for air-dispersion). Adapted from Nienow (2010). Data from McFarlane and Nienow (1995) and Nienow (1997)

where A_p is the projected area of one blade on a plane of a hydrofoil type impeller, and n is the number of blades. An impeller with a high value of SR stalls less easily. Stalling occurs when the boundary layer on the rear (suction) side of the blade separates. This leads to disorderly recirculation around the blade, and most of the pumping capacity is lost.

For all impellers the power number N_p is a function of the Reynolds number for the pump Re_s which is defined differently from Re in Table 10.6, but it is still the ratio between inertial and viscous forces:

$$Re_s = \frac{\rho_l N d_s^2}{\eta}. \tag{11.13}$$

For non-Newtonian liquids the apparent viscosity η_{app} = (shear stress τ)/(shear rate $\dot{\gamma}$) is used instead of η in (11.13), see Sect. 11.1.4.

N_p can be conceived as a friction- (or a drag-) factor, and from Fig. 11.4 it follows that the friction factor becomes independent of Re_s when the flow is turbulent. Here, physical parameters (ρ_l and η), and design (d_s) or operation (N) variables have no influence on N_p.

The constant value of N_p in the turbulent regime is obtained for all impellers, and it is the values of N_p for high values of Re_s which are listed in Fig. 11.3.

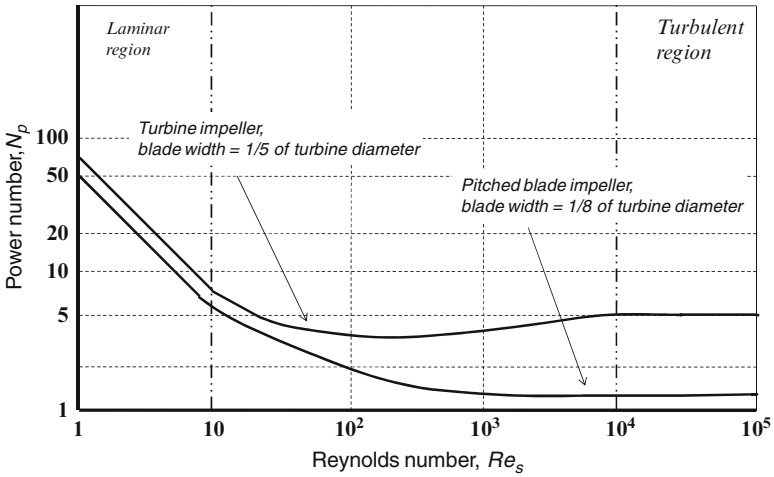

Fig. 11.4 The power number N_p as a function of Re_s for a Rushton turbine and a pitched blade impeller. Laminar flow is found for $Re_s < 10^2$ and fully turbulent flow for $Re_s > 10^4$. Curves very similar to those of this figure are found in textbooks on fluid flow through different types of pipes. Here the abscissa is the Reynolds number used in Table 10.6, and the ordinate is the "friction factor"

In the laminar flow region N_p is seen to be inversely proportional to Re_s which means that it is proportional to the viscosity of the liquid: To stir a viscous fluid in the laminar flow region is really costly in power consumption, and as mentioned earlier, a high power number does not indicate that the mixing is effective, as it certainly is not for viscous fluids in the laminar region.

The transition region on Fig. 11.4 is only indicative for mechanically stirred tanks. For mixing by liquid jets the transitional regime (where Re_s is defined slightly differently, see Sect. 11.1.5) extends between approximately $Re_s = 100$ and 1,500 (Revill 1992).

The mixing produced by a Rushton turbine is excellent in the radial direction of the tank, but the zone of mixing does not extend far in the axial direction. Hence for long, slim tanks several Rushton turbines must be used. On Fig. 11.2a the distance ΔC between turbines is indicated for typical low viscosity media. When more than 1 turbine is used the power input P can approximately be calculated by multiplication of the result in (11.10) by the number of turbines (Nienow and Lilly 1979). When the Rushton turbine has a number of blades different from 6 the power number N_p is different from ≈5.2, e.g., 7.5 for 12 blades. Similar values for varying P and N_p with nonstandard design of other agitators can be found in the literature.

Up to now the power requirement for mixing a *liquid medium* has been considered.

When the stirred tank is aerated the power requirement also depends on the amount of gas that is to be dispersed in the medium. The *aeration number* N_A (also dimensionless) is defined as

$$N_A = \frac{v_g}{N d_s^3} = \frac{v_g}{v_{pump}} N_f. \tag{11.14}$$

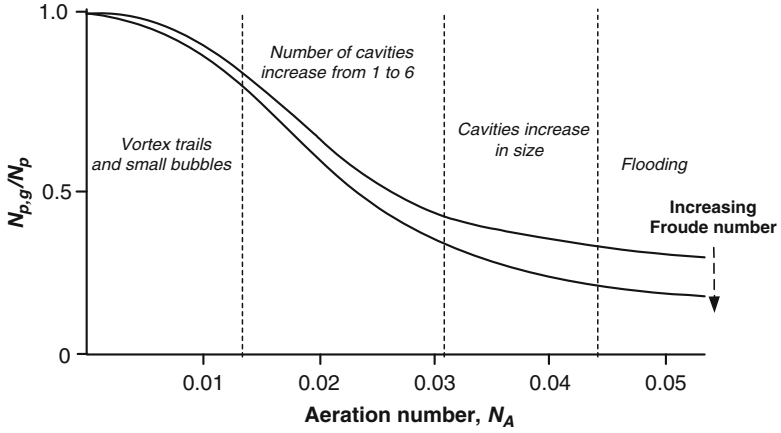

Fig. 11.5 $N_{p,g}/N_p$ sketched as a function of N_A for a six-bladed Rushton turbine. Adapted from Ekato Handbook of Mixing Technology (http://www.EKATO.com)

In (11.14) v_g is the volumetric gas flow rate and v_{pump} is the liquid flow delivered by the mixer. N_f is the (gas) flow number which was introduced in (11.6).

Figure 11.5 shows an empirical relation between the power number $N_{p,g}$ for the gassed liquid and N_p for the un-gassed liquid at the same value of Re_s, but at different values of the aeration number N_A. The data are valid for Rushton turbines only. For example, the Lightnin impeller (Fig. 11.3d) $N_{p,g}/N_p$ is ≈ 1 until $v_g/V \approx 1.5$ vvm (or $N_A N \approx 1.5\pi\,(d_s/T)^3$, where N has the unit min^{-3}).

The ratio between the two power numbers clearly decreases with increasing N_A, i.e., it decreases with increasing v_g for constant N (and d_s). For very high gas loads the mixing region at the pump becomes flooded with gas, the power input becomes very low, and the gas rises by buoyancy along the mixer shaft without much dispersion. In this region the gas–liquid mass transfer coefficient must be very low. For a very small gas load $N_{p,g}/N_p$ approaches 1, and the gas is fully dispersed, both above the mixer and in the volume below the sparger. Here mass transfer is good.

For a fixed gas load one can move from the right to the left on Fig. 11.5 by increasing N, an easily visualized result. The figure also displays an effect of the Froude number, i.e., of the ratio between inertial and gravitational forces acting on the liquid, on the ratio $N_{p,g}/N_p$:

$$\text{Fr} = \frac{N^2 d_s}{g}. \tag{11.15}$$

With increasing value of Fr flooding is reached at a lower value of N_A. The implication of this observation is discussed below.

Nienow (2010) gives the following relations for the gas load v_g at which respectively flooding and full gas dispersion occurs:

$$\text{Flooding}: (N_A)_F = v_g/N_F d_s{}^3 = 30(d_s/T)^{3.5} Fr = 30(d_s/T)^{3.5} N_F{}^2 d_s/g \quad (11.16)$$

$$\text{Fully dispersed}: (N_A)_{Disp} = 0.2(d_s/T)^{0.5} \mathrm{Fr}^{0.5} \quad (11.17)$$

Equations (11.16) and (11.17) can be rearranged to the following explicit expressions for $[N_{F,} N_{Disp}]$:

$$N_F = \left(\frac{g}{30} v_g\right)^{1/3} T^{7/6} d_s{}^{-2.5}, \quad (11.18)$$

$$N_{Disp} = \left(5 g^{1/2} v_g\right)^{1/2} T^{1/4} d_s{}^{-2}. \quad (11.19)$$

For a fixed tank diameter T and a fixed gas flow v_g the two equations imply that the critical N values for flooding and "full dispersion" decrease very fast for increasing d_s which also means that much more gas can be dispersed for a given N.

Note that when g is inserted as 9.81 m s^{-2}, $[N_F, N_{Disp}]$ have the unit s^{-1}. The unit for "length" (m) cancels.

The maximum gas flow at which flooding occurs depends on the impeller type. The Rushton turbine is especially poor (see Fig. 11.5), whereas, e.g., the Scaba hollow blade mixer (Fig. 11.3c) permits at least twice as high v_g to be dispersed at the same (small) power input before flooding occurs. The difference between the two mixer types is clearly seen if the gas dispersion is filmed: In the Rushton turbine the gas collects behind the blades, and flooding easily occurs, while the gas bubbles *leave* the blades of the Scaba mixer as a spiraling string.

Also, the typical radial mixing pattern of the Rushton turbine is a disadvantage at high aspect ratio H/T of the tank The hydrofoil mixers on Fig. 11.3 which resemble propellers with curved blades – see Fig. 11.3 – are much better for axial mixing. Using several Rushton turbines as shown on Fig. 11.2 will increase the mixing in each zone, but still transport between zones is slow. The power input increases approximately proportional to the number of turbines (Nienow and Lilly 1979).

This criticism of the Rushton turbine should, however, not be overemphasized. For really heavy gas–liquid mixing duties the Rushton turbine may be the only feasible mixer type since much power can be delivered.

To complete the picture of gas dispersion in liquids one also needs to include Bubble Columns, where at isothermal dispersion of gas at pressure p to the liquid:

$$P = v_g \Delta p = u_g \rho_l g \; V_l \quad (11.20)$$

In (11.20) u_g and Δp are respectively superficial linear gas velocity and pressure loss over the tank (including hydrostatic pressure loss).

Consequently, the total power input to an aerated, mechanically stirred tank is equal to P determined from (11.10) + the contribution from (11.20). This last term is, however, very small compared to the term from (11.10), but for bubble columns (11.20) is of course the only contribution to the power input. It is not strange that, e.g., $k_l a$ in bubble columns is smaller than what can be obtained in mechanically stirred tanks.

Example 11.4 *Power required for liquid mixing and for gas dispersion at the sparger.* The V_l = 600-L tank in Example 11.1 is sparged with 100 L air min^{-1}. Determine the power input when the tank diameter is $T = 0.25$ m, and the sparger is placed 1.2 m below the surface of the (aqueous) medium. First the power input due to gas-sparging alone is calculated using (11.20):

$$u_g = \frac{0.1}{60 \times (\pi/4 \times 0.25^2)} = 0.034 \text{ m s}^{-1}; \quad p/p_0 = 1.12 \text{ bar}. \tag{1}$$

From (11.20) the power used to release the gas into the tank is $P = 200$ W (= 333 W m^{-3} liquid), and $\Delta p = 200/(0.1/60) = 120000$ N m^{-2} = 1.2 bar.

From (11.18) $N_F = 0.000545^{1/3} \times 0.25^{7/6} \times 0.1^{-2.5} = 5.12$. $N = 2$ is clearly too small to avoid flooding of the impeller.

The conclusion is that the tank is poorly constructed. With 600 L medium and a tank diameter of 0.25 m the height of the medium in the tank is $4 \times 0.6/(\pi \times 0.25^2) = 12.2$ m, i.e., the aspect ratio $H/T = 49$, and with 1 Rushton turbine most of the tank is not well mixed (see Fig. 11.2).

The diameter of the tank should be larger, e.g., $T = 0.9$ m for which $H/T = 1.05$, and one could reasonably expect that one Rushton turbine could do the mixing. Next the impeller diameter is considered. According to Fig. 11.2 d_s/T should be around 0.35. When $T = 0.9$ m an impeller diameter $d_s = 0.35$ m is about adequate.

Consequently, one chooses a tank with $T = 0.9$ m, and d_s is increased to 0.35 m.

With respect to Example 11.1 the new choice of d_s will, according to (11.7), give a circulation time $t_c = 9.7$ s for the unaerated liquid. Hence, with the semiquantitative formula $t_{mix,0.95} = 4t_c$ one obtains "complete mixing" after 38 s. More important, N_F, calculated from (11.18), decreases from 5.12 to 0.996 s^{-1} while N_{Disp} calculated from (11.19) is 1.28 s^{-1}. Now a speed of rotation $N = 2$ s^{-1} is clearly satisfactory. With $N = 2$ (11.14) gives $N_A = 0.02$. Figure 11.5 indicates that $N_{p,g}/N_p$ is around 0.5 for $N_A = 0.02$, and with $N_p \approx 5.2$ for a Rushton turbine one calculates $N_{p,g} = 0.5\ N_p = 2.6$. This power number is used to calculate the necessary power input to the aerated 600 L tank.

One may increase N somewhat from 2 s^{-1} to be quite sure that the value of $N_{p,g} \approx N_p$, but the important message of the example is that *the basic design of the reactor and its mixing equipment must be right*.

For a tank with diameter $T = 0.9$ m the value of u_g in (1) is decreased to 0.00262 m s^{-1}.

The Rushton turbine is placed 0.45 m below the liquid surface and the sparger 0.2 m below the turbine.

Consequently, using (11.10) the power input to the Rushton turbine is $2.6 \times 10^3 \times 2^3 \times 0.35^5 = 109$ W (compared with 218 W for the unaerated reactor). The power input to push the gas through the sparger is (at least) $2.62\ 10^{-3} \cdot 10^3 \cdot 9.81 \cdot 0.6 = 15$ W.

The total power input of 124 W is not high, and a low mass transfer coefficient can be expected. This expectation is confirmed using any of the formulas of Table 10.4, e.g., that of van't Riet which gives $k_l a = 0.026 \times (0.00262)^{0.5} \times (124/0.6)^{0.4} = 0.011\ s^{-1} = 40\ h^{-1}$. Once the tank and the mixing aggregate is installed the only way to increase P is to increase N.

In Example 11.3 the very simple formula (11.7) was used to calculate the time to "full mixing" in a baffled tank as $t_{mix,0.95} \approx 4t_c = 4 \times {N_f}^{-1} \times (N)^{-1} \times {d_s}^{-3}\ V$.

Newer research, reviewed by Nienow (1997), has shown that the design variables d_s, T and H influence the result. Thus, data from the 1980s and 1990s for mixing of water-like media can be correlated by (11.21) for $H = T$:

$$t_{mix,0.90} = 5.3N^{-1}{N_p}^{-1/3}(d_s/T)^{-2}(\text{for } H = T) \tag{11.21}$$

In (11.21) N_p is the power number $= P\left(\rho_l N^3 {d_s}^5\right)^{-1}$. The constant 5.3 is correct for $H = T$, and $t_{mix,0.90}$ has the same dimension as N^{-1}. The equation is found to hold quite well for all impeller types at equal P/M, the power input per unit mass of the medium.

Thus, it is advantageous to use an agitator with a small N_p, since the torque on the shaft is smaller for a small N_p.

Equation (11.21) can be rewritten into a relation between $t_{mix,0.95}$ and P/M:

$$\begin{aligned} t_{mix,0.90} &= 5.3N^{-1}\left(\frac{P\frac{\pi}{4}T^3}{N^3 M {d_s}^5}\right)^{-1/3}\left(\frac{d_s}{T}\right)^{-2} \\ &= 5.74\left(\frac{P}{M}\right)^{-1/3}\left(\frac{d_s}{T}\right)^{-1/3}T^{2/3}. \end{aligned} \tag{11.22}$$

Whereas (11.21) confirms the result of (11.5) that $t_{mix} \propto N^{-1}$ it also tells how the proportionality constant depends on the ratio between d_s and T, and on the choice of agitator type. (11.22) relates t_{mix} to the power input per unit mass and the design variables d_s and T.

An interesting observation is, that the relation also tells how t_{mix} increases with scale, namely as $T^{2/3}$ (or $V^{2/9}$). Both (11.21) and (11.22) are derived for nonaerated media and for $H = T$. Aeration contributes somewhat to the mixing, but no reliable literature references are available to quantify the effect.

Also, one would like to have a formula like (11.22) embellished by a factor $\left(\frac{H}{T}\right)^{\beta}$ that describes how $t_{mix,0.95}$ depends on the aspect ratio of the reactor. Again, little of general nature has yet been reported, but Cooke et al. (1988), in a study of a 60 L tank with $H/T = 3$, stirred with 3 Rushton turbines found:

$$t_{mix,0.90} = 3.3N^{-1}{N_p}^{-1/3}\left(\frac{d_s}{H}\right)^{-2.43} \tag{11.23}$$

Equation (11.23) resembles (11.21) in the sense that each of the three turbines operates in a tank volume of height T, but the influence of H seems to be more pronounced than the influence of T. In any case, the somewhat spurious information

concerning the influence of H shows that the poor axial mixing quality of Rushton turbines requires that one turbine should be installed at each increment $\Delta H = 0.5–1\ T$ as shown on Fig. 11.2a. Even so, it appears that axial flow impellers do a better job than multiple Rushton turbines. Otomo et al. (1995) worked with a 0.59 m^3 tank where H/T was 2. He found that when two down-pumping Lightnin 315 hydrofoils (Fig. 11.3a) were used instead of two 6-bladed Rushton turbines the mixing time decreased by a factor 2.

The issue of poor axial mixing should be of real concern in fed-batch fermentation. The mixing aggregate is usually installed in the bottom part of the tank, and mixing needs to be efficient in the batch phase where biomass is grown up at high O_2 consumption rate. In the fed-batch phase the medium volume may increase by a factor 3 or 4, but although the O_2 demand is often much lower in the production phase the concentrated feed of substrate and of pH regulator is poorly mixed into the bulk medium when the feed-from-the-top operation is chosen.

Example 11.5 *Calculation of mixing time in Stirred Tank Reactors*. In the unaerated reactor of Example 11.4 ($T = 0.9$ m, $H = 0.94$ m, $d_s = 0.35$ m, and $N = 2\ s^{-1}$) the power input from the Rushton turbine is $5.2 \times 1{,}000 \times 2^3 \times 0.35^5 = 218.5$ W for an aqueous medium.

Using (11.22) one obtains:

$$t_{mix,0.90} = 5.74\left(\frac{218.5}{600}\right)^{-1/3}\left(\frac{0.35}{0.9}\right)^{-1/3} 0.9^{2/3} = 10.3\ s$$

This is just a little above t_c calculated by (11.7). It is probably safer to trust (11.22) than the simple relation t_{mix} "complete" $= 4\ t_c$, since (11.22) is based on a large experimental material.

11.1.4 Power Input and Mixing for High Viscosity Media

Rheology is concerned with the study of flow and deformation of matter. Strictly defined, a *fluid* is a material phase which cannot sustain *shear stress* τ, i.e., forces acting in the tangential direction of the surface. (The forces acting in the normal direction of the surface are the pressure forces.) A fluid will respond to shear stress by continuously deforming, i.e., by flowing. The *shear rate*,$\dot{\gamma}$ in stationary, two-dimensional flow is defined as

$$\dot{\gamma} = \frac{du_y}{dz}, \tag{11.24}$$

where z is the direction perpendicular to the flow direction y, u_y the linear velocity ($m\ s^{-1}$) in the y direction, and the derivative shows how u_y varies in the z direction.

In flow through a cylinder z is the radial distance r from the axis of the cylinder axis.

Isaac Newton was the first to propose (in 1687) a relation between shear stress and shear rate. He stated that "the resistance (*sic* the shear stress) which arises from the

lack of slipperiness originating in a fluid, other things being equal, is proportional to the velocity by which parts of the fluid are being separated from each other (*sic* the shear rate)." The *dynamic viscosity*,η (kg m^{-1} s^{-1}), of a fluid is the fundamental property which relates the *shear stress,* τ, (N m^{-2}) or (kg m^{-1} s^{-2}), to the shear rate $\dot{\gamma}$ (s^{-1}). For the one-dimensional case described in (11.24) the relation is:

$$\tau = -\eta\dot{\gamma} \tag{11.25}$$

We will in the following simply call η "viscosity," but it is important not to confuse the dynamic with the *kinematic viscosity* ν. The latter is the ratio between the dynamic viscosity and the density ρ_l of a fluid. The kinematic viscosity has the unit (m^2 s^{-1}).

Note 11.1 *Shear stress as a tensor property*. In many textbooks outside the field of fluid mechanics, the concept of stress is mathematically abused much in the same way as done above. Stress should properly be treated as a tensor property. The state of stress in a material phase is fully described by the stress tensor, $\mathbf{T}$ (N m^{-2}). The stress tensor includes both normal stress (i.e., pressure) and shear stress and can be written:

$$\mathbf{T} = -p\mathbf{I} - \boldsymbol{\tau}. \tag{1}$$

In (1) p is the pressure (N m^{-2}), $\mathbf{I}$ is the identity matrix, and $\boldsymbol{\tau}$ is *the shear stress tensor* (N m^{-2}). The stress acting on a surface at any point, characterized by a normal vector, $\mathbf{n}$, can be found from the stress tensor by scalar multiplication according to

$$\mathbf{t_n} = \mathbf{n} \times \mathbf{T} \leftrightarrow \mathbf{t_n} = -\mathbf{n} \times (p\mathbf{I} + \boldsymbol{\tau}). \tag{2}$$

In (2) $\mathbf{t_n}$ is the state of stress. Note that $\mathbf{t_n}$ has the same unit as $\mathbf{T}$, i.e., N m^{-2}, but is a vector instead of a tensor. For a Newtonian, incompressible fluid, the shear stress tensor can be written:

$$\boldsymbol{\tau} = -\eta(\nabla\mathbf{u} + \nabla\mathbf{u}^T). \tag{3}$$

Here $\nabla\mathbf{u}$ is the velocity gradient (s^{-1}), which can be said to be the tensor counterpart of the previously defined shear rate $\dot{\gamma}$.

For *Newtonian fluids* the viscosity is independent of the shear rate – i.e., it is constant – whereas for *non–Newtonian fluids* it is a function of the shear rate. The viscosities of fluids vary over a wide range, as seen in Table 11.1. Water, and many fermentation broths containing yeasts or bacteria, can be considered to be Newtonian fluids. However, fermentations involving filamentous fungi, or fermentations in which polymers are excreted, will often exhibit non-Newtonian behavior.

There are several different kinds of non-Newtonian behavior. The most important type is the s*hear rate-dependent* viscosity. A fluid for which the viscosity decreases with increasing shear rate is called a *pseudoplastic* (or *shear-thinning*) *fluid*. The opposite, i.e., a fluid with an increasing viscosity with increasing shear rate, is called a

Table 11.1 Viscosity of some Newtonian fluids (Adapted from Johnson 1999)

Fluid	Temperature (°C)	η (kg m^{-1} s^{-1})
Water	0	1.793×10^{-3}
	21	9.84×10^{-4}
	100	5.59×10^{-4}
Ethanol	20	1.20×10^{-3}
Glycerol	60	0.98
Sucrose solution (20 wt%)	21	1.92×10^{-3}
Sucrose solution (60 wt%)	21	6.02×10^{-2}
Olive oil	30	8.40×10^{-2}
Molasses	21	≈6.6

dilatant fluid. Polymer solutions, or solutions containing filamentous fungi, are often pseudoplastic, whereas, e.g., rice straw soaked in water, or whipped cream exhibit dilatant behavior.

There may also be *time-dependent effects* on the viscosity, so-called thixotropy. In this case, the viscosity changes as a function of time due to, e.g., alignment of fibers in the flow direction. At changing conditions, the initial viscosity may therefore be much different than the "steady-state" value. This is important to consider when the rheological properties of materials are determined.

Certain materials do not flow until a threshold shear stress is exceeded. This is true for, e.g., cheese and – quite important – pretreated, water-soaked lignocellulosic biomass. Although they are not, in a strict sense fluids, they behave like fluids once the yield stress is exceeded. These materials are called Bingham plastics or Bingham fluids.

A typical functional relationship for shear rate-dependent viscosity is the so-called *power law model* (or *Ostwald-de Waele model*):

$$\tau = -K|\dot{\gamma}|^n. \tag{11.26}$$

In analogy with (11.25) one defines the *apparent* viscosity η_{app} by

$$\eta_{\text{app}} = K|\dot{\gamma}|^{n-1}, \tag{11.27}$$

where K is the *consistency index* and n is the *power law index*. For $n = 1$ the fluid is Newtonian, and the viscosity η is a constant, independent on the shear rate $|\dot{\gamma}|$. For $n > 1$, the fluid is dilatant, and the apparent viscosity increases with increasing shear rate. If $n < 1$, the fluid is pseudoplastic, and the apparent viscosity η_{app} decreases with increasing when $|\dot{\gamma}|$.

For Bingham fluids, the shear stress is given by

$$\tau = \tau_0 - \eta\dot{\gamma}. \tag{11.28}$$

Here τ_0 is the *yield stress*. Also (11.26) can be supplemented with a constant term τ_0 to obtain a nonlinear relation between shear stress and shear rate with a

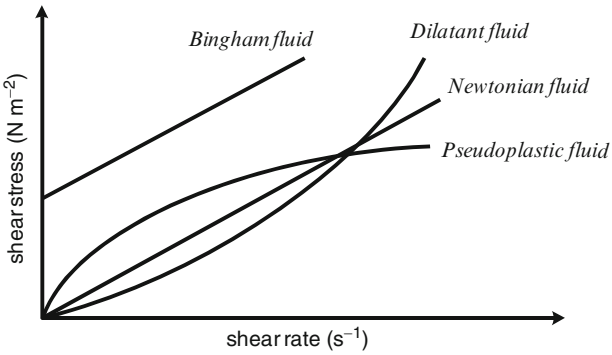

Fig. 11.6 Shear stress τ as a function of shear rate $\dot{\gamma}$ for different fluids

non-zero yield stress. The different kinds of shear rate-dependent rheological behavior are schematically shown in Fig. 11.6.

In order to find the linear velocity u_y for flow in the axial direction of a cylindrical tube one must set up a differential momentum balance and integrate the balance as shown in Bird et al. (2002). For *laminar* flow of Newtonian flow, i.e., (11.25) the momentum balance integrates to the well-known parabolic velocity profile:

$$u_{\mathrm{y}} = \frac{p_0 - p_{\mathrm{L}}}{4\eta L}\left(1 - \left(\frac{r}{R}\right)^2\right). \tag{11.29}$$

In terms of mass flow through the tube one obtains:

$$M = \frac{(p_0 - p_{\mathrm{L}})\pi R^4 \rho_{\mathrm{l}}}{8\eta L}\left(\mathrm{kg\ s^{-1}}\right). \tag{11.30}$$

In (11.29) and (11.30) L is the length of the tube, $(p_0 - p_{\mathrm{L}})$ the pressure difference between inlet and outlet, and R is the radius of the tube. (11.30), the Hagen–Poiseuille equation, is used in determination of η using a capillary viscosimeter. To be exact one must also incorporate the gravitational force acting on the liquid ($\rho_{\mathrm{l}}\ h\ \mathrm{g}$) when the ends of the tube differ in height by h, but $p + \rho_{\mathrm{l}}\ h\ \mathrm{g}$ is usually $\approx p$.

A large number of commercial instruments, *rheometers*, are available for the study of the rheological properties of fluids. Among the "conventional" rheometers designed with very accurate geometric dimensions the cone-and-plate rheometer (Example 11.6) is popular for studies of the rheology of simple fluids. Conventional rheometers are, however, difficult to apply for studies of fermentation media which contain air bubbles, more or less clumped biomass or even pellets of biomass, as is the case for cultivations of filamentous fungi.

Impeller type rheometers are used to characterize the rheology of fungal suspensions by measuring the torque To on the impeller at different rotational speeds N. To determine the apparent viscosity η_{app} (11.9) and (11.10) are combined

to eliminate the power input P. Thereafter, N_p is eliminated using (11.13), and the final result is (11.31):

$$To = \frac{N_p \rho_l N^2 {d_s}^5}{2\pi} = \frac{f(\mathrm{Re}_s)\rho_l N^2 {d_s}^5}{2\pi} = \frac{c}{2\pi}\eta_{app} N {d_s}^3. \tag{11.31}$$

In the last expression of (11.31) it is assumed that the flow is in the laminar region (which is often true for highly viscous fluids). The parameter c is obtained by measuring To as a function of N for a Newtonian liquid with known viscosity η.

Metzner and Otto (1957) found the approximate relation (11.32) for the mean shear rate $\dot{\gamma}_{av}$ in a stirred vessel:

$$\dot{\gamma}_{av} = kN. \tag{11.32}$$

Consequently, for power-law fluid where $\eta_{app} = K\dot{\gamma}^{n-1} = K(kN)^{n-1}$, one can obtain the value of k in (11.32) by measuring To as a function of N for a liquid with known values of n and K.

For many fluids k in (11.32) is between 10 and 13, but for a particular fluid the value can be found as described above.

Finally, to circumvent all the problems associated with settling biomass in off-line measurements, online rheometers mounted inside the bioreactor have been developed.

Picque and Corrieu (1988) used a "vibrating rod" sensor to characterize the medium in a *Xantomonas campestris* cultivation (producing xanthan). Kold (2010) used a commercial instrument (Marimax VA-300 from Marimax Industries, Canada) for rheological characterization of a *Xantomonas campestris* and an *A. oryzae* cultivation. In both cases, the rheometer was installed in the recirculation loop of a Rotating Jet Head fermentor (see Sect. 11.1.5).

Example 11.6 *Rheological characterization of xanthan solutions.* Kold (2010) compared different instruments for rheological characterization of fermentation media, both off-line and during cultivations of *Xantomonas campestris* and *A. oryzae*.

Figure 11.7 shows the average result of five sweeps τ *vs.* $\dot{\gamma}_{av}$ in a cone-and-plate rheometer. In this instrument, a very flat cone resting on a horizontal plane is rotated. The fluid to be investigated is between the cone and the horizontal plane, and the distance b between the cone and the plate is $b = R \sin\theta \approx R\,\theta$, where θ is the (small) angle between the cone and the plate.

Bird et al.(2002) derive the formulas for determination of $\dot{\gamma}_{av}$ and the torque To in a cone-and-plate rheometer:

$$\dot{\gamma}_{av} = \omega/\theta = N/(2\pi\theta), \text{ where } \omega \text{ is the angular velocity of the rotating cone} \tag{1}$$

$$\tau(\text{shear stress}) = \frac{3To}{2\pi R^2}. \tag{2}$$

When the torque acting on the shaft is measured for different N, the ordinate and abscissa on Fig. 11.7 are determined from (1) and (2).

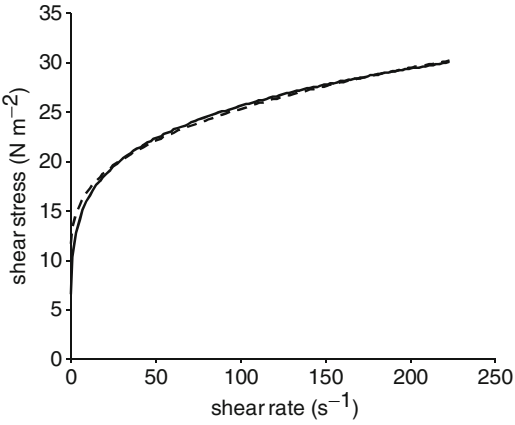

Fig. 11.7 Rheological characterization of a 1.50 wt% aqueous xanthan solution. *Solid line*: $\tau = 10.21\dot{\gamma}^{0.199}$, *Dashed line*: $\tau = 10.2 + \dot{\gamma}^{0.35}$. The data are from Kold (2010)

From the 5 sweeps Kold (2010) determined $n = 0.199 \pm 0.002$ and $K = 10.21 \pm 0.33$ in a power law expression (11.26) for a 1.50 wt% xanthan solution.

Whereas K increased almost proportional to the xanthan concentration c_{Xa} from 0 to 1.50 wt%, the value of n showed an irregular behavior as a function of c_{Xa} with a maximum (0.37) for $c_{Xa} = 0.25$ wt%, a minimum (0.1) at 0.75 wt%, and thereafter increasing to 0.2 at 1.50 wt%.

One may speculate that the power law model for xanthan solutions in water is not really good.

Thus, on Fig. 11.7 the decrease of τ for $\dot{\gamma}_{av} \to 0$ is very rapid (as ${\dot{\gamma}_{av}}^{-0.8}$), and the data could equally well be represented by a yield stress τ_0 + a power law term:

$$\tau = \tau_0 + K{\dot{\gamma}_{av}}^{n} \quad \text{with} \quad \tau_0 = 10.2 \text{ and } n = 0.35. \tag{3}$$

It should finally be mentioned that all five rheometers used in the study of Kold (2010) gave nearly the same values of n for all xanthan concentrations measured. The value of K differed by a few per cent.

It is obvious that the flow of viscous fluids is very different from that of nonviscous fluids like water. With apparent viscosities of xanthan solutions being 2 to 3 orders of magnitude higher than for water at small values of $\dot{\gamma}_{av}$(i.e., for small values of N) the flow is probably in the transitional region. For fluids with even higher viscosity the flow is laminar, and according to Fig. 11.4, N_p is very large. This results in a very high power requirement P, unless one accepts a very long mixing time t_{mix}. The apparent viscosity η_{app} decreases rapidly with increasing N, especially when $n \ll 1$ and the fluid exhibits strong pseudoplastic behavior. But the torque To on the shaft may become unacceptably high for high N, and one will have to turn to special agitators with low N_p to obtain a satisfactory mixing time (and hence also an acceptably high mass and heat transfer coefficient).

The phenomenon of "*cavern formation*" may ruin every hope of obtaining a satisfactory mixing of a highly viscous fluid: Due to the high mixing intensity near the impeller the fluid viscosity is low in this region while the fluid at some distance from the stirrer remains almost stagnant If $\tau < \tau_0$, the yield stress, the fluid does not move at all.

This results in the formation of a well-mixed cavern around the agitator.

The cavern is centered on the agitator, and its dimensions H_c and T_c are related by $H_c/T_c \approx 0.4$ for most agitators (e.g., Rushton turbines).The influence of N and of power input per mass, P/M on the size of the cavern are given by the following relation (Nienow (2010)):

$$\left(\frac{T_c}{d_s}\right)^3 = 0.138 N_p \left(\frac{\rho_l N^2 {d_s}^2}{\tau}\right). \tag{11.33}$$

The relation holds for $H_c/T_c = 0.4$. τ is determined from the relation between N (i.e., the shear rate) and the shear stress.

When $T = T_c$ the cavern extends to the reactor wall. Equation (11.33) is used to calculate the value of N required for this to happen. Once the cavern extends to the reactor wall its height H_c only increases slowly with N (from $\approx 0.4\ T$). Since P increases as N^3 by (11.10) it is definitely advantageous to install multiple agitators at a vertical distance of $\approx 0.4\ T$.

Thus, in cultivations where the medium becomes very viscous with increasing conversion of the substrate (either by the growth of a branched, entangled mycelium or by excretion of a viscous product such as a polysaccharide) it is advisable to use a large agitator diameter d_s to reduce the power (the N in (11.33)) to reach $T_c = T$. Multiple agitators should be used to counteract the effect of the slow increase of H_c with increasing power input.

11.1.5 Rotating Jet Heads: An Alternative to Traditional Mixers

In 2004, a mixing system based on rotating jets was patented (Hummer 2004). The use of rotating jet heads for mixing liquid, liquids and gas, and liquids and solids was a spin-off from the tank cleaning system of the Danish Toftejorg company. Effective cleaning-in-place (CIP) of, e.g., large oil tanks was achieved by sprinkling the walls with powerful jets of cleaning fluid. The construction of the sprinkling system allowed the liquid jets to change direction in a pattern which was repeated every 2–3 min. This enabled every part of the tank to be hit by the powerful jets, following a regular time-schedule. The house of a Toftejorg® rotating jet head (RJH) is shown in Fig. 11.8.

The characterization of RJH for *submerged mixing* was done during 2001–2003 at DTU (Nordkvist et al. 2003), and after the formation in 2003 of the Iso-Mix company (since 2009 a part of Alfa Laval) RJH mixers have been used in a large number of, particularly food related, industries.

De-oxygenation of vegetable oils and water for beer production, mixing of ingredients and dissolution of solids in large liquid volumes are typical applications. The RJH has not yet received widespread use in bioreactors, but a considerable number of RJH are installed in the large bioreactors of the brewing industry.

Lactobionic acid production by Novozymes (see Example 6.4) is another bioprocess application, and the study of Kold (2010) indicates that also in filamentous fermentations advantages may be obtained by the use of RJH rather than mechanical mixers – see Fig. 11.15.

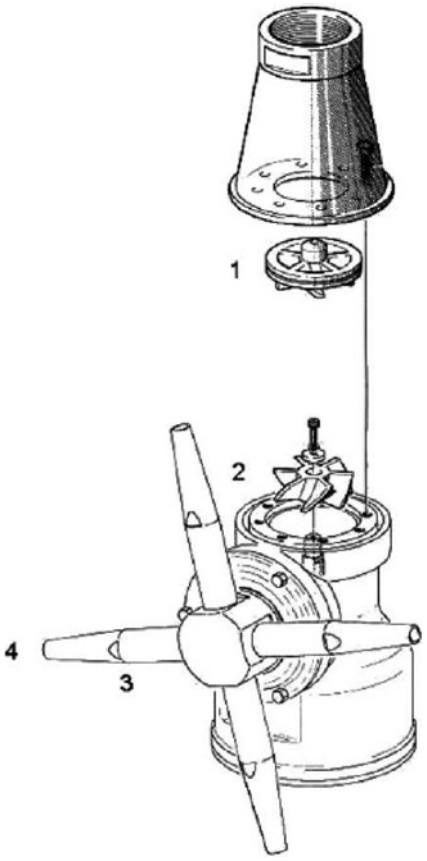

Fig. 11.8 IM 20 Rotary Jet Head (http://www.Iso-Mix.com). Liquid is pumped from the bottom of the tank and circulated to the top of the mixer. (1) Flow guide (2) Turbine which makes the RJH rotate slowly in the horizontal plane. (3) The four distributor arms are also set into a slow rotation, but the distributor arms rotate in a vertical plane. (4) Jets of liquid are sprayed into the tank through four nozzles. The jets uniformly sweep the reactor volume. Length of machine 356 mm (top to bottom) Weight 12.2 kg. Nozzle-diameter: 8, 9, or 10 mm (interchangeable). $N = 3.5$ rev min^{-1}at 10 bar gauge pressure, and $v_l = 46$ m^3 h^{-1}.

The reason for including a discussion of RJH in the present chapter is to show that the same basic principles for mixing that have been outlined earlier in this section also apply to a mixing system which is based on a completely different mixing concept than that of rotating mechanical stirrers. There are advantages in both systems, but despite the obvious differences between stirrers and RJH the power input to achieve a certain degree of mixing or a certain mass transfer rate is determined by analogous formulas.

Figure 11.9a is a schematic representation of the 3.4 m^3 pilot plant used to characterize the RJH in Nordkvist et al. (2003). Hua et al. (2006) used a 600 L pilot plant to study lactobionic acid production, as a preliminary to an industrial production (by Novozymes). A 20 m^3 plant has also been used to study mixing in near-industrial scale. Figure 11.9b shows the four sweeping jets in a 400 L transparent tank which was used for visualization of the mixing process.

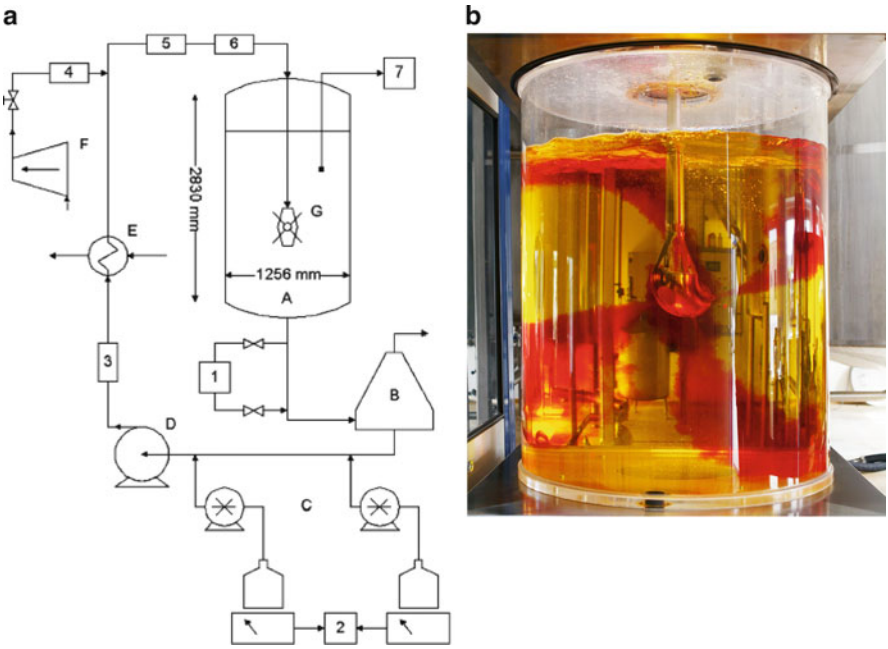

Fig. 11.9 (**a**) 3.4 m^3 (maximum working volume) tank used to characterize mixing by RJH. The circulation loop has a volume of 70 L when the degasser *B* is bypassed. *A* Tank, *B* Degasser used when gas is injected into the loop from the compressor *F*, *C* Positive displacement pumps for injecting tracers, *D* Centrifugal pump, *E* Heat exchanger, *G* Rotating jet head. Instruments: (1) pH electrode, (2) Balances for chemicals, (3) and (4) Mass flow-meters for liquid and gas. (5) Temperature sensor, (6) Pressure transmitter, (7) Oxygen electrode. (**b**) 400 L transparent tank used for visualization of the mixing process. A base-pulse is injected through the RJH, and the color of the acid base indicator (methyl-orange) in the tank changes from yellow to red

An energy balance which equates the potential energy of the liquid that reaches the nozzles to the kinetic energy of the jets injected into the liquid gives the following relation for *unaerated* liquid flow:

$$v_l \Delta p = \frac{1}{2}\rho_l v_l \left(\frac{v_l}{A_d}\right)^2, \text{ where } \rightarrow \Delta p = \frac{1}{2\pi^2}\rho_l n^{-2} {v_l}^2 d^{-4} \text{ since } A_d = 4n\left(\frac{\pi}{4}d^2\right), \tag{11.34}$$

Δp is the pressure difference between the pressure in the loop after the pump D on Fig. 11.9a and the pressure at the point of injection into the liquid. A_d is the total nozzle area with n RJH, each of which has four nozzles as shown on Fig. 11.9a. d is the diameter of each nozzle at the point of injection.

The pump is required to deliver the following power input:

$$P = \Delta p v_l = \frac{1}{2\pi^2}\rho_l n^{-2}\left({v_l}^3 d^{-4}\right) = 1,086 {v_l}^3 d^{-4} n^{-2} (\mathrm{W}). \tag{11.35}$$

The factor 1,086 is obtained when the medium is water ($\rho_l = 1{,}000\ \mathrm{kg\ m^{-3}}$), and [$v_l$, d, P] are in units of [$\mathrm{m^3\ h^{-1}}$, mm, W].

Equation (10.35) shows that the power input P to discharge the liquid at a given rate v_l depends very strongly on the nozzle diameter d. If v_l is discharged through n RJH, each with four nozzles and the same d, the power requirement decreases appreciably, compared to using one RJH.

When gas is pumped at a volumetric rate v_g from the compressor F into the circulating liquid on Fig. 11.9a and dispersed with the liquid into the tank Nordkvist et al. (2003) derived the following expression for the volume v_l of *liquid* dispersed into the tank:

$$v_l = 0.1599 n d^2 \Delta p^{1/2} \frac{\sqrt{1 + \alpha \frac{n_t p_t}{\Delta p} \ln((\Delta p + p_t)/p_t)}}{1 + \frac{n_t p_t}{\Delta p + p_t}((\Delta p + p_t)/p_t)^{\beta}}. \tag{11.36}$$

In (11.36) n_t is the ratio between v_g and v_l *at the pressure* p_t *of the tank*. α and β are empirical constants to be found by flow experiments. For water $\alpha = 1.41$ and $\beta = 0.587$ based on regression of many data obtained in the tank, Fig. 11.9a, at different v_g and v_l. The last factor in (11.36) is a (dimensionless) correction factor to (11.35). It is a weak function of Δp, and to find the required Δp for a given v_l and n_t, a good first approximation is obtained from (11.35). The constant 0.1599 requires [v_l, d, Δp] in units [$\mathrm{m^3\ h^{-1}}$, mm, bar].

Derivation of the somewhat complicated semiempirical relation (11.36) assumes that the gas expansion at the nozzles is neither completely isothermal nor reversible. This is the reason for the two empirical constants α and β. With v_l given by (11.36) – and assuming that all power input results from the pumping of the liquid at rate v_l, the power input for a certain n_t is given by the last expression in (11.35), where Δp is found by solution of (11.36) for each [v_l, n_t].

Formulas (11.35) and (11.36) are shown to fit experimental data very well in the range $3 < v_l < 45\ \mathrm{m^3\ h^{-1}}$, with $3.9 < d < 10$ mm, and with one or two RJH to dispense the liquid (a large v_l will require more than one RJH to avoid an excessive Δp).

Mixing experiments were carried out (Nordkvist et al. 2003) to obtain a relation between $t_{\mathrm{mix},0.95}$ and v_l or P for Newtonian liquids with η in the range 10^{-3} $\mathrm{kg\ m^{-1}\ s^{-1}}$ (water) to 137 $\mathrm{kg\ m^{-1}\ s^{-1}}$ (1.5 wt% carboxy-methyl cellulose (CMC)).

When the tracer (acid or base as described in Example 11.3) was added to the liquid (water) surface of the $V = 3.4\ \mathrm{m^3}$ tank of Fig. 11.9a one obtained

$$\begin{aligned} t_{\mathrm{mix},0.95}(\mathrm{s}) &= 1{,}600\left(v_l\left(\mathrm{m^3 h^{-1}}\right)\right)^{-0.925} \\ &= 9.45 \times 10^3 d(\mathrm{mm})^{-1.23} n^{-0.616}\left(P/V\left(\mathrm{W\ m^{-3}}\right)\right)^{-0.308}. \end{aligned} \tag{11.37}$$

The second expression was found when v_l was expressed in terms of P using (11.35). In (11.37) P is scaled by V (= 3.4 $\mathrm{m^3}$), and although (11.37) is based on measurements in large P/V interval ($0.05 < P/3.4 < 3.2$ kW $\mathrm{m^{-3}}$) and nozzle

diameter ($5.5 < d < 10$ mm), only one liquid volume ($V = 3.4$ m^3) was used. Hence, the scaling of P shown in (11.37) is not proved by this series of experiments.

Note 11.2 *In the design of RJH: Can power input P be scaled with medium volume V?* In another set of experiments with the 3.4 m^3 tank where the liquid was 1.5 wt% CMC, and the tracer was added to the surface, Nordkvist et al.(2003) found that for $d = 7$ mm, $n = 1$, and $V = [1.7, 2.2, 3.4]$ m^3 the mixing time was very well fitted by

$$\begin{aligned} t_{\mathrm{mix},0.95}(\mathrm{s}) &= 4,947\left(P/V\left(\mathrm{W\ m^{-3}}\right)\right)^{-0.463} \\ &= 54.2 \times 10^3 d(\mathrm{mm})^{-1.23} n^{-0.616}\left(P/V\left(\mathrm{W\ m^{-3}}\right)\right)^{-0.463}. \end{aligned} \tag{1}$$

The result (1) might indicate that the relation (11.37) between power input P/V and t_{mix} is true: The power input needed to obtain a certain value of t_{mix} is proportional to the liquid volume V.

Later studies by Nordkvist et al. (2008) have slightly modified this conclusion, and it seems that an influence of the nozzle diameter d should also be included in (1).

The exponent of P/V in (11.37) is derived for water as medium. In (1) the medium is the much more viscous 1.5 wt% CMC solution. This explains the different exponents to (P/V) and also the large difference between the two constants in the expressions. More important, the Re number for the two fluids is quite different. When working with water Re was $\approx 10^5$, i.e., the flow was fully turbulent. For the experiments with 1.50% CMC solution Re is estimated to be ≈2,000, and the flow was in the transient region. Only at high v_{l} (or P/V) will the turbulent region be reached for the 1.50% CMC solution.

Since the flow regime for the CMC experiments is different from that used in the experiments with water, one is not really sure that the result of (1) carries over to aqueous solutions. More experiments with tanks of varying V and H/T must be performed to prove wheather the scaling of P with V is correct or not. If it is correct, it would greatly simplify the design of RJH mixers, but unfortunately large scale pilot-plant research in the mixer industry is rare.

Addition of the tracer to the top of the liquid is, of course, not the right thing to do in a RJH system, especially since the mixing must be very fast when the liquid is injected as a powerful jet into the reactor medium. With $v_{\mathrm{l}} = 20$ m^3 h^{-1} the holding time in a tank with 3.4 m^3 liquid is 0.17 h = 612 s. A tracer added at the top is diluted by the bulk mixing action of the jets (see Fig. 11.9b) and slowly transported to the bottom of the tank to be mixed efficiently by the passage through the loop and reinjection into the tank.

Hence, in the study made by Nordkvist et al. (2003) mixing experiments were also made, where tracer was added to the loop before the pump D on Fig. 11.9a.

The result is dramatic for water, and for $0.5 < P/V < 2.5$ kW m^{-3} the mixing time $t_{\mathrm{mix},0.95}$ was approximately constant at about 20 s. Since the time for a pulse injected in the loop to reach the pH electrode is of the same order of magnitude one concludes that even a small P/V is sufficient to fully mix a tracer into 3.4 m^3 water. For viscous liquids the difference in t_{mix} between "feed at the top of the reactor" and "feed in the loop" is relatively much smaller.

In (11.10) the power input to a mechanically stirred tank is given. When N is substituted by the expression in (11.6) one obtains

$$P = N_p \rho_l N^3 d_s{}^5 = (N_p N_f{}^{-3} \rho_l) v_{pump}{}^3 d_s{}^{-4}. \tag{11.38}$$

The power input to a mechanically stirred tank is determined by an expression which is structurally the same as that for a RJH and given by (11.35). The variables have different interpretation ($v_{pump} \rightarrow v_l$ and $d_s \rightarrow d$), and the numerical constants are different.

This observation confirms the previously given statement that all mixing equipment basically have a power input that depends in the same fashion on operation and design variables, although the power drawn to obtain a given performance (mixing time, $k_l a$, etc.) differs between different mixers.

When (11.6) is inserted in (11.21) one obtains for a mechanically stirred tank with $H = T$:

$$t_{mix,0.95} = 5.3\ N_p{}^{-1/3} N_f \frac{d_s T^2}{v_{pump}} = \left(5.3\pi N_f N_p{}^{-1/3}\right)\left(\frac{v_{pump}}{V}\right)^{-1}\left(\frac{d_s}{T}\right). \tag{11.39}$$

Again the structure of (11.39) is very similar to that of (11.37) (assuming that the proportionality between P and V found in the CMC experiments holds). The exponent of (v_{pump}/V) is not quite -1 as it should be to make (11.37) dimensionless, but this is due to the regression of t_{mix} on v_l obtained from the experimental data.

Comparison of (11.39) and (11.37) shows that whereas t_{mix} for the mechanically stirred tank depends on the design of the agitator through d_s/T this may not be not the case for the RJH.

The rotation of the jets in a more or less spherical volume around the jet head creates a uniform mixing pattern that is independent of the tank dimensions as long as the jets do not reach the tank walls, or d_s is so large that the jets loose their kinetic energy very close to the jet head. This would be the rationale for placing multiple RJH in a large reactor.

Note 11.3 *Mixing with stationary jets.* For a stationary jet head (usually inserted through the tank wall at an angle of $\approx 45^o$) Grenville and Tilton (1996) obtained the following three different scales:

$$t_{mix,0.95} = 1.95 \frac{Z^2}{u_d d}, \tag{1}$$

where Z is the free path of the jet (m). d is the nozzle diameter (m) and u_d the linear velocity in m s^{-1} at the nozzle outlet. The range of $f = u_d\ d/Z$ that was tested is $0.013 < f < 0.137$ m s^{-1}.

Again, one will find that the power input to reach a certain t_{mix} for a stationary jet is given by a formula with the same structure as (11.10) and (11.35). In (1) t_{mix} is inversely proportional to $u_d\ d$ (Z is a function of the tank geometry), while t_{mix} for the RJH is inversely proportional to v_l, i.e., to $u_d\ d^2$ when the tracer is added to the top of the tank as in (11.37). When tracer is added to the loop of the RJH system t_{mix} depends somewhat on d (apart from

on v_l^{-1}), but not nearly enough to explain the difference between (11.41) and (11.37) (unpublished results).

It is concluded that the RJH operates differently from the stationary jet, and the reason is probably that large, almost stationary unmixed zones develop when a fixed-position jet is used. This subject was further investigated in Nordkvist et al. (2008) by artificially blocking the two-dimensional rotating pattern of the RJH machine on Fig. 11.8.

The discussion of mixers based on stirrers and on jets leads to the following conclusions:

1. Mixers of widely different design concept have a power input that depends in much the same way on key design and operation values. The outcome of the power consumption can vary considerably depending on the mixing concept. This is an incentive to strive for better designs.
2. Compared to mechanical stirrers, in particular Rushton turbines, baffles are unnecessary in RJH mixers. The operation of a RJH does not require a shaft with sterile inlet from the motor, since the power to dispense liquid and gas in the bulk volume is provided by a stand-alone pump. The RJH is in hydrodynamic balance when hung at the end of the loop (one hardly feels the motion of the RJH from outside the tank).When several RJH mixers are evenly distributed in the tank volume one overcomes the main disadvantage of Rushton turbine, the formation of axial compartments for large H/T. Thus, RJH can be used in fed-batch cultivation, and the mixers in the upper level of the reactor are started when the liquid level rises.
3. Mechanically stirred mixers, especially the Rushton turbine, can deliver a higher power input than other mixer types, e.g., the RJH. When a very high $k_l a$ is desired the power input to reach a given $k_l a$ is smaller in Rushton turbines than in RJH, unless the high v_l (calculated from (11.35)) is obtained using several RJH with a large d. This point was discussed in Nordkvist et al. (2003) where several expressions from Table 10.4 and other references were compared with rotating jet heads. A really high value of $k_l a$ can probably best be obtained using static mixers placed rather close in a loop as discussed in Example 9.12 in the design of a commercial plant for SCP production. Here, the issue becomes to balance the power cost with the loss of a substrate (O_2 in Example 9.12) or a higher capital cost (more reactors than the 35×30 m^2-reactors calculated in Example 9.12). Static mixers are not discussed in the present text, but design information can be obtained, e.g., from the homepage of Sulzer Chemtech.
4. The choice between mixers can also depend on less tangible quality criteria. One of these is the degree to which integrity of the culture is protected during the mixing process.

   Whereas bacteria and yeast are unlikely to be damaged by the mixing aggregate due to their size and very stable cell wall this may not be the case for filamentous fungi, and mammalian cells are definitely susceptible to shear stress damage. Some filamentous fungi, such as *A. oryzae*, function equally well also when the hyphae are ruptured while penicillin production by *P. crysogenum* is severely compromised when the hyphae break due to stirrer-induced

mechanical stress (see Figure 8.7). On the other hand, the break up of clumps or pellets of hyphae enhances substrate transfer to the cells. Rushton turbines may damage cells in the cavities behind the blades, but the passage of cells through the pump and the narrow apertures in the RJH are possibly equally damaging, and clumps of cells might stick in these tight locations. Another issue is the manner in which a mixing aggregate influences the shear thinning of highly viscous liquids or slurries, both locally and globally. Formulas similar to those of Table 10.4 for calculation of $k_l a$ are supplemented by a factor ${\eta_{app}}^{\beta}$ with β anywhere between -0.5 and -1, but the accuracy of the prediction is poor and different results are obtained for different mixers due to the uncertainty by which the "true" η_{app} has been obtained. When gas is to be transferred to a viscous medium, large bubbles (most of the v_g) occur together with many small bubbles. The distribution between small bubbles and large bubbles is different in different mixing aggregates, and consequently it is difficult to predict $k_l a$ based on the few, generally accepted variables used in the text. As a rule one should, however, avoid mixing systems in which very viscous liquids are re-circulated to the tank by means of centrifugal pumps. Many small bubbles are entrained in the circulated liquid and they may severely compromise the function of the circulation pump. Here, positive displacement pumps should be used.

11.2 Scale-Up Issues for Large Industrial Bioreactors

In Sect. 11.1 the (mostly) empirical tools for design of mixing aggregates have been discussed, namely their power requirement and the mixing efficiency for a given power input. In several places it was apparent that the geometrical dimensions of the reactor had a crucial effect on the power input needed to achieve a given goal, e.g., a high value of a mass transfer coefficient.

In the present section these observations will be collected with the intention of showing the best possible way to reach a certain objective, given the restrictions that are imposed by the available power input and mechanical stability of the tank + mixer construction. The discussion will at best be qualitative, mostly because the science of mixing has not yet reached maturity, but some guidelines will be provided. Also, techniques which in the past have often been used to predict the effect of scale-up, namely *scale down* and *regimen analysis* will be discussed.

11.2.1 Modeling the Large Reactor Through Studies in Small Scale

In principle the velocity field for any fluid can be derived from Newton's second law applied to fluid motion, assuming that fluid stress is the sum of a diffusive

(viscous) term and a pressure term. This fundamental relation between the pressure, velocity, and the material properties viscosity and density, is the Navier–Stokes equation[2] which states that the time rate of change of momentum in a fluid volume is the sum of pressure forces, viscous forces and gravity forces acting on that volume. For a one-phase incompressible flow, i.e., when $\nabla \mathbf{u} = 0$, the equation can be compactly written using vector notation as

$$\rho_\mathrm{l} \frac{D\mathbf{u}}{Dt} = -\nabla p + \eta_\mathrm{l} \nabla^2 \mathbf{u} + \rho_\mathrm{l} \mathbf{g} \tag{11.40}$$

where p is the pressure, $\mathbf{g}$ is the gravity vector, ∇ is the gradient operator, and ∇^2 is the Laplacian operator. (For translation of these operators into the correct component equations for the respective coordinate system, see, e.g., Bird et al. 2002).

The left hand side of (11.40), the so-called material derivative, can be expanded into

$$\frac{D\mathbf{u}}{Dt} = \frac{\partial \mathbf{u}}{\partial t} + \mathbf{u} \cdot \nabla \mathbf{u}. \tag{11.41}$$

The Navier–Stokes equation can be transformed into dimensionless form, in which the Reynolds and Froude numbers, Re and Fr, occur. The choice of characteristic length depends on the geometry of the system studied. For a stirred tank reactor, the impeller diameter is often chosen. The dimensionless form of the Navier–Stokes equation reads

$$\frac{D\mathbf{u}^*}{Dt} = -(\nabla p)^* + \frac{1}{\mathrm{Re_s}} \nabla^2 \mathbf{u}^* + \frac{1}{\mathrm{Fr}} \mathbf{g}^*, \tag{11.42}$$

where

$$\mathbf{u}^* = \frac{\mathbf{u}}{N d_\mathrm{s}} \mathbf{g}^* = \frac{\mathbf{g}}{g}; \ \mathrm{Re_s} = \frac{\rho_\mathrm{l} N {d_\mathrm{s}}^2}{\eta}, \mathrm{Fr} = \frac{d_\mathrm{s} N^2}{g}. \tag{11.43}$$

From (11.42), the Reynolds number is seen to be a parameter in the governing flow equation, which further justifies its appearance in simplified correlations for flow-related phenomena. In baffled reactors, the influence of the Froude number, i.e., the influence of gravitational forces, on the flow pattern is normally small.

[2]Claude Louis Navier and George Gabriel Stokes probably never met. Stokes (1819–1903) matriculated (Pembroke College, Cambridge) in 1837, the year after the death of Navier (1785–1836), but both contributed greatly to the development of Fluid Dynamics. In 1822, Navier who had little knowledge of the shear stress concept, i.e., on motion with friction, still developed the correct form of the equation. Stokes who held the Lucasian professorship at Cambridge from 1849 to his death put Fluid Dynamics on the right physical foundation in a series of papers from the 1840s. Both Navier and Stokes are to be counted among the giants of Applied Science and they were experts in many fields of Engineering, e.g., bridge-building.

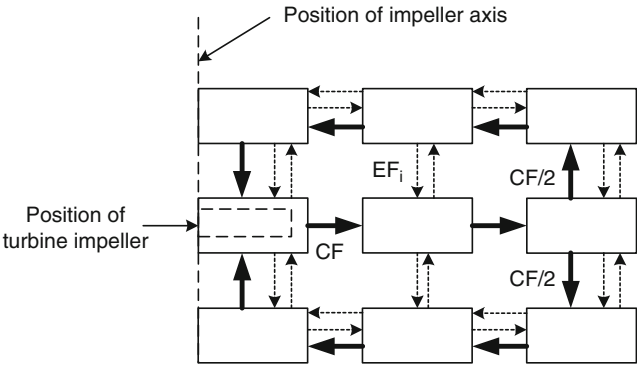

Fig. 11.10 Representation of an axial-symmetric compartment model of a stirred tank reactor equipped with one turbine impeller giving a radial flow pattern. Each compartment is assumed to be ideally mixed. The picture shows the right half of the reactor cross-section. The *thick arrows* represent the main circulation pattern (flow rate = CF along the central axis, which is split into two flows CF/2 at the reactor wall), and the *dotted arrows* represent the exchange flows between the compartments. The exchange flows, EF_i, need to be modeled for each individual compartment

For flow in stirred tank bioreactors, two important complications arise:

1. The flow is normally turbulent, and numerical calculation of a stable solution to Navier–Stokes equation for turbulent flow is difficult since the very different mixing lengths scales requires a fine-mesh resolution.
2. The flow is not a one-phase flow, since both gas and liquid are present. This makes it necessary to introduce modeling assumptions concerning both turbulence and two-phase flow before a numerical flow pattern can be calculated.

In many recent papers on bioreactors, simulated flow patterns are shown. These patterns result from numerical simulations using Computational Fluid Dynamics (CFD) which again is based on (11.40). The pictures give a very good visual representation of the velocity field, and may help to focus on scale-up issues, but they are only approximations of the true velocity field, and it may be difficult to apply simulation results from one reactor configuration to the design of even a slightly different reactor configuration.

For these reasons many studies – e.g., the yeast and *E. coli* investigations mentioned in the introduction to Sect. 11.1 – have approached the challenge of scale-up by analyzing the process in small scale. They use experiments to fit the parameters in a model which, at least to some extent describes the reactor by means of a number of *compartments* with different environmental conditions (e.g., oxygen tension or glucose concentration). The compartments exchange matter by simple "diffusion" mechanisms.

Figure 11.10 shows a typical compartment model which suggests an exchange of flows in the regions around each Rushton turbine (Vrabel et al. 2000).

The exchange flows EF_i on Fig. 11.10 can be driven by turbulent diffusion or by the dispersion of gas in the medium. Although helpful in visualizing the mixing

Table 11.2 Design data for the reactor modeled by Oosterhuis and Kossen (1983)

Property	Notation	Value
Ratio: stirrer to tank diameter	d_s/T	0.32
Number of impellers	n	2
Stirrer rate	N	2.6 s^{-1}
Baffle diameter/vessel diameter	d_{baffle}/T	0.09
Number of baffles		4
Liquid volume	V_l	varying – up to 25 m^3

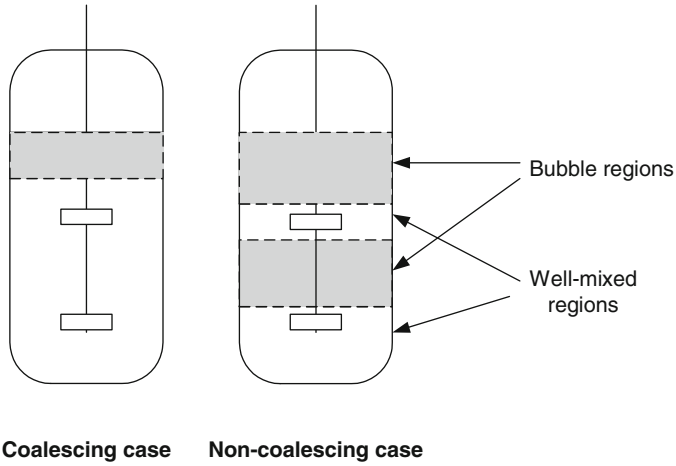

Fig. 11.11 The compartments defined in the Oosterhuis and Kossen model

processes, the models used to describe the exchange flows are speculative, and scale-up based on the modeling study is at best risky.

Example 11.7 *A two-compartment model for oxygen transfer in a large bioreactor.* An illustration of the usefulness of a simple compartment model is given by Oosterhuis and Kossen (1983). These authors were concerned with the validity of using (10.26) for calculation of oxygen transfer rates with the same parameter values in widely different scales. A bioreactor equipped with two Rushton turbines was used in the study, and the basic data for the reactor is given in Table 11.2 (Fig. 11.11).

The specific aerobic reaction is not stated in the paper, but it is described by Monod type kinetics. The dissolved oxygen concentration was measured in the reactor by a movable oxygen electrode, which allowed measurement at different axial positions. Furthermore, the overall oxygen transfer rate was calculated. The measurement showed (as could be expected) that the oxygen concentration was not constant throughout the reactor space. Furthermore, the oxygen transfer rate was overestimated using a single correlation for k_la of the type given by (1) or (2).

To better model the oxygen transfer rate, the reactor was divided into one or two well-mixed regions close to the impellers and one or two bubble regions (i.e., regions which

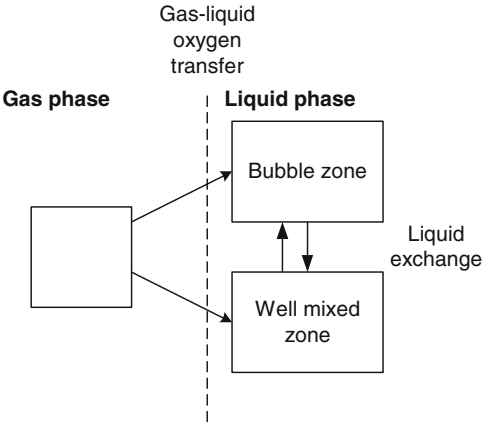

Fig. 11.12 Schematic representation of the oxygen transport processes

behave like bubble columns) one located in the top part of the reactor and the other located in the region between the turbines as shown in Fig. 11.12. For a coalescing medium, i.e., for the case where the time for coalescence was lower than the circulation time, only one well-mixed region and one bubble region was used. For the case of a non-coalescing medium, the time for coalescence to occur was expected to be larger than the circulation time. Here, two mixed regions and two bubble regions were used. The main reason for making this compartment division was that the oxygen transfer rate could be expected to be higher in the well-mixed region close to the impellers and somewhat lower in the bubble region, and two different correlations should be used for the gas–liquid mass transfer to the well-mixed and bubble regions, respectively (see Fig. 11.12).

The correlations for $k_l a$ for the well-mixed region (subscript m), and for a coalescent medium was

$$k_l a_m = 2.6 \times 10^{-2} u_s^{0.5} \left(\frac{P_g}{V}\right)^{0.4}. \tag{1}$$

For a non-coalescent medium the following relation (see Table 10.4) was used:

$$k_l a_m = 2 \times 10^{-3} u_s^{0.2} \left(\frac{P_g}{V}\right)^{0.7}. \tag{2}$$

The $k_l a$ value in the bubble region (subscript b) was given by

$$k_l a_b = 0.32 u_s^{0.7}. \tag{3}$$

The top bubble region was assumed to start just above the top impeller in both cases. For the non-coalescing case, the volume of the well-mixed region, V_m, was assumed to be

$$V_m = n d_h T^2 \frac{\pi}{4} \tag{4}$$

where n was the number of stirrers (=2), d_h was the impeller blade height, and T was the tank diameter.

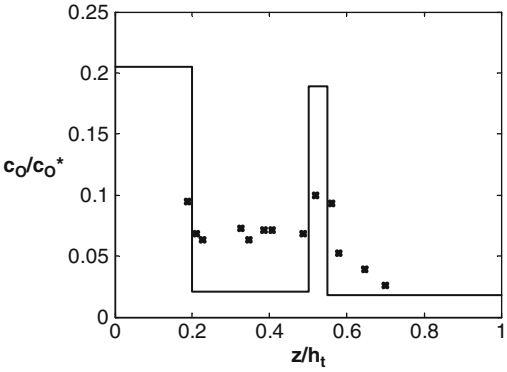

Fig. 11.13 Calculated O_2 concentration for coalescing case compared to O_2 concentration as a function of axial position in the reactor (Data from Oosterhuis and Kossen 1983)

The liquid flow between the compartments was estimated from the pumping capacity, v_{pump}, which was given by

$$v_{\text{pump}} = 0.2 N_{\text{A}} d_{\text{s}}^3 N. \tag{5}$$

In (5) N_{A} is the aeration number defined by (11.14). To make a balance for the gas phase, the gas hold-ups in the different compartments are needed. These were estimated from the power input in the impeller region and from the superficial gas velocity in the well-mixed region according to

$$(1 - \varepsilon_{\text{m}}) = 0.13 \left(\frac{P_{\text{G}}}{V_{\text{l}}} \right)^{0.3} u_{\text{s}}^{0.67}, \tag{6}$$

$$(1 - \varepsilon_{\text{b}}) = 0.6 u_{\text{s}}^{0.7}. \tag{7}$$

In the well-mixed regions steady-state conditions requires

$$k_{\text{l}} a_{\text{m}} (c_{\text{O}}^* - c_{\text{O,m}}) + \frac{v_{\text{pump}}}{V_{\text{m}}} (c_{\text{O,b}} - c_{\text{O,m}}) + q_{\text{O,m}} = 0. \tag{8}$$

Similarly for the bubble regions:

$$k_{\text{l}} a_{\text{b}} (c_{\text{O}}^* - c_{\text{O,b}}) + \frac{v_{\text{pump}}}{V_{\text{b}}} (c_{\text{O,m}} - c_{\text{O,b}}) + q_{\text{O,b}} = 0. \tag{9}$$

The oxygen concentration predicted by the compartment model in the non-coalescing case as well as the measured oxygen concentration are shown in Fig. 11.13.

Obviously, this simple compartment model will not be able to predict the observed, gradually changing oxygen concentration in the axial direction. However, qualitatively, the increased dissolved oxygen concentration close to the impellers is predicted. With respect to the overall oxygen transfer rate in the entire reactor volume, a better agreement was found using the compartment model than with either of the equations (1) or (2) – see Fig. 11.14.

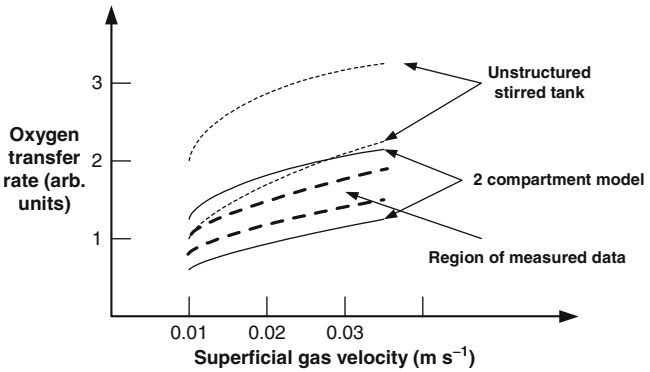

Fig. 11.14 Predicted O_2 profiles for different models as a function of u_s

Table 11.3 Characteristic times for important processes in fermentations

Process	Variable
Circulation	t_c
Mixing	$t_m \approx kt_c$ $(k = 4?)$
Gas flow	$t_{gas} = (1 - \varepsilon)V/v_g$
Gas–liquid mass transfer	$t_{otr} = 1/k_l a$
Biomass growth	$t_{bio} = 1/\mu$
Substrate consumption	$t_{sc} = s/(-q_s)$
Substrate addition	$t_{sa} = v_s/v_f s_f$

Figure 11.14 includes predictions (dotted lines) for an unstructured model (upper line) of one stirred tank based on (2) – and (lower line) a non-coalescent liquid. Results for a two-compartment model are shown with solid lines: non-coalescing, upper curve, and coalescing, lower curve. The experimental values of $q_o{}^t$ for $1.35 < H/T < 1.75$ are in the range shown on the figure.

This example shows that a better accuracy of predicted oxygen transfer rates may be obtained using a physically motivated compartment model of low complexity in combination with standard correlations for $k_l a$.

In *regimen analysis*, a popular method both in academia and in industry, one tries to identify limiting process steps through a study of the individual time constants, see Table 11.3 for a selection of time constants that are likely to be significant in scale-up.

Example 11.8. *Regimen analysis of penicillin fermentation.* In the literature, one finds many applications of time-scale analysis to identify the limiting regime in a given process (see Sweere et al. 1987 for a review). Here, we will consider the penicillin fermentation for which Pedersen (1992) found the characteristic times listed in Table 11.4. The characteristic times are given for the two different phases of a typical fed-batch fermentation (i.e., the growth phase and the production phase), carried out in a 41-L pilot plant bioreactor. The smallest characteristic time is certainly t_m (which was experimentally determined using isotope techniques). This indicates that no mixing problems arise during the fed-batch fermentation in the pilot plant bioreactor. Thus there will not be any concentration gradients for the substrates (glucose and oxygen). This conclusion will, however, definitely be different in a

Table 11.4 Characteristic times for a penicillin fermentation in a 41-L pilot plant bioreactor

Characteristic time	Growth phase (s)	Production phase (s)
t_m	1.5	1.5
t_{gas}	60.3	60.3
t_{otr}	22.2	22.2
t_{sa}	95.6	126.7
t_{oc}	11.5	12.4
t_{sc}	189.3	102.2

Table 11.5 Scale-up by a factor 125 from pilot reactor to industrial reactor

Property	Pilot scale (100 L)	Plant scale (12.5 m^3)			
P	1	125	3125	25	0.2
P/V	1	**1**	25	0.2	0.0016
N	1	0.34	**1**	0.2	0.04
d_s	1	5	5	5	5
v_{pump}	1	42.5	125	25	5
t_c	1	2.94	**1**	5	25
Nd_s	1	1.7	5	**1**	0.2
Re_s	1	8.5	25	5	**1**

All numbers are scaled to 1 in the pilot plant, while the numbers fixed in each column for the large reactor are shown in bold

Note that $d_s = 5$ (scaled value) in all four cases studied. Adapted from Oldeshue (1966)

large production vessel, where the mixing time may approach 20–50 s. The characteristic mixing time for mixing in the gas, t_{gas}, is high, indicating that this mechanism is slow. The characteristic times for glucose addition, t_{sa}, and glucose consumption, t_{sc}, are of the same order of magnitude. This is of course no surprise, since it was intended to keep the glucose concentration at a constant level by controlling the feed addition. Also, the characteristic times for oxygen supply, t_{otr}, and oxygen consumption, t_{oc}, are of the same order of magnitude. This indicates that oxygen limitations may occur if the oxygen supply for some reason fails or the oxygen requirements increase (e.g., due to an increasing feed addition of glucose). Thus the gas liquid mass transfer seems to be the limiting regime for this process, and this conclusion would be even more pronounced in a production-scale vessel.

Table 11.5 is based on a classical table published by Oldeshue (1966). It compares the values of eight important design variables when results obtained in a 100-L tank are to be used for design of a 12.5 m^3 tank. d_s is scaled by a factor 5 (linear scaling). In each of the four columns pertaining to the 12.5 m^3 tank one or (in one case two) of the variables have the same value 1 as in the 100-L tank. These variables are shown in bold numbers. The other variables now attain the values shown in the rest of the column, e.g., when P/V is kept at the same value as in the 100 L tank the power input increases by a factor 125, N decreases from 1 to $(125/5^5)^{-1/3} = 0.342$, etc.

The disturbing side of these, at most semiquantitative, methods is that the characteristic times for the separate processes tell nothing about the effect of, e.g., P/V on the productivity of penicillin in Example 11.8. Still, in Sect. 11.2.2,

we shall show two examples of design of a large reactor based on results from a smaller reactor. The tools we use are the quantitative scale-up rules of Sect. 11.2, illustrated by (11.6), (11.7), (11.10), (11.21), (11.35), and (11.37). Many of these expressions are of course used to obtain the numbers of Table 11.5.

11.2.2 Scale-Up in Practice: The Desirable and the Compromises

In Sect. 11.2.1 it was argued that calculation of mixing and mass transfer based on fundamental mechanisms and assisted by CFD computation of the velocity field is, *as yet*, not possible with any kind of confidence. The experimental and model-driven investigation of a small-scale look-alike of the large bioreactor is also fraught with approximations. Sometimes – e.g., with a nonlinear relation between shear stress and shear tension – the small-scale study must also be made with a medium very different from the actual medium, since the flow behavior in the large-scale reactor is governed by Re or Fr numbers that are much larger than in the small scale.

In the following section some general, but only semiquantitative, rules for scale-up will be discussed. Some of these rules follow from the discussion of the design equations for mixing systems in Sect. 11.1, and others will be introduced here.

A fool-proof method is to increase the production capacity by simply multiplying the number of small-scale, or pilot reactors. This is clearly safe in terms of the performance of each reactor. Unfortunately, the cost of building and servicing, say 20 reactors each of 5 m^3 working volume, is surely much larger than that of one 100 m^3 reactor. Consequently, one will have to rely on the results obtained in the small reactors, and attempt the physical scale-up, using the more or less accurate predictions suggested by, e.g., Table 11.5.

The data of Table 11.5 show that it will be impossible to maintain the same mixing time, mass transfer coefficient, etc., as were found in the small scale, and compromises will have to be made as shown in Examples 11.9 and 11.10.

The large reactor will typically be desired to have the same H/T and the same d_s/T as the smaller reactors, since intuitively this will make the scale-up more trustworthy. But as indicated above this may lead to quite unacceptable designs: d_s/T may have to be changed, and one may also have to accept that due to larger mixing time, mass- or heat exchange in the large scale may become less favorable than in small scale.

Example 11.9 *Scale-up of a 600-L pilot plant reactor to 60 m^3 for unaerated mixing*. In Examples 11.4 and 11.5 it was found that a tank with $T = 0.9$ m ($H = 0.94$ m) and with $d_s = 0.35$ *m* did a reasonable job for mixing an *unaerated* medium volume of 0.6 m^3 ($t_{mix,0.95} = 10.3$ s for a power input of 218.5 W or 0.364 W/kg).

When the reactor volume is increased by a factor 100–60 m^3 in a design where all linear dimensions are increased by a factor $100^{1/3} = 4.64$, one will obtain $T = 4.18$ m and $d_s = 1.624$ m.

Let us first assume that N is kept equal to 2 s^{-1}.

According to (11.10) the power input now needs to be $P = 470$ kW or 7.83 W kg^{-1}, i.e., not only has the total power input increased dramatically, but this is also the case for the specific power input P/M. This is due to the dependency of P/M on V which is as $(V/V_0)^{5/3}(V/V_0)^{-1} = (V/V_0)^{2/3} = 100^{2/3} = 21.5 = 7.83/0.364$.

A power input of 7.83 W kg^{-1}, or 7.83 kW t^{-1} is unacceptably high. In industrial practice 5 kW m^{-3} is considered an upper limit, and conversion of the mechanical energy to heat will also lead to high cooling costs. If, in attempt to avoid the high power cost, one decides to use the same power input 0.364 W kg^{-1} as in the pilot plant, then by (11.22) the mixing time increases by a factor $(T/T_0)^{2/3} = (V/V_0)^{2/9} = 100^{2/9} = 2.78$ from 10.3 s (Example 11.5) to 29 s. This, considerably longer mixing time may, as discussed in the introduction to Sect. 11.1, give rise to formation of undesired byproducts, but the total power input is now $0.364 \times 60 = 21.84$ kW, i.e., a factor 21.5 lower than the 470 kW calculated above. The example shows that in the large scale it costs a fortune to keep the mixing time low. A compromise must be made between operating costs and product quality.

If (11.21) is used to calculate t_{mix} rather than the identical formula (11.22), then t_{mix} remains constant if N^{-1} $(d_s/T)^{-2}$ is constant. If N is reduced from 2^{-1} to 1 s^{-1} and d_s increased from 1.624 m to $1.624 \times \sqrt{2} = 2.296$ m then t_{mix} remains the same, namely 10.3 s, for the 60 m^3 reactor as was found for the 0.6 m^3 reactor. $d_s/T = 0.55$ with the larger stirrer. In (11.10) P increases with N^3 and with ${d_s}^5$. Thus, a reduction of N by a factor 2 while d_s increases by a factor $\sqrt{2}$, leads to a *decrease* in energy input by a factor $2^3 \times 2^{-5/2} = \sqrt{2}$ to obtain *the same value of* t_{mix} as was found in the smaller scale reactor.

Thus, *in any mixing operation the power input to obtain a given quality of mixing decreases significantly when the stirrer diameter increases and the speed of rotation of the stirrer is simultaneously decreased*. In the example, the energy savings is formidable. For $[d_s, N] = [2.3\text{ m}, 1\text{ s}^{-1}]$ P is reduced to 332 kW and P/M to the more amenable 5.53 W kg^{-1}.

One could also use an agitator concept quite different from that of the Rushton turbine.

Consider the choice of 5 RJH with $d = 15$ mm. Five RJH are chosen, since one RJH with at most a nozzle diameter of 10 mm was used to cover the volume 3.4 m^3 in the pilot plant tank of Fig. 11.9a. The volume 60 m^3 can be expected to be covered by the overlapping jets of 5 RJH. A nozzle diameter $d = 15$ mm will give a reasonably small Δp even for the large v_1 used in the 60 m^3 tank, and still the flow field around the jet will be turbulent for several meters from the nozzle.

Assume that we wish to obtain the mixing time 29 s which was obtained with the Rushton turbine with a power input 0.364 W kg^{-1}.

Equation (11.37) can be solved to find P/V (=P/M for a water-like medium):

$$\frac{P}{V} = 8.08 \times 10^{12} \times n^{-2} d^{-4} {t_{mix}}^{-3.25}. \tag{1}$$

With $t_{mix} = 29$ s, $V = 60$ m^3, $d = 15$ mm and $n = 5$ machines one obtains

$$\frac{P}{V} = 8.08 \times 10^{12} \times 4 \times 10^{-2} \times 1.975 \times 10^{-5} \times 1.77 \times 10^{-5} = 113\text{ W m}^{-3}. \tag{2}$$

For $V = 60\ \mathrm{m}^3$ one obtains $P = 6.78$ kW. v_l is determined by inserting P in (11.35):

$$v_\mathrm{l} = \left(\frac{6,780}{1,086}15^4 5^2\right)^{1/3} = 199.2\,\mathrm{m}^3\mathrm{h}^{-1} \text{ distributed equally between the five RJH.} \quad (3)$$

Finally Δp is determined from (11.34):

$$\begin{aligned}\Delta p &= \frac{1}{2\pi^2} \times 1,000 \times \left(\frac{199.2}{5 \cdot 3600}\right)^2 (15 \times 10^{-3})^{-4} = 122,541\ \mathrm{N\ m}^{-2} \\ &= 1.23\ \mathrm{bar}.\end{aligned} \quad (4)$$

Even with feed to the top of the liquid (the best researched situation in Nordkvist et al. (2003)), the RJH solution seems to offer a reduction of P/M by a factor 364/113 = 3.2 compared to the Rushton turbine.

Also when a constant $t_\mathrm{mix} = 10.3$ s as obtained in the 600-L pilot plant is considered, the RJH seems to be a better solution than the Rushton turbine. Inserting $t_\mathrm{mix} = 10.3$ s in (1) gives

$$\frac{P}{V} = 3261\,\mathrm{W\ m}^{-3} \rightarrow P = 195.6\ \mathrm{kW}, v_\mathrm{l} = 611\,\mathrm{m}^3\mathrm{h}^{-1}, \text{ and } \Delta p = 11.6\ \mathrm{bar}. \quad (5)$$

Compared to the result for the Rushton turbine, the power input per m^{-3} is reduced by a factor 7.83/3.26 = 2.40. One might contemplate to use more RJH (or a larger d) for this demanding mixing situation with $t_\mathrm{mix} = 10.3$ s. In particular, the large Δp may be a problem.

Example 11.10 *Oxygen transfer to a 60 m³ industrial reactor*. In continuation of Example 11.4 we shall now scale-up the mass transfer from 0.6 to 60 m^3 scale.

The reactor has the dimensions $T = 4.18$ m and $H = 4.36$ m used in Example 11.4.

In the scale-up, the gas flow v_g is 100 times as large as in the pilot plant, corresponding to the larger medium volume $V = 60\ \mathrm{m}^3$. Consequently,

$$u_\mathrm{g} = 4\frac{v_\mathrm{g}}{\pi T^2} = 100^{1/3} \times 0.00262 = 0.0122\,\mathrm{m\ s}^{-1}. \quad (1)$$

It is seen that scale-up results in an increase of the superficial gas velocity by a factor $\left(\frac{V}{V_0}\right)^{1/3}$. This will increase the mass transfer coefficient, but also the risk of flooding the stirrer.

Consider the impeller diameter $d_\mathrm{s} = 1.624$ m calculated in Example 11.8 for $N = 2\ \mathrm{s}^{-1}$.

According to (11.18) flooding will occur for

$$N < N_\mathrm{F} = \left(\frac{9.81 \times 10}{60 \times 30}\right)^{1/3} 4.17^{7/6} \times 1.624^{-2.5} = 0.60\ \mathrm{s}^{-1} \quad (2)$$

N_Disp is calculated to $0.88\ \mathrm{s}^{-1}$, and for $N = 2\ \mathrm{s}^{-1}$, $N_\mathrm{A} = 0.019$. Compared with the small scale, both N_F and N_Disp have decreased on scale-up. *Thus, in a linear scale-up much more*

gas can be handled without risk of flooding. According to Fig. 11.5, $N_{p,g}/N_p$ is still about 0.5, but the figure is of qualitative character only since no values are stated for Fr on the two curves shown on the figure. With one Rushton turbine $N_{p,g} \approx 2.6$ and $P = 235$ kW or 3.91 kW m^{-3}.

One might follow the advice of (11.11) and install a mixing system with a smaller N_p than the Rushton turbine to increase the stirrer diameter, and thereby allow even more gas to be effectively dispersed *without changing N or P*. Thus, if a four-bladed Lightnin A 315 (Fig. 11.3a) is chosen, the diameter d_s can be changed to $1.624 \times (5.2/0.8)^{1/5} = 2.36$ m (=0.56 *T*) without incurring higher power costs.

Now, according to (11.14) the aeration number

$$N_A = \frac{v_g}{N d_s^3} = \frac{10}{60 \times 2 \times 2.36^3} = 0.0064 \tag{3}$$

Since N_A is very small $N_{p,g}/N_p$ is not much below 1, and the Lightning hydrofoil probably works quite efficiently. If the gas feed is increased from 10 m^3 min^{-1} the stirrer would still disperse the gas effectively without incurring further power costs. One should, of course be aware that the hydrofoil may not be able to draw the high power (235 kW) required. This would make the change in stirrer type impossible.

Finally, one may calculate the value of k_la in the 60 m^3 tank. Since the superficial gas velocity u_g is much higher in the large scale, *mass transfer will improve with increasing scale*.

Using the van't Riet expression, Table 10.4, for a coalescing liquid (water) one obtains $k_la = 0.026 \times 0.0122^{0.5} \times (235000/60)^{0.4} = 0.078$ s^{-1} = 283 h^{-1}, i.e., a mass transfer rate 7.25 times as large as in the 600 L scale.

Nordkvist et al. (2003) found relation (4) for mass transfer to an aqueous medium for $V = 3.4$ m^3:

$$k_la\left(s^{-1}\right) = 0.0958 {u_g}^{0.764} {v_l}^{0.700} \left(\left[u_g, v_l\right] \text{ in } \left[\text{m s}^{-1}, \text{m}^3 \text{h}^{-1}\right]\right). \tag{4}$$

For $t_{mix} = 29$ s, $v_l = 199.2$ m^3 h^{-1}. Each RJH is serviced by 199.2/5 m^3 h^{-1}, and when this volumetric flow is inserted in (4) together with $u_g = 0.0122$ m s^{-1}, one obtains $k_la = 0.0428$ s^{-1} = 154 h^{-1}. This result is lower than the result 283 h^{-1} obtained with the Rushton turbine, but following the results from Example 11.9, *P* is only 6.78 kW against 21.84 for the Rushton turbine, i.e, a factor 3.2 times smaller. If only 3 RJH had been used *P* had increased by the factor $(5/3)^2$ to 18.8 kW, and at the same time k_la increases by a factor $(5/3)^{0.7}$ to 220 h^{-1}. This result underlines the previously made statement, that *to obtain the same quality of the mixing one must use more or less the same power input in any sort of mixing equipment*.

The result (4) is, of course only true if each of 5 (or 3) RJH in the 60 m^3 tank cover the same volume as in the 3.4 m^3 tank–see Note 11.2. One needs to make more mass transfer experiments with RJH, both in large-scale reactors and with varying number of RJH in the tank. As yet the result obtained is only indicative of what one may expect to find in such experiments.

The two Examples 11.9 and 11.10 illustrate the main consequences of scale-up for key variables, such as the effect of power input on mixing time and mass transfer in different scales, and the formulas used are based on large experimental investigations in equipment that is often used in industrial practice.

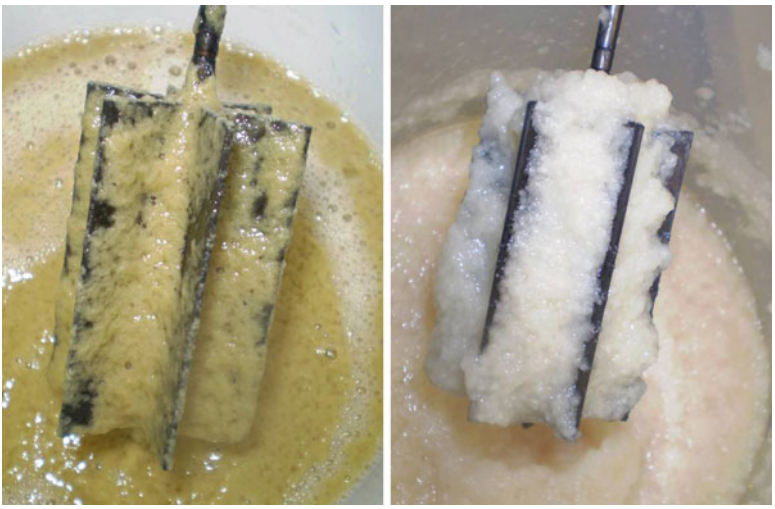

Fig. 11.15 *Aspergillus oryzae* cultivation in a 200-L working volume reactor. *Left picture*: One RJH (IM 15, $d = 7$ mm), $P = 1.6$ kW m^{-3} (at $t = 57$ h and 28.6 g X/kg medium). *Right picture*: Intermig-mixer, $P = 2.6$ kW m^{-3} (at 45 h cultivation and 22 g X/kg medium). Pictures from Kold (2010)

But new mixing equipment turns up in the market, such as the hydrofoils shown in Fig. 11.3 and the RJH of Fig. 11.8, and each new type of mixer must be evaluated to find its advantages compared to standard mixers. This evaluation must be done for both nonviscous, Newtonian fluids and for non-Newtonian fluids. Pseudoplastic fluids are common in industrial bioproduction. They always present problems due to our lack of understanding of the influence of the governing variables. We may not even find mixing equipment that does not break down due to excessive power input.

Figure 11.15 illustrates how difficult it is to conclude what each type of mixer does. The difference in rheology and morphology between cultivation with a RJH and another relatively new mixer-design, the Intermig, is clearly seen on the figure. The pellets in the porridge-like fluid on the right hand picture are not seen in the smooth, much less viscous fluid on the left hand picture. The color of the biomass is also different.

The simple, quantitative data, P and biomass produced after about 50 h cultivation, are easily compared, and especially in the power input the RJH has an advantage.

But the more important yield and productivity data for the recombinant protein produced by the fungus are not discussed in Kold (2010). The cells may have been much more damaged in the RJH then by the Intermig – thus explaining the much lower apparent viscosity. Other data do, however, show that *A. oryzae* produces many recombinant proteins equally well if the mycelial culture is severely broken up, but this is not the case when other filamentous fungi are used.

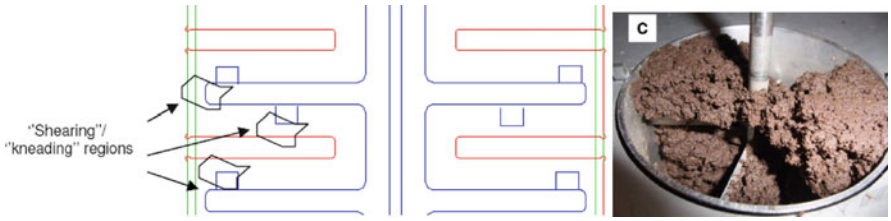

Fig. 11.16 Mixing of hydrolytic enzymes into pretreated barley straw (Andric 2010)

One must conclude, that the quality criteria used to compare different mixing systems (P, $t_{mix,}$ k_la) are not always sufficient to judge between different mixing systems. Many, and especially fundamental studies on metabolic behavior of the culture must be made, before the problems of mixing in industrial scale have been characterized.

Andric (2010) made a comprehensive study of the mixing aspects of enzymatic hydrolysis of pretreated wheat and barley straw using an enzyme cocktail of cellulases from Novozymes and a β-glucosidase, also from Novozymes.

The most expensive step in ethanol production from lignocellulosic biomass is most likely the hydrolysis step in which the sugars are released from cellulose (and the hemicelluloses). The process time for the hydrolysis step may be 20–40 h, and a large fraction of the added enzymes never contribute to the hydrolysis, since they are either deactivated or do not come into close enough contact with the cellulose fibers. This is entirely a problem caused by unsatisfactory mixing of the water-swollen pretreated biomass.

A high cellulose content of the slowly liquefying biomass–water mixture (15–25 wt%) is necessary in order to make the ensuing recovery of ethanol from the fermentation medium profitable, but initially the mixture has the appearance of a thick dough.

Conventional mixing aggregates will never work, from a mechanical or a power consumption point of view. Hence, completely new mixing aggregates must be invented, and the new mixers will always operate in the laminar flow region.

In his study of robust mixers that in large scale and with an acceptable power input could handle hydrolysis of lignocellulosic biomass Andric looked at the Paper and Pulp Industry where similar but less demanding mixing processes are made in large scale. Inspired by processes used in the bakery, Andric also looked at machines in which tearing of the semisolid biomass, combined with kneading (the folding and refolding of thin layers of the material) is the mixing concept.

Figure 11.16 shows one of his (home-made) stirrers with a set of partly overlapping stirrer arms that almost touch the cylindrical tank wall. Here tearing and kneading are combined, and most of the sugars were released after 6–10 h of "kneading-tearing-and hydrolysis" from the still semisolid residue (see photo on Fig. 11.16). Still, the power input was way too high.

The conversion of polymeric carbohydrates to monomers by the mixing-assisted enzymatic hydrolysis is one of the most challenging mixing processes in present

day bioproduction. As discussed in Chap. 2, enormous advances have been made during the last 20 years concerning effective production of the hydrolytic enzymes, their productivity and their stability at the hydrolysis temperature. The outstanding challenge is to make the enzymes work, not on artificial cellulose substrates, but on real lignocellulosic biomass. Here, new process technology and new equipment will certainly have to be developed.

Problems

Problem 11.1 *Scale-up without maintaining geometrical similarity*. In Example 11.9 and 11.10, linear scale-up of a stirred tank bioreactor from 600 L to 60 m^3 was considered. It was found that the mixing time increased by a factor of ≈3. Suppose now instead that the impeller diameter of the 60 m^3 reactor is chosen to 1.4 m (i.e., the reactor geometry is changed), but the requirement of a constant P/V (113 W m^{-3}) is maintained.

(a) How much larger is the mixing time in the large-scale bioreactor now?
(b) Determine the value of N that would give the same t_{mix} as in Example 11.9 with $[P/V, d_s] = [113\ Wm^{-3}, 1.4\ m]$.
(c) Would the choice of $[N, P/V, d_s]$ in (b) increase or decrease the risk of flooding?
(d) At a certain t_{mix}, and for n RJH with nozzle diameter d you have calculated a power input P/V and a corresponding liquid flow ${v_l}^0$ for $V = V^0$. Show that for the same P/V, but at a different medium volume V^1 the liquid flow must be ${v_l}^1 = {v_l}^0\ (V^1/V^0)^{1/3}$. Use the data from Example 11.9 to calculate v_l for $V^1 = 3.4\ m^3$ based on $v_l = 199.2\ m^3\ h^{-1}$ that was obtained for $V^0 = 60\ m^3$.

Problem 11.2 *Exchanging impellers*. One drawback of the traditional Rushton impeller is that the ratio between aerated and unaerated power consumption falls rapidly with an increased aeration rate. The hydrofoil impeller typically has a lower power number, but the aerated power consumption falls less rapidly with increasing aeration rate. For a Rushton turbine and a Prochem impeller, and for stirring speeds close to 300 rpm, the ratio between aerated and unaerated power consumption is given in the figure shown below.

You are replacing a Rushton turbine in a 100 m^3 reactor ($T = 3$ m, $d_s = 1$ m) by a Prochem impeller. Assume that the stirring rate should be maintained the same.

(a) What diameter of the Prochem impeller will give the same unaerated power consumption as the Rushton turbine? The values of N_p for the Rushton turbine and the Prochem impeller are 5.2 and 1.5, respectively.
(b) How much higher (approximately) will the k_la value be for the Prochem impeller at an aeration rate of 0.5 vvm under the conditions in (a), (i.e., the same unaerated power consumption is achieved)? The k_la value for the same specific power input has been found to be identical for the two impeller types. Assume a non-coalescing medium.

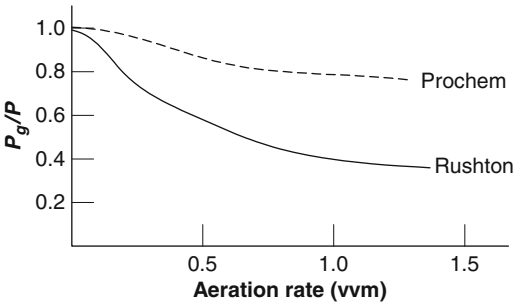

Problem 11.3 *Design of a pilot plant bioreactor*. In connection with the purchase of a new pilot plant bioreactor (41 L) to be used for penicillin fermentation, it is desired to examine whether one of the manufacturer's standard-design bioreactors (equipped with Rushton turbines) can be used. The dimensions of this bioreactor are specified in the table below.

Aspect ratio (T/d_s)	3
Tank diameter (T)	0.267 m
Stirrer diameter (d_s)	0.089 m
Number of impellers[a]	3
Maximum stirring speed (N_{max})	600 rpm

[a]The impellers are six-bladed Rushton turbines.

(a) Show that with a non-Newtonian medium, for which the rheology is described by a power law expression (11.26), Re_s is given by (1)

$$\mathrm{Re}_s = \frac{\rho_l N^{2-n} d_s^2}{K k^{n-1}}, \tag{1}$$

where $k = 10$ is the constant used for calculation of the average shear rate in (11.32). For a medium containing, respectively, 0, 20, and 40 g L^{-1} biomass (of the fungus *P. chrysogenum*) you are required to plot Re_s vs. the stirring speed. Discuss the results.

(b) Determine the power number with $N = 600$ rpm for the three cases considered in (**a**), and calculate the power input per unit volume when the bioreactor contains 25 L of medium. Calculate the average viscosity in the bioreactor.

(c) For non-Newtonian media and the 41 L bioreactor, the following correlation was found:

$$k_l a = 0.226 \times 10^{-3} u_s^{0.4} \left(\frac{P_g}{V}\right)^{0.6} \eta^{-0.7}. \tag{2}$$

Can the dissolved oxygen concentration in the reactor be maintained above 30% (which for some strains is a critical level for penicillin production) when the oxygen requirement for a *rapidly growing* culture of *P. chrysogenum is*

$r_o = 2.3$ mmol of O_2 (g DW)$^{-1}$ h^{-1} Discuss how the bioreactor can be modified to satisfy the oxygen requirement.

(d) You decide to examine the effect of increasing the stirrer diameter. Start with $d_s/T = 0.4$. Can the critical level of dissolved oxygen concentration be maintained with this diameter ratio?

Problem 11.4 *Scaled-down experiment*. The pH value is often controlled using only a single pH electrode and a single point of addition of base or acid, also in large-scale bioreactors. The pH electrode is typically located in a well-mixed region, and addition of base or acid is typically made at the liquid surface. Since concentrated solutions are used, pH gradients in large-scale reactors are likely to be present.

Amanullah et al. (2001) used of a scaled-down system to study effects of pH gradients. The scaled-down system consisted of a 2 L standard stirred tank reactor, with a working volume of 1 L, equipped with two Rushton turbines ($d_s/d_t = 0.33$). To the reactor was connected a piece of tubing ($L = 2.75$ m, $d_i = 4.8$ mm), through which liquid from the reactor was pumped. The pH value in the reactor was measured, and pH control was achieved by adding base to a small mixing bulb (volume about 1.5 ml) located just before the tubing (see figure below).

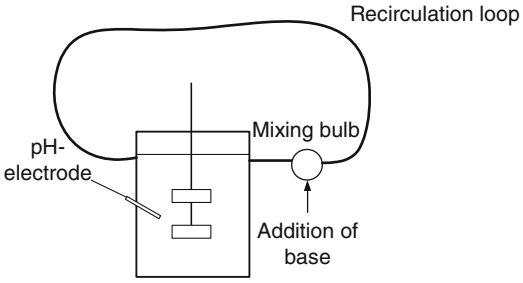

This system was used to experimentally simulate a three compartment reactor model, with a direct feed zone (bulb), a poorly mixed zone (tubing part), and a well-mixed zone (the reactor).

(a) Discuss what residence time in the tubing that should be chosen to simulate a large-scale reactor (100 m^3). The same residence time in the tube can be achieved by different ratios of tube volume, V_{tube} and recirculation flow, v_{rec}. Discuss how the values of V_{tube} and v_{rec} should be chosen.

In their study, Amanullah et al. (2001) used a strain of *Bacillus subtilis*. This organism produces acetoin and 2,3 butanediol under oxygen-limited conditions. The formation of acetoin and butanediol is described by:

$$2 \text{ pyruvate} \rightarrow CO_2 + \text{ acetolactate} \rightarrow (\text{acetolactate synthase})$$

$$\text{Acetolactate} \rightarrow CO_2 + \text{ Acetoin} \rightarrow (\text{acetolactate decarboxylase})$$

$$\text{Acetoin} + \text{NADH} + H^+ \leftrightarrow 2,3 \text{ butane-diol} \rightarrow (\text{butanediol dehydrogenase})$$

At pH values higher than 6.5 also acetate is formed.

(b) Compare the residence time in the tube to the characteristic times for oxygen consumption and substrate consumption. Assume that the dissolved oxygen concentration in the reactor is 10% of DOT, and that the system is to be operated as a chemostat with a glucose concentration = 10 mg L^{-1} and a biomass concentration of 4 g L^{-1}.

What are your conclusions?

(c) The experiments by Amanullah et al. were in fact made as batch cultivations, with oxygen-limited conditions also in the stirred tank reactor. A control experiment, in which base addition was made in the reactor instead of in the loop was also made. The following yields were found

Residence time in loop (s)	Yield of acetic acid (g g^{-1})	Sum of yields of acetoin and butanediol (g g^{-1})	Biomass yield (g g^{-1})
(no loop)	0	0.30	0.49
30	0.002	0.31	0.52
60	0.023	0.29	0.51
120	0.076	0.23	0.50
240	0.083	0.22	0.50
120[a]	0	0.30	0.50

[a]pH control made in the stirred tank reactor instead of in the loop

Discuss the results.

Problem 11.5 *Calculation of the true v_l and the true power input for Rotating Jet Heads*. In Example 11.10 the mass transfer coefficient k_la was calculated from (4), assuming that for a given Δp, v_l was given by (11.37) and (11.35).

When the medium is aerated with $v_g/v_l = n_t$ then, for a given Δp one must use (11.36) to calculate v_l rather than (11.35) which is derived for unaerated medium. v_l will be smaller than when calculated from (11.35), and consequently P will be smaller when calculated from (11.35). Since the power input is smaller the value of k_la will be smaller for the given Δp.

The present problem will calculate the true value of v_l and the ratio between the "true" P and $P = P_0$ calculated from (11.35). This will give us an analogue to $N_{p,g}/N_p$ of Fig. 11.5.

(a) For a fixed $p_t = 1.04$ and a fixed $\Delta p = 1.23$ bar, $v_l = 199.2$ m^3 h^{-1} (the result for v_l in Example 10.9 for $t_{mix} = 29$ s, when the correction factor in (11.36) is not included). But $n_t = 10/199.2 = 0.0502$, and when $[n_t, p_t, \Delta p] = [0.0502, 1.04, 1.23]$ the correction factor is slightly smaller than 1, and $v_l < 199.2$ m^3 h^{-1}.

For different values of $n_t \subset (0,1)$ calculate the true v_l by iteration of (11.36) – at most two iterations is enough to obtain convergence. Start with $n_t = 0.0502$, but use also other values of v_g at $\Delta p = 1.23$ bar to cover at least part of the interval $0 < n_t < 1$.

Calculate P for the series of v_g values used, and thereafter P/P ($v_l = 199.2$ m^3 h^{-1}).

How do these results influence k_la for increasing v_g?

(b) The results in (a) can be plotted in the same fashion as on Fig. 11.5.
What is a reasonable variable to plot on the abscissa?
Make your own conclusions concerning an analogue for N_A in the RJH-mixer.

References

Amanullah, A., McFarlane, C.M., Emery, A.N., and Nienow, A.W. (2001). A scale-down model to simulate spatial pH variations in large-scale bioreactors. *Biotechnol. Bioeng.* **73**:390–399.

Andric, P. (2010). Reactor design for improved enzymatic hydrolysis of lignocellulose. PhD thesis, DTU (DK).

Bird, R.B., Stewart, W.E., and Lightfoot, E.N. (2002). Transport phenomena, 2nd ed., John Wiley & Sons, New York.

Brown, D.A.R., Jones, P.N., and Middleton, J.C. (2004) Experimental methods, part A: Measurement tools and techniques for mixing and flow-visualization studies. In *Handbook of Industrial Mixing* (E.L. Paul, V.A Atiemo-Obeng and S.M. Kresta, *eds.*) Wiley Interscience 145–202.

Bylund, F., Castan, A., Mikkola, R., Veide, A., and Larsson, G. (2000). Influence of scale-up on the quality of recombinant human growth hormone. *Biotechnol. Bioeng.* **69**:119–128.

Cooke, M. Middleton, J.C., and Bush, J. (1988). Proceedings 2nd Int. Conf. Bioreactor fluid dynamics, BHR group 37–64.

Crank, J. (1956). *The Mathematics of Diffusion*, 1st edition Oxford (UK).

Delaplace, G., Bouvier, L., Moreau, A., Guérin, R., and Leuliet, J.C. (2004). Determination of mixing time by colorimetric diagnosis-application to a new mixing system. *Exp. Fluids*, **36**: 437–443.

Dominguez, J., Abreu, A.M., McCalla, R., Borroto, J. Ortueta, M., and Perez, E. (1999). Mixing characterization in batch reactors using the radiotracer technique. *J. Radioanal.& Nucl. Chem*, **241**:337–340.

Einsele, A., Ristroph, D.L., and Humphrey, A.E. (1978) Mixing times and glucose uptake measured with a fluorometer. *Biotechnol. Bioeng.* **20**:1487–1492.

Enfors, S.O. (ed) 2001. Physiological responses to mixing in large scale reactors. *J. Biotechnol*, **85**: 175–185.

George, S., Larsson G., Olsson, K., and Enfors, S.-E. (1998) Comparison of the Baker's yeast process performance in laboratory and production scale. *Bioproc. Eng.* **18**:135–142.

Grenville, R.K., and Tilton, J.N. (1996). A new theory improves the correlation of blend time data from turbulent jet mixed vessels, *Chem Eng Research Design*, **74**:390–396.

Hua, L., Nordkvist, M., Nielsen, P.M., and Villadsen, J. (2006). Scale-up of enzymatic production of lactobionic acid using the Rotary Jet Head System, *Biotechnol. Bioeng.* **97**:842–849.

Hummer, J.S. (2004). A method and a process plant for treating a batch of liquids. European Patent 1,324,818.

Johnson, A.T. (1999). Biological process engineering, John Wiley & Sons, New York.

Kold, D. (2010). Study of mass transfer in viscous fermentation – using a Rotating Jet Head mixing system. PhD thesis DTU (DK).

Leib, T.M., Pereira, C.J., and Villadsen, J. (2001). Bioreactors, a chemical engineering perspective. *Chem. Eng. Sci.* **56**:5485–5497.

Masiuk, S. (2000). Mixing time for reciprocating plate agitator with flapping blades. *Chem. Eng. J.* **79**:23–30.

McFarlane, C.M., and Nienow, A.W. (1995). Studies of high solidity ratio hydrofoil impellers for aerated bioreactors, part I and II, *Biotechnol. Prog.* **11**:601–607 and 608–618.

Melton, L.A., Lipp, C.W., Spralding, R.W., and Paulson, K.A. (2002). DISMT determination of mixing time through color changes. *Chem. Eng. Commun.* **189**:322–338.

Metzner,A.B., and Otto, R.E. (1957). Agitation of non-Newtonian fluids, *AIChE J*, **3**:3–10.

Nienow, A.W. (1997). On impeller circulation and mixing effectiveness in the turbulent flow regime, *Chem. Eng. Sci.* **15**:2557–2565.

Nienow, A.W. (2010). Stirred tank bioreactors, and Scale-up and scale down of stirred bioreactors (in *Comprehensive Bioprocess Engineering*, Berovic, M. and Enfors S.O.(editors), University of Ljubljana (Slo), 135–159 and 179–199.

Nienow, A.W., and Lilly, M.D. (1979). Power drawn by multiple impellers in sparged vessels. *Biotechnol. Bioeng.* **21**:2341–2345.

Nordkvist, M., Grotkjær, T., Hummer, J.S., and Villadsen, J. (2003). Applying rotary jet heads for mixing and mass transfer in a forced recirculation tank reactor system, *Chem. Eng. Sci.* **58**:3877–3890.

Nordkvist, M., Nielsen, P.M., and Villadsen, J. (2006). Oxidation of lactose to lactobionic acid by a *Microdochium nivale* carbohydrate oxidase; Kinetics and operational stability. *Biotechnol. Bioeng.* **97**:694–707.

Nordkvist, M., Vognsen, M., Nienow, A.W., Villadsen, J. and Gernaey K.V. (2008). Mixing by Rotary Jet heads: Indications of the effect of rotation at turbulent and transitional flow conditions. Transactions, 6th symposium on mixing in industrial process industries, Niagara Falls (Ca) 17–21 August 2008.

Oldeshue, J. (1966). Fermentation mixing scale-up techniques, *Biotechnol. Bioeng.* **8**:3–24.

Oosterhuis, N.M.G., and Kossen, N.W.F. (1983) Oxygen transfer in a production scale bioreactor. *Chem. Eng. Res. Dev.* **61**:308–312.

Otomo, N., Bujalski, W., and Nienow, A.W. (1995). The application of a compartment model to a vessel stirred with either dual radial or dual axial flow impellers. 1995 *IChemE Research Event*, *Proceedings*, 829–831.

Otomo, N., Bujalski, W., Nienow, A.W., and Takahashi, K. (2003). A novel measurement technique for mixing time in an aerated stirred vessel. *J. Chem. Eng. Japan*, **36**:66–74.

Parente, E. and Ricciardi, A. (1999). Production, recovery and purification of bacteriocins from lactic acid bacteria. *Appl Microbiol.* Biotechnol. **52**:628–638.

Pedersen A.G. (1992). Characterization and modeling of bioreactors. PhD thesis, DTU (DK).

Pedersen, A. G., Bundgård-Nielsen, M., Nielsen, J., Villadsen, J (1994).Characterization of mixing in stirred tank bioreactors equipped with Rushton turbines. *Biotechnol. Bioeng.* **44**:1013–1017.

Picque, D., and Corrieu, G. (1988). New instrument for on-line viscosity measurement of fermentation media. *Biotechnol. Bioeng.* **31**:19–23.

Revill, B.K (1992). Jet mixing (in *Mixing in the Process Industries*, Harnby, N., Edwards, M.F., and Nienow, A.W. (editors), Oxford, UK) 159–183.

Rushton, J.H., Costich, E.W., and Everett, H.J. (1950a). Power characteristics of mixing impellers – Part I. *Chem. Eng. Prog.* **46**:395–404.

Rushton, J.H., Costich, E.W., and Everett, H.J. (1950b). Power characteristics of mixing impellers – Part II. *Chem. Eng. Prog.* **46**:467–476.

Schweder, T., Kruger, E., Xu, B., Jurgen, B., Blomsten, G., Enfors, S.-E., and Hecker, M. (1999). Monitoring of genes that respond to process-related stress in large-scale bioprocesses. *Biotechnol. Bioeng.* **65**:151–159.

Sweere, A.P.J., Luyben, K.Ch.A.M., and Kossen, N.W.F. (1987). Regimen analysis and scale-down: tools to investigate the performance of bioreactors. *Enz. Microb. Technol.* **9**:386–398.

Villadsen, J. (1997). Putting structure into Chemical Engineering. *Chem Eng Sci*, **97**: 2857–2864.

Vrabel, P., van der Lans, R.G.J.M., Luyben, K.Ch.A.M., Boon, L., Nienow, A.L. (2000). Mixing in large-scale vessels stirred with multiple radial or radial and axial up-pumping impellers: modelling and measurements. *Chem. Eng. Sci.* **55**: 5881–5896.

Index

J. Villadsen et al., *Bioreaction Engineering Principles*,
DOI 10.1007/978-1-4419-9688-6, © Springer Science+Business Media, LLC 2011

D

M